19TH INTERNATIONAL COSMIC RAY CONFERENCE

LA JOLLA, USA AUGUST 11-23, 1985

NASA-CP-2376-VOL-5
19850026678

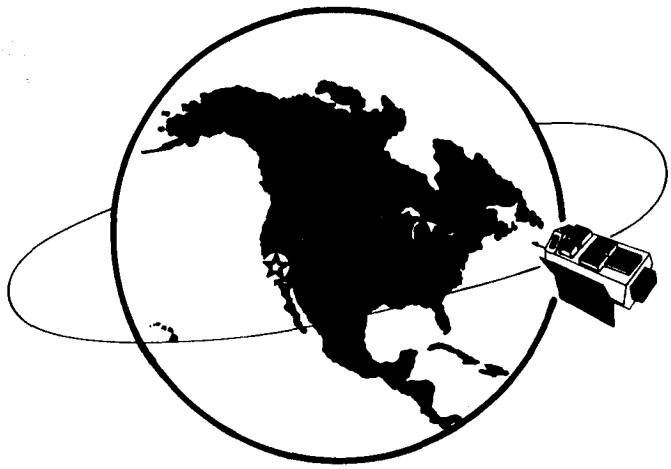

CONFERENCE PROGRAM SESSIONS VOL. 5

19TH INTERNATIONAL COSMIC RAY CONFERENCE

LA JOLLA, USA AUGUST 11-23, 1985

CONFERENCE PAPERS

SH

SESSIONS
VOL. 5

NASA Conference Publication 2376

Published by
Scientific and Technical Information Branch
National Aeronautics and Space Administration
Washington, D.C. 20546

August 1985

For sale by the National Technical Information Service, Springfield, VA 22151

PREFACE

The 19th International Cosmic Ray Conference, under the auspices of the Cosmic Ray Commission of the International Union of Pure and Applied Physics, is being held on the campus of the University of California, San Diego, on 11 through 23 August 1985. In keeping with the tradition begun in 1971 by the Australian organizers of the 12th ICRC, the Proceedings of this conference are appearing in two sets of volumes. The first set, consisting of volumes 1 through 8, is being distributed to all participants at the beginning of the conference. This set contains the contributed papers. The second set, distributed after the conference, contains invited, rapporteur, and highlight papers. The papers are reproduced here exactly as they were received from the authors, without refereeing.

For the 19th ICRC, the scientific program was organized according to three major divisions-- OG (cosmic rays and gamma rays of Galactic Origin), SH (Solar and Heliosphere), and HE (High Energy). Technical papers are included in each of the three divisions.

This conference depended on funds from several agencies of the United States government, including major financial support from the National Aeronautics and Space Administration and support from the National Science Foundation, the Department of Energy, and the Air Force Geophysics Laboratory. Important financial support also came from the Center for Astrophysics and Space Sciences of the University of California, San Diego, from the California Space Institute of the University of California, from the Department of Physics and Astronomy of the University of Maryland, College park, from the International Union for Pure and Applied Physics, and from several corporate sponsors who will be acknowledged by name in the post-conference volumes.

We appreciate the confidence placed in the conference organizers by the Cosmic Ray Commission, and acknowledge with thanks the role of the Commission members in setting up the rules for the conference and in advising the organizers during its planning.

We are grateful to all of the members of the various organizing committees listed at the front of this volume. The three Program Committees went to great effort to organize a coherent scientific program and to schedule four parallel sessions with a minimum of conflicts. The Local Organizing Committee has worked long and hard to ensure efficient and hospitable accommodations for all the participants, both in the scientific sessions and outside them. The Publications Committee not only took great pains to assemble these volumes but also maintained an orderly data base of papers and authors which was extremely helpful to the program committees. The General Organizing Committee made important contributions of ideas and efforts to make the conference possible; this committee included international representation from all of North America, thus the departure from the traditional name of National Organizing Committee. And the entire effort was coordinated by the dedicated members of the Steering Committee.

Martin H. Israel, Chairman
General Organizing Committee

August, 1985

LETTER FROM THE EDITORS

This conference marks a departure from previous conferences in this series in that the publication of the Conference Papers was carried out an entire continent away from the activities of Local Organizing Committee. This posed some problems but, to the considerable surprise of the Publications Committee members, the one that was expected to be the most trouble turned out not to be significant. The overwhelming majority of those submitting papers and abstracts sent them to the correct address, not to La Jolla as was feared. We wish to thank our many authors for their alertness and commend them for handling a complicated situation so well.

There are eight volumes to be distributed to the conference participants in addition to the Conference Program and Author Index: three volumes for OG, two for SH and three for HE. the detailed makeup of these volumes is described in the prefaces written by the Scientific Program chairmen for their respective volumes. Out of some 1100 abstracts that were accepted by the Scientific Program Committees for inclusion in the conference some 929 papers were finally received in time for inclusion in the Conference Papers. This represents a response of approximately 84 percent, a modest improvement. Even if one excludes the 42 one page papers that should be considered as "confirming abstracts", even though there was no such formal category, the response was somewhat higher than that of recent years. We attribute this to the carrot of a later deadline than before coupled with the stick of there being no printing of post deadline contributed papers. We believe that this decision of the General Organizing Committee was a wise one. Of course invited, rapporteur, and highlight talks will be printed in volumes to be distributed to the participants after the conference as usual.

The Publications Committee had much generous help in performing its duties: from Goddard Space Flight Center we had the help of B. Glasser, L. Harris, E. Schronce, N. Smith, J. Esposito and T. Smith. From the Naval Research Laboratory we were helped by T. Mazzotta, and at the University of Maryland M. L. Snidow and J. Mucha gave much needed assistance. Special thanks are due to Caryl Short, the lone staff member of the Publications Committee. She maintained the computer data base, organized the abstracts as they arrived, and kept track of the papers themselves to see that the finally arrived in the right place at the right time. Without her help the job would have been far more difficult than it was.

PUBLICATIONS COMMITTEE August, 1985

Frank C. Jones, Chm.
Jim Adams
Glen M. Mason

SH SESSIONS
VOLUME V

19th INTERNATIONAL COSMIC RAY CONFERENCE
LA JOLLA, USA
AUGUST 11-23, 1985

INTERNATIONAL UNION OF PURE AND APPLIED PHYSICS
MEMBERS OF THE COMMISSION ON COSMIC RAYS OF IUPAP

A.E. Chudakov, Chm.
F.B. McDonald
G.C. Castagnoli
P.H. Fowler
D. Hovestadt
J. Kota
T.O. Montmerle
H. Moraal
J.R. Prescot
B.V. Sreekantan
K. Suga
J. Wdowczyk

STEERING COMMITTEE

F. McDonald, Chm.
G. Burbage
M. Forman
T. Gaisser
M. Israel
F. Jones
R. Lingenfelter
R. Mewaldt
L. Peterson

GENERAL ORGANIZING COMMITTEE

M. Israel, Chm.
M. Bercovitch
P. Freier
R. Gall
R. Jokipii
L. Jones
V. Jones
S. Krimiges
J. Kurfess
J. Lockwood
P. Meyer
B. Price
R. Ramaty
F. Reines
M. Shapiro
M. Shea
J. Simpson
E. Stone
D. Venkatesan
J. Waddington
S. White

PROGRAM COMMITTEES

OG SESSIONS
R. Mewaldt, Chm.
G. Cassiday
C. Fichtel
A. Harding
J. Matteson
D. Muller
W. Webber

SH SESSIONS
M. Forman, Chm.
H. Hudson
G. Mason
B. McKibben
M. Pomerantz

HE SESSIONS
T. Gaisser, Chm.
K. Lande
J. Linsley
E. Loh
G. Yodh

PUBLICATIONS
F. Jones, Chm.
J. Adams
G. Mason

LOCAL ORGANIZING COMMITTEE

L. Peterson,Chm.
G. Burbidge
R. Lingenfelter
R. Rothschild
J. Arnold
W. Baity
A. Buffington
M. Burbidge
W. Fillius
R. Gall
R. Gould
H. Hudson
J. Linsley
K. Marti
G. Masek
J. Matteson
C. McIlwain
R. Mewaldt
O. Piccioni
M. Thiemens
W. Thompson
H. Ticho
R. White

Sponsored by
National Aeronautics and Space Administration
National Science Foundation
Department of Energy
Center for Astrophysics and Space Science, University of California, San Diego
California Space Institute, University of California
Department of Physics and Astronomy, University of Maryland, College Park

PREFACE TO THE VOLUMES 4 AND 5 (SH)

The category SH includes all papers on solar and heliospheric energetic particle phenomena. SH combines the MG (modulation of galactic) and SP (solar particles) categories used in previous conferences, with papers on particles accelerated in the solar wind. Papers about techniques and instrumentation for science in the SH category are now included in SH. Cosmogenic nuclide studies, formerly in OG (origin and galactic) are also in the new SH category. Papers on particles of strictly magnetospheric origin were not included in this conference.

The SH heading numbers are :

SH1. Particle Acceleration on the Sun and in the Heliosphere
SH2. Composition, Spectra and Anisotropy
SH3. Propagation of Solar and Interplanetary Energetic Particles
SH4. Solar-Cycle Modulation and Propagation of Galactic Particles in the Heliosphere
SH5. Transient Modulations
SH6. Geomagnetic and Atomospheric Effects and Response Functions
SH7. Cosmogenic Nuclides
SH8. Solar Neutrinos
SH9. Techniques
SH10. Others

Papers appear in this volume in a numerical sequence determined primarily by this numbering system. For example, paper number SH2.1-8 is the eighth paper in the first session formed of papers in category SH2.

We thank the SH program committee for devising this numbering system, for reading every abstract submitted and for organizing on the basis of their content coherent sessions with reasonable length for presentation. We thank them also for selecting the rapporteurs and for advice in the selection of invited and highlight speakers. The committee members are: Hugh Hudson (UCSD), Bruce McKibben (U. of Chicago), Glenn Mason (U. of Maryland), Martin Pomerantz (Bartol Res. Foundation, U. of Delaware) and alternate Walker Fillius (UCSD).

These contributed papers are reviewed in plenary session by a team of expert rapporteurs at the end of the Conference. These extremely useful reports can only be prepared during the Conference, and so their written versions will be included in a later volume. We thank the rapporteurs in advance for their willing service.

Miriam A. Forman, Chairman
Solar - Heliospheric Program Committee

This conference is the 19th in a series. Previous conferences in this series were held at:

Cracow, Poland	–	1947
Como, Italy	–	1949
Bagneres–de–Bigorre, France	–	1953
Guanjuato, Mexico	–	1955
Varenna, Italy	–	1957
Moscow, USSR	–	1959
Kyoto, Japan	–	1961
Jaipur, India	–	1963
London, UK	–	1965
Calgary, Canada	–	1967
Budapest, Hungary	–	1969
Hobart, Australia	–	1971
Denver, USA	–	1973
Munchen, FRG	–	1975
Plovdiv, Bulgaria	–	1977
Kyoto, Japan	–	1979
Paris, France	–	1981
Bangalore, India	–	1983

VOLUME 5

SH 4.3
GRADIENTS AND NORTH-SOUTH ANISOTROPIES

SH 4.4
SIDERIAL AND LONG TERM MODULATION

SH 4.5
DIURNAL VARIATIONS

VOLUME 5

SH 4.6
THE ANOMALOUS COMPONENT

SH 4.7
INTENSITY GRADIENTS AND THE OUTER HELIOSPHERE

SH 5.1
TRANSIENT MODULATION (FORBUSH DECREASES)

SH 6.1
GEOMAGNETIC AND ATMOSPHERIC EFFECTS AND RESPONSE FUNCTIONS

VOLUME 5

SH 7.1
COSMOGENIC NUCLIDES

SH 8.1
SOLAR NEUTRINOS

SH 9.1
TECHNIQUES AND INSTRUMENTATION

SH 10.
OTHER TOPICS

GRADIENTS AND ANISOTROPIES OF HIGH ENERGY COSMIC RAYS IN THE OUTER HELIOSPHERE

Fillius, Walker [1], E. C. Roelof [2], Edward J. Smith [3], David Wood [1], and Wing-Huen Ip [4]

1 University of California, San Diego, La Jolla, CA 92093
2 Johns Hopkins University Applied Physics Laboratory, Laurel, MD
3 Jet Propulsion Laboratory, Pasadena, CA 91103
4 Max Planck Institut fur Aeronomie, Katlenburg-Lindau 3, Germany

Introduction Two cosmic rays which pass through the same point going in opposite directions will, in the absence of scattering and inhomogeneities in the magnetic field, trace helices about adjacent flux tubes, whose centerlines are separated by one gyrodiameter. A directional anisotropy at the point suggests a difference in the number of cosmic rays loading the two flux tubes; that is, a density gradient over the baseline of a gyrodiameter. The anisotropy produced by such a gradient can be written

$$\xi = \rho_g \hat{B} \times G = P/B^2 \; B \times G \qquad (1)$$

where ξ is the anisotropy, ρ_g the gyroradius, P the rigidity, B the field, and G the gradient. It is convenient to express ξ in %, G in %/AU, B in nT, and P in nT-AU.

Previous studies at lower energies have shown that the cosmic ray density gradients vary in space and time [1], and many authors currently are suggesting that the radial gradient associated with solar cycle modulation is supported largely by narrow barriers which encircle the sun and propagate outward with the solar wind. If so, the anisotropy is a desirable way to detect spatial gradients, because it can be associated with the local solar wind and magnetic field conditions.

With this in mind we are studying the anisotropy measurements made by the UCSD Cerenkov detectors on Pioneers 10 and 11. This is a progress report in which we show that the local anisotropy varies greatly, but that the long-term average is consistent with the global radial gradient measured between two spacecraft over a baseline of many AU.

Instrumentation Our Cerenkov detectors register cosmic rays with velocity > 3/4c, corresponding mainly to hydrogen and helium above an energy of ~500 MeV/nucleon. In this study we will consider only protons. Alpha particles are counted, in proportions exceeding their abundance, because the solid angle of the acceptance lobe is larger for multiply charged particles. However, for the same reason, the alpha particle response is less directional than the proton response, and so these particles do not have a great effect on the anisotropy measurements.

Integrating the cosmic ray proton spectra of Meyer et al [2] above our threshold, we estimate that the detector responds to protons with a mean rigidity, P, of 0.14 nT-AU at solar maximum and 0.10 at solar minimum. For a normal Parker spiral field with magnitude of 6 nT at one AU, the average gyroradius for a proton in our counter is then R*0.032

(AU) and R*0.023, respectively, and the expected north-south anisotropy, for a gradient of 2%/AU as measured over a two-spacecraft baseline, is R*0.064% and R*0.046%. Statistically we can resolve an anisotropy of 10% in 10 minutes, 1% in 18 hours, and 0.1% in 75 days, when the telemetry coverage is good. Thus it takes many days to resolve the expected effect.

As the Cerenkov detector is mounted perpendicular to the spacecraft spin axis, which points at earth, we obtain the unidirectional flux of high energy cosmic rays in a plane perpendicular to the spacecraft-earth line. When the gradient effect is dominant, a north-south anisotropy normally represents a radial gradient, and an east-west anisotropy reflects a latitude gradient.

Method The east-west and north-south components of equation (1) give usable relationships between the radial gradient and its contribution to the anisotropy.

$$\xi_{EW} = G_r * P * B_z / B^2 - [G_z * P * B_r / B^2] \quad (1a)$$

$$\xi_{NS} = -G_r * P * B_y / B^2 + [G_y * P * B_r / B^2] \quad (1b)$$

We expect the last terms to be negligible, because, as G_y is the longitudinal and G_z the latitudinal gradient, they tend to cancel themselves when averaged over a solar rotation or longer. Besides, B_r is small in the outer heliosphere, and also tends to cancel itself over a number of magnetic sector reversals.

The self-cancellation of unwanted terms becomes the basis of a powerful detection method, because, as the gradient-related anisotropy does change sign with B, we can average the data in such as way as to preserve this effect alone. Multiply equations (1a and b) by B_z and B_y.

$$B_z * \xi_{EW} = G_r * P * (B_z/B)^2 + \text{self-cancelling terms} \quad (2a)$$

$$-B_y * \xi_{NS} = G_r * P * (B_y/B)^2 + \text{self-cancelling terms} \quad (2b)$$

Adding (2a) and (2b) produces an expression relating the radial gradient, G_r, to its associated anisotropy in the scan plane.

$$B_z * \xi_{EW} - B_y * \xi_{NS} = G_r * P * (B_\perp/B)^2 + \text{self-cancelling terms} \quad (3)$$

We recognize the LHS of (3) to be $(\xi \times B)_r$. From a general expression for ξ, it can be shown [3] that $(\xi \times B)_r = (G_\perp P)_r$ + a scattering term that is proportional to the inverse of the diffusion tensor. The differences between this and equation (3) are negligible when we average over sufficiently long intervals and assume weak scattering.

Observations The scatter in the data is amply demonstrated in Figure 1, where we test for the linear relationship between ξ_{NS} and B_y/B^2 given by equation (1b). The data points are one-day accumulations, and so their accuracy is limited statistically to $\pm$ 1%. Clearly the variability of the data points exceeds this measurement limit by a large factor. We interpret this result as evidence that either the gradient is not uniform and homogeneous (it might be time dependent, or localized spatially), or the density gradient effect does not always dominate the anisotropy.

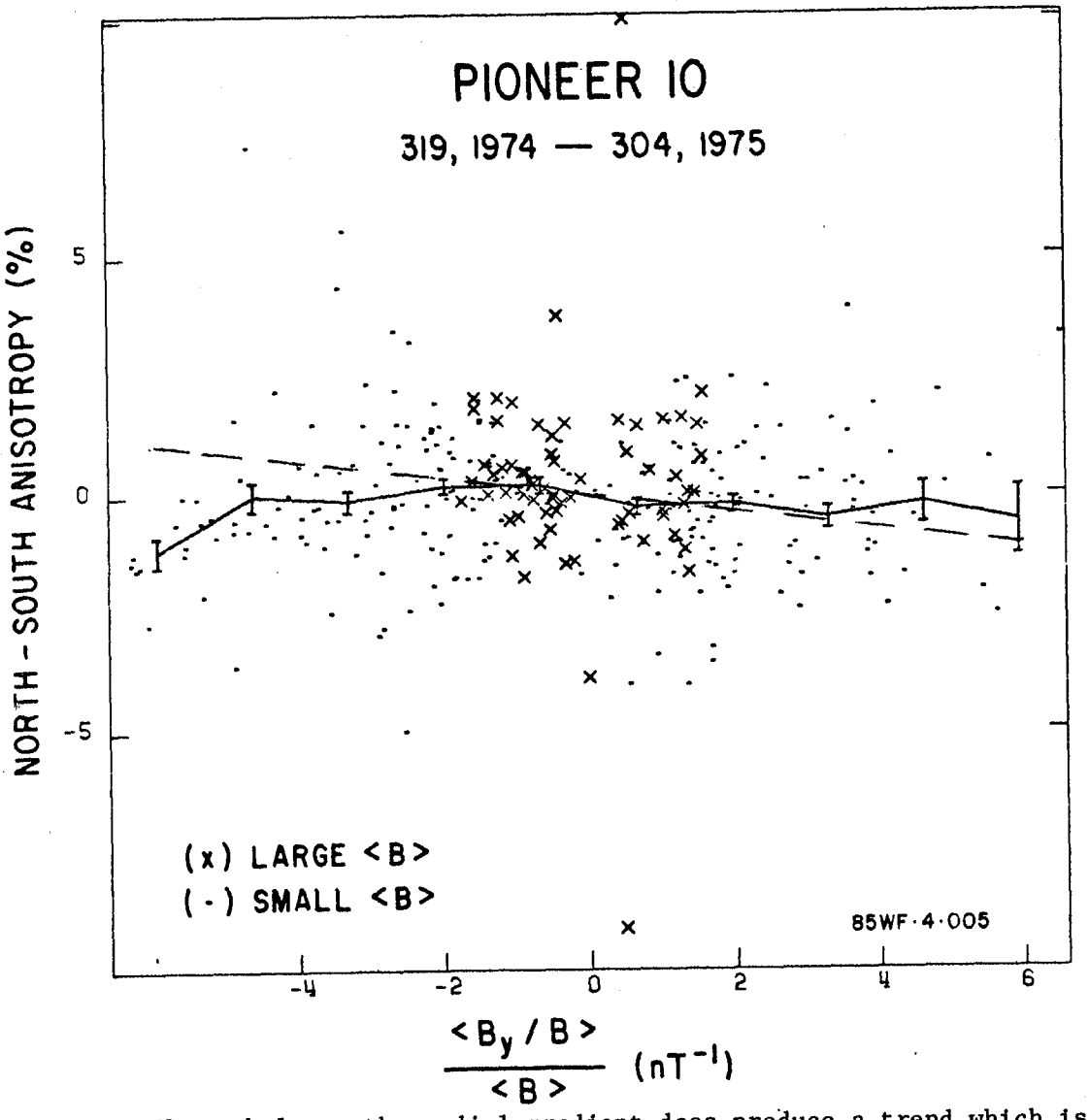

Nevertheless, the radial gradient does produce a trend which is discernible with enough data. The abscissa was divided into ten intervals, and the anisotropies averaged over each interval, as shown by the ten points with error bars. The five points at the center fall close to the expected relationship, given by the dashed line for 1.8 %/AU [4], and it is only the fringe intervals that deviate from expectations. As these intervals represent days when B is low, a possible interpretation is that the gradient is small inside rarefaction regions.

Although the gradient-related anisotropy is submerged in highly variable data, it is a robust effect. Figure 2 demonstrates how this signal persisted for 1000 days during an interval when we had adequate data coverage. Here we have solved equations (2b) and (3) for the gradient, and plotted this quantity vs time. We used equation (2b) before January, 1975 because Jovian electrons were present up to that

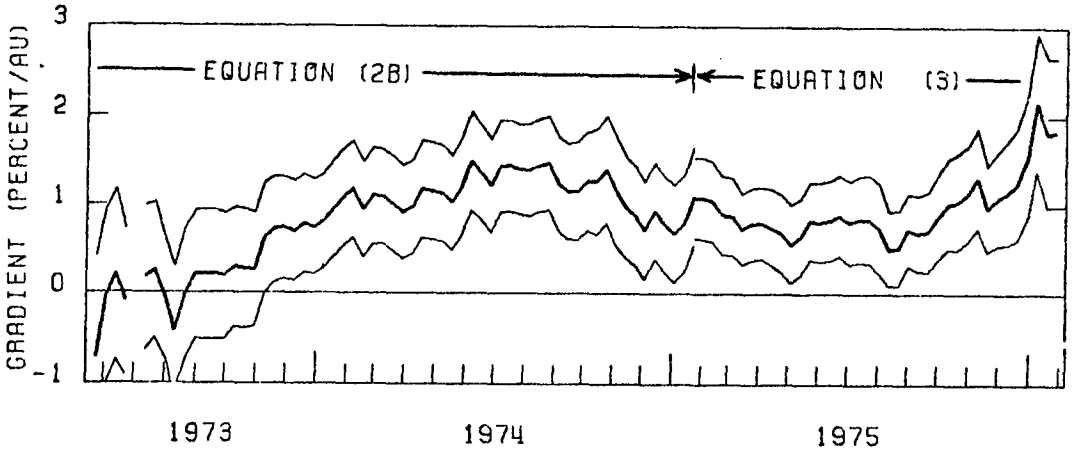

time in the east-west anisotropy, and affected the results from equation (3). These equations were evaluated every 10 days using 300 day boxcar averages to beat down the statistics and allow the extraneous effects to cancel.

Discussion The gradient values of 1-2 %/AU in Figure 2 are close to those obtained by comparing omnidirectional counting rates on two widely separated spacecraft [4,5]. Thus, the anisotropy method works for obtaining the radial gradient from a single spacecraft. This method was anticipated by Ip et al [6], but the present application is the most successful yet.

It is clear that other effects are present, over and above statistical errors, which cause the microscopic measurement to deviate from the global value. We hope to learn more about these effe`cts with further study.

Acknowledgement This work was supported in part by NASA Grants NAS 2-153 and NGL 05-005-007, and by Task ZF10 and contract N00024-85-C-5301 between the Johns Hopkins University and the Department of the Navy.

References

[1] Roelof, E. C., R. B. Decker, and S. M. Krimigis, "Latitudinal and Field-Aligned Cosmic Ray Gradients 2-5 AU: Voyagers 1 & 2 and IMP-8," J. Geophys. Res., Vol 88, 9889, Dec. 1, 1983.

[2] Meyer, P., R. Ramaty, and W. R. Webber, "Cosmic Rays -- Astronomy With Energetic Particles," Physics Today, 23-32, October, 1974.

[3] Zwickl, R. D., and E. C. Roelof, "Interplanetary Propagation of <1 MeV Protons in Nonimpulsive Energetic Particle Events," J. Geophys. Res., Vol 86, 5449-5471, July 1, 1981.

[4] Fillius, W., B. Wake, W.-H. Ip, and I. Axford, "Cosmic Ray Gradients in the Out`er Heliosphere," Proc. 18th I.C.R.C., Vol 3, p 55, 1983.

[5] Fillius, W., I. Axford, and D. Wood, "Time and Energy Dependence of the Cosmic Ray Gradient in the Outer Heliosphere," Paper SH 4.7-2, This Conference, 1985.

[6] Ip, W.-H., W. Fillius, A. Mogro-Campero, L. J. Gleeson, and W. I. Axford, "Quiet Time Interplanetary Cosmic Ray Anisotropies Observed From Pioneer 10 and 11," J. Geophys. Res., 83, 1633-1640, April 1, 1978.

ISOTROPIC INTENSITY WAVES AND FEATURES OF THEIR OCCURRENCE.

M.L. Duldig and R.M. Jacklyn
Antarctic Division, Department of Science, Australia.

and

M.A. Pomerantz
Bartol Research Foundation, University of Delaware, U.S.A.

ABSTRACT

Waves of daily average cosmic ray intensity, dependent on IMF polarity, have been observed in 1982 (Jacklyn and Pomerantz, 1983) and again in 1983 and 1984. These waves at first appeared to be due to the North-South anisotropy. Further investigation has revealed that the waves comprise two components, a large isotropic and a smaller anisotropic component. The anisotropic part is attributed to the North-South anisotropy and is in phase with the larger isotropic component in the Southern hemisphere. Unlike the North-South anisotropy which is a permanent feature of cosmic ray modulation, the isotropic phenomenon appears to be episodic in character. When present it is clearly dependent on IMF polarity but does not correlate well with IMF field strength. It is conjectured that the phenomenon might indicate some difference between the intensity regimes above and below the neutral sheet.

Introduction.

Isotropic intensity waves were first observed in variations of neutron intensity which followed the cosmic ray storm of September 1978 (Pomerantz and Duggal, 1979). The spectrum of these waves was found to be similar to that for a Forbush decrease, namely p^{-1} (Duggal et al., 1981). Since that time no further examples of this phenomenon have been observed.

During the latter months of 1982, 1983 and 1984 waves of variation occurred again. On each of the three occasions the waves were similar to each other, but were different in character from the 1978 waves. They consisted of two components, one isotropic and a second smaller anisotropic component, each having a hard rigidity spectrum. The analysis of the 27-day waves observed in 1982 have been described earlier (Jacklyn and Pomerantz, 1983; Jacklyn and Duldig, 1983; Jacklyn et al., 1984a, 1984b). In this paper we reiterate the two-component structure of the 1982 intensity waves, describe the intensity waves observed in 1983 and 1984 and discuss the field dependence of the isotropic component.

The 1982 Two Component Intensity Waves.

The discovery of prominent 27-day waves of the daily average cosmic ray intensity between July and October 1982 was described at the Bangalore Conference (Jacklyn and Pomerantz, 1983). It was clear that these waves had a relatively hard spectrum and seemed to represent waves of the interplanetary North-South asymmetry. Furthermore there was a very strong linear correlation between the waves and the proven index of variation of the North-South asymmetry, namely GG Nagoya (Mori and Nagashima, 1979).

It was later realized that these waves, now referred to as A_1 waves, were far too large in relation to the GG variations to be due solely to

the North-South asymmetry. By employing a constant of proportionality k_2, obtained from the CRRL tables of coupling coefficients for unidirectional anisotropies with a power index $\gamma=0.0$ and upper limiting rigidity Pu=200 GV, it was possible to remove the North-South asymmetry component through the GG variations (Jacklyn, Duldig and Pomerantz, 1984a and 1984b). The resulting residual variations, after p^{-1} isotropic and p^0 anisotropic variations had been removed, are referred to as A_2 variations and are given by

$$A_2 = A_1 - k_2 {}^{\Delta I}/_{I_o}(GG)$$

$$= {}^{\Delta I}/_{I_o}(MAW.UGN) - k_1 {}^{\Delta I}/_{I_o}(McMURDO\ NM) - k_2 {}^{\Delta I}/_{I_o}(GG)$$

A Chree method of superposition of epochs was employed (Figure 1) to compare the two wave components A_1 and A_2. Clearly the variation is mainly due to the A_2 component which is encompassed in the A_1 variations. Furthermore there was a strong correlation between sectorized field direction and the waves.

When underground data from the Misato multi-directional telescope system became available it appeared that, unlike the North-South asymmetry component, the A_2 variations were isotropic, being in phase worldwide. Using the appropriate coupling coefficients together with the GG data the asymmetric component was removed from 4 northern and 3 southern hemisphere asymptotic latitudes of viewing and the isotropic nature of the variations was confirmed (Figure 2).

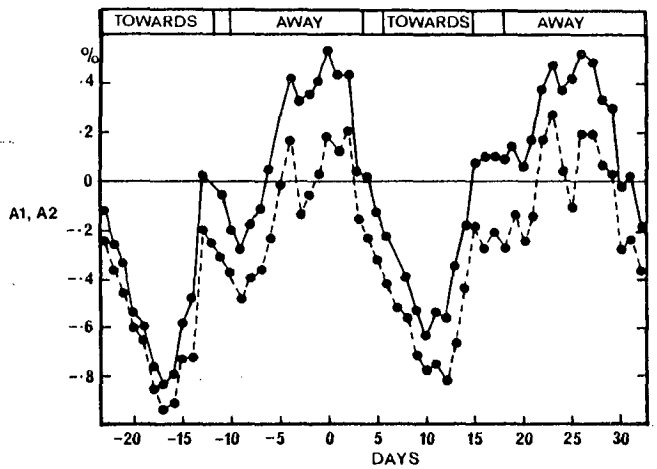

Figure 1. A 54-day Chree analysis of A_1 and A_2 using the days of maximum A_1 on 16 July and 12 August 1982 as key days. The averaged Towards and Away Periods are shown. A_1: full lines A_2: dashed lines.

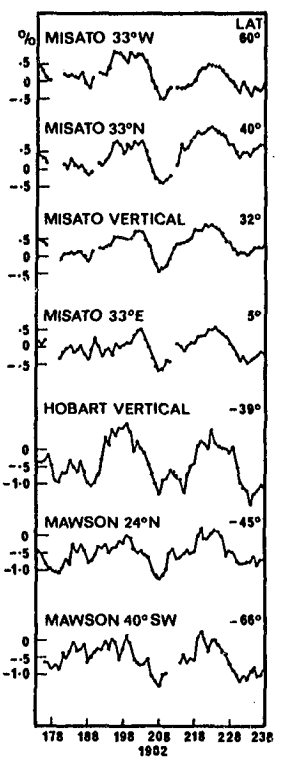

Figure 2. The A_2 intensity waves, derived from observations underground at depths of 40-60 hg cm^{-2}, July - August 1982. The asymptotic latitudes of viewing at the median rigidities of response are shown at the right of the figure.

The Intensity Waves of 1983 and 1984.

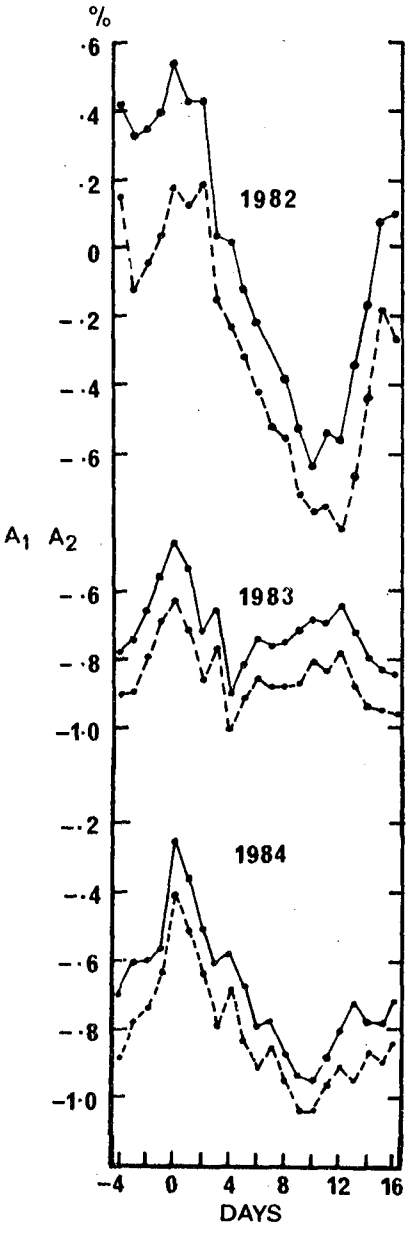

Figure 3. A 21-day Chree analysis of A_1 and A_2 in 1983 and 1984, compared with the results from 1982 (see Fig.1). Peak days in the waves of A_1 are used as key days.
A_1: full lines
A_2: dashed lines.

Figure 3 shows the 21-day Chree analysis of A_1 and A_2 waves for 1982, 1983 and 1984, on the same scale. The 1983 intensity waves were of the same intrinsic character as those of 1982 given that a 4-sector IMF structure had replaced the earlier 2-sector structure. Thus in 1983 the waves show a periodicity of 13.5 days. In 1984 a two-sector structure was again apparent. However, the A_1 and A_2 waves were significantly smaller than those of 1982.

Summary and Discussion.

Two kinds of intensity wave occuring together have been observed over the last 3 years. The first is due to the well known North-South asymmetry and can be extracted from the combined (A_1) wave. The residual waves (A_2) are much larger and are isotropic with a hard ($\gamma \gtrsim 0$) rigidity spectrum. These isotropic waves correlate well with the IMF sector direction.

Attempts to correlate the A_2 intensity waves with IMF field strength gave conflicting results. Over short time scales (single periods of waves) the correlation was good but over several periods the correlation disappeared. The delay required to optimize the correlation was different for each period. Furthermore, periods of strong IMF field strength with clearly defined sector structure early in 1983 and 1984 showed no A_2 waves in the daily average cosmic ray observations from Mawson.

A possible explanation may relate to the extent of the IMF sector structure away from the heliomagnetic equator and to an omnidirectional cosmic ray intensity that is presumed to be greater at times below the neutral sheet than above it. During periods of large amplitude of the waves in the neutral sheet, the particle radiation would tend to be confined within the wave boundary of a sector and to exhibit the intensity characteristics of either the southern or northern space of the heliosphere. When the wave amplitude of the neutral sheet is small, particle modulation should be less effective (Yasue, 1980) and confinement to a particular helio hemisphere should

be less pronounced within a sector. Thus the size of the A_2 waves may give some indication of the neutral sheet amplitude.

Acknowledgements.

Professor S. Mori, Shinshu University and Dr. A. G. Fenton, University of Tasmania are thanked for their kind assistance in providing underground data for Misato and Hobart respectively. This research is supported in part by the National Science Foundation, Division of Polar Programs Grant No. DDP-8300544, Division of Atmospheric Sciences Grant No. AAM-8303758 and Division of International Programs Grant No. INT-8114863.

References.

Duggal S.P., Jacklyn, R.M., Pomerantz, M.A. and Tsao, C.H. (1981) Proc. 17th Int. Cosmic Ray Conf., Paris, 10, 179.

Jacklyn, R.M. and Pomerantz, M.A. (1983) Proc. 18th Int. Cosmic Ray Conf., Bangalore, 3, 206.

Jacklyn, R.M. and Duldig, M.L. (1983) Proc. Astron. Soc. Aust., 5, 2, 262.

Jacklyn, R.M., Duldig, M.L. and Pomerantz, M.A. (1984a) Proc. Astron. Soc. Aust., 5, 4, 581.

Jacklyn, R.M., Duldig, M.L. and Pomerantz, M.A. (1984b) Proc. Int. Symp. on Cosmic Ray Modulation in the Heliosphere, Morioka, p76.

Mori, S. and Nagashima, K. (1979) Planet. Space Sci., 27, 39.

Pomerantz, M.A. and Duggal, S.P. (1979) Proc. 16th Int. Cosmic Ray Conf., Kyoto, 3, 428.

Yasue, S. (1980) J. Geomag. Geoelectr., 32, 617.

IMF-SENSE-DEPENDENT COSMIC RAY ANISOTROPY PRODUCED FROM DIFFUSION-CONVECTION IN HELIOSPHERE

K. Nagashima*, K. Munakata and R. Tatsuoka

*Cosmic Ray Research Laboratory, Nagoya University
Nagoya 464, Japan
Department of Physics, Nagoya University, Nagoya 464, Japan

1. Introduction. An IMF-sense-dependent first order anisotropy of solar origin, which is produced perpendicularly to the ecliptic plane from the radial density gradient, was first pointed out by Swinson.

In addition to this anisotropy, the existence of IMF-sense-dependent higher order anisotropies has recently been suggested by Munakata and Nagashima([1]), based on the simulation of cosmic ray diffusion-convection in the heliomagnetosphere.

In this paper, we discuss the characteristics of the daily variations caused by the IMF-sense-dependent 2nd order anisotropy obtained on the same condition as adopted by Munakata and Nagashima([1]). A brief comparison of these variations with observations will also be made in order to demonstrate their existence.

2. Daily Variation and its Seasonal Variation. Munakata and Nagashima obtained a stationary cosmic ray anisotropy of solar origin which is expressed in the IMF-polar-coordinate system defined at any point fixed in space(cf. fig.1), as

$$\eta(\boldsymbol{r},\boldsymbol{p})=\sum_{n=1}^{\infty}\sum_{m=0}^{n}\{\eta_n^{mc}(\boldsymbol{r},p)\cos m\Phi'+\eta_n^{ms}(\boldsymbol{r},p)\sin m\Phi'\}P_n^m(\cos\Theta'), \qquad (1)$$

where the angles Θ' and Φ' express the incident direction of cosmic rays with momentum p at a point r, and $P_n^m(\cos\Theta')$ is the semi-normalized associate Legendre function([3]).

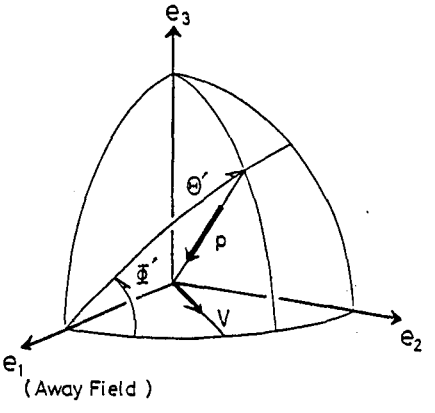

Fig. 1. The IMF-POLAR-COORDINATE SYSTEM.
p: Momentum of particle.
V: Solar wind velocity.
e_1 : Unit vector in the direction of "away" magnetic field.
e_3 : Unit vector in the direction of $e_1\times V$.
$e_2=e_3\times e_1$.

The terms with coefficients η_n^{ms} in eq.(1) are called IMF-sense-dependent terms, because η_n^{ms}'s change their sign according to the sense of IMF. The IMF-sense-dependent 2nd order anisotropy is composed of two kinds of term ($\eta_2^{ms}P_2^m(\cos\Theta')\sin m\Phi'$; $m=1,2$) which are not symmetric for an arbitrary rotation around any axis. This anisotropy produces two kinds of daily variation at the Earth; one is a solar(SO) diurnal variation and the other is an extended sidereal($SI_{1/2}$) semi-diurnal variation([2]).

The solar diurnal variation changes the sign for a sign change of the

geographic latitude($\frac{\pi}{2}-\theta$) of the viewing direction of the telescope. We call this type of variation the north-south(N-S) asymmetric type or $P_2^1(\cos\theta)$-type. For the positive and negative polarity states, fig.2(a) shows the dependence of the solar diurnal space harmonic vector(^{2}) on the diffusion parameters(λ_0 and α_λ) which are related to the scattering m.f.p (λ) as,

$$\lambda=\lambda_0(R/GV)\exp\left(\frac{r-r_e}{33\text{a.u.}}\right)(1+\alpha_\lambda\cos\theta_H). \qquad (2)$$

In the equation, R is the cosmic ray rigidity, r_e=1a.u. and θ_H is the heliographic co-latitude. In fig.2, the arabic numerals express the values of α_λ and the roman numerals I and II express, respectively, the cases of λ_0=0.016a.u. and λ_0=0.032a.u.

On the other hand, the extended sidereal semi-diurnal variation is N-S symmetric or $P_2^2(\cos\theta)$-type and represents the annual variation of the solar semi-diurnal variation whose yearly average is zero. This space harmonic vector(^{2}) is also shown in fig.2(b).

It is noteworthy that these two kinds of vector show remarkable polarity state dependences (cf. fig.2).

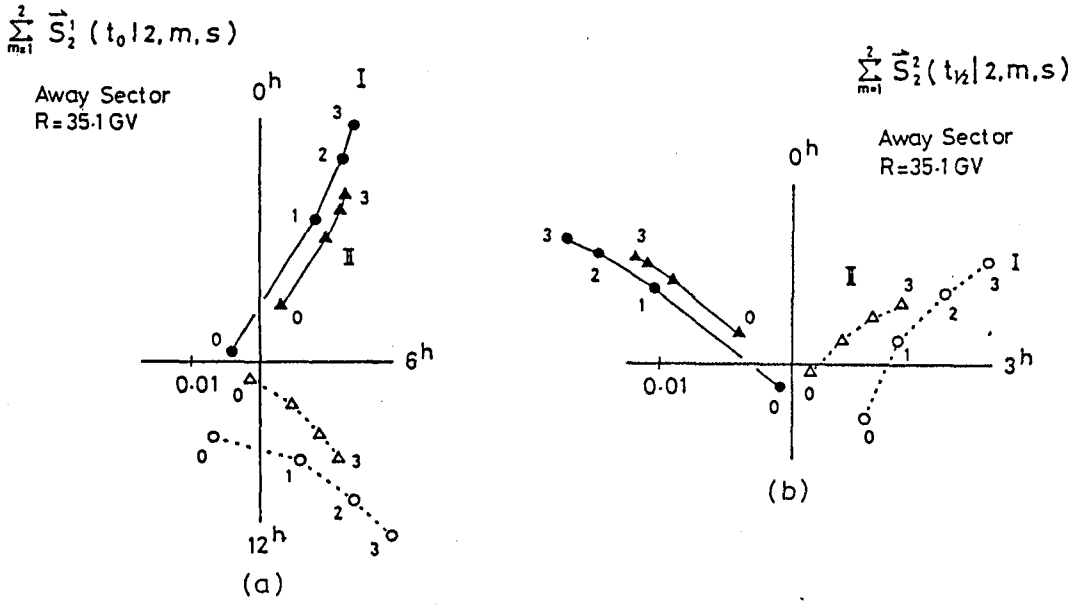

Fig. 2. PARAMETER DEPENDENCE OF THE (a) SOLAR DIURNAL AND (b) EXTENDED SIDEREAL SEMI-DIURNAL SPACE HARMONIC VECTOR IN THE AWAY SECTOR. The solid and open symbols represent the positive and negative polarity states, respectively.

3. Comparison with Observations. Fig.3 shows the observed *SO* difference vectors(T-A) between the corresponding harmonic vectors in the toward(T) and away(A) sectors in the positive polarity state(1971-1979) of the multi-directional muon telescope at Nagoya. In the figure, the symbols(V,N,S,E,...) denote respectively the 17 directional component telescopes(^{4}).

The theoretical *SO* vectors to be compared with the observed vectors are shown in fig.4 and are obtained by assuming that the phase of space harmonic vector is 0hr(^{4}).

The relative configuration of the observed vectors in fig.3 bears a

striking resemblance to that of $P_2^1(\cos\theta)$-type not to that of $P_1^1(\cos\theta)$-type (N-S symmetric) shown in fig.4.

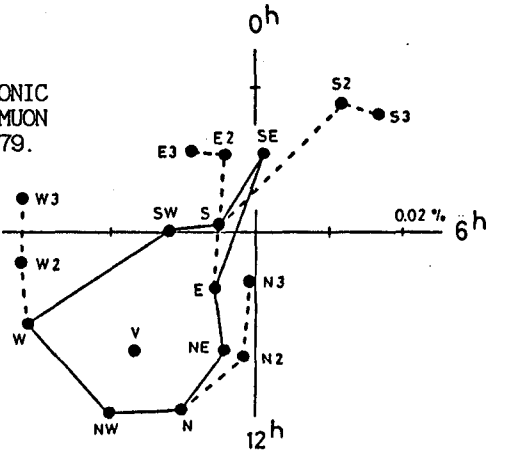

Fig. 3.
SOLAR DIURNAL "TOWARD-MINUS-AWAY" HARMONIC VECTORS (T-A) OBSERVED BY MULTI-DIRECTIONAL MUON TELESCOPE AT NAGOYA FOR THE PERIOD OF 1971-1979.

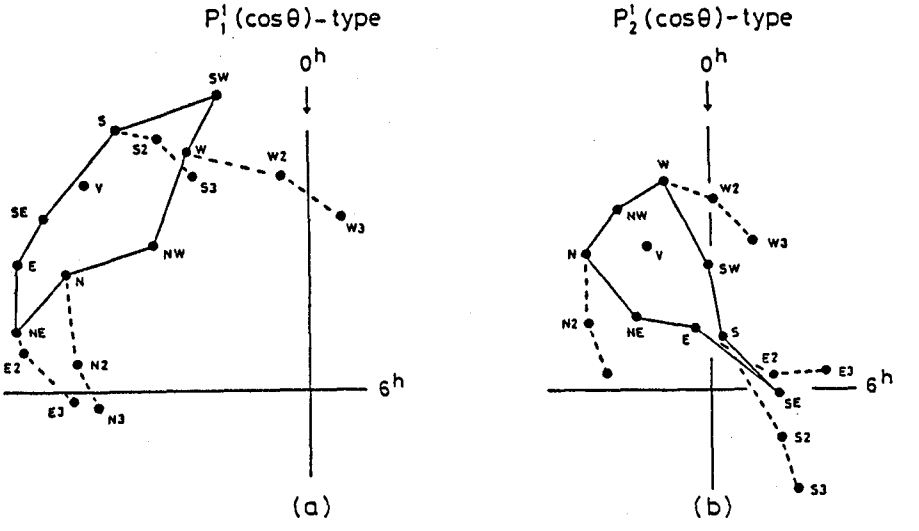

Fig. 4. RELATIVE CONFIGURATION OF EXPECTED DIURNAL HARMONIC VECTORS OF $P_1^1(\cos\theta)$- AND $P_2^1(\cos\theta)$-TYPE FOR COMPONENT TELESCOPES OF MULTI-DIRECTIONAL MUON TELESCOPE AT NAGOYA.
The spectrum of the vector is assumed to be of power-type $[(R/10GV)^{0.5}]$ with upper limiting rigidity (100GV).

In addition to the above solar diurnal variation, the present anisotropy produces also $SI_{1/2}$ vector. Fig.5 shows the T-A vectors in positive polarity state, and the theoretical vectors are shown in fig.6 in the same manner of fig.4. Although the observed vectors $SI_{1/2}$'s are not very significant statistically, their relative configuration is systematic and bears a resemblance to that of $P_2^2(\cos\theta)$-type in fig.6(a) not to that of $P_3^2(\cos\theta)$-type (N-S asymmetric).

In fig.5, we show also the observed $AS_{1/2}$ vectors which must be very small ($\sim$ one sixth) in comparison with $SI_{1/2}$ vectors from the theoretical point of view ([2]). The observed vectors $AS_{1/2}$'s are evidently small as expected.

These comparison with observations strongly suggest the existence of the 2nd order IMF-sense-dependent anisotropy. For confirmation, however, detailed analysis of the observed vectors SO and $SI_{1/2}$ is required.

4. Conclusion. It has been demonstrated that an IMF-sense-dependent 2nd order anisotropy is produced by the diffusion-convection of cosmic rays in the heliomagnetosphere. The result implies that the anisotropy cannot be expressed only by the pitch angle ($\mu=\cos\Theta'$) with respect to the IMF-axis (cf. eq. (1)). In this respect, it is not suitable to discuss the 2nd and 3rd order anisotropies, based on the diffusion equation with respect to the pitch angle ([5]).

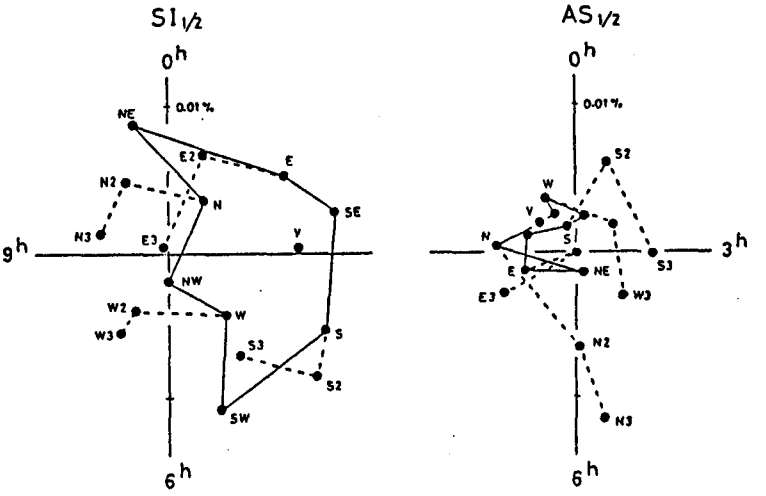

Fig. 5. EXTENDED SIDEREAL ($SI_{1/2}$) AND ANTI-SIDEREAL ($AS_{1/2}$) SEMI-DIURNAL "TOWARD-MINUS-AWAY" HARMONIC VECTORS (T-A) OBSERVED BY MULTI-DIRECTIONAL MUON TELESCOPE AT NAGOYA FOR THE PERIOD OF 1971-1979.

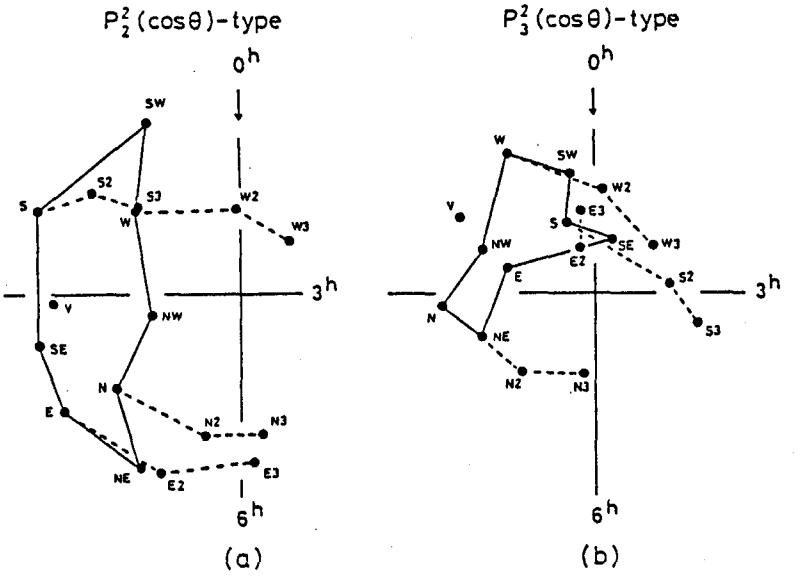

Fig. 6. RELATIVE CONFIGURATION OF EXPECTED SEMI-DIURNAL HARMONIC VECTORS OF $P_2^2(\cos\theta)$- AND $P_3^2(\cos\theta)$-TYPE FOR COMPONENT TELESCOPES OF MULTI-DIRECTIONAL MUON TELESCOPE AT NAGOYA.
The spectrum of the vector is assumed to be of power-type $[(R/10GV)^{0.5}]$ with upper limiting rigidity (100GV).

References

([1]) K. Munakata and K. Nagashima: *Proc. Int. Cosmic Ray Symposium* (Morioka, Japan, 1984), p.144; This Conference SH 4.5-1.
([2]) R. Tatsuoka and K. Nagashima: This Conference SH 4.5-2.
([3]) S. Chapman and J. Bartels: *Geomagnetism*, Vol.2 (Oxford, 1940), p.61; K. Nagashima: *Rep. Ionos. Space Res.*, Japan, **25**, 189 (1971).
([4]) K. Fujimoto et al.: *Rep. of Cosmic-Ray Research Lab.*, No.9 (Nagoya Univ., 1984).
([5]) J.W. Bieber and M.A. Pomerantz: *J.G.R. Lett.*, **10**, 920 (1983).

13

Influence of the Neutral Sheet on the Swinson's Type North-South Anisotropy of Cosmic Rays

Y.Munakata, S.Shibata* and K.Hakamada

College of Engineering, Chubu University, Kasugai, 487,Japan
*Department of Physics, Nagoya University, Nagoya, 464,Japan

Abstract

We examine the relations between the north-south anisotropy of cosmic rays and/or nucleonic intensity variation and the latitudinal angular distance (λ) of the earth from the neutral sheet, using the data in the period from Apr. 1976 to Aug. 1977 at the solar minimum.

It is found that the nucleonic intensity variation of the cosmic rays has no correlation with $\sin\lambda$ in this period as shown in Figure 1; but the amplitude of the north-south anisotropy is fairly correlated with $\sin\lambda$ as shown in Figure 2.

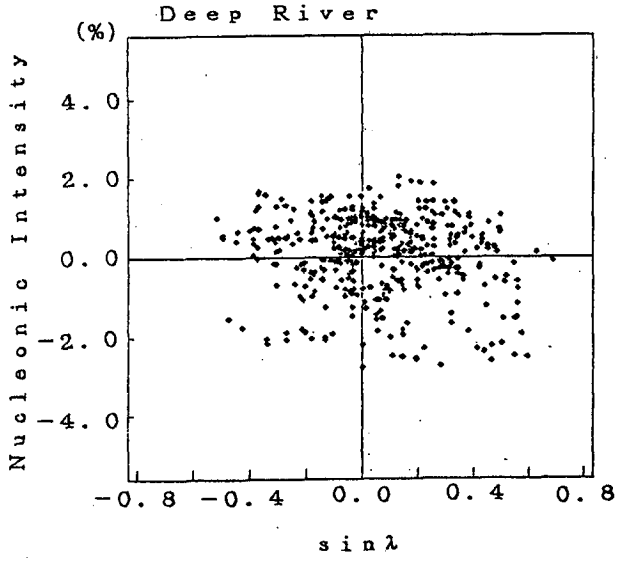

Figure 1. The correlation diagram between nucleonic intensity variation and $\sin\lambda$.

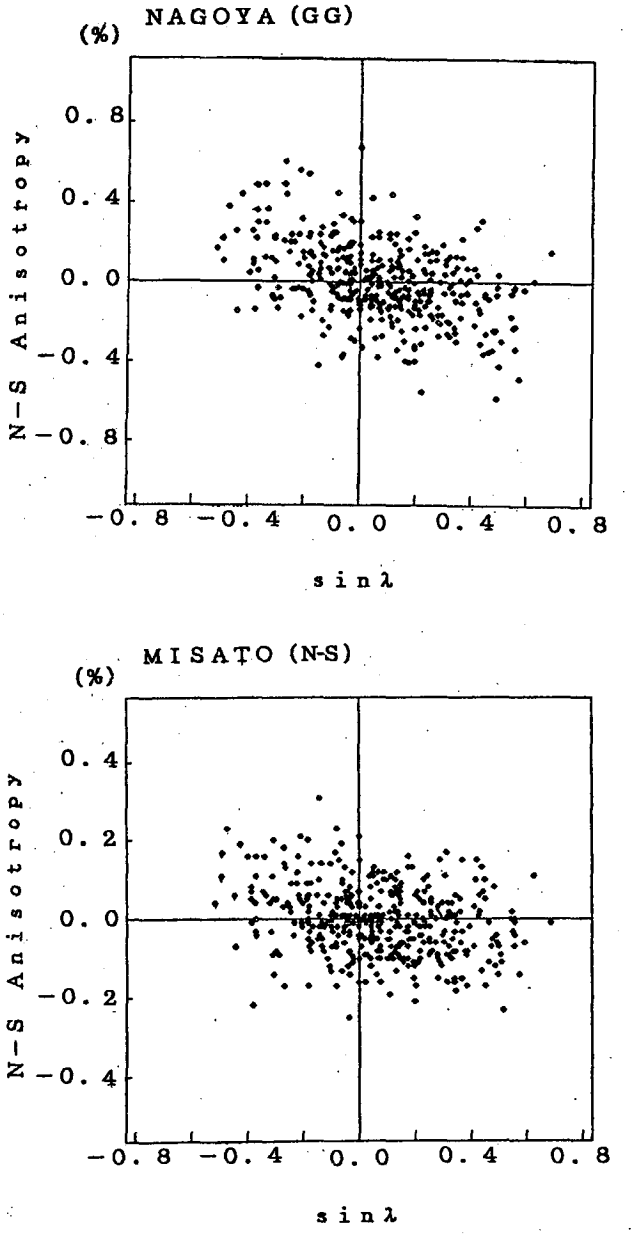

Figure 2. The correlation diagrams between north-south anisotropy and $\sin\lambda$. The figures at the top and the bottom correspond to the data observed at Nagoya (85 GV) and at Misato (150 GV). The resultant correlation coefficients are -0.42 and -0.26 respectively.

CHARACTERISTICS OF COSMIC RAY POLE-EQUATOR ANISOTROPY DERIVED FROM SPHERICAL HARMONIC ANALYSIS OF NEUTRON MONITOR DATA

H. Takahashi and N. Yahagi
Department of Physics, Iwate University
Morioka 020, Japan

ABSTRACT

We have carried out the spherical hamonic analysis of cosmic ray neutron data from the worldwide network neutron monitor stations during the years, 1966-1969. The second zonal harmonic component obtained from the analysis corresponds to the Pole-Equator anisotropy of the cosmic ray neutron intensity. We have reported some preliminary results on such an anisotropy. In this paper, further studies on this subject are presented. The results obtained confirms our earlier results: Such an anisotropy makes a semi-annual variation. In addition to this, in this paper, it is shown that the Pole-Equator anisotropy makes a variation depending on the IMF sector polarities around the passages of the IMF sector boundary. A mechanism to interpret these results is also discussed.

1. Introduction. The method of spherical harmonic analysis of cosmic ray neutron data from the worldwide network stations is developed extensively by Nagashima (1971). The second zonal harmonic component obtainable from the analysis corresponds to the Pole-Equator anisotropy of the cosmic ray neutron intensity. We have carried out such an analysis and obtained the second zonal harmonic component, using cosmic ray neutron data in the years, 1966-1969. The preliminary results on the Pole-Equator (P-E) anisotropy obtained from the cosmic ray data in 1966 and 1967 were reported (Takahashi et al.,1974, 1975, 1977, 1981, 1984). This paper presents characteristics of time variations of the P-E anisotropy during the three years, 1966, 1967 and the additional year in this study, 1969. The relationship of the P-E anisotropy to the polarity of the IMF sector is also given and discussed.

2. Analysis. Cosmic ray neutron data in daily mean from the worldwide network cosmic ray stations ($\sim$40 stations) in 1969 in addition to 1966 and 1967 which were analysed previously are analyzed on the 27 day basis by means of the three-dimensional analysis method by Nagashima, which is given in detail in the papers (Takahashi et al., 1974, 1975, 1977).

3. Results and Discussion. Hereafter, as in our previous papers, a_2^2 means the second zonal harmonic component, i. e. the P-E anisotropy, and also a_2^s's for which the power expo-

nential type spectrum having γ=2.0 and P_0 =100 GV was best-fit in the analysis are used throughout this study.

i) Variation of P-E anisotropy, a_2°

The results obtained are shown in Figs. 1 - 4. Fig. 1 shows the variation of the mean value, $\overline{a_2^\circ}$, of a_2°'s during each solar rotation interval during the year, 1969. Figs.2 -3, which have appeared in the papers (Takahashi et al., 1983) are shown again in order to compare the result obtained here with our previous results.

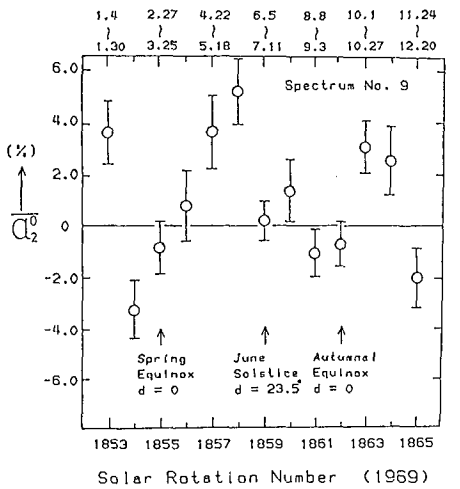

Fig.1. The variation of $\overline{a_2^\circ}$, which indicates the mean value of a_2°'s during each solar rotation interval in 1969.

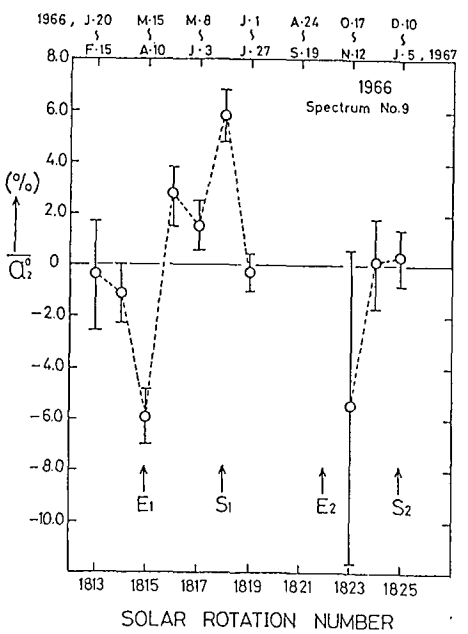

Fig.2. The variation of $\overline{a_2^\circ}$ in 1966 (Takahashi et al., 1983).

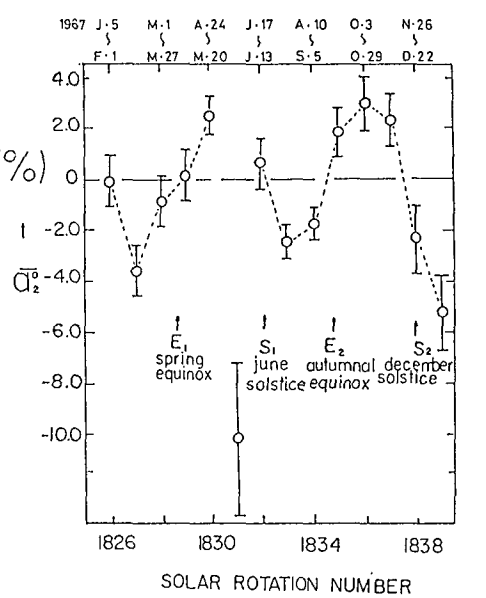

Fig.3. The variation of $\overline{a_2^\circ}$ in 1967 (Takahashi et al., 1967).

It will be found that Figs.1 - 3 are similar to each other. This establishes that a_2° makes a semi-annual variation such as pointed out in our previous papers (Takahashi et al., 1981, 1983, 1984). The suggested mechanism in our last paper also holds good for this phenomenon.

ii) Relationship of a_i°'s to the IMF sector structure

Fig.4 shows that a_2° is related to the IMF sector sturcture. It should notice that the relationship of a_2° to the IMF sector polarity as shown in Fig.4 is reversed to the contrary to that of the N - S anisotropy, a_1°, in other wards, the P - E anisotropy is, on an average, negative in the toward (-) sector, where -as the P - E anisotropy is positive in the away (+) sector.
Ely (1977) found the equatorial modulation, EqM, from the analysis of the cosmic ray data obtained from the measurements of galactic cosmic rays, and also has given a mechanism for the EqM, in which he predicts that the EqM would reverse its phase with respect to the sector polarity at each equinox if the mean IMF is parallel to the plane of the ecliptic. The Ely's EqM is not the same as our a_2°. Nevertheless, such a mechanism as proposed by him may give an important hint for interpreting physically our results obtained here.

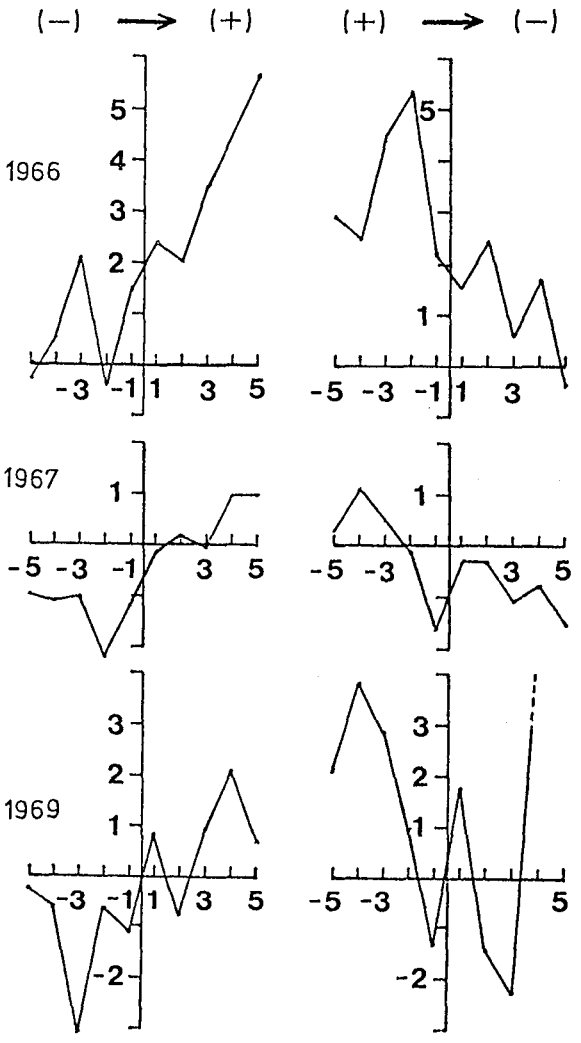

Fig.4. The variation of a_2° around the passages of the positive and negative IMF sectors.

4. Conclusions. The following conclusions from the results and discussion mentioned above may be drawn:

1) The P - E anisotropy makes a semi-annual variation.
2) The P - E anisotropy is related with the IMF sector structure and it is positive in the positive (away) sector, whereas it is negative in the negative (toward) sector.
3) The mechanism to interpret physically these results is not yet made clear, but, the mechanism to interpret the EqM by Ely may be applicable for the results obtained here.

5. Acknowledgments. The authors wish to express their sincere appreciation to Prof. K. Nagashima, Nagoya University, Japan, for his stimulating suggestions and kind support throughout this study. They are also indepted to Mr. S. Oikawa for his help in preparing the data. They also wish to thank to the directors of the cosmic ray stations, espesially Dr. M. Wada, The Inst. Phys. Chem. Res. Tokyo for supplying the cosmic ray data through WDC-2 in Japan. The calculations were made at computer center of Iwate University.

References.

Ely John T. A., 1977, J. Geophys. Res., 82, 343.
Nagashima, K., 1971, Rep. Ionos. Space res. Japan, 25, 189.
Svalgaard, L., 1975, SUIPR Report No. 629, Institute for Plasma Research, Stanford University.
Takahashi, H., N. Yahagi,and K. Nagashima, 1974, Proc. Int. Symp. on STP, Sao Paulo, 1, 431.
Takahashi, H., N. Yahagi,and K. Nagashima, 1975, Proc. Int. Cosmic Ray Conf., München, West-Germany, 4, 1236.
Takahashi, H., N. Yahagi, and K. Nagashima, 1977, Proc. 15th Int. Cosmic Ray Conf., Plovdiv, Bulgaria, 3, 284.
Takahashi, H., N. Yahagi, and K. Nagashima, 1979, Proc. Int. Cosmic Ray Conf.,Kyoto, Japan, 3, 284.
Takahashi, H., N. Yahagi, and K. Nagashima, 1981, Proc. Int. Cosmic Ray Conf., Paris, France, 10, 197.
Takahashi, H., and N. Yahagi, 1983, Proc. 18th Int. Cosmic Ray Conf., Bangalore, India, 10, 148.
Takahashi, H., N. Yahagi, and K. Nagashima, 1984, Proc. Int. Cosmic Ray Modulation in the Heliosphere, Morioka, Japan, p.156.
Tolba, M. F., 1984, Proc. Int. Symp. on Cosmic Ray Modulation in the Heliosphere, Morioka,Japan, P. 69.

First Zonal Harmonic Component of Cosmic Ray Neutron Intensity

H. Takahashi, N. Yahagi and T. Chiba
Department of Physics, Iwate University
Morioka 020, Japan

Abstract

Cosmic Ray neutron data from the cosmic ray stations from the worldwide network in 1966, 1967 and 1969 are analysed by means of the three-dimensional analysis method by Nagashima. The variations of the north-south anisotropy, which is the first zonal harmonic component obtained from the analysis are studied. The result obtained confirms our earlier findings. Relationship of the anisotropy to the IMF sector polarity is also studied.

1. Introduction

We have carried out the analyses of the neutron monitor data in daily mean on the 27 day basis during the years 1966-1969 by means of the Nagashima's method (1971). The first zonal harmonic component of cosmic ray intensity is observed as the North-South (N-S) Asymmetry of cosmic ray intensity and interpreted as the cosmic ray flow in the direction of the earth's rotation axis (Nagashima et al., 1968). We have studied previously such a N-S anisotropy by the method and reported some results (Takahashi et al., 1974: 1979: 1981) on that matter. In this paper, further studies on the subject will be given and discussed in comparison with our earlier results (Takahashi et al., 1974: 1979: 1981). In addition to the above, in this paper, the relationship of a_1^0's to the sector polarity of IMF will be also given and discussed.

2. Method

The method of the analysis has been given previously (Takahashi et al., 1974; 1975; 1984) with particulars. In this paper, a_1^0's for which the power exponential type spectrum having $\gamma = 2.0$ and $P_0 = 100$GV was best-fit in the analysis are used similarly to those in our previous papers (Takahashi et al., 1974; 1975) as a matter of convenience for comparing the results obtained with our earlier results. The data of the Interplanetary magnetic sector polarity are taken from Svalgaard's paper (Svalgaard: 1975).

3. Results and Discussion

(i) Variation of N-S anisotropy, a_1^0

The results obtained are shown in Figs. 1-4. Fig. 1

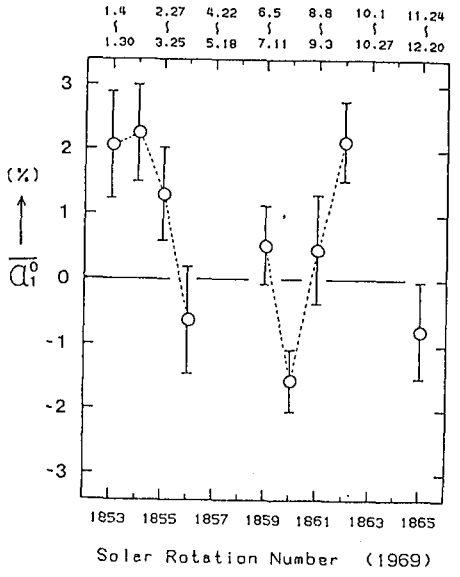

Fig. 1

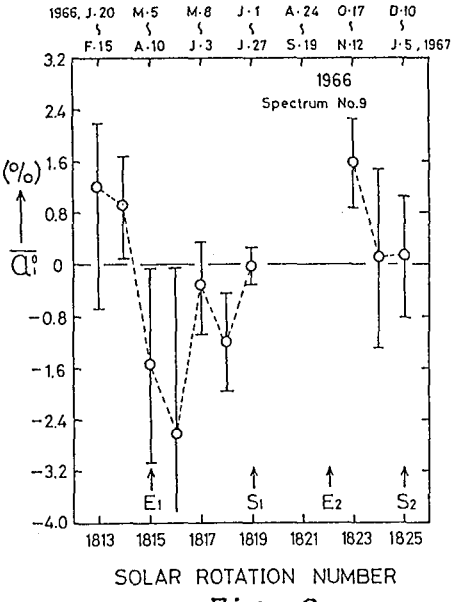

Fig. 2

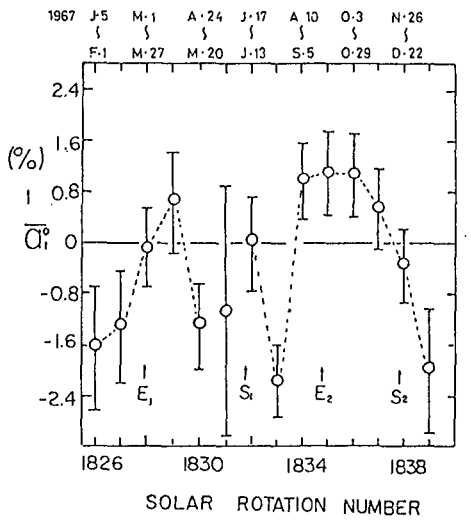

Fig. 3

Fig. 1: The Variation of $\overline{a_i^0}$. $\overline{a_i^0}$ indicates the mean value of a_i^0's during each solar rotation interval in 1969.

Fig. 2: The Variation of $\overline{a_i^0}$, which indicates the mean value of a_i^0's during each solar rotation interval in 1966 (Takahashi et al., 1981).

Fig. 3: The Variation of $\overline{a_i^0}$, which indicates the mean value of a_i^0's during each solar rotation interval in 1967 (Takahashi et al., 1981).

shows the variation of the mean value, $\overline{a_i^0}$, of a_i^0's during each solar rotation during the year 1969. Figs. 2 and 3 are given for comparison of the results obtained here with our earlier results. It will be found that the variation of $\overline{a_i^0}$ shown in Fig. 1 is very similar to that in Fig. 2, whereas there is a marked discrepancy at the period from Rot. No. 1826 to No. 1830 in Fig. 3 between the variations in 1967 and 1969, and at the period from Rot. No. 1831 to 1838, there is a close correlation between them. Although the reason of such a discrepancy is not made clear, it may be due to the difference of physical condition in Space.

(ii) Relationship of a_1's to the passages of the positive and negative interplanetary sectors.

Fig. 4 shows the variations of $\overline{a_1}$, for the two types of the passages of the interplanetary magnetic sectors, where $\overline{a_1}$ indicates the average value of a_1 during each solar rotation interval in 1966 and 1969. The figure (Fig.4) is obtained from the Chree analysis, in which the day of passage of the sector boundary is selected as zero day.

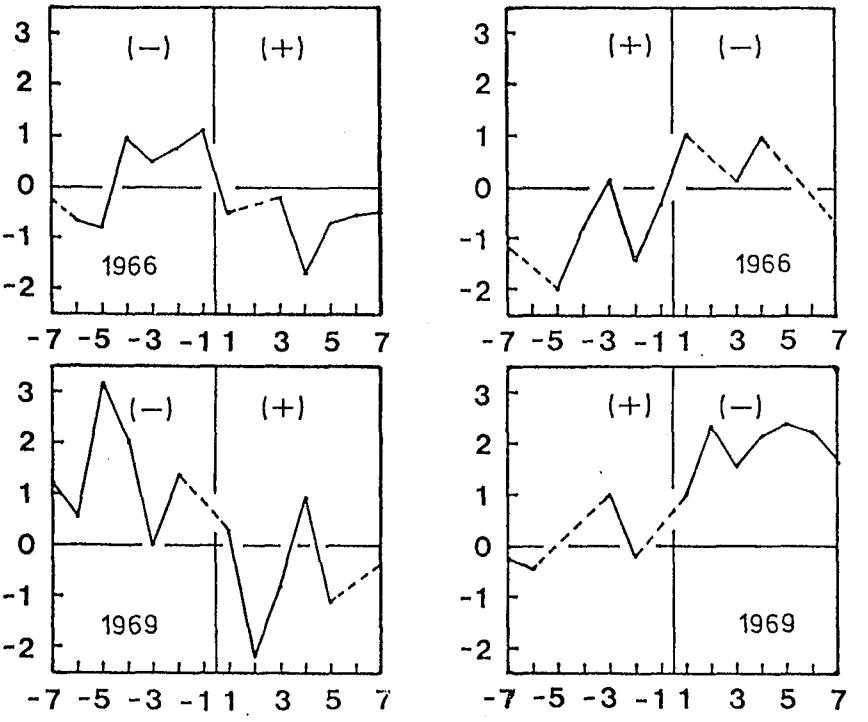

Fig. 4. The variation of $\overline{a_1}$ around the passages of the positive and negative interplanetary magnetic sectors where $\overline{a_1}$ indicates the average value of a_1 during each solar rotation interval in 1966 and 1969.

Yoshida et al. (1971) reported that the N-S anisotropy is related to the interplanetary magnetic sector structure. They also showed that the N-S anisotropy is, on an average, positive in the toward (-) sector (i. e. excess fluxes from the northern polar region), whereas the N-S anisotropy is negative in the away (+) sector (i. e. excess fluxes from the southern polar region (Yoshida et al., 1973). Our results (Fig. 4) are consistent with those by Yoshida et al. (1973). As for the mechanism of the N-S anisotropy, it is reported that the Bx∇n mechanism gives a negative N-S anisotropy due to the outward direction of $B_{//}$ (positive $B_{//}$). Also the inward $B_{//}$ produces a positive N-S anisotropy (Tolba, 1974). Pomerantz and Bieber (1984) also showed that the N-S anisotropy is prepondarantly positive, as expected if it arises from a positive radial gradient via the Bx∇n

drift mechanism. Such a mechanism is also applicable to our results obtained here.

4. Conclusions

The following conclusions from the results shown the above may be drawn:

(1) The first zonal harmonic component (N-S anisotropy) derived from the three-dimensional analysis method by Nagashima makes a yearly variation on an average during a solar rotation interval.

(2) The first zonal harmonic component (N-S anisotropy) derived from the three-dimensional analysis by Nagashima's method makes a variation closly related to the passages of the interplanetary magnetic sectors on an average during a solar rotation interval. The variation depends on the sector polarity.

(3) Such a variation may be interpreted by the Bx∇n mechanism.

5. Acknowledgements

The authers wish to express our sincere appreciation to Prof. K. Nagashima, Nagoya University, for his stimulating suggestions and kind support throughout this study. They also wish to thank to the Directors of the cosmic ray stations, especially Dr. M. Wada, The Inst. Phys. Chem. Res. Tokyo, for supplying the cosmic ray data through WDC-2 in Japan. They are also indebted to Mr. S. Tashiro for his help in computer calculations. The calculations were made at computer Center of Iwate University.

References

Nagashima, K., S. P. Duggal, and M. A. Pomerantz, 1968, Planet. Space Sci., 16, 29.

Nagashima, K., 1971, Rep. Ionos. Space Res. Japan, 25, 189.

Pomerantz, M. A., and J. W. Bieber, 1984, Proc. Int. Symp. Cosmic Ray Modulation in the Heliosphere, Morioka, p. 39.

Svalgaard, L., 1975, SUIPR Report No. 629., Institute for Plasma Res., Stanford Univ.

Takahashi, H., N. Yahagi, and K. Nagashima, 1974, Proc. Int. Symp. on STP, São Paulo, 1, 431.

Takahashi, H., N. Yahagi, T. Chiba, and K. Nagashima, 1979, Proc. 16th Int. Cosmic Ray Conf. Kyoto, Japan, 3, 514.

Takahashi, H., N. Yahagi, T. Chiba, and K. Nagashima, 1981, Proc. 17th Int. Cosmic Ray Conf., Paris, 10, 193.

Tolba, M. F., 1984, Proc. Int. Symp. on Cosmic Ray Modulation in the Heliosphere, Morioka, Japan, p. 69.

Yoshida, S., N. Ogita, S-I. Akasofu, and L. J. Gleeson, 1973, J. Geophys. Res. 78, 6409.

Yoshida, S., S-I. Akasofu, N. Ogita, and A. Outi, 1971, J. Geophys. Res., 76, 1.

SH 4.3-14

COSMIC RAY INTENSITY DISTRIBUTION PERPENDICULAR TO SOLAR EQUATORIAL PLANE AT 1 A.U. DURING 1978-83.

S.P.Pathak*, S.P.Agrawal, and P.K.Shrivastava
Physics Department (Vikram Space Physics Centre)
A.P.S.University, Rewa(M.P.),486003, India.

and

R.S. Yadav
Cosmic Ray & Space Physics Group,
Aligarh Muslim University,
Aligarh (U.P.),202001,India.

ABSTRACT

The distribution of cosmic ray intensity perpendicular to solar equatorial plane, has been investigated by using its yearly variation with respect to the helio-latitudinal position of the earth, for the two intervals 1978-80 and 1981-83. The monthly mean values of two high latitude stations along with the solar and geomagnetic indices are used to derive the cosmic ray intensity distribution free from the changes due to variation in solar activity. The correction is found to be significant only during the interval 1978-80. The results indicate a significant linear increase in cosmic ray intensity from north to south of solar equator, contrary to that observed during 1973-75. No symmetrical gradients are found during the period of study, in agreement with earlier results.

1. Introduction.

The helio-latitude of the earth changes by $\pm 7.25^{\circ}$ with respect to solar equatorial plane during the period September to March each year. Any cosmic ray density gradient perpendicular to the solar equatorial plane will therefore, cause yearly variation in cosmic ray intensity. Earlier results, using high latitude neutron monitor data have failed to provide any evidence of the presence of symmetrical cosmic ray density gradients perpendicular to the solar equatorial plane, which are predicted to explain

---

* Also at, Physics Department, Govt. Science College, Rewa (M.P.), 486 001.

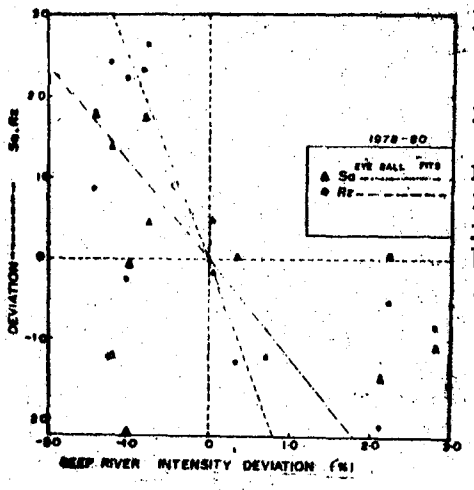

Fig.1 Cross-plot between the average percent deviation of the cosmic ray intensity, with mean deviation of sunspot number (Rz), and solar radio flux (Sa) for the interval 1978-80. Eye-ball linear fits for Sa and Rz are also drawn.

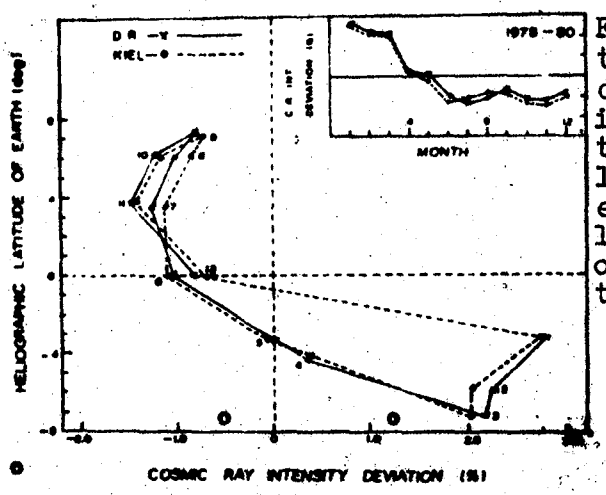

Fig.2 (a) Cross-plot between the observed average percent deviation of cosmic ray intensity for 1978-80 for two stations and helio-latitudinal position of earth. The inset shows the linear time-intensity plot of cosmic ray intensity for the 12 month period.

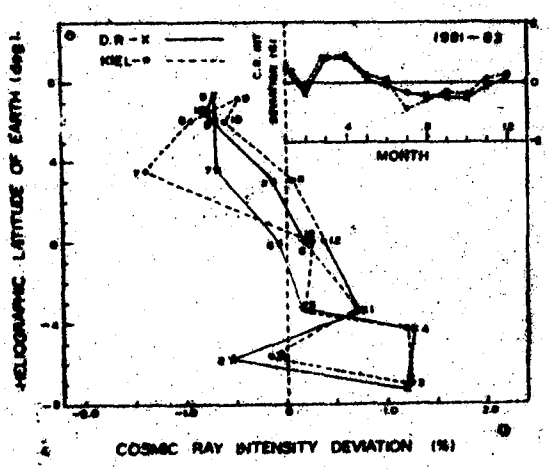

Fig.2 (b) Same as in figure 2a, for the interval 1981-83.

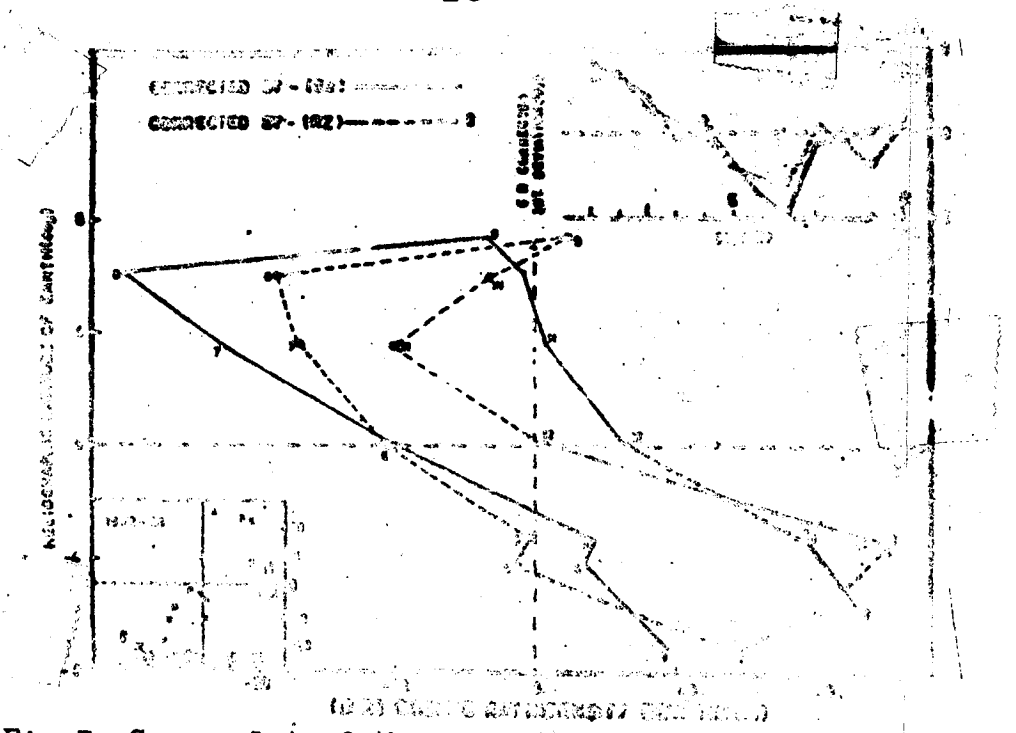

Fig.3 Cross-plot of the corrected average percent deviation of Deep River cosmic ray intensity for the interval 1978-80. The correction has been applied by using Sa & Rz separately.

the semi-diurnal anisotropy observations. In an earlier study (Pathak and Agrawal, 1982; and references there-in) for the interval 1973-75, during which the amplitude of semi-diurnal anisotropy was largest, no evidence was found for the presence of any symmetrical or linear cosmic ray gradients in the helio-latitude range $\pm 7.25^{0}$. Moreover, it is known that the semi-diurnal anisotropy exists during all the years of the sunspot cycle; the amplitude increases during the declining phase of the solar activity. In this paper, the analysis has been extended to include the period of maximum solar activity (1978-80) and the period of declining solar activity (1981-83), to derive the helio-latitudinal gradients by using the procedure adopted by Pathak and Agrawal (1982).

2. Method of analysis.

The corrected monthly average cosmic ray intensity values for two neutron monitor stations (Deep River and Kiel) have been used to determine the helio-latitudinal gradients, separately for the interval 1978-80 and 1981-83. Similar calculations have been performed for sunspot number (Rz), 2800 MHz solar radio flux (Sa), and for geo-magnetic field variability index (Ap), for both the intervals. The mean deviations have been obtained to derive the gradients after correcting the percent deviations of cosmicray intensity for variations in the solar indices.

3. Results and Discussion.

Earlier studies have shown significant correlation between the solar activity and the cosmic ray intensity during the 11-year period of a sunspot cycle, particularly on a long term basis (Rao, 1972). Therefore, to derive the gradient of cosmic ray intensity, it is necessary to remove the effect of solar activity from the observed cosmic ray intensity. Figure 1 shows the relationship between the percent deviation of cosmic ray intensity for Deep River neutron monitor and the deviations for Sa and Rz, for the interval 1978-80. The figure depicts significant correlation between the cosmic ray intensity and solar indices Sa and Rz. The lines drawn across them are the eye-ball fits, showing negative correlation. Such a fit has been used to correct for the effect of solar activity changes in the observed cosmic ray intensity deviations. However, a similar plot (not shown here), for interval 1981-83 does not show any relationship between these quantities; the points are observed to be randomly distributed. Therefore, no correction is applicable in the cosmic ray intensity deviations for the interval 1981-83. We have also investigated the effect of Ap on cosmic ray intensity deviations, which shows almost random changes, for both the intervals. Next we depict, the observed cosmic ray intensity deviations for both the intervals against the heliographic latitude of the earth for each month. Figures 2(a) and 2(b) show such a cross-plot, as well as the cosmic ray intensity deviations in a linear fashion. The observations indicate a rising density gradient from north to south with a small super-position of symmetrically rising density gradients with respect to solar equatorial plane. Nevertheless, the changes observed in the northern helio-latitudes are small. Moreover, these observations are affected by the changes in solar activity (see figure 1) and hence are re-plotted in figure 3, after correcting thecosmic ray intensity deviations for the effect of solar activity changes. The bottom inset shows the relationship between Sa and Rz in which months 8 and 11 do not show concurrent variability of Sa and Rz. This has resulted in two graphs in fig.3, for the corrected intensity for the same station Deep River. It is seen that the cosmic ray intensity in both the cases, is minimum in northern hemisphere, whereas it increases linearly with a maximum in southern hemisphere; the total percent change in cosmic ray intensity is $\approx$ 3% during 1978-80, for the helio-graphic latitude of $\pm$ 7.25°. Similarly, the total change for the interval 1981-83 is $\approx$ 2%. The values of the linearly increasing gradient observed here are found to be quite significant and are much larger as compared to that reported earlier for intervals 1973-75. It is further noted that the smaller densities observed in northern hemisphere could be due to the presence of more abundant larger area solar polar coronal holes in the northern hemisphere as compared to southern hemisphere.

References.

Pathak, S.P. and Agrawal S.P., Indian J. Radio & Space Physics, Vol. 8 (1982), 140.

Rao, U.R. Space Science Rev.(Netherlands), 12 (1972) 719.

SH 4.3-15

THE COROTATING VARIATION OF THE NORTH-SORTH ANISOTROPY OF COSMIC RAYS

Xue Shunsheng Zhang Gongliang Xao Shaoyu
(Institute of Space physics, Academia Sinica)

Correlation analysis on the relation of the north-south (N-S) anisotropy of cosmic rays, observed by the Nagoya multi-directional meson telescope, with the IMF as well as the solar wind velocity within solar Carrington rotation for the period 1971-1976.

It is found that the N-S anisotropy of cosmic rays correlates quite well with the Bx component of the IMF. The correlation coefficient nearly equalsto 0.8.

1. Introduction. Since the cosmic ray N-S anisotropy was discovered, a number of studies about it have been published. The drift due to the radial gradient of cosmic ray density n derives the N-S anisotropy in the presence of the IMF intensity B, as interpreted by Swinson[1]. The correlation of the cosmic ray anisotropic index GG([4], [5]) with the daily average direction of the IMF was studied by Yasue et al.[2], and a good correlation coefficient (~0.75) was obtained. But they did not give the quantitative analysis between the GG and magnetic field intensity. Fujimoto et al.[3] pointed out that the GG value decreased, as the IMF sector boundary changes its polarity from toward to away the sun, and vice verse. Munakata et al.[4] found that N-S anisotropy correlated somewhat with the solar wind velocity, as well as the Bx component of the IMF.

We made the correlation analysis between the N-S anisotropy and solar flare, and found the flare of importance ≥ 2 with duration ≥ 1.5 hours could change significantly the anisotropy[5]. The present paper studies the relation of the corotating variation of cosmic ray N-S anisotropy with solar wind velocity, as well as the parameters of the IMF with the sun.

2. Data and Method. The cosmic ray data used are the daily average values taken from the multi-directional meson telescope at Nagoya for the period 1971-1976[6]. The cosmic ray N-S anisotropic indexes A and AA are defined below,

$$A=(N-S)/2 \quad (1)$$

$$AA=(N-S)+(N-E) \quad (2)$$

Another parameter I is defined as

$$I=(N+S)/2 \quad (3)$$

Each term from formula (1) to (3) denotes a directional component of the cosmic ray intensity having its central direction of the viewing cone pointing toward the zenith angle of 30° in the north (N), the south (S), and the east (E)-directions, different from that adopted by Munakata et al.. The solar wind velocity and the IMF data are taken from

that compiled by King, J. H.[7].

Analysis of cosmic ray data are made by applying Chree superposed epoch method with reference to their ordinal day in a solar rotation[8]. An accurate Carrimgton rotation period is divided into 27 round days. It avoids not only the drifting error caused by adopting Bartel's rotation, but also the difficulty produced by decimal Carrington rotation. Such a converted round day is called the "Carrington Day", with length approximately equal to 1.01 calender days. After taken the nearest whole number, the day at which the zero Carrington longitude crossing the solar central meridian is regard as the beginning day of each Carrington rotation.

In all figures of this paper the absissas represent the Carrington ordinal day from the first day to the 27th day corresponding the solar longitude from 360° to 0°. The ordinates show the parameters concerned, i.e. A, AA and I, as well as the solar wind velocity V, IMF total intensity B, its components Bx and By and its azimuthal angle φ in the ecliptic plane. In order to making the figures more clear, the values of the first three days are drawn repeatedly after the 27th day

3. Analysis and results. The distributions of cosmic ray N-S anisotropy and IMF Bx component in the Carrington rotation have been calculated. Simply shown are the results for 1973 and 1974 in Fig. 1. In Fig. 1b, two steady corotating structures of the IMF can obviously be seen. Also noted are the variations of A and AA being similar to that of Bx component. In other years, the steady corotating structures still exist, but not as clear as in 1974. Because the correlation coefficient between the A and AA is almost closed to 1, only the AA is discussed in following.

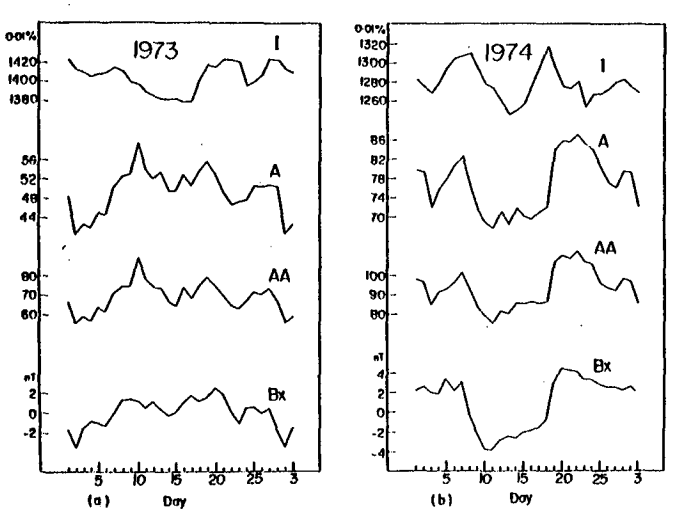

Fig. 1. Corotating variations of I, A, AA and Bx.

The single and bi-correlation between AA and Bx and By can be expressed as the following formulas,

$$AA = a_{01} + a_{1x} B_x \quad (4)$$

$$AA = a_{02} + a_{1y} B_y \quad (5)$$

$$AA = a_0 + a_{11} B_x + a_{12} B_y \quad (6)$$

Table 1 summarizes the yearly coefficients in formula (4) to (6) and respective correlation coefficients r_x, r_y and r_{xy}, as well as the I and AA. It is striking that AA correlates quite well with the Bx component with a high correlation

coefficient r_x 0.8 The r_y is negative, its magnitude is a bit less than r_x. The bi-correlation coefficient r_{xy} is a little higher than r_x. The r_x obtained here is much higher than that by Munakata et al.. This is because the present correlation coefficients are calculated on a yearly beses, while the previous ones using five year data altogether, and the change of the AA following the solar cycle reduced

Table 1. Values of various coefficients, as well as the I and AA during 1971-1975

year	a_{01}	a_{1x}	r_x	a_{02}	a_{1y}	r_y	a_0	a_{11}	a_{12}	r_{xy}	I	AA
1971	14	4.2	0.86	14	-4.1	-0.80	14	3.0	-1.4	0.87	1705	3
1972	38	4.2	0.71	39	-4.1	-0.63	39	3.1	-1.7	0.74	1557	38
1973	69	4.0	0.73	70	-4.3	-0.69	69	3.4	-0.8	0.73	1400	64
1974	90	3.4	0.88	92	-3.6	-0.88	91	1.8	-1.6	0.88	1294	91
1975	114	3.3	0.82	113	-3.3	-0.78	114	3.5	-0.3	0.82	1187	97

the statistical accuracy. Meanwhile the superposed epoch method has filtered the short term vaviation and raised also the statistical accuracy. The coefficients a_{1x}, a_{1y}, a_{11} and a_{12} do not change very much, but a_{01}, a_{02} and a_0 increase approximately from 14 to 114 with the decreasing solar activity during 1971-1975. This fact illustrates that the variation of N-S anisotropy is due to not only $\overline{B}\times\nabla n$, but other factor, for example, the variation solar general magnetic field.

We have also calculated the distributions of cosmic ray N-S anisotropy, solar wind velocity and the IMF parameters in the Carrington rotation for this period. For simplicity only the results for 1971 and 1974 are shown in Fig. 2. Table 2 summarizes the correlation coefficients of the AA with the V, φ and B respectively. The magnitude of r_V, r_φ and r_B are much lower than those of Bx and By. Hence it is the best to study the correlation of AA with IMF component.

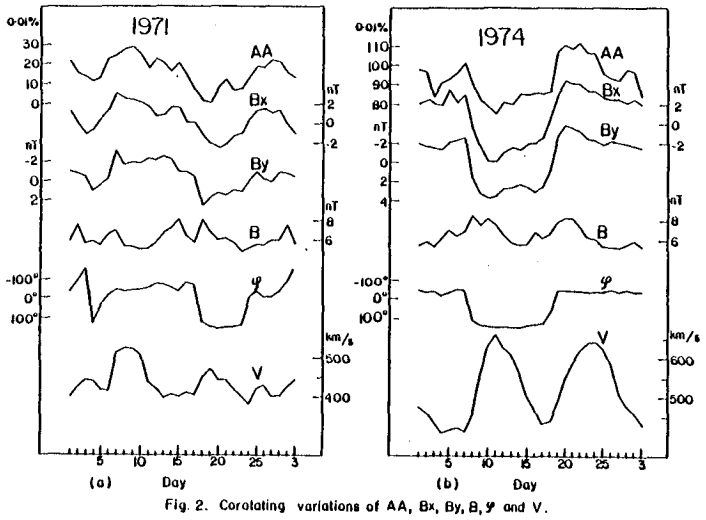

Fig. 2. Corotating variations of AA, Bx, By, B, φ and V.

It is well known that the solar activity weekens from 1971-1974, the solar modulation of cosmic rays increases, and the omnidirectional intensity of cosmic rays increases

Table 2. The r_V, r_φ and r_B for 1971 and 1974

Year	r_V	r_φ	r_B
1971	-0.33	-0.61	0.29
1974	0.21	-0.75	0.02

every year. The present results show the AA follows a similar trend, however, it is unexpected that the I decreases from year to year, quite different from the variation of omnidirectional intensity.

4. Conclusion. The cosmic ray N-S anisotropy correlates quite well with the IMF components Bx and By with a correlation coefficient nearly equal to 0.8, a positive one for the Bx component and negative for the By. The bi-correlation coefficient with both Bx and By is almost closed to 0.8. The variation of the regressive coefficients illustrates that the cosmic ray N-S anisotropy, in addition to the gradient drift effect, is controlled by some kinds of long term variayion of the solar cycle.

5. Acknowledgements. The authors are grateful to Prof. K. Nagashima for providing the valuable Nagoya multi-directional meson telescope data.

References

1. Swinson, D.B., (1969), J. Geophys. Res., 74, 5591
2. Yasue, S., Mori, S. and Munakata, Y., (1981), 17th ICRC, Paris, 4, 88
3. Fujimoto, K., Kojima, H., Murakami, K. and Nagashima, K., (1981), 17th ICRC, Paris, 4, 72
4. Munakata, Y., Mori, S. and Nagashima, K., (1979), 16th ICRC, Kyoto, 4, 131
5. Xao, S., Xue, S. and Zhang, G., (1985), to be published
6. Sekido, Y. et al., Report of Cosmic-Ray Laboratory, Multi-Directional Cosmic-Ray Intensities, No. 1
   Nagashima, K. et al., Report of Cosmic-Ray Laboratory, Multi-Directional Cosmic-Ray Intensities, No. 3
7. King, J. H., Interplanetary Data Book, NSSDC/WDC-A-R & S, 77——04, 1977
8. Zhang, G., Yang, G. and Lu, C., (1985), Acta Astrophys. Sinica, Vol. 5, No. 2, 140

SH 4.4-2

COSMIC RAY SIDEREAL DIURNAL VARIATION OF GALACTIC ORIGIN OBSERVED BY NEUTRON MONITORS

Y. Ishida, K. Nagashima*, S. Mori** and I. Morishita***

Department of Physics, Fukushima University, Fukushima 960-12, Japan
*Cosmic-ray Research Lab., Nagoya University, Nagoya 464, Japan
**Department of Physics, Shinshu University, Matsumoto 390, Japan
***Gifu College of Dentistry, Hozumi-cho, Gifu 501-02, Japan

ABSTRACT

Cosmic ray sidereal diurnal variations observed by neutron monitors are analyzed for the period 1961-1978, by adding 134 station-years data to the previous paper (Nagashima et al., 1983). Also the dependence of the sidereal variations on Sun's polar magnetic field polarity is examined for two periods; the period of negative polarity in the northern region, 1961-1969 and the period of positive polarity, 1970-1978. It is obtained that for the former period, the amplitude A=0.0203±0.0020% and the phase ϕ=6.1±0.4 h LST and for the latter period, A=0.0207± 0.0020% and ϕ=8.6±0.4 h LST, respectively.

1. Introduction

In the previous paper (Nagashima et al., 1983; hereafter referred to as Paper I), we presented the analyzed results of the cosmic ray sidereal diurnal variations observed by neutron monitors, by using 620 station-years data from a worldwide network for the period 1958-1979. It was shown that the sidereal variations averaged over the above period for the Northern Hemisphere are significantly different from the corresponding variations in the Southern Hemisphere. Both difference and average between two hemispheres were analyzed. The results were interpreted on a theoretical basis of the three-dimensional anisotropy and its annual modulation model (Nagashima and Ueno, 1971; Nagashima et al., 1972a, b) that the former (difference) can be identified with the spurious sidereal diurnal variation arising from annual modulation of 2nd order anisotropy in space responsible for the solar semi-diurnal variation. And the latter could be regarded as being due to uni-directional galactic anisotropy (see detail, Paper I). In the present work, we analyze the neutron monitor data by adding 134 station-years to the previous ones, in the same manner as in Paper I for the period 1961-1978.

Cini-Castagnoli et al. (1975) pointed out the association of the sidereal diurnal variations at deep underground stations in the northern hemisphere with changing Sun's polar magnetic field polarity. For the period of negative polarity in the northern region, the observed sidereal vectors were around 20 h LST, while for the period of positive polarity, the vectors were observed at $\sim$3 h LST. Very recently, Nagashima et al. (1984) pursued this problem in detail, and demonstrated that Cini-Castagnoli et al.'s finding is not real, but virtual even for the deep underground observations (rigidity region $\lesssim$500 GV) due to modulation with the spurious sidereal diurnal variation of solar origin, based on the three-dimensional anisotropy and its annual modulation. In the present analysis, we examine the dependence of the sidereal variations on Sun's polar

magnetic field polarity for two periods; for the negative period in the northern region (1961-1969) and for the positive period (1970-1978).

2. Analysis

The data used in the present analysis are those of neutron monitors from a worldwide network for the period 1961-1978. The total amount of data in the Northern and Southern Hemispheres are respectively 544 and 142 station-years by adding 134 station-years to them. The added data are mostly concentrated on 1974 to 1977.

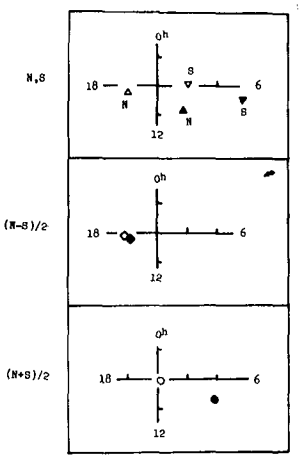

Fig. 1 The first haronic of observed sidereal daily variations for the Northern (N) and Southern (S) Hemispheres, together with their difference (N-S)/2 and their average (N+S)/2 with solid marks. The corresponding expected variations are also shown with open marks.

The analysis is made in the same manner as in Paper I. The top panel of Fig. 1 show the first harmonics of the observed daily variations for Northen (N) and Southern (S) Hemispheres and are; for the (N), the amplitude A=0.0123±0.0019% and the phase ϕ=9.0±0.3 h LST and for the (S), A=0.0286±0.0037% and ϕ=6.7±0.4 h LST, respectively.

Fig. 1 shows their difference first harmonics (N-S)/2 and average (N+S)/2 for two Hemispheres; for (N-S)/2, A=0.0099±0.0014% and ϕ=17.3±0.5 h LST and for (N+S)/2 A=0.0196±0.0014% and ϕ=7.4±0.3 h LST, respectively. For comparision, the corresponding expected variations are shown for flat rigidity spectrum with an upper cut-off rigidity of 300 GV. The present results reconfirm the previous results and support the conclusion in Paper I.

In order to examine the dependence of the sidereal diurnal variation on Sun's polar magnetic field polarity in neutron monitor rigidity region, we separate the variations into two groups according to Sun's polar field polarity; the negative period showing toward field polarity in the northern region (1961-1969) and the positive period showing away field polarity (1970-1978). The number of data used and their average cut-off rigidities are tabulated in Table 1. These are not necessarily balanced for both hemispheres, but we regard them almost conjugate with respect to the north-south. The sidereal diurnal variations of all the station-years for N

Table 1 Number of data and average cut-off rigidity.

	Negative period (1961-1969)		Positive period (1970-1978)	
	Station-years	Cut-off (GV)	Station-years	Cut-off (GV)
Northern Hemisphere	253	2.86	291	3.66
Southern Hemisphere	78	4.07	64	3.68

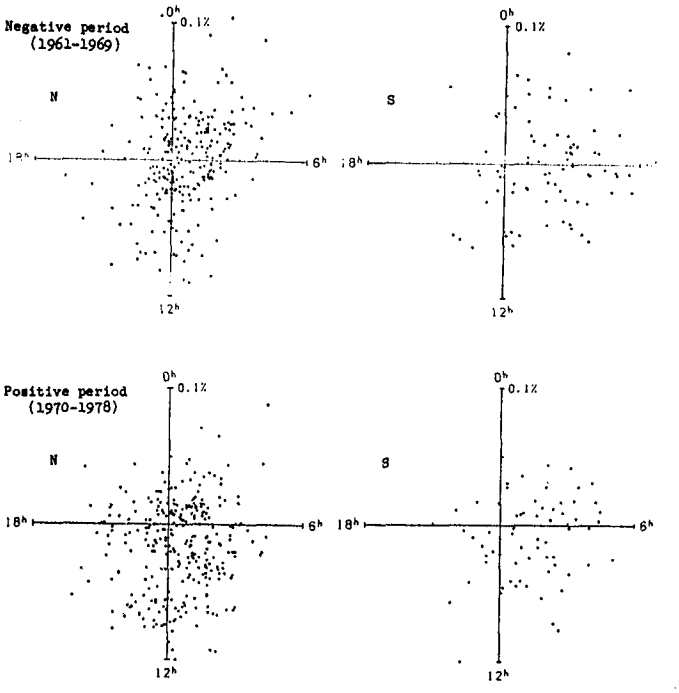

Fig. 2 Sidereal diurnal variations of all the station-years for N and S for two periods; negative (1961-1969) and positive (1970-1978) periods.

and S for two periods are shown in Fig. 2. In the figure, the distributions of variations of N are different from those of S for both periods

Fig. 3 shows the mean vectors for N and S for these two periods, N_1 and S_1 for the negative period (1961-1969) and N_2 and S_2 for the positive period (1970-1978), respectively. The numerical values; their averages and each dispersions are tabulated in Table 2. In the vectors with a notation (N+S)/2 expresses the variation common to both hemispheres of north-south symmetric type. This could be regarded as being due to uni-directional galactic anisotropy as has been discussed in Paper I, and is shown Fig. 4. It is obtained that for the negative period, the

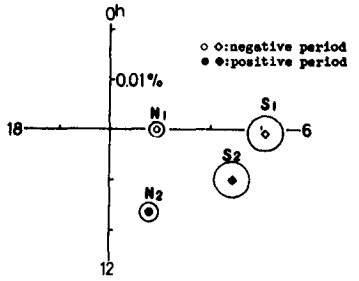

Fig. 3 Averaged sidereal diurnal variations for N and S for two periods; ○◇ with figure 1 for negative period (1961-1969) and ●◆ with figure 2 for positive period (1970-1978).

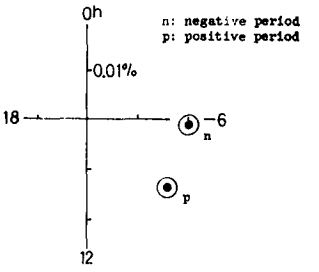

Fig. 4 Sidereal diurnal variations (N+S)/2 for two periods; negative (n) and positive (p) period.

	Negative period (1961-1969)		Positive period (1970-1978)	
	Amp.(%)×10^{-4}	Phase(h)	Amp.(%)×10^{-4}	Phase(h)
N	94 (16)	6.0 (0.6)	182 (19)	10.3 (0.4)
S	312 (36)	6.2 (0.4)	261 (36)	7.5 (0.5)
(N+S)/2	203 (20)	6.1 (0.4)	207 (20)	8.6 (0.4)

Table 2 Observed sidereal diurnal variations for N and S for two periods. Also (N+S)/2 is shown. Figures in the parentheses express the dispersions.

amplitude A=0.0203±0.0020% and the phase ϕ=6.1±0.4 h LST and for the positive period, A=0.0207±0.0020% and ϕ=8.6±0.4 h LST. It is noteworthy that the present averages are exceptionally significant from the statistical point of view.

3.Discussion and Conclusion

The present results of the sidereal diurnal variation, (N+S)/2, common to both hemispheres are statistically significant for two periods; the negative (1961-1969) and the positive (1970-1978) period of Sun's polar magnetic field as shown in Fig. 4. In these variations, the spurious sidereal variations may be eliminated by taking a long-term average. And also the spurious sidereal diurnal variation caused by annual modulation of the solar diurnal variation produced from a stationary anisotropy responsible for the solar semi-diurnal variation (Nagashima, 1984), can be eliminated due to its north-south asymmetric nature.

Also as shown in Fig. 4, the sidereal diurnal variations for these two periods are significantly different from each other (several times larger than the dispersion error). On the other hand, a recent work of Nagashima et al. (1984) demonstrated that the sidereal diurnal variations observed at deep underground stations in both hemispheres almost coincide with each other, after correcting for the annual modulation effect of the solar diurnal variation for the negative and positive period mentioned above. And they showed that these resultant variations are stationary throught the periods 1958-1983, regardless of Sun's polar magnetic field polarity reversal. The present result msy somewhat contradict their conclusion, which may be due to rather larger errors in underground data.

As far as these two periods and the neutron energy regions are concerned, a clear phase difference between two periods; negative and positive periods, was obtained. A further analysis is necessary to derive a definite conclusion.

4.Acknowledgements

The authors wish to express their sincere appreciation to all the directors of the observation stations for providing invaluable neutron monitor data. These data are obtained through WDC-C2. A large part of the present calculations were made of Computer Center Fukushima University.

References

Cini-Castagnoli, G., Marocchi, D., H. Elliot, R.G. Marsden and T. Thambyahpillai, Proc. 14th Int. Cosmic Rays Conf. (Munich). 4, 1453 (1975).

Nagashima, K. and H. Ueno, Rep. Ionosph. Space Res., Japan, 25, 212 (1971).

Nagashima, K., H. Ueno, K. Fujimoto, Z. Fujii and I. Kondo, Rep. Ionosph. Space Res., Japan, 26, 1 (1972a).

Nagashima, K., H. Ueno, K. Fujimoto, Z. Fujii and I. Kondo, Ibid., 26, 31 (1972b).

Nagashima, K., S. Sakakibara, A.G. Fenton and J.E. Humble, Planet. Space Sci., (in press, 1984).

Nagashima, K., Proc. Int. Symp. Cosmic Ray Modulation Heliosph. (Morioka), 309 (1984).

Sidereal Anisotropies in the Median Rigidity Range 60-600GV in 1978-1983

H.Ueno, Z.Fujii, S.Mori*, S.Yasue* and K.Nagashima
Cosmic Ray Res. Lab., Nagoya Univ., Nagoya 464, Japan
*Depart. of Physics, Shinshu Univ., Matsumoto 390, Japan

1. Introduction

A great many observation has been made of the sidereal time variations of cosmic rays with various detectors in a wide range of rigidities from neutron monitors(effective primary rigidity 10^{10}V), surface and underground muon telescopes to small air shower arrays($10^{13} \sim 10^{14}$V), and much data have been accumlated to explore the nature of the galactic anisotropy, such as its origin and its propagation inside and outside the heliomagnetosphere.

In low rigidity region, the observed sidereal diurnal variations contain not only those of galactic origin but also those of solar and atmospheric origin. The variations of the latter origin are called the spurious sidereal variations, and almost all of them can be eliminated by taking the difference between the variations observed by two component telescopes pointing different directions (cf. Elliot and Dolbear, 1950). This elimination method, however, cannot be applied to the variation arising from the seasonal variation of solar anisotropy. A typical example for this can be seen in the spurious sidereal diurnal variation arising from the solar anisotropy of the 2nd order responsible for the solar semi-diurnal variation(Nagashima and Ueno, 1971).

In the present paper, the observed sidereal variations are corrected for the influence of this spurious variation by a method using the anti-sidereal diurnal variations produced from the same 2nd order anisotropy (Nagashima et al., 1983). It is demonstrated that the corrected variations are a resultant product of two constituents of galactic origin: one is north-south(N-S) symmetric and the other is N-S asymmetric.

2. Data Analysis and Discussions

In the present analysis, we use the data from surface(NAgoya) and underground(Misato and Sakashita) muon telescopes. Hereafter we abbreviate these stations to NAMS by picking up the top letter of the name of the stations. These data cover the rigidity range of 60 to 600GV, and the present work is concerned with 6-year averages of these data in the period of 1978-1983.

In Table 1, 6-year averages of the observed sidereal diurnal variations of NAMS are listed, together with those of the anti-sidereal diurnal variations and are shown in Fig.1 and Fig.2. Also listed in the table are some characteristics of the telescopes(Fujimoto et al., 1984). Errors of the amplitudes are derived from the dispersion of yearly vectors.

The spurious sidereal diurnal variations are produced by various noises such as the atmospheric effects and also transient cosmic ray intensity variations. In the present analysis, these noises can be eliminated statistically by taking 6-year averages and also by introducing the unknown vector common to all directional components at each station in the best fit calculation. The spurious sidereal diurnal variation is also produced from cosmic ray flow perpendicular to the solar equatorial plane. This variation is sector-structure dependent and is called Swinson-type(cf. Swinson, 1969). This variation could

Table 1 6-year averages of observed sidereal diurnal variations of NAMS for 1978-1983, together with those of associated anti-sidereal diurnal variations and also corrected variations for Nagashima's component (see text). Some characteristics of the telescopes are also shown. Errors of the amplitudes are derived from the dispersion of yearly vectors.

		Zenith & Azimuth		Geographic Direction		Median Rigidity	Counting Rate	Amplitude(%) & Phase(hr) of Harmonics of 6 Years Averages 1978-1983					
STATION	TELESCOPE	Z	A	λ	ψ	P_{ME}(GV)	$\times 10^4$/hr	Anti-Sidereal 1st		Sidereal 1st		Corrected Sidereal 1st	
NAGOYA 0mwe	V	0°	-	35°N	137°	60	276.0	.034±.008	20.8	.011±.008	16.1	.021±.011	4.4
	N	30°	0°	65°N	"	66	125.0	.037±.008	19.5	.018±.007	14.5	.018±.010	3.3
	E	"	90°	30°N	172°	67	120.0	.026±.008	19.7	.002±.008	3.8	.026±.009	3.2
	S	"	180°	5°N	137°	64	123.0	.014±.009	21.3	.009±.008	4.2	.022±.011	4.5
	W	"	270°	30°N	102°	63	126.0	.035±.007	22.3	.016±.007	18.7	.018±.011	5.0
MISATO 34mwe	V	0°	-	36°N	138°	145	28.0	.032±.007	21.9	.028±.007	19.0	.012±.008	0.9
	N	33°	39°	57°N	177°	155	10.7	.033±.007	19.5	.030±.007	15.8	.007±.009	21.9
	E	"	129°	12°N	164°	143	14.2	.012±.007	21.7	.018±.008	21.9	.018±.008	0.3
	S	"	219°	9°N	117°	155	10.7	.025±.005	23.6	.019±.007	23.9	.022±.008	4.6
	W	"	309°	51°N	95°	156	9.8	.037±.006	23.3	.025±.006	19.5	.012±.007	5.1
SAKASHITA 80mwe	V	0°	-	36°N	138°	331	39.0	.032±.004	23.0	.017±.004	22.9	.028±.004	4.2
	N	41°	346°	73°N	104°	401	6.2	.023±.004	22.6	.008±.004	17.6	.015±.005	6.4
	E	"	76°	35°N	188°	384	7.6	.021±.004	21.2	.021±.004	22.6	.029±.003	1.5
	S	"	166°	5°S	147°	387	6.7	.018±.004	1.3	.054±.004	2.6	.056±.005	3.8
	W	"	256°	18°N	96°	444	5.6	.019±.004	2.2	.040±.005	3.8	.043±.004	5.4
	NN	60°	346°	77°N	26°	595	2.4	.002±.004	6.4	.002±.004	13.2	.004±.006	13.5
	SS	"	166°	23°S	151°	540	2.7	.015±.005	8.1	.086±.005	2.6	.072±.006	2.4

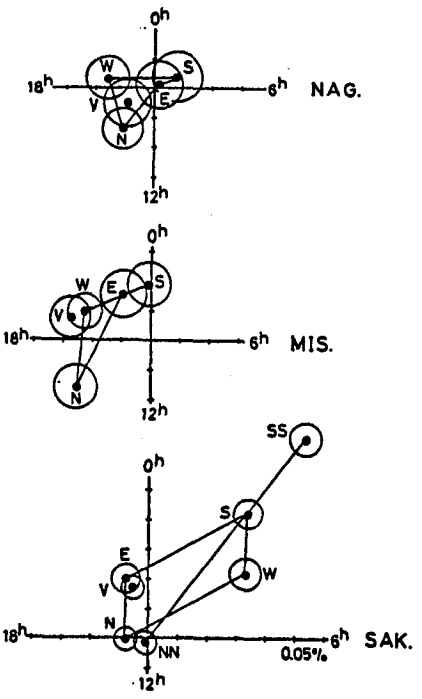

Fig.1 6-year averages of observed sidereal diurnal variations of NAMS telescopes at Nagoya (NAG), Misato (MIS) and Sakashita (SAK) for 1978-1983.

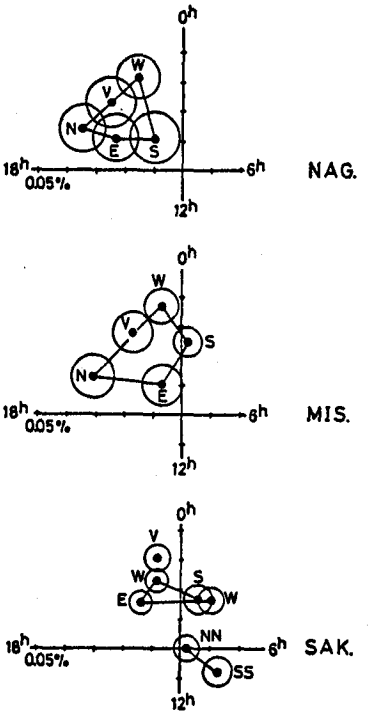

Fig.2 6-year averages of observed anti-sidereal diurnal variations of NAMS telescopes for 1978-1983.

be canceled by taking averages of the all period due to almost equal appearance of the toward and away sectors.

Spurious sidereal diurnal variation is also produced by a systematic annual variation of the solar diurnal variation arising from a solar diurnal variation caused by a stationary anisotropy responsible for the solar semi-diurnal variation(Nagashima and Ueno, 1971). According to the recent study(Nagashima et al., 1983), the spurious variation can be eliminated by multiplying the observed anti-sidereal diurnal variation by 0.947, rotating the vector counterclockwise by 68°, and subtracting it from the observed sidereal diurnal vector.

The corrected sidereal diurnal variations of NAMS are also listed in Table 1 and are shown in Fig.3. As is seen in the figure, the corrected sidereal diurnal variations at Sakashita station are statistically significant, while the variations at Misato and Nagoya stations are comparable with the corresponding dispersion errors. As the counting rates at Misato and Nagoya are large, the large errors are supposed to be caused by the scattering of year-to-year vectors mainly due to the insufficient correction for transient solar diurnal variations. On the other hand, the relative configuration of the vectors of each station seems to be reasonable from the standpoint of geometrical setting of the component telescopes. This implies that real errors may be smaller than the dispersion errors, and in this respect it is worthwhile examining the rigidity dependence of the corrected sidereal diurnal variations including those of the two stations.

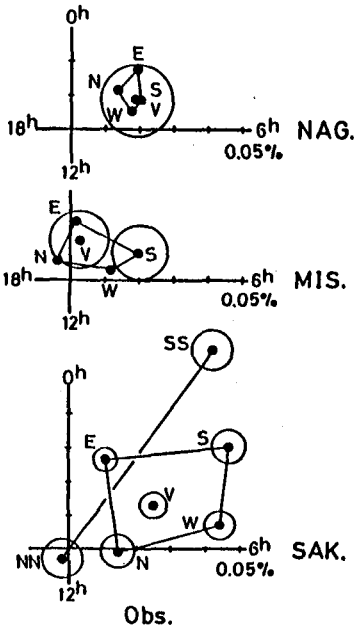

Fig.3 6-year averages of corrected sidereal diurnal variations of NAMS telescopes for 1978-1983.

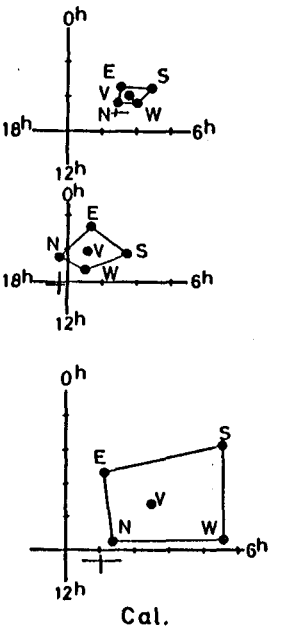

Fig.4 Best fit case of corrected sidereal diurnal variations of NAMS telescopes for 1978-1983. The cross marks are the common vector for each station calculated by the least squares method.

In order to derive the anisotropy, we assume the following in the best fit method as

1) two terms of N-S symmetric and N-S asymmetric types are assumed in the anisotropy for a better fitness between the observed and the expected variations,
2) from the observed fact that the amplitudes are larger for the deeper underground stations, we reasonably assume the low cutoff rigidity P_L in the flat rigidity spectrum, and
3) the unknown vectors are introduced to eliminate the spurious noises as mentioned above.

Tentative results using coupling coefficients given by Fujimoto et al. (1984) are obtained;

N-S symmetric term (P_1^1-type)
the amplitude 0.079+0.007%, the phase 3.5hr and P_L=200GV
N-S asymmetric term (P_2^1-type)
the amplitude 0.035+0.007%, the phase 14.9hr and P_L=200GV

In the present calculation, SS-component at Sakashita station is not included because of larger risidual error probably due to some heliospheric effect which occurs in sidereal semi-diurnal variations (Fujii et al., 1984). The calculated variations in the best fit case are shown in Fig.4.

3. Summary

1. The correction for the spurious sidereal variation using the anti-sidereal variation is indispensable to the study of sidereal anisotropy in low rigidity region.
2. Galactic sidereal anisotropy can be explained better with two terms of N-S symmetric and N-S asymmetric types than the usual uni-directional anisotropy only.

References

Elliot,H. and Dolbear,D.W.N. (1950) Proc. Phys. Soc. A, 63, 137.
Fujii,Z. et al. (1984) Proc. Int. Symp. CR Mod. Morioka, 364.
Fujimoto,K. et al. (1984) Rep. CR Res. Lab., Nagoya Univ., No.9.
Nagashima,K. and Ueno,H. (1971) Rep. Ionos. Space Res. Japan, 25, 212.
Nagashima,K. et al. (1983) Nuovo Cimento, 6C, 550.
Swinson,D.B. (1969) J. Geophys. Res., 74, 5591.

SIDEREAL VARIATIONS DEEP UNDERGROUND IN TASMANIA

J.E.Humble, A.G.Fenton and K.B.Fenton
Physics Department, University of Tasmania
Box 252C, G.P.O., Hobart, Tasmania, Australia, 7001

1. Introduction. Data from the deep underground vertically directed muon telescopes at Poatina, Tasmania, have been used since 1972 for a number of investigations, including the daily intensity variations, atmospheric influences, and checking for possible effects due to the interplanetary magnetic field (1-3). These telescopes have a total sensitive area of only $3m^2$, with the result that the counting rate is low (about 1680 events per hour) and the statistical errors on the results are rather large. Consequently, it was decided several years ago to construct larger detectors for this station. The first of these telescopes has been in operation for two complete years, and the results from it are presented here.

2. Site and Equipment. The equipment is located at a vertical material depth of 139.4m underground in a hydro-electric power station. The mean density has been estimated as 2.56g cm^{-2}, giving a vertical absorber of 357hg cm^{-2}. This corresponds to a muon cut-off of about 100 GV and median primary rigidity $\sim$ 1200 GV. The geographic coordinates are 41.8^0S, 146.9^0E.

When fully operational, there will be three proportional counter telescopes each having a sensitive area of approximately $4m^2$ and semi-cubical geometry (2mx2mx1m). In each telescope there are four trays of 10cm diameter proportional counters made from thin-walled copper water pipe, with soldered brass ends and glass-metal seals. These were given a prolonged outgassing at temperatures close to 100^0C before being filled with standard P-10 gas (90% argon plus 10% methane) at atmospheric pressure. Each counter was tested by pulse-height analysis of the background radiation soon after filling and again several months later as a check for leaks. During the two year period there have been no counter replacements, and no evidence for loss of detecting efficiency, a problem frequently experienced with GM counter telescopes. The four trays of counters are arranged in two crossed pairs at the top and bottom of the telescope frame so that there is a possibility of looking for narrow angle effects or grouping the data into broader directions e.g. east and west of the vertical, and for studying multiple particle events.

3. Results. The first and second harmonics for each of the years 1983 and 1984 separately, and the totals for the two-year period are shown in Table 1, analysed according to solar, sidereal and anti-sidereal time. In this Table the Poisson errors are shown; these are somewhat smaller than the standard errors obtained from the scatter in the individual values arising during analysis of a year's data.

As may be seen from the Table, the first harmonic in solar time is not convincingly different from zero; nor is there a significant anti-

sidereal variation. None of the second harmonics are significantly different from zero. On the other hand, the first harmonic in sidereal time is significant during both years as well as in the total. On estimating the errors from the scatter in the values of the components of the vectors we find the amplitude of the first harmonic for the total period 1983-1984 to be (0.081±0.045)% with its maximum at 2.43±2.25 hours.

TABLE 1

	First Harmonic		Second Harmonic	
	Amplitude(%)	Max (hr)	Amplitude(%)	Max (hr)
Solar				
1983	0.053±0.035	3.14± 2.77	0.024±0.035	10.80±6.00
1984	-0.006±0.035	10.59±12.00	0.036±0.035	1.30±2.70
Total	0.026±0.025	3.63± 4.94	0.024±0.025	0.63±6.00
Sidereal				
1983	0.111±0.035	4.41± 1.23	0.022±0.035	1.40±6.00
1984	0.058±0.035	1.92± 2.46	0.005±0.035	8.11±6.00
Total	0.081±0.025	2.43± 1.20	0.009±0.025	2.37±6.00
Anti-sidereal				
1983	0.032±0.035	7.37±12.00	0.038±0.035	10.20±2.34
1984	0.026±0.035	23.41±12.00	0.023±0.035	5.77±6.00
Total	0.019±0.025	4.41±12.00	0.014±0.025	5.86±6.00

4. Discussion. Results from the new, more stable equipment at Poatina appear to confirm the existence of a first harmonic in the daily variation in sidereal time reported earlier, and are consistent with small or non-existent first harmonics in solar and anti-sidereal time. All the second harmonics appear to be small, if not zero at these energies. It will be important to establish the magnitude and phase of any of the variations (other than the 24-hour sidereal wave) which turn out to be present, since these will be crucial in testing models of the anisotropy by comparison with northern hemisphere results. Since these are evidently of very small amplitude, a long period of observation will be required using the full $12m^2$ detector system. The higher total counting rate available with the complete system should assist also in our investigation of the reasons for the observed standard errors being appreciably larger than from counting statistics alone. Systematic influence such as uncorrected atmospheric effects or year to year variations in the anisotropy itself may be responsible, apart from instrumental variability which is thought to be very small in the new designs.

5. Acknowledgements. We wish to thank the Hydro-Electric Commission of Tasmania and its staff for the excellent facilities provided at Poatina. This work is supported in part by the Australian Research Grants Scheme.

6. References.

1. Fenton A G and Fenton K B (1975). 14th Int.Cos.Ray Conf., Munich, Conference Papers 4, 1482-1484.
2. Fenton A G, Fenton K B and Humble J E (1977). 15th Int.Cos.Ray Conf. Plovdiv, Conference Papers 11, 242-244.
3. Humble J E, Fenton A G, Fenton K B and Lyons P R A (1979). 16th Int. Cos.Ray Conf., Kyoto, Conference Papers 4, 258-262.

THE EFFECT OF THE INTERPLANETARY MAGNETIC FIELD ON SIDEREAL VARIATIONS OBSERVED AT MEDIUM DEPTH UNDERGROUND DETECTORS

J.E.Humble and A.G.Fenton
Physics Department, University of Tasmania
Hobart Tasmania Australia 7001

1. Introduction. It has been known for some years that the intensity variations in sidereal time observed by muon detectors at moderate underground depths are sensitive to the polarity of the interplanetary magnetic field (ipmf) near the earth (1-5). There are differences in the response to these anisotropies as observed in the northern and southern hemispheres (6, 7). When fully understood, the nature of the anisotropy seems likely to provide information on the 3-dimensional structure of the heliomagnetosphere, its time variations, and its linking with the local interstellar field - difficult to obtain by other means.

2. Data. The data were obtained from vertically-pointing wide angle (semi-cubical) G-M counter muon telescopes at the underground station near Hobart, located at a depth of 46hg cm^{-2} below the top of the atmosphere (geographic coordinates 42.9^0S, 147.4^0E). The inferred ipmf data used in the analysis were mainly those published in 1972 by Svalgaard (8), Wilcox et al in 1975 (9) or from Solar Geographical Data Bulletins. Unfortunately, in recent years the inferred field directions have been based only on the southern polar station at Vostok, whereas previously data from Thule were also included. This has led to a decrease in the percentage of days for which ipmf data are available.

3. Results. At the time of writing, analysis for the years 1983 and 1984 has not been completed, due to delays in acquiring the ipmf data; however, the results for the period 1958-1982 are unlikely to be altered dramatically by the addition of these two years, or by the re-analysis of data for the whole period. To date, the main results are as follows:

(i) The summation harmonic dials for the sidereal diurnal variation during 1958-1982 show that there is a strong dependence on whether the ipmf near the earth is directed outwards (away, A) from the sun or inwards (towards, T) it (see Figure 1).

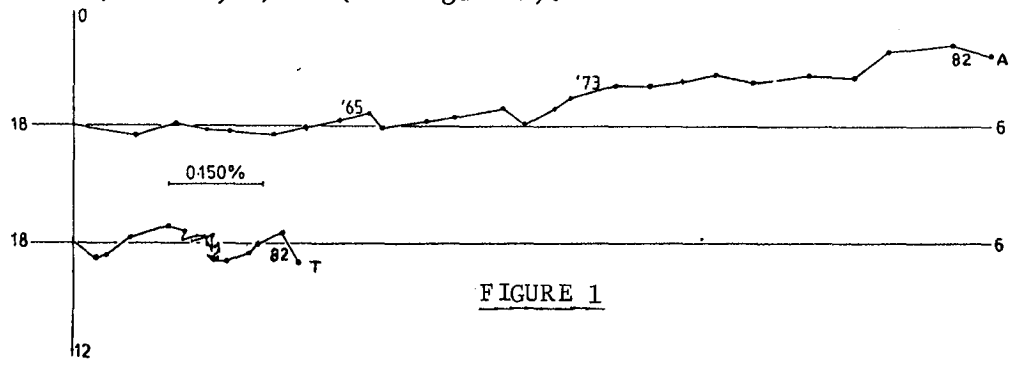

FIGURE 1

(ii) There are significant differences in the amplitude of the sidereal daily variation within the two data sets if these are divided into regimes based on the solar activity cycles (5). For example, before solar minimum in 1965 and after 1977 the amplitudes were relatively large, whereas between 1965 and 1977 the amplitudes were small.

(iii) The variation in anti-sidereal time is significant, but seems to be independent of the ipmf direction.

4. Discussion. The results for the whole period do not seem to agree with those obtained in the northern hemisphere nor are they consistent with some of the interpretations. For example, Thambyahpillai (10) concluded that the shift in position of the viewing cone on the celestial sphere accompanying solar polar field reversals accounts for the London 60 mwe observations. However, the Hobart results group better according to solar minimum years than to the times of solar magnetic field reversals. A more recent explanation of the observations in both hemispheres by Nagashima et al (11, 12) seems to be more satisfactory at the present time. The basis of this model is that the solar semidiurnal variation undergoes an annual modulation due to the excursions in heliolatitude made by the earth; this in turn leads to a diurnal variation in anti-sidereal time which can be used to correct the observed sidereal variation. After such correction, the London and Hobart sidereal variations are more consistent. A more detailed investigation of the Hobart results is in progress.

5. Acknowledgements. The Hobart observations were assisted by grants received from the Australian Research Grants Scheme.

6. References.

1. Swinson D B (1969) J.Geophys.Res. 74, 24, 5591-98
2. Swinson D B (1971) J.Geophys.Res. 76, 19, 4217-23
3. Humble J E, Fenton A G, Speller R D, Otaola J A, Thambyahpillai T, Dutt J C, Mathews T, Miyazaki T and Peacock D S (1973), 13th Int.Cosmic Ray Conf., Denver, Conference Papers 2, 976-81
4. Humble J E and Fenton A G (1977), 15th Int.Cos.Ray Conf., Plovdiv, Conference Papers 11, 245-250
5. Humble J E and Fenton A G (1983), 18th Int.Cos.Ray Conf., Bangalore, Conference Papers 10, 214-217
6. Cini-Castagnoli G, Marocchi D, Elliot H, Marsden R G and Thambyahpillai T (1975) Paper MG10-2, 14th Int.Cosmic Ray Conf., Munich, Conference Papers 4, 1453-7
7. Humble J E and Fenton A G (1975) Paper MG10-8, 14th Int.Cosmic Ray Conf., Munich, Conference Papers 12, 4226-8
8. Svalgaard L (1972) J.Geophys.Res. 77, 4027-34
9. Wilcox J M et al (1975) J.Geophys.Res., 80, 3685-3688
10. Thambyahpillai T (1983), 18th Int.Cos.Ray Conf., Bangalore, Conference Papers 3, 383-386
11. Nagashima K et al (1984) Proc.Int.Symp.Cosmic Ray Modulation in the Heliosphere, Morioka, Japan, 337 (Abstract)
12. Nagashima K et al (1985) Planetary & Space Science, in press

THE SIDEREAL SEMI-DIURNAL VARIATION OBSERVED AT HIGH ZENITH ANGLES AT MAWSON, 1968-1984, AND THE POLARITY OF THE SOLAR MAIN FIELD.

R.M. Jacklyn and M.L. Duldig
Antarctic Division, Department of Science, Australia.

ABSTRACT.

High zenith-angle North/South telescopes viewing equatorially and at mid-latitudes through 40 MWE of atmosphere have been operating at Mawson since early 1968. It is evident that a sidereal semi-diurnal component of galactic origin has been observed, over and above a possible spurious component proposed by Nagashima, arising from a bi-directional component of the solar anisotropy. Although a very pronounced reduction in the semi-diurnal galactic response followed the reversal of polarity of the solar main field during 1969-1971, so far the observations indicate that there has been no recurrence of a larger galactic response following the reversal of polarity around 1981. The possible role of the latitudional extent λ_o of the wavy neutral sheet is discussed.

Introduction.

There is now considerable evidence for the existance of a sidereal semi-diurnal variation of galactic origin at the low end of the high energy spectrum, from detecting systems whose median rigidities of primary response, Pm, to the omnidirectional intensity range from $\sim 10^{14}$v down to $\sim 10^{11}$v (Jacklyn, 1970; Gombosi et al., 1975; Sakakibara et al., 1976, 1979, 1984; Bergeson, 1979). From the underground vertical detectors at Hobart (Pm $\approx 10^{11}$v), for instance, the long-term average amplitude, 1958-1963, has the reported value of 0.0084 $\pm$0.0014%, far in excess of the estimated spurious amplitude of 0.0036 $\pm$0.0002% that is due to seasonal modulation of the solar semi-diurnal variation (Nagashima et al., 1984).

What is at issue in this paper is the role of the alternating +ve and -ve polarity states of the solar main field in affecting observations of the sidéreal semi-diurnal component through associated changes in the heliomagnetic modulating regime. The extensive calculations of Nagashima et al. (1982) have shown that heliomagnetic modulation may differ considerable between the two polarity states. There are indications from his work that in the +ve polarity state (field directed away from the sun in the northern space of the heliosphere) a semi-diurnal galactic response may be relatively suppressed at the field-sensitive rigidities. It has seemed that this might explain why it was that relatively large variations characteristic of a bi-directional sidereal anisotropy were observed with detectors of the shallow-depth type, underground and at the surface, between 1958 and 1969, when the polarity state was -ve, whereas they were very much smaller in the following years of +ve polarity (Jacklyn and Duldig, 1983). More than that, in the earlier years the second harmonic observed with detectors viewing equatorially was significantly larger than that observed at mid-latitudes (Jacklyn, 1970). This suggests that heliomagnetic modulation at that time may not have seriously affected the characteristic latitude dependence of the second harmonic.

Observations now available from successive -ve, +ve and -ve polarity states are discussed here. They concern mainly the results from high zenith-angle telescopes that have been operating at Mawson since 1968.

Observations.

Equatorial and mid-latitude observations have been obtained from Geiger counter telescopes, one group located underground at Hobart (43°S) and the other at the surface at high zenith-angles at Mawson (67°S). All inclined telescopes were aligned in the geographic meridian plane. The mean absorber depth at Hobart was approximately 50 MWE. At Mawson the absorber depth of 40 MWE was entirely atmospheric. Telescope characteristics and the data periods used in the present comparison are listed in Table 1. Further details have been published elsewhere (Jacklyn, 1970; Jacklyn and Vrana, 1969).

TABLE 1.

Telescope Characteristics.

Period	Place	Site	Geometric aperture zenith	azimuth	Inc.	Asympt.* Lat.	Count rate (10^3/hr)
1958-65	Hobart	UG	126°	126°	Vert.	-39°	70
1961-62	Hobart	UG	90°	90°	30°N	-20°	17
1968-69	Mawson	Surface	20°	126°	76°N	10°	6
			20°	126°	76°S	-42°	6
1974-84	Mawson	Surface	20°	126°	76°N	-6°	40
			20°	126°	76°S	-47°	40

*Mean asymptotic latitude of viewing at median rigidity Pm.

The size of the surface telescope system at Mawson was increased from one to three crossed telescopes between 1969 and 1974 and the geometry modified to improve the counting rate and to allow the North asymtotic cone to straddle the equator more effectively. In the result there was an insignificant improvement in the coupling cinstants of response to a second harmonic. That is, the response characteristics that are of relevance here were unchanged.

In Figure 1, the results of observations of the sidereal second harmonic are shown in relation to the succession of polarity states of the heliosphere that occurred between 1958 and 1984, as shown at the foot of the Figure. Consider first the period, 1958-1968, of -ve polarity. Although the counting rate of the single high zenith-angle telescope at Mawson was very low, there was remarkable similarity between the equatorial and mid-latitude vectors at Mawson (amplitudes 0.051 ±0.015% and 0.016 ±0.015%. during 1968-69 and the more significant vectors (amplitude 0.024 ±0.010% and 0.006 ±0.002%) observed at Hobart during 1958-63. At both places the equatorial amplitudes in particular were each greatly in excess of that of the spurious component of solar origin (0.005 ±0.0008% at Hobart and 0.005 ±0.002% at Mawson).

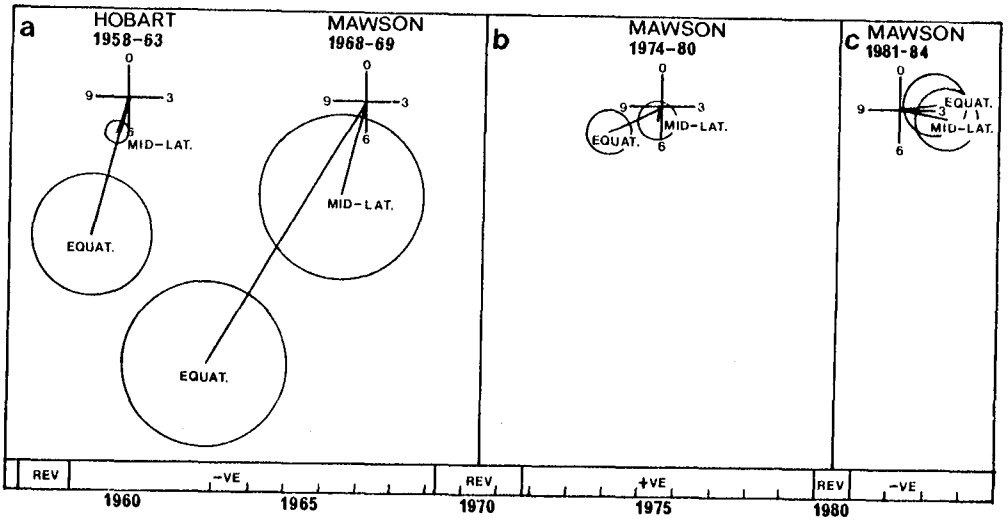

Fig. 1. Sidereal semi-diurnal vectors observed with the telescope systems at effective depths of 40-50 MWE.

(a) within the period of -ve polarity, 1958-1970, from Hobart underground vertical (mid-latitude), Hobart underground 30°N (equatorial), Mawson surface 76°S (mid-latitude) and Mawson surface 76°N (equatorial).

(b) within the period of +ve polarity, 1971-1980, from Mawson surface 76°S and 76°N.

(c) within the period of -ve polarity, 1981-1984, from Mawson surface 76°S and 76°N.

The SD circles are derived from observed fluctuations in the data.

Observations with a seven-fold increase in counting rate of the high zenith-angle equipment commenced at Mawson in 1973, after the heliomagnetic field polarity had reversed. Averaged over the following years of +ve polarity, 1974-1980, the sidereal second harmonics in the north and south directions were very small (Fig. 1b). However, the equatorial amplitude (0.010 ±0.004%) was significant and almost twice the amplitude of the estimated spurious component (0.005 ±0.0004%). The result tended to support the evidence for a latitude dependence of amplitude found in the earlier period of -ve polarity.

The most recent results, 1981-1984, relate to the present conditions of -ve polarity. There are no indications (Fig. 1c) of a return to the large equatorial amplitudes that seemed to be characteristic of the earlier period of -ve polarity. In fact, the average amplitudes to date are not greater than the estimated spurious effect.

Discussion.

Further evidence for the reality of a bi-directional galactic response at shallow depths during 1958-1970 was presented at the previous Conference from observations of the characteristic diurnal counterpart of the second harmonic (Jacklyn and Duldig, 1983). It was suggested there that suppression of response might have occurred in the epoch of +ve polarity that followed. This was apparent not only because of the reduction of the Mawson equatorial semi-diurnal amplitude, but because there was no associated reduction of the solar semi-diurnal amplitude, thus indicating that there had been suppression not of the spurious but of a genuine galactic response.

It seems now that suppression of semi-diurnal response has continued into the present epoch of -ve polarity, at least up to the end of 1984. The possibility is in accord with the evidence given by Bercovitch that the magnitude of change in sidereal diurnal response of the Ottawa Horizontal Muon Array that was predicted to follow the latest reversal of polarity did not occur (Bercovitch, 1984). That this might have been due to increased scattering in the -ve polarity state was discounted. However, he has pointed out, on the basis of the heliomagnetic model of Nagashima et al. (1982), that if the latitudinal amplitude λ_o of the wavy neutral sheet was sufficiently large in both polarity states the expected change in the diurnal response should be small. Thus, as Nagashima et al. (1984) have noted, characteristic differences between the two polarity states tend to become lost as λ_o increases.

It seems, then, that λ_o might be the critical factor. Perhaps it was a smaller latitudinal extent of the waviness of the neutral sheet during 1958-1969 that resulted in the larger galactic semi-diurnal response evidenced during that period of -ve polarity.

Conclusion.

Although there is persistant evidence in the long term for a semi-diurnal variation of galactic origin at the shallow depths of observation, it now appears that there are groups of years when the response is suppressed and that they are not necessarily associated with a particular polarity state of the heliosphere. When large amplitudes were observed, during 1958-1969, notably in the equatorial direction, the polarity was -ve, but some other factor or factors must have favoured the increased response. It is suggested that a possible factor might have been a relatively small amplitude λ_o of the neutral sheet.

References.

Bercovitch, M. (1984) Proc Int. Symp. on Cosmic Ray Modulation in the Heliosphere, Morioka, 329.

Bergeson, H.E. et al. (1979) Proc. 14th. Int. Cosmic Ray Conf., Munich, 2, 586.

Gombosi, T., et al. (1975) Proc. 14th Int. Cosmic Ray Conf., Munich, 2,586.

Jacklyn, R.M. and Vrana, A. (1969) Proc Astron. Soc. Aust., 1, 6, 278.

Jacklyn, R.M. (1970) ANARE Sci. Rep. Series C(II), Pub. 114, Australia.

Jacklyn, R.M. and Duldig, M.L. (1983) Proc. 18th Int. Cosmic Ray Conf., Bangalore, 3, 391.

Nagashima, K. et al. (1982) Planet. Space Sci., 30, 898.

Nagashima, K., Sakakibara, S., Fenton, A.G. and Humble, J.E. (1984) Planet. Space Sci., in press.

Sakakibara, S. et al. (1976) Proc. Int. Symp. on High Energy Cosmic Ray Modulation, Tokyo, 316.

Sakakibara, S. et al. (1979) Proc 16th Int. Cosmic Ray Conf., Kyoto, 4, 216.

Sakakibara, S. et al. (1984) Proc. Int. Symp. on Cosmic Ray Modulation in the Heliosphere, Morioka, 329.

CORRECTED SIDEREAL ANISOTROPY FOR UNDERGROUND MUONS

D. B. SWINSON[1] and K. Nagashima[2]

[1] Department of Physics and Astronomy, The University of New Mexico, 800 Yale N.E., Albuquerque, New Mexico 87131

[2] Cosmic Ray Research Laboratory, Faculty of Science, Nagoya University, Chikusa-Ku, Nagoya, 464 JAPAN

ABSTRACT

Data from underground muon telescopes in New Mexico and Bolivia are analyzed in sidereal time and anti-sidereal time in the rigidity range 20 GV to a few 100's of GV. Using both vertical and north- and south- pointing telescopes in both hemispheres, a latitude range of 70°N to 50°S is covered. It is shown that there is an anti-sidereal variation of the P^1_2 type, having opposite phase in the northern and southern hemispheres, and maximum amplitude at mid latitudes. The anti-sidereal data are used to correct the sidereal data, using the Nagashima method (Nagashima, 1984); the resulting corrected sidereal vectors for northern hemisphere telescopes have their sidereal maxima close to 3h sidereal time, in reasonable agreement with sidereal data at higher energies from small air showers. The Nagashima correction also eliminates effects due to the reversal of the sun's polar magnetic field which show up in the uncorrected sidereal data.

INTRODUCTION: This paper presents data from the vertical and north- and south-pointing telescopes of the underground cosmic ray muon detectors at Embudo Cave (35.2°N, threshold rigidity 19 GV, median rigidity 132 GV), Socorro (34.04°N, threshold rigidity 45 GV, median rigidity 305 GV) and Bolivia (16.31°S, threshold rigidity 16 GV, median rigidity 125 GV). The asymptotic directions of viewing for these nine telescopes are given by Regener and Swinson (1968); they cover a range in latitude from 70°N to 50°S. Data from Embudo for 1965 to 1983, Socorro for 1968 to 1983, and Boliva for 1965 to 1976 are used in this analysis. The data are analyzed both in sidereal time and in anti-sidereal time, and the nature of the anti-sidereal diurnal variation is examined; the anti-sidereal data are then used to apply the Nagashima correction to the observed sidereal data.

Nagashima et al. (1983, 1985) have shown that, owing to the Earth's orbital motion through the interplanetary magnetic field (IMF), the geographical direction of the field at the earth is subject to a systematic arrival variation; as a result, the solar diurnal and semi-diurnal cosmic ray intensity variations produced from this effect show an annual modulation which can be decomposed into sidereal and anti-

sidereal diurnal and semi-diurnal components. The anti-sidereal diurnal variation is expected to vary with latitude according to the relation (Nagashima et al., 1983).

$$P_2^1 (\sin \lambda) = \sqrt{3}. \text{ Sin } \lambda. \text{ Cos } \lambda \qquad (1)$$

Where λ is the geographic latitude (positive in the northern hemisphere and negative in the southern hemisphere). This function has opposite signs in the two hemispheres, so the expected phases of the anti-sidereal diurnal cosmic ray variation should differ by 180° in the two hemispheres. Note that, in outer space, these phases show eigen values 23.3 h ($\lambda>0$) and 11.3 h ($\lambda<0$), respectively (Nagashima, 1984).

ANTI-SIDEREAL DATA: Figure 1 presents data from the nine telescopes listed earlier, displayed as harmonic dials in anti-sidereal time. Each vector represents an average for all available data (19 years for Embudo, 16 years for Socorro, and 12 years for Bolivia). The error circles are determined on the basis of the scatter of the individual daily vectors which are used to arrive at the various resultant vectors. Errors calculated on the basis of counting rate alone are appreciably smaller. The capital letters E, S and B are for Embudo, Socorro and Bolivia, respectively, and the subscripts V, N and S represent vertical, north- and south-pointing telescopes, repectively at each location. With the exception of the Bolivia north-pointing telescope, the northern latitude telescopes are clustered near 21h anti-sidereal time, and the southern latitude telescopes are clustered near 9h anti-sidereal time, thereby showing the ex-

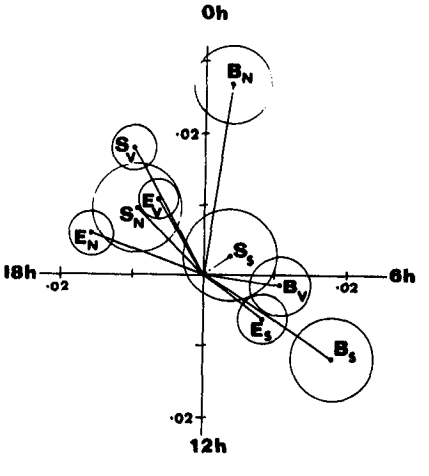

Fig. 1: Harmonic dial in anti-sidereal time for Bolivia, Embudo and Socorro North, South and Vertical Telescopes. Amplitudes are in percent.

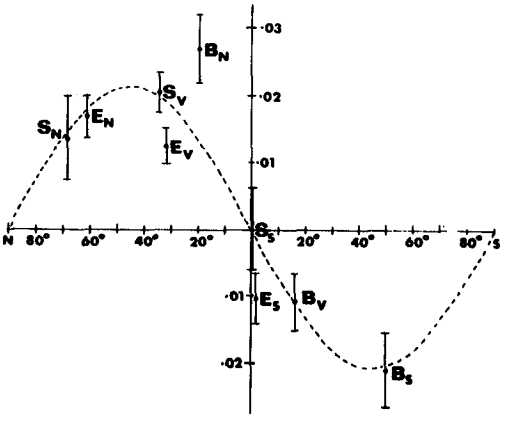

Fig. 2: Amplitude data from Fig. 1 plotted against viewing latitude λ; dashed curve is the function A sinλ Cosλ fitted to the data. Amplitudes are in percent.

pected 180° phase difference between the two hemispheres; the deviations from the corresponding eigen values (23.3 h and 11.3 h) are consistent with the cosmic ray orbital deflection in the geomagnetic field (Fujimoto et al., 1984).

In Figure 2, the data from Figure 1 are displayed in terms of the anti-sidereal amplitude for each of the nine telescopes, plotted as a function of its asymptotic latitude. Superimposed upon the diagram is a graph of the function A $\sin\lambda.\cos\lambda$ (dashed line), with the amplitude A adjusted to provide the best fit to the experimental points. The data conform very well the theoretical expectation (equation 1).

CORRECTED SIDEREAL DATA Nagashima et al [1985] have demonstrated that the anti-sidereal data can be used to remove the related spurious sidereal diurnal variation from the observed diurnal variation in sidereal time. The correction is achieved by rotating the observed anti-sidereal vector by 4.53 hours counter-clockwise, reducing its amplitude by a factor of 0.947, and then subtracting it from the observed sidereal vector. This method has been applied to the data from the nine telescopes used here, and the resulting corrected sidereal diurnal variation vectors for each telescope, for all available data, are presented in Figure 3 as harmonic dials in sidereal time. The vectors for the northern hemisphere telescopes (Embudo and Socorro) all lie in the first quadrant, in the vicinity of 3h sidereal time. The amplitude for the Socorro telescope (median regidity 305 GV) is significantly greater than that of the Embudo telescope (median rigidity 132 GV). These results are consistent with the observations by Bercovitch [1984], using surface telescopes detecting muons arriving at large zenith angles, in which, as the median rigidity increased beyond about 100GV, the sidereal amplitude increased with rigidity, with the phase remaining consistently near 3h sidereal time. The northern hemisphere data in Figure 3 are also consistent with the corrected sidereal data presented by Nagashima et al. [1985], in which the London telescope had a maximum at about 3h sidereal time, with the Hobart telescope observing a somewhat later maximum near 6h sidereal time. The Bolivia (southern hemisphere) data in Figure 3 show a maximum close to 9h sidereal time, which is even later than what is seen at Hobart; at the moment there is no clear explanation for the later phase in the southern hemisphere.

When the Nagashima correction is applied to the observed sidereal data, the correction is relatively effective in reducing or removing phase changes which occur in uncorrected data upon the reversal of the sun's polar magnetic field in 1969-71 and 1980-81 [Swinson, 1976, 1984]. Data from the Socorro vertical telescope (where the sidereal anisotropy is greatest) are shown in Figure 4. In the uncorrected data, a clear phase change can be seen in 1971 and 1981, after the

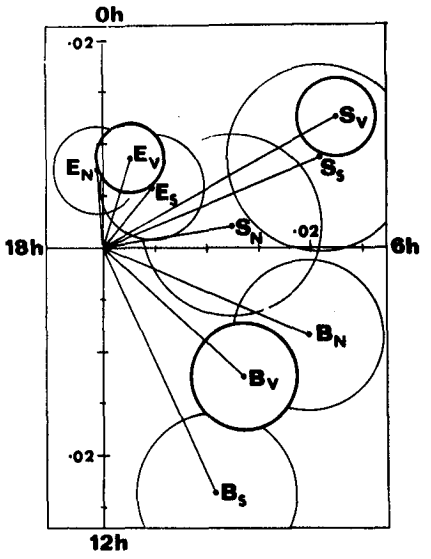

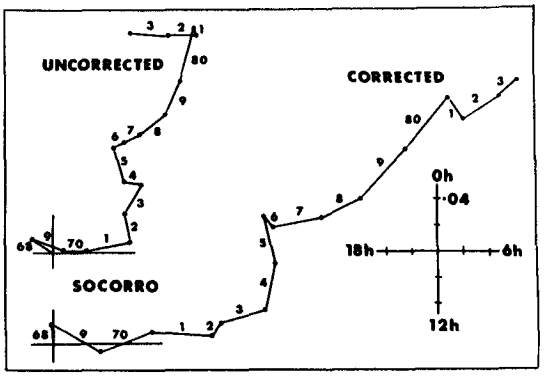

Fig. 4. Yearly harmonic dials in sidereal time for the Socorro vertical telescope, uncorrected and with the Nagashima correction.

Fig. 3. Harmonic dial in sidereal time for Bolivia, Embudo & Socorro North, South and Vertical telescopes with the Nagashima correction. Amplitude scale is in percent.

two most recent solar field reversals. The data corrected by the Nagashima method, however, show very little change, with the yearly vectors remaining relatively consistent, regardless of the magnetic configuration of the heliosphere. This gives one more confidence that the data, corrected in this fashion, are representative of a truly galactic anisotropy.

ACKNOWLEDGEMENTS: The work of one of the authors (DBS) was supported by the Atmospheric Sciences Section, National Science Foundation, under grant ATM-8305098.

REFERENCES

Bercovitch, M., Proc. Int. Symposium on Cosmic Ray Modulation in the Heliosphere, Morioka, Japan, p. 329, 1984.

Fujimoto, K., A. Inoue, K. Murakami and K. Nagashima, Rep. of Cosmic-Ray Research Laboratory, Nagoya University, No. 9, 1984.

Nagashima, K., Proc. Int. Symposium on Cosmic Ray Modulation In The Heliosphere, Morioka, Japan, p. 309, 1984.

Nagashima, K., R. Tatsuoka and S. Matsuzaki. Nuovo Cim., 6C, No. 5, p. 550, 1983.

Nagashima, K., S. Sakakibara, A. G. Fenton, and J. E. Humble, Planet. Space Sci., 1985 (in press).

Regener, V.H. and D.B. Swinson, Can. J. Phys., 46, S784, 1968.

Swinson, D.B., J. Geophys. Res., 81, 2075-2081, 1976.

Swinson, D.B., Proc. Int. Symposium on Cosmic Ray Modulation in the Heliosphere, Morioka, Japan, p. 338, 1984.

SIDEREAL ANISOTROPY OF COSMIC RAYS

A.I.Kuzmin

Yakutsk State University, 677007 Yakutsk, USSR

P.A.Krivoshapkin, G.V.Skripin, G.V.Shafer

Institute of Cosmophysical Research & Aeronomy
Lenin Ave., 31, 677891 Yakutsk, USSR

ABSTRACT

The data of the ionization chamber in Yakutsk for 1954-1984 are analyzed. A false sidereal variation caused by the second spherical harmonic in cosmic ray distribution was found and it has the amplitude 0.020±0.002%. The sidereal anisotropy with a very small amplitude (not more than 0.005%) was observed to exist.

In Table 1 the characteristics of the first harmonic of the solar-diurnal, sidereal and anti-sidereal variations of cosmic rays on data of the ionization chamber in Yakutsk from 1954 to 1984 are given. The data are pressure corrected.

From Table 1 it is evident that all the three variations significantly change from year to year. The solar-diurnal variation phase in 1954 and 1955 shifted to very early time as compared with other years. This tendency manifested in 1976 which evidences the 22-year recurrence of this variation.

The sidereal variation is ~ 3 times less than the solar-diurnal one. Its maximum time, on average, is 21 hr of the sidereal time varying 2-3 hours from it at various years. Sidereal variation in 1958 was somewhat anomalous with a very small amplitude (0.009%) and early maximum time (14.7 hr).

The anti-sidereal variation suffers the stronger changes from year to year either on amplitude or on phase. Its amplitude is ~ 2.5 times less and the maximum time is at earlier hours (13.8 hr) in comparison with the sidereal variation.

In Table 1 data separately for two periods 1958-1968 and 1972-1981 being characterized by various polarity of the general magnetic field of the Sun are also shown. It is evident that phases of sidereal and anti-sidereal variations at these periods are almost invariable. And the phase of the solar-diurnal variation in the second period 2,4 hr to the earlier time is shifted. The amplitudes of all the variations in 1972-1981 increased by 15-30%.

In Table 2 the characteristics of all the three variations corrected to pressure, influence of atmospheric temperature and the Earth's magnetic field (J_{hTM}) are presented. Contribution of the temperature (T) was determined by the

method described in [1] . Vectors T were substracted from the average observed vectors of the intensity anisotropy of of corresponding variations presented by the last three lines in Table 1. Then using receiving vectors [2] for the ionization chamber the correction to the influence of the geomagnetic field was introduced.

Table 2

Characteristics of solar, sidereal and anti-sidereal vectors of diurnal variation of ground temperature (t), of the contribution of the whole atmosphere (T) and of cosmic ray intensity corrected to atmospheric effects and to geomagnetic field (J_{hTM})

Vector	Period	Solar-diurnal		Sidereal		Anti-sidereal	
		Amp.	φ,h	Amp.	φ,h	Amp.	φ,h
t, °C	I*	3.9±0.1	15.2	1.4±0.1	8.1	1.1±0.1	21.5
T, %·10⁻³	II	40 ±3	4.7	14 ±1	21.9	11 ±1	10.2
J_{hTM}, %·10⁻³	I	244 ±8	16.8	24 ±2	21.7	20 ±2	20.3
t, °C	III	3.8±0.1	15.1	1.4±0.1	8.1	1.1±0.1	21.3
T, %·10⁻³	III	60 ±4	4.8	22 ±1.5	21.8	17 ±1.1	11.0
J_{hTM}, %·10⁻³	III	265 ±8	17.4	15 ±3	15.9	20 ±2.2	21.4
t, °C	IV	3.9±0.1	15.4	1.3±0.1	8.1	1.1±0.1	21.8
T, %·10⁻³	IV	24 ±4	4.7	8 ±1.3	21.4	7 ±1.1	11.3
J_{hTM}, %·10⁻³	IV	239 ±8	15.9	33 ±3	23.0	19 ±2.3	18.0

* I - 1954-1983, II - 1958-1979, III - 1958-1968, IV - 1972-1981

From Table 1,2 it is evident that after the corrections J_{hTM} were made the solar diurnal variation amplitude at all the observation periods increased by ~3 times and the phase had shifted 4 hr to later time. As for above two periods the amplitude of solar diurnal variation at the first period (1958-1968) in comparison with the second period became larger and the phase difference remained almost invariable. The phases of the solar-diurnal variation vectors of ground temperature (t) and of vectors T do not change on time. However, the T vector amplitude in the second period is more than twice larger than in the first one.

The J_{hTM} vectors of sidereal and anti-sidereal variations for 30-year period are equal on the value and differ significantly on the phase. Such a behaviour of the variation can be explained as it was shown in [3] by antisymmetric diurnal variation caused by the second spherical harmonic of the cosmic ray distribution in the interplanetary magnetic field. Due to this reason a false sidereal variation with the amplitude 0.020±0.002% and phase 21.7 hr occurs. After substraction of anti-sidereal variation from

Table 1

Amplitudes and phases of solar-diurnal, sidereal and anti-sidereal variations on data of ASK-1 ionization chamber in Yakutsk

Years	Solar-diurnal		Sidereal		Anti-sidereal	
	$A \cdot 10^{-3}$,%	φ,h	$A \cdot 10^{-3}$,%	φ,h	$A \cdot 10^{-3}$,%	φ,h
1954	55±2	5.8	70±2	22.0	29±2	4.1
1955	71	8.9	48	21.7	10	5.6
1956	107	12.2	34	20.8	16	14.3
1957	95	13.6	34	18.0	34	13.3
1958	90	13.6	9	14.7	15	14.2
1959	93	14.7	31	19.3	29	13.3
1960	95	14.9	37	19.7	14	15.3
1961	55	14.8	33	18.9	19	22.9
1962	96	14.8	27	19.4	8	13.3
1963	80	13.8	21	22.3	22	12.3
1964	72	13.3	15	21.9	9	13.8
1965	58	12.2	17	19.5	14	17.3
1966	89	13.7	15	20.5	7	15.8
1967	83	13.3	35	23.8	14	10.3
1968	87	14.3	23	23.9	3	18.2
1969	89	14.3	12	23.0	10	8.4
1970	87	13.5	15	01.4	5	9.8
1971	109	12.3	19	23.2	3	22.8
1972	91	11.4	35	22.2	6	13.0
1973	98	11.3	20	23.7	11	13.1
1974	95	12.6	24	18.5	18	17.6
1975	96	10.4	34	20.7	18	11.1
1976	84	9.9	21	23.0	10	13.2
1977	108	11.0	25	17.5	39	14.1
1978	117	11.0	18	21.7	15	18.1
1979	106	12.9	29	21.2	23	11.4
1980	91	13.1	24	22.6	22	18.2
1981	89	12.7	26	22.3	18	12.0
1982	87	14.7	26	19.4	3	13.9
1983	84	13.7	42	19.0	24	15.8
1984	105	14.7	35	21.7	15	12.5
1954-1983	78±0.3	12.8	24±0.3	21.0	9±0.3	13.8
1958-1968	80±0.5	14.0	20±0.5	20.6	10±0.5	14.3
1972-1981	93±0.5	11.6	23±0.5	21.3	13±0.5	14.2

sidereal one by means of mirrow reflection of anti-sidereal variation relative to the 21 hr direction (as in [4]) the galactic sidereal variation within the errors is not found.

Anti-sidereal variation on amplitude and phase does not change. This feature can be interpreted by the influence of the second harmonic in the cosmic ray distribution.

The sidereal variation suffers significant changes either on amplitude or on phase. Substracting anti-sidereal variation from sidereal one by the above method we obtain the galactic sidereal variation for 1958-1968 with an amplitude 0.018±0.002% and a phase 11.0±0.4 hr and for 1972-1981 - 0.015±0.002% and 22.0±0.4 hr. The vectors are equal on the value but their phases are almost opposite. It indicates the significant influence of sign change of the solar magnetic field upon galactic sidereal variation.

In conclusion it should be noted that on data of the ionization chamber in Yakutsk it was found: 1) the existence of false sidereal variation with an amplitude 0.020±0.002% and a phase 21.0±0.4 hr from contribution of the second spherical harmonic. 2) at periods of various polarities of the solar magnetic field the similar on the amplitude (0.005%) sidereal variation but with opposite phase was observed to exist.

References

1. Kuzmin, A.I. i dr.,(1971) Geomagnetizm i aeronomiya, 11, 523.
2. Fujimoto, K. et al.,(1984) Report of Cosmic Ray Research Laboratory, No.9, Nagoya, Japan, 185.
3. Krivoshapkin P.A.,(1970) Geomagnetizm i aeronomiya, 6, 761.
4. Elliot, H., et al.,(1970) Proc.11-th ICRC, Budapest, Acta Phys.Hung., 29, Suppl.1, 491.

COSMIC RAY INTENSITY VARIATIONS OBSERVED AT MATSUSHIRO (220 M.W.E. IN DEPTH)

S. Yasue, S. Mori and S. Sagisaka
Department of Physics, Faculty of Science
Shinshu University, Matsumoto 390, JAPAN

ABSTRACT

Cosmic ray data from Matsushiro underground station have been analyzed for four years (1981-84). It is found that a marked semi-annual intensity variation has been observed in this period. Solar diurnal and semi-diurnal variations have also been observed. After correcting for the spurious sidereal diurnal variation arising from the anisotropy responsible for the solar semi-diurnal variation (Nagashima et al., 1983), it is found that the corrected siderial diurnal variation is consistent with those so far reported.

1. Introduction. Deep underground observation of the cosmic ray intensity variation provides valuable information as to the nature of modulation in the heliosphere. Matsushiro underground cosmic ray station has been in operation since Aug. 1980 at the depth of 220 m.w.e. (Yasue et al., 1981a). The median primary rigidity of the vertical telescope is about 700 GV (Fujimoto et al., 1984), and its counting rate is 2.1×10^4/h. The analyses of the observed intensity variations of the vertical telescope for four complete years (1981-84) are presented.

2. Semi-annual intensity variation. At the Paris Conference, we have reported that the most part of the unexpectedly large barometric coefficient ($\sim$-0.05%/mb) observed at deep underground stations (Humble et al., 1979; Yasue et al., 1981b) can be attributed to the atmospheric temperature effect (Yasue et al, 1981b). In this report, we present another phenomenon which also seems to be caused by the atmospheric temperature effect. Fig. 1 shows the monthly averaged intensity varia

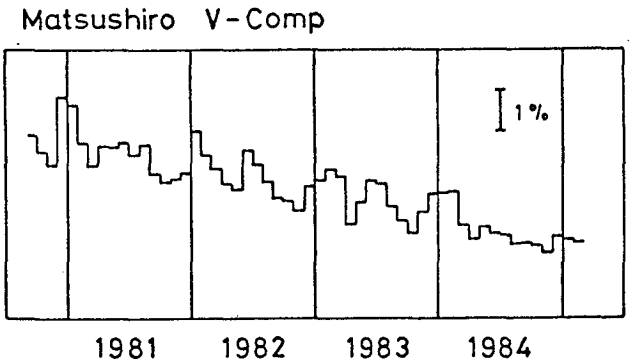

Fig.1 Monthly averaged intensity variation.

tion of the vertical telescope (abbreviated as V-Comp) observed at Matsushiro. In the figure, we can notice a marked semi-annual intensity variation superposed on a gradual intensity decrease. The intensity decrease (about 1 % per year) may be due to the decrease in detector efficiency of the scintillation counters (Ueno, private communication). The semi-annual intensity variation takes the maximum value both in summer and in winter. Such a variation has not been observed at the shallower underground stations than Matsushiro (Ueno et al., 1979). The most part of this variation can be explained quantitatively in terms of the variation of the upper atmospheric temperature (Sagisaka, 1984).

3. Observed daily variations. Fig. 2 shows the daily variations of V-Comp (top) and atmospheric pressure (bottom) averaged over four years (1981-84) for solar (SO), sidereal (SI) and anti-sidereal (AS) time. Cosmic ray data are not corrected for pressure. In the figure, V-Comp shows not only significant SI daily variation but also SO and AS daily variations. It is noted, however, that the atmospheric temperature effect described in the previous section may contaminate also the daily variations.

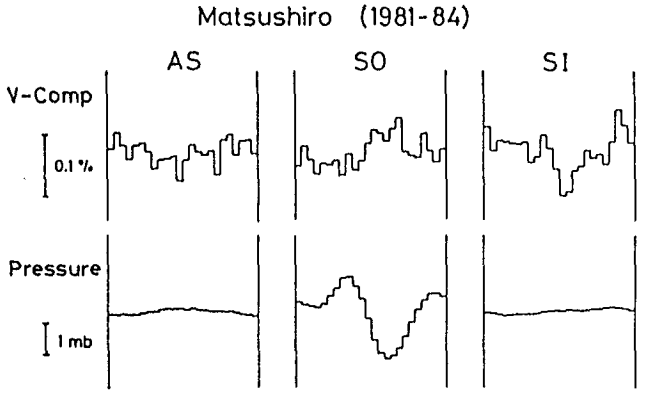

Fig.2 Averaged daily variation of V-Comp and atmospheric pressure for solar(SO), sidereal(SI) and anti-sidereal(AS) time.

We can find in Fig. 2 that the daily variations of pressure in SI and AS time are negligibly small (about one-tenth) compared with that in SO time. This fact implys that we may reasonably assume that the influence of the atmospheric effects becomes serious only in SO time and can be neglected in SI and AS time.

4. Solar daily variation. The heavy solid lines in Fig. 3 show the 1st and 2nd harmonic vectors of the daily variation (SO) of V-Comp shown in Fig. 2. The error circles are the standard error of each mean vector estimated from the dispersion of yearly vectors. In the following, we try to estimate SO harmonic vectors caused by the temperature effect. By analyzing observed data from multi-directional

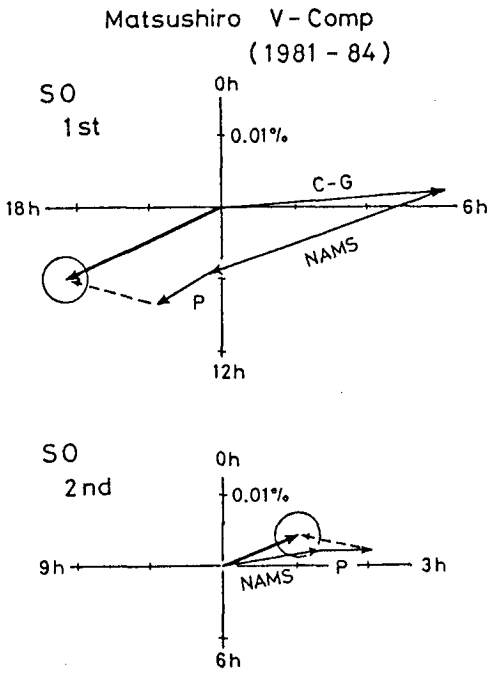

Fig. 3 Solar 1st and 2nd harmonic vectors.

muon telescopes at Nagoya and underground telescopes at Misato and Sakashita (NAMS) in the period of 1978-83, Ueno et al. (1984) and Morishita et al. (1984) determined, respectively, the characteristics of the anisotropies responsible for the solar diurnal and semi-diurnal variations. Assuming those anisotropies obtained by them, and using the coupling coefficients (Fujimoto et al, 1984), we can estimate the expected solar diurnal and semi-diurnal variations at Matsushiro in this period. The obtained vectors are shown in Fig. 3 with the vectors 'NAMS'. These vectors are free from the atmospheric effects. The vectors 'P' in the same figure show SO 1st and 2nd harmonics produced from the daily variation of the atmospheric pressure shown in Fig. 2. Here, we assume the genuine barometric coefficient of -0.01%/mb (Sagisaka et al., 1979). The vector 'C-G' in Fig. 3 shows the 1st harmonic vector originated from the Compton-Getting effect due to the Earth's revolution around the Sun. Composing the above vectors on the respective harmonic dials, and comparing the resultant vectors with the observed ones, we can obtain the residual vectors (dashed line) shown in Fig. 3. One might expect that these vectors are produced from the atmospheric temperature effect. (It is noted that other unknown vectors, one of which may be originated from the galactic anisotropy (Nagashima et al., 1982), might also be included in these vectors.)

5. SI and AS daily variations. It is emphasized that the solar daily variation is observed even at this depth (220 m.w.e.) in this period. As has been described by Nagashima et al. (1983, 1985), the second order solar anisotropy responsible for the observed semi-diurnal variation produces the AS 1st harmonic vector with the phase of 0h, due to the tilt of the spin axis of the Earth to the ecliptic plane. The present observation seems to support his expectation. Namely, the observed AS vector in Fig. 4 seems to be interpreted as the side-band vector produced from the 2nd order anisotropy at 3h-21h. In this case, another side-band vector (spurious sidereal vector) should be observed according to his theory. This vector can be derived from the observed AS vector (Nagashima et al., 1983), and is shown by the dashed line (amplitude and phase of the vector is 0.014% and 19.4h, respectively) on the SI harmonic dial (see Fig. 4). If we subtract this spurious SI

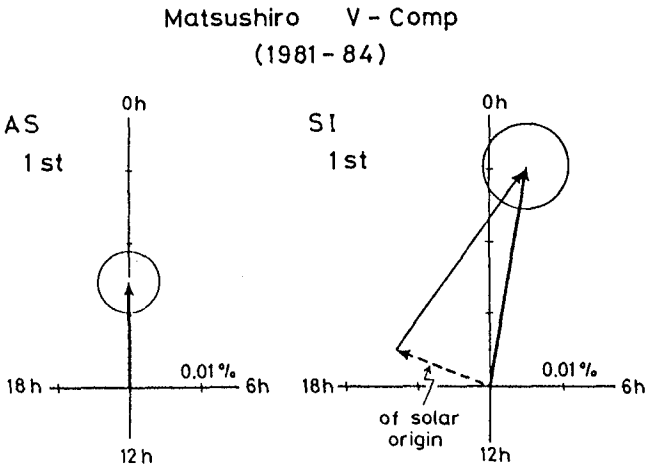

Fig.4 Sidereal and anti-sidereal harmonic vectors.

vector from the observed SI vector, we can obtain the true SI vector of galactic origin. The resultant vector has the amplitude of 0.031% and the phase of 2.3h. The present result seems to be consistent with those so far reported (Nagashima et al., 1985).

Acknowledgements. The authors express harty thanks to Prof. K. Nagashima for his encouragement and discussions with them. Thanks are also due to Mr. K. Chino for his help in data processing.

References

Fujimoto, K. et al. (1984), Rep. of C. R. Res. Lab. Nagoya Univ. No.9.
Humble, J.E. et al. (1979), Proc. 16th ICRC (Kyoto) 4, 258.
Morishita,I. et al. (1984), Proc. Int. Symp. C.R. Mod. (Morioka), p130.
Nagashima, K. et al. (1982), Planet. Space Sci. 30, 879.
Nagashima, K. et al (1983), Nuovo Cimento 6C, 550.
Nagashima, K. et al. (1985), Planet. Space Sci. (in press).
Sagisaka,S. et al. (1979), Proc. 16th ICRC (Kyoto) 4, 235.
Sagisaka, S. (1984), Proc. Int. Symp. C. R. Mod. (Morioka), p360.
Ueno, H. et al. (1979), Proc. 16th ICRC (Kyoto) 12, 228.
Ueno, H. et al. (1984), Proc. Int. Symp. C. R. Mod. (Morioka), p109.
Yasue, S. et al. (1981a), Proc. 17th ICRC (Paris) 4, 304.
Yasue, S. et al. (1981b), Proc. 17th ICRC (Paris) 4, 308.

LONG-TERM MODULATION OF COSMIC RAYS DURING SOLAR CYCLE 21

A.G.Fenton, K.B.Fenton and J.E.Humble
Physics Department, University of Tasmania
Hobart Tasmania Australia 7001

1. Introduction. In recent years we have reported (1, 2, 3) results from the Australian chain of neutron monitors relating to Forbush-type decreases observed during Solar Cycle 21. It was concluded that the rigidity dependence of the decreases observed in the southern hemisphere during this period is essentially the same now as it was in the previous cycle. Fitting the data from ten Forbush-type decreases of amplitude $\geq 4\%$ during the period September 1977 to January 1983 to a modulation function of the form $\exp(-K/P^{\gamma})$ showed that these events were consistent with $0.5<\gamma<0.9$, with the mean γ-value close to 0.7. In this paper we report a preliminary result concerning the rigidity dependence of the longer-term solar cycle modulation.

2. Neutron Monitors, Data and Methods. The neutron monitors chiefly referred to in this paper are 9NM64-type, located near sea level at Hobart (42.9°S, 147.3°E, vertical cut-off 1.89 GV), Brisbane (27.4°S, 153.1°E, 7.24 GV) and Darwin (12.4°S, 130.9°E, 14.07 GV). The neutron monitor at The Springs at an altitude of 725m on the slopes of Mt.Wellington, overlooking Hobart, is currently a 6NM64, but before 1967 there was a 12-counter IGY-type monitor at this site. By careful normalisation of data from different neutron monitors operated in the Hobart area it has been possible to obtain a continuous record of intensity back to July 1956. Other monitors operated by the Hobart group include a 12-counter IGY-type at Mawson, Antarctica (67.6°S, 62.9°E, 0.22 GV) and IGY-type monitors operated at Lae, New Guinea (6.7°S, 147.0°E, 15.52 GV) for some years beginning with the IGY period, and at Brisbane from 1960 until the 9NM64 was installed. It is hoped that it will be possible in the near future to coordinate the results from these stations to determine the solar cycle modulation during Solar Cycle 20, as observed by these southern recorders.

The 11-year solar cycle modulation was assumed to be of the exponential form with exponent $-K/P^{\gamma}$, as discussed in earlier papers (1, 2, 3). An attempt was made to find a best-fit γ, using monthly mean data selected to be relatively free from Forbush-type decreases. Figures 1 and 2 show respectively the long term changes observed at Mt.Wellington, and daily mean intensities over the 4-months period including the major transient event of July, 1982.

3. Results. The long-term modulation, using monthly mean intensities selected as above, and referred to November 1977 as a normalising level, appear to be in accordance with the exponent $\gamma = 1$, provided only Brisbane and Hobart data are used. Darwin data do not conform to this pattern except perhaps during the early years of the cycle until about the end of 1980, since when the Darwin long-term intensity has been largely steady, apart from Forbush-type decreases and as yet unidentified

small changes of the order of 1%. Thus these results must be regarded as preliminary.

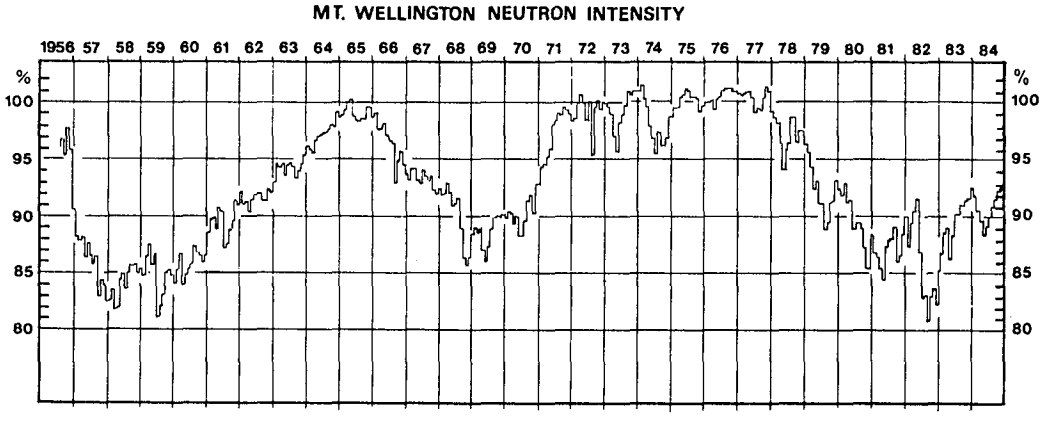

FIGURE 1

Monthly mean neutron intensities relative to May, 1965.

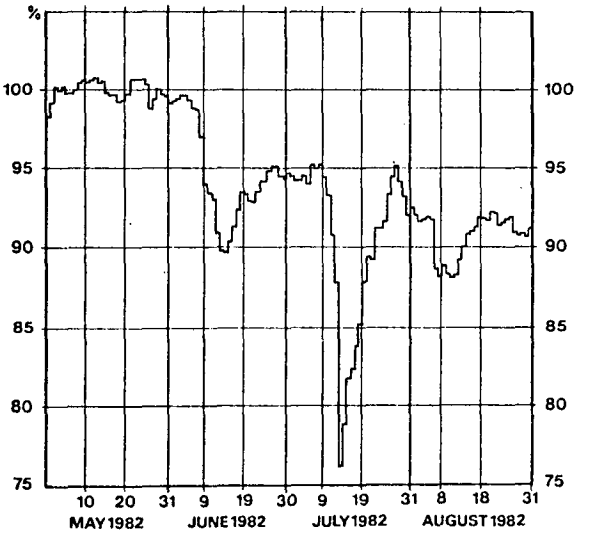

FIGURE 2

Daily mean pressure-corrected Mt.Wellington neutron intensities for May-August 1982, expressed as percent of mean level for May.

4. Discussion. The results seem to confirm the conclusion reached earlier that the Forbush-type modulation and the 11-year cyclic changes have a different rigidity response, and thus is probably caused by different mechanisms under solar influence; however, from our preliminary analysis it may be that the long-term changes have been limited to rigidities below about 10 GV since solar maximum, which occurred in December 1979. This observation would agree with a report by Lockwood and Webber (4) that the observed hysteresis effect between the integral intensity measured by satellite cosmic ray telescopes and Mt.Washington neutron monitor counting rates can be explained by a change in the rigidity dependence of the diffusion coefficient during Solar Cycle 20, 1965-1976, and suggests that similar changes in rigidity response are occurring in the current cycle.

Semi-quantitative evidence against the contention that the long-term solar cycle modulation is made up from superimposed Forbush-type decreases may be obtained from data such as displayed in Figure 2. Here, it may be seen that the very large transient event in July 1982 completely recovered by late July, and that the intensity changes during the period May-August may be considered to be composed of long-lasting possibly stepwise decreases on which the shorter transients are superimposed. Indeed, if the Forbush-type decreases are considered separately, the total 'count' removed by them is only about half the total removed by the longer-term effect.

5. Acknowledgements. We wish to thank the staff of the Bureau of Meteorology stations at Brisbane and Darwin airports for their valuable assistance in the operation of these neutron monitors. The neutron monitor programme at Hobart, Brisbane and Darwin has been supported in part by grants from the Australian Research Grants Scheme.

6. References.

1. Fenton A G, Fenton K B and Humble J E (1983). Proc.18th Int.Cosmic Ray Conf., Bangalore, 10, 164-167
2. Fenton A G, Fenton K B and Humble J E (1984). Proc.Int.Symposium on Cosmic Ray Modulation in the Heliosphere, Morioka, Japan, 1984, 191-196
3. Fenton A G, Fenton K B and Humble J E (1984). Proc.ASA 5 (4), 590-593
4. Lockwood J A and Webber W R (1979) J.Geophys.Res. 84, 197-202

SH 4.4-12

ROLE OF SOLAR FLARE INDEX IN LONG TERM MODULATION OF COSMIC RAY INTENSITY

P.K.Pandey*, A.K.Jain, P.K.Shrivastava, S.P.Pathak**
and S.P.Agrawal
Physics Department (Vikram Space Physics Centre)
A.P.S.University, Rewa (M.P.) 486003, India.

ABSTRACT

Recently, the importance of the occurrence of solar flares in the long-term modulation of cosmic ray intensity has been re-emphasized. For this purpose, the data of solar flares have been used from various publications, such as Solar Geophysical Data books, U.A.G. reports and Quarterly Bulletin Of Solar Activity. Our investigation, very clearly reveals that even the periodic changes in the solar flare observations, obtained from the four different data sources, for the same interval, differ significantly from one another; this is evident even on an average basis. Hence, in any study using solar flares, the importance of selecting a single compilation of the solar-flare data for the entire period of investigation is stressed.

1. Introduction. The study of the long term records of cosmic ray measurements, extending to energies beyond 100 Gev., have confirmed the eleven year solar cycle variation of cosmic ray intensity. Recent results (Hatton, 1980; Hatton and Bowe, 1981; Hatton and Bowe, 1983) using the number of solar flares, of importance $\geqslant 1$, and the cosmic ray intensity deviations, have provided an empirical relation with better correlations for a time lag of ≈ 10 months. Such a time lag corresponds to a value of ≈ 70 A.U. for the solar modulating boundary. The goodness of fit has been shown to be quite satisfactory. The use of solar flares for such a correlation studies, often assumes that the total number and importance of solar flares would be the same, irrespective of the source of data of the solar flares. In this paper, we define a more realistic index for using the solar flare data, and then derive the monthly solar flare indices (SFI) for an extended period of time, from 1957-84, to compare it with the monthly averages of the cosmic ray intensity. During the course of investigation, we have found very significant difference in the solar flare indices, when derived from the tabulation of solar flares published in different data sources. These differences are quite large, hence need to be emphasized.

---

* Also at - Govt.Girls Degree College, Rewa (MP.) 486001.
** Also at - Govt.Science College, Rewa (MP.) 486001.

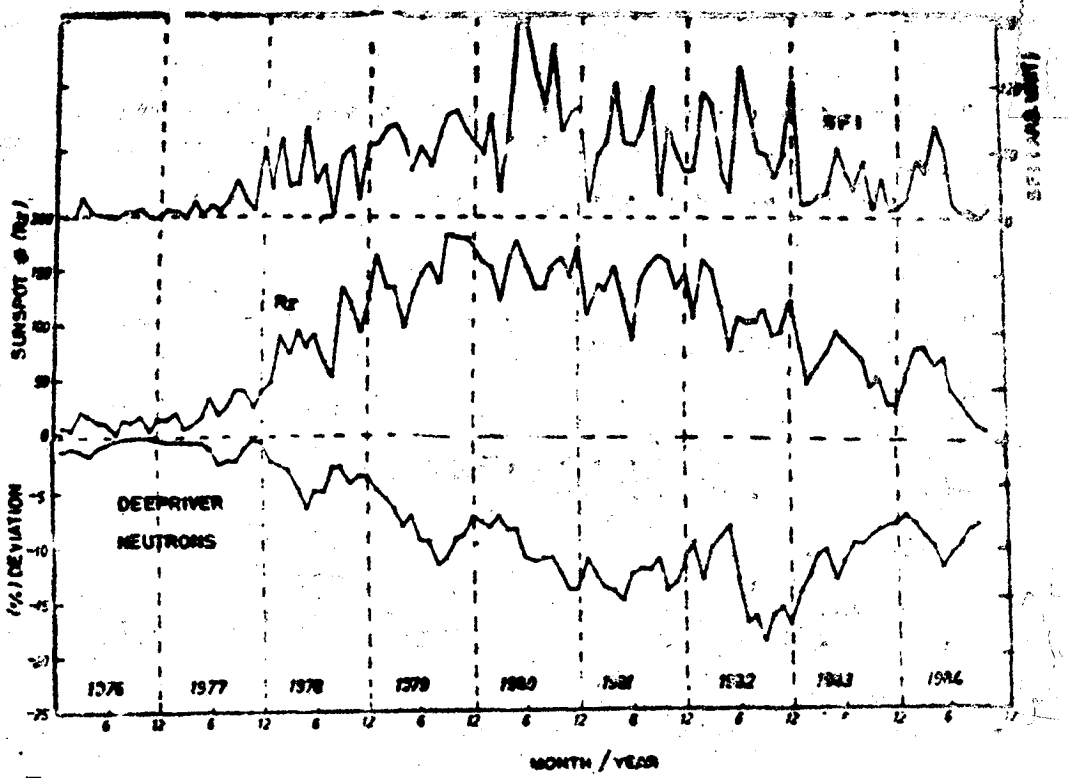

Fig. 1 Shows the percent deviation of monthly mean cosmic ray intensity observed by Deep River Neutron monitoring station. The 100% level is taken as the average for the month, Sept.-Nov. 1976. The monthly values of sunspot number (Rz) and solar flare index (SFI; see text for details for computing SFI) are also plotted for the year 1976-84.

2. Solar flare index. The occurrence of the solar flares are routinely published in solar Geophysical Data, both in the prompt reports as well as in the comprehensive reports. The solar flares are also listed in the quarterly Bulletin of solar Activity as well as in a slightly modified form in the UAG reports of World Data Centre-A. From these listing, various investigators have used the information of the occurrence of solar flares for comparison, with other observations. Usually, for most of the studies the solar flares of importance ≥ 1 are selected (as was done by Hatton, 1980; for Cosmic ray investigations). In these studies the number of solar flares were added without giving any weight either to the importance of the flares or to their brightness. The solar flare brightness is usually represented by B, N and F, whereas the flare-importance is represented by numerical numbers 1, 2, 3 and rarely also 4. We have therefore, generated a

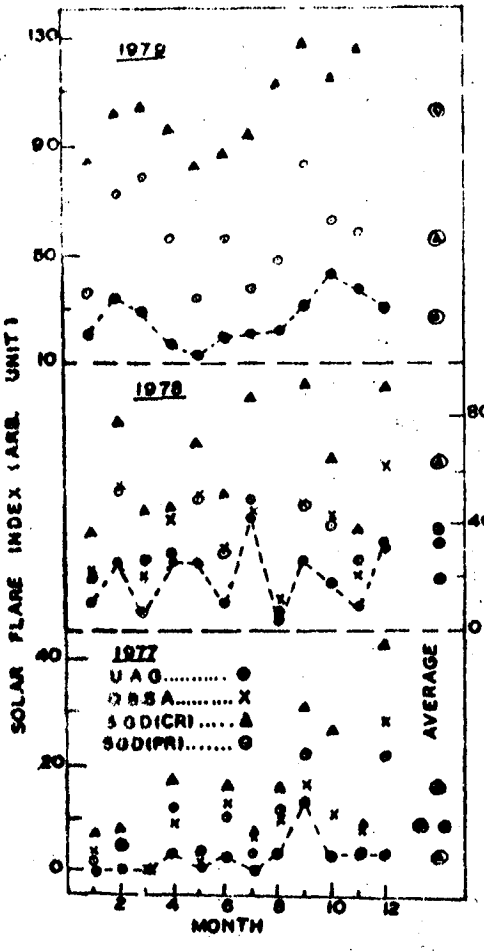

Fig.2 Shows the solar flare index for each month for the three years of high solar activity period 1977,78,79, for four different data sources, which are routinely published. The month to month changes are distinguished by joining the line for the solar flare computed from UAG report. The averages are shown in the right most part of the figure.

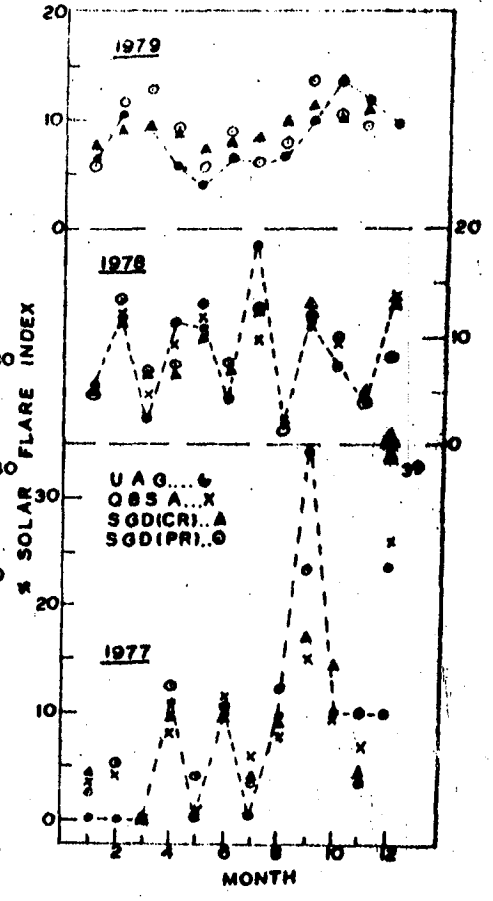

Fig.3 Shows the normalised values of solar flare index for all the monthly data sets and the time interval shown in figure 2. In each case the yearly sums are normalised to 100, to derive the percent solar flare index for each month.

Solar Flare Index (SFI) for each flare, for the interval for which the solar flare data from various sources (mentioned earlier) are available. In generating the new flare index (SFI) the reported importance of the solar flare is used as a numerical weight i.e. the SFI increases with the importance of the flare. Moreover, the brightness level, F, N, and B (Faint, Normal and Bright) are used to additionally weight the numeric value of the importance of the solar flares, by adding to it - 0.3, 0 and + 0.3 respectively. Such a solar flare index (SFI) has been computed for each solar flare of importance ≥ 1. These are then added to form monthly solar flare indices.

3. Results and Discussion. By the method described earlier, we have computed the solar flare index (SFI) using the data of solar flares published in the prompt report of the Solar Geophysical Data (SGD). By using the average of 3 monthly (Sept.-Nov., 1976) values of cosmic ray intensity (when the maximum intensity for the solar cycle occurred), the percent deviations for each month has been obtained for the period 1976-84. These are plotted in fig. 1, along with Rz and SFI (obtained from prompt reports) for 1976-84. In general, from this figure we observe an anti-correlation of both Rz and SFI with percent deviation of Deep River neutrons. However, the significant departure during the year 1980, is clearly evident in the figure.

The solar flare data are also published in the comprehensive reports (C.R.) of SGD. Therefore, the value of SFI calculated from comprehensive reports have been compared with the values of SFI computed earlier from the prompt reports (PR) for the same interval. From this comparison, we notice very significant differences, both in their absolute magnitude as well as in the variations observed from one month to another. Similar differences are noted when we make use of the solar flare listings from other two sources, viz. Quarterly Bulletin of solar Activity and UAG report. Figure 2 shows the monthly values of SFI derived from four different data sources. The annual averages are also marked, to show the difference in their absolute values. It is apparent from the figure that the changes from one month to another are not always similar. As mentioned earlier, if one uses different data sources to compute SFI for different periods, it is necessary to normalise the indices. This has been done for each year by using the yearly sums which are each normalised to 100. The percent solar flare index for each month, has been computed and plotted in figure 3, by using the absolute values plotted in figure 2. From this figure, the large differences in % SFI, from one month to another, comes out in a very significant manner. We conclude therefore, that the solar flare indices generated by either giving weight or otherwise, one should use only one type of data source.

4. References.

Agrawal, S.P.; 1983. Space Science Rev. 34 p. 127.
Hatton, C.J.; 1980 Solar Physics, 66 p. 159.
Hatton, C.J. and Bowe, G.A.; 1981. Proc. 17th ICRC Paris 3 p. 255.
Hatton, C.J. and Bowe, G.A. 1983. Proc. 18th ICRC Bangalore 3, p. 68.

A STUDY OF PERIODICITIES AND RECURRENCES IN SOLAR ACTIVITY AND COSMIC RAY MODULATION

Attolini M. R., Cecchini S.
Istituto TE.S.R.E -C.N.R., Bologna, Italy

Galli M.
Dipartimento di Fisica dell'Università,Bologna, Italy

1. Introduction. Time variability on a wide range of time scales is the main characteristic of cosmic rays observed inside the solar cavity. As the intensity of galactic cosmic rays is assumed to be essentially constant outside the heliosphere, the temporal changes observed must be due to the interaction of CR particles with the IMF which is carried by the solar wind.

The question is then to find out the pattern of the IMF and its flow, to determine the time and spatial evolution of their configurations and to relate them to CR variations.

Unfortunately the direct measurements of the IMF and of the solar wind plasma are insufficient because they are limited to a region close to the ecliptic plane as compared to the vast 3-dimensional extension of the heliosphere. On the other hand CR particles provide an indirect measurement of the global structure of IMF since they sample a large volume of the solar cavity in their travel from its boundary to the Earth.

Yet one can tentatively try to derive important parameters of the interplanetary medium by means of the observations of the source itself, the Sun.

Solar output during the 11yr activity cycle has many different aspects such as the sunspot area and number, the development of polar coronal holes, the solar flares and the solar wind.

Furthermore among the cyclic variations of the various kinds of solar activity one has to distinguish the ones having same period but differing in phase, amplitude and pattern.

It is common practice to use the sunspot number variation as the standard of the solar cycle and to compare to it all the other relevant parameters, even though this approach has not a good physical ground. The same is true for CR intensity since Forbush (1954) discovered an inverse correlation between this latter and the sunspot number. On the other hand the changes in the solar wind characteristics are related to the temperature variations of the corona, which in turn depend on different solar features such as sunspots, flares, polar coronal holes, plages etc. It is then extremely interesting to investigate the possible relationship between these phenomena and the CR intensity.

The spectral and cross-spectral power analysis is the tool that can be used to consider over a wide range of frequencies in a global way correlations on the same time scale between two time series.

We have already analyzed CR variation of ergodic nature (Attolini et al., 1984) but we cannot exclude variations corresponding to spectral lines.

From the operational point of view the best way to study line spectrum is to obtain estimates of the power trough the periodograms and average

them on a band as narrow as possible.

This has been done by averaging each periodogram to its consecutive and then repeating this operation six time. in that way we obtain a binomial smoothing which preserve the frequency information over 7 periodograms corresponding to the average of 4.43 independent data equivalent. Since before performing the FFT operation the number of data has been increased to 1024 via zero padding, each coherency value corresponds to 2.13 independent data equivalent. The coherency figure (Y12) is the one defined by Jenkins and Watts (1968). The 95% significance level has been found using simulations on random data series with the same number of data.

In our analysis we have used the monthly data series of the following relevant parameters: *sunspot number* (Rz) from 1944 to 1984 (Solar Geophys. Data); *CR intensity* (RC) from 1944 to 1984 (Huancayo-Climax pressure crrected counting rates); *aa indexes* (aa) from 1944 to 1984 (Mayaud,1973,1975); *major flares* from 1955 to 1979 (Dodson et al.,report UAG N.14,19,52,80).

2. Computations and Results.

a) RC vs Rz

The first thing to note in the comparison of the coherency spectra in Figure 1a-c computed for three different time intervals, is that we can identify two regions,the first one with frequencies higher than 1c/yr, the other one with frequencies lower than 1c/yr. The first one contains few peaks that exceed the 95% confidence level, which do not shift in frequency when increasing the length of the series and whose amplitudes remain the or at least increase with the increase of the number of data. In the other range the peaks slightly wander in frequency and in amplitude; the long wave of 22yr appears only in the longer data set and with low significant level. All the peaks in this region correspond to nearly all possible harmonics up to 10th order of the 11yr cycle in all the series as it can be better seen in the computation with zero padding of the data up to 2048. The other significant peaks of the second region are at periodicities 10.4m, 156.5d, 70.9d.
The correlation is negative (Θ) in the first two and positive (⊕) in the last case. The 156.5 days may be related to the flare occurrence.

b) RC vs aa

Since solar wind plasma drives geomagnetic activity the aa index has been used to investigate CR intensity variations caused by solar wind changes. Following the study by Feynman(1982) we have considered the aa and the aa_I (i.e. aa corrected for Rz) monthly indexes. The results are shown in Figure 2. One can see that the coherencies between CR and either aa or aa_I do not differ very much. The only difference between the two is the 11yr cycle periodicity. The significant peaks are, however, different from the RC vs Rz and the correlation is always negative. More meaningful is to compare the CR intensity deduced after the subtraction of the sunspot correlation computed according to Nagashima and Morishita (1980). In that case the coherency (Figure 3) is significant in a greater number of frequencies. These periodicities are linked to the polarity of the IMF and possibly some of them represent the aliased peaks of more fundamental periodicities such as 28.2,27.15 and 26.85 days typical either of sector structure as described by Svalgaard and Wilcox (1975) or of the recurrent decreases in CR intensity in correspondence to aa_I increases. This last fact can be consistent with the description of high speed stream effects on CR (Iucci et al.,1979). In fact the analysis by Feynman (1982) has put in evidence that the property

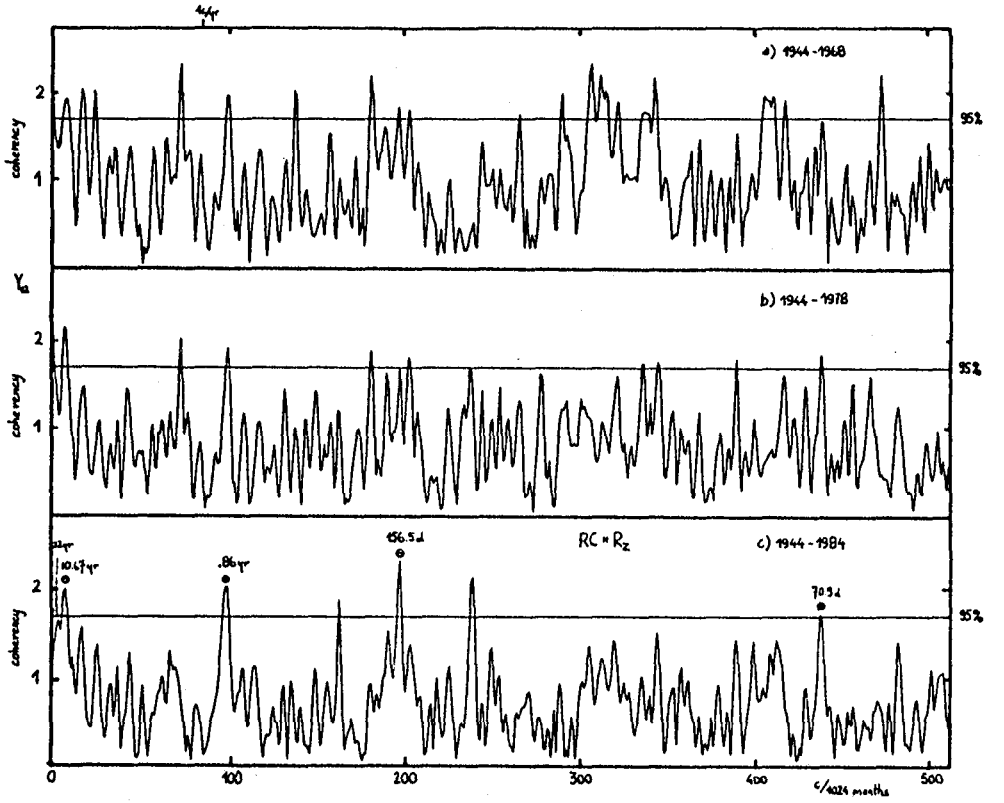

Fig.1

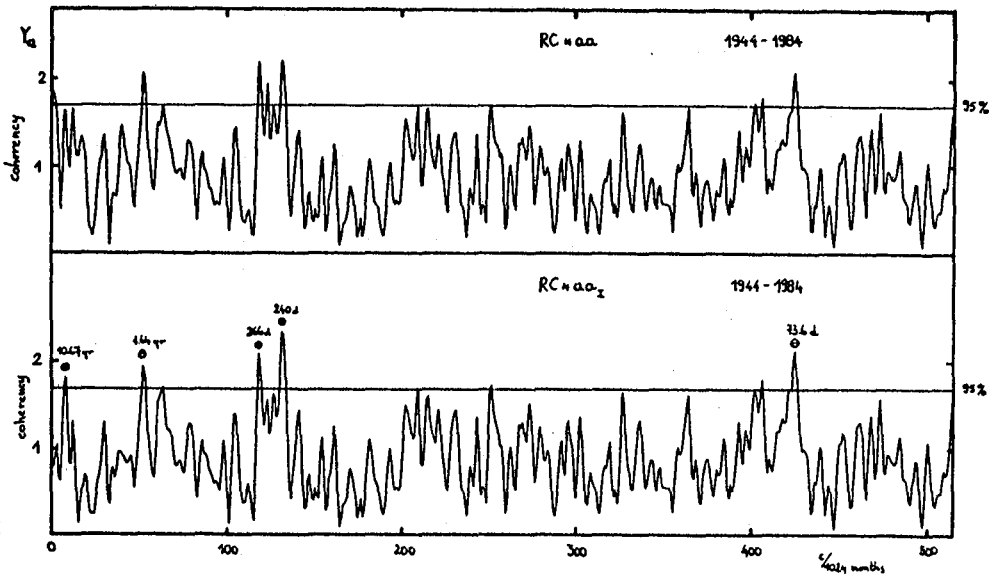

Fig.2

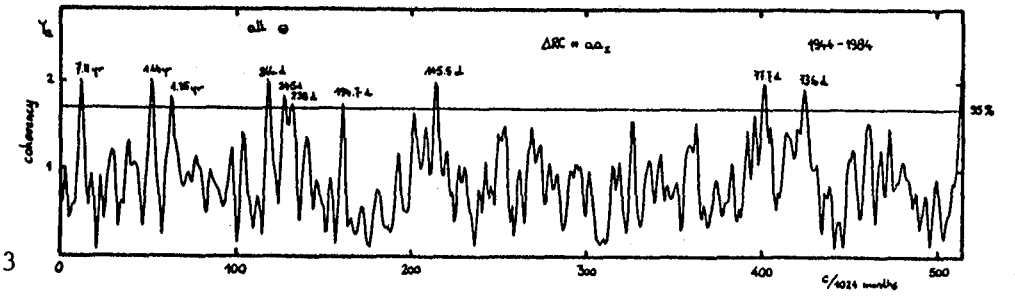

Fig.3

of the aa_I is the high recurrence probability.

It should be remarked that a plasma stream that do not engulf the Earth can nevertheless affect CR that reach us by inducing changes in the 3-dimensional IMF configuration.

c) RC vs Flares

Here the most outstanding periodicity is the one at 66.2 d and the most interesting is the one at 153.4d which is similar to the one found in hard solar flares (Rieger at al.,1984) and near to the 156.4d of RC vs Rz (Figure 4). However the Rz vs Flare coherency does not show such a correlation.

3. Conclusion. We want to stress that our work is aimed to find the correlation of two data series in narrow frequency bands. The fact that does not exist a correlation on a 2 periodogram band does not imply that a very high correlation does not exist on a much wider frequency band (e.g. CR vs Flares,Rz,aa as a whole). The existence of a narrow band correlation, on the other hand, means only that a particular type of variation in a series corresponds, with a very high probability, to a variations on the same time scale in the other series.

Among the results here reported we have found the 154d periodicity in the RC vs Flares, and some other peaks of coherency in the RC vs aa_I that when interpreted as aliased values might correspond to recurring IMF structures and solar wind streams. We cannot exclude however that some of the correspondence with aa are of terrestrial origin.

This study cannot be considered exhaustive due to the fact that other solar variables, such as polar hole size, are possibly correlated to CR intensities,however the number of observations is small so that the interpretation of the results is very difficult.

4. References. Attolini,M.R.,et al.,Nuovo Cim.,7C,413,1984// Dodson,H.W. et al.,Report UAG Nos.14,19,52,80// Feynman,J.,J.Geophys.Res.,87,6153,1982// Forbush,S.E.,J.Geophys.Res.,59,525,1954// Iucci,N. et al.,Nuovo Cim.,26,421, 1979// Jenkins,G.M. and Watts,D.G.,Spectral Analysis and Its Applications, Holden-Day,1968// Mayaud,P.N., IAGA Bulletin Nos.33,39// Nagashima,K.,and Morishita,L.,Planet.Space Sci.,28,177,1980//Rieger,E.,et al.,Nature,312, 623,1984.

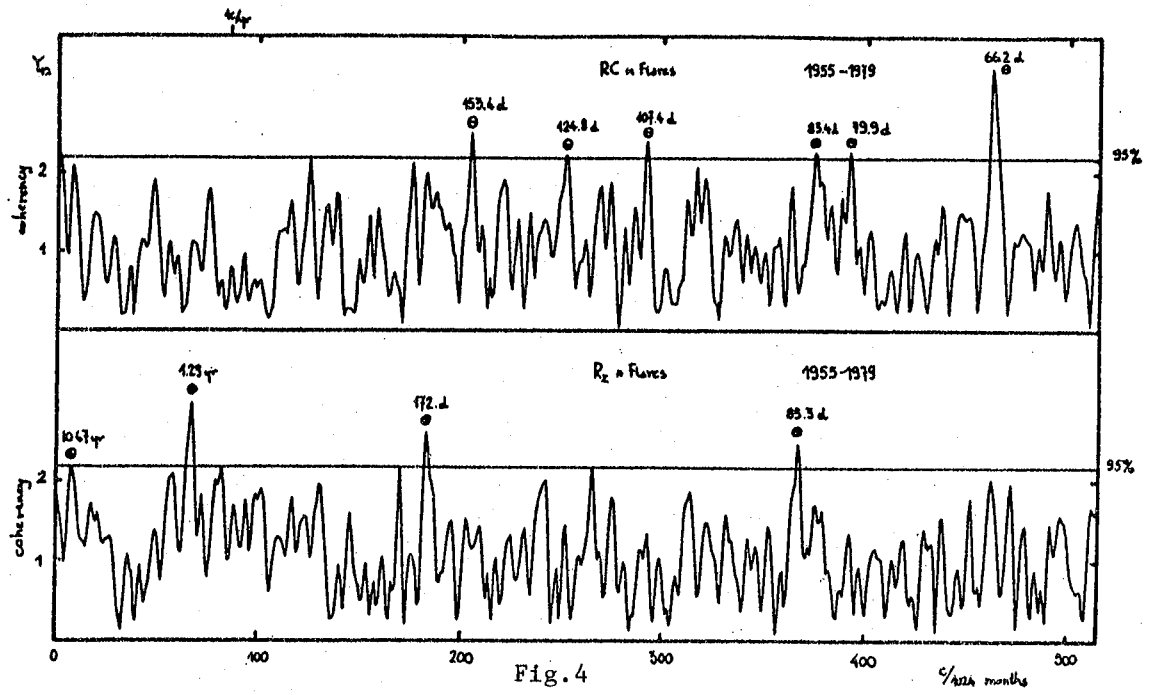

Fig.4

COSMIC RAY BIANNUAL VARIATION

Attolini, M.R., Cecchini, S.
Istituto TE.S.R.E.- C.N.R.,Bologna, Italy

Cini Castagnoli, G.
Istituto di Cosmogeofisica - C.N.R.,Torino, Italy
Istituto di Fisica Generale dell'Università,Torino, Italy

Galli, M.
Dipartimento di Fisica dell'Università, Bologna, Italy

ABSTRACT

The study of the CR power spectrum (Attolini et al., 18th ICRC, Conf.Papers, 10,174,Bangalore 1983) has revealed a significant variation with a period around 2 yr that cannot be explained as a high order harmonic of the 11 yr solar cycle. Comparative study of the correlation on different time scales between CR intensity and Rz, aa, high speed streams and polar hole size (SH 4.4-14, this conference) has put in evidence that a high degree of coherency exists between each couple of variables at 1.58-1.64 yr, except between CR and Rz. On the other hand cyclic variation on a short time scale, around 26 months, has been claimed (Sakurai, 18th ICRC,Conf. Papers, 4,210,Bangalore 1983) to be present in the neutrino flux (Davis et al.,AIP Conf. Proceedings,No.96, 1983). Critical tests of this hypothesis are considered and a preliminary result seems to indicate that the hypothesis of the existence of a 1.6 yr periodicity in the neutrino data during the measurement time interval, has a significance $\geq$ 99.9 %.

The posssible origin of this variation as due to a contribution either of CR interactions in the upper atmosphere or to the solar dynamics,will be discussed.

COSMIC RAY POWER SPECTRAL VARIATIONS: 3. SOLAR ROTATION PERIODICITIES

S. P. Agrawal
Department of Physics (Vikram Space Physics Centre)
A.P.S. University, Rewa (M.P.) 486003, India

ABSTRACT

Earlier studies of the periodic changes in cosmic ray intensity by power spectral analysis provided some understanding of the daily variation in terms of ambient power. The solar rotation periodicities are investigated here using daily means of Calgary neutron monitor data during 1965-76. Significant peaks with periods of 27 and 13.5 days with varying magnitudes are observed.

1. Introduction. It is generally accepted that the galactic cosmic radiation is modulated by the continuously varying solar plasma and fields of the modulating region within the heliosphere. Most cosmic ray variational studies (1-1000 Gev), have used 4 decades of ground-based measurements. These include ~ eleven-year solar cycle variation, Forbush decreases, 27-day variation and the various harmonics of the daily variation.

The 27-day variation has direct bearing on the solar features, on or above the solar surface and remain stable for more than one solar rotation of average period 27 days. The solar modulation is a continuous process and any variations in solar output will affect the interplanetary plasma and field, and in turn upon the flow of cosmic rays. Thus a study of the 27-day recurrence in cosmic ray intensity can provide us with information on solar output and its propagation in the interplanetary medium. Here we derive the 27-day rotation periodicities by power spectral analysis during the interval 1965-76, using the procedure adopted by Lanzerotti et al., (1981).

2. Spectral analysis of cosmic ray data. Daily mean values of Calgary neutron monitor data have been used over the interval 1965-76, for power spectral analysis, to investigate the 27-day periodicies and its harmonics. The Galgary neutron monitor is an 18-NM-64 type detector with statistical fluctuations of 0.02% in daily means. Initially the computations were carried out using one year's data at a time; however the peaks under investigation, were not very clear. Hence we combined 2 3 years of data for deriving the power spectra. The choice of 2 years of data at a time was found optimum to look for individual peaks and to compare their variations during the solar cycle.

3. Results and Discussion. The results of the power spectral analysis are shown in Figure 1. Over a sunspot cycle, the cosmic ray intensity changes (at median energies ~ 10-15 Gev) by about 15-20%, and any two successive years combined here generally correspond to similar solar conditions, with very small changes in cosmic ray intensity. However, large changes in cosmic ray intensity, which occur over periods of days (Forbush type decreases), do affect to some extent the overall spectral

shape, but are not effective in modulating the peaks observed. The vertical dashed lines indicate frequencies corresponding to peaks at 27 and 13.5 days. Note that the main peaks occur for the 27-days period and is quite significant for all the years, except for 1973-74. However, the 13-14 day peak is not very significant for a number of years, such as 1965-66, 1967-68 and 1975-76. These results were essentially confirmed by Sulphur Mountain Cosmic ray data. The power associated with the 27-day peak in 1973-74 is quite low and indicates the possibility that even the stable periodic features of the solar surface were not effective in producing any significant changes in the cosmic ray intensity. Solar coronal holes are quite abundant during 1973-74 and also in 1975-76, and thus an absence of any solar rotation periodicity in 1973-74 perhaps indicated that some other solar feature may be responsible. Venkatesan et al., (1982) have shown that only small changes occur in cosmic rays due to coronal holes. The Chree type of analysis involving some specific solar features, in future, may provide the answer for the observations reported here. It is likely that the solar flares/solar active centres could be the source for the solar rotation periodicity observed. The reason for this is not obvious at present.

4. Acknowledgement. The assistance of Messrs. Arun Tiwari and Vishwarnath Khare in data reduction, etc. is acknowledged. I also wish to acknowledge the Calgary data kindly provided by D. Venkatesan and T. Mathews.

5. References.

Lanzerotti, L. J., Maclennan, C. J., Agrawal, S. P. and Venkatesan, D., (1981), J. Geophys. Res., 86, 6951.

Venkatesan, D., Shukla, A. K., and Agrawal, S. P., (1982), Solar Physics, 81, 375.

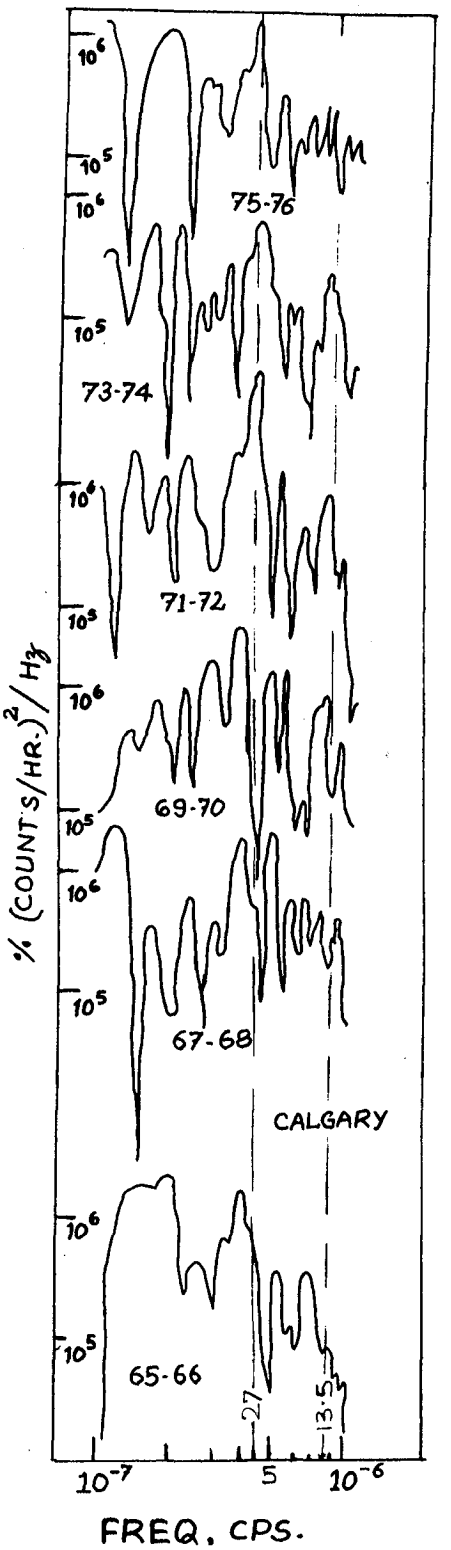

Figure 1. Power spectra for the Calgary neutron monitor for the interval 1965-76. Vertical dashed lines indicate the 27 and 13.5 day period.

SH 4.4-17

VARIATIONS OF THE COSMIC RAY GENERAL COMPONENT IN ANTARCTICA

T.N. Charakhchyan, A.F. Krasotkin, A.I. Kurguzova
Institute of Nuclear Physics, Moscow State University, Moscow 119899, USSR

N.S. Svirzhevsky
P.N.Lebedev Physical Institute of the Academy of Sciences of the USSR, Moscow, USSR

ABSTRACT

The report treats the cosmic ray variations connected with the changes of atmospheric temperature and solar activity level and the variations which are probably due to zonal cosmic ray modulation.

A new type of cosmic ray variations, so called zonal cosmic ray modulation, was found in the lower atmosphere from the sonde measurement results /1/. The new variations give rise to anomalies in the latitude distributions of the cosmic ray charged component and the anomalous north-south asymmetry. To find the nature of the variations, we began measuring the cosmic ray general component with the same detectors as in the sonde measurements (the STS-6) gas-discharge counters and the counter telescopes with 7-mm Al filters detecting the electrons of energy above 200 keV and 5 MeV).

In this report the measurement data obtained in Antarctica (Mirny) in the years 1978-1983 are presented and discussed.

Measurement results. Two B-1 instruments described in /2/ are in operation at Mirny. The measurements are taken daily for two hours (0800-1000 UT). The data on the time dependence of the cosmic ray global component are obtained using six independent units (the unit consists of ten STS-6 counters with a 16 cm^2 geometric factor each). The monthly means of charged-particle number per minute corrected for barometric effect (-0.16%/mb) are shown in Fig. 1 (curve C). The data on time dependence of the cosmic ray vertical component are obtained using three independent units. These data corrected for barometric effect (-0.24%/mb) are shown in Fig. 1 (curve T).

Considering that radioactive background is in practice absent at Mirny /3/(the charged particle flux is

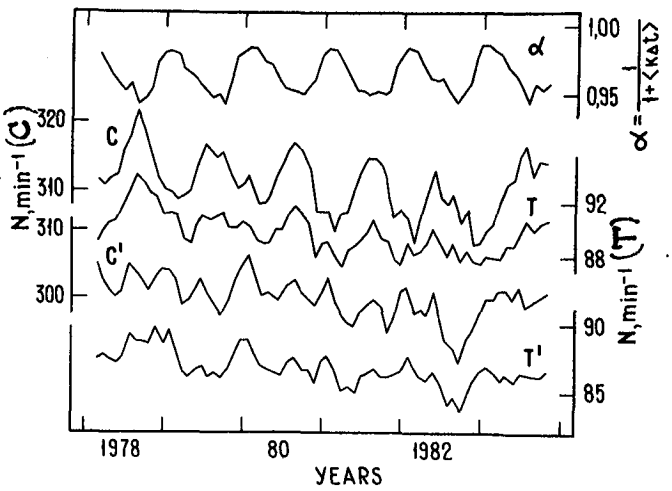

Fig.1. Time dependences at Mirny (x=1030 g/cm^2). C and T- cosmic ray global and vertical components correlated for barometric effect; α -correction coefficient for temperature; C' and T'-cosmic ray global and vertical components corrected for barometric and temperature effects.

about 300 m^{-2}s^{-1}), the observed variations are mainly due to cosmic ray variations.

Seasonal cosmic ray variations. As it should be expected, the main variations of the measured particle number on the Earth's surface in Antarctica are due to the seasonal temperature variations. The seasonal variation amplitude (3-4%) is in a good agreement with the calculated values because of the muon component intensity variations /4/. Curve α in Fig. 1 presents the values of the correction factors calculated allowing for the atmospheric temperature distribution inferred from meteorological sounding data and of the partial temperature coefficients for the cosmic ray general component at sea level. The correction factor $\alpha = 1/(1+K\Delta t)$, where K is a partial temperature coefficient, Δt is the difference between the temperature measured at a given isobaric level and the temperature of the standard atmosphere at the same level; $\langle K\Delta t\rangle$ is the mean of the 10 isobaric levels in the 10-1000 g/cm^2 interval. Curves C' and T' in Fig. 1 show the data corrected for the temperature effect. It is seen that, apart from the temperature-induced variations, the general component suffers other types of variations.

The variations due to changes of solar activity level. From 1978 to 1982, the mean level of the charged-particle number at Mirny has changed by $\sim$3%. The same change of the particle number was inferred from the data of the vertical telescope with the 7-mm Al filter at Murmansk. The changes are in a good agreement with the nucleon component variations inferred from the data of high-latitude neutron monitors (see Fig. 2).

During the above mentioned period the sunspot number increased markedly, so the observed cosmic ray intensity decrease was mainly due to the rise of solar activity level. From Fig. 2 it may be seen that the amplitude of these variations in the nucleon component (NM) is 4 times greater than the amplitude in the general component (T) of cosmic rays at sea

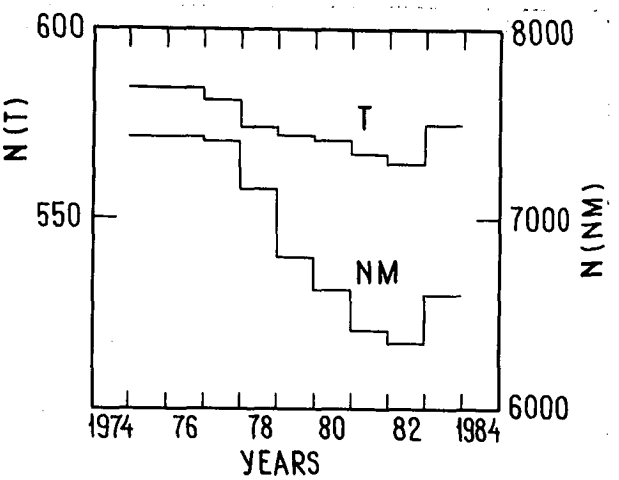

Fig. 2. The yearly means of the detected particle number at sea level. T-charged component (7-mm Al filter); NM-nucleon component (the data of the Apatity neutron monitor).

level. Once the continuous series of the nucleon component data from Apatity are available, the cosmic ray variations due to solar activity changes may be excluded from the data shown in Fig. 1 C' and T'. The time dependences of cosmic rays at Mirny after excluding the temperature variations and the variations due to solar activity are shown in Fig. 3 (Curves C'' and T''). The residual variations may be thought to be due mainly to the measurement errors and to the errors in introducing the corrections for the barometric and temperature effects. It should be noted, however, that the found variations resemble the variations in the lower atmosphere inferred from the sonde measurements of cosmic rays.

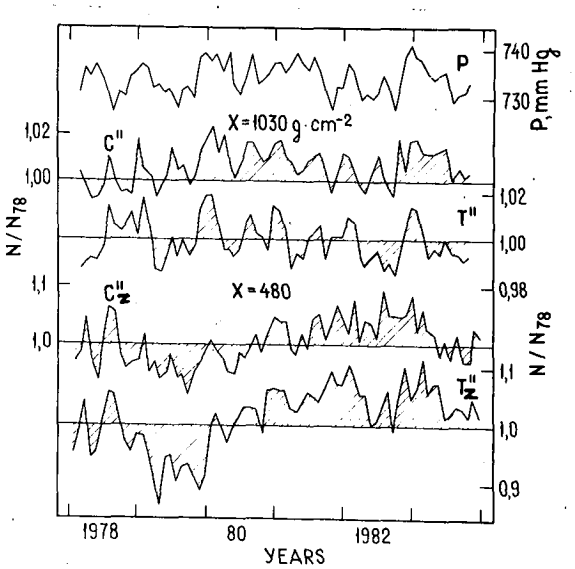

Fig. 3. The corrected time dependences of the cosmic ray charged component at Mirny. C'' and T'' - at sea level; C''_z and T''_z - at the level x=480 g/cm^2; P - atmospheric pressure at Mirny.

The variations due to the zonal cosmic ray modulation. During the studied period, the zonal cosmic ray modulation was clearly expressed in the lower atmosphere over Mirny, which can be seen in Fig. 3 where curves C''_z and T''_z show the time dependence of the cosmic ray charged component inferred from the gas-discharge counter and telescope measurements at the level x=480 g/cm^2 over Mirny after excluding the variations due to solar activity changes. Here the cosmic ray intensity variations are significant. The particle number changes by up to 10%. The changes at sea level are 1-2%, i.e. 5 times as small as the changes at 500 g/cm^2 level. In both cases, however, we can clearly see the variations of some half-year period with 1-1.5% amplitude at sea level and 2-5% amplitude at 480 g/cm^2 level. At the same time, the variations with characteristic times of 2-3 years can be seen. The found variations can hardly be accounted for by incorrect inclusion of the barometric and temperature effects because such variations are absent both in pressure (curve P in Fig. 3) and temperature (curve α in Fig. 1). In this case the annual variations would have been most probably found because they show the largest amplitudes in both pressure and temperature.

Thus, the measurements of the cosmic ray charged component at Mirny have shown that the zonal cosmic ray modulation seems to exist also at sea level, but its amplitude is about an order as low as at $\sim$ 500 g/cm^2 level. The same conclusion can essentially be drawn from the analysis of the neutron monitor data made in /5/ for the solar minimum of 1964-1965.

References

1. Charakhchyan A.N., et al.(1979), Proc. 16th ICRC, Kyoto, v. 3, p. 277.
2. Altukhov A.M. et al. (1984), Geomagn. i Aeron., 24, 386.
3. Charakhchyan A.N. et al. (1979), Proc. 16th ICRC, Kyoto, v. 4, p. 253.
4. Kurguzova A.I., Charakhchyan T.N. (1983), Geomagn. i Aeron., 23, 715.
5. Charakhchyan A.N. et al. (1979), Proc. 16th ICRC, Kyoto, v. 3, p. 271.

THE DIFFERENCE IN THE ENERGY SPECTRA OF GALACTIC COSMIC RAYS AT THE MINIMA OF THE 19TH AND 20TH SOLAR ACTIVITY CYCLES

A.K. SVIRZHEVSKAYA, N.S. SVIRZHEVSKY, YU.I. STOZHKOV,

P.N.LEBEDEV Physical Institute of the Academy of Sciences of the USSR, Leninsky Prospect, 53, 117924, Moscow, USSR

T.N. CHARAKHCHYAN

Institute of Nuclear Physics, Moscow State University, 119899, Moscow, USSR

ABSTRACT

The absorption curves of the cosmic ray charged component for solar minima in 1965 and 1975-1977 are analysed on the basis of daily stratospheric measurements in Murmansk, Moscow, Alma-Ata and Mirny (Antarctic).

Two distinct features in the energy spectra of galactic cosmic rays are revealed during these periods.

1. At the 20th solar activity minimum there was the additional short range component of cosmic rays. Additional fluxes in the stratosphere at high latitudes (Murmansk, Mirny) caused by this component are probably protons and He nuclei with the energy 100-500 MeV/n. The fluxes are estimated as $\sim 300\ m^{-2}s^{-1}sr^{-1}$.

2. At the minimum in 1975-1977 the proton intensity in the energy range 1-15 GeV is 10-15% lower than that in the 1965 solar activity minimum.

Numerous experimental evidences are indicative of a significant role of the solar general magnetic field in the cosmic ray modulation effects /1,2/. The magnetic field direction in the polar regions of the Sun proves to be of importance for the formation of the energy spectra of galactic cosmic rays in the Earth's vicinity.

The differences in the primary cosmic ray energy spectra in the consecutive solar minima are pointed out in particular by the short range component detected in the stratosphere /3,4/. Although the nature of the particles of this component is not clear yet at middle latitudes (Moscow, Alma-Ata), at the same time the data obtained in /5/ suggest that the short range component at high latitudes (Murmansk, Mirny) should be associated probably with the protons and helium nuclei of energies below 500 MeV/n.

Information on the variations of the primary cosmic ray energy spectrum may be derived from the altitude dependence of the relative variations of the cosmic ray intensity $\Delta N/N$ in the stratosphere. In the case of the 11-year cosmic ray modulation the variation amplitude decreases with increasing the primary particle energy, and then the value of $\Delta N/N$ decreases with rising the atmospheric pressure X. Over Murmansk, for example, $\Delta N/N$ at X=10 g/cm^2 is two times as high as that at X=150 g/cm^2. However the shape of the dependence $\Delta N/N(X)$ in the years near the 20 solar activity minimum proved to be quite different.

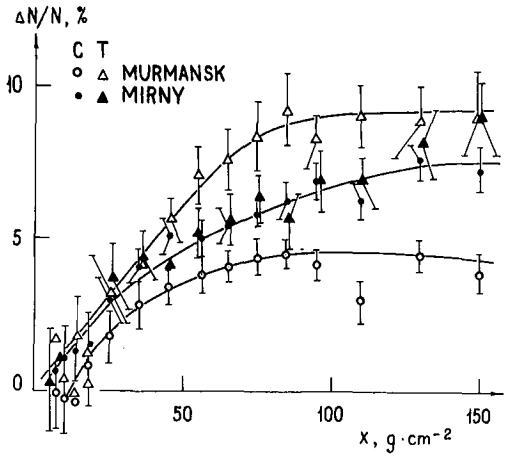

Fig.1. $\Delta N/N$ versus the atmospheric pressure in 1976 for a Geiger counter (C) and counter telescope (T) at Murmansk and Mirny.

Fig.1 shows the variations of the cosmic ray intensity $N_{76}(X)$ in 1976 relative to the intensity in 1965, $\Delta N/N=(N_{65}-N_{76})/N_{65}$, over Murmansk and Mirny. In a broad interval of pressures the cosmic ray intensity in the stratosphere and hence the primary particle intensity in 1976 was lower than that in 1965. The character of the dependence $\Delta N/N$ at $X > 70$ g/cm^2 indicates that the primary spectrum variation in a certain energy range is independent of the particle energy. The decrease of $\Delta N/N$ at $X < 70$ g/cm^2 may be explained by the existence of the cosmic ray short range component in 1976. The same situation took place also in 1975 and 1977.

The data presented in Fig.1 were used to obtain the absorption curves for the additional short range component of cosmic rays (see Fig.2). The absorption curves are actually identical at high latitudes in the nothern and southern hemispheres. The energy spectrum of the additional proton flux, which is also shown in Fig.2, was determined assuming that the additional component consists of protons. The value of the additional 100-400 MeV proton flux is ~ 300 m^{-2}s^{-1}sr^{-1}. Taking into account the fact that He nuc-

lei make a definite contribution to the particles detected in the stratosphere, the flux obtained proves to be in a good agreement with the additional flux of protons and He nuclei in 1977 (compared with 1965) according to /5/. The short range particles at high latitudes in the stratosphere appeared in 1972 and disappeared practically after 1979 /4/, that is they existed during about the same period as the anomalous He component of cosmic rays detected by space probes /6/.

Another important conclusion can be drawn from the data presented in Fig.1, namely, the 1-12 GV rigidity cosmic ray fluxes were much lower in 1976 than in 1965. The same conclusion may be drawn from the analysis of the data of latitude stratospheric measurements in the years 1965, 1969 and 1975 /7/. Fig.3 shows the energy spectra of the variations of primary cosmic rays in 1969 and 1976 relative to 1965 inferred from the latitude measurements. From Fig.3 it seen that the primary cosmic ray intensity in the 4-12 GV was 10-15% lower in 1976 than that in 1965. In the examined energy range the cosmic ray intensity in 1976 was essentially the same as during the solar activity maximum of 1969. The dashed line in Fig.3 presents the spectrum of the variations $\Delta I/I(R)$

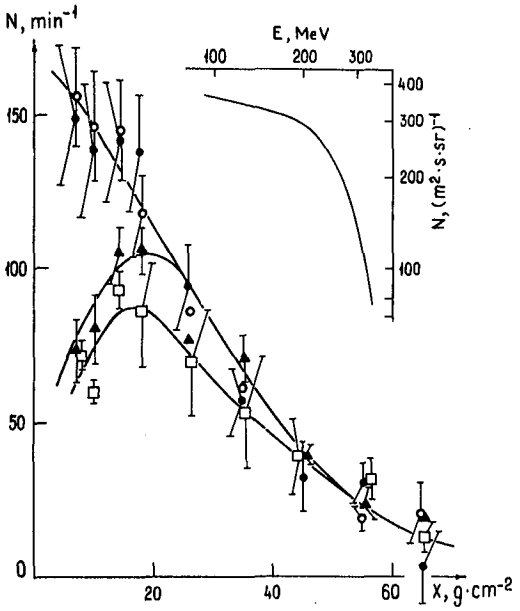

Fig.2. Additional fluxes of the cosmic ray short range component in the stratosphere over Murmansk (○), Mirny (●), Moscow (▲) and Alma-Ata (□). At the top right-hand corner the energy spectrum of the additional proton flux is shown.

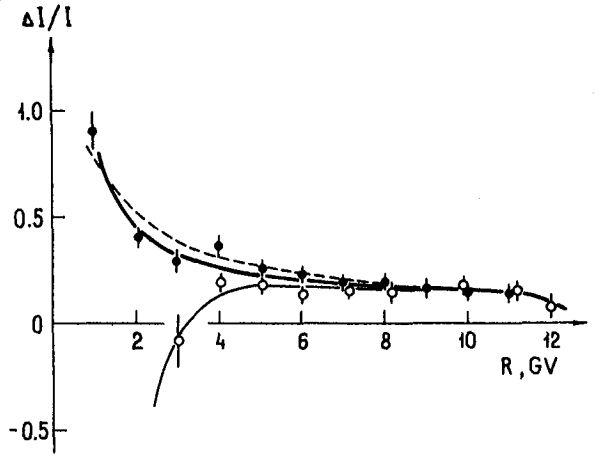

Fig.3. The spectra of the primary cosmic ray variations $\Delta I/I=(I_{65}-I_i)/I_{65}$ in 1969 and 1976 (the dark and light dots respectively). The dashed line shows the variation spectrum in 1969 calculated using the values of $\Delta N/N$ at high latitudes.

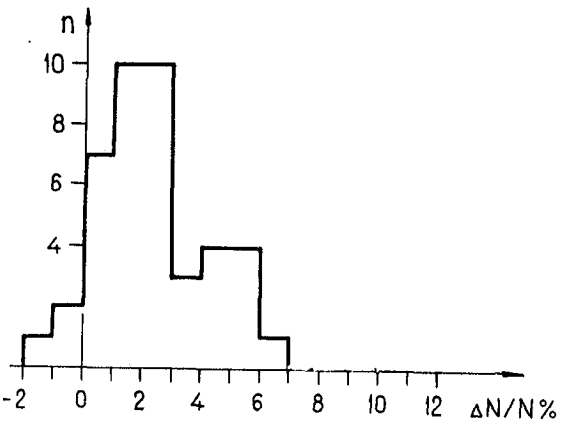

Fig.4. The distribution of Δ N/N for high latitude neutron monitors (R ≤ 2.3 GV) in 1975-1977.

calculated for 1969 using Δ N/N at Murmansk and Mirny. The spectrum presented is in a good agreement with the spectrum inferred from the latitude measurements.

Fig.4 shows the distribution of $\Delta N/N=(N_{65}-N_i)/N_{65}$ for several neutron monitors located at high latitudes (R ≤ 2.3 GV). The mean value of Δ N/N for neutron monitors is 2.3±0.3 per cent, but Δ N/N appears to be 5-7 % for some of them (for example, Mt. Washington, Durham). The conclusion that the cosmic ray intensity was lower in 1976 than in 1965 is generally confirmed by the neutron monitor data. The broad distribution of Δ N/N inferred from the neutron monitor data and the difference in Δ N/N over Murmansk and Mirny together with the difference in Δ N/N from the data of a Geiger counter and counter telescope (Fig.1) seems to indicate that the modulation mechanism in the solar activity minima is different from the mechanism of the 11-year cosmic ray modulation.

References

1. Charakhchyan A.N. et al., (1973), Izv. Akad. Nauk SSSR, ser.fiz., v. 37, p. 1258.
2. Nagashima K. et al., (1977), Proc. 15th ICRC, v. 10, p.380.
3. Svirzhevskaya A.K. et al., (1981), Proc. 17th ICRC, v. 3, p. 187.
4. Svirzhevskaya A.K. et al., (1983), Proc. 18th ICRC, v. 3, p. 43.
5. Webber W.R. et al., (1983), Proc. 18th ICRC, v. 3, p. 35.
6. Garcia-Munoz M. et al., (1981), Proc. 17th ICRC, v. 3, p. 270.
7. Svirzhevsky N.S., (1983), Thesis, FIAN, Moscow.

COSMIC RAY VARIATIONS WITH THE PERIOD CLOSE TO 27 DAYS AND THEIR CONNECTION WITH SOLAR ACTIVITY LONGITUDINAL DISTRIBUTION

G.A.Bazilevskaya

P.N.Lebedev Physical Institute of the Academy of Sciences of the USSR, Moscow, USSR

M.I.Tyasto, E.S.Vernova

Leningrad Branch of IZMIRAN, Leningrad, USSR

ABSTRACT

The amplitude and phase changes of the 27 day cosmic ray variation from 1958 to 1975 were studied. The comparison between cosmic ray intensity characteristics and longitudinal distribution of solar activity ones for different stages of the solar cycle were made.

1. Introduction

In some cases the longitudinal redistribution of the solar activity (SA) leads to the changes in 27 day cosmic ray (CR) variations connected with the solar rotation period / 1 /. The purpose of this paper is to analyse in detail the amplitude and the phase evolution of CR 27 day variations along with the longitudinal redistribution of SA. The neutron monitor data I of Thule and the sunspot group area Sp from 1958 to 1975 (except for 1964) were processed.

2. Method

As a result of the sunspot group area treatment for each solar rotation, the polar vector with the amplitude ρ_{SA} and the phase λ_{SA} was obtained, which characterized the non-uniformity of the sunspot longitudinal distribution / 2 /. Indeed, the existence of a longitudinal interval with increased activity means the increased value of ρ_{SA}, and the movement of this interval on the solar surface causes the changes of λ_{SA} from one rotation to another. The amplitude ρ_{CR} and the phase λ_{CR} of the first harmonic of the 27 day CR variation was used for comparison with ρ_{SA} and λ_{SA} of SA / 1 /. The 11-year CR variation, which plays a part of the trend for the present analysis was firstly withdrawn from the primary CR data.

3. Results

Fig. 1 shows the correlation coefficient values R (λ_{SA} , λ_{CR}) between time series of the phases of 27

day SA variations and CR ones with the zero shift between these two series. The horizontal bars correspond to the time intervals, for which these correlation coefficients were obtained. Fig. 1 shows $R(\lambda_{SA}, \lambda_{CR})$ keep the high values during the long time intervals; but for two time intervals from 1970 to 1973 correlation coefficient sharply fell. For these two time intervals (III 1970 - IX 1971, II 1972 - VIII 1973) $R(\lambda_{SA}, \lambda_{CR})$ were computed with the time shift between time series of the phases of 27 day SA variations and CR ones.

Fig. 2 shows the dependence of the $R(\lambda_{SA}, \lambda_{CR})$ on the time shift. It can be seen in Fig. 2 the $R(\lambda_{SA}, \lambda_{CR})$ reached the maximum value $R \approx 0.86$ for the time shift equal to about three months CR variations being prior to the SA ones. It should be noted that not far from 1970-1973 the polarity reversal of the Sun's general magnetic field took place / 3 /, thus we may expect the redistribution of solar magnetic fields among these the SA longitudinal redistribution. The corresponding changes of interplanetary magnetic fields and 27 day CR variations may be expected. To check this assumption we consider the 27 day variation cyclogram of sunspot group areas shown in Fig.3 / 4 /. As could be expected the SA amplitude of variations decreased and the phase became unstable (region A in the cyclogram). When SA is high the phase of variations is more stable, except for time intervals B and C which concerned with the polarity reversal of the Sun's general magnetic field. This result is confirmed by Table 1 where the parameter of the phase conservation is presented which is the relation $|\Sigma\vec{\rho}_i|/\Sigma|\vec{\rho}_i|$ in percent / 5 /. This parameter was more than 58% during the years of high SA except for XI 1959 - VIII 1960 and II 1970 - III 1972, when it fell abruptly.

Table 1

Year	$\lvert\Sigma\vec{\rho}_i\rvert/\Sigma\lvert\vec{\rho}_i\rvert$, %	Year	$\lvert\Sigma\vec{\rho}_i\rvert/\Sigma\lvert\vec{\rho}_i\rvert$, %
II-V 1958	85	VIII 1961 - IV 1962	89
VI-X 1958	95	VII 1966-V 1967	87
XI 1958-X 1959	65	VI 1967-II 1968	60
XI 1959-VIII 1960	58	III 1968-I 1970	58
IX 1960-VII 1961	76	II 1970-III 1972	5

4. Conclusion

The strong variability of the longitudinal distribution of SA took place near the polarity reversal of the Sun's general magnetic field. The disturbance of 27 day CR variations may be expected in turn.

Nevertheless from the point of view of current ideas about the solar modulation of CR intensities it is difficult to explain a high value of $R(\lambda_{SA}, \lambda_{CR})$ between the time series of the phases of 27 day SA variations and CR ones for 1970-1973 with CR variations being prior to the

Fig. 1. Correlation coefficients between the 27 day variation phases of CR intensity and sunspot area with zero shift between time series.

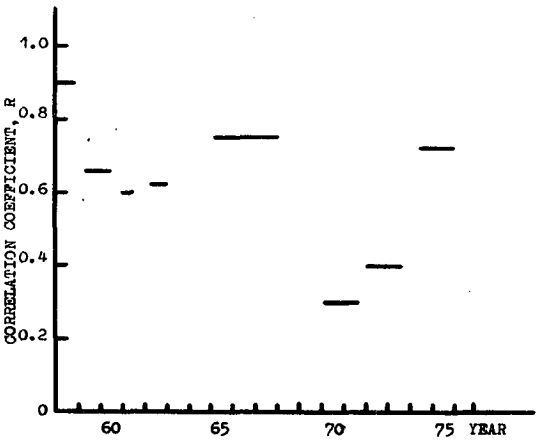

Fig. 2. Correlation coefficient R(λ_{SA} , λ_{CR}) versus the time shift between the series.

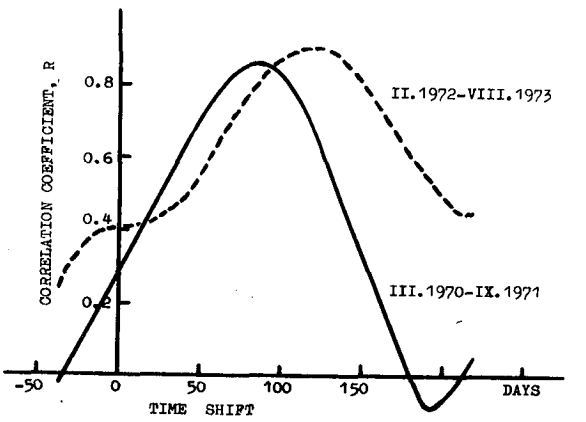

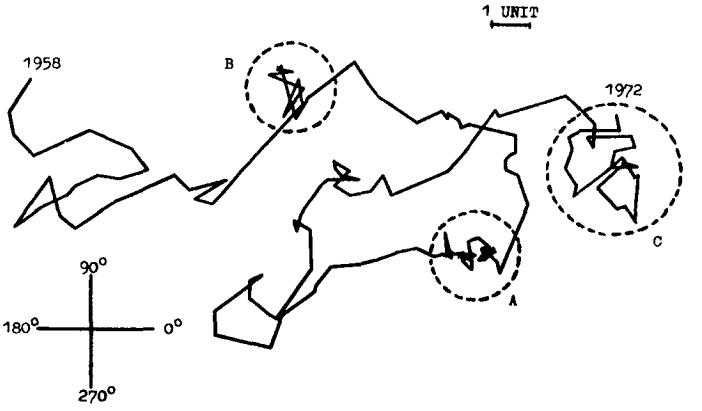

Fig. 3. The cyclogram of sunspot area for 1958-1972 (1 unit is equal to 20 000millionths of the solar hemisphere).

SA. At the same time it is unlikely to obtain such a high value of $R(\lambda_{SA}, \lambda_{CR})$ by chance because of rather long time intervals under consideration (each of them being of order 1.5 year).

5. References

1. Bazilevskaya, G.A. et al., (1984), Izv. Akad. Nauk, ser. fiz., v.49, p.2117.
2. Bazilevskaya, G.A. et al., (1979), 16th ICRC, v.3, p.385.
3. Howard, R. (1974), Solar Phys., v.38. p.283.
4. Chapman, S., Bartels, Y. (1951), Geomagnetism, Oxford University press, v.2, p.569.
5. Attolini, M.R., Cecchini, S., Galli, M., (1981), 17th ICRC, v.4, p.171.

AZIMUTHAL AND MERIDIONAL ASYMMETRIES OF THE SOLAR WIND AND QUASIPERIODIC VARIATIONS OF INTENSITY OF GALACTIC COSMIC RAYS (GCR)

L.Kh.Shatashvili, T.V.Djapiashvili, B.G.Kavlashvili, B.D.Naskidashvili, O.G.Rogava, G.V.Shafer

The Institute of Geophysics, Georgian Academy of Sciences, Z.Rukhadze str. I, 380093, Tbilisi, USSR

ABSTRACT

The results of analysis of 27-day, annual and quasi-two-year variation of GCR are presented. The dependence of the periods of 27-day GCR variation on the energy of ini - tial radiation is discovered, according to the data during I980 of the World network of station in sufficiently wide range of the observed threshold energy. The dependence of the annual variation of GCR is established, according to the data of the Huancayo station in conformity with the change of the polarity of the General Magnetic Field of the Sun (GMFS).

I. 27-day variation of GCR intensity

In paper /1/, the supposition, that the duration τ of 27-day oscillation of GCR ought not depend on the stage of development of the 11-year cycleness was expressed and in average τ =9÷I0 Sun's rotation time was addmited. However, observations on the wider intervals of time show that these confirmations are true not for all cycles of Solar activity, in particular, it appeared, that for the period of I962-I964 $\tau \approx 22$ Sun's rotation time. At present we have the data for 20-2I cycles of Solar activity, which show that τ is changing in a quite wide range of time.

We have made complex analysis of Solar activity data; geomagnetic activity(Solar Geophysical data) of neutron component of GCR Kiel(FRG), Tokyo(Japan), Sanae(antarctica) South Africa, the vertical direction of GCR rigid component of supertelescopes on ground station at Nagoya and the underground station at Sakashita (80 m.w.e. underground) Not so often we meet the case, when the duration of 27-day variations of GCR intensity is very long. Particular interest has been attached to the epoch I980 when τ was quite big and at the same time it was possible to correlate the GCR data with the change of Solar wind characteristics, made directly in cosmic space. The results of calculation by the method of superposition analysis for several stations of CR are presented in Fig.I. The stations are chosen so that the difference in the cut-off of initial radiation could be noticable. The attention must be paid to the extremly interesting observed phenomena- the dependence of the period of the reccurent change of GCR intensity on the cut-off energy. The period, determined in first rotations

of the Sun according to the data with less cutoff of CR is essentialy longer than according to the data with the big cutoff. It is difficult to ascribe the above mentioned dependence to the not considered temperature effects in the rigid component data at Nagoya and Sakashita stations, as the analogic phenomenon is observed in the neutron data at Tokyo station, where the temperature effect is obsviously small, at the cutoff energy is essentialy more than at Kiel station.

In a number of papers the change of periods of 27-day GCR variation was investigated. In paper /4/ it is established that the average period of 27-day GCR variation depends on the polarity of GMFS. In the present paper the dependence of period of 27-day GCR variation on the cycle phase of Solar activity (SA) is investigated. The investigation was made by the method of Fourier transform /5/ using the Han windows, on the basis of hour data of neutron monitor at Kiel station.

The period of 27-day variation- T_{27} of GCR intensity is defined by 2-year data with the subsequent drifts of number of datum for a year. The value of the period T_{27} was determined by Fourier spectrum function $F(T)$ so that T_{27} -corresponded to the maximum of function $F(T)$ in the interval of period $T = 25 \div 32$ days.

In Fig. 2 the change of the period T_{27} in time is presented. It is possible, to notice that the period T_{27} 27-day GCR variation in the maximum epoch of SA reaches the synodic period of the Sun's rotation, but in minimum of SA T_{27} is maximum.

2. Annual variation

In paper /6/ the annual variation of GCR intensity was investigated, according to the data of CR neutron component in connection with the polarity of GMFS. We've made the analogical analysis, using the data of ionic chamber (IC) at stations, Iakytsk and Huancayo for the other epochs. The averaging of vectors of the annual variation was made in conformity with the direction of GMFS (I946-I955 and I960-I968). The results of harmonic analysis of the average monthly data of these stations, show that the IC data at Iakytsk contains the influence of the seasonal temperature change. It is due to expect that so far as the Huancayo station is equatorial, the seasonal change is not essential. Indeed the results of harmonic analysis according to the data of Huancayo station, show that supposed in /6/ the effect observed in the neutron component of high latitudinal station, connected with the change of GMFS polarity is as well clearly expressed in the data of IC equatorial station at Huancayo /Fig.3/.

3. GCR quasi-two-year variations

In paper /7/ it was noticed, that the observed quasi-two-year variations of neutron and μ -meson components of CR are caused not only by the cycle changes of parameters of solar modulation of CR, but at the expense of two-year variations of meteorological parameters of the Earth atmosphere.

For the present moment we've widened our analysis. For the more assurance we used the Forbush data too /2/.

Then we obtained that the quasi-two-year variations of intensity of rigid μ -meson component of CR, corrected on the temperature and barometric effects of IC-I(Iakytsk) for the period 1954-1976 are synchronous with the quasi-two-year variations of SA. Quasi-two-year variations corrected on the meteorological effects, are apparently caused /7/ rather by the quasi-two-year variations of the meridional asymmetry of Solar wind velocity /8/.

REFERENCES

1. Dorman L.I., Shatashvili L.Ch., sb. "Cosmicheskie luchi" 1965, Izd-vo "Nauka", № 7, Str.161.
2. Forbush S.E., Cosmic Ray Results. vol.XX 1957.
3. Bazilevskaya G.A., Okhlopkov B.P., Charakchyan T.N. Tr. FIAN, 1976, 88, 94.
4. Bazilevskaya G.A., Vernova E.S., Grigoryan M.S., Sladkova A.I., Tiasto M.N., Charakchyan T.V., Geomagnetizm i aeronomia" № 4, 1984.
5. Bendat J., Pyrsol A., Primenenie correlatsionnogo i spectralnogo analyza. "Mir", 1983.
6. Krimsky G.F., Krivoshaphin P.A., Mamrukova V.P., Skripin G.V., Geomagnetizm i aeronomia, 21, 823, 1981.
7. Djapiashvili T.V., Rogava O.G., Shatashvili L.Kh., 18th ICRC, v. 10, p.235, 1983.
8. Djapiashvili T.V., Rogava O.G., Shatashvili L.Kh. Shafer G.V., Geomagnetizm i aeronomia, 24, c. 680.

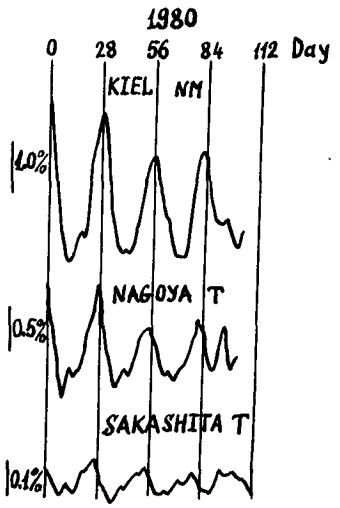

Fig. 1

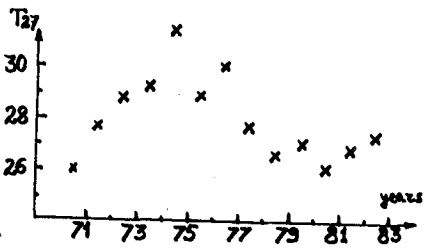

Fig. 2

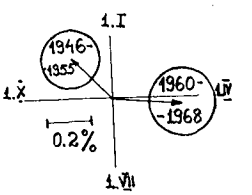

Fig.3

DYNAMICS OF TWO-YEAR COSMIC RAY VARIATIONS INFERRED FROM THE DATA OF SPACECRAFT AND STRATOSPHERIC MEASUREMENTS AND FROM THE NEUTRON MONITOR DATA IN 1959-1981

T.N. Charakhchyan, E.V. Gorchakov, V.P. Okhlopkov,
L.S. Okhlopkova, M.V. Ternovskaya
Institute of Nuclear Physics, Moscow State University,
Moscow 119899, U S S R

ABSTRACT

The two-year cosmic ray variations are studied using the spacecraft measurements of 1967-1976, the sonde measurements at high latitudes in the stratosphere (Murmansk, Mirny), and the neutron monitor data of 1959-1981. The two-year variations are most pronounced from 1967 to 1975. An anticorrelation is observed between the two-year variations in cosmic rays and in geomagnetic activity.

In work /1/ the two-year cosmic ray variations were singled out from the stratospheric sounding data and were shown to be of isotropic character. The variation amplitude and phase are the same in the southern and northern hemispheres, they are also the same for the global and vertical fluxes of cosmic rays. The nature of the two-year variations is still obscure. Although the energy spectrum of the variations is close to the energy spectrum of the 11-year variations, but their relevance to solar activity parameters is not so obvious as in case of the 11-year variations. The problem of the stability of the variation period and phase has not been resolved either. Therefore, the information derivable from the satellite measurements beyond the Earth's magnetosphere gets essential in understanding the nature of the variations.

In the present work, the two-year variation was sought in the low-energy cosmic ray intensity beyond the Earth's magnetosphere. We processed the $\geqslant$60 MeV proton detection data (the Explorer satellites data in May,1967- May 1973/2/ and, the Soviet space probes data in June 1973-March,1976/3/).

The method of mathematical selective filter used in/1,4/ can hardly be used to discriminate the two-year variations in such a comparatively small series of experimental data because the information for two years is lost at the ends of the series, so but a single period of the two-year variation may be singled out from the satellite data. Therefore, the peculiar method based on the difference in the approximation of the data by the Fourier series was developed /5/ for small data series. If the Fourier series with different numbers of harmonics are used, they will have different cut frequencies and the difference of transforms will discriminate a narrow frequency band. Such a transform is a selective filter. The method was used to process the spacecraft data. Fig. 1 shows the results of the processing.

Fig. 1 shows also the two-year cosmic ray variations inferred from the data of stratospheric sounding at a 20 g/ /cm^2 layer at Murmansk and Mirny (Antarctica) and the neutron component data at Deep River and Climax discriminated using the numerical selective filter /4/.

It is seen that the two-year cosmic ray intensity variation was in practice absent in 1959-1965 and was pronounced in 1966-1976 when its amplitude was 4-7% on spacecraft,2-4% in the stratosphere, and 1-1.4% in the neutron component. All the cosmic ray data show a good coincidence of the variation phases. The fact that the two-year variation appeared in the spacecraft data is worth noting because it demonstrates that the variation is actually due to the two-year variation of the interplanetary medium parameters rather than to some geophysical effect.

A change should be noted in the variation period which was 24-25 months in 1966-1972 and 19-20 months in

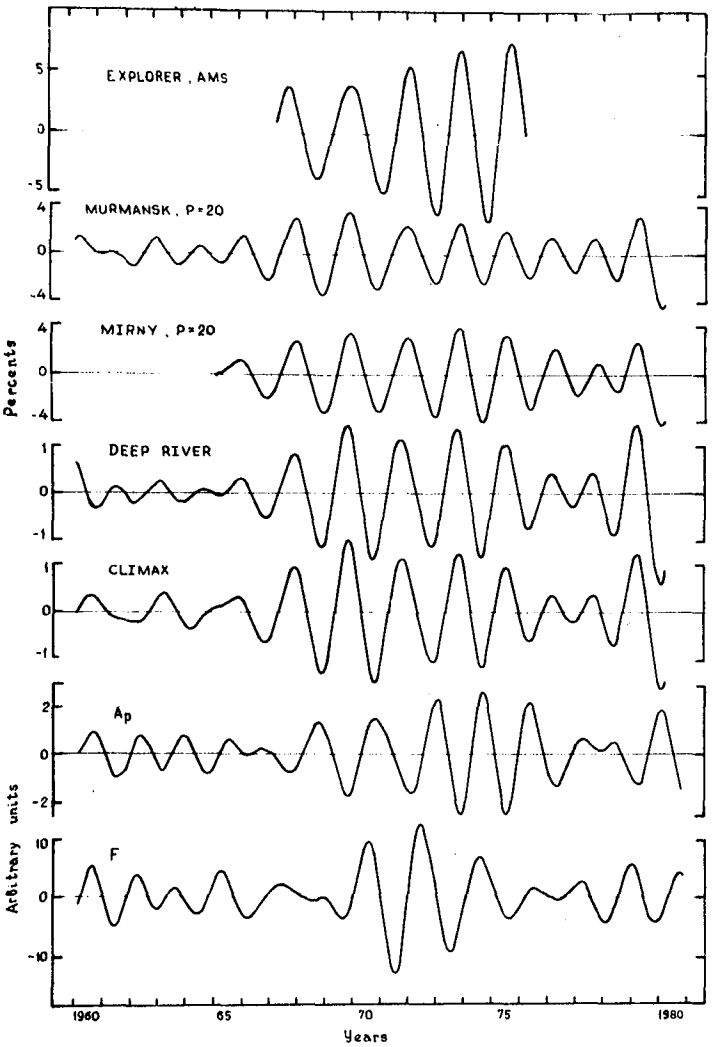

Fig. 1.

The twoyear variations obtained using the selective filter. The upper curve shows the data from the Explorer satellite and from the Soviet space probes. The stratospheric data at 20 g/cm^2 level over Murmansk and Mirny. The neutron component at Deep River and Climax. The Ap-index. F is the 10.7 cm radio emission from the Sun.

1973-1977. Since the change is seen in all the data, it is not accidental and reflects the real changes of the character of the variations in the interplanetary medium parameters. Fig. 1 also shows the two-year variations inferred from the solar 10.7 cm radio emission (F) and from the Ap-index. Although the two-year variation was felt in solar activity, its dynamics differs much from the two-year cosmic ray variation. The two-year wave in solar ativity was in practice absent in 1966-1969. Considering that the variations in solar activity and cosmic rays must be of opposite phase, the phase shift between solar activity and cosmic rays was about half-year in 1970-1975. This fact should have meant that a large modulation region is responsible for the cosmic ray variation, but such a conclusion is at variance with the data on the two-year geomagnetic activity variations.

From Fig. 1 it is seen that the pronounced two-year variation was observed simultaneously in the Ap-index and in cosmic rays. It is worth noting that the waves in the Ap-index and in cosmic rays are clearly of opposite phase. Both the Ap-index and cosmic rays exhibit the trend in the variation period to change from 24-25 months to 19-20 months. All the above means most probably that the two-year cosmic ray variation is due to the changes in the properties of the near region of interplanetary space and is contingent upon the variations of the same parameters which give rise to the geomagnetic activity variations (solar wind velocity and density, interplanetary magnetic field).

The preliminary processing of the data obtained before 1984 has shown that the amplitude of the two-year cosmic ray variation increased markedly after 1979, so in 1980-1983 it was closer to the variation amplitude in 1968-1974.

Thus, the two-year variation dynamics is characterized by significant changes in the amplitude, phase, and period of the variation. Since the significant decreases of the variation amplitude occur during the periods close to the solar minima (1964-1965, 1975-1977) and in the periods close to the solar maximum (1959-1982), the dynamics of the two-year variations does not seem to depend on the phase of the 11-year solar activity cycle, but is most probably determined by the state of the heliosphere, the approach adopted, for example, in /6/.

References

1. Charakhchyan T.N. et al. (1979), Proc. 16th ICRC, Kyoto, v.3, p.297.
2. Solar Geophysical Date, Boulder, USA, 1967-1973.
3. Ignatiev P.P., Shvidkovskaya T.E. (1980). In: Cosmic Rays, No. 27, p. 57.
4. Charakhchyan T.N. et al. (1979). Proc. 16th ICRC, Kyoto, v.3, p.308.
5. Okhlopkov V.P. VINITI AN USSR, No.7382-85 DEP.
6. Dorman L.I., Ptuskin V.S. (1981). Astrophys. and Space Sci. v. 179, p.397.

LONG-TERM MODULATION OF GALACTIC COSMIC RAYS IN HIGH-ENERGY REGION

P.A.Krivoshapkin, A.N.Prikhodko, G.V.Skripin, I.A.Transky, G.V.Shafer

Institute of Cosmophysical Research & Aeronomy
Lenin Ave., 31, 677891 Yakutsk, USSR

ABSTRACT

The results of continious registration of the cosmic ray muon intensity on the ground and underground at 7, 20 and 60 m w.e. depths in Yakutsk for 1957-1983 are presented. In years of the solar activity maximum in cosmic ray density were found two minima or two-stepped decrease. The second intensity minimum appears to be not the result of the inversion of the general magnetic field of the Sun but caused by the increase of the solar wind speed.

In [1] it was shown that the galactic cosmic ray intensity in even cycles of the solar activity is associated mainly with the number of sunspots and in odd ones - with the solar wind speed.

In [2] to describe the galactic cosmic ray density the index is suggested which is as a function of the number of sunspot groups and of their average heliolatitude. In [2] it was found as well that correlation of the galactic cosmic ray intensity with the above index is violated during the periods of the inversion of the general magnetic field of the Sun. The violation of the close correlation between the temporal behaviour of high- and low-energy galactic cosmic rays at this period has been explained by the decrease of the regular interplanetary magnetic field intensity.

In [3] it is obtained that on the 11-year galactic cosmic ray intensity variation the effect of interaction of the general magnetic field of the Sun and of the galactic magnetic field is superimposed. The dependence of the galactic cosmic ray intensity on the solar activity in even and odd

cycles forms a narrow and a wide loops of hysteresis, respectively.

The cosmic ray muon intensity by telescopes at 0, 7, 20 and 60 m w.e. depths in Yakutsk beginning from 1957 is continuously registered. The median values of energy for coupling coefficients at the above levels are 40, 78, 123 and 260 GeV, respectively. The average monthly statistical accuracy for vertical telescopes at these levels was 0.014, 0.017, 0.017 and 0.025%, respectively. In 1963-1964 the pit was reconstructed, i.e. the area at all the three underground levels was significantly enlarged. Because of this reason the telescopes at 7 and 20 m w.e. operated with breaks. Beginning from 1970 to 1982 at all the depths two and more telescopes were in operation. At present the statistical accuracy increased by ~ 2 times as compared with 1957. Beginning from June 1953 to present the ionization chamber of a large volume (the mean monthly statistical accuracy is 0.003%) is continiously operating [4] .

In the Figure the geomagnetic activity (A_p-index), sunspot numbers R_z, the galactic cosmic ray density smoothed in an annual interval on measurements by the muon vertical telescopes at 0, 7, 20, 60 m w.e. and by the ionization chamber in Yakutsk for the recent three solar cycles are presented.

During the 19-th solar activity cycle three peaks in geomagnetic activity were observed. The first increase of A_p was early in 1958 and it coincides with the maximum of R_z. The second peak is when the R_z started to decrease, the third one - near the minimum of the solar activity. The increases of A_p coincided with decreases of the galactic cosmic ray intensity at all the depths up to 60 m w.e. (in the Figure a scale for 60 m w.e. is twice larger in comparison with other levels).

In the 20-th cycle the two peaks in A_p were observed. The first peak coincides with the solar activity maximum, the second one was caused by the occurence of high-speed stationary solar wind streams with regular magnetic field in 1973-

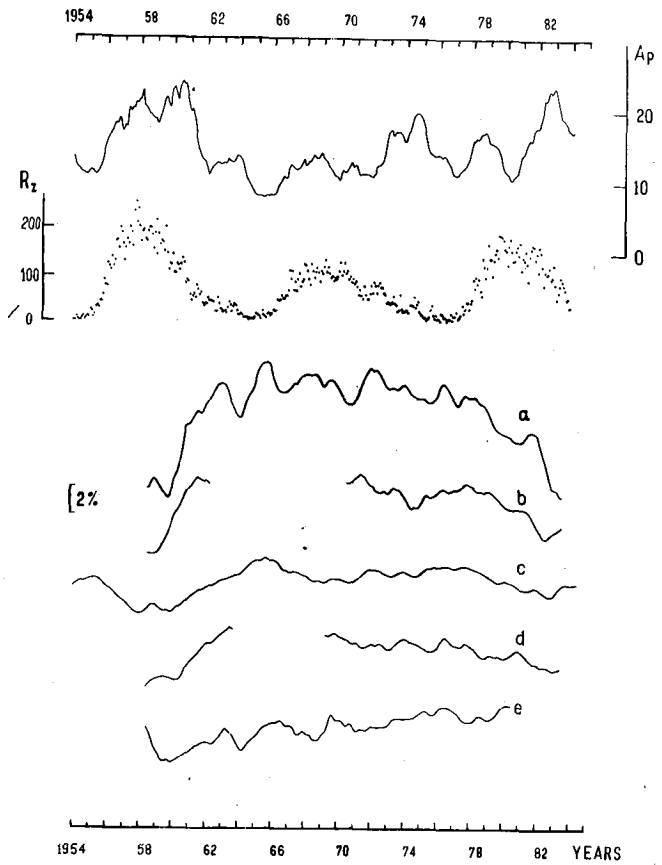

Geomagnetic activity (A_p-index), sunspot number R_z and the galactic cosmic ray intensity smoothed in annual interval on Yakutsk measurements by the muon telescopes (vertical) at 0, 7, 20 and 60 m w.e. depths (a,b,d,e, respectively) and by ionization chamber (c)

1974. In the galactic cosmic ray density the two minima are observed. The first (deep) minimum was in 1970, the second one (less deep) - was in 1974.

In the 21-st cycle also two peaks in A_p were observed. The first peak coincides with the phase of the solar activity increase, the second one was at the R_z decrease. A_p minimum coincided with the R_z maximum. In the galactic cosmic ray density the two-stepped decrease is revealed. The first decrease appears to be caused by the solar activity maximum, the second one - by the A_p increase in 1982.

The moments of the galactic cosmic ray density maxima delay by 9-12 months with respect to the solar activity minima. The geomagnetic activity minima in the 19-20-th cycles coincide with the galactic cosmic ray density maxima. In the years of the solar activity maxima in the high-energy

galactic cosmic ray density the two minima or two-stepped decrease were observed. The second minimum in the galactic cosmic ray intensity appear to be not the result of the inversion of the general magnetic field of the Sun. This fact confirms the results of [1] . The enrgy spectrum of 11-year variation in the galactic cosmic ray density obtained based on underground data is of the form $\sim E^{-1.0}$.

References

1. Chirkov, N.P. Solnechnyi veter i variatsii plotnosti kosmicheskikh luchei. - V kn.: Variatsii kosmicheskikh luchei i solnechnyi veter, (1980), Yakutsk, 25.

2. Krainev, M.V., Stozhkov, Yu.I., Charakhchyan, T.N., (1983), Proc. 18-th ICRC, Bangalore, 3, 23.

3. Nagashima, K. and Morishita, I. Twenty-Two Modulation of Cosmic Rays Associated with Polarity Reversal of Polar Magnetic Field of the Sun, (1979), Nagoya, Japan, 24.

4. Shafer, G.V., Shafer, Yu.G. Pretsizionnye nablyudeniya kosmicheskikh luchei v Yakutske, (1984), Novosibirsk, Nauka. 734 p.

THE FIRST THREE HARMONICS OF SOLAR DAILY VARIATION CAUSED BY THE DIFFUSIVE PROPAGATION OF GALACTIC COSMIC RAYS THROUGH THE HELIOSPHERE

K. Munakata and K. Nagashima*

Department of Physics, Faculty of Science,
Nagoya University, Nagoya 464, JAPAN

*Cosmic Ray Research Laboratory, Faculty of Science,
Nagoya University, Nagoya 464, JAPAN

Introduction

Forming a complement to our preceeding paper(1), we present some results for the first three harmonics derived from the simulation of diffusion-convection of galactic cosmic rays. We present also some dependences of the results to the modulation parameters. The results are discussed in comparison with observations and with the former studies of higher order anisotropy.

In addition to this, we suggest the existence of the IMF-sense-dependent anisotropy of higher order which is discussed in detail in a separate paper(2).

Theory and Model

The cosmic ray anisotropy $\eta(r,p)$ can be expressed as

$$\eta(r,p)\sim 1+\sum_{n=1}^{3}\sum_{m=0}^{n}\{\eta_n^{mc}(r,p)\cos(m\Phi')+\eta_n^{ms}(r,p)\sin(m\Phi')\}P_n^m(\cos\Theta'), \quad (1)$$

where Θ' and Φ' express the incident direction of cosmic rays, defined as(cf. Fig.1)

$$\Theta'=\pi-\Theta, \qquad \Phi'=\pi+\Phi,$$

and

$$\eta_n^{mc}(r,p)=(-1)^n F_n^{mc}(r,p)/F_0^{0c}(r,p),$$

$$\eta_n^{ms}(r,p)=(-1)^n F_n^{ms}(r,p)/F_0^{0c}(r,p).$$

As shown in our preceeding paper(1), F_n^{mc} and F_n^{ms} in Eq.(1) are given by the cosmic ray density U, stream S_i, stress tensor T_{ij} and heat flow tensor H_{ijk} which are governed by the following equations.

$$\nabla\cdot(CUV-\underline{\kappa}^{(1)}\cdot\nabla U)=-\frac{\partial}{\partial p}\left(\frac{1}{3}pV\cdot\nabla U\right), \quad (2)$$

$$S=CUV-\underline{\kappa}^{(1)}\cdot\nabla U, \quad (3)$$

$$T_{ij}=-\kappa^{(2)}_{ijfg}\overline{\overline{(\nabla S)_{fg}}}, \quad (4)$$

$$H_{ijk}=-\kappa^{(3)}_{ijkfgh}\overline{\overline{\overline{(\nabla\underline{T})_{fgh}}}}. \quad (5)$$

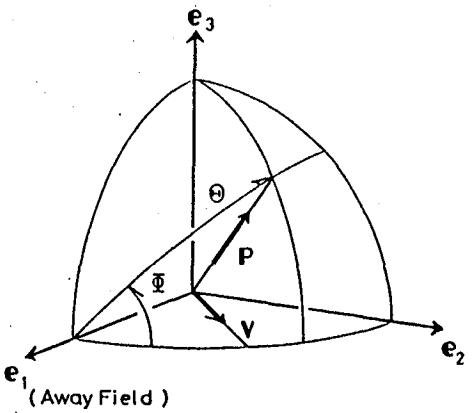

Fig.1 IMF-COORDINATE SYSTEM

p ; Particle's momentum.
V ; Solar wind velocity.
$\mathbf{e}_1$; Unit vector in the direction of B in the 'away' sector.
$\mathbf{e}_3=\mathbf{e}_1\times\mathbf{V}/|\mathbf{e}_1\times\mathbf{V}|$.
$\mathbf{e}_2=\mathbf{e}_3\times\mathbf{e}_1$.

where

$$\overset{\circ}{(\nabla S)}_{fg}=\frac{1}{2}\left[\frac{\partial S_f}{\partial x_g}+\frac{\partial S_g}{\partial x_f}+S_q(Z_{qfg}+Z_{qgf})\right]-\frac{1}{3}(\nabla\cdot S)\delta_{fg}, \qquad (\nabla\cdot S)=\frac{\partial S_q}{\partial x_q}+S_qZ_{qrr},$$

and

$$Z_{ijk}=\frac{\partial \boldsymbol{e}_i}{\partial x_j}\cdot\boldsymbol{e}_k=-Z_{kji}. \qquad (6)$$

Note that, in the IMF-coordinate system, Z_{ijk}'s in Eq.(6) represent the IMF-curvature and focusing. We first solve Eq.(2) in the model heliosphere and, starting from the solution for U, we can calculate successively S_i, T_{ij} and H_{ijk} by Eqs.(3)-(5). In these calculations, the following scattering m.f.p. is assumed.

$$\lambda=\lambda_0(R/GV)\exp\left(\frac{r-r_e}{33\text{a.u.}}\right)(1+a_\lambda\cos\theta_H), \qquad (7)$$

where λ_0 and a_λ are the parameters, R is the rigidity and θ_H is the polar angle in the heliocentric polar coordinate system. The calculations were carried out for various values of λ_0 and a_λ and, in this paper, the results in the following two cases will be presented.

case I .... λ_0 = 0.016 a.u. and $0\leqq a_\lambda\leqq 3$,

case II .... λ_0 = 0.032 a.u. and $0\leqq a_\lambda\leqq 3$.

It is noteworthy that, in Eqs.(3)-(5), S_i, T_{ij}, H_{ijk} having subscript '3' odd times are IMF-sense-dependent and their associated anisotropies symbolized by η_n^{ms} with mark 's' change their signs according to the alteration of the 'away' and 'toward' sectors whereas η_n^{mc} with mark 'c' do not. In this paper, we restrict ourselves only to η_n^{mc}, and the natures of η_n^{ms} mentioned above will be discussed in a separate paper(2).

Results and Discussions

The anisotropies η_n^{mc}'s in space can be expressed by the surface harmonics in the equatorial coordinate system and can be observed as solar daily variations at the Earth(3).

The resultant first space harmonic vectors for cases I and II are shown in Fig.2, with black characters in the positive state and white characters in the negative state. It can be clearly seen that the harmonic vector in the positive state changes its phase toward earlier hours from that of 18h in the negative state, in accordance with the observed 22-year variation of the diurnal variation(4,5,6).

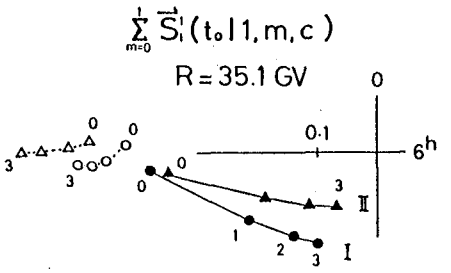

Fig.2 FIRST SPACE HARMONIC VECTORS

Arabic numerals represent the value of a_λ in Eq.(7). The black and white characters represent the positive and negative polarity states, respectively.

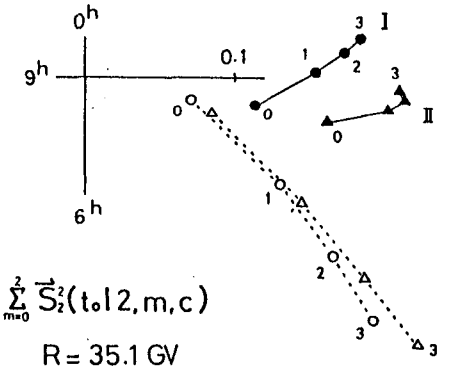

Fig.3 SECOND SPACE HARMONIC VECTORS

The resultant second space harmonic vectors are shown in Fig.3. These vectors in both polarity states are mainly due to the η_2^{0C}-type anisotropy which is independent of Φ (cf. Eq.(1)). The magnitude η_2^{0C} of the anisotropy includes three terms expressing, respectively, the spatial derivatives of S_i, the IMF-curvature effect and the IMF-focusing effect. On the basis of simulations, it is found that all these terms have significant contribution to the anisotropy and the IMF-focusing effect is not always most predominant. A similar Φ- independent anisotropy was obtained also by Bieber and Pomerantz(7), on the basis of the following diffusion equation with respect to the pitch angle cosine ($\mu=\cos\Theta$).

$$\frac{\partial f(\mu,x_1,t)}{\partial t}+\mu v\frac{\partial f(\mu,x_1,t)}{\partial x_1}-\frac{\partial}{\partial \mu}D_{\mu\mu}\frac{\partial f(\mu,x_1,t)}{\partial \mu}+\frac{v}{2L}(1-\mu^2)\frac{\partial f(\mu,x_1,t)}{\partial \mu}=0, \qquad (8)$$

where $D_{\mu\mu}$ is the Fokker-Planck coefficient for pitch angle scattering and L is the focusing length of IMF(8). They concluded that the anisotropy is principally a result of the focusing effect of IMF represented by the last term in Eq.(8). This anisotropy can be regarded as a special case which is applicable only for one dimensional diffusion along the IMF with infinite radius of curvature in the equatorial plane. In other words, this special anisotropy lacks the term expressing the IMF-curvature effect which has a dominant influence on the anisotropy as pointed out previously.

Turning to the third order anisotropy, we obtained two dominant terms η_3^{0C} and η_3^{1C}. The eigen phases of the tri-diurnal variation arising from these two terms are almost orthogonal to each other, that is, (1h,5h) from η_3^{0C} and (3h,7h) from η_3^{1C}. It is noteworthy that one of the eigen phases(3h,7h) arising from η_3^{1C} coincides with the observed phase around 7h in local time(9,10). Since the η_3^{1C}-type distribution is not symmetrical with respect to the field, this implies that the angular

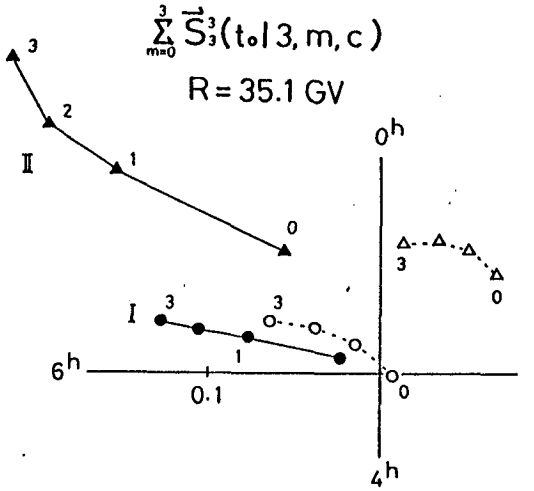

Fig.4 THIRD SPACE HARMONIC VECTORS

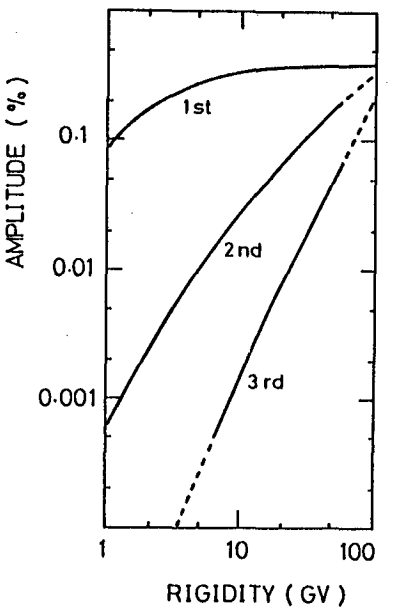

Fig.5 RIGIDITY SPECTRA OF THE FIRST THREE HARMONICS

distribution of the third order anisotropy can not expressed generally in terms of only the pitch angle cosine μ. In this respect, it is not suitable to discuss the third order anisotropy on the basis of the diffusion equation of Eq.(8). Fig.4 shows the resultant tri-diurnal variations which are mainly composed of the above mentioned two types of distribution, i.e., η_3^{0c} and η_3^{1c}. It is noted that the tri-diurnal variations obtained show polarity dependence. This dependence, however, is sensitive to the modulation parameters and, for instance, in case I we can get almost a polarity independent variation with increasing a_λ.

Lastly, Fig.5 shows the rigidity spectra of the first three harmonics obtained in case I for $a_\lambda = 0$. The spectrum of the higher harmonic rises more steeply than that of the lower harmonic, and in the high rigidity region, the spectra of the second and third harmonic are almost proportional, respectively, to R and R^2. This is due to λ linearly increasing with rigidity R(cf. Eq.(7)). Such a rigidity dependence is consistent with the observations(*10*,*11*).

References

1. Munakata,K. and Nagashima,K.(1984)
   Proc. Int. Sympo. on Cosmic Ray Modulation(Morioka), p144.
2. Nagashima,K. et al.(1985)
   paper code SH 4.3-9, in this conference.
3. Tatsuoka,R. and Nagashima,K.(1985)
   paper code SH 4.5-2, in this conference.
4. Thambyahpillai,T. and Elliot,H.(1953)
   Nature,171, p918.
5. Forbush,S.E.(1969)
   J. Geophys. Res., 74, p3451.
6. Mori,S. et al.(1979)
   Proc. 16th Int. Cosmic Ray Conf.(Kyoto), 4, p64.
7. Bieber,J.W. and Pomerantz,M.A.(1983)
   J. Geophys. Res. Lett., 10, p920.
8. Earl,J.A.(1976)
   Astrophys. J., 205, p900.
9. Nagashima,K. et al.(1977)
   Proc. 15th Int. Cosmic Ray Conf.(Plovdiv), 4, p72.
10. Mori,S. et al.(1984)
    Proc. Int. Sympo. on Cosmic Ray Modulation(Morioka), p138.
11. Morishita,I. et al.(1984)
    Proc. Int. Sympo. on Cosmic Ray Modulation(Morioka), p130.

FORMULATION OF COSMIC-RAY SOLAR DAILY VARIATION AND ITS SEASONAL VARIATION, PRODUCED FROM GENERALIZED STATIONARY ANISOTROPY OF SOLAR ORIGIN

R. Tatsuoka and K. Nagashima*

Department of Physics, Nagoya University, Nagoya 464, Japan
*Cosmic Ray Research Laboratory, Nagoya University
Nagoya 464, Japan

1. Introduction. In the previous papers([1-3]), we presented a formulation of cosmic-ray daily variations produced from solar anisotropies stationary through a year, and also of their annual (or seasonal) modulation caused by the annual variation of the rotation axis of the Earth relative to that of the Sun. These anisotropies are symmetric for an arbitrary rotation around an axis. On the other hand, from observations of the tri-diurnal variation([5]), it has been suggested that solar anisotropies also contain some axis-asymmetric term of the third order with respect to the IMF-axis. This suggestion has recently found support in a theoretical study by Munakata and Nagashima([4]). According to their results, the terms of axis-asymmetry with respect to IMF-axis appear also in the 2nd order anisotropy, together with some different kinds of axis-symmetric terms.

The contribution of these anisotropies to the daily variation is different from that of those discussed previously. In the present paper, we extend the above mentioned formulation to a case of a generalized anisotropy.

2. Formulation. Following after the formulation by Munakata and Nagashima([4]), we express the stationary anisotropy $\eta(\boldsymbol{r},p)$ through a year in the IMF-polar-coordinate system defined in fig. 1, as

$$\eta(\boldsymbol{r},p)=\sum_{n=1}^{\infty}\sum_{m=0}^{n}\{\eta_n^{mc}(\boldsymbol{r},p)\cos m\Phi'+\eta_n^{ms}(\boldsymbol{r},p)\sin m\Phi'\}P_n^m(\cos\Theta'), \tag{1}$$

where $\eta_n^{mc}(\boldsymbol{r},p)$ and $\eta_n^{ms}(\boldsymbol{r},p)$ are coefficients, and the angles Θ' and Φ' express the incident direction of cosmic rays with momentum p at a point $\boldsymbol{r}$. $P_n^m(\cos\Theta')$ in the equation is the semi-normalized associate Legendre function([6]). It is noted that the terms with coefficients $\eta_n^{0c}(\boldsymbol{r},p)$'s have a symmetry with respect to the IMF-axis, and have been discussed in the previous papers([1-3]). In eq.(1), each term with the coefficient η_n^{mc} or η_n^{ms} can be expressed in the equatorial coordinate system, as

$$\begin{cases}\eta_n^{mc}(\boldsymbol{r},p)P_n^m(\cos\Theta')\cos m\Phi'=\sum_{k=0}^{n}P_n^k(\cos\theta)S_n^k(\alpha\,|\,n,m,c)\\ \eta_n^{ms}(\boldsymbol{r},p)P_n^m(\cos\Theta')\sin m\Phi'=\sum_{k=0}^{n}P_n^k(\cos\theta)S_n^k(\alpha\,|\,n,m,s),\end{cases} \tag{2}$$

where

$$S_n^k(\alpha\,|\,n,m,\sigma)=\eta_n^{m\sigma}\{a_n^k(\alpha_S\,|\,n,m,\sigma)\cos k(\alpha-\alpha_S+\pi)+b_n^k(\alpha_S\,|\,n,m,\sigma)\sin k(\alpha-\alpha_S+\pi)\}, \tag{3}$$

in which the angles α and θ are, respectively, the right-ascension and the co-declination ($\theta=\pi-\delta$) of the particle's incident direction. α_S in eq.(3) is the right-ascension of the Sun, and $\alpha-\alpha_S+\pi$ is related to solar local time t as $\alpha-\alpha_S+\pi=2\pi(t/24\mathrm{hr})$. Using this relation, the incident

direction can be expressed in terms of θ and t instead of θ and α. The coefficients a_n^k and b_n^k in eq. (3) vary with α_S, owing to the seasonal variation of the relative configuration between the equatorial- and IMF-coordinate systems arising from the Earth's revolution around the Sun. Applying the frequency modulation method([2]), S_n^k of eq. (3) can be transformed as

$$S_n^k(\alpha|n,m,\sigma)=\sum_{l=-\infty}^{\infty} S_n^k(t_{l/k}|n,m,\sigma) \quad \text{for } \sigma=c \text{ or } s, \text{ and } k\neq 0, \tag{4}$$

where

$$S_n^k(t_{l/k}|n,m,\sigma)=x_n^k(l|n,m,\sigma)\cos(2k\pi t_{l/k}/24\text{hr}) + y_n^k(l|n,m,\sigma)\sin(2k\pi t_{l/k}/24\text{hr}), \tag{5}$$

where

$$\begin{cases} x_n^k(l|n,m,\sigma)=T_x(k,l|n,m,\sigma)\eta_n^{m\sigma} \\ y_n^k(l|n,m,\sigma)=T_y(k,l|n,m,\sigma)\eta_n^{m\sigma}, \end{cases} \tag{6}$$

in which T_x and T_y are called the transformation coefficients. In eqs. (4) and (5), $t_{l/k}$ is the time in hours (0~24hr) in a day defined by $1\text{year}/(365+l/k)$ and therefore $P_n^k(\cos\theta)S_n^k(t_{l/k}|n,m,\sigma)$ expresses the k-th harmonic of the daily variation in the time frame of $t_{l/k}$ observed by a vertical telescope pointing toward the θ-direction in the outer space of the Earth.

The terms with $l=0$ are the yearly averaged solar k-th harmonic variations and are expressed by the symbol "*SO*", while those for $l\neq 0$ are called the extended sidereal ($l>0$) and anti-sidereal ($l<0$) daily variations([2]) and are expressed by the symbol "$SI_{l/k}$" for $l>0$ and "$AS_{|l|/k}$" for $l<0$.

Assuming that the anisotropy is stationary through a year, all the transformation coefficients $T_x(k,l|n,m,\sigma)$ and $T_y(k,l|n,m,\sigma)$ in eq. (6) are obtained for $n\leq 3$ and $|l|\leq 3$ and are shown in Tables I, II and III. In the calculations, B, assumed to have Parker's Archimedian spiral structure, is expressed in the heliographic polar co-ordinate system (r, θ_h, φ_h) as

$$\begin{aligned} B_r &= B_0(1\text{a.u.}/r)^2, \\ B_{\theta_h} &= 0, \\ B_{\varphi_h} &= -B_0(1\text{a.u.}/r)\sin\theta_h, \end{aligned} \tag{7}$$

where B_0 is positive(negative) for the away (toward) sector. The inclination of the solar equatorial plane with respect to the ecliptic plane is also taken into account in the calculations([3]).

3. Discussion and Conclusion. The terms with a mark "c" in tables express the IMF-sense-*independent* terms, as the corresponding coefficients η_n^{mc}'s in eq. (2) are independent of IMF-sense([4]). On the contrary, the terms with a mark "s" express the IMF-sense-*dependent* terms, as η_n^{ms}'s change their sign with the change of IMF-sense.

The No.1 and No.2 terms in Table I produce the solar diurnal variation of north-south symmetric type, whereas the No.3 term produces the IMF-sense-dependent sidereal diurnal variation of Swinson type([7]).

The most important term in Table Ⅱ is that of No.1. It is noteworthy that the No.4 and No.5 terms are IMF-sense-dependent and will be discussed in detail in a separate paper([8]).

The importance of the No.1 term in Table Ⅲ has been well acknowledged for the explanation of the solar tri-diurnal variation from the theoretical point of view, whereas the existence of the No.2 term has recently been pointed out by Munakata and Nagashima([4]).

In conclusion, it is emphasized that the transformation coefficients(T_x and T_y) in these tables enable us to connect solar anisotropies produced from the diffusion-convection process with the observed cosmic-ray solar daily variation and its seasonal variation and, as the result, enable us to obtain the information of electromagnetic state in interplanetary space from the observation of solar daily variation of cosmic rays.

References

([1]) K. Nagashima: *Rep. Ionos. Space Res.*, Japan, 25, 189 (1971).
([2]) K. Nagashima and H. Ueno: *Rep. Ionos. Space Res.*, Japan, 25, 212 (1971).
([3]) K. Nagashima, R. Tatsuoka and S. Matsuzaki: *Nuovo Cim.*, 6C, 550 (1983).
([4]) K. Munakata and K. Nagashima: *Proc. Int. Cosmic Ray Symposium* (Morioka, Japan, 1984), p.144; This Conference SH 4.5-1.
([5]) K. Nagashima et al.: *Proc. Int. Conf. Cosmic Rays*, Vol.4 (Plovdiv, 1977), p.72; S. Mori et al.: *Proc. Int. Cosmic Ray Symposium* (Morioka, Japan, 1984), p.138.
([6]) S. Chapman and J. Bartels: *Geomagnetism*, Vol.2 (Oxford, 1940), p.611.
([7]) D.B. Swinson: *J. Geophys. Res.*, 76, 4217 (1971).
([8]) K. Nagashima, K. Munakata and R. Tatsuoka: This Conference SH 4.3-9.

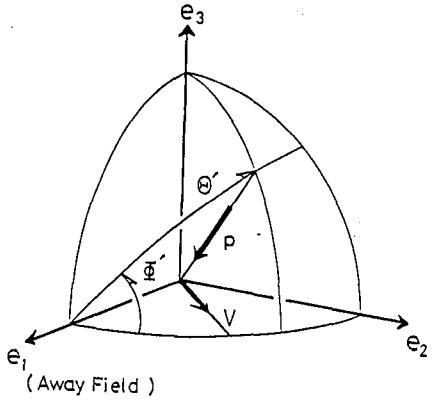

Fig. 1. The IMF-POLAR-COORDINATE SYSTEM.
p: Momentum of particle.
V: Solar wind velocity.
e_1 : Unit vector in the direction of "away" magnetic field.
e_3 : Unit vector in the direction of $e_1 \times V$.
$e_2 = e_3 \times e_1$.

Table Ⅰ. The transformation coefficients $T_x(k,l|n,m,\sigma)$ and $T_y(k,l|n,m,\sigma)$ in eq.(6) for n=1, in units of 10^{-3}.

No.	nmσ	k	l = 3 T_x T_y	l = 2 T_x T_y	l = 1 T_x T_y	l = 0 T_x T_y	l = -1 T_x T_y	l = -2 T_x T_y	l = -3 T_x T_y
1	10c	1		-3, 47		696, -668		16, -15	
2	11c	1		32, -46		660, 671		13, 16	
3	11s	1	-4, 9		62, -410		-57, -25		-1, 0

Table Ⅱ . The transformation coefficients $T_x(k,l|n,m,\sigma)$ and $T_y(k,l|n,m,\sigma)$ in eq.(6) for n=2, in units of 10^{-3}.

No.	nmσ	k	l = 3 T_x T_y	l = 2 T_x T_y	l = 1 T_x T_y	l = 0 T_x T_y	l = -1 T_x T_y	l = -2 T_x T_y	l = -3 T_x T_y
1	20c	1	-8, -12		-55, 285		-300, 59		-7, 1
		2		51, 60		34, -804		2, -36	
2	21c	1	-9, 16		57, 1		-45, -395		0, -9
		2		-41, -25		907, 25		40, 4	
3	22c	1	23, -8		-80, 579		266,		6, 1
		2		134, 17		8, 421		-3, 17	
4	21s	1		22, 102		591, -553		28, 6	
		2	22, 13		-230, -330		-61, 13		-2, 1
5	22s	1		121, -100		531, 522		-12, 28	
		2	-25, -13		313, -227		-13, -59		-1, -2

Table Ⅲ . The transformation coefficients $T_x(k,l|n,m,\sigma)$ and $T_y(k,l|n,m,\sigma)$ in eq.(6) for n=3, in units of 10^{-3}.

No.	nmσ	k	l = 3 T_x T_y	l = 2 T_x T_y	l = 1 T_x T_y	l = 0 T_x T_y	l = -1 T_x T_y	l = -2 T_x T_y	l = -3 T_x T_y
1	30c	1		-35, -110		-291, 274		82, 46	
		2	-30, -7		167, 247		-186, 276		-9, 12
		3		103, 10		-466, -532		-31, -36	
2	31c	1		-61, 40		-127, -101		-70, 122	
		2	10, 15		-60, 46		-343, -267		-14, -13
		3		-47, 51		627, -568		44, -36	
3	32c	1		-42, -132		-342, 293		-117, -75	
		2	-38, -15		268, 390		238, -228		12, -9
		3		104, -96		353, 350		19, 25	
4	33c	1		-223, 161		-342, -314		59, -74	
		2	52, 53		-410, 306		102, 139		3, 7
		3		84, 128		-113, 140		-9, 5	
5	31s	1	-19, -26		-83, 449		-373, 75		-9, -7
		2		137, 85		42, -563		28, -22	
		3	39, -15		-368, -77		-41, 46		-1, 3
6	32s	1	-25, 47		75, 11		-60, -537		12, -12
		2		-30, -57		655, 14		23, 38	
		3	-21, 28		84, -451		-57, -49		-4, -2
7	33s	1	63, 0		-83, 639		389, -8		8, 11
		2		256, 48		27, 345		-25, 9	
		3	2, -51		261, 38		27, -34		1, -2

SOLAR TRI-DIURNAL VARIATION OF COSMIC RAYS IN A WIDE RANGE OF RIGIDITY

Mori, S., H. Ueno*, Z. Fujii*, I. Morishita** and K. Nagashima*

Department of Physics, Shinshu University, Matsumoto 390, Japan
*Cosmic-Ray Research Lab., Nagoya University, Nagoya 464, Japan
**Department of Physics, Asahi University, Hozumi-cho, Gifu 501-02, Japan

ABSTRACT

Solar tri-diurnal variations of cosmic rays have been analyzed in a wide range of rigidity, using data from neutron monitors, and the surface and underground muon telescopes for the period 1978-1983. The rigidity spectrum of the anisotropy in space is assumed to be of power-exponential type as $(P/\gamma P_0)^{\gamma}\exp(\gamma-P/P_0)$. By means of the best-fit method between the observed and the expected variations, it is obtained that the spectrum has a peak at P $(=\gamma P_0)\cong 90$ GV, where $\gamma\cong 3.0$ and $P_0\cong 30$ GV. The phase in space of the tri-diurnal variation is also obtained as 7.0 hr (15 hr and 23 hr LT), which is quite different from that of $\sim$1 hr, arising from the axis-symmetric distribution of cosmic rays with respect to the IMF.

1. Introduction

Studies of higher harmonics in the daily variation of cosmic rays provide valuable infromations as to the nature of the cosmic ray modulation in the heliosphere. So far a great many investigation has been performed of the solar tri-diurnal variation, and some of its characteristic natures have been revealed; its extra-terrestrial origin and also its rising spectrum with rigidity (e.g., Bieber et al., 1983; Mori et al., 1984; hereafter referred to as Paper I).

These results, however, have not yet been firmly founded because of the statistical uncertainty of the data used which is largely due to limited rigidity range. In particular, there is a wide divergence of opinion as to the direction of the anisotropy; some analyses reported $\sim$1 hr direction, while some obtained $\sim$7 hr direction. This discrepancy is crucial for determining the modulation mechanism; 1 hr direction is in favor of the 'loss-cone' model (Fujii, 1971) or the model of Bieber et al. (1983), whereas 7 hr direction requires other kind of model such as the one presented by Munakata and Nagashima (1985; in this issue).

In the present analysis, we try to obtain a definite form of the anisotropy responsible for the averaged tri-diurnal variations over 6 years (1978-1985), using data in a wide range of rigidity from neutron monitors to underground muon telescopes, which respond to the effective rigidity of 10 to 600 GV.

2. Analysis of Data

The present experimental data include 2 to 6-year averages of neutron monitor data in a worldwide network (36 stations from the polar to the equatorial regions) and 6-year averages of the surface (NAGOYA) and underground (MISATO and SAKASHITA) muon telescopes for the period 1978-1983.

Fig. 1 illustrates the summation harmonic dial, showing clearly the persistency of year-to-year changes of the observed tri-diurnal variations of three muon telescopes at NAGOYA (surface) for 1971-1983, at MISATO (34 m.w.e. in depth underground) for 1974-1983 and at SAKASHITA (80 m.w.e. in depth underground) for 1978-1983. In the present analysis, 6-year averages over 1978-1983 were used; of 13 directional components at NAGOYA, 9 components at MISATO and 10 components at SAKASHITA, and these are listed in Paper I.

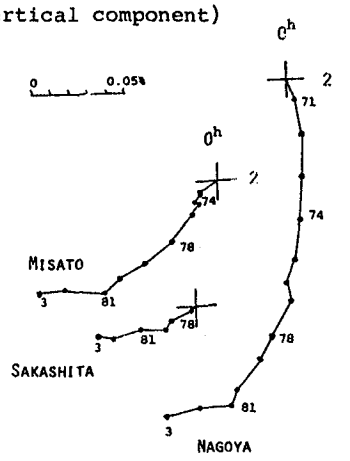

Fig. 1 Observed solar tri-diurnal variations of V-component at NAGOYA, MISATO and SAKASHITA in summation dial.

In order to derive the 3rd order anisotropy, the tri-diurnal variation produced by the anisotropy with a certain form of the rigidity spectrum G(P), will be compared with the observed results. In the anaysis, G(P) is assumed to be of power-exponential type as

$$G(P)=(P/\gamma P_0)^{\gamma}\exp(\gamma-P/P_0) \quad (1)$$

Evidently, G(P) becomes maximum at $P=\gamma P_0$ for $\gamma>0$, and is normalized to unity.

The expected 3rd harmonic components (A_{ij}, B_{ij}) for j-th components telescopes of i-th station including neutron monitor station, are related to the space harmonic components (X, Y) by the following equations with coupling coefficients c_{ij} and s_{ij} as

$$A_{ij} = (c_{ij}X + s_{ij}Y), \qquad B_{ij} = (-s_{ij}X + c_{ij}Y) \quad (2)$$

The coefficients c_{ij} and s_{ij} were derived from the differential coupling coefficients dc_{ij} and ds_{ij} given by Fujimoto et al. (1984). The best-fit parameters satisfying the following equation are determined.

$$\Sigma_{ij} w_{ij}\{ (A_{ij} - a_{ij})^2 + (B_{ij} - b_{ij})^2 \} = \text{minimum} = \delta^2 \quad (3)$$

In Eq. (3), the weight w_{ij} is given for the observed a_{ij} and b_{ij} so as to balance the difference in the number of the data used in the rigidity interval; 6 divisions in all the ranges of 10 to 600 GV to have equal weight. Also each vector in all the muon components was subtracted from the reference component to eliminate the atmospheric temperatute effect; in this analysis, V-component for NAGOYA and MISATO and SE-component for SAKASHITA were taken as the reference.

3. Results and Discussions

The contour map of equal δ^2's obtained from the residual sum of the

observed vectors and the expected vectors computed by Eq. (2), is shown against γ and P_0 in Fig. 2. As is seen in the figure, minimal δ^2 region locates in relatively narrow regions of γ and P_0-value. It is noted that in these regions the product of γ and P_0 keeps almost invariant as $\gamma P_0 \cong 90$ GV. The best-fit parameters were obtained as that $\gamma \cong 3.0$ and $P_0 \cong 30$ GV.

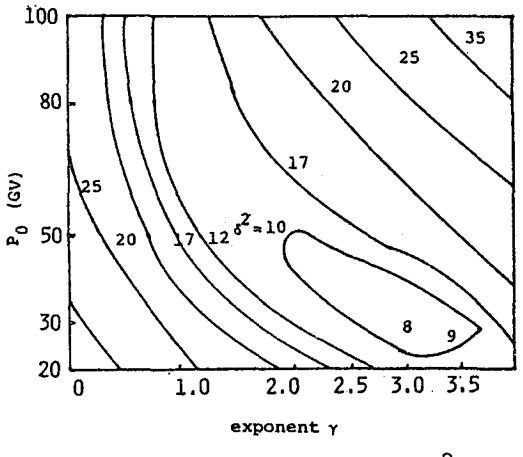

Fig. 2 Contour map of equal δ^2 plotted against γ and P_0, showing minimal δ^2 ($\cong$8) for $\gamma \cong 3.0$ and $P_0 \cong 30$ GV.

The direction (phase) of the anisotropy was obatined as 7.0 hr. It is also noted that this direction shows almost constant value for the above minimal region.

The fitness of the reproduced variations computed by Eq. (2) in the best-fit case to the observed ones is shown in Fig. 3; (a) for NAGOYA, (b) for MISATO and (c) for SAKASHITA, respectively. The observed vectors are shown with the solid circles (●) and the reproduced ones with the open circles (○). Also the reference component mentioned above is shown by the symbol (⊙) and the origin of the diagram in the best-fit case is given by the cross (✖). A fairly good agreement can be seen between two patterns drawn by connecting each observed point (solid line) and each reproduced point (dotted line) for each station.

The present anaysis can obtain a definite parameter set as; $\gamma \cong 3.0$ and $P_0 \cong 30$ GV. As shown in Paper I, where only muon data at the above three stations (NAGOYA, MISATO and SAKASHITA) were used, parameter set (γ,P_0) rather spereads as; $\gamma = 2 \sim 12$ and $P_0 = 50 \sim 8$ GV. The present form can be derived by adding neutron monitor data to Paper I. Note that the observed vectors of neutron monitors from 36 stations are so divergent even if in the best-fit case, which may be largely due to inaccurate barometric correction in the data.

On the other hand, the direction (phase) of the anisotropy in space was obtained as $\sim$7 hr ($\sim$15 hr and $\sim$23 hr LT). So far there has been a wide divergence of opinion as to the direction; $\sim$1 hr direction was reported by the analyses of neutron monitor data alone, while $\sim$7 hr direction was reported by using muon data. The former is in favor of the 'loss-cone' model (Fujii, 1971) or the model of Bieber et al. (1983), arising from the axis-symmetric distribution of cosmic rays with respect to the IMF. On the other hand, the latter requires other kind of model such as the one preseneted by Munakata and Nagashima (1985, in this issue). The present result provides a firm basis for the latter model.

A further analysis would be necessary to derive the detailed form and its year-to-year variation.

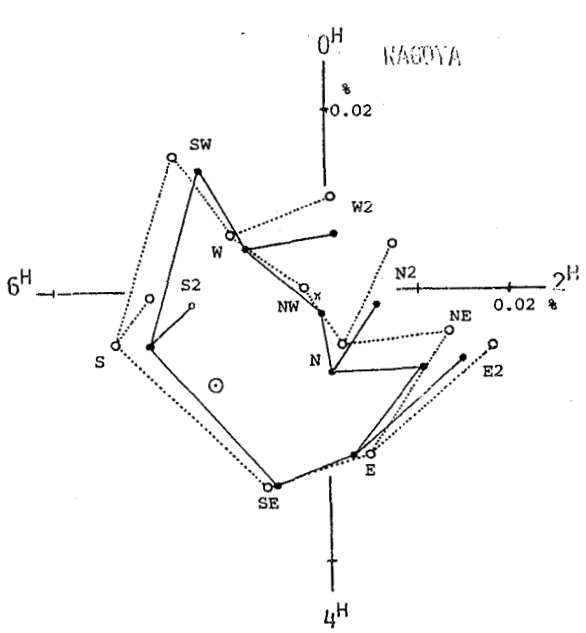

(a) for NAGOYA

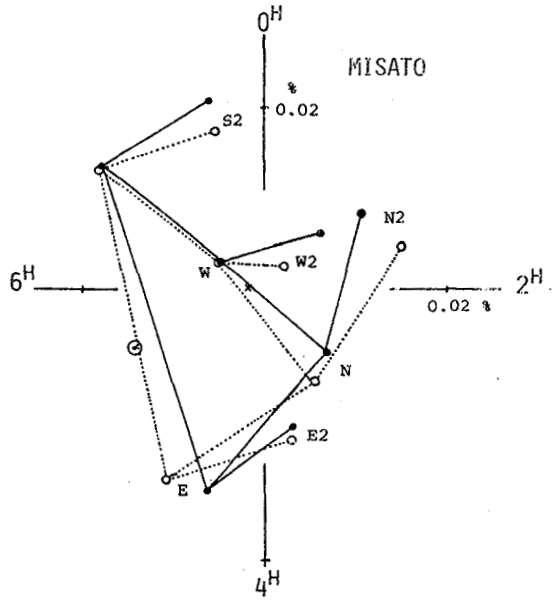

(b) for MISATO

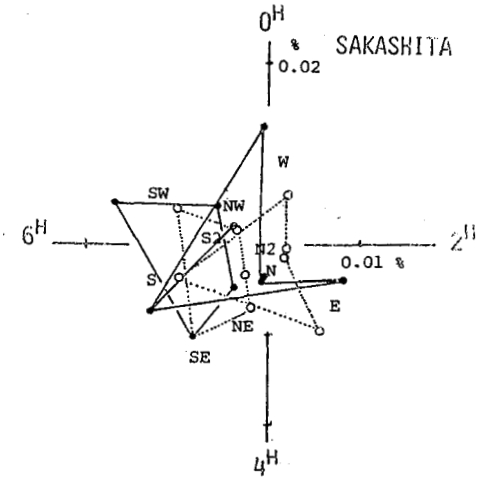

(c) for SAKASHITA

Fig. 3 Fitness between the observed (●) and the reproduced (○) variations; (a) for NAGOYA, (b) for MISATO and (c) fro SAKASHITA for the period 1978-1983.

4. Acknowledgements

The authors express their appreciation to Messrs. K. Chino and S. Nakamura for their computational help. Neutron monitor data were obtained through WDC-C2, whom we acknowledge much.

References

Bieber, J.W. et al., (1983), 18th ICRC (Bangalore), 3, 289.
Fujii, Z., (1971), Rep. Ionos. Space Res., Japan, 25, 242.
Fujimoto, K. et al., (1984), Rep. of CR-Lab,, Nagoya Univ., No. 9.
Mori, S. et al., (1984), Int. CR-Symp. (Morioka), p138.
Munakata, K. and K. Nagashima, (1985), in this issue (SH 4.5-1).

UPPER CUT-OFF RIGIDITY FOR COROTATION ANISOTROPY DURING SOLAR ACTIVITY CYCLES 20 AND 21

H. S. Ahluwalia[1] and J. F. Riker[2]

[1] Department of Physics and Astronomy, The University of New Mexico, Albuquerque, N.M. 87131, U.S.A.

[2] B.D.M. Corporation, Albuquerque, N.M., 87106, U.S.A.

ABSTRACT

At the Eleventh International Conference on Cosmic Rays held at Budapest in 1969, we discussed the results of our study of the solar diurnal variations of cosmic rays observed during the ascending phase of solar activity cycle twenty (Ahluwalia and Ericksen, 1970). We reported that the diurnal variation, observed underground during 1965-68 period, results from an extra-terrestrial anisotropy having a continuously increasing upper cut-off rigidity R_c. However, the coupling functions applicable to underground telescopes were controversial then. This situation has improved now. So we have re-examined those results and extended them to cover the period 1965-78. In this study we have used the coupling functions given by Murakami et al. (1979) for underground muons and those given by Lockwood and Weber (1967) for neutron monitors. We show that a great deal of care should be exercised in calculating the value of R_c. Although numerical values of R_c are a little different, the trend for 1965-68 period remains unchanged. Highest value of R_c occurs in 1970 and the lowest value occurs in 1976. Our results are discussed.

Ahluwalia, H.S., and Ericksen, J.H., 1970, Acta Phys. Acad. Scient. Hung., 29, Suppl. 2, 139.

Murakami, K., Nagashima, K., Sagisaka, K., Mishima, Y., and Inoue, A., 1979, Nuovo Com., 2C, 635.

Lockwood, J.A., and Weber, W. R., 1967, J. Geophys. Res., 72, 3395.

22-YEAR CYCLE OF THE UPPER LIMITING RIGIDITY OF DALY WAVES

G. Erdős, J. Kóta and E. Merényi

Central Research Institute for Physics, Budapest, Hungary

Abstract. The method of calculating energy losses along regular particle trajectories is applied to obtain the predicted cosmic ray anisotropies from 200 to 500 GV. The tilt angle of the interplanetary neutral sheet varies to simulate a 22-year cycle magnetic cycle. The calculated values of solar diurnal and semidiurnal, and siderial diurnal intensity waves are compared with observations.

1. Introduction. Earlier we suggested (Erdős and Kóta 1979, 1980) that the cosmic ray anisotropies observed at underground energies can be interpreted in terms of regular particle motion in the Interplanetary Magnetic Field (IMF) incorporating a wavy neutral sheet. At high rigidities, the effects of small-scale irregularities should be negligible and, being the dominant large-scale feature of the IMF, the wavy neutral sheet plays the decisive role.

In this paper we investigate how cosmic ray anisotropies change during a 22-year magnetic cycle. We consider the 200 - 500 GV range which represents the high rigidity tail of the modulation spectrum. The state of the heliosphere changes in a complex way during a solar cycle. From this complexity, the only feature we consider here is the variation of the inclination of the tilted heliospheric neutral sheet. The tilt angle is minimal around solar minimum and increases with increasing solar activity (Thomas and Smith 1981). As a crude approximation, we simulate the 22-year cycle by simply changing the tilt angle.

2. The Model. The IMF model and the method of calculation are described in detail elsewhere (Erdős and Kóta 1979, 1980, 1981). Briefly, a conventional Parker spiral field is applied with a 5 gamma field strength at the earth. The wavy neutral sheet dividing the opposite polarities is given by

$$\sin\theta = \sin\alpha \cdot \cos(\varphi + r) \qquad (1)$$

where θ and φ are heliographic latitude and longitude, respectively, r is heliocentric distance in units of AU. The tilt angle, α, gives the maximum latitudinal excursion of the neutral sheet. The configuration of away polarity above the sheet and toward polarity below the sheet will be referred to as $A > 0$.

We note that equation (1) does not exactly correspond to a tilted plane at the sun. Calculations were also carried out for a tilted plane of 90° inclination. This case of indefinite A, where the two configurations merge, will be labelled with 90*.

The theoretical results to be presented always give the full free-space anisotropy that would be observed by an equatorial observer in the absence of geomagnetic deflection. Calculations do not include the Compton-Getting effect due to the orbital motion of the earth.

3. Results. In this paragraph we briefly report on the daily intensity waves predicted for 200, 300 and 500 GV at various values of the tilt angle, α.

The harmonic dial of the solar daily variation calculated for 200 GV is shown in Figure 1. For comparision, Figure 2 (taken from Benkő et. al., 1984) shows the year-to-year daily vectors observed by the Budapest underground telescopes (median energy: 180 GeV) in the period of 1976 (A>0, low solar activity) to 1983 (A<0). We find a remarkable agreement if correction is made to the 1.5 hr geomagnetic deflection, the Compton-Getting effect due to the earth's orbital motion, and the $\cos 47^\circ \approx 0.68$ attenuation factor due to the 47° N geografical latitude of the station.

The amplitudes of the solar daily waves calculated for 200, 300 and 500 GV are shown in Figure 3.

The predicted harmonic dial of the semidiurnal variation of 200 GV cosmic rays is shown in Figure 4, while the calculated amplitudes are given in Figure 5. A charge asymmetry can clearly be seen: for $A > 0$, an earlier phase and a smaller amplitude is to be expected. These findings are in general agreement with numerous observations (see, for example, Morishita et. al., 1984).

As expected, the phase of the sidereal daily wave was always found to be close to either 6 hr or 8 hr, depending on the polarity of the magnetic sector. Figure 6 gives the calculated sidereal amplitudes. Our theoretical results suggest a hard energy spectrum; the spectrum of the sidereal variation turns out markedly harder than the solar diurnal and semidiurnal spectra. This finding also suggests that a sidereal variation of solar origin may still be present at rigidities where solar diurnal and semidiurnal waves already diminish. Thus, in searching for a genuine galactic anisotropy of cosmic rays one should be cautious in establishing the upper rigidity limit of the heliospheric effects.

References:

Benkő, G., Kecskeméty, K., Kóta, J., Somogyi, A., Varga, A., 1984: Proc. Int. Symp. on CR Modulation, Morioka, p104

Erdős, G. and Kóta, J., 1979: Proc. 16th ICRC, Kyoto, 4, 45

Erdős, G. and Kóta, J., 1980: Astrophys. Space Sci., 67, 45

Erdős, G. and Kóta, J., 1981: Proc. 17th ICRC, Paris, 10, 105

Morishita, I., Ueno, H., Fujii, Z., Mori, S. and Nagashima, K., 1984: Proc. Int. Symp. on CR Modulation, Morioka, Japan, p130.

Thomas, B. T. and Smith, E. J., 1981: J. Geophys. Res., 86, 11105

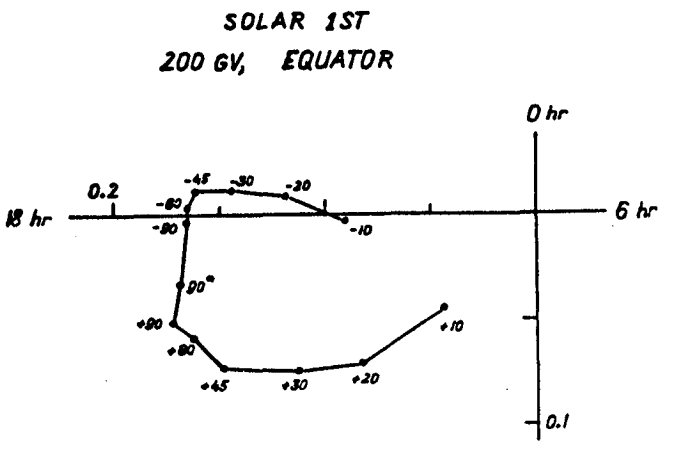

Figure 1. Calculated harmonic dial of the solar daily waves of 200 GV cosmic rays. Numbers stand for the tilt angle, α, in degrees (negative values refer to A < 0).

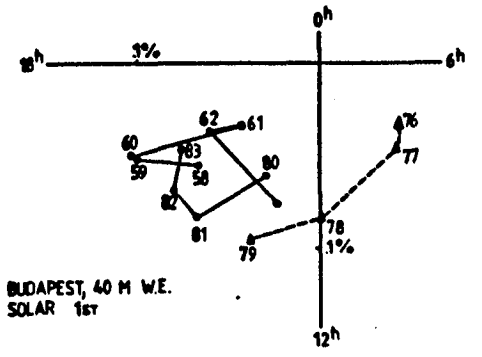

Figure 2. The Budapest solar daily vectors without geomagnetic correction. Numbers stand for the year of observation. Results are grouped according to the polarity state (triangles and dashed lines refer to A > 0).

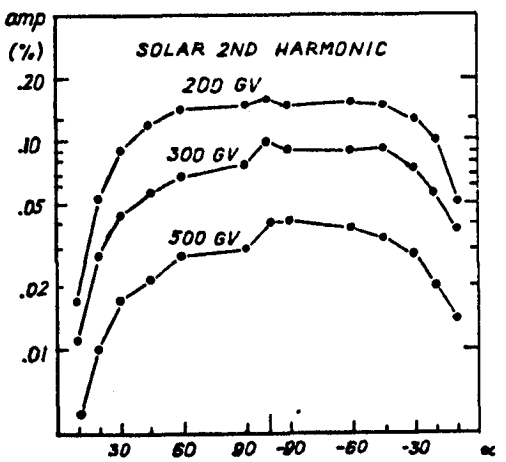

Figure 3. Calculated amplitudes of the solar daily vectors of 200, 300 and 500 GV cosmic rays vs the tilt angle, α, in degrees. (Negative values of α refer to A < 0.)

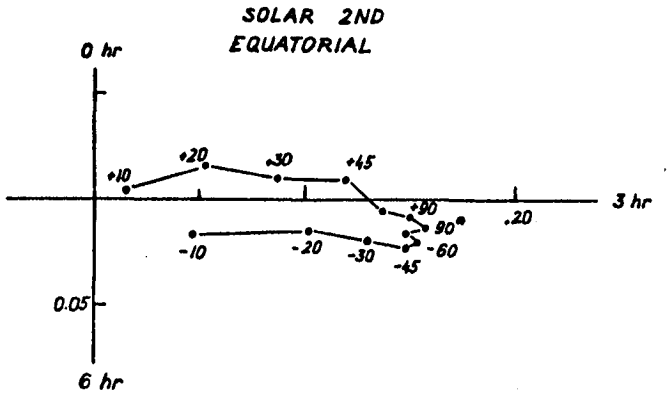

Figure 4. Same as Fig. 1., for semidiurnal vectors.

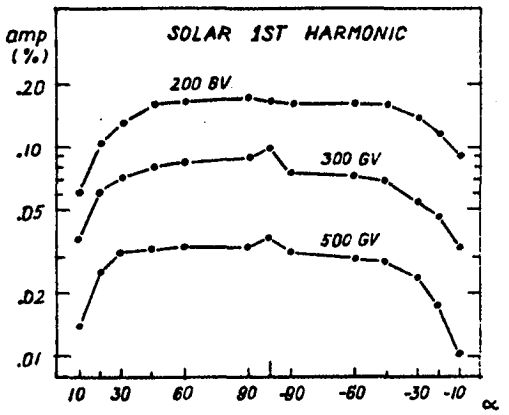

Figure 5. Same as Fig. 3., for semidiurnal vectors.

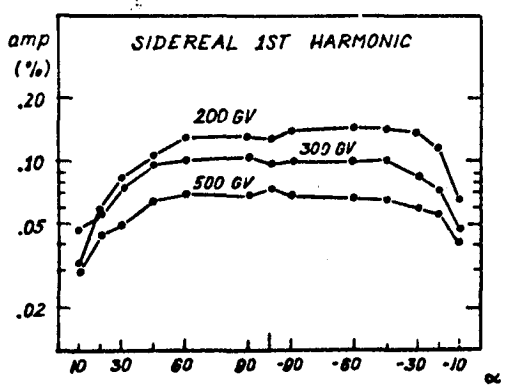

Figure 6. Same as Fig. 3., for sidereal daily vectors.

SOLAR WIND VELOCITY AND DAILY VARIATION OF COSMIC RAYS

H. S. Ahluwalia[1] and J. F. Riker[2]

[1] Department of Physics and Astronomy, The University of New Mexico, Albuquerque, N.M., 87131, U.S.A.

[2] B. D. M. Corporation, Albuquerque, N.M. 87106, U.S.A.

ABSTRACT

Recently parameters applicable to the solar wind and the interplanetary magnetic field (IMF) have become much better defined (King, 1981). Superior quality of data bases that are now available, particularly for post-1971 period, make it possible to believe the long-term trends in the data. These data are correlated with the secular changes observed in the diurnal variation parameters obtained from neutron monitor data at Deep River and underground muon telescope data at Embudo (30 MWE) and Socorro (82 MWE). The annual mean amplitudes appear to have large values during the epochs of high speed solar wind streams. Our results are discussed.

King, J. H., 1981. J. Geophys. Res., 86, 4828.

DIURNAL ANISOTROPY DURING SOLAR ACTIVITY CYCLE TWENTY AND DIFFUSION-CONVECTION MODEL

H. S. Ahluwalia and J. F. Riker

Department of Physics and Astronomy, The University of New Mexico, Albuquerque, N.M., 87131, U.S.A.

ABSTRACT

Underground muon telescope data obtained at Embudo and Neutron monitor data obtained at Deep River are divided into two sets; one covers the ascending phase of the cycle (1965-70) and the other covers the descending phase (1971-76). The amplitude of diurnal anisotropy calculated from the data does not agree with the value predicted by the simplified version of the Diffusion-Convection Model (DCM); the discrepancy is worse for neutron data.

INTRODUCTION. We report here an extension of our earlier study (Ahluwalia and Ericksen, 1970, 1971). Coupling functions (W) given by Murakami et al. (1979) and those given by Lockwood and Weber (1967) are used to calculate the amplitude of diurnal anisotropy. Median rigidity of response (R_m) $\sim$ 16 GV for Deep River neutrons and $\sim$ 134 GV for Embudo muons. Unlike Subramanian (1971) we are not able to reconcile our calculations with the predictions of the simplified version of Diffusion-Convection Model (Forman and Gleeson, 1975).

DATA. Figure 1 summarizes the available data on the annual mean amplitudes of the diurnal variation observed at Embudo (open circles) for the period 1965-79 and at Deep River (solid dots) for the period 1962-79. The flags indicate the standard deviation, computed from the observed scatter in the data for a given year. Zurich sunspot numbers (R_z) indicate the level of solar activity. Epoch of solar polar field reversal is also shown; after 1970 the solar polar field is directed out of the sun in the northern hemisphere. In

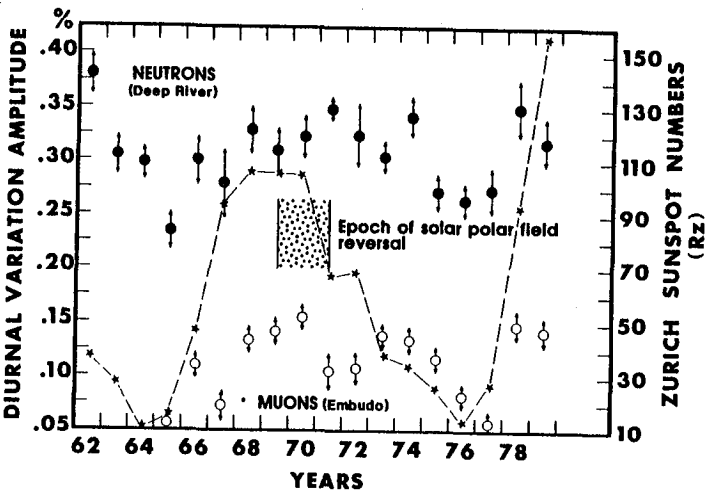

FIG 1

general the amplitudes have the lowest values during activity minima and large values during activity maximum. In particular, we wish to point out that the amplitudes at Embudo have large values for the years 1973, 1974 and 1975 during which the mean level of the solar activity is only about one third of the maximum value in 1968. Bulk velocity (V) of solar wind is high during these years.

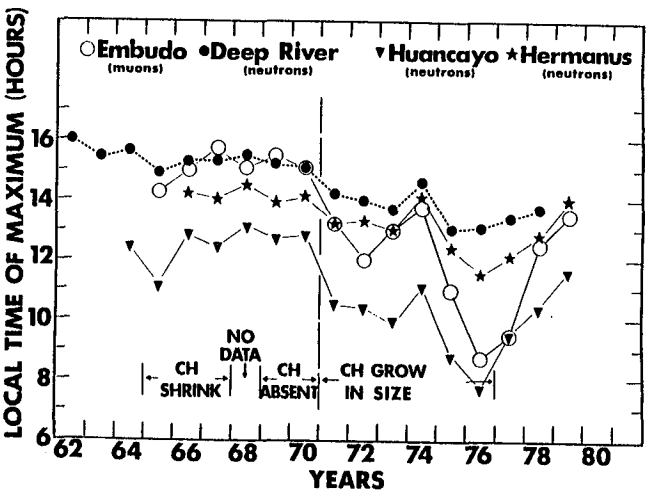

FIG 2

Another important feature of the dependence of the diurnal variation on the solar activity is shown in Figure 2. It gives the annual mean time of maximum of the diurnal variation observed at Embudo, Deep River, Hermanus ($R_m \cong 20$ GV) and Huancayo ($R_m \cong 30$ GV). The data exhibit a remarkable, worldwide, systematic, rigidity-dependent shift of the time of maximum of diurnal variation to early hours, during the period 1971-76. The data for Huancayo and Hermanus are staggered in time, with respect to Deep River, to minimize an overlap. The rigidity dependent nature of this effect was emphasized by us elsewhere (Ahluwalia, 1976). Note that prior to 1971 the observed time of maximum at Embudo is nearly steady at about 15 hours (LT) but in 1976 the time of maximum is at 8.7 hours (LT). The diurnal times of maximum return to pre-1971 values by about 1979, at all stations. Agrawal (1983) has reported similar behavior for neutron and surface-level muon detectors at sites in Canada. Also summarized in Figure 2 is the information about the size of the coronal holes during solar activity cycle (SAC) 20.

ANALYSIS. We subdivide the data into two sets; one set covers the period 1965-70 and the other set covers the period 1971-76. The reader is reminded that the observed diurnal variation is rather steady, on a year to year basis, during the first period and undergoes a remarkable systematic change during the second period. The characteristics of the annual mean diurnal variation observed at Embudo and at Deep River for the two periods are displayed in Fig. 3 on the harmonic dial. The error circles are for 2σ. One can see that the amplitudes for the two periods remain the same for both Embudo muons and Deep River neutrons. However, the time of maximum is significantly early for both detectors, for the second period (1971-76). The fact that the ampli-

tudes are the same for muons as well as neutrons, implies that upper cut-off rigidity R_c has the same average value for both periods; in fact $R_c \sim 70$ GV. Also the fact that the vectors for the two periods, for both detectors, are well-resolved implies that some new effects contribute to the observed diurnal variation during 1971-76 period.

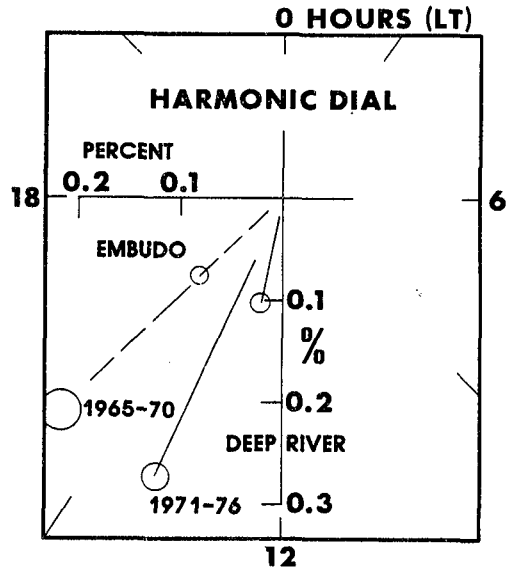

FIG 3

Diffusion-Convection Model (DCM) predicts that if $K_\perp = 0$ and there is no net radial streaming (S_r) and if perpendicular gradient is zero, cosmic rays undergo corotation. In this case the anisotropy (δ) recorded by a detector with a mean asymptotic latitude λ of viewing is given by

$$\delta = 0.6 \cos \lambda, \ \%$$

So we expect that δ should be independent of solar wind bulk velocity (V). An obvious limitation of the model is that it does not contain the concept of R_c. Somehow the diffusion coefficients $K_{\parallel}$, $K_\perp$ must depend upon primary rigidity (R) in such a way as to lend some physical significance to the concept of R_c. The theory in its present state is obscure on this point. Let us assume that,

$$\delta_{theo} = \begin{cases} 0.6 \cos \lambda \ \%, & \text{if } R \leq R_c \\ 0.0, & \text{if } R > R_c \end{cases}$$

This form of variational spectrum is consistent with the results obtained in our analyses earlier, for the first period (1965-70). Table 1 gives a summary of results for the two detectors, for the three periods, assuming $R_c = 70$ GV. The direction of anisotropy in free space is calculated after applying corrections for the "orbital-effect" and for the "geomagnetic bending" of the primaries. These corrections are model independent.

RESULTS. (1) Diurnal Anisotropy in free-space is in the direction of 18 hours (LT) for the first (1965-70) and third periods (1965-76), but the direction is significantly earlier for the second period (1971-76).

(2) Within errors of observations the amplitudes of diurnal variations for the two detectors, for the three periods, are the same. The amplitude of the anisotropy, calculated from the data for the two detectors, is tabulated in the last column of Table 1. The calculated value is about 33% less for neutrons and about 8% less for muons when compared to the theoretical value. So our results do not

TABLE 1

Station	λ deg	$\int_{R_o}^{R_c} WdR$ %	Free Space Direction of Diurnal Anisotropy hours (LT) 1965-70	1971-76	1965-76	δ calc %
Deep River	11.8	0.78	18.21 ± 0.12	16.87 ± 0.12	17.54 ± 0.12	0.43 ± 0.01
Embudo	19.1	0.28	17.83 ± 0.11	16.87 ± 0.11	17.74 ± 0.11	0.55 ± 0.02

agree with the predictions of the simplified DCM, for SAC 20. However in practice we may not have $K_\perp = 0$. Also $K_\perp$ may be inversely proportional to the square of the particle rigidity (Jokipii, 1971). If we follow Jokipii's suggestion and take $(K_\perp/K_{||}) \simeq 0.15$ and further note that median primary rigidity of response for muons is about a factor of eight larger than for neutrons, the calculated values agree much better with the theoretical value. But this does not explain why the direction of anisotropy is significantly earlier in the second period (1971-76). Also it is hard to believe that the ratio $K_\perp/K_{||}$ is invariant in time.

(3) In recent years Jokipii has emphasized very strongly that drifts should play an important role in the modulation of cosmic rays (Kota and Jokipii, 1983 and references therein). It would be interesting to see if one obtains a better agreement between theory and observations by invoking charged particle drifts.

REFERENCES.

Agrawal, S. P., 1983. Space Sci. Rev., 34, 127.
Ahluwalia, H. S. and Ericksen, J. H., 1970. Acta. Phys. Acad. Scient. Hung., 29, Suppl. 2, 139.
Ahluwalia, H. S., and Ericksen, J. H., 1971. J. Geophys. Res., 76, 6613.
Ahluwalia, H. S., 1976. Proc. Intern. Cosmic Ray Symp. on High Energy Cosmic Ray Modulation, Tokyo, p. 260.
Forman, M. A., and Gleeson, L. J., 1975. Astrophys. Space Sci., 32, 77.
Jokipii, J. R., 1971. Rev. Geophys. Space Phys., 9, 27.
Kota, J., and Jokipii, J. R., 1983. Astrophys. J., 265, 573.
Lockwood, J. A., and Weber, W. R., 1967. J. Geophys. Res., 72, 3395.
Murakami, K., Nagashima, K., Sagisaka, K., Mishima, Y., and Inoue, A., 1979, Nuova Cim. 2C(5), 635.
Subramanian, G., 1971. J. Geophys. Res., 76, 1093.

SH 4.5-8

DIURNAL EFFECT IN COSMIC RAYS AT MIDDLE LATITUDES ACCORDING TO STRATOSPHERIC MEASUREMENTS

Asatryan G.A., Babayan V.Kh.
Yerevan Physics Institute, Markarian st.2
375036, Yerevan, Armenia, USSR

Stozhkov Yu.I.
P.N. Lebedev Physical Institute of the Academy of Sciences of the USSR, Leninsky prospect,53, 117924, Moscow, USSR

ABSTRACT

Results of measurements of the diurnal wave of the cosmic ray (CR) intensity in stratosphere at the latitude with the geomagnetic cutoff rigidity R_c = 7.6 GV are presented.

Measurements of diurnal variation of the CR intensity were carried by means of radiosondes - by a detector composed of a gas-discharge counter CTC-6 and a telescope containing two counters with a 7 mm aluminium filter between them. Radiosondes were launched in Yerevan daily during a month (May 23 to June 23, 1984) at the following hours: 2,5,8,11,14,17,20,23 LT. The period of time during which the measurements were carried out is characterized by a quiet situation: the average three-hourly value $K_p < 3$ [1]. The CR intensity fluctuations in the absorption curve maximum in stratoaphere did not exceed $\sim 2.5\%$

at high altitudes (R_c = 0.5 GV) and $\sim$ 1% at the latitude with R_c = 2.5 GV.

Experimental data allowed to obtain the altitude dependence of the CR intensity on the atmospheric depth, N(x), for eight different times of LT. To reveal the diurnal wave of the CR intensity in stratosphere, we have used the following method of processing of altitude dependences for a vertical CR flux. Three pressure intervals X = 8 + 50, 50 + 100 and 100 + 150 g/cm^2 were analyzed, each of which was in its turn divided into several subintervals. Then the mean for the daily CR intensity for each interval, $\overline{N}(x)$, was found. After that the value $\delta = \frac{N_i(x) - \overline{N}(x)}{\overline{N}(x)}$, %, was defined, where i is the time of measurements. To improve the accuracy, values of δ were averaged for each interval. Mean values of $\overline{\delta}$ are presented in figs. 1a,b,c for the above three pressure intervals. A diurnal wave is observed with the amplitude which decreases from $\sim$ 4% to $\sim$ 2% with the increase in the atmosphere pressure from $\sim$ 30 g/cm^2 to $\sim$ 130 g/cm^2. The time of maximum is $11 \div 14^h$ LT. These results agree with measurements of the diurnal wave in stratosphere carried out in 1981 [2]. The daily wave of the CR intensity on the neutron monitor in Tbilisi (R_c = 7.4 GV) is presented in fig.1d for the same period of the time (23 May $\div$ 23 June 1984).

The dependence of the diurnal wave amplitude on the atmospheric depth X is shown in fig.2. A substantial decrease in the value of $\overline{\delta}$ is observed with the increase in

the atmospheric depth.

Certain difficulties arise in trying to give a correct explanation of a large amplitude of the CR intensity diurnal amplitude in stratosphere (~ 4%) and of the early time of maximum ($11^h \div 14^h$ LT). The presence of such a large anisotropy of CR in stratosphere may be connected to the anisotropic pitch-angular distribution of particles in the interplanetary space and possible to the large contribution of nuclei of galactic cosmic rays in the diurnal wave. It is difficult to explain the obtained results by the temperature effect in cosmic rays or by the drift radiosondes during the flight and appropriate variations of the value of R_c.

References:

1. Solar Geophysical Data.(1984), N° 479, part 1, p.91, N° 480, part 1, p.86, Boulder, USA.
2. G.A. Asatryan, Yu.I. Stozhkov, (1983), 18-th ICRC, Bangalore, India, v.3, p.299.

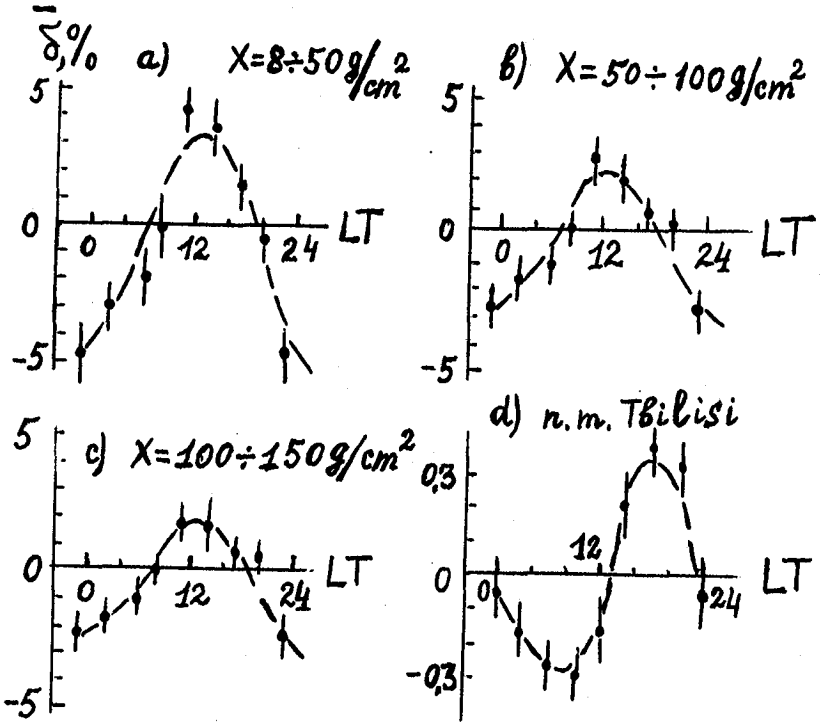

Fig.1. The diurnal wave of CR intensity according to the measurements in 23 May ÷ 23 June 1984 in the stratosphere (Yerevan, R_c=7,6 GV) at the atmospheric pressure X=8÷50 g/cm (a), X=50÷100 g/cm (b), X=100÷150 g/cm (c) and on the neutron monitor Tbilisi, R_k=7,4 GV (d).

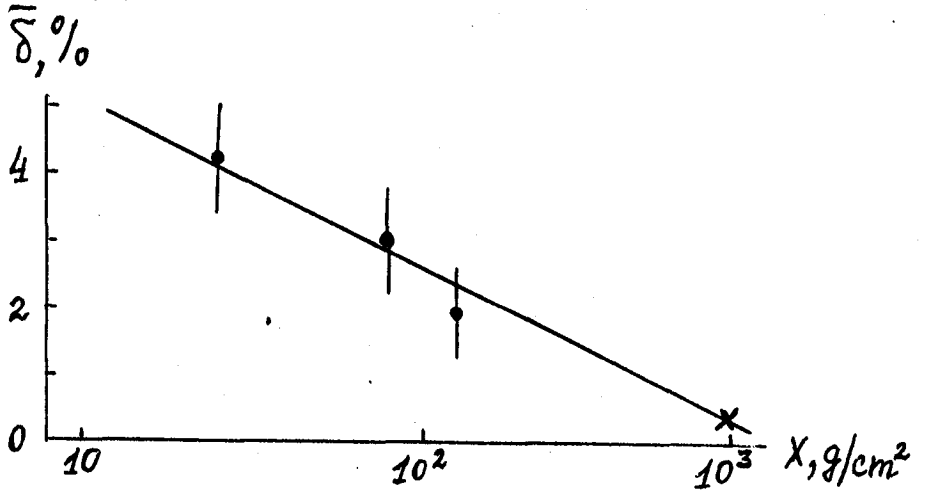

Fig.2. The diurnal wave amplitude at the different atmospheric data; X - neutron monitor Tbilisi, • - stratospheric data.

SH 4.5-9

COMPARATIVE STUDY OF THE PHASE OF DIURNAL ANISOTROPY ON QUIET AND DISTURBED DAYS ON A LONG TERM BASIS UPTO RECENT PERIOD

Santosh Kumar
Rani Durgavati University, Jabalpur.India.

ABSTRACT

The data from the world-wide grid of neutron monitoring stations have been analysed for a comparative study of the phase of diurnal anisotropy on quiet and disturbed days on a long term basis upto recent period. It has been observed that the phase of the diurnal anisotropy on disturbed days where the value of the Ap-index is higher, is found to shift towards earlier hours in comparison to the phase of the diurnal anisotropy on quiet days where the value of Ap-index is lower on all the stations from 1965 to 71. Such a trend is not observable for the later period. This affect is found to be more pronounced on equatorial stations, in particular, in comparison to high latitude stations. It has been derived from these observational facts that the relationship between Ap-index and the phase of the diurnal anisotropy is not invariant throughout the period of consideration. Furthermore, the exact cause of such a drastic change is not known, but it demonstrates very clearly that the interplanetary conditions which are responsible for both, diurnal anisotropy of cosmic ray intensity and the geomagnetic Ap-index variation, have drastically changed during the period 1971 and onwards.

Key words: Ap-index, latitude, phase

☐ Theoretical ☐ Observational ☒ Both

Paper to be presented by : Dr.Santosh Kumar

Name and address for scientific correspondence :

Dr.Santosh Kumar
Department of Post Graduate Studies and
Research in Physics,
Rani Durgavati University,
Jabalpur (M.P.)- 482001 (INDIA)

SH 4.5-10

STUDY OF SPECTRAL EXPONENT ON QUIET AND DISTURBED DAYS

Santosh Kumar
Rani Durgavati University, Jabalpur.India.

ABSTRACT

The spectral exponents of the diurnal and semi-diurnal anisotropies are studied on quiet and disturbed days for a period from 1964 to 75. It has been observed for the diurnal anisotropy that the spectral exponent for quiet days is 0.0 from 1964 to 70, however during 1971 and onwards its value is found different from zero and is -0.4; for disturbed days the spectral exponent is observed to be 0.0 from 1964 to 75 with an exception of the year 1966. Further, it has been observed for the semi-diurnal anisotropy that the best value for the spectral exponent on quiet days being + 0.6 from 1964 to 74; however on disturbed days the value of spectral exponent is sometimes negative or positive but different from zero. It has been derived from the present investigation that superimposed on the corotational anisotropy, expected from a balance between outward radial convection and inward field alligned diffusion, there is an additional component operating during the period under consideration.

Key words: Spectral exponent, quiet days, diurnal, semi-diurnal

☐ Theoretical ☐ Observational ☒ Both

Paper to be presented by : Dr. Santosh Kumar

Name and address for scientific correspondence :

Dr.Santosh Kumar
Department of Post Graduate Studies and Research in Physics,
Rani Durgavati University,
Jabalpur (M.P.) - 482001 (INDIA)

SH 4.5-11

DIURNAL VARIATION OF GALACTIC COSMIC RAY INTENSITY ON QUIET DAYS

Santosh Kumar, S.C.Datt
Department of P.G.Studies & Research in Physics,
Rani Durgavati University, Jabalpur. India.

R.S.Yadav
Department of Physics, A.M.U., Aligarh. India.

S.P.Agrawal
Vikram Space Physics Centre, A.P.S. University, Rewa. India.

ABSTRACT

A detailed study of the diurnal variation on long term basis has been performed on geomagnetically quiet days using the experimental data of the cosmic ray intensity from the world-wide neutron monitoring stations. During the period when the polarity of the solar magnetic field in the northern hemisphere of the sun is negative the phase and amplitude of the diurnal anisotropy on quiet days has been observed to remain almost constant. When the polarity of solar magnetic field in northern hemisphere changes from negative to positive, a shift in the phase of the diurnal anisotropy on quiet days towards earlier hours is observed and the shift is found to be maximum during minimum solar activity periods 1953-54 and 1975-76. Further, when the polarity of solar magnetic field changes from positive to negative in the northern hemisphere of the sun the phase of the diurnal anisotropy on quiet days recovers to its usual direction of corotational anisotropy and is observed to remain almost constant till the polarity of the solar magnetic field does not change. Furthermore, during the period when the polarity of solar magnetic field in the northern hemisphere of the sun is negative the amplitude of the diurnal anisotropy on quiet days is observed to remain almost constant. And when the polarity of the solar magnetic field in the northern hemisphere of the sun changes from negative to positive the amplitude of the diurnal anisotropy on quiet days is observed to decrease quite significantly. The decrease in the amplitude of the diurnal anisotropy on quiet days is maximum during 1976. Further, when the polarity of the solar magnetic field changes from positive to negative the amplitude of the diurnal anisotropy on quiet days recovers to its usual value and is observed to remain almost constant.

1. Introduction. It has been shown (Kumar et al., 1981, and references therein) that daily geomagnetic index A_p correlates

well with both the diffusive as well as the convective components of the convection-diffusion theory. Also, this is a parameter which is least affected on quiet days in particular, evenwhen the days with abrupt fluctuations in IMF are quite frequent. This has led for the study of the diurnal variation of galactic cosmic ray intensity on quiet days on a long as well as short term basis.

2. Experimental Data and Analysis. The data of the neutron monitors for the stations, shown in figure-1, are used in the analysis. The data has been corrected for meteorological effects. The long term effects have been removed by the method of trend correction. Thus obtained magnetically most quiet days cosmic ray intensity data is subjected for the harmonic analysis and the average values of the amplitude,the phase of the first harmonic component of neutron intensity for different stations are obtained. Essentially, whole of the period has been divided into four parts- (i) before 1956 including 1953-54; (ii) after 1971 and earlier than 1978; (iii) after 1960 upto 1968 and (iv) 1981 and onwards. During the periods (i) and (ii) the polarity of the solar magnetic field in the northern hemisphere is positive, where as during the periods (iii) and (iv) the polarity of the solar magnetic field in the northern hemisphere is negative.

3. Results and Discussion. The long term plots of yearly average values of the geomagnetic disturbance index-A_p for the interval 1957-81 for all the days as well as for sixty most geomagnetic quiet days and sixty most geomagnetic disturbed days are represented in figure-2. It is apparent from the figure-2 that there is a marked variation in the plots for all days and disturbed days from year to year, particularly, for years of high sunspot activity. However, we noticed a very smooth and small variations for the quiet days which proves the importance of selecting most quiet days and in deriving the daily variations for these days only, to represent the long term or short term behaviour.

The interstation dispersion for the yearly average values for the magnetically most quiet days have already been plotted and shown (Kumar et al.,1981). It has been noted that the dispersion is small as compared to changes fron one year to another. This is found to be true even for the most recent period for which we have limited amount of data.

In this presentation we have used the data for Deep River neutron monitoring station for which the pressure corrected hourly cosmic ray intensity is available for an extended period of time. The average values derived for each year for the neutron monitoring station Deep River have been shown in figure-3 without making any correction for the effect of the geomagnetic field. Earlier[1]the vectors derived for different stations were corrected to derive the space vectors to facilitate comparison between different stations. The interstation agreement can not be judged by comparing the observed

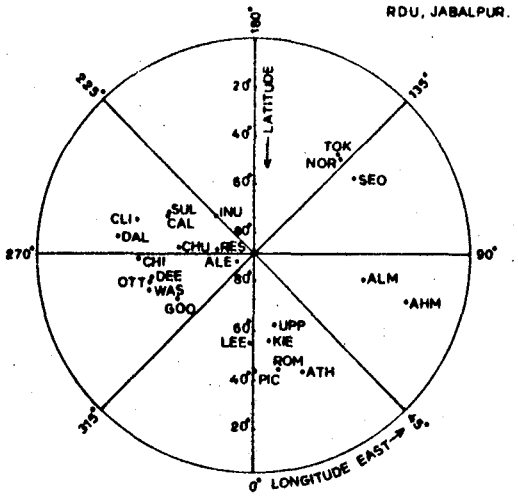

FIG. 1. ILLUSTRATES THE GEOGRAPHICAL LATITUDES AND LONGITUDES OF THE NEUTRON MONITORING STATIONS USED IN THE ANALYSIS.

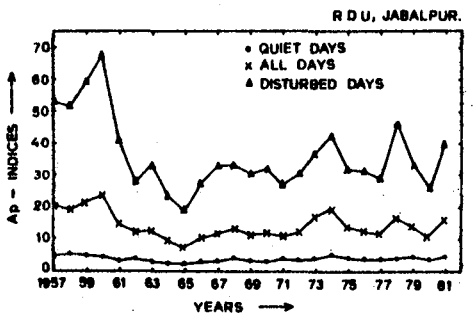

FIG. 2. VARIATION OF Ap-INDEX DURING THE PERIOD 1957-81 ON QUIET DAYS, ALL DAYS AND DISTURBED DAYS.

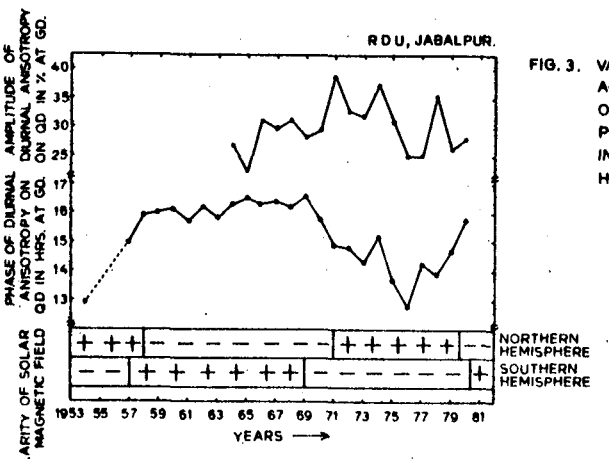

FIG. 3. VARIATION OF THE AMPLITUDE AND PHASE OF DIURNAL ANISOTROPY ON QUIET DAYS AT GROUND AND POLARITY OF SOLAR MAGNETIC FIELD IN NORTHERN AND SOUTHERN HEMISPHERES DURING DIFFERENT YEARS.

amplitude and phase in space because the geomagnetic corrections are different for different stations. So far, it is not clear that β and R_{max} are constant during period of 11-year or more, and hence the constant geomagnetic corrections generally applied on a long term basis is not very effective.

It is quite apparent from the figure-3 that during the period when the polarity of the solar magnetic field in the northern hemisphere of the sun is negative the phase and amplitude of the diurnal anisotropy on quiet days are almost constant. When the polarity of solar magnetic field in northern hemisphere changes from negative to positive, a shift in the phase of the diurnal anisotropy on quiet days towards earlier hours is observed and the shift is found to be maximum during minimum solar activity periods 1953-54 and 1975-76. Further, when the polarity of solar magnetic field changes from positive to negative in the northern hemisphere of the sun the phase of the diurnal anisotropy on quiet days recovers to its usual direction of corotational anisotropy and is observed to remain almost constant till the polarity of the solar magnetic field does not change.

Earlier results (Yadav and Badruddin, 1983) have indicated that on an average the two solar cycles when the northern hemisphere of the sun is dominated with negative polarity and when the northern hemisphere of the sun is dominated with the positive polarity, show different behaviour of diurnal anisotropy. This was done by considering all the 365 days in the year. We have considered the average of only magnetically most quiet days for the same interval (1964-68) and (1972-76) as well as for (1960-68) and (1972-78) to compare the effect of polarity reversal on diurnal anisotropy during magnetically most quiet days. Here again the vectors are drawn for the diurnal amplitude and phase observed at the station Deep River.

The results show that, in general, magnetically most quiet days are slightly more effective by the polarity reversal as compared to all days. The significance of magnetically most quiet days comes from the fact that these are least affected days due to disturbances in the interplanetary medium and hence are best suited for understanding the anisotropy on long as well as short term basis. It has been visualised further that if the similar trend exists, one should observe a steady variation in the diurnal amplitude and phase on magnetically most quiet days during 1981 and onwards till the polarity of the solar magnetic field in the northern hemisphere remains negative.

References

1. Kumar, S. et al., 1981, Proc. 17th Int.Conf.Cosmic Rays., France (Paris). pp.226-229.

2. Yadav, R.S. and Badruddin, 1983, Proc. 18th Int.Conf. Cosmic Rays, Bangalore (India) pp.366-369.

DIURNAL VARIATIONS FROM MUON DATA AT TAKEYAMA UNDERGROUND STATION

K.Takahashi, K.Imai, T.Imai, S.Kudo, and M.Wada
The Institute of Physical and Chemical Research
7-13 Kaga-1, Itabashi, Tokyo 173, Japan

ABSTRACT

An underground station, Takeyama, is introduced, and some results of the solar diurnal and semi-diurnal variations for the period between 1967 and 1984 are presented. There are clear tendency of double and single solar cycle variations in the daily variations which are in good accord with those detected by other underground and neutron monitor observations.

1. Introduction. Takeyama is the first Japanese underground station for the study of the time variations of cosmic ray intensity. The depth is 54 *mwe* which is equivalent to the median rigidity of primary cosmic rays around 200 GV. The geographic latitude and longitude are 35.22° N and 139.62° E, respectively. The continuous observation was started in September 1967. The operation was stopped in September 1981. It was restarted in June 1982. The area of detector has been increased from 9 m^2 to 16 m^2. The detector consists of 2 layers of 16 plastic scintillators, 1 m^2 each.

Since the station is situated a few tens km apart from the main laboratory, the memorized data are communicated through public telephone lines. The recording and communication modes are controled through the terminal computers set at both sites. The computer at the observation site can memorize one week data. The data are read out at the laboratory by the command. Generally the coincidence counts per hour of 256 combinations (16 × 16) are communicated. They are rearranged in the laboratory to get the counts of directional components, i.e., vertical and four azimuthal directions inclined around 30° from zenith. The observed counting rates are corrected for the pressure effect with the coefficient, -0.035 %/mb.

2. Daily variations. The yearly average solar diurnal and semi-diurnal variations are presented here. Figs.1a and 1b show the summation diagrams of the diurnal vectors of the vertical component, without and with the correction for Compton-Getting effect, respectively, for the earth's revolution around the sun. The correction values have been given by Prof. H.Ueno of Nagoya University. He has calculated them using the listed coupling coefficients (Fujimoto et al. 1984) for the variation spectrum which is flat upto essentially infinite rigidity. They are listed in Table 1.

It is clearly seen from the figures that the phases are earlier during the period from 1969 to 1980 compared with those after 1982. This tendency has already been pointed out by Swinson (1983) from his underground observations. There is a period, 1975-77, when virtually no diurnal variation is seen if Compton-Getting effect is concerned as Fig.1b. The phases of diurnal variations detected by neutron monitors are also relatively earlier in this period as seen in Fig.2. The level of cosmic ray intensity is highest and the variations are calm in the same period when the sunspot numbers are minimum.

Figs.3a and 3b show the vector diagrams of directional components for three year periods, 1978-80 and 1981-83, respectively. It is clear that the phases are later for the latter case as expected from those illustrated in Fig.1. Those results can be added on Ueno and others' "NAMS" analysis (1984) which utilizes the muon data from Nagoya, Misato, and Sakashita, and may become "NAMTS".

Fig.4 shows the summation diagram of solar semi-diurnal variation. The phases are nearly at 1.5 hour. There again some tendency of advancing the phases during the years in 1970's comparing with the periods before and after that.

Table 1. Correction values for Compton-Getting effect in percent. (after H.Ueno)

Axis	Vert.	North	East	South	West
0 hr	0.0073	0.0088	0.0227	0.0053	-0.0093
6 hr	0.0351	0.0232	0.0316	0.0422	0.0335

3. Summary. The underground observation at Takeyama is presented, with some information of the restart of observation with somewhat larger area than before. The solar diurnal and semi-diurnal variations are analyzed. The double solar cycle variation in the diurnal variation is seen. The diurnal variations in 1975-77 indicate the character of single solar cycle variation, for the period corresponds to the sunspot minimum years. Those double and single solar cycle variations are in good accord with those detected by the muon and neutron monitors.

The multi-component or multi-station analysis will give more information about the anisotropy in space. Further observation, at least until the next solar minimum with better quality, will result much complete conclusion of the analysis given above.

4. Acknowledgment. The earlier observation was performed by Prof. K.Murakami and others in the laboratory and the technical team in the Institute. The revised observation has been operated under the same members of the laboratory and of the technical workshop, specially K.Nishi and H.Kato. Prof. H.Ueno has provided us Compton-Getting values of Takeyama. We are grateful to them all.

References

Fujimoto,K., A.Inoue, K.Murakami, and K.Nagashima, (1984), *Coupling Coefficients of Cosmic Ray Daily Variations for Meson Telescopes*, Rep.Cosmic-Ray Res.Lab., CRRL., Nagoya Univ., Nagoya, Japan.

Swinson,D.B., (1983), *Long Term Change in the Solar Diurnal Variation of Cosmic Rays and Cosmic Ray Density Gradients at High Rigidities*, 18th ICRC, Bangalore, 10, 55-58.

Ueno,H., Z.Fujii, S.Mori, I.Morishita, and K.Nagashima, (1984), *Solar Diurnal Variations Observed at Nagoya, Misato, and Sakashita Stations (NAMS)*, Proc.Int.Symp.Cosmic Ray Mod.Heliosphere, Morioka, Iwate Univ. Japan, 109-113; and will be given in this conference.

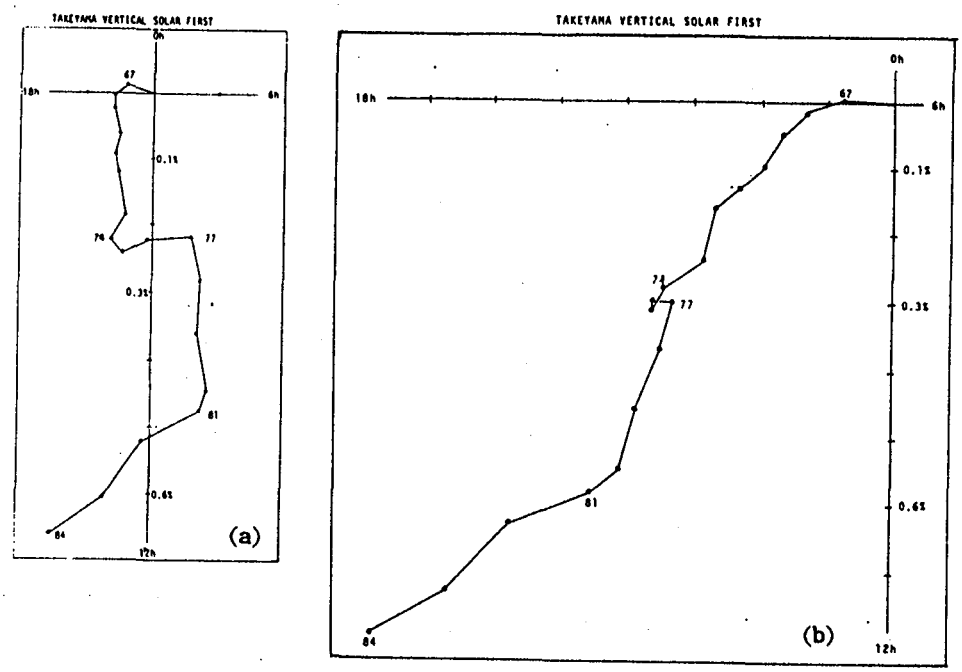

Fig.1. Summation diagrams of yearly solar diurnal variation, vertical component observed at Takeyama underground station from 1967 to 1984: (a): without, and (b): with the correction for Compton-Getting effect, respectively.

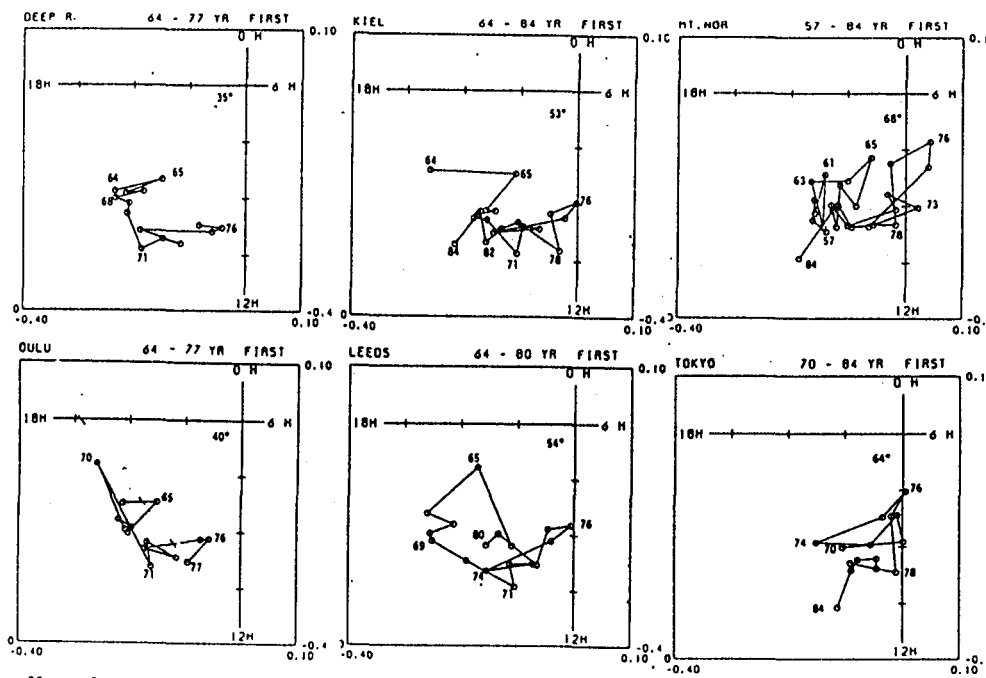

Fig.2. Yearly solar diurnal vectors of the neutron monitors. Each vector is drawn from the origin, and the lines connect the vectors to show the year to year changes. Notice the vector of 1976 which is at the upper right corner of the evolution in each graph.

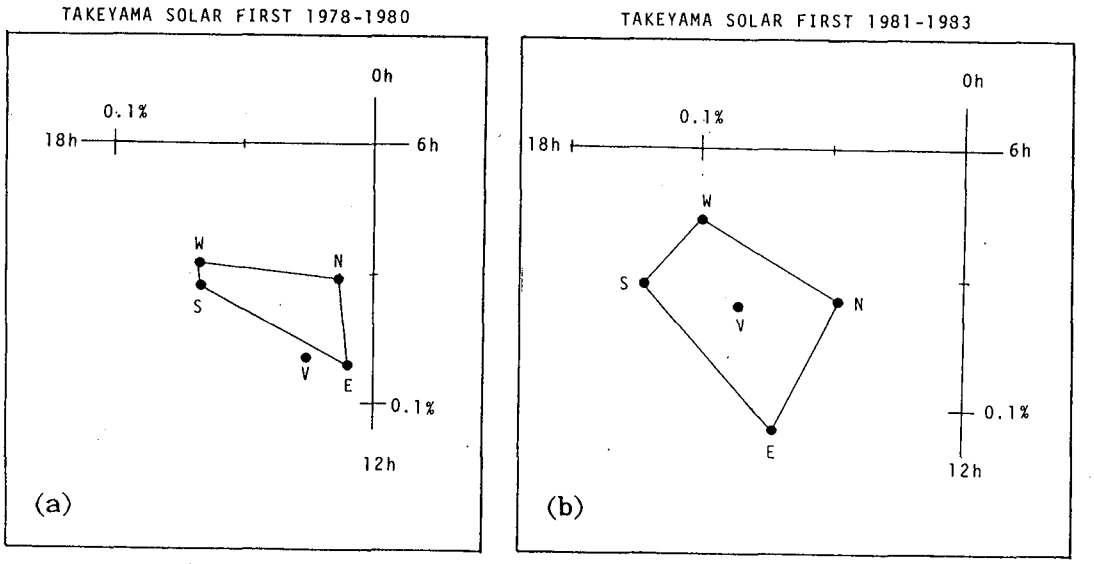

Fig.3. Solar diurnal vectors of directional components at Takeyama for the periods: (a): 1978-80, and (b): 1981-83, respectively.

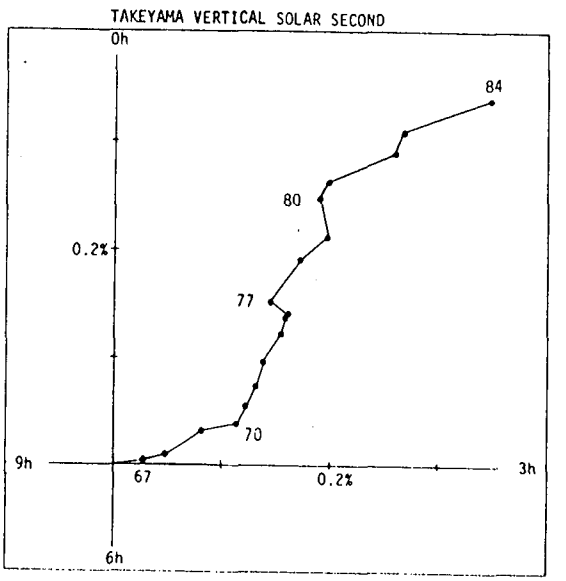

Fig.4. Summation diagrams of yearly solar semi-diurnal variation, vertical component at Takeyama for 1967-84.

SH 4.5-14

LONG TERM CHANGES IN COSMIC RAY DIURNAL VARIATIONS OBSERVED BY ION CHAMBERS IN HONG KONG AND JAPAN

L.S. Chuang, M. Kusunose*, and M. Wada**

Department of Physics, the Chinese University of Hong Kong, Shatin, New Territories, Hong Kong

* Department of Physics, Faculty of Science, Kochi University, 5-1 Akebono-2, Kochi 780, Japan

** Cosmic Ray Laboratory, Institute of Physical and Chemical Research, 7-13 Kaga-1, Itabashi-ku, Tokyo 173, Japan

ABSTRACT

Yearly average solar diurnal variations of cosmic ray ion chamber data are inspected from a view point of the eleven and the 22 year solar activity cycle modulations. The ion chamber data are from Tokyo for 1948-77, Mt. Norikura for 1958-77, and Hong Kong for 1970-83. Those of Carnegie Institution of Washington are also used. The neutron data from various stations are further added. From an inspection of observed data, we propose a simplest approximation that the 11 year and the 22 year variations of the solar diurnal variation are along 18-hour and 12-hour axes, respectively. The 18-hour component of diurnal variation in the 11 year cycle increases toward the solar active years. The 12-hour component is enhanced when the solar general magnetic field is parallel to the rotation vector, and is almost zero for the other state. The transition occurs when the amplitude of the 18-hour component is greater owing to the transition of the field during the maximum phase of solar activity. The 22 year shift is consistent with the drift modulation model in heliosphere. While the 11 year variation along the 18-hour axis is not interpreted yet.

1. Introduction. The present paper follows after the discovery of the 22 year variation in the phase of solar diurnal variation by Thambyahpillai and Elliot (1953), the invariant 18-hour anisotropy which is agreeable with the Axford-Parker theory (McCracken and Rao, 1965), and the two component analysis of the eleven and the 22 year variation in the diurnal variation by Forbush (1969).

Continuous observations of cosmic ray intensity by means of identical ion chambers have been started in 1948 at Tokyo, then Mt. Norikura, Sapporo (now stopped), Hong Kong, and Kochi. Though the observation accuracy is not so high as current muon telescopes and the neutron monitors, the data can be used as tools to inspect the diurnal variations in yearly basis for long time period.

If the deflection of the cosmic ray particles through the geomagnetic field, and the background diurnal variation due to, say, the

temperature effect are taken into account, the observed diurnal variation can be converted to the anisotropy detectable in space. The greatests of all the yearly average diurnal variations are the eleven year solar cycle variation and that related to the reversal of the solar general magnetic field at nearly the years of maximum activity which makes the 22 year variation.

Though there are fluctuations, from an inspection of the vector diagrams of diurnal variation, the eleven year and the 22 year variation can be separated into the amplitude variations along 18-hour and 12-hour axes, respectively. Such an approximation is given from a very rough idea, but the shift along 12-hour axis accords with the drift model of heliospheric modulation.

2. Display of the diurnal variations. Fig. 1 shows the vector diagram of the solar diurnal variation observed at Tokyo. Hong Kong data are added to extend the years. The data have only been corrected for the barometer effect. The broken lines indicate expected observations if the direction of anisotropy in space is 18 hour. The variation spectrum is assumed to be flat upto rigidity given in the figure. The values with % in the figure is the amplitude observable in space. If the diurnal variation due to the temperature effect is concerned, the origin of the observed vectors must be shifted, though the amount of shift can not reasonably be given, for the temperature diurnal variation is not known accurately. It can be allowed, however, the origin can be shifted so that the pattern becomes similar to those observed by the neutron monitors. The diagrams for other stations including those of the Carnegie Institution (Forbush, 1969) and of some neutron monitors are seen in the following Figs. 2-5.

3. Discussion. The hand writing drawing in Fig. 6 indicates our idea to interpret approximately the variations during 11 and 22 year periods. It can be shifted and rotated to fit the observed diagram of the anisotropy. There are appreciable scatter around the proposed simple variation, but one can see this kind of interpretation is possible. It is seen that the transition from different 12-hour states occur at around years of the reversal of the solar general magnetic field. This situation is understandable if the drift effect of modulation in heliosphere is concerned (Jokipii and Kopriva, 1979).

Kadokura and Nishida (1984) have simulated the anisotropy of cosmic rays in heliosphere putting the effect of drift as well as the diffusion through the interplanetary magnetic field (IMF) and Compton-Getting effect in the system of solar wind. They compared the results for different states of the solar general magnetic field which is parallel or anti-parallel to the rotation vector. The difference appears in the term of diffusion if restricted the position at the earth orbit. The anisotropy due to the diffusion is enhanced during the anti-parallel state. Since the diffusion is along IMF, the anisotropy is along 21-hour axis. That makes the 18-hour component greater than that of the other state. On the other hand, because of the enhancement of 0-hour component, the overall effect of the 12-hour component is almost canceled out, while that in the parallel state remains to be significant. It appears as the enhancement of the 12-hour component during the parallel state compared with that of the anti-parallel state.

As for the eleven year variation of the diurnal variation, though the observed variation is clearly seen, the model for that has not been fixed yet. One point which should be examined further is the distribution of the diurnal vectors in daily basis. While the average amplitude changes, at least two patterns can exist. The one is that the total distribution shifts without change in shape. The other is that the shape of distribution is distorted; for example, the frequencies at greater amplitudes increase compared with those at lower amplitudes. If the latter is a real case, there are various origins which enhance the amplitude during the solar active years. For example, the frequencies of occurrence of solar flares, Forbush decreases and so on are greater during the active years. Still, why the enhancement occurs along the 18-hour direction during the active years is an open question. We leave this problem for further studies

Fig.1. Observed yearly average diurnal vectors for ion chambers in Tokyo and Hong Kong. The broken lines indicate expected observations if the direction of anisotropy is 18 hour in space The spectrum is flat upto GV written inside. The % values correspond to the amplitude in space.

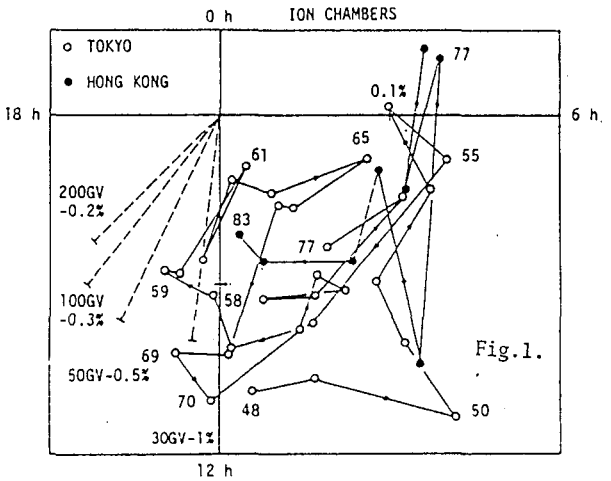

Figs.2-5. The same as Fig.1, but for ion chambers at Mt.Norikura, Huancayo, and Cheltenham (Forbush, 1969), and neutron monitor at Mt.Norikura (Kawasaki et al. 1983), respectively.

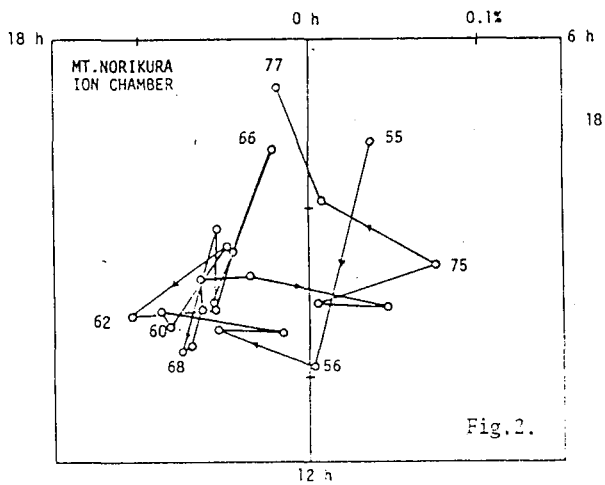

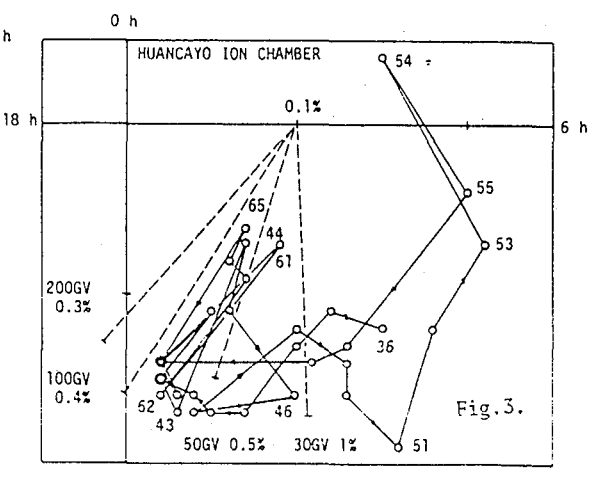

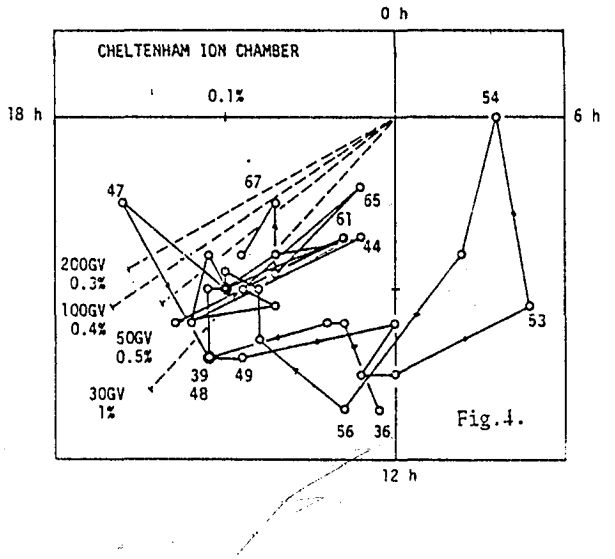

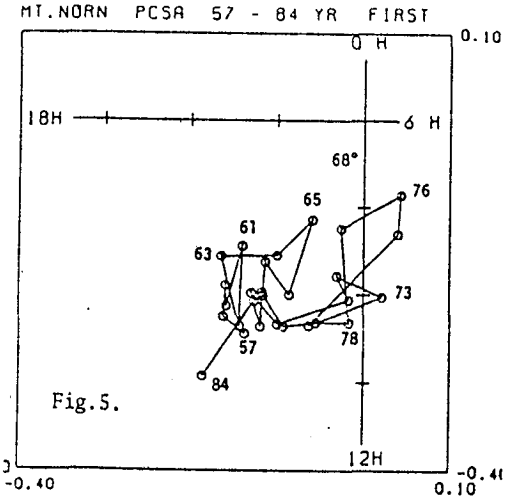

Fig.6. Simplest and approximate aspect of the 11 and the 22 year variations of the solar diurnal variation. See text.

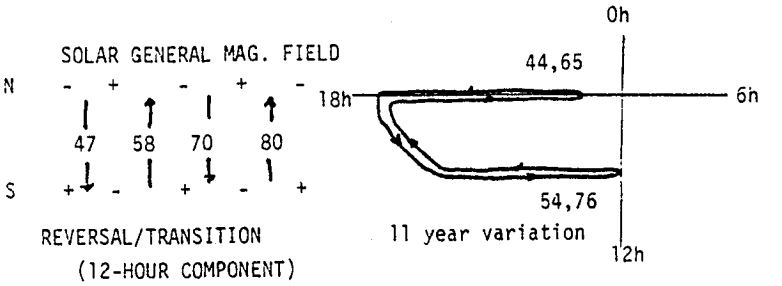

4. Acknowledgements. We are grateful to all the investigators who continued to operate and to process data for such long periods as shown here.

References

Forbush, S.E., (1969), Variation with a Period of Two Solar Cycles in the Cosmic-Ray Diurnal Anisotropy and the Superposed Variations Correlated with Magnetic Activity, J. Geophys. Res. 74, 3451-3468.

Jokipii, J.R. and Kopriva, D.A., (1979), Effects of Drift on the Transport of Cosmic Rays, III. Numerical Models of Galactic Cosmic-Ray Modulation, Astrophys. J. 234, 384-392.

Kadokura, A. and Nishida, A., (1984), private communication.

Kawasaki, S., Imai, K. and Wada, M., (1983), Cosmic-Ray Data at Mt. Norikura, Neutron Monitor 1968.9-1980.12, ICR-Report 109-83-03, Inst. Cosmic Ray Res. Univ. Tokyo.

McCracken, K.G. and Rao, U.R., (1965), A Survey of the Diurnal Anisotropy, Proc. Int. Conf. Cosmic Rays, London, 1, 213-218.

Thambyahpillai, T. and Elliot, H., (1953), World-Wide Change in the Phase of the Cosmic-Ray Solar Daily Variation, Nature, 171, 918-920.

THE MODULATION FEATURES OF THE LONG - PERIOD COSMIC RAY VARIATIONS IN CONNECTION WITH THE SING CHANGE OF THE GENERAL MAGNETIC FIELD OF THE SUN

Iskra K. Agriculture - Teacher University, Physics and Biophysics Dep. 08-110 Siedlce, ul. 3 Maja 54 POLAND

In the paper on the basis of the model and experimental investigations the spatial distribution of cosmic ray anisotropy for the different epochs of solar activity is studied.
A solution is offered to the anizotropic diffusion equation with regard to the electro-magnetic conditions for the periods of minimum and maximum solar activity and cosmic ray particle drift in a regular interplanetary magnetic field.
It is shown that the long-period changes amplitude and phase of the diurnal variations of cosmic rays is limited not only by convection and diffusion of particles but also by the drift effect before and after the sing change of the general magnetic field of the sun.
The calculated model is compared with the results obtained on the basis of an analysis of the experimental data from the neutron super-monitor station at Kiel, and it is shown that for the periods when the lines of magnetic force of the sun come from the northern hemisphere the phase of the first harmonic diurnal variation is shifted forwards to an earler time.
It can be argued that the 22-year change in the diurnal variation of cosmic rays is generally caused by cosmic-ray particle drift in a regular magnetic field.
The 22-year change of shift in the first harmonic diurnal variation is of 2-3 hours and the change of amplitude between twenty and thirty percent.

THE COSMIC RAY DIFFERENTIAL DIURNAL VARIATION DEPENDENCES ON THE ZENITH ANGLE AND THE GEOMAGNETIC DISTURBANCE

S. Kavlakov and L. Georgiev

INSTITUTE FOR NUCLEAR RESEARCH AND NUCLEAR ENERGY.
BULGARIAN ACADEMY OF SCIENCES. SOFIA 1784. BULGARIA.

1. INTRODUCTION.

Simultaneous and continuous muon measurements in two opposite azimuthal directions under equal zenith angles [1] demonstrated the importance of this method for cosmic ray diurnal variation investigations. Lately these measurements were extended by means of improved telescopes [2,3]. The obtained cosmic ray diurnal variations were presented as intensity differential curves.

Theoretical investigations [4] connected the properties of these curves with some interplanetary space parameters. The harmonics of these curves were interpreted [5] physically. Second order difference curves were introduced [6].

In our earlier works [7,8,9] some dependences between the parameters charachterizing the first and the second harmonics of the differential intensity curves and the geomagnetic activity were found. Then all measurements were carried out under only one zenith angle.

Here we presented the results of investigations of similar dependences using data of simultaneous measurements under three different zenith angles.

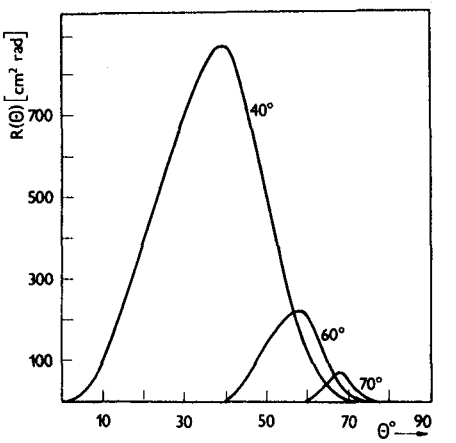

Fig. 1.

2. EXPERIMENT.

The measurements were carried out on p. Musala ($\varphi = 42^{\circ}11'N$; $\lambda = 23^{\circ}35'E$; $H = 2925$ m.a.s.l.) by means of a multidirectional counter telescope [10]. After the connection of a supplementary electronic circuit it became possible to measure simultaneously in the four cardinal azimuthal directions (East(E), West(W), North(N), South(S)) under three different zenith angles (40°; 60°; 70°) [11].

On fig. 1. are shown the zenith angle sensitivities for the telescopes inclined under 40°; 60°; 70°.

On fig. 2. are plotted in polar coordinates the azimuth angle sensitivities for all our 12 telescopes measuring simultaneously.

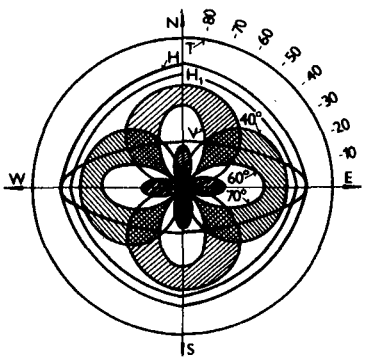

Fig. 2.

3. ASYMPTOTIC DIRECTIONS.

If the energy is sufficiently grate the particle's primery direction does not change when it moves through the earth megnetosphere. On fig. 3. the small circles present the asymptotic directions $(\vartheta_{E=\infty}, \lambda_{E=\infty})$ calculated following I12I for our telescopes and projected on the extended map of the Globe surface. There p. Musala is shown with a triangle.

The asymptotic directions for the same telescopes computed I13I for different lower energies are shown on the same figure as separate points. The points are connected with suitable curves for every one of the telescopes.

Because of the considerable width of the distributions of $R(\theta)$ and $P(\alpha)$ for the real telescopes, the points corresponding to all asymptotic direction projections for a certain energy cover a considerable area on the Globe surface. Then the curves plotted on fig. 3. form large strips.

It could be accepted that the differences of intensity data obtained simultaneously from two inclined telescopes, detecting under equal zenith angles in different azimuthal directions eliminate particles with energy below 18 - 20 GeV. So these differences are independent not only on meteorological changes, but on the changes in the low energy part of the cosmic ray spectrum.

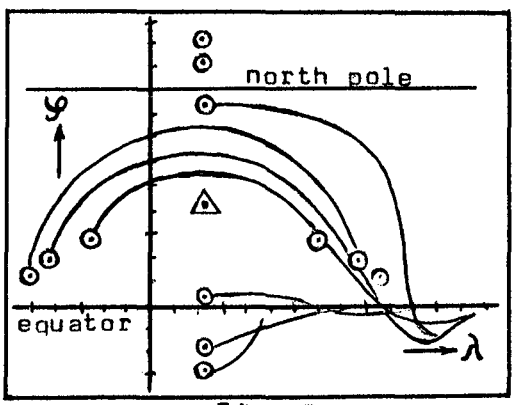

Fig. 3.

4. DATA TREATMENT.

From all the data obtained on p. Musala in the period June 1,1981 - April 30,1983 only "complete" data days were used. For these days all the 24 separate hourly measurements for all the 12 telescopes were available. From the measured hourly intensities for every separate day, for every separate zenith angle the following 8 differences were formed

I ordre: E - W; E - N; E - S; W - N; W - S; N - S;
II ordre: G = (N - S) - (E - N); K = (N - S) - (W - N).

To present the deviations in percentage arround a zero average the formula

$$(1) \quad (E-W)_{ij} = 2\,\frac{E_{ij} - W_{ij} - (\overline{E}_j - \overline{W}_j)}{\overline{E}_j + \overline{W}_j}\,100\,\%$$

was used. Here i (i = 1,2...24) was the index of the i-hour measurement in the j-day. $\overline{E}_j$ and $\overline{W}_j$ are the corresponding dayly averages. Analogically all other differences were formed.

To every one of the chosen days the indexes m and n were appropriate. So j = j(m,n). The index m charachterized the degree of the corresponding day magnetic activity. The values of m were chosen according I14I. The index n specified the continuity of the days arround the beginning of the magnetic storm.

The combinations between m and n are classified on table 1.

Table 1.

	quiet m = 0	weak m = 1	moderate m = 2	intense m = 3	strong m = 4	All for the row
PRECEDING n = -1	——	1,-1	2,-1	3,-1	4,-1	N =-1
BEGINNING n = 0	——	1, 0	2, 0	3, 0	4, 0	N = 0
FOLLOWING n = 1	——	1, 1	2, 1	3, 1	4, 1	N = 1
For the column	——	M = 1	M = 2	M = 3	M = 4	MN

For every one of the three zenith angles (40^0;60^0;70^0), for every one of the 21 index combinations (table 1.) the average diurnal variation of every one of the 8 differences was investigated. Fourier analysis was applied for every one of these 3 x 21 x 8 = 504 cases to compute the amplitudes A1; A2; A3 (in percents) and the phases t1; t2; t3 (in hours Local Solar Time (LST)) of the first (I), the second (II), and the third (III) harmonics.

5. RESULTS.

The first (I) and the second (II) harmonics for some of the computed differences for magnetically quiet days (m = 0), for the zenith angles 40^0,60^0,70^0 are presented on fig. 4. as vector-hourly diagrams. The phases of the first harmonics remain grouped arround 6 h.LST and the phases of the second harmonics - arround 9 h.LST. That is valid for all the three zenith angles and prctically for all other differences (not shown on the figure).

If these vectors are compared with those obtained 10 years ago on the same place, with the same apparatus (measureing then only under zenith angle of 60^0) it could be assumed that they are rather stable in time

The amplitudes A1 and A2 increase with the zenith angle. As an example that is shown for G on fig. 5.

The first harmonic amplitude dependences on the magnetic disturbance degree are shown for K on fig. 6. for the three zenith angles. This amplitude, as well as the amplitudes of the other differences (not shown on the figure) increases with m. The increase is rather faster for greater zenith angles.

An interesting phenomena - the first harmonic amplitude increase in the days preceding the beginning of the magnetic storm observed in our earlier investigation I9I for zenith angle 60^0,now is clearly expressed for all the three zenith angles (40^0,60^0,70^0). On fig. 7. are presented the changes of the first harmonic amplitude of the difference K in the days arround the beginning of the magnetic storm compared with its value during magnetically quiet days. If the statistical accuracy of the separate diurnal measurement is sufficient then after a sudden jump in the amplitude's value, some short time forcast for a forthcomming magnetic disturbance could be done. This dependence is not well expressed for the second amplitudes.

In our case the third harmonics are generally small and their changes are practically in the limits of the statistical accuracy.

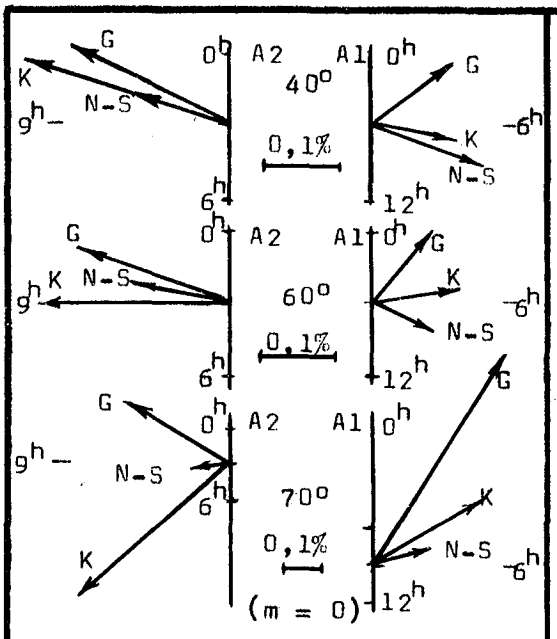

Fig. 4.

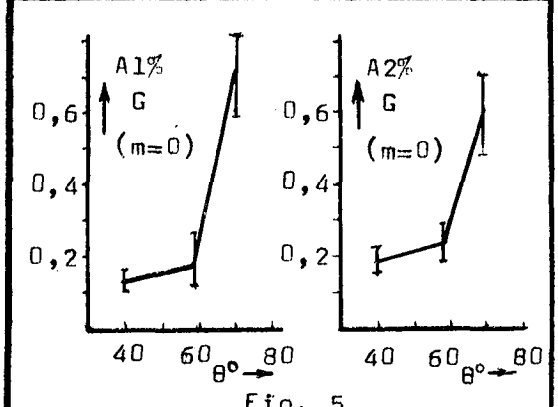

Fig. 5.

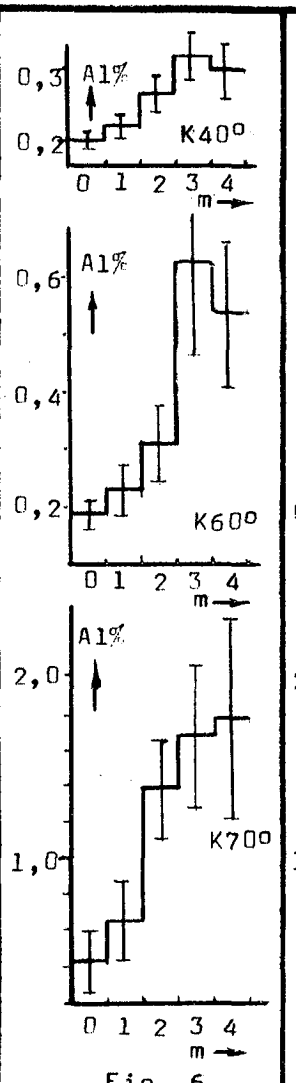

Fig. 6.

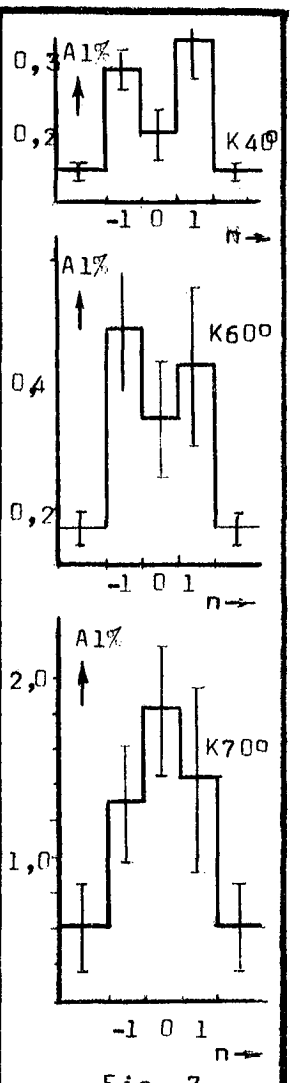

Fig. 7.

REFERENCES.

1. Kohlhörster W., Phys. Zs., 42 55 1941.
2. Elliot H., D. Dolbear, Proc. Phys. Soc., 63A 137 1950.
3. Sekido Y. et all. Multidirectional C.R.Intensity, Nagoya, 1975.
4. Nagashima K., Rep. Ionos. Space Res. Japan, 25/3 189 1971.
5. Nagashima K. et all.,Rep. Ionos. Space Res. Japan, 26/1 1 1972.
6. Kondo I. et all., Proc. 14 ICRC München, 4 1182 1975.
7. Kavlakov S., Izv. Acad. Nauk USSR (Physics), 40/3 607 1976.
8. Kavlakov S., Proc. ICR Symp., Tokyo, 285 1976.
9. Kavlakov S., Proc. 15 ICRC, Plovdiv, 4 82 1977.
10. Kavlakov S., Compt. Rend. Acad. Bulg. Sci. 18/8 731 1965.
11. Kavlakov S., Thesis, Sofia, 1977.
12. Kavlakov S. et all. Proc. 17 ICRC, Paris, 4 237 1981.
13. Shea M. A. and D. F. Smart, Tables, Private communication.
14. Cosmic Data (in rushan) Moscau, 1981, 1982, 1983.

SH 4.5- I7

COSMIC RAY DENSITY GRADIENT AND ITS DEPENDENCE ON THE NORTH-SOUTH ASYMMETRY IN SOLAR ACTIVITY

Badruddin, R.S.Yadav and N.R.Yadav
Space Science Group, Dept. of Phys., A.M.U., Aligarh (India).

ABSTRACT

An analysis of the diurnal anisotropy on geomanetically quiet days has been performed using neutron monitor data at Deep River($R_c \sim 1.02$GV), Leeds($R_c \sim 2.20$GV), Rome($R_c \sim 6.32$GV) and Tokyo ($R_c \sim 11.61$GV), well distributed in latitude and longitude for the period 1964-79. The days have been separated according to the polarity of IMF on that day. A significant difference in the amplitude and phase has been found on towards and away polarity days particularly during the years of high solar activity and large north-south asymmetry. These results (particularly time of maximum) on geomanetically quiet days show some better relationship to the expected results as compared to the results obtained using all the days in a year.

I. Introduction. The existence of perpendicular gradient has been studied by separating the cosmic ray diurnal vectors into groups corresponding to the direction of IMF. This method has been recently applied (Kananen et al. 1981; Swinson and Kananen, 1982) by using the neutron and meson monitor data for the period 1965-75. These authors have found that the amplitude of the diurnal anisotropy on away polarity days exceeds those of towards polarity days during year 1965-68 and that the reverse is generally the case after the reversal of sun's polar magnetic field in 1969-71. These data points to a cosmic ray gradient, perpendicular to the ecliptic plane, pointing southward prior to 1969 and there was some evidence about northward pointing gradient after the reversal of sun's polar magnetic field in 1969-71 except in 1974. However, the phase does not show the effect expected from the amplitude behaviour. They found no significant difference, in the amplitude and phase both, of the away and towards polarity days in 1969-71, at neutron monitor energies.

We found in our paper that on day-to-day basis the coherence for the cosmic ray anisotropy is better for days of low to average solar wind speed, which also is related to geomagnetically quiet days, and it would be more meaningful to use only these days for determining the annual average of the cosmic ray daily variation particularly for sunspot maximum activity period, during which one observed large number of cases of time varying isotropic changes in cosmic ray intensity. In this paper we have analysed the neutron monitor data for 1964-79 period for the stations mentioned above on magnetically most quiet days and determined the amplitude and phase for away and towards polarity days separately. On the basis of these results the perpendicular density gradient are discussed. Some indirect information about the three dimensional structure of the heliosphere especially current sheet has been inferred from these results.

2.Result. Fig.I shows that the amplitude on away polarity days is ,in general, higher than on towards polarity days during I964-68.But the phase on towards polarity days is higher than the away polarity days during this period.The difference in amplitude and phase on away & towards polarity days are more pronounced during the higher solar activity period I967 and I968.These results are in agreement with the results of the earlier workers(Hashimand Bercovitch,I972; Kananen et al.,I98I;Swinson &Kananen,I982).However the results of Kananen et al.(I98I) for the time of maximum does not show the right type of effect as expected.We found using the data from three neutron monitors, for geomanetically quiet days that the results for the time of maximum are also generally in agreement to that expected from the amplitude behaviour during I964-68,especially in I967 and I968.To give a better representation,we have plotted the average vectors for the period I964-68,separately on away and towards polarity days (Fig.2).

Kananen et al.(I98I) and Swinson & Kananen(I982) do not found any significant difference in the amplitude and phase on away and towards polarity days during I969-7I.Their results imply no density gradient (pointing northward or southward)during this period of reversal of sun's polar magnetic field.The solar activity was high and north-south asymmetry was also quite large(and positve)throughout the period I966-70(Badruddin et al.,I983).We see from Fig.I that the amplitude at Deep River and Leeds,which was higher for away polarity days than for towards polarity days during the year I964-68,changed to higher value for towards polarity days than away polarity days in I969 though at Rome similar change has been observed in I970.However,as far as phase is concerned,it has changed to later hours for towards polarity days than the away polarity days in I969 at all the three stations Deep River,Leeds,& Rome.In I970,the amplitude was much higher for towards polarity days than away polarity days and the time of maximum was quite significantly changed towards later hours for away polarity days than towards polarity days.These results are also shown on the vector diagram in Fig.2.In many earlier studies it has been assumed that the IMF in northern and southern hemispheres have reverse configurations in I964-68 and I969-79.The north-south asymmetry in solar activity in I969-70 was of the same sign(positive) as it was in I967-68.Thus if the current sheet was displaced downward due to positive north-south asymmetry in I967-68,it will be the same case in I969-70.But since the IMF polarity may be different in northern and southern hemispheres in I967-68 and I969-70,the reverse behaviour of diurnal amplitude and phase on away and towards polarity days in I967-68 and I969-70 may be due this reason. However,in I97I,when solar activity was lower as compared to I969 and I970 and north-south asymmetry was also small in this year,no significant difference in amplitude and time of maximum for towards and away polarity days is observed at

all the four stations(only the amplitude at Deep River shows some diffrence).Similar difference at Deep River was also reported by Swinson and Kananen (I982).

During the period I971, I972 and I973 there is some difference in the amplitude at towards and away polarity days only at Deep River.The average vectors for the period I97I-I973 have also been shown in Fig.2 for all the four stations.During these periods there was no marked north-south asymmetry as evidenced form solar flares.Swinson and Kananen (I982)did not found a consistent northward gradient at meson monitor energies during I97I-73, though their results point to a northward gradient in I972 and in I973 for Deep River and Oulu neutron monitors.

In I974 the amplitude on away polarity days is higher than the towards polarity days.Various arguments have been advanced to explain the observed amplitude and phase behaviour in I974(Swinson &Kananen,I982;Ahluwalia & Riker,I98I).It is to be mentioned here that the north-south asymmetry in solar activity was some-what negative as evidenced from solar flares and moreover in I973-75 the monster type solar wind straams were prominently observed.

In the solar activity minimum period I975-76, there is no appreciable difference in the amplitude and phase values for towards and away polarity days.The north-south asymmetry was also very small during these years.However, in I977,there is some evidence for a northward pointing gradient as seen from amplitude at Deep River and the amplitude and phase at Tokyo for towards and away polarity days.The solar activity in I977 was not high and north-south asymmetry was also small.However there was an accelerated increase in solar activity after mid-I977.

In I978 & I979 the solar activity was very high.However, the north-south asymmetry was small.We see from results for amplitude and phase on away and towards polarity days that there is no appreciable difference in amplitude and phase for the two types of days both at Deep River and Tokyo.

3.Conclusion. From the above results we see that there is an appreciable difference in the amplitude and/or phase on towards and away plarity days during years of high solar activity and large north-south asymmetry.During the years of lower solar activity and/or small north-south asymmetry this difference is not appreciable.These results support the view that at least during the period of high solar activity and appreciable north-south asymmetry,either the density gradient pointing away from the solar equatorial plane is not symmetric or the current sheet might have been displaced from the ecliptic plane.Thus it seems right to suggest(Swinson,I983) that in order to detect any $\vec{B} \times \vec{\nabla} N$ anisotropy the position of the current sheet(on average)would have to be displaced from the ecliptic plane due to asymmetric activity on the sun.

References

Ahluwalia,H.S.and Riker,J.F.,(I98I),I7th ICRC,IO,230.
Badruddin,Yadav,R.S.and Yadav,N.R.(I983),Ind.J.Radio Space,

Phys.,I2,I24.
Hashim,A.and Bercovitch,M.(I972),Planet.Space Sci.,20,79I.
Kananen,H.,Komari,H.,Tamskanen,P.and Oksman,J.,(I98I),
I7th ICRC,IO, I90 .
Swinson,D.B.and Kananen,H.,(I982),J.Geophys.Res.,87,I685.
Swinson,D.B.,(I983),I8th ICRC, IO, 55 .

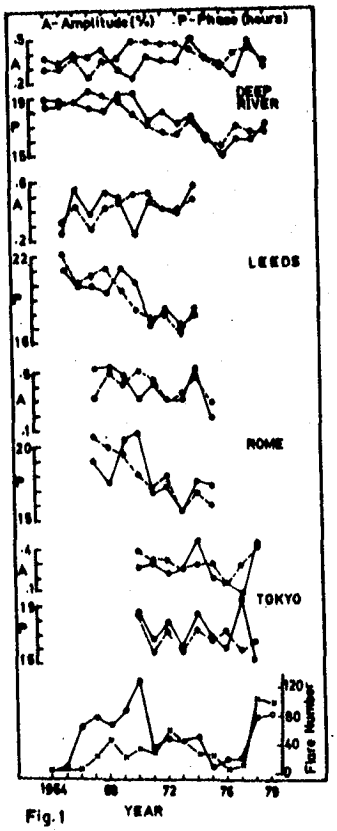

Fig.1

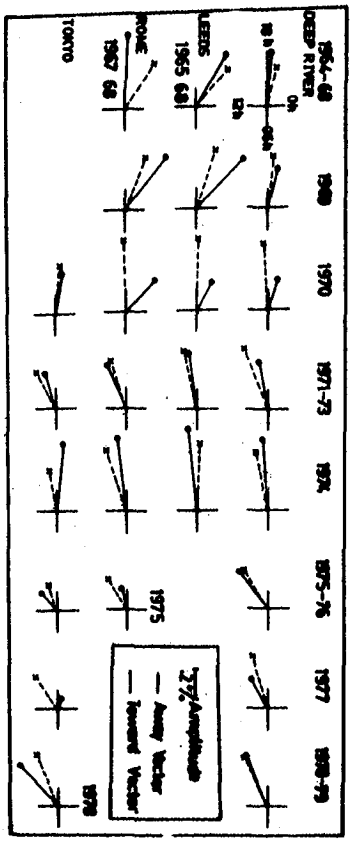

Fig.2

Fig.I shows average amplitude(A) and phase(P) of away polarity days(solid line) and towards polarity days(broken line)from I964-79.The diagram in the bottom shows the major solar flares numbers in respective years in northern(circle) and southern(crosses) hemispheres.
Fig.2 shows the average diurnal vectors on away polarity days(solid line)and towards polarity days(broken line) for the years and stations indicated.

Anomalous Increase of Solar Anisotropy above 150GV in 1981-1983

H.Ueno, Z.Fujii, S.Mori*, I.Morishita** and K.Nagashima
Cosmic Ray Res. Lab., Nagoya Univ., Nagoya 464, Japan
*Department of Physics, Shinshu Univ., Matsumoto 390, Japan
**Gifu College of Dentistry, Gifu 501-02, Japan

Abstract

An analysis was carried out of the observed data with Nagoya(surface), Misato(34mwe) and Sakashita(80mwe) multi-directional muon telescopes, for the solar activity maximum period of 1978-1983. These data respond to primaries extending over the median rigidity range 60GV to 600GV.

The observed amplitude at Sakashita station in 1981-1983 increased, especilly in 1982; the amplitude is twice as large as that in 1978-1980, when those at Nagoya and Misato stations are nearly the same as those in 1978-1980.

Uni-directional anisotropy is derived by the best fit method by assuming the flat rigidity spectrum with the upper cutoff rigidity Pu. The value of Pu obtained is 270GV in 1981-1983 and 150GV in 1978-1980.

1. Introduction

Earlier analyses (e.g., Rao et al.; 1963, Jacklyn et al.; 1970) have shown that the steady-state solar diurnal anisotropy of cosmic rays is rigidity independent up to the upper cutoff rigidity Pu which varies from 50GV to 100GV according to the characters of solar-controlled electromagnetic conditions in the heliomagnetosphere. So far, the obtained values of Pu were dependent on the rigidity range of the data used. To investigate the year-to-year changes of Pu, an analysis over a wide range of rigidities is most necessary during various levels of solar activity.

Since 1978, Sakashita underground multi-directional muon telescope has been in routine operation at the depth of 80mwe and 6-year data have been accumulated. The following observed fact is obtained that the amplitude increases for the period of 1981-1983, especially in 1982. This shows a very remarkable contrast to rather invariant variations at Nagoya and Misato for these years. On the other hand, the observed phases are gradually recover to the 18 hr direction from 1978 due to systematic changes by 22-year modulation.

In the present report, we try to derive the solar diurnal anisotropy responsible for the observed variations showing the above mentioned characteristics.

2. Data and Analysis

In the present analysis, the observed data from Nagoya, Misato and Sakashita stations are exclusively used, then these data are hereafter abbreviated as NAMS by picking up the top letter of these NAgoya, Misato and Sakashita stations. The observed variations are corrected for the Compton-Getting effect due to Earth's orbital motion (.046%,6hr in space), and the corrected variations are used as the basic data in the present analysis.

In Table 1, 3 year averages of the observed solar diurnal variations of NAMS are shown, together with some characteristics of the component

Table 1 NAMS solar diurnal variations corrected for Compton-Getting effect due to earth's orbital motion and the characteristics of NAMS telescopes. Errors in the amplitudes are determined by the dispersion of yearly vectors.

		Zenith & Azimuth		Geographic Direction		Median Rigidity	Counting Rate	3 Years Averages of Amplitude(%) & Phase(hr) of Solar 1st Harmonics	
STATION	TELESCOPE	Z	A	λ	ψ	$P_{ME(GV)}$	$\times 10^4$/hr	'78-'80	'81-'83
NAGOYA	V	0°	-	35°N	137°	60	276.0	.218±.035 12.0	.207±.014 13.3
0mwe	N	30°	0°	65°N	"	66	125.0	.204±.063 10.8	.189±.031 12.0
	E	"	90°	30°N	172°	67	120.0	.225±.072 10.6	.221±.034 11.9
	S	"	180°	5°N	137°	64	123.0	.214±.024 12.7	.212±.028 14.1
	W	"	270°	30°N	102°	63	126.0	.182±.016 13.3	.170±.030 14.8
MISATO	V	0°	-	36°N	138°	145	28.0	.136±.015 13.4	.145±.024 14.9
34mwe	N	33°	39°	57°N	177°	155	10.7	.131±.042 11.4	.152±.018 12.8
	E	"	129°	12°N	164°	143	14.2	.151±.032 12.3	.175±.018 13.9
	S	"	219°	9°N	117°	155	10.7	.124±.025 15.3	.157±.048 16.9
	W	"	309°	51°N	95°	156	9.8	.090±.010 14.5	.091±.012 15.9
SAKASHITA	V	0°	-	36°N	138°	331	39.0	.066±.015 14.2	.091±.013 15.8
80mwe	N	41°	346°	73°N	104°	401	6.2	.030±.026 12.8	.037±.015 15.6
	E	"	76°	35°N	188°	384	7.6	.064±.027 12.3	.086±.014 13.5
	S	"	166°	5°S	147°	387	6.7	.061±.014 14.8	.097±.015 15.7
	W	"	256°	18°N	96°	444	5.6	.046±.013 16.4	.068±.008 19.2
	NN	60°	346°	77°N	26°	595	2.4	.017±.028 12.4	.002±.031 6.9
	SS	"	166°	23°S	151°	540	2.7	.028±.011 14.0	.065±.029 16.1

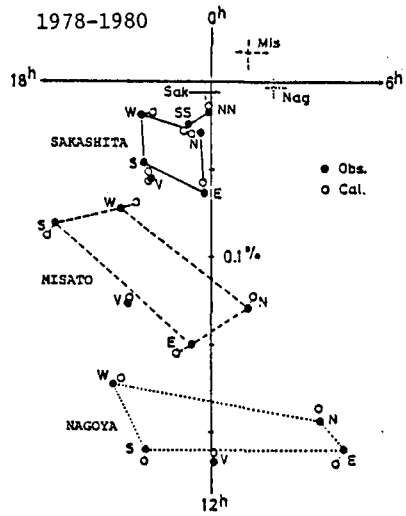

Fig.1(a)

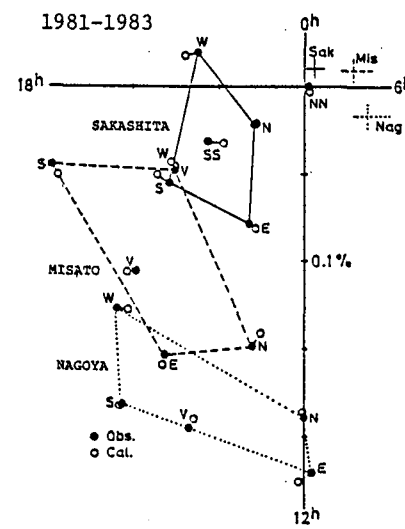

Fig.1(b)

Fig.1 Solar diurnal variation of NAMS in the period of 1978-1980 (Fig.1 a) and of 1981-1983(Fig.1 b).
Solid circles represent the vectors observed, and open circles are those reproduced from the best fit anisotropies. The three kind of cross are respectively the common vectors of each station calculated by the least squares method.

telescopes used and are plotted in Fig.1(a) for 1978-1980 and in 1(b) for 1981-1983 with dotted circles(•).

The solar diurnal anisotropy responsible for the observed variations was determined. Space harmonic vector(X,Y) responsible for the diurnal variation is related to the observed harmonic vector(a_{ij}, b_{ij}) of the j-th component telescope at the i-th station by the following equation with coupling coefficients c_{ij} and s_{ij}.

$$a_{ij} = (c_{ij}X + s_{ij}Y) + a_{ci}, \quad b_{ij} = (-s_{ij}X + c_{ij}Y) + b_{ci} \qquad (1)$$

where (a_{ci}, b_{ci}) represents the unknown vector common to all the components for i-th station. By the least squares method with equal weight for each component, the unknown quantities(X,Y) and (a_{ci}, b_{ci}) were determined for the flat rigidity spectrum with the upper cut-off rigidity Pu, which is taken every 10GV from 50GV to 200GV and so on. The coupling coefficients were referred to the table presented by Fujimoto et al. (1984).

Table 2 Best-fit quantities of anisotropy

	1978-1980	1981-1983
Amplitude in space	0.377 ± 0.016 %	0.320 ± 0.010 %
Direction of anisotropy	15.8 ± 0.2 hr	17.0 ± 0.1 hr
Upper cut-off rigidity	150 ± 10 GV	270 $\pm \frac{35}{20}$ GV

The best-fit parameters are obtained for two periods; 1978-1980 and 1981-1983 and these are shown in Table 2. Also in Figs. 1(a) and 1(b), the reproduced vectors for each component in the best fit case computed by eq.(1) are shown with open circles(○), where the cross marks (⋯, ⋯, ⊥) represent the common vector (a_{ci}, b_{ci}) for each station. As is shown in Figs. 1(a) and 1(b), a good agreement between the observed and the reproduced vectors is clearly seen, suggesting uni-directional anisotropy having the characteristics given in Table 2, is well consistent with the present observations.

Year-to-year basis calculation was also performed by the same method. Best-fit quantities

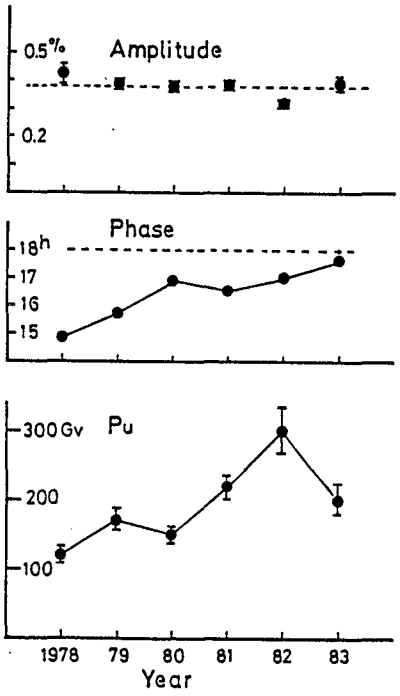

Fig.2 Year-to-year variations of the obtained amplitude, the phase and the upper cutoff rigidity of the solar diurnal anisotropy. Errors in P_U are replaced from the errors of the amplitudes of the anisotropy obtained by the least squares method.

of the anisotropy are shown in Fig.2 as a function of time from 1978 to 1983. As seen in the figure, the amplitude of the anisotropy remains invariant with time for these 6 years. The direction of the anisotropy gradually recovers to 18 hr level. The upper cutoff rigidity varies with time from 100GV to 300GV, particularly Pu in 1982 is extremely higher than those so far reported (Davies et al., 1977, Fenton et al., 1983).

3. Discussions

The increase of solar diurnal variation around 1982 has been observed at London(Thambyahpillai; 1983), Socorro(Swinson; 1983) and Takeyama (Wada et al.; 1985), by the underground muon telescopes at the depth deeper than 60mwe, where the amplitudes are nearly twice as large as in 1978-1980 similar to that at Sakashita station. The origin of the increase of Pu from 150GV to 300GV is yet unknown, but it may be considered to be due to some effect of strong solar activity or the influence of the field reversal resulted in the transition of the heliomagnetosphere from positive state to the negative.

Solar activity of the cycle 21 reaches its first maximum at the end of 1979 and increases again with the second maximum at about Sep. 1981. The cosmic ray intensity minima observed by neutron monitors which correspond to the solar activity maxima are in the middle of 1980 and much lower in July of 1982. In 22-years ago after the period of the maximum solar activity since the start of the cosmic ray observation and at the same phase of the field reversal as in 1981-1983, the cosmic ray neutron intensity had the double minima in Apr. 1958 and in July 1959. At that time, the solar diurnal variations did not increase at London(60mwe, Thambyahpillai et al.; 1965). These facts are very important for the interpretation of the increase of Pu and also for the study of the heliomagnetosphere.

4. Summary

1. The solar diurnal variations observed at Sakashita station remarkably increased in 1981-1983, especially 1982.
2. Uni-directional anisotropy is well consistent with the observed variations, the direction of which gradually recovers to 18 hr level from 1978 to 1983.
3. The upper cutoff rigidity is obtained as 300GV in 1982.

References

Davies S.T. et al., (1977) ICRC(Plovdiv), 4, 7.
Fenton A.G. et al., (1983) ICRC(Bangalore), 10, 186.
Fujimoto K. et al., (1984) Rep. CRRL, Nagoya Univ., No.9.
Jacklyn R.M. et al., (1970) Acta Physica Hungaricae, 39 Suppl. 2, 47.
Rao U.R. et al., (1963) J. Geophys. Res., 68, 345.
Swinson D.B., (1983) ICRC(Bangalore), 10, 55.
Thambyahpillai T. et al., (1965) ICRC(London), 1, 138.
Thambyahpillai T. et al., (1983) ICRC(Bangalore), 3, 383.
Wada M. et al., (1985) Private Communication.

DIAGNOSTIC OF ELECTROMAGNETIC CONDITIONS IN SPACE USING COSMIC RAYS

V.M.Dvornikov, V.E.Sdobnov, A.V.Sergeev

Siberian Institute of Terrestrial Magnetism, Ionosphere and Radio Wave Propagation, USSR Academy of Sciences, Irkutsk 33, P.O.Box 4, USSR

Abstract. The method of spectrographic global survey was used to study the time variations in parameters of cosmic ray (CR) pitch-angle anisotropy and their relationship with the variations of some solar wind characteristics under different electromagnetic conditions in interplanetary space. A classification is made of the conditions that are accompanied by the increase in CR anisotropy.

According to the new ideas, under development now, of the physics of modulational effects of cosmic rays (CR) in the heliosphere /1, 2/, the crucial influence upon the CR distribution function in interplanetary space is exerted by effects that are accumulated during a multiple rotation of particles in a Larmor circumference: drift motions, variations in pitch-angle due to an approximate conservation of the transverse adiabatic invariant and particle energy variations in regular fields of solar wind (SW).

The development of these ideas has been stimulated by the obtained phenomena of strong pitch-angle anisotropy of CR during Forbush-effects /3/ whose explanation in terms of a convection-diffusion model /4/ renders itself impossible.

In the context of the model under development, strong pitch-angle CR anisotropy is a reflection of structural features of large-scale fields in interplanetary space due to dynamical processes in the heliosphere, i.e. it is some kind of an indicator of these processes.

The aim of the present work is to study the time variations in parameters of CR pitch-angle anisotropy and their relationships with the variations in some SW characteristics under different electromagnetic conditions in interplanetary space. The analysis has been carried out using the method of spectrographic global survey (SGS) that has been devised using the physics, under development now, of CR modulational effects in the heliosphere, according to which the variations in particle flux density in interplanetary space can be described by a function of the form

$$\frac{\delta J}{J}(R,\Psi,\lambda) = \sum_{n=0}^{N}\Big(\sum_{k=1}^{m_n} a_{nk} R^{-k}\Big) P_n(\mu) =$$

$$= \sum_{n=0}^{N}\Big(\sum_{k=1}^{m_n} a_{nk} R^{-k}\Big)\Big[P_n(\sin\lambda)\,P_n(\sin\lambda_0) +$$

$$+ 2\sum_{m=1}^{n}\frac{(n-m)!}{(n+m)!}\,P_n^m(\sin\lambda)\,P_n^m(\sin\lambda_0)\cos m(\Psi-\Psi_0)$$

Here $\mu = \cos\theta$, θ is the pitch-angle of a particle in

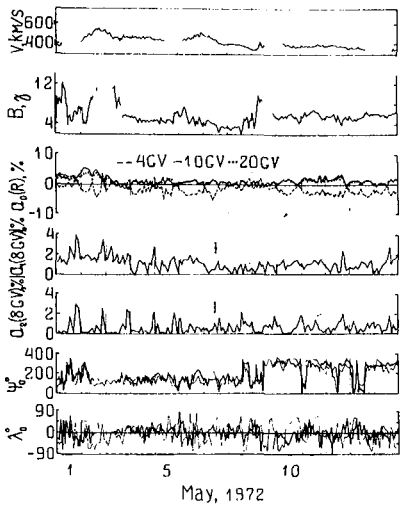

Fig. 1

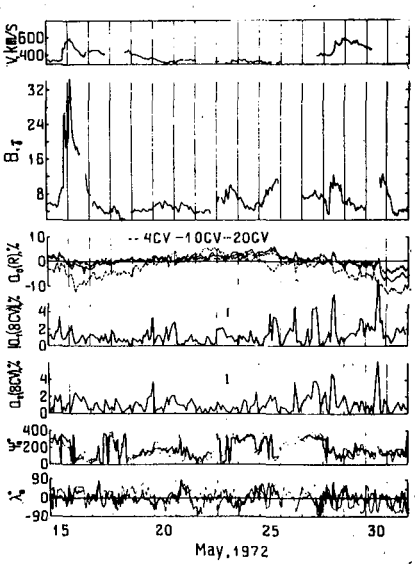

Fig. 2

the IMF, R is the magnetic rigidity of the particles, $P_n(\mu)$ and $P_n^m(\sin\lambda)$ are polynomials and associated Legendre polynomials, ψ and λ are asymptotic angles that determine the direction of the particles outside the magnetosphere in some selected system of coordinates, ψ_0 and λ_0 are the angles that characterize the direction of the IMF vector in this same system, and a_{nk} are the parameters characterizing the amplitudes and rigidity dependences of the isotropic component, and of the first and second harmonics of CR pitch-angle anisotropy. The SGS method makes it possible to determine using ground-based CR observations from the world-wide network of stations, the parameters a_{nk}, ψ_0, and λ_0 (accurate to within π) as well as the variations of the planetary system of geomagnetic cut-off rigidities for each hour of the observations.

The SGS method was used to analyze the variations of the CR distribution function for the periods 1 May through 30 June and 1 through 15 August 1972. The analysis results as well as direct measurements of SW characteristics are presented in Figs 1-5 in the following order (from top to bottom); V - SW velocity, B - IMF modulus; $a_0(R)$-amplitudes of the isotropic component of CR intensity variations for particles of different rigidity; a_1(8GV) and a_2(8GV) are respectively the amplitudes of the first and second harmonics of CR pitch-angle distribution (for R = 8 GV); and ψ_0, λ_0-angles characterising the IMF direction (heavy lines - direct measurements /5/, thin lines - CR data); in addition, Fig. 4 shows the variations in geomagnetic cut-off rigidity ΔR_c at Irkutsk, determined from CR variations, and D_{st} - index).

The comparison between the variations in CR pitch-angle anisotropy and SW characteristics has led to the following classification of the events accompanied by the increase in CR anisotropy of the type considered:

1. Anisotropy increases during powerful SW disturbances (see Figs 2, 4, and 5). During the growth phase of the IMF modulus, the amplitude of the first harmonic ($a_1 \gtrsim 3\%$) increases while during the declining phase, the amplitude of the second harmonic does ($a_2 \gtrsim 3\%$). A minimum flux density of

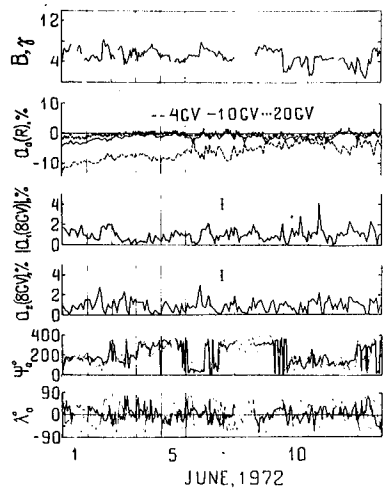

Fig. 3

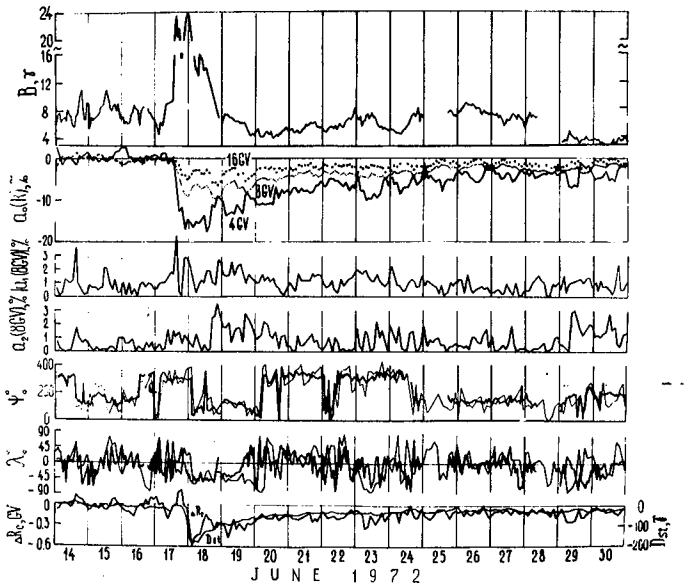

Fig. 4

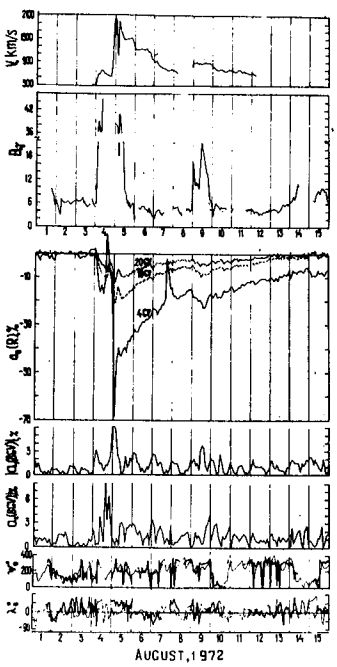

Fig. 5

flow is observed for particles with large pitch-angles. A likely reason might be the influence upon the CR angle distribution of large-scale magnetic traps that form in interplanetary space at propagation of high-speed solar wind streams.

II. Anisotropy increases at places of local decreases in IMF strength (a_1 and $a_2 \sim 2\%$). The character of pitch-angle distribution is the same as for type I events. The likely reason might be trapping and deceleration of particles with large pitch-angles in the traps between the maxima of a random field.

III. Anisotropy increases at places of local increases in IMF strength accompanied by an increase in flux density by 5-15% from some selected direction. In the opposite direction, throughout the entire hemisphere the intensity remains unaltered and is almost independent of the CR direction. This type of anisotropy was observed during 25 to 30 May 1972 (see Fig. 2), with a maximum of the flux density from directions 120-150° westward of the Earth-Sun line and 50-70° southward of the helioequatorial plane. A likely cause of the observed anisotropy may be IMF structures arising as the azimuthal and meridional components of the magnetic field are carried away from the corona. In this case, arrival of CR along the IMF flux tubes is possible from interplanetary space regions (for example, from middle heliolatitudes) where the CR density exceeds significantly the observed density in the helioequatorial region.

IV. Recurrent double enhancements of pitch-angle anisotropy were found assuming that geoeffective regions on the Sun have their mappings in the IMF structure corresponding to their structures. In this connection, an attempt was made to trace, using CR, from rotation to rotation the development of processes in the heliosphere prior to some geoeffective phenomenon with the aim to find distinctive features of the active region that is responsible for a given event. As the object of study, we selected one of the events of most geoeffective interest, the solar proton flares.

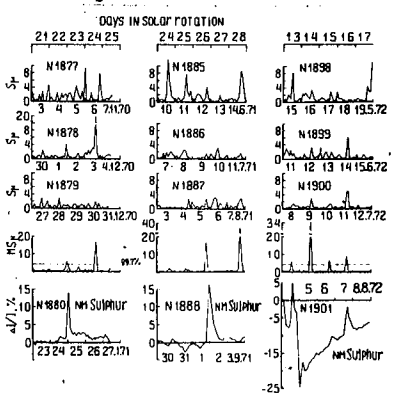

Fig. 6

The SGS method was used to analyze the fluctuations of CR pitch-angle anisotropy in three solar rotations preceding four powerful solar CR enhancements (outbursts) in 1971 and'72.

In order to simplify the analysis we introduced two indices, S_μ and MS_μ. The S_μ-index defines the amplitude of pitch-angle anisotropy at time t_i of the observation; it is calculated in the following way

$$S_\mu(t_i) = \int_R \int_\mu \left\{ \frac{\partial}{\partial \mu} \left[\frac{\delta J}{J}(t_i, R, \mu) \right] \right\}^2 dR\, d\mu$$

We used as the indicator of the recurrent event the multiplicative index $MS_\mu(t_i) = \prod_{k=0}^{2} S_\mu(t_i + k\tau)$, where τ is the period of solar rotation.

The analysis (see Fig. 6) revealed that three or four rotations before the onset of a solar proton event (SPE), two comparatively narrow recurrent IMF structures spaced by 15-30° in heliolongitude and causing recurrent double outbursts of CR pitch-angle anisotropy, form in interplanetary space. The character of pitch-angle distribution of the particles at these moments is the same as for type III events.

The four SCR outbursts were all observed on the ground at moments of passage through one of the detected structures. The fact that these structures are identifiable using CR pitch-angle anisotropy in solar rotations preceding SPE can be used for long-term prediction of regions of localization of radiation-dangerous zones in interplanetary space and of times when the Earth enters these zones.

REFERENCES

1. V.M.Dvornikov, Yu.G.Matyukhin, 1976, Izv.AN SSSR, ser.fiz. 40, 624.
2. V.M.Dvornikov, Yu.G.Matyukhin, Izv.AN SSSR, ser.fiz. 43, 2573.
3. V.M.Dvornikov, V.P.Karpov, A.V.Sergeev, 1978, Izv.AN SSSR, ser.fiz., 42, 1043.
4. E.N.Parker. "Dynamical Processes in the Interplanetary Medium", Moscow, Mir, 1965, 216.
5. J.H.King, 1977, Interplanetary Medium Data Book, NSSD C/H--C4.

CHANGE OF COSMIC RAY ANISOTROPY WITH SOLAR ACTIVITY

N.G.Kravtsov, P.A.Krivoshapkin, A.I.Kuzmin,
G.V.Skripin, I.A.Transky, G.V.Shafer

Institute of Cosmophysical Research & Aeronomy
Lenin Ave., 31, 677891 Yakutsk, USSR

ABSTRACT

Muon telescope data at various depths underground in Yakutsk within energy range 10-300 GeV for 1957-1984 are analyzed. 22-year variation of the interplanetary magnetic field aligned component is found. The variation is caused by interaction of heliomagnetosphere with the local galactic field and interstellar wind.

In [1,2] was convincingly shown the existence of 22-year variation of cosmic ray anisotropy aligned with the interplanetary magnetic field. Unfortunately, there are no reliable results on data of ground and underground registration during the end of the 20-th and the beginning of the 21-st solar activity cycle which confirm the result of [1,2].

Here we investigate the long-term variations of cosmic ray anisotropy for 1937-1984 and define the energy range at which the variation is observed. For the analysis were used the Fourier components of mean annual diurnal variation of muon intensity on data of ionization chambers at Cheltenham, Huancayo (1937-1972) and at Yakutsk (1954-1983) and muon telescopes of the Yakutsk underground complex at depths 0, 7, 20 and 60 m w.e. (1958-1984). Data are pressure corrected. To estimate the contribution of the atmospheric temperature into the observed diurnal variation on data of ionization chambers we used the indirect methods. Firstly, we supposed the mean-annual total vector of diurnal temperature fluctuations on the whole depth of atmosphere is practically invariable, at least, for 22 years. In this case the difference vector of the cosmic ray diurnal variation $\Delta \vec{r}_i = \vec{r}_i - \vec{r}_{aver}$ ($\vec{r}_i$ is the observed vector of the diurnal variation for i-year, $\vec{r}_{aver}$ is the average vector for 22 years) is of extra-atmospheric origin.

The observed vector for 1951-1972 at Huancayo and Cheltenham and for 1954-1975 at Yakutsk as $\vec{r}_{aver}$ was taken. We calculated the receiving vectors of the diurnal variation for various mechanism of formation of the cosmic ray anisotropy. In the given case the receiving vectors were

used: for Huancayo $z = 0.80e^{-i\cdot 51^\circ}$, for Cheltenham $z = 0.82\ e^{-i\cdot 31^\circ}$; for Yakutsk $z = 0.72\ e^{-i\cdot 31^\circ}$. Secondary, one of the reliable methods of exclusion of the temperature effect is the crossed telescope method which allows to obtain the absolute anisotropy value. In the Table are presented the amplitude and the maximum time of primary anisotropy for 1958-1980 obtained on difference of telescope readings directed southward and northward at an angle 30° relative to vertical at depths 0, 7, 20 and 60 m w.e.

m w.e.	0	7	20	60
Amp., %	0.194±0.008	0.149±0.006	0.118±0.005	0.050±0.009
t_{max}, h	16.0±0.1	15.4±0.2	16.1±0.2	14.8±0.7

It is clear from the Table that at all the levels the maximum time differs significantly from 18^h.

Then we consider the problem on the separation of 11- and 22-year variations of the cosmic ray anisotropy. Two versions of decomposition of the primary anisotropy vector into two components on clock-dial were considered: the first version - into components along $9\text{-}21^h$ and $6\text{-}18^h$ lines (in Figures 1 and 2 the open circles), the second version - along $9\text{-}21^h$ line and the line of anisotropy maximum time for 22 years (the Table and closed circles in Figures 1,2).

In Fig.1 and 2 the ionization chamber data for 1937-1953 are for Huancayo and Cheltenham stations and for 1954-1983 are for ASK-1 Yakutsk. The statistical accuracy of determination of anisotropy components for the first period is ±0.01%, for the second one is ±0.004%.

In Fig.1 the 22-year cosmic ray anisotropy variation is shown. As seen from the Fig.1 it is observed at all the registration levels except 60 m w.e. At the 20 m w.e. depth where the effective energy of registered patricles is ~ 70 GeV, its amplitude is 0.05%.

Note that in the case of the first version of decomposition the point scattering increases. More pronounced variation is observed at a longer set of data of ionization chambers. The magnetic field of the northern solar hemisphere (a dashed line in Fig.1) which was estimated on a number of polar faculaes [3] evidences the negative correlation with 22-year anisotropy variation along the $9\text{-}21^h$ line. When the interplanetary magnetic field being in the north part of the ecliptic is directed from the Sun the cosmic ray anisotropy is field-aligned to the Sun. If in the same region the field sign changes to opposite then the anisotropy will be directed field-aligned from the Sun. At the moment of

sign-change of general magnetic field of the Sun the 22-year wave in Fig.1 crosses the zero line. It is clear from Fig.2 that the 11-year cosmic ray anisotropy variation is observed as well at all the depths which is probably caused by the decrease of regularity degree of the interplanetary magnetic field at solar activity minima. From the Table it follows that the maximum time of anisotropy caused by convective-diffusive process for 23 observation years is $15\text{-}16^h$. It means that the inhomogeneous solar wind is of a flattened form.

The obtained temporal change of the galactic cosmic ray anisotropy can be caused by the peculiarities of interaction of the heliomagnetosphere with the local interstellar magnetic field. It is known that the local galactic magnetic field (Orion's arm field) is oriented in the direction of solar apex ($\alpha = 20°$, $\delta = 35°$) and the speed vector of the interstellar wind ($\sim$ 20 km/s) lies in the plane of the ecliptic at the angle 53° with respect to the direction of the field (see references in [4]).

In [5,6] a model of opened and closed configurations of the heliosphere was proposed. The opened heliosphere is formed if the solar magnetic field in the northern hemisphere is derected outward, the closed one - at the opposite field orientation. In the first case the galactic cosmic rays penetrate into the heliosphere along force lines in polar regions, in the second case the penetration occurs by a diffusion way.

In the given here model it is not taken into account that the solar wind speed increases while moving away from the solar equator [7] and the magnetic field in heliosphere polar regions forms a structure of magnetic cork type. Therefore even in the case of the "opened" heliosphere the galactic cosmic rays penetrate mainly by a diffusive way. Besides, particle transfer within the inner part of the heliosphere from high latitudes to low ones is rather slow due to a small ratio of perpendicular diffusion coefficient to the parallel one ($D_\perp/D_\parallel \ll 1$). On the whole the approach to be solution of considered problem can be retained if to assume that at the opened configuration the local galactic field and the heliosphere field under interaction dissipate in a restricted narrow layer enveloping the part of the heliosphere where the interstellar wind blows. The energy of magnetic fields passes to the plasma of the interaction region and spreads along force lines [8] .

Thus in the case of the opened heliosphere an additional diffusion outflow of particles from the heliosphere in the plane of ecliptic can be formed which compensates the wind speed increase at high latitudes. Due to the condition $D_\perp/D_\parallel \ll 1$ the additional current for particles, at least, at 20 m w.e. will be directed along force lines, mainly. At the opposite orientation of the magnetic field

of the heliosphere the supersonic interstellar wind causes the field increase (beyond the region of a possible heliomagnetosphere "tail") and therefore some excess of cosmic rays. It leads, in its turn, to the increase of the diffusive stream of cosmic rays directed inside the heliosphere.

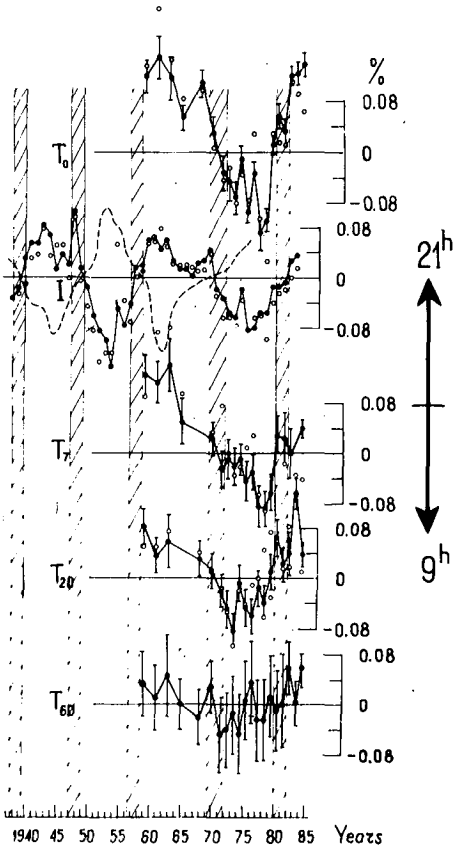

Fig.1. 22-year variation of cosmic ray anisotropy. T_o, T_7, T_{20}, T_{60} are muon telescope data at the 0, 7, 20 and 60 m w.e., I is ionization chamber data. Dashed line - magneric field of northern hemisphere of the Sun

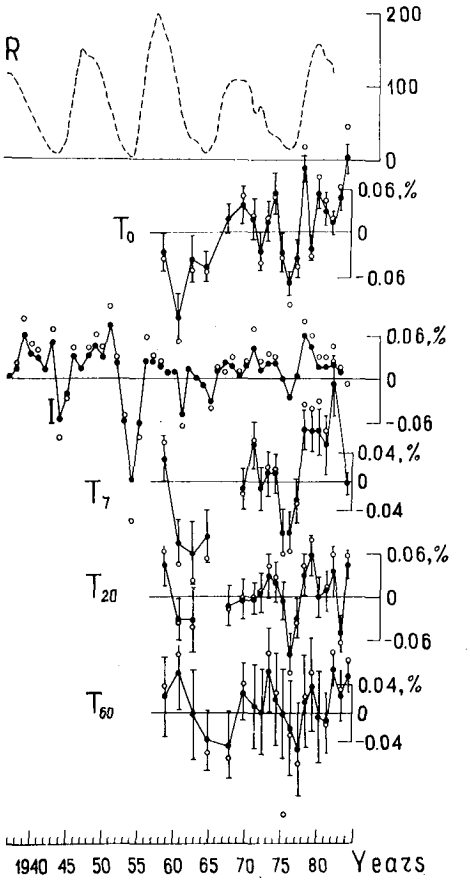

Fig.2. 11-year variation of cosmic ray anisotropy. R is solar activity (sunspot numbers). I, T_o, T_7, T_{20}, T_{60} the same as in Fig.1

References

1. Forbush, S.E., (1969) J.Geophys.Res., 74, 3451.
2. Forbush, S.E., (1972) J.Geophys.Res., 78, 7933.
3. Sheeley, N.R., Jr., (1976) J.Geophys.Res., 81, 3462.
4. Baranov, V.B., Lebedev M.G. et al., (1979) Astrophys.Space Sci., 66, 429.
5. Shatten, K.H., Wilcox J., (1969) J.Geophys.Res., 74, 4157.
6. Ahluwalia, H.S., (1979) Proc.16-th ICRC, Kyoto, 12, 216.
7. Efimov, A.I., Lotova, N.A., (1975) Kosmich.issled., 13, 603.
8. Parker, E.N. Kosmicheskiye magn.polya, I, (1982) M.:Mir.

MAGNETIC FLUCTUATIONS AND COSMIC RAY DIURNAL VARIATIONS

J. W. Bieber and M. A. Pomerantz
Bartol Research Foundation of The Franklin Institute
University of Delaware, Newark, Delaware 19716

ABSTRACT

A unified theory of cosmic ray diurnal variations has been proposed in which the first 3 harmonics of the cosmic ray daily variation all result from a single anisotropy produced by the combined effects of adiabatic focusing and anisotropic pitch angle scattering. The purpose of the present report is twofold: (1) to simplify and improve the theoretical description of steady-state cosmic ray anisotropies, and (2) to present and discuss, in light of the theory, preliminary results of a study of correlations between cosmic ray diurnal variations and the fluctuation characteristics of the interplanetary magnetic field.

1. Theory. Several theoretical investigations of energetic particle anisotropies (Roelof, 1969; Kunstmann, 1979; Earl, 1981) suggest that observed anisotropies may appropriately be cast in the form of a simple analytic solution of the steady-state Boltzmann equation, which, according to Earl (1981), is given by

$$f = c_0 + c_1 B \exp\left\{\frac{(4-q)\lambda}{3L}\,\mu\,|\mu|^{1-q}\right\}. \qquad (1)$$

Here, f is the phase space density, c_0 and c_1 are constants, B is the magnetic field magnitude, q is a parameter characterizing the anisotropy of pitch angle scattering, λ is the scattering mean free path, L is the focusing length (~ 0.94 AU for the nominal Parker field at Earth), and μ is the cosine of the particle pitch angle. The property of (1) relevant to the present work is that it has a non-sinusoidal form, and hence will naturally contribute higher order harmonics to the cosmic ray daily variation observed by ground-based instrumentation.

For reasons connected with geomagnetic correction of neutron monitor observations (Yasue et al., 1982), it is convenient to express the free space anisotropy as a Legendre series. Figure 1 shows the relationship between the parameters λ/L and q and the coefficients a_i of the Legendre expansion of (1). Note that a measurement of the 3 coefficients a_1, a_2, and a_3 serves to determine uniquely the values of both λ/L and q. Figure 1 thus allows values of interplanetary scattering parameters to be inferred from measurements of cosmic ray diurnal variations.

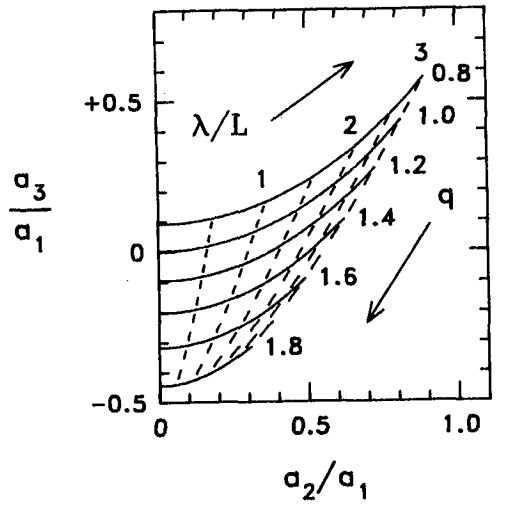

Fig. 1. Lines of constant λ/L (dashed) and constant q (solid) are plotted in a coordinate system representing ratios of the coefficients a_i of a Legendre series expansion of the exponential anisotropy (1). The coefficients a_1, a_2, and a_3 are closely related to the first, second, and third harmonics, respectively, of the cosmic ray diurnal variation.

Bieber and Pomerantz (1983) used essentially this procedure to infer values for λ and q from an analysis of 12 years of neutron monitor data. However, that earlier analysis expressed the anisotropy as a first-order focusing eigenfunction, which is closely related to the exponential (1), but which differs somewhat in the quantitative prediction of harmonic amplitudes. Because the exponential anisotropy is derived from the steady-state Boltzmann equation which includes the effect of a field-aligned density gradient, as well as the effects of focusing and scattering, it should be the more accurate approximation to actual cosmic ray anisotropies in most circumstances. If the observational results of Bieber and Pomerantz are re-interpreted in terms of the exponential anisotropy, then the long-term average of the scattering mean free path at 10 GV changes from 0.5 to 0.3 AU, while the long-term average of q remains unchanged at 1.1.

2. Magnetic Fluctuations and Diurnal Variations. In light of the theory described above, it might be expected that cosmic ray diurnal variations would be correlated with the fluctuation characteristics of the interplanetary magnetic field. In particular, one might expect the amplitude of the second harmonic relative to the first to decrease as the fluctuation level increases, since an increase in fluctuations should correspond to a decrease in λ and, according to Figure 1, a decrease in a_2/a_1.

A thorough investigation of this effect would require that the scattering mean free path be calculated from the observed power spectrum of the magnetic field (e.g., Jokipii, 1971). However, for this preliminary study a simpler procedure was chosen in which the fluctuation level is characterized by the relative variance of the magnetic field. Relative variance was calculated on a daily basis by taking the vector variance of observed hourly field vectors and dividing this by the mean-square field. For days in which both toward and away field polarities occurred, the direction of toward vectors was reversed before the variance was taken. Days with fewer than 12 hours of data were excluded from the analysis. The remaining days were then

divided into 7 groups according to relative variance, and the first 3 harmonics of the cosmic ray daily variation observed at Swarthmore over the period 1965-1978 were averaged separately for each group.

Results of the analysis appear in Figure 2, where the amplitudes and phases of the first 3 harmonics of the diurnal variation are displayed as a function of relative variance. The only quantity to exhibit a strong dependence upon magnetic fluctuation level is the amplitude of the second harmonic, which decreases significantly at the higher fluctuation levels.

After correction for geomagnetic effects and for the Compton-Getting anisotropy (Bieber and Pomerantz, 1983), the data of Figure 2 may be used to infer values of the interplanetary scattering parameters λ/L and q, as described above. For relative variances in the range 0-0.5, λ/L remains nearly constant at a value ~ 0.35, while for ranges 0.5-0.7 and 0.7-1.0 λ/L decreases to 0.27 and 0.19, respectively. For all values of relative variance the q parameter remains near a value of 1.1.

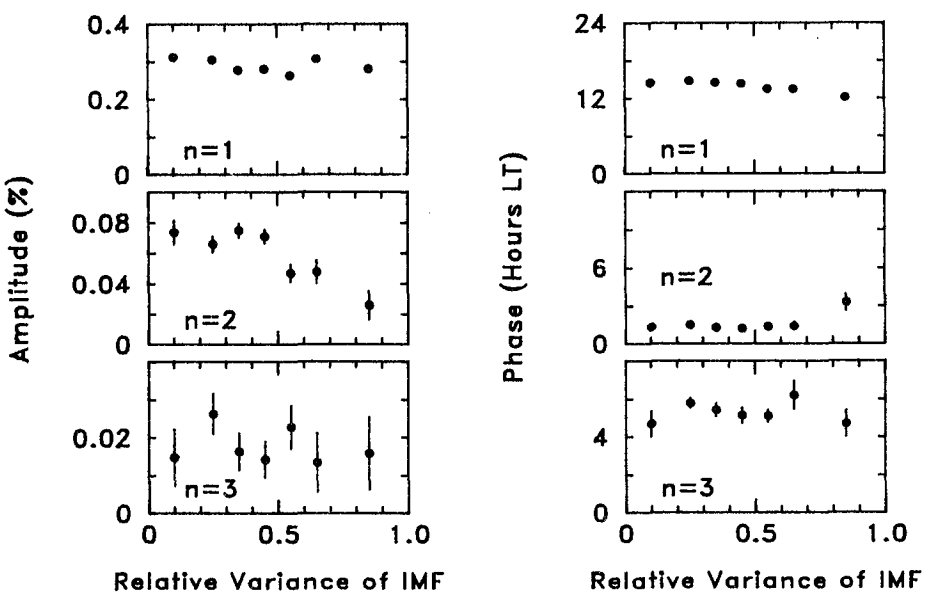

Fig. 2. The amplitudes and phases of the first (top panels), second (middle panels), and third (bottom panels) harmonics of the cosmic ray daily variation observed at Swarthmore are plotted as a function of the relative variance of the interplanetary magnetic field. Data are not corrected for geomagnetic effects or for the Compton-Getting anisotropy. Error bars are $\pm 1\sigma$.

3. Discussion. The daily variance calculated from hourly-averaged magnetic field vectors will naturally be most influenced by fluctuations with time scales in the range of 1 to 24 hours. This, it turns out, is a very suitable range insofar as the scattering of cosmic rays of neutron monitor energies is concerned, as a cosmic ray of 10 GV rigidity is resonant with waves that have periods ~ 24 hours in the spacecraft frame. Thus, it is reasonable to suppose that the relative variance provides a rough measure of the scattering rate that would be calculated from the actual power spectrum of fluctuations.

Under this hypothesis, the results described above show general agreement with theoretical expectation, in that the mean free path inferred from particle anisotropies decreases at the higher fluctuation levels. There is also a hint of a possible discrepancy, however, in that the inferred mean free path seems to be independent of fluctuation level for relative variances < 0.5.

Further analysis is required to see whether any significance can be attached to this puzzling result. In particular, the characterization of fluctuation level by daily relative variance should be replaced by a careful evaluation of observed magnetic power spectra. This will allow the relationship between interplanetary scattering parameters and the fluctuation characteristics of the magnetic field to be studied quantitatively at a level of detail that has not heretofore been possible.

4. Acknowledgments. C. H. Tsao contributed significantly to the extensive computer analysis involved in this work. This research was supported by the National Science Foundation under grant ATM-8303758.

References

Bieber, J. W., and M. A. Pomerantz, (1983), A unified theory of cosmic ray diurnal variations, Geophys. Res. Lett., 10, 920-923.

Earl, J. A., (1981), Analytical description of charged particle transport along arbitrary guiding field configurations, Astrophys. J., 251, 739-755.

Jokipii, J. R., (1971), Propagation of cosmic rays in the solar wind, Rev. Geophys. Space Phys., 9, 27-87.

Kunstmann, J. E., (1979), A new transport mode for energetic charged particles in magnetic field fluctuations superposed on a diverging mean field, Astrophys. J., 229, 812-820.

Roelof, E. C., (1969), Propagation of solar cosmic rays in the interplanetary magnetic field, Lectures in High-Energy Astrophysics, NASA Spec. Publ. 199, edited by H. Ogelman and J. R. Wayland, National Aeronautics and Space Administration, Washington, D.C.

Yasue, S., S. Mori, S. Sakakibara, and K. Nagashima, (1982), Coupling coefficients of cosmic ray daily variations for neutron monitor stations, Report of Cosmic-Ray Research Lab, No. 7, Nagoya, Japan.

Changes in the Energy Spectrum of Anomalous Oxygen and Helium During 1977-1985

A. C. Cummings and E. C. Stone

California Institute of Technology, Pasadena, CA 91125 USA

W. R. Webber

University of New Hampshire, Durham, NH 03824 USA

We have used data from the cosmic-ray experiment on the Voyager spacecraft to measure the energy spectrum of anomalous O and He during the period 1977 to 1985. We find that these spectra change dramatically after the middle of 1980, with the peak or plateau region of the differential spectrum shifting to a higher energy. This change appears to be related to the reversal of the solar magnetic field and could imply that particle drifts are important to the acceleration or propagation of these particles.

1. Introduction. The study of the anomalous component of cosmic rays over the solar cycle may prove to be key to the understanding of the role of drifts in cosmic-ray modulation. *Pesses et al.* [1981] have suggested that the acceleration site of the anomalous component is most likely in the polar regions of the solar wind termination shock. In their model the particles drift latitudinally toward the neutral sheet from the polar regions during the last solar cycle, but drift radially inward along the neutral sheet during the current solar cycle. Consequently, they predict a strong dependence of the intensity of the anomalous component near the solar equator on solar magnetic field polarity. In this analysis we make use of measurements of the spectra of O and He from the Cosmic Ray Subsystem (CRS) [*Stone et al.*, 1977] on the Voyager 1 (V1) and 2 (V2) spacecraft to address whether or not these spectra exhibit changes associated with the polarity of the solar magnetic field.

2. Observations. The general features of the 11-year cosmic-ray modulation cycle are evident in the counting rate of the particles which penetrate the high energy telescope on V1, shown in Fig. 1 for 1977-1985. In order to minimize the contamination by solar and interplanetary energetic particles, quiet times were selected by setting limits to the maximum low-energy He flux, in a manner similar to that described in *Cummings et al.* [1984]. The six quiet-time periods that were selected for analysis for V1 are shown as horizontal bars in Fig. 1 and are labeled A through F. Also shown are the approximate times of the reversal of the solar polar magnetic fields [*Webb et al.*, 1984]. Note that the field reversal occurs approximately between periods C and D.

The anomalous O spectrum for the Voyager measurements is derived from the observed total O spectrum for a particular time interval by subtracting a low-energy solar or interplanetary component and the high-energy galactic cosmic-ray component. This subtraction procedure is illustrated in Fig. 2 for two extreme examples. The low-energy component is scaled and extrapolated from a power-law fit to the observed He spectrum in the energy range 3-6.1 MeV/nuc using a ratio He/O = 100 ± 50 (see *Gloeckler et al.* [1979]). The galactic cosmic-ray O component is estimated by normalizing the observed carbon spectrum to the O intensity in the 66-125 MeV/nuc energy interval.

Figure 3 shows the spectra of anomalous O for the six quiet-time intervals A through F derived from the V2 observations in the manner just described. The a and b panels show the spectra for the three intervals before and after the solar magnetic field reversal in 1980, respectively. The spectra for intervals A, B, and C are essentially monotonic with a tendency to flatten into a peak or plateau at less than $\sim$6 MeV/nuc. It is clear from Fig. 3b that the energy dependence of the spectra for the intervals after the field reversal (D, E, and F) is significantly different, having a peak or plateau at $\sim$10-20 MeV/nuc.

A similar change in the energy spectrum is also apparent in the V1 data. In Fig. 4a we show the V1 observed O spectra for intervals B and F. The galactic cosmic-ray intensity is dom-

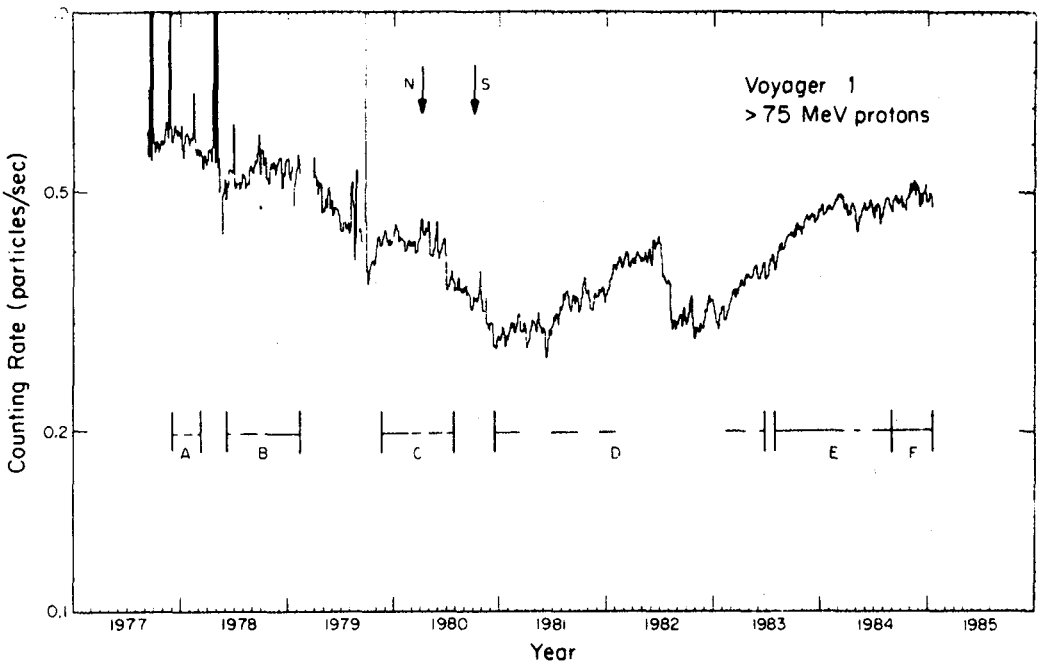

Fig. 1. Three-day average counting rate of penetrating particles in the HET 1 (High-Energy Telescope number 1) of the V1 CRS instrument from 1977 to 1986. The rate is dominated by protons with energy > 75 MeV. The bars and arrows are described in the text.

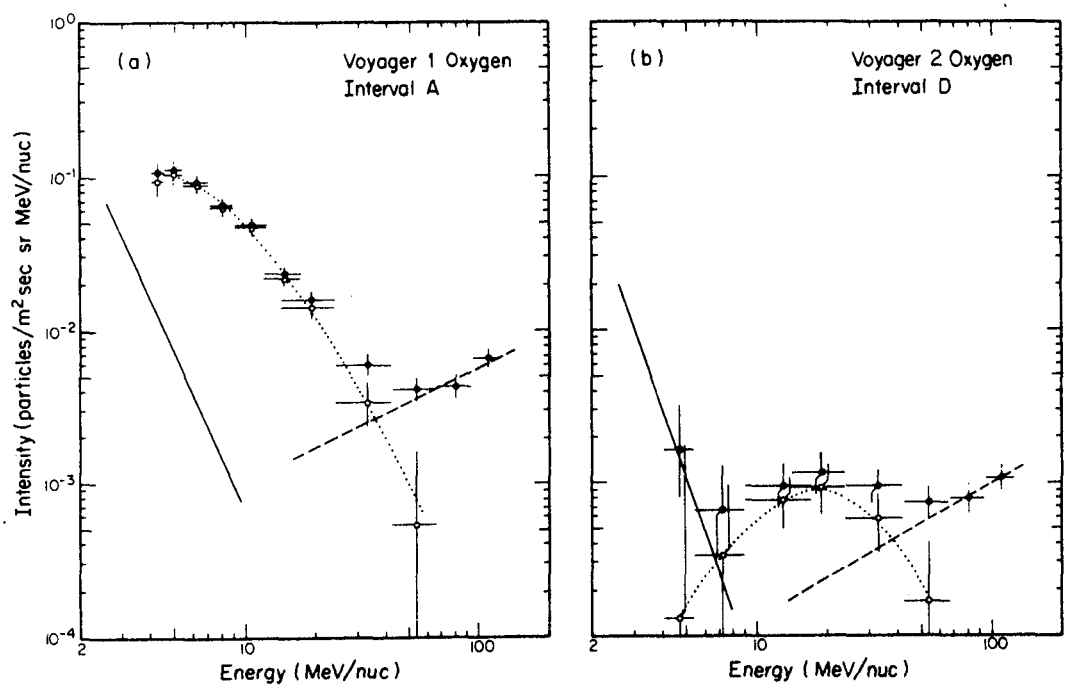

Fig. 2. Quiet-time energy spectra of O from Voyager data for two sample time intervals. The observed spectra are shown as the solid circles. Estimated spectra of interplanetary and galactic components are shown as solid and dashed lines, respectively. The spectra of anomalous O are indicated by the open squares which are joined by the dotted lines.

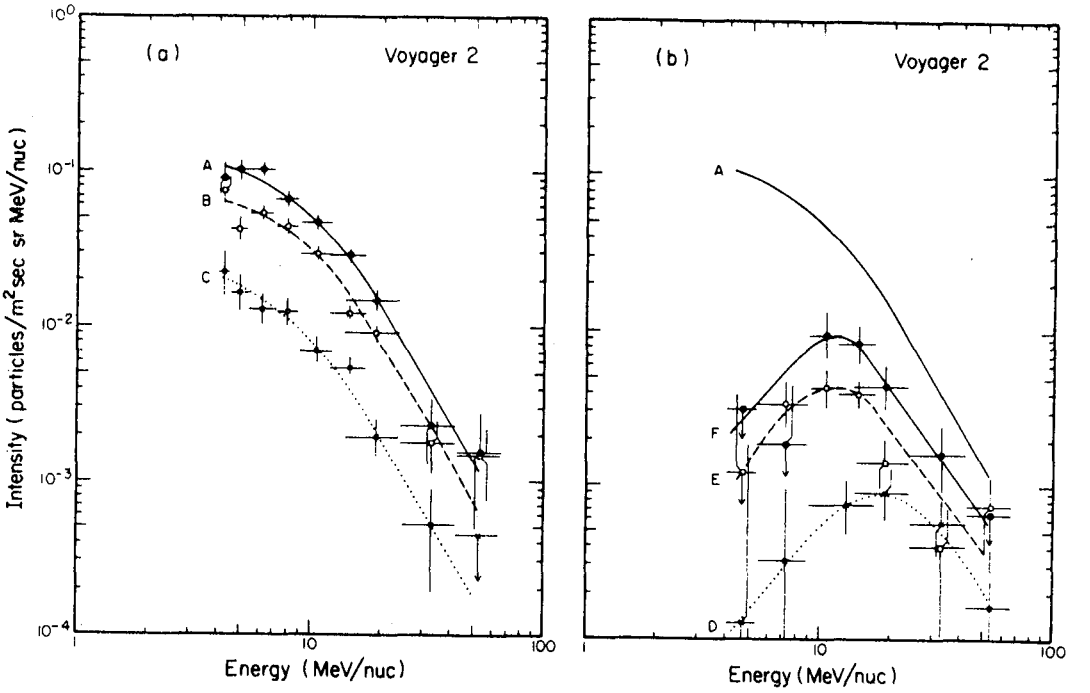

Fig. 3. Spectra of anomalous O from V2 for the six quiet-time intervals. Panels a and b show the spectra for periods before and after the solar magnetic field reversal, respectively. The smooth curves are drawn to aide the eye and are not functional fits to the data. The dashed line labeled "A" in panel b is copied from panel a to facilitate comparison. Note the higher energy of the peak (or plateau) intensity of the spectra in panel b when compared to those of panel a.

inant in the 50-125 MeV/nuc energy range for both time intervals. The intensity in this energy range is only ~20% higher for interval B than for interval F, indicating that a similar level of modulation has been reached. Similarly, the anomalous O intensity in the 10-30 MeV/nuc energy range is approximately the same for the two time intervals. However, below 10 MeV/nuc there is a factor of 10 difference in intensity producing a striking difference in the spectrum.

This change in the energy spectrum is also evident in the He data. We show in Fig. 4b the observed He spectrum for the same two intervals as for Fig. 4a. Below ~8 MeV/nuc a low-energy solar or interplanetary component is dominant and causes a sharp upturn in the spectrum. For interval B the flat region of the spectrum from ~8 to 50 MeV/nuc indicates that anomalous He is the primary component, dominating the flux of solar and galactic cosmic rays. The period F spectrum has a much lower intensity than the period B spectrum below ~30 MeV/nuc suggesting that the anomalous He spectrum has shifted to higher energies. If the particles are singly ionized, the energy dependence of the He spectrum is expected to be obtained by shifting the anomalous O spectrum by a factor of ~4 in energy [*Cummings et al.*, 1984], so that the absence of anomalous He below 30 MeV/nuc is consistent with the reduced intensity of anomalous O below 8 MeV/nuc.

3. **Discussion.** If the changes in the energy spectra of the anomalous component are to be explained by "conventional" modulation theory, in which the effects of diffusion, convection, and adiabatic deceleration are considered, and the effects of drifts ignored (see *Fisk* [1980], for a review of solar modulation theory), then it would require either a very prolonged "hysteresis" effect or a significant change in the rigidity dependence of the diffusion coefficient between halves of the solar cycle. A hysteresis effect (phase-lag between intensity variations of low-rigidity and high-rigidity particles) has been reported for the anomalous O component by *Klecker et. al* [1980] for the 1974-1975 period. They found a phase lag of 72 days between the intensity of

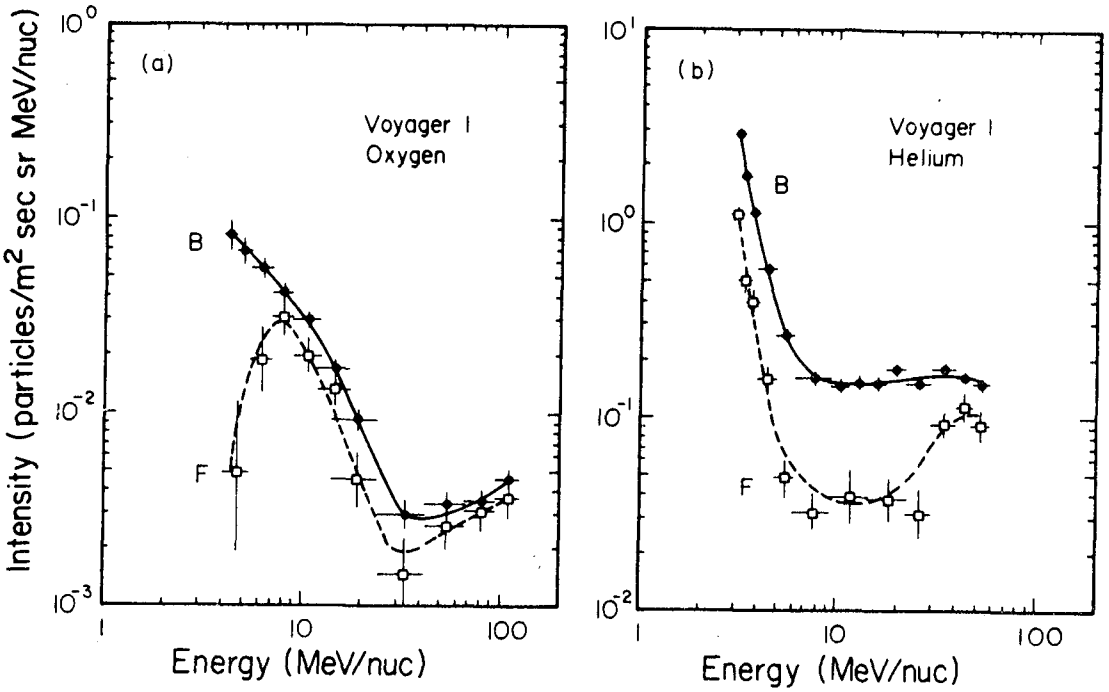

Fig. 4. Spectra of observed O (a) and He (b) for time intervals B and F from V1.

anomalous O with 7.6-24 MeV/nuc and the intensity of galactic cosmic rays with energy >10GeV. If the energy spectrum changes in our study are to be ascribed to hysteresis, then a phase lag of ~ 4 years would be required between particles with only modestly different rigidities and velocities. If changes in the diffusion coefficient between halves of the solar cycle are to account for our observations then the spectra of other cosmic-ray species would show pronounced effects at the corresponding rigidities.

It appears more likely, therefore, that the observed time variation of the energy spectra of anomalous O and He may be related to changes in the acceleration of particles at the termination shock due to the change in the polarity of the solar magnetic field. Recently, *Jokipii* [1985] has used a model of the anomalous component which includes acceleration at the termination shock and particle drifts and has calculated spectra of anomalous O and He in the two halves of the solar cycle with different field polarity that resemble the observations reported here.

4. Acknowledgments. We are grateful to R. E. Vogt and other CRS team members at the California Institute of Technology, the Goddard Space Flight Center, the University of Arizona, and the University of New Hampshire. This work was supported in part by NASA under contract NAS 7-918 and grant NGR 05-002-160.

5. References.

Cummings, A. C., E. C. Stone, and W. R. Webber, *Ap. J. (Letters), 287*, L99, 1984.

Fisk, L. A., *Proc. Conf. Ancient Sun,* edited by R. O. Pepin, J. A. Eddy, and R. B. Merrill, (Pergamon Press : New York), 103, 1980.

Gloeckler, G., D. Hovestadt, and L. A. Fisk, *Ap. J. (Letters), 230*, L191, 1979.

Jokipii, J. R., submitted to *J. Geophys. Res.*, 1985.

Klecker, B., D. Hovestadt, G. Gloeckler, and C. Y. Fan, *Geophys. Res. Letters, 7*, 1033, 1980.

Pesses, M. E., J. R. Jokipii, and D. Eichler, *Ap. J. (Letters), 246*, L85, 1981.

Stone, E. C., R. E. Vogt, F. B. McDonald, B. J. Teegarden, J. H. Trainor, J. R. Jokipii, and W. R. Webber, *Space Sci. Rev., 21*, 355, 1977.

Webb, D. F., J. M. Davis, and P. S. McIntosh, *Solar Phys., 92*, 109, 1984.

SOLAR CYCLE VARIATIONS OF THE ANOMALOUS COSMIC RAY COMPONENT

R. A. Mewaldt and E. C. Stone

California Institute of Technology
Pasadena, California 91125 USA

The intensity of the "anomalous" cosmic ray component, consisting of He, N, O, and Ne, has long been known to be especially sensitive to the effects of solar modulation. Following its discovery in 1972, this component dominated the quiet-time flux of cosmic ray nuclei below ~30 MeV/nucleon during the 1972-1978 solar minimum, but then became essentially unobservable at 1 AU with the approach of solar maximum conditions. One recent theoretical model predicts substantial differences in the intensity of the anomalous fluxes from one solar minimum period to the next because of the reversal of the solar magnetic field. Using data from the Caltech experiments on IMP-8 and ICE (ISEE-3), we report on the intensity of anomalous O and He at 1 AU during the years 1972 to 1985. In particular, we hope to determine whether the anomalous fluxes will return to their 1972-1978 levels, as predicted by spherically symmetric modulation models, or whether they will fail to return to 1 AU, as suggested by modulation models in which gradient and curvature drifts dominate.

Our preliminary analysis of data from 1984 shows that the intensity of 8 to 27 MeV/nucleon O is still more than an order of magnitude below its 1972 to 1978 levels, while the intensity of 25 to 43 MeV/nucleon He is a factor of ~8 below its maximum level in 1977. Data from 1985 is now being analyzed.

This work was supported in part by NASA under grant NGR 05-002-160 and contracts NAS5-28441 and NAS5-28449.

TEMPORAL VARIATIONS OF THE ANOMALOUS OXYGEN COMPONENT, 1977 - 1984

G.M. Mason[1], B. Klecker[2], A.B. Galvin[1], D. Hovestadt[2], and F.M. Ipavich[1]

[1]Dept. of Physics & Astronomy, Univ. of MD, College Park, MD 20742 USA
[2]MPI fur Extraterrestrische Physik, 8046 Garching, FRG

ABSTRACT

We present a survey of the long term temporal variations of 6.6-12 MeV/nucleon anomalous oxygen at 1 AU covering the period 1977-1984. This time interval included the recent solar maximum, with the recovery at neutron monitor energies beginning in 1982. During this time interval, 6.6-12 MeV/nucleon O fluxes decreased by at least a factor of 50, and indeed remained below our instrumental detection threshold after 1979. By late 1984, neutron monitors had recovered to roughly 1979 levels from the 1982 solar maximum, and anomalous O still remained below our detection threshold.

1. Introduction. The 1972 discovery of the anomalous components of He (4), N, O and Ne (1,5,8) added a new particle population to the set available to probe acceleration and transport processes in the heliosphere. Observed over the energy range from a few to a few 10s of MeV/nucleon during the 1972-77 solar minimum, these components display an unusual composition resembling neither galactic cosmic rays nor solar energetic particles. Of the many models suggested to explain the anomalous components, perhaps the most attractive is that by Fisk, Kozlovsky and Ramaty (3), who proposed that the particles begin as interstellar neutrals which are ionized and accelerated in the heliosphere, yielding a particle population in which high ionization potential elements are favored.

A key prediction of this model (3) is that the particles are singly ionized. However, a direct test of this prediction remains beyond the capabilities of any instruments flown to date. Temporal variations, however, may offer clues pertinent to this question. For example, a special temporal behavior has been predicted by Pesses, Jokipii and Eichler (10) in a model where the anomalous component is accelerated at the solar wind termination shock over the solar poles, and the particles subsequently flow down to the ecliptic plane. In this case, particle drifts yield a 22-year modulation cycle, and thus the component would not be expected to re-appear during the upcoming solar minimum. In order to probe these questions we present measurements of ~10 MeV/nucleon oxygen over the period 1977-1984, thus updating our previous report for the years 1974-79 (7).

2. Instrumentation. The measurements presented here were carried out in interplanetary space with the Ultra Low Energy Wide Angle Telescope (ULEWAT), which is part of the MPI/UMD experiments on the ISEE-1 and ISEE-3 spacecrafts. Figure 1 shows a cross sectional view of the ULEWAT, which identifies particle type and energy by the dE/dx versus residual energy method. For the particles discussed in this paper, the flow-through proportional counters P1 and P2 serve as dE/dx elements, and the silicon detector D1 is the residual energy detector. The

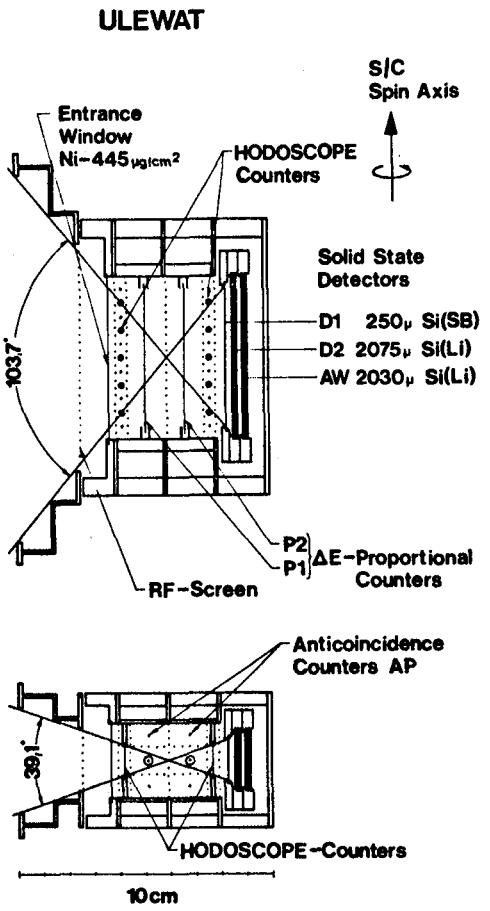

Figure 1

hodoscope detectors shown in the Figure permit correction of the ΔE signals for particles entering the telescope at different angles, thus allowing a wide opening angle while preserving instrument resolution. For the present study, particles with incident angles up to ~25° were accepted, resulting in a geometrical factor of ~1.3 cm^2 sr. A complete instrument description has been published elsewhere (6).

In order to remove the possibility of contamination by, e.g., solar flare particles, a strict criterion was adopted wherein observation times were used only if the counting rate channel for $Z \geq 6$ particles above 300 keV/nucleon counted less than 30 particles in 24 hours of observing time. Assuming E^{-3} spectra, this criterion extrapolates roughly to a level of 10^{-4} particles/sec-m^2-sr-MeV/nuc at 10 MeV/nucleon, a factor of ~500 below anomalous O flux levels during solar minimum. Table 1 lists the observing time periods and number of hours observing time for each point. High levels of solar activity decreased the number of hours of quiet time in some intervals, and, after ISEE-3 was targeted for comet encounter, spacecraft tracking coverage was an important factor.

3. Observations. Figure 2 shows the fluxes and upper limits of 6.6-12 MeV/nucleon quiet time O during the survey period. Note that after the end of 1978, only upper limits are shown. In the figure, upper limit data points plotted with positive standard deviation bars indicate finite O measurements where the spectral information was not sufficient to conclusively identify the particles as part of the anomalous component. Points that are shown as upper limits only are 1-count upper limits. For comparison with the solar modulation at high energies, the lower panel shows 3-month averages of the Deep River neutron monitor as compiled from Solar-Geophysical Data. While the neutron monitor has been increasing since its 1982 minimum, by late 1984 it has not surpassed 1979 levels, and thus it is not surprising that even in 1984 anomalous O remained below our detection threshold.

Table 1

OBSERVATION PERIODS AND COLLECTION TIMES

Spacecraft	Period	Hours	Spacecraft	Period	Hours
ISEE-1	10/26/77 - 12/30/77	343	ISEE-3	7/01/81 - 12/31/81	635
ISEE-1	01/01/78 - 08/08/78	368	ISEE-3	1/01/82 - 06/30/82	734
ISEE-3	08/14/78 - 12/30/78	784	ISEE-3	7/01/82 - 12/31/82	758
ISEE-3	01/01/79 - 06/30/79	709	ISEE-3	1/01/83 - 07/01/83	1299
ISEE-3	07/01/79 - 12/31/79	684	ISEE-3	7/01/83 - 12/31/83	2058
ISEE-3	01/01/80 - 06/30/80	1148	ISEE-3/ICE	1/01/84 - 06/30/84	418
ISEE-3	07/01/80 - 12/31/80	686	ISEE-3/ICE	7/01/84 - 09/28/84	172
ISEE-3	01/01/81 - 07/01/81	586			

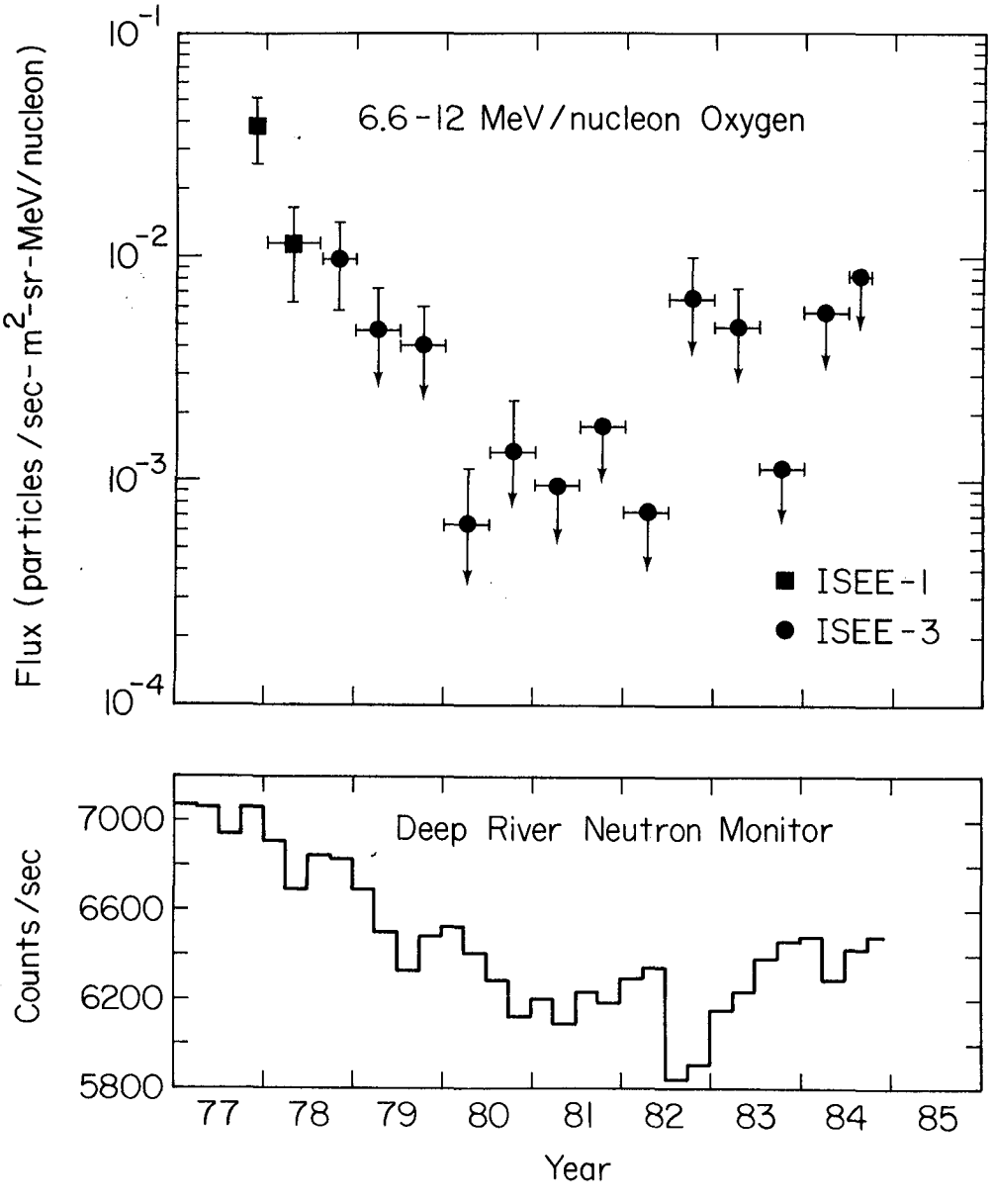

Figure 2

4. Discussion. From Figure 2 it is clear that at 1 AU anomalous O decreased by at least a factor of 50 between 1977 and solar maximum levels in 1981-82. This is much larger than the factor of ~10 observed for cosmic ray protons near 100 MeV (13), but is comparable to the factor of ~30 decrease in 10-20 MeV/nucleon anomalous He between 1977 and 1981 (9). The fact that the anomalous components show greater sensitivity to the solar cycle than galactic cosmic rays may be due to a combination of source (acceleration) and modulation effects; however, the unique spectral shapes of the anomalous components may also play an important role (11).

During the 1977-81 time period the ~10 MeV/nucleon O flux observed on the Voyager spacecrafts decreased also by a factor of ~50 (12), almost the same as the upper limits shown in Figure 2. However, since the Voyagers were at ~10 AU in 1981, the measurements cannot be directly compared with the results presented here. Indeed, since the anomalous He component has typically shown rather large positive radial gradients, the Voyager results could imply an anomalous O flux level at 1 AU a factor of 2 or more below our upper limits--yielding an overall modulation factor of >100 between 1977 and 1981.

Since the neutron monitors have not returned to levels at which our instrumental sensitivity would allow us to see anomalous O based on an 11-year cycle, we are not yet able to address the predictions of a 22-year cycle as in the model in reference (10). Recently, the anomalous O fluxes have been increasing at large distances from the sun (2), so it may be soon possible to address this question with measurements at 1 AU.

5. Acknowledgements. We are grateful to the MPI and UMD individuals responsible for the success of the ISEE instruments. This work was supported by NASA under contract NAS5-28704, grants NGR 21-002-224/316 and NAGW-101, by the NSF under grant ATM-84-07546, and by the Bundesministerium fur Forschung und Technologie, contract RV 14-B8/74.

References

1. Chan, J.H. and Price, P.B. 1974, Ap.J. (Letters), 190, L39.
2. Cummings, A.C. et al. 1984, EOS, 65, 1035.
3. Fisk, L.A. et al. 1974, Ap.J. (Letters), 190, L35.
4. Garcia-Munoz, M. et al. 1973, Ap.J. (Letters), 182, L81.
5. Hovestadt, D. et al. 1973, Phys. Rev. Letters, 31, 650.
6. Hovestadt, D. et al. 1978, IEEE Trans. Geo. El., GE-16, 166.
7. Hovestadt, D. et al. 1979, 16th ICRC, Kyoto, 3, 255.
8. McDonald, F.B. et al. 1974, Ap.J. (Letters), 187, L105.
9. McKibben, R.B. et al. 1982, Ap.J. (Letters), 257, L41.
10. Pesses, M.E. et al. 1981, Ap.J. (Letters), 246, L85.
11. von Rosenvinge, T.T. and Paizis, C. 1981, 17th ICRC, Paris, 10, 69.
12. Webber, W.R. and Cummings, A.C. 1983, Solar Wind V, NASA CP-2280, 435.
13. Webber, W.R. et al. 1983, 18th ICRC, Bangalore, 3, 35.

Radial and Latitudinal Gradients of Anomalous Oxygen During 1977-1985

W. R. Webber

University of New Hampshire, Durham, NH 03824 USA

A. C. Cummings and E. C. Stone

California Institute of Technology, Pasadena, CA 91125 USA

We find that the radial gradient of anomalous O remains constant during 1977-85 at $\sim$10-15%/AU although the intensity changes by more than a factor of 100. These results can be used to deduce that most of the modulation of the intensities of these particles is occurring beyond 27AU. We also find evidence for a latitudinal gradient of $\sim$+3%/degree at low energies (7.1-10.6MeV/nuc).

1. Introduction. In this analysis we make use of measurements of the spectrum of O nuclei from the Cosmic Ray Subsystem (CRS) on the Voyager 1 (V1) and 2 (V2) spacecraft [*Stone et al.*, 1977] and from the Goddard-University of New Hampshire experiment on Pioneer 10 [*McDonald et al.*, 1977] to study the radial and latitudinal gradients and temporal variations of anomalous O. Quiet-time data from 1977 to 1985 are utilized.

2. Observations. The general features of the 11-year cosmic-ray modulation cycle may be examined by using the counting rate of particles which penetrate the high-energy telescope on V1 as shown in Fig. 1 (curve "P", mainly protons >75 MeV). A change in this rate by a factor $\sim$2 is observed between 1977 and the minimum in 1981-82. This change is mainly due to solar modulation; however, some gradient effects are present in the data as well since V1 is moving outward from 1 to $\sim$22AU during this time period. Figure 1 also shows a similar plot for 40-106MeV/nuc C+O nuclei for 24 quiet-time intervals between 1977-85 (curve "C+O"). Here the change in intensity between 1977 and the minimum in 1981 is a factor $\sim$5. Finally, in Fig. 1 the temporal variations for 5.6-17.2 MeV/nuc anomalous O are shown for the same 24 quiet-time intervals (curve "O"). All three components show a similar pattern of variations but for the anomalous O the overall intensity variation is larger than the others, approaching a factor $\sim$100.

In order to minimize contamination by solar and interplanetary particles and to help separate temporal and radial variations, six quiet-time intervals labeled A-F in Fig. 1 were selected by setting limits to the maximum low-energy helium flux, in a manner similar to that described in *Cummings et al.* [1984]. The anomalous O spectrum is derived from the observed total O spectrum for a particular time interval by subtracting both a low-energy solar or interplanetary component and the high-energy galactic cosmic-ray component [*Cummings et al.*, 1985].

In Fig. 2a, b, c we show the differential intensities of anomalous O nuclei in three separate energy intervals for each of the six quiet-time intervals at each of the spacecraft as they moved outward from the sun. The solid lines are least-squares fits to the data points, except for the lowest energy interval for periods E and F when V1 is at $\sim$24 degrees north heliographic latitude. (V1 left the ecliptic plane after encounter with Saturn in 1980.) In these two cases the V1 points, connected by the dashed lines, are significantly above the straight lines (representing a constant radial gradient) connecting the V2 and P10 points. We attribute the deviation to a latitude gradient at low energies having a weighted average value of 3.0 ± 1.0%/degree for the combined two periods E and F.

In Fig. 3 we show the calculated radial gradient (slope of solid lines in Fig. 2) for each of the three energy intervals. In the lowest energy interval (7.1-10.6MeV/nuc) the spectrum of anomalous O is changing with time [*Cummings et al.*, 1985], which may contribute to the observed variation in the radial gradient. Above 10.6 MeV/nuc no such energy spectral changes are found and the resulting gradient is remarkably constant. In the 10.6-17.1MeV/nuc interval the average value of the gradient is 10.7 ± 0.6%/AU, somewhat lower than the 15 ± 3%/AU found by

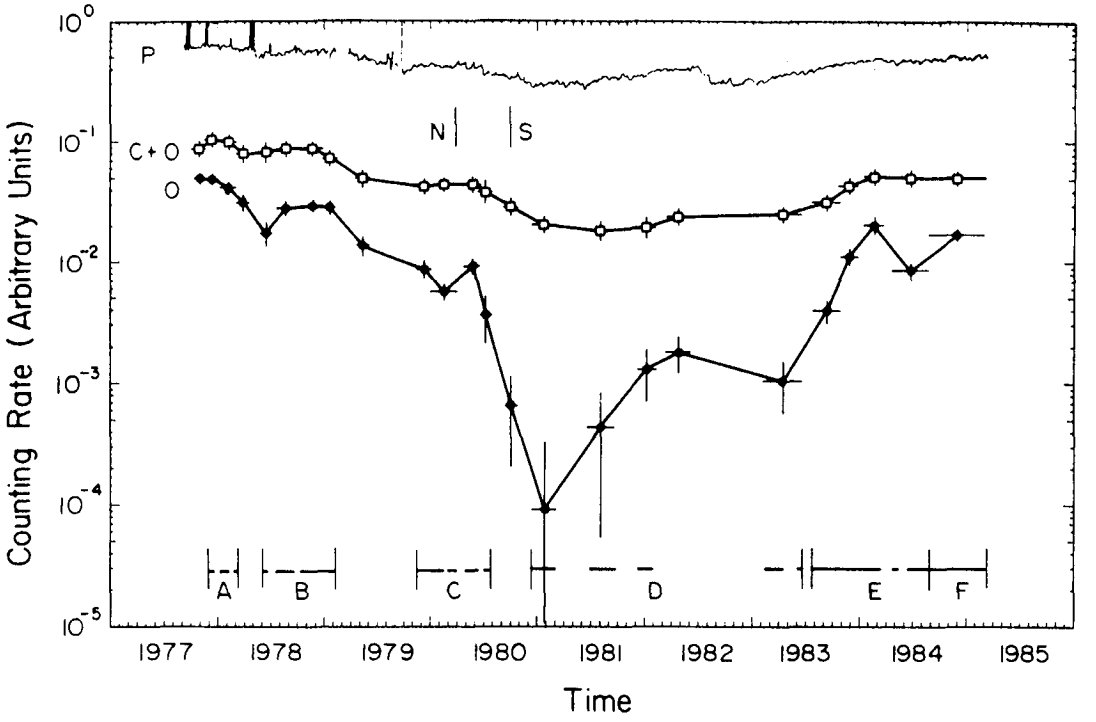

Fig. 1. Counting rates of three particle types from Voyager 1 telescopes. P labels the penetrating rate from the high-energy telescope (mainly protons > 75 MeV), C+O labels the rate of 40-106 C+O, and O labels the rate of 5.6-17.2 MeV/nuc anomalous oxygen. The approximate times of the solar magnetic field reversal in the northern (N) and southern (S) polar regions are indicated by the vertical bars [*Webb et al.*, 1984]. The horizontal bars represent quiet-time intervals as discussed in the text.

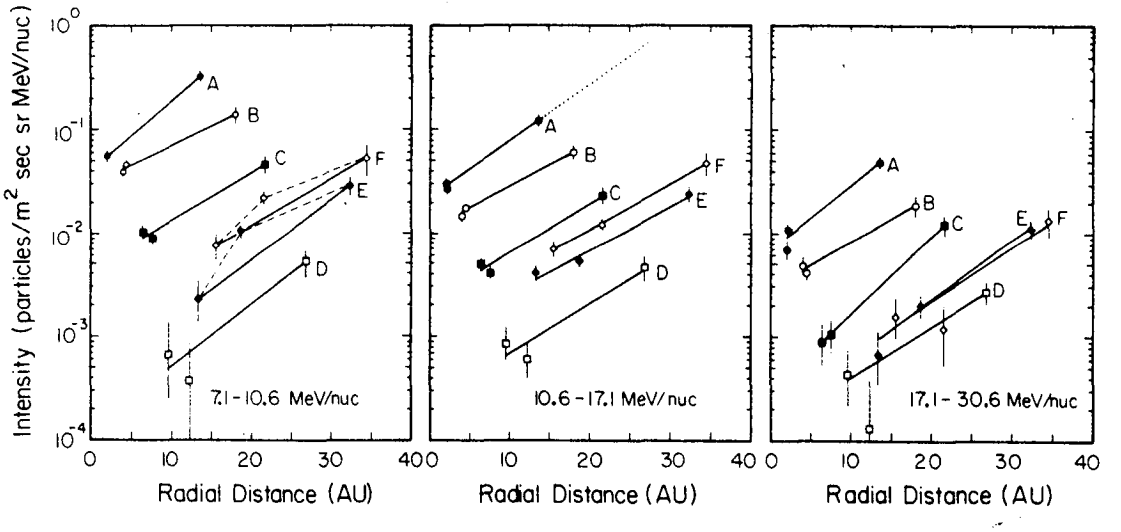

Fig. 2. Intensity of anomalous O versus heliocentric radial distance in three energy intervals from the V1, V2, and P10 cosmic-ray instruments. The labels A-F refer to the six quiet-time intervals chosen for analysis. The lines are described in the text.

Webber et al. [1981] for the period 1972-79. It is clear from Figs. 2 and 3 that the radial gradient for all three energy intervals has not changed appreciably with time or radial distance, maintaining a value between ~10-15%/AU despite the fact that the intensity has varied by more than a factor of 100.

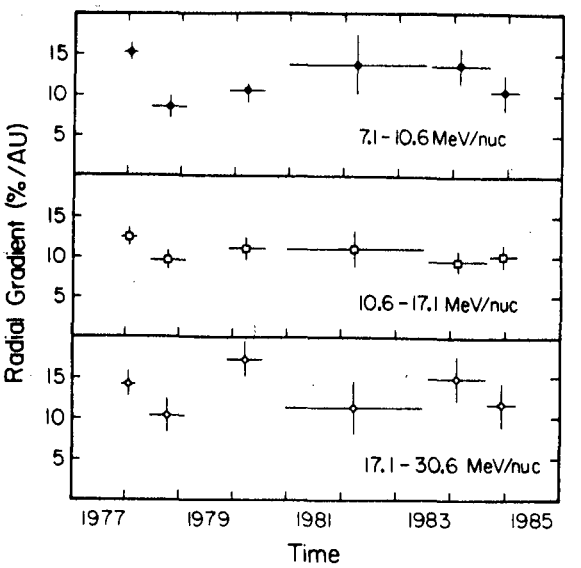

Fig. 3. Measured radial gradients of anomalous O versus time for the three energy intervals of Fig. 2.

3. Discussion. We believe that the constancy of the gradient with respect to time both before and after the solar magnetic field reversal in 1980, and during a period when the intensity change was a factor ~100 is an important clue and constraint on the solar modulation process. In conventional modulation theory, if the effects of particle streaming in the interplanetary medium can be neglected, then the radial gradient, G_r, and the radial diffusion coefficient, κ_r, are related by $G_r = CV/\kappa_r$. The average solar wind velocity, V, and κ_r change only slightly over a solar cycle (see *Hedgecock* [1974] and *Feldman et al.* [1979]). Also the Compton-Getting coefficient C, which is related to the spectral shape, does not change appreciably since the spectral shape remains similar above ~10 MeV/nuc. Thus, if the gradient can be described by these local parameters, it would be expected to be constant as observed.

In this simple conventional modulation model in which κ_r is independent of radial distance r, the particle intensity j at r is given by $j = j_b \exp[CV(r-r_b)/\kappa_r]$, where j_b is the intensity at the modulation boundary. Since C, V, and κ_r are not changing appreciably with time, and assuming j_b is constant, the large modulation at a given position would require a time variation in the boundary location r_b. The magnitude of the required change in the boundary distance can be estimated from Fig. 2b. The dotted line is an extrapolation of the intensity in the 10.6-17.1 MeV/nuc energy range during the time of solar minimum to the position of P10 (27 AU) during the solar maximum period of interval D. The implied intensity change from period A to D at 27 AU is a factor of 136 ± 52, indicating that most of the modulation during period D is occurring beyond 27 AU. Using the average radial gradient for this energy interval we find that the required change in the boundary distance r_b is 46 ± 4 AU. A similar boundary shift has been suggested by *Evenson et al.* [1979] to explain electron observations.

Such a boundary shift would also produce changes in the intensity of other particle species. For example, the penetrating particle rate (P) in Fig. 1 shows a variation from solar minimum to solar maximum of a factor ~2. The median rigidity of the particles dominating this rate is ~1.8 GV, the same rigidity as 7 MeV/nuc anomalous O if O is singly charged (as expected if they are freshly-ionized neutrals [*Fisk et al.*, 1974]). The spectral shapes of the anomalous O (above 10 MeV/nuc) and high-energy protons are similar (spectral index ~-2) implying they have similar values of C. Since $\kappa_r \propto \beta f(R)$, where β is the particle velocity and R is the rigidity, the expected gradient for the P rate can be scaled from the gradient of anomalous O by $G_r(P) = G_r(O)(\beta_O/\beta_P) \sim 10(.12/.89) = 1.5\%$/AU, a value in approximate agreement with observations by others (see *McKibben et al.* [1982] and *Lockwood and Webber* [1984]). The intensities at two different times are related by $j_1/j_2 = \exp(G_r(\delta r_b))$ Therefore, a boundary change of 46 AU and a radial gradient of 1.5-3%/AU would result in $j_1/j_2 = 2$-4 for the penetrating particles, similar to what we observe.

An alternative way to accomplish the same modulation without changing the boundary distance is to decrease κ_r, and thus increase the gradient, in a localized shell of turbulence in the outer heliosphere, as suggested by *Burlaga et al.* [1984]. The observed change in modulation

would require, for example, an increase in the anomalous O gradient from 11%/AU to 44%/AU in a shell 15 AU thick.

It is also possible that variations in the source of the anomalous O may contribute to the observed solar cycle variation. We note that *Jokipii* [1985], using a model of the anomalous component in which the particles are accelerated at the polar termination shock and drift to the solar equatorial regions, has calculated spectra of anomalous O that depend on the polarity of the magnetic field and which are in reasonable agreement with observations of changes in the spectra associated with the magnetic field reversal (see *Cummings et al.* [1985]). However, we find no evidence of a change in the gradient of the anomalous O at the time of the solar magnetic field reversal as would presumably be expected from such a model.

4. Acknowledgments. We are grateful to R. E. Vogt and other CRS team members consisting of scientists and engineers at the California Institute of Technology, the Goddard Space Flight Center, the University of Arizona, and the University of New Hampshire. This work was supported in part by NASA under contract NAS 7-918 and grant NGR 05-002-160.

5. References.

Burlaga, L. F., F. B. McDonald, N. F. Ness, R. Schwenn, A. J. Lazarus, and F. Mariani, *J. Geophys. Res., 89,* 6579, 1984.

Cummings, A. C., E. C. Stone, and W. R. Webber, *Ap. J. (Letters), 287,* L99, 1984.

Cummings, A. C., E. C. Stone, and W. R. Webber, *19th Internat. Cosmic-Ray Conf., La Jolla,* paper SH4.6-1, 1985.

Evenson, P., J. Caldwell, S. Jordan, and P. Meyer, *J. Geophys. Res., 84,* 5361, 1979.

Feldman, W. C., J. R. Asbridge, S. J. Bame, and J. T. Gosling, *J. Geophys. Res., 84,* 7371, 1979.

Fisk, L. A., B. Kozlovsky, and R. Ramaty, *Ap. J. (Letters), 190,* L35, 1974.

Hedgecock, P. C., *J. Geophys. Res., 79,* 4775, 1974.

Jokipii, J. R., submitted to *J. Geophys. Res.*, 1985.

Lockwood, J. A., and W. R. Webber, *Ap. J., 279,* 151, 1984.

McKibben, R. B., K. R. Pyle, and J. A. Simpson, *Ap. J. (Letters), 254,* L23, 1982.

McDonald, F. B., N. Lal, J. H. Trainor, M. A. I. Van Hollebeke, and W. R. Webber, *Ap. J., 216,* 930, 1977.

Stone, E. C., R. E. Vogt, F. B. McDonald, B. J. Teegarden, J. H. Trainor, J. R. Jokipii, and W. R. Webber, *Space Sci. Rev., 21,* 355, 1977.

Webb, D. F., J. M. Davis, and P. S. McIntosh, *Solar Phys., 92,* 109, 1984.

Webber, W. R., F. B. McDonald, T. T. Von Rosenvinge, and R. A. Mewaldt, *17th Internat. Cosmic-Ray Conf., Paris, 10,* 92, 1981.

OBSERVATION OF PICK-UP IONS IN THE SOLAR WIND: EVIDENCE FOR THE SOURCE OF THE ANOMALOUS COSMIC RAY COMPONENT?

D. HOVESTADT, E. MÖBIUS, B. KLECKER, M. SCHOLER,
Max-Planck-Institut für extraterrestrische Physik, 8046 GARCHING, Germany
G. GLOECKLER and F.M. IPAVICH
Dept. of Physics and Astronomy, University of Maryland, COLLEGE PARK, MD 20742, USA

ABSTRACT. Singly ionized energetic helium has been observed in the solar wind by using the time-of-flight spectrometer SULEICA on the AMPTE/IRM satellite between September and December, 1984. The energy-density spectrum shows a sharp cut-off which is strongly correlated with the four-fold solar wind bulk energy. The absolute flux of the He^+ ions of about 10^4 ions/cm^2·s is present independent of the IPL magnetic field orientation. The most likely source is the neutral helium of the interstellar wind which is ionized by solar UV-radiation. It is suggested that thes particles represent the source of the anomalous cosmic ray component.

1. Introduction. In 1972 anomalous features in the low energy quiet time cosmic ray energy spectrum have been detected for helium, oxygen, nitrogen, and neon by GARCIA-MUNOZ et al.(1972), HOVESTADT et al.(1973), and Mc DONALD et al.(1974). These four elements are known to have a high first ionization potential compared to other elements like carbon, magnesium, silicon and iron (e.g ALLEN (1973)). This fact lead FISK et al.(1974) to suggest that the source of the particles is the interstellar neutral wind which becomes ionized in the inner heliosphere by interaction of the atoms with solar ultra-violett radiation and/or solar wind ions. The newly created ions then are picked-up by the interplanetary magnetic field. With their gyro-motion in the solar wind frame they represent a distinguished population which is subsequently convected into the outer heliosphere while being accelerated within the turbulent magnetic fields of the heliosphere (e.g. FISK 1976a,b) or at the terminating shock (PESSES et al. (1981)). The resulting energy spectrum is then reshaped to the observed spectrum by modulation and propagation effects in interplanetary space. This paper presents first direct observations of the distribution function of freshly ionized helium in the solar wind which likely has its origin in the neutral interstellar wind and probably represent the source of the anomalous helium component in cosmic rays.

2. The Pick-Up Process. Freshly ionized helium atoms are locally subjected to the combined forces of the interplanetary $V_{SW} \times B$ field of the solar wind and the Lorentz-force in the magnetic field, B, where V_{SW} is the solar wind velocity; i.e. in the inertial-system (which nearly coincides with the spacecraft-system) the particles undergo initially a cycloidal motion in a plane perpendicular to the local magnetic field, B, with a minimum velocity which is equal to the velocity of the neutral wind(assumed to be < 20 km/s and therefore being neglected in the following).The maximum velocity which these ions can obtain in the pick-up process is determined by the solar wind velocity and the angle α between its flow direction and the direction of the local magnetic field:

$$v(max,loc) = 2 \cdot V_{SW} \cdot \sin\alpha \qquad (1)$$

. This leads to an energy of

$$E(max,loc) = 4 \cdot M/2 \cdot V_{SW}^2 \cdot \sin^2\alpha \qquad (2)$$

In the solar wind frame the motion initially leads to a conical pitch-angle distribution with the pitch angle α. The velocities parallel and perpendicular to the local magnetic field are given by

$$v(par) = V_{SW} \cdot \cos \alpha \quad (3) \quad \text{and}$$

$$v(perp) = V_{SW} \cdot \sin \alpha \quad (4) .$$

Therefore the total ion velocity in the solar wind frame is given by

$$v = (v_{par}^2 + v_{perp}^2)^{1/2} = |V_{SW}| \quad (5)$$

If the interplanetary medium were homogenious with parallel magnetic field lines and if there were no scattering imposed by intrinsic or self-generated waves, the distribution function would remain gyrotropic and ring-shaped in the three-dimensional velocity space.

In the real world ,however, the motion of the particles is subjected to effects generated by temporal and spatial magnetic irregularities in the expanding interplanetary medium. While energy-changing wave-particle interactions can be neglected, pitch-angle scattering and adiabatic deceleration can greatly influence the particle distribution. Within a scattering mean free path-length λ the initially ring-type velocity distribution is expected to be reshaped by pitch-angle diffusion into a spherical-shell type distribution which is fully convected with the solar wind . The orbital velocity $|v| = |V_{SW}|$ remains constant in the solar wind frame as long as adiabatic deceleration does not play a significant role. In the inertial system the expected velocities range from zero to $2 \cdot V_{SW}$ with corresponding observable energies between zero and four times the solar wind bulk energy ($0 < E_{pick-up} < 4 \cdot M/2 \cdot V_{SW}^2$).The energy spectrum should show a clean cut-off at that energy value . The spectrum below cut-off should reflect the effect of adiabatic deceleration in the expanding interplanetary medium upstream of the observer.

3. INSTRUMENTATION and SATELLITE. The data presented here are obtained with the suprathermal particle spectrometer SULEICA of the Max-Planck-Institute/ University of Maryland onboard the IRM spacecraft of the Active-Magnetospheric-Particle-Tracer Explorer project (AMPTE), launched on 11. August 1984 into a highly elliptical orbit with an apogee of 18.9 earthradii. During the time period from launch until December 1984 the S/C spent a large fraction of each orbit in the solar wind upstream of the bow-shock of the earth. The SULEICA spectrometer is based on the techniques of electrostatic deflection followed by a time-of-flight and residual energy measurement(for details see MÖBIUS et al.1985). The electrostatic deflection analyser, represented by two concentric segments of a sphere, selects incoming ions according to their energy per charge in 24 logarithmically spaced voltage steps corresponding to an energy range from 5 to 226 keV/charge. After passing through the analyser the ions enter the time-of-flight section where the velocity of the ions is measured. The ions are stopped in a Silicon surface barrier detector where the residual energy is determined. The geometrical factor of the instrument is $4.3 \cdot 10^{-2}$ cm ^{2}sr and the energy resolution is $\Delta E/E \approx 0.097$.
For the investigation presented here the energy of the pick-up ions is too low to create a sufficiently high energy signal in the solid-state detectors. Therefore we identify the ion-species only by combining the electrostatic deflection (E/Q)and the time of flight signal (TOF). For a given E/Q step the TOF histogram as shown in figure 1 therefore represents a mass-per-charge histogram which is taken in the direction of the solar wind.

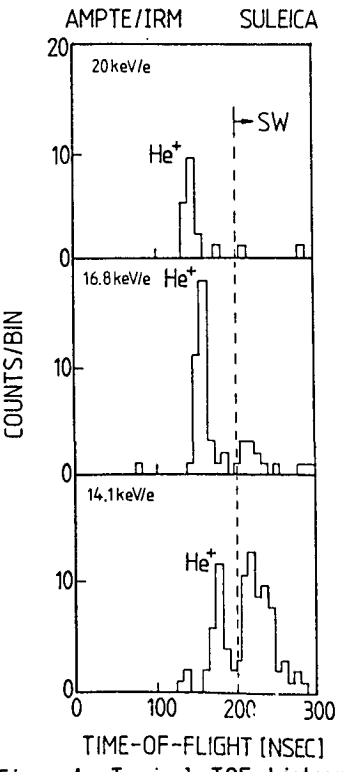

Figure1: Typical TOF-histogram at three different energy steps, takenin the solar sector.Data are obtained on Nov.11,1984 at ≈18 R_E in front of the bow- shock

4. OBSERVATIONS. A limited number(ten) of observational periods were chosen in the solar wind between launch of the S/C and December,15, 1984. During all periods we observed a peak in the TOF-histograms at M/Q = 4 at E/Q steps which are significantly higher than we would expect for genuine solar wind particles. Depending on the E/Q step and the solar wind velocity, we also observe in addition a broad and variable peak at TOF values which correspond to the solar wind velocity. These ions with M/Q values above 5 correspond to solar wind heavy ions. Figure 1 shows a typical example of TOF histograms for three different E/Q steps obtained on November11, 1984. It should be noted, that the He^+ peak is visible at all orientations of the interplanetary magnetic field no matter wether bow-shock accelerated ions are present or not.

Figure 2 shows the energy-density spectrum of the M/Q = 4 peak as measured during a sample period of 40 minute duration on Novenber 11,1984, when there are no bow-shock accelerated particles present. The spectra are taken from the directional sector which also contains the solar wind. Except the two neighbouring sectors all other sectors do not show any counts in the M/Q = 4 bin.There is a sharp cut-off at an energy of about 23 keV/e which corresponds to four time the bulk-energy of the solar wind. Below the cut-off energy we observe a more or less flat distribution which ends at a sharp rise of the spectrum at about 8 keV/e. We attribute the rise to solar wind particles of M/Q = 4 which will be not discussed in this paper.

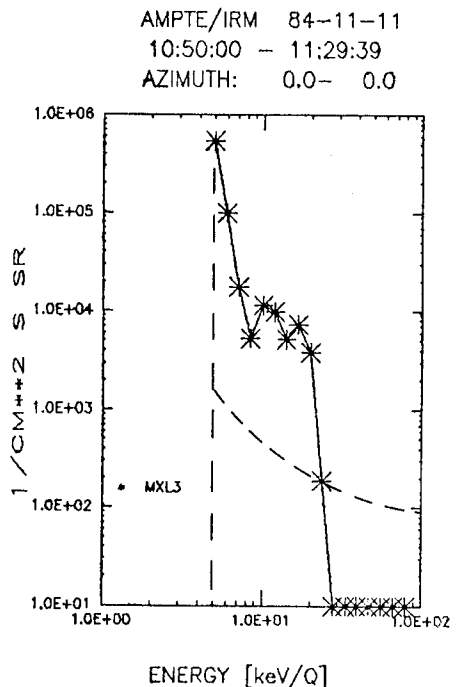

Figure 2:Example of an energy-density spectrum of the M/Q=4 ion channel accu- mulated over 40 minutes. Dashed curved line represents the 1 count/step level.

5. Discussion. Following the arguments in section 2 we tried to correlate the experimental cut-off energies, firstly (figure 3) with the full four-fold solar wind bulk-energy for mass M = 4 (Helium), and secondly (figure 4) with the four-fold component perpendicular to the local interplanetary magnetic field (eq. (2)).

There is an excellent correlation with the full energy (correlation coefficient = 0.98) while the correlation with the perpendicular component is rather poor (correlation coefficient = 0.26). This result suggests that the originally injected ions have lost their directional information in the solar wind frame due to pitch angle scattering, while maintaining their injection energy. The poor correlation with the perpendicular component shows that the ions have lost their directional information and therefore suggests that the source region of the ions extends beyond one mean free scattering length upstream of the observer. The magnetic rigidity of suprathermal singly ionized helium of a few keV/nucleon is in the order of 5 to 10 MV. The mean free path is known to be of the order of 0.05 AU during quiet interplanetary conditions (e.g.compilation in MASON et al.(1983)). The apparently large extent of the source region excludes a terrestrial origin of the ions.

The effect of adiabatic deceleration is expected to be high due to strong coupling of the particles to the solar wind. This sets an upper limit for the distance between point of origin and observer. Ions originating too far upstream (or too close to the sun) loose so much energy that they become indistinguishable from the solar wind itself.

To get a rough estimate of the source strength of the pick-up ions we use the energy spectrum (figure 2) and argue that the energy channels below the cutoff energy are populated via adiabatic deceleration , the rate of which is assumed to vary as 1/r with heliocentric distance. The measured

quantity $E \cdot dj/dE \cdot d\Omega$ in each energy channel in figure 3 is related to the relevant source- quantities as: $E \cdot dj/dE\, d\Omega \approx E \cdot S(r) \cdot \Delta r \cdot 4 \cdot \Delta\Omega_{SULEICA}/(4\pi \cdot \Delta E \cdot \Delta\Omega) = S(R) \cdot \Delta r/\pi \cdot (E/\Delta E)$

where $S(r) = N_{He} \cdot \nu_{ion}$ is the source strength of singly ionized helium. For a relative energy width of the instrument of $\Delta E/E = 0.1$ the length of the source column upstream of the S/C translates into $\Delta r = 0.2$ AU $= 3 \cdot 10^{12}$cm. Using an average value of $7 \cdot 10^{3}$ for the energy density of the pick-up ions(from figure 2) we obtain a source strength $S(r=1\ AU) \approx 8 \cdot 10^{-10}$ /cm^{3}s. For an ionization rate of $8 \cdot 10^{-8}$/s (e.g.Holzer 1977) we arrive at a neutral interstellar helium density $N_0 = 10^{-2}$ /cm^3, a value which is fully compatible with results from optical EUV measurements of He II resonantly scattered EUV-lines (WELLER and MEIER 1974; DALAUDIER et al.1984) in the heliosphere. These measurements represent the first direct observation of energetic helium ions picked-up by the solar wind from the interstellar neutral wind thereby filling one more gap in the hypotheses to explain the anomalous cosmic ray component.

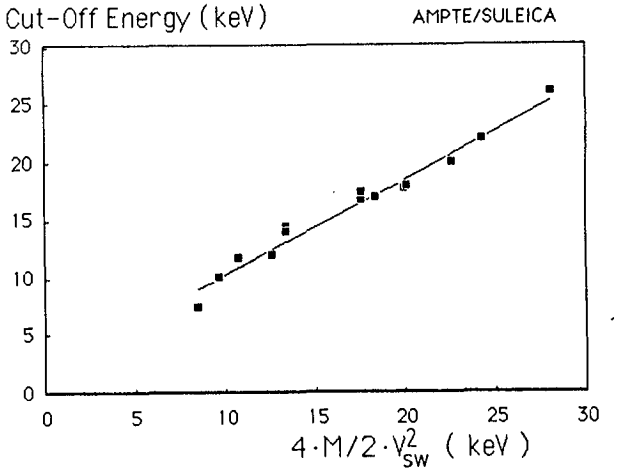

Figure 3: Correlation between experimenmtal cut-off energies and the four-fold solar wind bulk-energy (Correlation coefficient = 0.98).

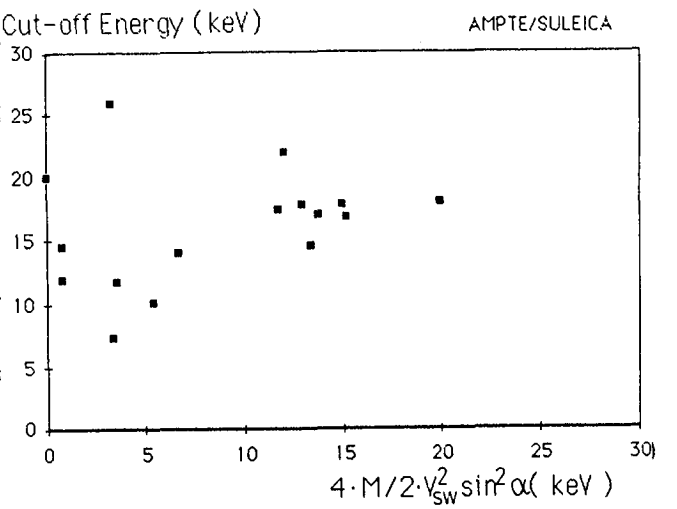

Figure 4: Same as figure 3, but abscissa is vertical-to-B component of the SW bulk-energy(Corr.coeff.=0.26).

Acknowledgement The authors are grateful to the many individuals at the Max-Planck-Institut and the University of Maryland who contributed to the success of the experiment and to the AMPTE project as a whole.

REFERENCES

Allen 1973, ASTROPHYSICAL QUANTITIES, The Athlone Press, London
Dalaudieretal. 1984, Astron. Astrophys., **14**, 171
Fisk et al. 1974, Ap. J. Letters **190**, L35
FiskL.A. 1976a, Ap.J. **206**, 333; 1976b, J.Geophys.Res. **81**, 4633,
Garcia-Munoz et al. 1973, Ap.J.Letters **182**, L81
Holzer 1977, Rev.Geophys. Space Phys., **15**, 467
Hovestadt et.al. 1973, Phys.Rev.Letters, **3**, 650
Mason et al. 1983, Ap.J. **267**, 844
Mc Donald et al. 1974, Ap.J. Letters **187**, L105
Möbius et al. 1985, IEEE Transactions on Remote Sensing, issue May 1985
Pesses et al. 1981, Ap.J.Letters, **246**, L85
Weller and Meier 1974, Ap.J. **193**, 471

ON THE ANOMALOUS COMPONENT

M. S. Potgieter, L. A. Fisk and M. A. Lee
Space Science Center, University of New Hampshire
Durham, NH 03824, USA

1. Introduction. The so-called anomalous cosmic ray component, which occurs at energies of about 10 MeV/nucleon and consists only of He, N, O, and Ne, has been a subject of interest for more than a decade. The origin of this component is generally considered to be interstellar neutral gas that is ionized and accelerated in the solar wind, as was proposed by Fisk et al. (1974). The mechanism and the location for the acceleration, however, remains an unsolved problem.

In this paper, we use a model which includes the effects of gradient and curvature drifts and consider the implications of observed spatial gradients of the anomalous component for the location of the acceleration region. We conclude that if drifts are important the acceleration region cannot lie at the solar poles. We also conclude that there is no single region for the acceleration which can account for both the observed intensities and gradients in models which include drift effects.

2. Results and Discussion. Pesses et al. (1981) proposed a mechanism for the acceleration of the anomalous component based on the acceleration of particles at the solar wind termination shock over the poles. They argue that once the particles are accelerated, gradient and curvature drifts will bring the particles downward from the heliospheric polar regions onto the equatorial plane. After a polarity reversal of the solar magnetic field, the oppositely directed drifts will restrict the passage of particles onto the equatorial plane. They therefore predict a dramatic change in the intensity of the anomalous component from cycle to cycle.

A complicating factor for drift models, however, is the small radial gradients these models predict for periods when the interplanetary magnetic field (IMF) is directed outwards in the northern heliosphere, as in 1970-80 (Potgieter, 1985). During this period the downward drifts of particles from the polar regions onto the equatorial plane tend to make the radial gradients in the equatorial plane small. The gradients also prove to be rather insensitive to changes in modulation parameters, for instance, the parallel diffusion coefficient. The question therefore arises whether a polar source for the anomalous component and strong drift effects can be compatible with the observed radial gradients of 10%-15%/AU for the anomalous component (Webber et al., 1981, 1985).

In this preliminary study we assumed a source spectrum for the anomalous oxygen which yields approximately the observed 1976-77 energy spectrum at Earth using a drift model for the modulation of cosmic rays (Potgieter and Moraal, 1985). To obtain a source which can be placed at various Θ-(polar angle) values at a radial distance of 50 AU, we used Gaussian spectra of the form

$$j_T^* = j_T \exp\{-0.028(\Theta - \Theta_o)^2\} \quad ,$$

with a half-width of 10° about Θ_o and j_T the assumed Θ-independent anomalous oxygen spectrum. We then solved the cosmic-ray transport equation,

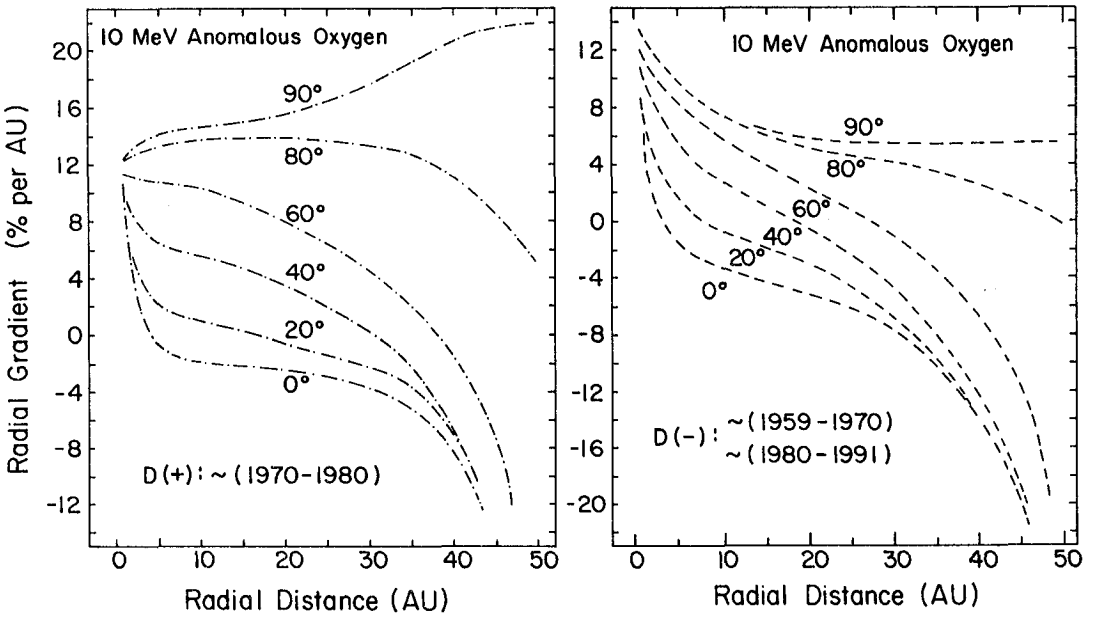

Fig. 1: Calculated radial gradients in the equatorial plane as a function of radial distance with a source at 50 AU and various polar angles; (a) for a D(+) cycle with drifts downward onto the equatorial plane at Θ = 90°, and (b) for a D(-) cycle that is with the polarity of the IMF reversed.

assuming a steady-state and azimuthal symmetry, shifted the source in 10° intervals from the pole to the equator at Θ=90°, and calculated the radial gradients in the equatorial plane for each location of the source. We repeated the calculations with the IMF polarity reversed, but otherwise unchanged modulation parameters. The diffusion coefficients used correspond to solar-minimum conditions (Potgieter and Moraal, 1985).

To distinguish between the two configurations of the IMF, we use the notation D(+) for ~1970-80 and D(-) for the 11 years before and after this period. Starting with a D(+) period, that is with drifts directed downward onto the equatorial plane, we show in Fig. 1a the radial gradients in the equatorial plane for 10 MeV anomalous oxygen as a function of radial distance with the source at 50 AU and various polar angles. The striking feature of this figure is the dramatic decrease of the radial gradient with increasing radial distance, from ~10%/AU at Earth to a negative gradient, with the source placed at 50 AU over the pole. With the source at the equatorial plane, the radial gradient steadily increases from 12%/AU at Earth to about 22%/AU at 50 AU. Fig. 1b shows the situation with the polarity of the IMF reversed, that is with drifts directed from the equatorial plane toward the polar regions. The radial gradients, with the source at the pole, again rapidly decrease with increasing radial distance. With the source at the equator, the radial gradients compared to Fig. 1a are smaller for most of the heliosphere out to 50 AU.

The results of Fig. 1 indicate the following. The radial gradients in the equatorial plane, with a source at the pole, are inconsistent with the observed radial gradients for the anomalous component, independent of the polarity of the solar magnetic field. By moving the source towards the equatorial regions, the calculated radial gradients become comparable to those observed. The calculated values, however, are significantly smaller, except in the inner heliosphere, for the present cycle as compared to the previous cycle, whereas the observed values seem to remain constant before and after the polarity change in 1980 (Webber et al., 1985).

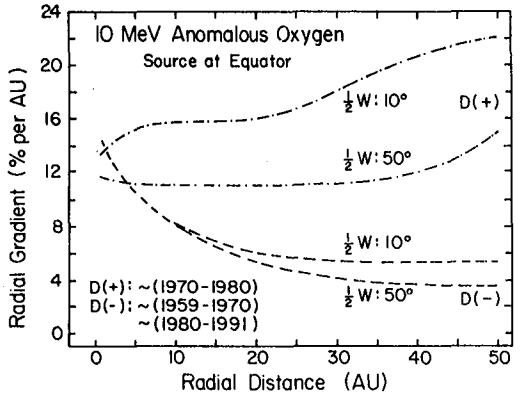

Fig. 2: The effect of increasing the half-width (W) of the source spectrum, from 10° to 50°, on the radial gradients in the equatorial plane with a source at the equator at 50 AU.

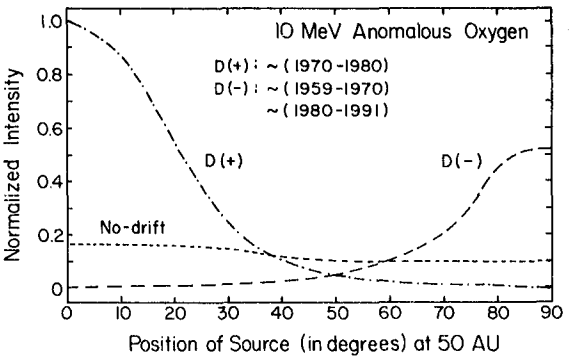

Fig. 3: The normalized intensity at Earth of 10 MeV anomalous oxygen as a function of various polar angle positions of the source at 50 AU for periods before and after a polarity reversal.

We also investigated the effect of increasing the half-width of the source spectra from 10°, in steps of 10°, to 50° to simulate an extended, less localized source. For both the D(+) and D(-) cycle of the magnetic field the radial gradients in the equatorial plane change insignificantly with the extended source over the polar regions. The effect of an extended source placed at the equator is shown in Fig. 2. For the D(+) period the radial gradients now seem compatible with those observed.

The intensity for the anomalous oxygen at Earth with a source at various latitudes should also be taken into consideration. The intensity of the 10 MeV anomalous oxygen at Earth, normalized to the intensity during a D(+) period with a source at the pole, is given in Fig. 3 as a function of the position of the source at 50 AU at various polar angles. For the D(+) period (downward drifts) the intensity at Earth decreases rapidly as the source is shifted from the pole to the equator. Comparing the intensity for the two periods, with the source at the pole, the D(-) intensity is substantially lower (a factor of 200) as was suggested by Pesses et al. (1981). For the D(-) cycle the intensity increases as the source is shifted toward the equator. It is interesting to compare this behavior, dependent on the polarity of the IMF, to the no-drift case shown in Fig. 3.

Our calculations show that, although the intensity of the anomalous oxygen, with a source at the pole, dramatically decreases after a change in the IMF polarity, the radial gradients in the equatorial plane are inconsistent to those observed. Furthermore, although the radial gradients for a D(-) cycle (the present cycle) with a source at 50 AU at the equator seem comparable to observations, the calculated intensity during this cycle exceeds the intensity during a D(+) cycle (the previous cycle), which is again contrary to what is observed.

3. Concluding Remarks. It should be noted that no attempt has been made in this preliminary study to include acceleration at the termination shock in a self-consistent manner. As has been pointed out recently by Jokipii (1985), drifts along the shock front and in the IMF can affect the spectrum and the spatial distribution of particles at the termination shock. When drifts are downward from the poles, they are poleward along the shock front. Both effects tend to limit the shock acceleration of particles that are injected near the poles. Conversely, when the drifts are towards the poles in the IMF, as they are in the current cycle, the drifts are downward from the poles along the shock front. These effects will increase the number of times particles interact with the shock, thereby increasing the energy they can gain, and will spread particles injected over the poles towards the equatorial region.

The complication of an accelerated spectrum which evolves with changing field polarity does not affect our conclusion that the injection and acceleration cannot occur primarily over the solar poles in models in which drift effects are important. During the last cycle, when drifts were downward from the poles, drifts along the termination shock front would concentrate the acceleration at the poles. However, as we demonstrated above, in this case the radial gradient seen in the equatorial plane is inconsistent with observations. An evolving spectrum at the termination shock could, however, affect the intensity seen at Earth.

In conclusion, we argued in this paper that the source for the acceleration of the anomalous component cannot lie at the solar poles in models that include gradient and curvature drifts. Such models will not yield the observed spatial gradients in the equatorial plane. We argued also that a source near the equatorial plane can yield the correct gradients, but in drift models will not yield the observed behavior in the intensity from cycle to cycle.

It would appear, therefore, that drift models may have significant difficulty in accounting for the observed features of the anomalous component.

References

Fisk, L. A., Kozlovsky, B., and Ramaty, R., 1974, Ap.J., 190, L35.
Jokipii, J. R., 1985, submitted to J. Geophys. Res.
Pesses, M. E., Jokipii, J. R., and Eichler, D., 1981, Ap. J., 246, L85.
Potgieter, M. S., 1985, Paper SH4.2-5, this conference.
Potgieter, M. S., and Moraal, H., 1985, Ap. J., in press.
Webber, W. R., McDonald, F. B., Von Rosenvinge, T. T., and Mewaldt, R.A., 1981, Proc. 17th ICRC (Paris), 10, 92.
Webber, W. R., Cummings, A. C., and Stone, E. C., 1985, this conference.

POSSIBLE ORIGIN OF THE ANOMALOUS COMPONENT OF COSMIC RAYS

Biswas, S., Durgaprasad, N., Singh, R.K.,
Vahia, M.N., and Yadav, J.S.
Tata Institute of Fundamental Research
Bombay 400 005, India

ABSTRACT

In this work we have studied the possible origin of the anomolous cosmic rays (ACR) in terms of stellar wind injection from O-type stars and their acceleration in shock fronts of SNR's. This is in continuation of our earlier work (Biswas,Durgaprasad, and Trevedi, Proc. Ind. Acad. Sci. 1981) in which we estimated that heavy ions of He^{+2},O^{+4},etc. of energy 10-100 KeV/N from the stellar wind will travel a distance of the order of (1-5) x 10^{2} pc in a hot and thin ISM. We assume that a fraction of these will encounter interstellar shock fronts of SNR's and these are accelerated to about 5-100 MeV/N and give rise to ACR's. Typically these ions would travel a distance of the order of a few 10^{3} pc. Therefore we estimate that O-type stars in a volume of radius of a few Kpc around the solar system are contributing to the intensity of ACR in the local ISM. From observational data, the intensity of ACR in the local ISM is estimated. It is suggested that these ACR ions enter the solar system along the solar dipole field lines connected to the interplanetary magnetic field lines.

THE COSMIC RAY INTERPLANETARY RADIAL GRADIENT FROM 1972 - 1985

Webber, W. R. and J. A. Lockwood
Space Science Center, University of New Hampshire
Durham, New Hampshire 03824 USA

1. Introduction It is now established that the solar modulation of the cosmic-rays is produced by turbulent magnetic fields propagated outward by the solar wind. Observations show that the modulation effects themselves propagate outward from the sun with speeds of the order of the solar wind speed [1, 2, 3, 4]. Therefore, changes in the cosmic-ray intensity are not simultaneous throughout the modulation region, thus requiring time-dependent theories for the cosmic-ray modulation [e.g., 5] . Fundamental to an overall understanding of this observed time-dependent cosmic-ray modulation is the behavior of the radial intensity gradient with time and heliocentric distance over the course of a solar modulation cycle.

We have focussed our attention primarily on the period from 1977 to 1985 when data are available from the cosmic-ray telescopes on Pioneer (P) 10, Voyager (V) 1 and 2, and IMP 8 spacecraft. Additional data from P10 and other IMP satellites for 1972 to 1977 can be used to determine the gradient (G_R) at the minimum in the solar modulation cycle and as a function of heliocentric distance R. All of these telescopes have thresholds for protons and helium nuclei of $E \gtrsim 60$ MeV/nucleon.

2. Observations In order to compare the cosmic-ray intensity at different heliocentric distances over a long time period we have calculated the 26-day average counting rates of the IMP 8, V1, V2 and P10 cosmic-ray telescopes. The normalized rates of these telescopes are shown in Fig. 1 along with the heliocentric distances of V1 and P10. There are several striking features about these normalized rates. First, the progressive separation of rates is a clear measure of a radial gradient. Second, time lags in specific decreases at the different spacecraft beginning about 1977 indicate an outward radial propagation speed for the solar modulation comparable to the solar wind speed [1,2]. Third, there is also an apparent time lag during the recovery phase seen in specific increases starting in early 1983. Fourth, the fractional decrease from late 1977 to the end of 1982 at earth and at P10 ($\sim$ 30 AU) are comparable in magnitude.

We can use the data shown in Fig. 1 to obtain the heliocentric radial gradient, keeping in mind that the gradient must be computed including the time delay noted above.

The differential radial gradient g_R is defined by:

$$g_R = 1/N \; (\partial N/\partial R) \qquad (1),$$

where N, the cosmic-ray intensity, is taken to be a separable function of R and t. Hence, N can be written:

$$N(R,t) = n_o f(R) h(t) \qquad (2),$$

where h(t) accounts for this delay time and f (R) represents the radial

dependence of the quasi-stationary intensity.

Thus,
$$g_R = \frac{1}{f(R)} \frac{df}{dR} \qquad (3),$$

In general, we use spacecraft at different R to determine the gradient, with one spacecraft remaining near earth (R = 1 AU). Then,

$$\int_{R_1}^{R_2} g_R dR = \int_{f_1}^{f_2} \frac{df}{f} = \ell n \frac{N(R_2)}{N(R_1)} = G_R(R_2 - R_1) \qquad (4),$$

where G_R is an integral gradient and $N(R_2)$ is taken at the time $t + (R_2-R_1)/V_{SW}$.

In Fig. 2 we have plotted G_R for P10/IMP as a function of R. There are several interesting features in this plot. First, G_R reaches a maximum around 5 AU, which is seen in all three panels of Fig. 2. Second, G_R is nearly constant as a function of both R (beyond $\sim$ 5 AU) and t between 1976-1982. During this period the cosmic-ray intensity at earth decreased in 1982 to 32% of the intensity in 1976 and the solar magnetic field reversed in 1980 with no apparent change in the gradient. Third, the decrease in G_R seen after 1982 indicates a different state in the cosmic-ray modulation in the heliospheric cavity.

3. Discussion There are several significant implications in the data shown in Figs. 1 and 2. We shall discuss two of them here.

a) The constancy of G_R over extended periods of time and radius as observed between 1976 and 1982 can be related to limits on the interstellar cosmic-ray intensity. Between 1976 and 1982 the normalized counting rate at earth decreased from 1.0 to 0.32, with a comparable decrease at P10 so that G_R remained essentially constant throughout this period. This behavior is indicated in Fig. 3 for six time periods of relatively constant intensity (no large transient variations propagating outward) between 1976 and 1984 as indicated by shaded areas in Fig. 1. We can use Fig. 3 to determine the fraction of total modulation beyond a given R. First, we need to estimate the residual modulation at earth at sunspot minimum [6]. We assume that the interstellar proton spectrum can be parameterized by the form $dJ/dT = \text{constant} \cdot T^{0.3} (T + T_o)^{-3.0}$, where T = kinetic energy and T_o is a variable parameter between 0.3 - 0.5 GeV/nuc. This corresponds to a residual modulation parameter ϕ = 450 ± 100 MV at sunspot minimum [7]. We have integrated interstellar spectra for this range of T_o to determine the expected rate for T > 60 MeV/nuc as indicated on Fig. 3. Thus, for 1976 the reduction in the intensity between the heliospheric boundary and earth is calculated to be a factor of 4.3 if T_o = 0.4 GeV/nuc. In 1977 when P10 is at $\sim$ 15 AU about 60% of the modulation must occur beyond this distance. During 1981-82 about 85% of the modulation must occur beyond 30 AU. Thus, at solar minimum, and even more so at solar maximum, most of the modulation is occurring in the outer heliospere beyond 15-30 AU!

b) It appears from Fig. 2 that the conditions in the heliospheric cavity were different after 1982 since G_R in the inner heliosphere decreased from $\sim$ 2.8%/AU to $\sim$ 1.8%/AU. This is shown more clearly in Fig. 3 where it is evident that this is a temporal effect and the

gradient remains relatively constant as a function of radius.

From a study of the heliocentric radial dependence of the characteristic recovery time t_o of 19 transient Forbush-type decreases occurring from 1980 to 1984 we found that t_o is about 20 times longer at 30 AU [8]. We would then expect that at R ∿ 30 AU a typical transient would take ∿ 100 days to recover to 1/e whereas near earth it is only ∿ 5 days. In a simple model then the intensity will recover first at earth as the transient decreases pass outward beyond earth and become less frequent. This more rapid recovery at earth produces a lower G_R. We would expect this situation of a smaller G_R to persist until the number and magnitude of the transient decreases are insignificant. At that time (∿ 1988) one might expect the gradient to return to its sunspot minimum value of ∿3%/AU. In 1988 when P10 will be at ∿ 45 AU we would estimate that the normalized intensity at 1 AU would be unity. If at that time G_R ∿ 3%/AU, the normalized intensity at P10 relative to earth would be ∿ 3.5, so P10 would then possibly be sampling the interstellar spectrum. However, if the gradient remains ∿ 2%/AU, P10 at 45 AU would still be well within the modulation region. An important clue as to the origin of the modulation in the distant heliosphere will be obtained from observations of this gradient between now and 1988.

4. Acknowledgements The authors thank Frank McDonald for making available the data from the Pioneer and Voyager spacecraft and Tycho vonRosenvinge for providing the IMP data. This study was supported by the NSF (ATM-8304486) and GSFC (NAS-24354).

5. References

1. McDonald, F.B., et al., (1981), Ap. J., 249, L71.
2. Webber, W.R. and J.A. Lockwood, (1981), J. Geophys. Res. 86, 11458.
3. McKibben, R.B., et al., (1982), Ap. J., 254, L23.
4. Lockwood, J.A., and W.R. Webber, (1984), J. Geophys. Res., 87, 17.
5. Perko, J. and L. Fisk, (1983), J. Geophys. Res., 88, 9033.
6. Webber, W.R., and J.A. Lockwood, (1983), 18th ICRC, 3, 59.
7. Webber, W.R., and S.M. Yusak, (1983), Ap. J., 275, 391.
8. Webber, W.R., et al., (1985), J. Geophys. Res., to be published.

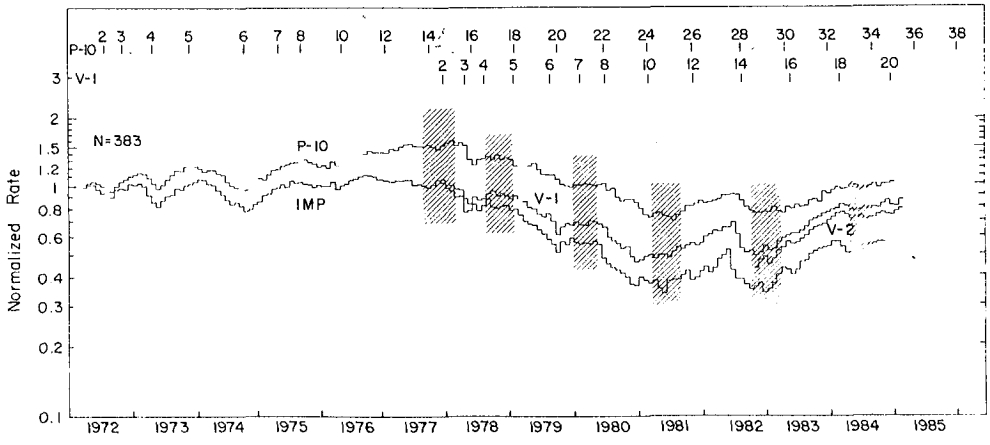

Fig 1: Normalized rates of > 60 MeV particles from IMP8, V1, V2 and P10. Heliocentric distances for V1 and P10 are shown.

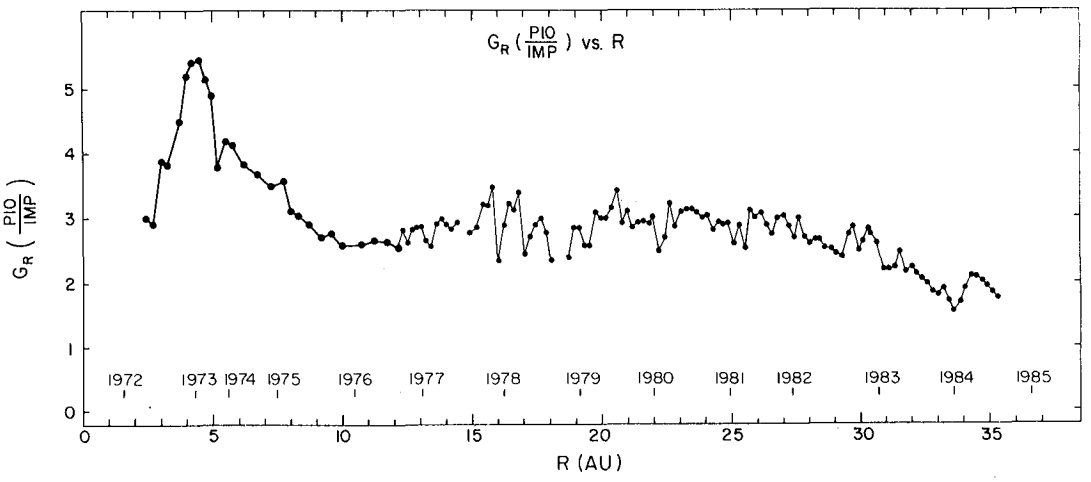

Fig. 2 G_R(%/AU) for P10/IMP8

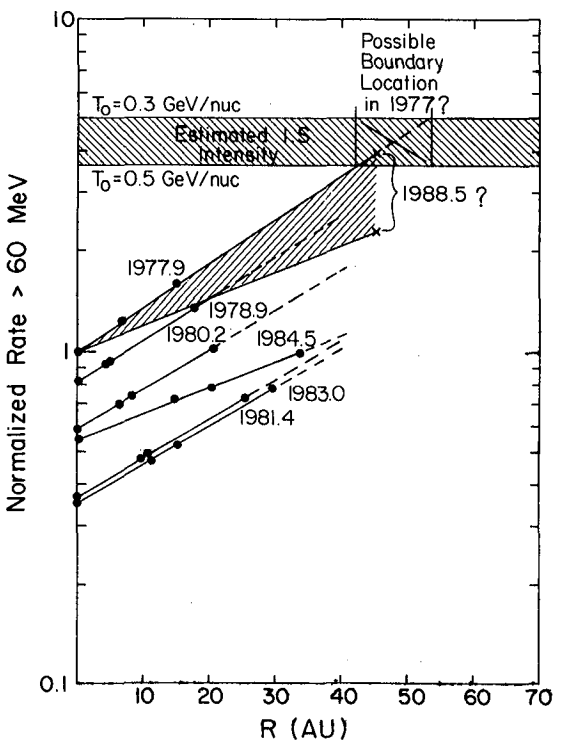

Fig 3: Radial variation of >60 MeV rate at various 26-day periods (see Fig. 1) from P10, V1, V2 and IMP8 data. Estimated interstellar rates are shown as described in text.

189

TIME AND ENERGY DEPENDENCE OF THE COSMIC RAY GRADIENT IN THE OUTER HELIOSPHERE

Fillius, Walker
University of California, San Diego, La Jolla, CA 92093

Axford, Ian
Victoria University of Wellington, New Zealand

Wood, David
University of California, San Diego, La Jolla, CA 92093

ABSTRACT

Pioneers 10 and 11, now 35 and 18 AU from the sun, continue to extend our knowledge of the spatial dependence of cosmic ray intensities in the heliosphere. We report radial gradients measured from these spacecraft by UCSD detectors which have integral energy responses above thresholds of 80 and 500 MeV/nucleon. An average gradient of ~ 2 %/AU typifies the data set as a whole, but there are time and energy dependences that deviate from this value.. With operating lifetimes of 13 and 12 years, respectively, for the two spacecraft, we have followed the time dependence for over a solar cycle.. The higher energy channel shows less modulation on all time scales.. At the start of the present cycle, the gradient is lower than the average value during the last solar cycle.

INSTRUMENTATION

Table I outlines the characteristics of the four UCSD data channels used in this report..

Table I

CHARACTERISTICS OF FOUR UCSD DATA CHANNELS

	Z = 1 Energy Range	Relative Response (Ratio)	Z > 1 Energy Range
M3	80<E<300 MeV	50 : 50	>80 MeV/nucl
M1	>80 MeV	90 : 10	>80 MeV/nucl
C1	>500 MeV	80 : 20	>500 MeV/nucl
C3	>500 MeV	30 : 70	>500 MeV/nucl

OBSERVATIONS

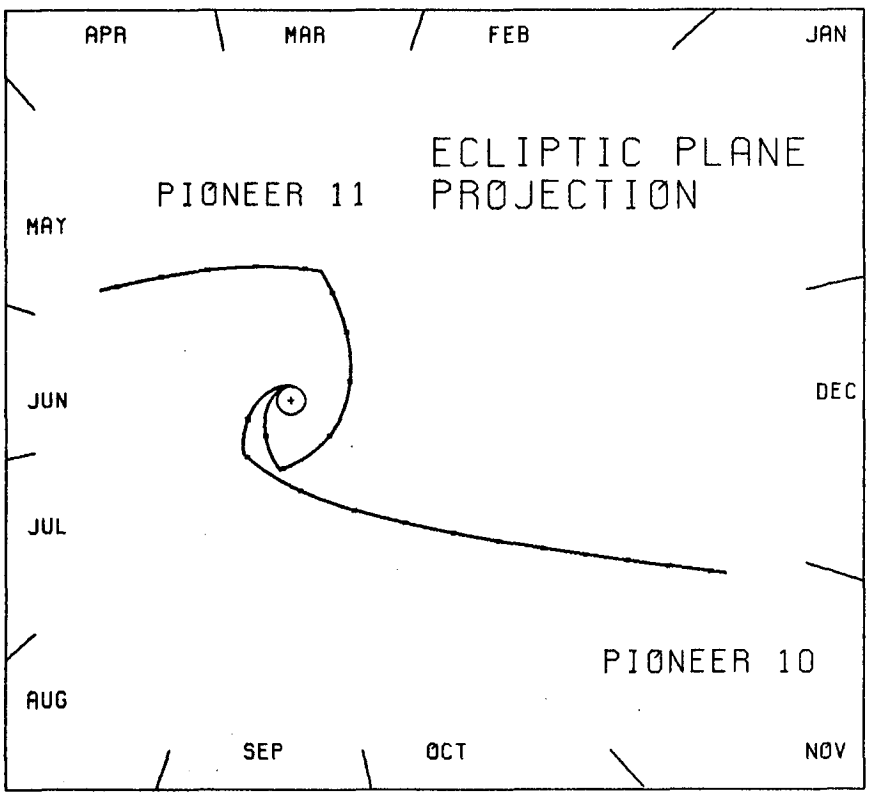

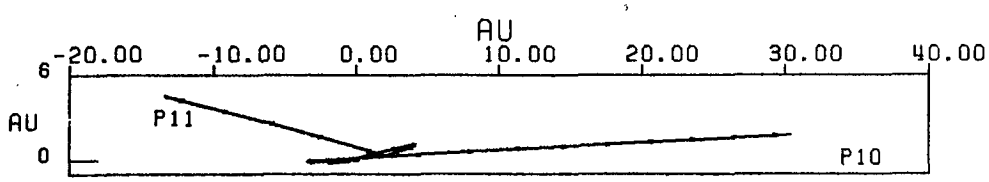

Figure 1 shows the positions of the two Pioneer spacecraft up to mid-1985..

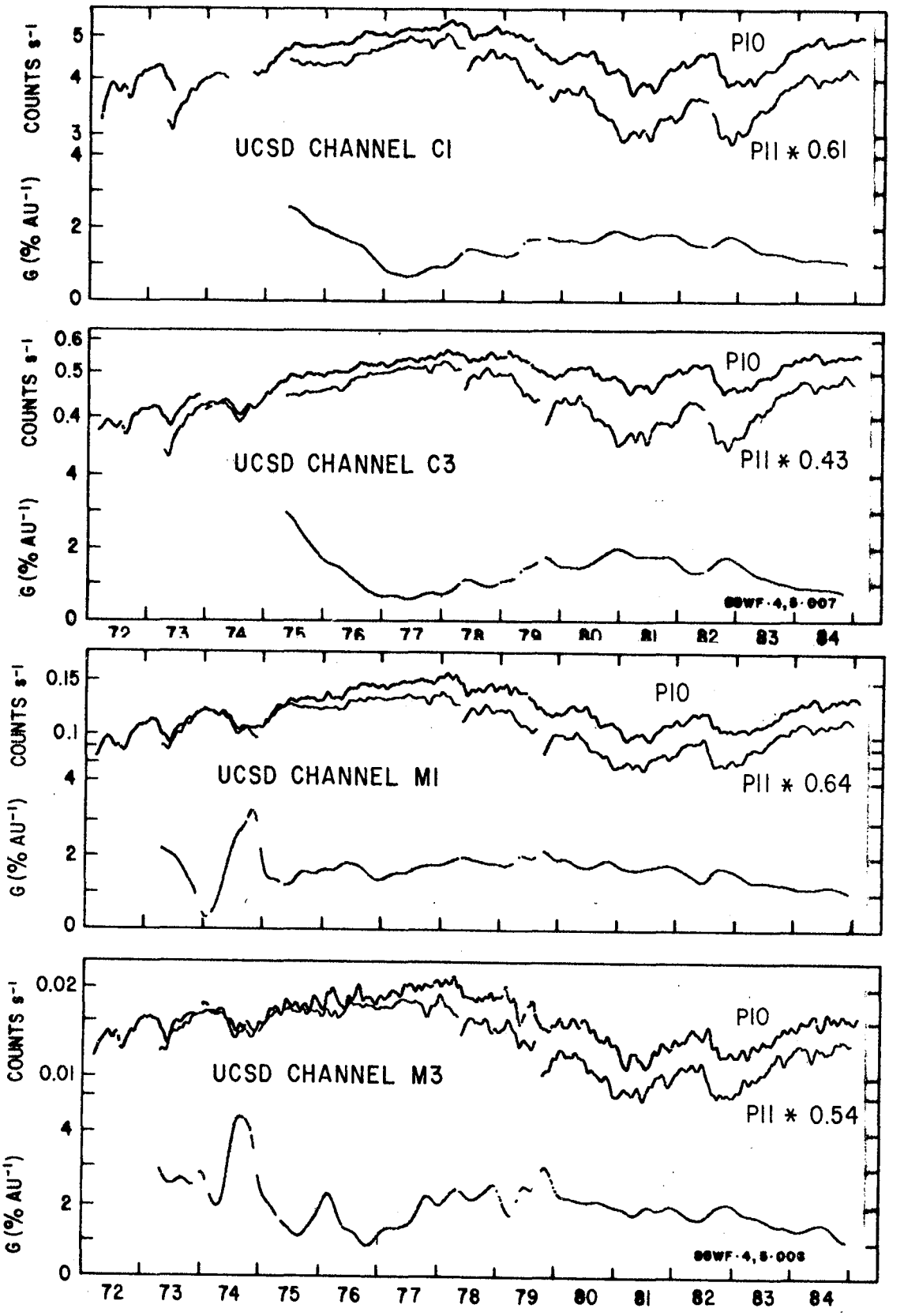
UCSD CHANNEL C1
P10
P11 * 0.61
UCSD CHANNEL C3
P10
P11 * 0.43
UCSD CHANNEL M1
P10
P11 * 0.64
UCSD CHANNEL M3
P10
P11 * 0.54
COUNTS s⁻¹
G (% AU⁻¹)
72 73 74 75 76 77 78 79 80 81 82 83 84

Figures 2 and 3 show the gradient as a function of time, for each channel in Table I, calculated from normalized counting rates from the two spacecraft.. The data have been passed through a gaussian low-pass filter to smooth the graphs..

ACKNOWLEDGEMENT

This work was supported in part by NASA Grants NAS 2-153 and NGL 05-005-007..

THE LARGE SCALE DYNAMICS OF THE OUTER HELIOSPHERE AND THE LONG-TERM MODULATION OF GALACTIC COSMIC RAYS

Frank B. McDonald, NASA Headquarters/Code P, Washington, DC 20546
T.T. von Rosenvinge, N. Lal, P. Schuster, J. H. Trainor,
NASA/GSFC, Greenbelt, MD 20770
M.A.I. Van Hollebeke, Musee National des Sciences, Technique et Industrie
PARC de La Villette, Paris, France

ABSTRACT

The network of cosmic-ray observatories reaching across the heliosphere has given new insight into the process of solar modulation, establishing that the decreases occur principally in the outer heliosphere and are produced by interplanetary flow systems; that the hysteresis effects appear to be produced by changes in the rigidity dependence of the diffusion coefficient and that the predicted effects on the cosmic ray gradients associated with the reversal of the solar magnetic field polarity are not observed.

1. Introduction. The study of cosmic ray modulation has traditionally been of importance in determining the local interstellar spectra of galactic cosmic rays and their transport in the heliosphere. The presence of a network of cosmic ray detectors at various heliocentric distances not only offers new insight into these areas but also offers a means of studying the dynamics of the interplanetary medium in the outer heliosphere. Pioneer 10 cosmic ray measurements now cover the period from 1972 to the present and extend to heliocentric distances beyond 32 AU (Fig. 1). Voyagers 1 and 2, launched in 1977, provide observations at intermediate heliocentric distances while Helios 1 and ISEE-3 provide "baseline" measurements at 1 AU. The data from the Goddard cosmic ray experiments (done in collaboration with the California Institute of Technology and the University of New Hampshire on Voyagers 1 and 2 and with the University of New Hampshire on Pioneers 10 and 11) on these missions give detailed differential energy spectra for galactic cosmic ray helium nuclei from 3-500 MeV/nuc and for hydroden nuclei from 3-250 MeV. The detector systems used on these various missions are similar in their method of operation but differ in detail and in their relative geometric factors. In this paper a summary overview is given of these observations along with differential measurements of the cosmic ray gradient over the last solar cycle.

2. Observations. Intensities of the higher energy He ($\sim$185-450 MeV/nuc) and H ($\sim$130-240 MeV) along with the integral measurements >70 MeV are shown in Fig. 2 in the form of 26 day averages. Lower energy data for 30-56 MeV/nuc H and He and the 10-21 MeV/nuc anomalous He interval are shown in Fig. 3 for Pioneer 10 and Voyager. The 1 AU data has not been included in this later plot because of the difficulty in removing the solar energetic particle contribution at low energies.

As noted previously (McDonald et al., 1981; Lockwood and Webber,

1984; McKibben et al.,1982; Van Allen and Randall, 1985) the long term decrease occurs in a series of three distinct steps between April 1978 and January 1981. These decreases propagate radially outward with a velocity of 400-500 km/sec. There is a recovery period starting in early 1981 which is interrupted by the onset of increased solar activity in 1982 which results in a fourth step decrease. In early 1981 at ∿24 AU and in late 1982 at 28 AU the galactic cosmic ray intensities at energies less than 500 MeV/nuc were distinctly lower than their 1 AU solar minimum values - suggesting that the bulk of the modulation must occur in the distant heliosphere.

The recovery is more complex and will have to be examined over a larger period of time to establish a pattern. One distinctive feature is a hysteresis effect as seen from the lag in the recovery of 10-21 MeV/nuc He and 30-56 MeV H (Fig. 3) as compared to the substantial recovery of the 185-450 MeV/nuc He (Fig. 2). If a clear rigidity

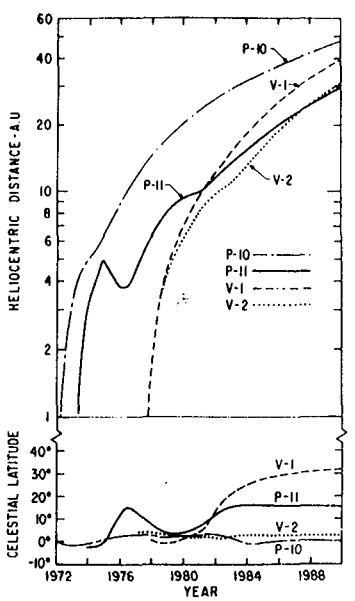

Fig. 1

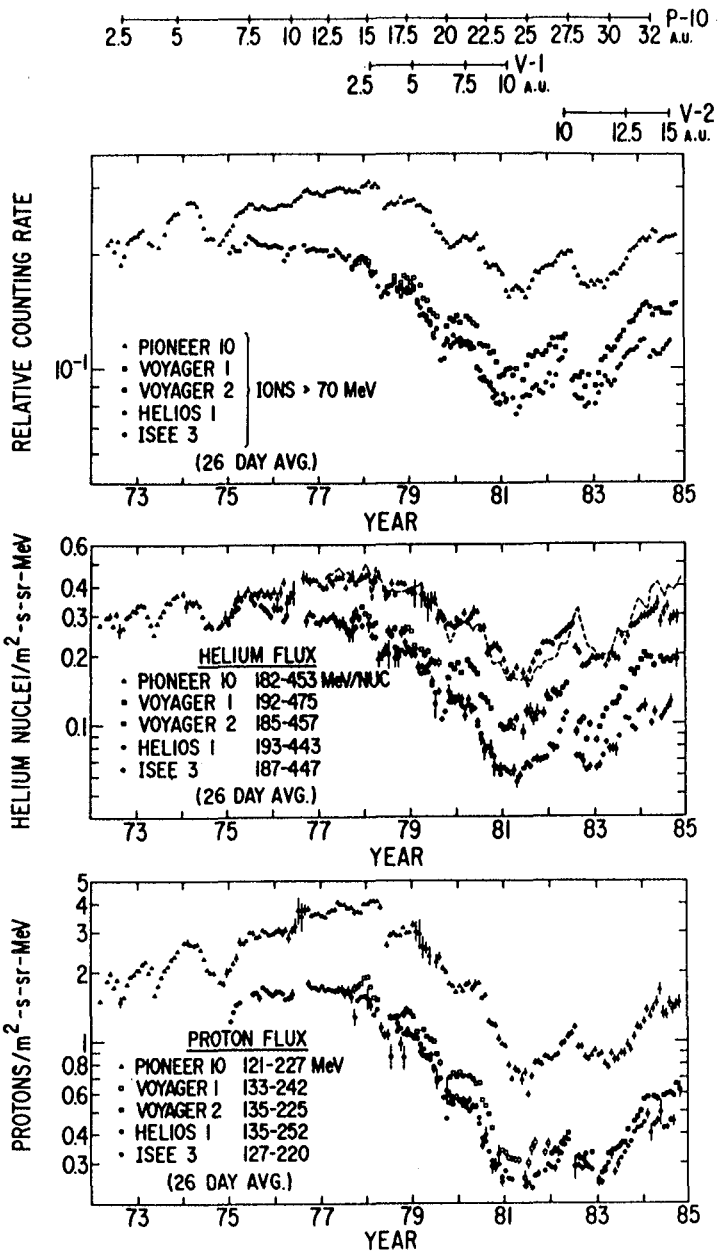

Fig. 2. The dashed line in the center panel is the extrapolation of the Helios/ISEE-3 data to the orbit of Pioneer 10 assuming a constant 4% AU gradient and a solar wind velocity of 550 km/sec.

dependence can be established for this effect it may offer a method of determining the charge state of the anomalous component (McKibben, 1973; Paizis and von Rosenvinge, 1981). It is also seen that the decreases propagate rapidly outward for the first three steps, this concept breaks down after ∿ 1982. This breakdown probably reflects large heliolongitude asymmetries resulting from a few very strong shocks.

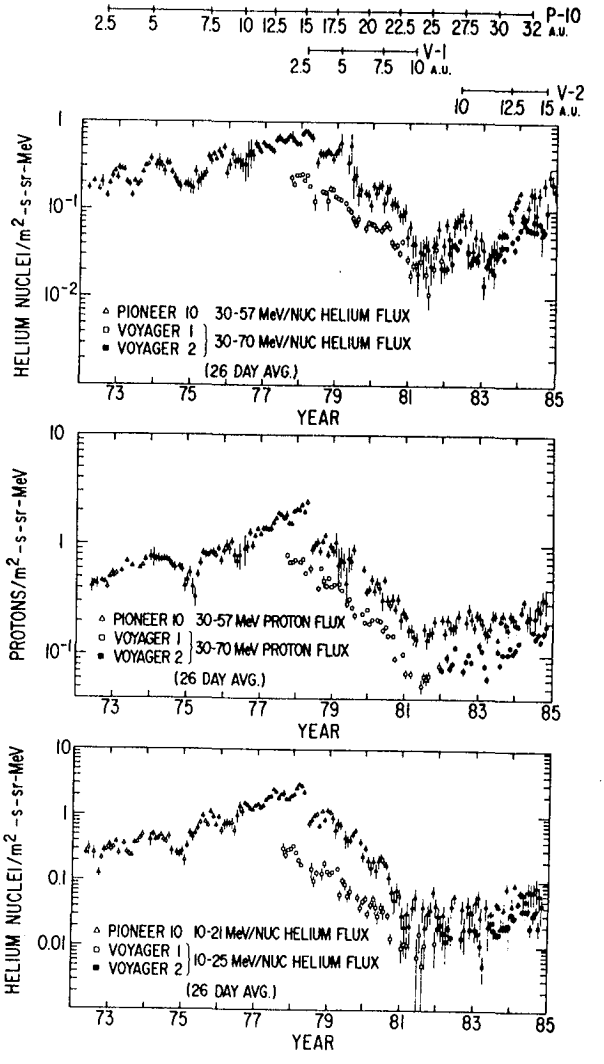

Fig. 3

Measurements of the differential gradient are shown for the solar minimum period (3/77, 12/77) and the plateau regions between the step decreases(Fig4). At solar minimum (3/77) the gradients in the inner solar system are substantially higher than those in the outer heliosphere. With the onset of increased solar activity, they show a complex change. For the high energy He (150-380 MeV/nuc), the gradient approaches a value of ∿4%/AU for both sets of measurements. A similar pattern is observed for 30-56 MeV/nuc H and He and in the outer heliosphere for the high energy protons. However this latter component has a very small gradient in the inner solar system after the onset of the first recovery period in early 1981. The anomalous He interval approaches a value of ∿10%/AU until this same recovery period and then also shows a sharp decrease in the outer heliosphere - in agreement with the observations of McKibben, et al., 1985.

3. Discussion. The step decreases have been explained in broad outline by Burlaga, et al., 1984, in terms of interplanetary flow systems containing a number of transient shocks and post shock flows. These systems of transient flows should evolve into expanding pressure waves such that the systems would merge and the outer heliosphere would be a region of enhanced turbulance. With such a system there would not be corresponding "step-increases" and the hysteresis effect would be explained by changes in the rigidity dependence of the diffusion coefficient in the outer region. If particle drifts play a major

role in the transport of galactic cosmic rays then an increase in the radial gradient is expected in the inner heliosphere at the time of the reversal of the solar magnetic field polarity (1980) (Jokipii and Kopriva, 1979). The gradient observations show either a decrease or no change. The failure of the anomalous He to recover has been predicted by drift models (Pesses et al., 1981) but there is no corresponding prediction for protons.

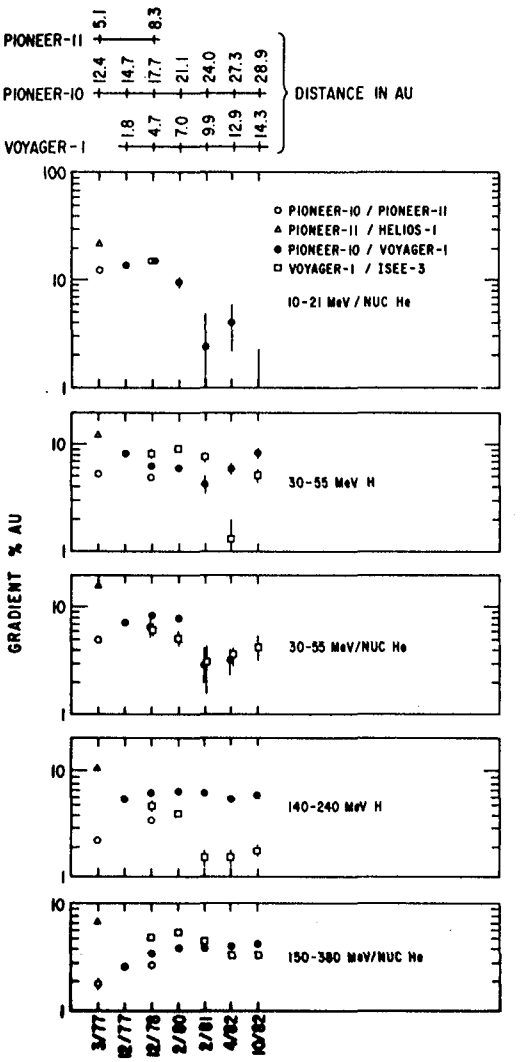

Fig. 4

References

1. Jokipii, J.R. and Kopriva, D.A., (1979), Ap.J., 234, 384.
2. Lockwood, J.A. and Webber, W.R., (1984), J. Geophys. Res., 89, 17.
3. McDonald, F.B., Lal, N., Trainor, J.H., Van Hollebeke, M.A.I., and Webber, W.R., (1981), Astrophys. J., 249, L71.
4. McKibben, R.B., Pyle, K.R., and Simpson, J.A., (1982), Astrophys. J., 254, L23.
5. McKibben, R.B., Pyle, K.R., and Simpson, J.A., (1985), Astrophys. J., 289, L35.
6. McKibben, R.B., (1977), Astrophys. J., 217, L113.
7. Paizis, C., and von Rosenvinge, T.T., (1981), Proc. 17th ICRC, 10, 73.
8. Pesses, M.E., Jokipii, J.R., and Eichler, D., (1981), Astrophy. J., 246, L85.
9. Van Allen, J.A. and Randall, B.A., (1985), J. Geophys. Res., 90, 1399.

197

Solar Modulation and Interplanetary Gradients of the Galactic Electron Flux 1977-1984

S. P. Christon, A. C. Cummings, and E. C. Stone

California Institute of Technology, Pasadena, CA 91125 USA

W. R. Webber

University of New Hampshire, Durham, NH 03824 USA

Previously, only one measurement of electrons at a location remote from earth has been reported [*Eraker,* 1982]. That measurement was made with a cosmic ray instrument on board the Pioneer 10 spacecraft during the period from 1972 - 1980, when Pioneer proceeded outward from 1 to 21.5 AU. Electrons of 1.75 - 25 MeV were observed. This energy range appears to be dominated by Jovian electrons, and no significant temporal or radial effects due to galactic electrons were observed.

In this paper we report on the flux of electrons with energy from ~ 10 - 180 MeV measured with the electron telescope on the Voyager 1 and 2 spacecraft [*Stone et al.,* 1977] in the heliocentric radial range 1 - 22 AU between 1977 and 1984. Jovian electrons were clearly observable between 1978 and 1983 (radial range 2 - 12 AU) at energies below ~ 50 MeV [*Christon et al.,* 1985]. Above ~ 50 MeV the electron intensity exhibited temporal variations generally related to the 11 year modulation of protons > 75 MeV. The overall magnitude of the electron intensity changes between the maximum intensity observed in 1977 and the minimum intensity in 1981 was a factor ~ 2, also comparable to that observed for > 75 MeV protons. By early 1985 the electron intensity had apparently recovered to the level observed in 1977 whereas the proton intensity was still about 20% lower. A detailed interpretation of these electron variations in all energy channels depends on an accurate subtraction of background induced by energetic protons of a few 100 MeV. This subtraction is facilitated by calibration results at several energies. Further results on these temporal variations and limits on possible interplanetary gradients will be reported.

This work was supported in part by NASA under contract NAS 7-918 and grant NGR 05-002-160.

References.

Christon, S. P., A. C. Cummings, E. C. Stone, and W. R. Webber, *19th Internat. Cosmic-Ray Conf., La Jolla,* paper SH1.5-18, 1985.

Eraker, J. H., *Ap. J., 257,* 862, 1982.

Stone, E. C., R. E. Vogt, F. B. McDonald, B. J. Teegarden, J. H. Trainor, J. R. Jokipii, and W. R. Webber, *Space Sci. Rev., 21,* 355, 1977.

GALACTIC COSMIC RAY RADIAL GRADIENTS AND THE ANOMALOUS He COMPONENT NEAR MAXIMUM SOLAR MODULATION AND TO RADII BEYOND 34 AU FROM THE SUN

R. B. McKibben, K. R. Pyle, and J. A. Simpson
Enrico Fermi Institute, The University of Chicago
Chicago, Illinois 60637 (U. S. A.)

ABSTRACT: Radial gradients for relativistic galactic cosmic rays (E > 70 MeV) remained nearly constant at ~2.5 %/AU from 1978-84, which includes the period of maximum solar modulation in 1981-82. For energies 30-70 MeV/n, gradients decreased at solar maximum to values of 1 %/AU (protons) and 4 %/AU (helium), and appear to be increasing again in 1983-84 toward the values found for solar minimum. The anomalous helium component has not reappeared, either at 1 AU or at Pioneer 10 at R > 34 AU.

1. INTRODUCTION: Our observations of the radial and temporal variations of the modulated cosmic radiation and anomalous helium to the time of maximum solar modulation in 1981-82 (McKibben et al., 1983, 1985) showed that, at solar maximum, radial gradients for low energy (E < 100 MeV/n) cosmic rays measured between 1 and 31 AU were sharply reduced from their values at solar minimum. At relativistic energies, however, the radial gradient was not strongly affected by the level of solar modulation. We now extend our observations to the end of 1984, by which time the cosmic ray intensity had begun to recover from maximum modulation both at 1 AU and in the outer heliosphere. The Pioneer and IMP instruments used in this study have been described by Simpson et al. (1980), and by Garcia-Munoz et al. (1977). By late 1984, Pioneer 10 had reached a radial distance of > 34 AU from the sun, as shown in Figure 1C.

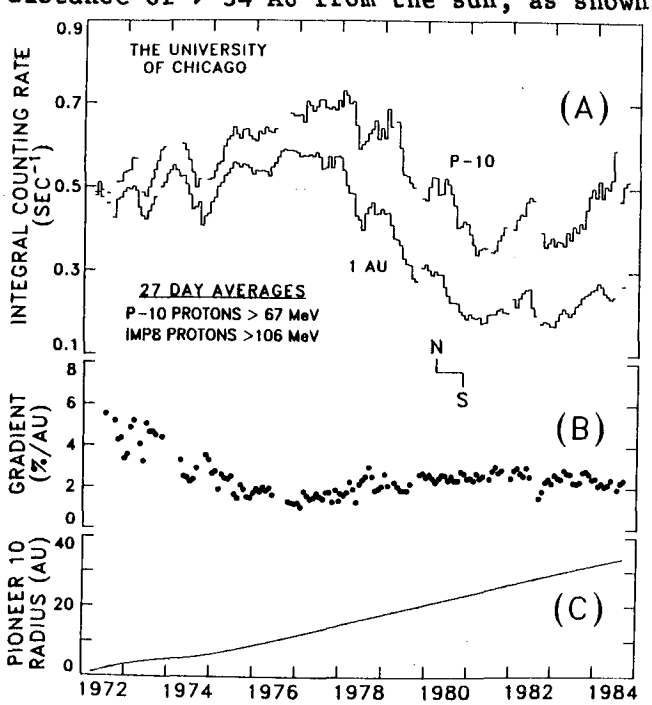

FIGURE 1

2. INTEGRAL GRADIENTS (E $\gtrsim$ 70 MeV): Figure 1A shows simultaneous 27 day averages of integral counting rates from Pioneer 10 (protons $\gtrsim$ 70 MeV) and IMP 8 (protons $\gtrsim$ 106 MeV), selected to exclude contributions from solar particles. These counting rates are dominated by relativistic particles with a mean energy of the order of 2 GeV. The time variations observed at Pioneer 10 remain well correlated with variations at 1 AU after a time shift corresponding to outward propagation at near the solar wind speed (McKibben et al. 1982). In late 1984, the flux at Pioneer 10 at 34 AU was increasing from the maximum modulation observed

in 1981-82, but was still not significantly greater than that observed at 1 AU at solar minimum in 1972. Therefore, the flux at Pioneer 10 remained heavily modulated in 1984.

Figure 1B shows the radial gradient of the integral intensity as a function of time. As in McKibben et al. (1983), a 400 km/s propagation delay from 1 AU to Pioneer 10 has been assumed. Although there are significant variations during the near-solar-minimum period (1972-1978), since 1978 the gradient has remained nearly constant at ~ 2.5 %/AU despite large changes in the intensity at both Pioneer and IMP. The transient decrease in the gradient in 1982 is an artifact of the high velocity [$\gtrsim$ 800 km/s (Lockwood and Webber, 1984)] of the shocks which produced the intensity decrease in 1982.

3. LOW ENERGY (E < 70 MeV/n) DIFFERENTIAL FLUXES: Figure 2A shows the low energy (30-70 MeV) cosmic ray proton flux as observed at Pioneer 10, Pioneer 11, and IMP 8 starting in 1977, shortly before the onset of renewed solar activity, continuing through solar maximum in 1981-82 and into 1984 when recovery of the cosmic ray flux had begun. After 1979, measurements in this energy range are not available from Pioneer 11 because a detector problem has blocked analysis of particles with energy > 20 MeV/n. As reported earlier (McKibben et al., 1985), at solar maximum (1981-82) for low energy protons, nearly the same flux was measured at Pioneer 10 (R > 20 AU) and at 1 AU. At both Pioneer 10 and IMP 8 the proton flux remained essentially constant during 1981-82, and the shocks that produced such strong effects at higher energies had little effect on the low energy proton flux. As the recovery began in 1983-84, the flux at Pioneer 10 once again increased above that at 1 AU.

Figures 2B-D show the 27-day-average radial gradients measured for 30-70 MeV protons, 11-20 MeV/n helium, and 30-70 MeV/n helium. The accuracy of the measurements is reflected in the scatter of the points. All three gradients decrease at solar maximum. The largest decrease is shown by the gradient of 11-20 MeV/n helium and corresponds to the disappearance of the anomalous helium in 1980-81. The shocks in 1982 appear to have produced a further decrease, lasting 6 months or more, in the 30-70 MeV/n helium gradient. No clear corresponding effects are observed for lower energy helium. After maximum modulation, the gradient of 30-70 MeV protons increased slightly, and the data also suggest an increase in gradients for helium.

The observations are summarized in Figures 3A-C, which contain yearly snapshots of the convection-corrected intensity of 30-70 MeV protons, and of 11-20 and 30-70 MeV/n helium. Open

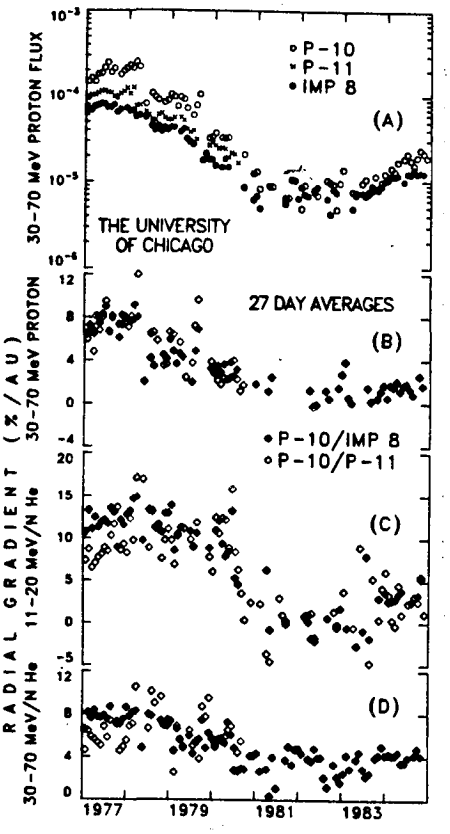

FIGURE 2

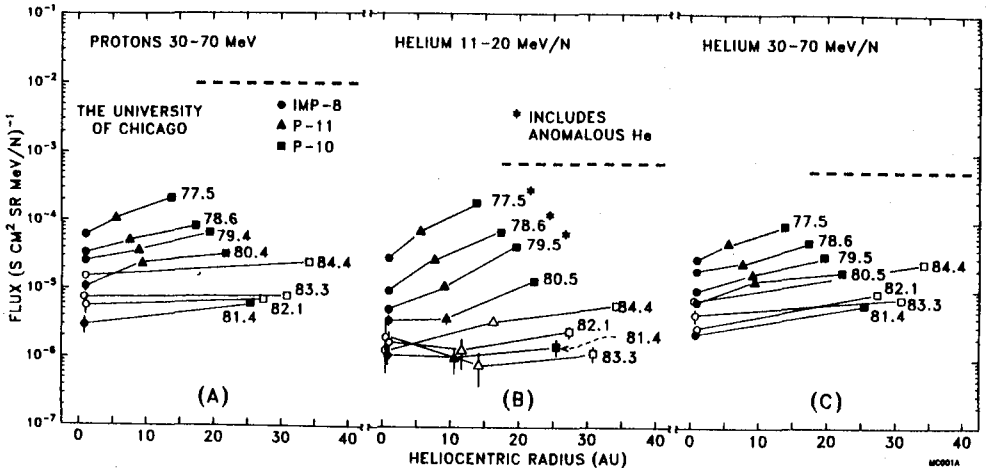

FIGURE 3

symbols correspond to data obtained since maximum modulation in 1981, and the heavy dashed lines indicate estimated interstellar galactic cosmic ray fluxes from the model of Evenson et al. (1983). For all three components, the flux measured in 1984 at Pioneer 10 remains below that measured at 1 AU at solar minimum in 1977. Comparing the observed fluxes in 1984 to the interstellar fluxes, at least 95% of the modulation takes place outside R = 34 AU. Linear extrapolation of the gradients observed in 1984 to the interstellar fluxes suggests modulation boundaries in the range 100-300 AU. However, modulation models suggest that the radial gradient may not remain constant to the boundary, so that linear extrapolation provides no reliable estimate of the boundary location. Furthermore, the radius of the boundary itself may vary with solar activity. Thus, based on our observations to date, we conclude only that the current radius of the modulation region is much larger than 35 AU.

IV. ANOMALOUS HELIUM: The anomalous helium component was present from 1972-79 at Earth and at Pioneer 10 and 11. It disappeared at 1 AU in 1979 and at Pioneer 10 (R > 20 AU) in 1980-81, at roughly the same time as the reversal of the sun's polar magnetic fields. Alternate models for the acceleration and modulation of this component predict either that it will be observed near the ecliptic only when the north pole of the sun is magnetically positive (Pesses et al., 1981), or that it will be observed whenever modulation is sufficiently weak (Garcia-Munoz et al., 1983).

The anomalous component helium spectrum is significantly softer than the spectrum of modulated galactic cosmic rays. Figure 4 displays the correlation observed at Pioneer 10 between the power law spectral index (i.e. γ for a spectrum of the form $dJ/dE \propto E^{+\gamma}$) for helium between 11 and 70 MeV/n, which indicates the strength of the anomalous component, and the flux of 29-67 MeV/n helium, which measures the level of solar modulation. From 1972-1980, the correlation is well defined, and weaker modulation corresponds to a larger contribution from the anomalous component. At solar maximum in 1981-82, the spectral indices cluster near the value of $\sim$+1.0 expected for normally modulated galactic helium. In 1983-84, as shown by the large unfilled data points, the helium flux began to recover, and by the end of 1984, the helium flux had reached levels where in previous years the spectrum had shown clear evidence of the anomalous component. As of late 1984, however, the spectrum remained

consistent with the presence only of galactic cosmic ray helium. These observations show that the presence of the anomalous component near the ecliptic is not a function only of the strength of modulation. Alternatives include 1) existence of a hysteresis effect, in which case the anomalous helium should reappear at Pioneer 10 in the near future, 2) sensitivity of the anomalous helium to the sign of the heliospheric magnetic field, as suggested by Pesses et al. (1981), or 3) dependence of acceleration or modulation of the anomalous helium on some as yet undefined characteristic of heliospheric structure.

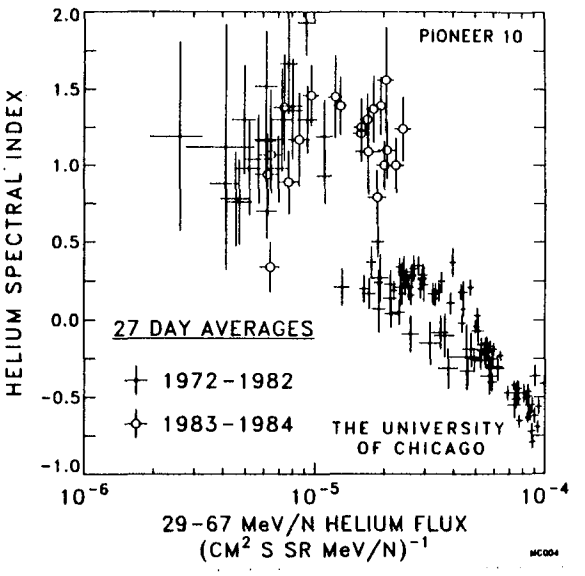

FIGURE 4

4. SUMMARY AND CONCLUSIONS: 1. For relativistic cosmic rays, the radial gradient measured between 1 AU and Pioneer 10 at R > 30 AU was nearly independent of the level of modulation throughout the period 1978-84, remaining approximately constant at $\sim$ 2.5 %/AU.
2. For cosmic rays below 100 MeV/n, the radial gradient was much smaller at maximum modulation than at solar minimum. As the flux increased in 1983-84 after solar maximum, the gradient also began to increase.
3. The cosmic ray flux at Pioneer 10 at > 34 AU remains as heavily modulated as it was at 1 AU in 1972, so that Pioneer 10 is still far from the boundary of the modulation region. Based on estimates of the interstellar spectra, for energies < 100 MeV/n more than 95% of the modulation was occuring beyond 34 AU in 1984.
4. The anomalous helium has yet to reappear at either 1 AU or Pioneer 10.

5. ACKNOWLEDGEMENTS: We are grateful to C. Lopate for his assistance in preparation of the data. This work was supported in part by NASA/Ames Contract NAS 2-11126, and by NASA Contract NAS5-28442.

REFERENCES:

Evenson, P., Garcia-Munoz, M., Meyer, P., Pyle, K.R., and Simpson, J.A., 1983, Ap. J. (Letters), 275, L15.
Garcia-Munoz, M., Mason, G.M., and Simpson, J.A., 1977, Ap. J., 217, 859.
Garcia-Munoz, M., Pyle, K.R., and Simpson, J.A., 1983, Ap. J. (Letters), 274, L93.
Lockwood, J.A., and Webber, W.R., 1984, J. Geophys. Res., 89, 17.
McKibben, R.B., Pyle, K.R., and Simpson, J.A., 1982, Ap. J. (Letters), 254, L23.
_____, 1983, Proc. XVIII ICRC, Bangalore, India, 3, 63.
_____, 1985, Ap. J. (Letters), 289, L35.
Pesses, M.E., Jokipii, J.R., and Eichler, D., 1981, Ap. J. (Letters), 246, L85.
Simpson, J.A., Bastian, T.S., Chenette, D.L., McKibben, R.B., and Pyle, K.R., 1980, J. Geophys. Res., 85, 5731.

VOYAGER 1 AND 2 MEASUREMENTS OF RADIAL AND LATITUDINAL COSMIC RAY GRADIENTS DURING 1981-84

D. Venkatesan[1,2], R.B. Decker[1] and S.M. Krimigis[1]
[1]The Johns Hopkins University, Applied Physics Laboratory,
Laurel, MD 20707 USA

[2]The University of Calgary
Calgary, Alberta, T2N 1N4 Canada

ABSTRACT

We have determined the cosmic ray radial gradient during 1981-84 using data from very similar detectors onboard spacecraft Voyagers 1 and 2 (radial separation ~ 6 AU, heliolatitude separation ~ 25^0)and from the earth-orbiting satellite IMP 8. The principal result is that the radial gradient over this period decreased at the rate ~ 0.4%/AU/year, reaching by the end of 1984 a value of ~ 2.0%/AU between 1 and 16 AU and ~ 0.6%/AU between ~ 16 and 22 AU.

1. Introduction: Measurements of galactic cosmic ray intensity gradients, radial as well as heliolatitudinal, play on important role in guiding theoretical models of cosmic ray propagation in the heliosphere. Determinations of integral radial gradients (for a summary, see Venkatesan et al., 1985) using data from Pioneers 10 and 11, Voyagers 1 and 2, and IMP 8 have revealed relatively small values of 2-4% per AU, thus questioning the concept of a spherically symmetric heliosphere. Decker et al. (1984) have estimated for the first time the heliolatitudinal gradient of galactic cosmic ray intensity during early-1981 through mid-1982, a period coinciding with the initial phase of cosmic ray recovery following the minimum reached in late-1980 to early-1981. They found that for all practical purposes, the heliolatitudinal gradient is 0%/deg over the 16° heliolatitudinal separation in the region 8-13 AU during that period of study. This was based on the assumption that the radial gradient during the 1981-82 recovery period remained at the same ~ 2-4%/AU level as determined from multi-spacecraft measurements during the 1977-80 cosmic ray intensity decay period.

2. Experiment: Our study has used the data from the cosmic ray channel (responding to protons integral above 70 MeV) provided by a heavily shielded solid state detector in the low-energy charged particle (LECP) instrument on both Voyagers. Total counts over a 26 day interval are typically $\gtrsim 2 \times 10^4$; thus the statistical error is $\lesssim 0.7\%$. We have also used the data from the charged particle measurement experiment (CPME) anticoincidence scintillator (Ep $\gtrsim$ 35 MeV) on IMP-8. For detector details and analysis refer to Venkatesan et al. (1985).

3. Observations:

(a) Differential Gradient: Figure 1 shows at the top a plot of the 26 day means of the cosmic ray intensity registered by both the Voyagers. Note that the Voyager 1 data has been shifted to the position of Voyager 2 using an average value of 500 km/sec for the solar wind. The

convection of cosmic ray features and the appropriateness of such a solar wind speed has been discussed in detail by Venkatesan et al. (1984, 1985). The close correspondence in the two intensity-time profiles is seen.

In the middle of Figure 1 we have plotted the values of the radial gradient G_r given by $G_r = \left((\ell n\ (R_1/R_2))/\Delta r\right) \times 100\%$, where R_1 and R_2 are the counting rates of Voyagers 1 and 2, and Δr is the radial separation. They are point-by-point computations which assume that the difference in intensity is entirely due to a radial gradient. The points are fitted with the line of least squares; note that G_r decreased from ~ 2.1%/AU to ~ 0.6%/AU over the four year period giving a value for $\dot{G}_r$ of 0.38 (± 0.09)%/AU/year.

In the bottom portion of Figure 1 we have plotted the values of the heliolatitudinal gradient G_ψ given by $G_\psi = \left((\ell n\ (R_1/R_2))/\Delta\psi\right) \times 100\%$ where $\Delta\psi$ is the latitudinal difference between the two spacecraft. Again, they are point-by-point computations based on the assumption that the difference in intensity is entirely due to a latitudinal gradient. The points are fitted with a line of least squares; note that G_ψ also decreased from ~ 0.42%/deg to ~ 0.13%/deg over the four year period giving a value for $\dot{G}_\psi$ of 0.06 (± 0.02)%/deg/year.

(b) Integral Gradient: We use the terminology "integral gradient" when we use a comparison detector located at 1 AU, such as IMP-8 and "differential gradient" when the two Voyagers are compared with each other. Figure 2 at the top shows the intensity time profiles for IMP-8 and the two Voyagers; the latter data were shifted to 1 AU to compensate for convection of cosmic ray features at the speed of 500 km/sec. Note the similarity among the three profiles.

The middle and lower part of Figure 2 show the integral radial gradient determined from the two pairs, Voyager 1-IMP-8 and Voyager 2-IMP-8. Again these are point-by-point computations and in the case of Voyager 1 (where only it is relevant) the assumption is made that the intensity difference arises entirely from the radial gradient. The values of G_r decreased from ~ 3.5%/AU to ~ 1.5%/AU and from ~ 3.8%/AU to ~ 2.0%/AU respectively; the decreases in the radial gradient are given by $\dot{G}_r$ = 0.48 (± 0.5)%/AU/year and $\dot{G}_r$ = 0.43 (± 0.07)%/AU/year respectively.

4. Discussion and Conclusions: The following points can be made.

(1) The choice of 500 km/sec for the average solar wind speed to correct the data for convection of cosmic ray features (from Voyager 1 to Voyager 2) in the heliospheric region ~ 8 AU to ~ 22 AU during 1981-84 is appropriate since the two intensity-time profiles at the top of Figure 1 agree fairly well.

(2) The similarity in the long-term trend of G_r and G_ψ in Figure 1 is indicative of the fact that the heliosphere, at least up to a radial distance of ~ 22 AU and heliolatitude of 25°, responds to cosmic ray modulation rather similarly. This is not surprising since it is clear from an earlier study (Decker et al., 1984) that no significant

latitudinal gradient exists. This is still our view, by virtue of the fact that the radial gradient G_r of ~ 2.0%/AU is evident from other multispacecraft studies as well.

(3) A decrease in the radial gradient as a function of increasing radial distance is clearly seen. Comparing the middle part of Figure 1 with the bottom portion of Figure 2, we see for example, at the end of 1984, we have IMP-8 (at 1 AU), Voyagers 1 and 2 at radial distances of 16 and 22 AU respectively. We find that the radial gradient G_r in the region 1-16 AU (IMP8-Voyager 2 pair) is ~ 2%/AU and that in the region 16-22 AU (Voyager 2-Voyager 1 pair) is ~ 0.6%/AU, a lower value. This clearly demonstrates that a comparison of integral radial gradient, over larger distances and at the same time later periods in the solar cycle is somewhat questionable. A value of say 2.0%/AU for the radial gradient over a complete solar cycle and out to a heliocentric distance of over 32 AU (Van Allen and Randall, 1985) could very well consist of the mean of the radial gradient G_r over different regions at different times including a 0.0%/AU gradient in the outermost region at the time of the approaching solar minimum. It is appropriate to mention that McKibben et al. (1985) have also observed a similar decrease in the radial gradient for low energy cosmic rays ($10 < E < 70$ MeV).

(4) The trend of G_r shows that we may be approaching a region of G_r = 0.0%/AU either at greater distances or at the sunspot minimum (~ 1987-88) at which time Voyager 2 would be at ~ 22-25 AU and Voyager 1 at ~ 30-31 AU. If the trend persists and our interpretation is correct, we may well be seeing the boundary of cosmic ray modulation at the solar minimum. We note that Voyager 1 is generally moving in the direction of the solar apex, while Pioneer 10 although at a greater radial distance, is moving in the opposite direction. It should be pointed out that this is the first time gradient measurement is being reported during the recovery period of the cosmic ray intensity eleven-year cycle at such large radial distances.

In summary, it seems reasonable to conclude that the region of cosmic ray modulation shrinks and expands possibly in step with the solar activity cycle (minimum and maximum). McDonald et al. (1981) have suggested the dominant source of solar cycle modulation as the "pile up" of propagating shocks in the outer heliosphere.

Acknowledgements: This work was supported in part by NASA under Task I of Contract N000024-78-C-5384 and by NSF under grant ATM-8305537.

References

1. Decker,R.B., S.M.Krimigis & D.Venkatesan, Ap. J., 278, L122, 1984
3. McDonald,F.B., N.Lal, J.H.Trainer,M.A.I. Van Hollebeke & W.R.Webber, Ap. J., 249, L71, 1981
4. McKibben,R.B., K.R.Pyle, & J.A.Simpson, Ap. J., 289, L35, 1985.
5. Van Allen,J.A., & B.A.Randall, J.G.R., 90, 1399, 1985
6. Venkatesan,D., R.B.Decker & S.M.Krimigis, J.G.R., 89, 3735, 1984
7. Venkatesan,D., R.B.Decker, S.M.Krimigis & J.A.Van Allen, J.G.R., 90, 2905, 1985

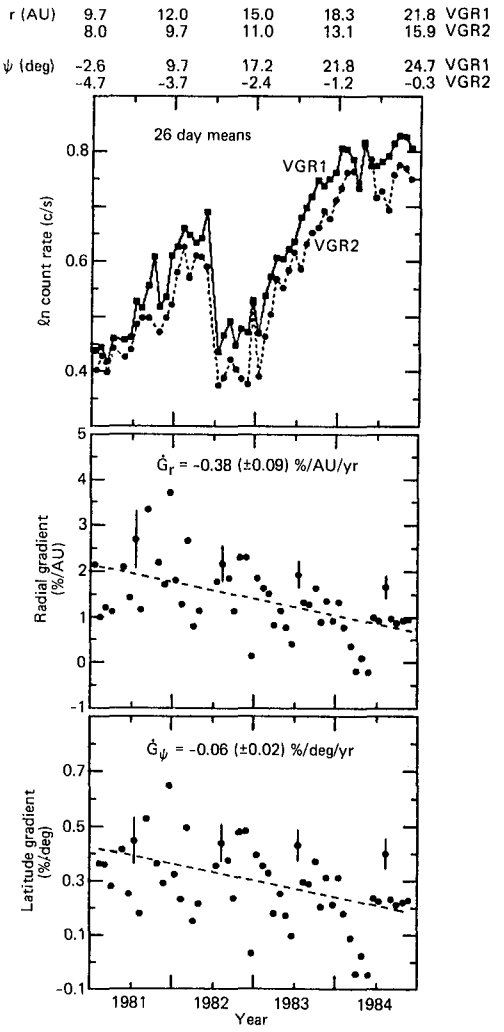

Figure 1

Intensity-time profiles of cosmic ray intensity at Voyagers 1 and 2; Voyager 1 data has been shifted to position of Voyager 2 using a solar wind speed of 500 km/sec. The middle and bottom portions provide the radial and heliolatitudinal gradients between the Voyagers.

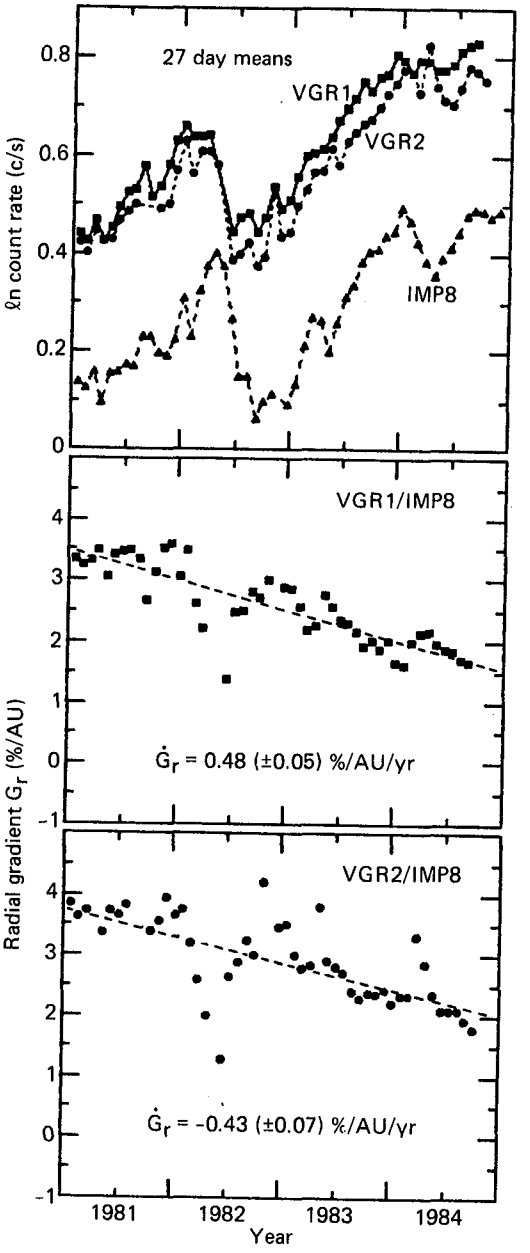

Figure2

Intensity-time profiles of cosmic ray intensity at the Voyagers duly shifted to 1 AU using a solar wind speed of 500 km/sec and IMP 8; the radial gradients are between Voyager 1 and IMP 8 and Voyager 2 and IMP 8.

THE RECOVERY OF THE COSMIC RAY FLUX FROM MAXIMUM SOLAR MODULATION AT IMP-8 (1 AU) AND AT PIONEER 10 (R > 30 AU)

R. B. McKibben, K. R. Pyle, and J. A. Simpson
Enrico Fermi Institute, The University of Chicago
Chicago, Illinois 60637 (U. S. A.)

ABSTRACT: In the period 1980-84, observations of relativistic and low energy ($30 \lesssim E \lesssim 70$ MeV/n) cosmic ray nuclei from Pioneer 10 in the outer heliosphere and from IMP-8 at 1 AU show that increases as well as decreases in intensity propagate outward at velocities equal to or greater than the average solar wind velocity.

INTRODUCTION: In the period of increasing and maximum solar modulation (1977-81), observations of the galactic cosmic ray intensity from Pioneer 10/11 and Voyager 1/2 have shown that intensity decreases propagate outward at near the average solar wind velocity (e.g. Lockwood and Webber, 1984; McDonald et al., 1981; McKibben et al., 1982, 1985a; Van Allen and Randall, 1985; Venkatesan et al., 1985). Since 1981, solar activity has been decreasing, and following a prolonged depression caused by a series of large interplanetary shocks in 1982, (Lockwood and Webber, 1984; Pyle and Simpson, 1985), the cosmic ray flux has been increasing towards solar minimum levels. Therefore, it is now possible to determine whether intensity increases propagate outward in the same manner as decreases. In earlier work dealing with relativistic cosmic rays, Van Allen (1979) has reported that the recovery from an isolated Forbush decrease was more rapid near 1 AU than in the outer heliosphere, and Fillius and Axford (1985) have reported that recovery from maximum solar modulation began earlier at 1 AU than in the outer heliosphere.

In this paper we use observations from University of Chicago instruments on Pioneer 10 and on IMP 8 (described respectively by Simpson et al. (1980) and Garcia-Munoz et al. (1977)) to investigate the radial propagation of the recovery for both relativistic cosmic rays and for low energy galactic protons and helium in the energy range $30 < E < 70$ MeV/n.

In comparing observations at 1 AU and at Pioneer 10, we have been careful to use well matched energy intervals from the two spacecraft. Under conditions of changing modulation, even at one location significant delays between changes in intensity for particles of different energies arise from energy dependent hysteresis effects (e.g. Cooper and Simpson, 1979). Thus, use of poorly matched energy intervals may lead to confusion between phase shifts caused by radial propagation and shifts arising from the energy dependent hysteresis.

RADIAL DEPENDENCE OF THE RECOVERY: In Figure 1A, we compare simultaneous 27 day gradient-corrected averages of the integral intensity of cosmic rays above 67 MeV from Pioneer 10 and above 106 MeV from IMP 8 in the period 1980-84. These counting rates are dominated by relativistic cosmic rays with a mean energy of ~ 2 GeV. During the period shown, Pioneer 10 moved outward from ~ 20 to ~ 34 AU from the sun. As a result of this motion, and of the measured radial gradient of 2.5 %/AU for the relativistic particles (McKibben et al. 1985b), increases in intensity in uncorrected data from Pioneer 10 are caused partly by Pioneer 10's outward motion, and partly by the decreasing level of solar

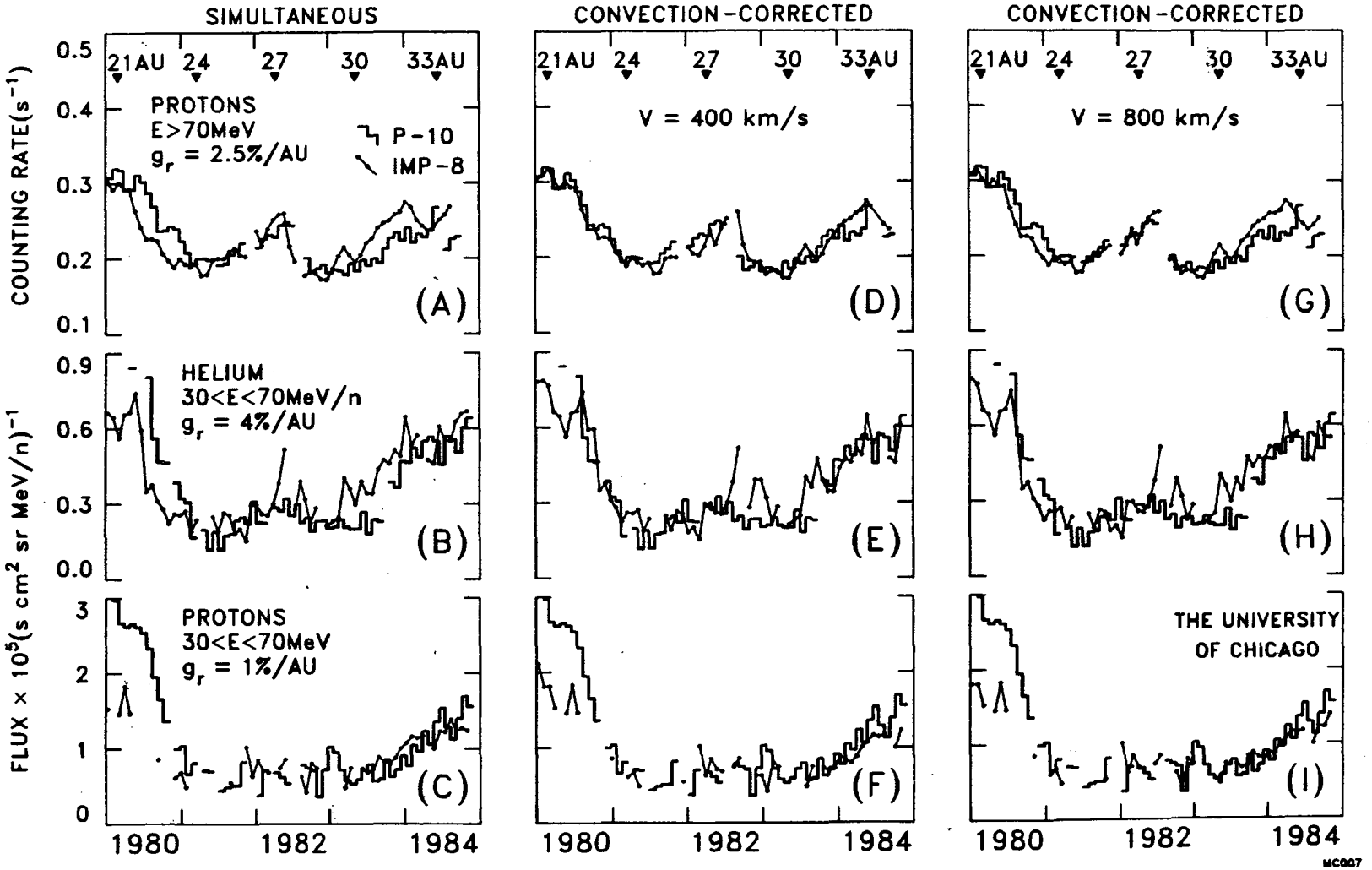
SIMULTANEOUS
CONVECTION-CORRECTED
CONVECTION-CORRECTED
21AU 24 27 30 33AU
PROTONS
E>70MeV
g_r = 2.5%/AU
P-10
IMP-8
V = 400 km/s
V = 800 km/s
(A)
(B)
(C)
(D)
(E)
(F)
(G)
(H)
(I)
HELIUM
30<E<70MeV/n
g_r = 4%/AU
PROTONS
30<E<70MeV
g_r = 1%/AU
COUNTING RATE(s^{-1})
FLUX × 10^5($s\ cm^2\ sr\ MeV/n$)$^{-1}$
0.5
0.4
0.3
0.2
0.1
0.9
0.6
0.3
0.0
3
2
1
0
1980
1982
1984
THE UNIVERSITY OF CHICAGO
MC007

FIGURE 1

modulation. To reduce the effects of the radial motion, we have extrapolated the intensity measured at Pioneer 10 back to 1 AU assuming a gradient of 2.5 %/AU. Thus, in Figure 1A we have plotted I(1) = I(R)exp(-0.025(R-1)) where I(R) is the counting rate measured by Pioneer 10 at radius R AU.

Figure 1A shows that during periods of increasing modulation (1980, 1982), intensity changes occur later at Pioneer 10 than at IMP 8. During the period of decreasing modulation in 1981, there is no clear delay between the recovery at 1 AU and at Pioneer 10, although the data suggest that the intensity increase began earlier at IMP 8 than at Pioneer 10. In 1983-84, on the other hand, the recovery from the effects of the 1982 shocks clearly began first at 1 AU, as reported by Fillius and Axford (1985) and Pyle and Simpson (1985). In Figure 1D, we show the same data, but with the IMP measurement shifted in time by an amount $\Delta t = (R-1)/V$, where V is taken to be 400 km/s, and Δt is taken to be the nearest integral multiple of 27 days. Over the period shown, Δt increases from 81 to 135 days. Compensating for propagation in this way greatly improves the agreement of the intensity profiles at the two spacecraft. The main exceptions are 1) the period of decreasing modulation in 1981-82, where agreement is better using simultaneous observations than shifted observations, and 2) the period in 1982 immediately following passage of the shocks, which propagated more rapidly than 400 km/s.

Figure 1(B, E) shows the same analysis for 30-70 Mev/n helium, assuming a constant gradient of 4 %/AU. As reported by McKibben et al. (1985b), the radial gradient was larger before the middle of 1980, so that the gradient correction is inadequate for the earlier data. After 1980, however, the gradient was nearly constant at $\sim$ 4 %/AU, and agreement between the intensity profiles for low energy helium at 1 AU and at Pioneer 10 is improved by assuming that all changes in modulation, both increases and decreases, propagate outward with a velocity of about 400 km/s. However, in 1982, there is a large increase in the helium flux at 1 AU that has no analogue at Pioneer 10.

Similar analysis for 30-70 MeV protons is shown in Figure 1(C, F), for a gradient of 1 %/AU. This value of the radial gradient was observed only from mid-1980 until late 1983, after which the gradient began a gradual increase (McKibben et al., 1985b). Therefore, since we have used a constant gradient of 1 %/AU to correct the Pioneer data to 1 AU, comparison between the gradient-corrected intensity profiles is meaningful only from mid-1980 to late 1983. In this period the low energy proton flux was nearly constant, and no conclusions can be drawn.

DISCUSSION: The observations may be summarized as follows. In the recovery from the modulation produced by the shocks in 1982, the intensity increase occurred first at 1 AU and propagated outward with a velocity near 400 km/s both for relativistic cosmic rays and for low energy (30-70 MeV/n) helium. In 1981-82, however, when the modulation was not dominated by any single event, the recovery was more nearly simultaneous at 1 AU and at Pioneer 10.

In considering the propagation of changes in modulation in the heliosphere, Forman and Jones (1985) have pointed out that for models in which the modulation at any point is produced by numerous scattering centers convected outward by the solar wind and distributed along the radial path of a particle inward from a fixed boundary of the modulation region, the recovery from maximum modulation should begin first in the

inner heliosphere. Their arguments show that individual features propagate outward at the solar wind velocity but that the overall pattern propagates twice as fast. These conclusions are also implicit in the work of Perko and Fisk (1983). Figure 1(G-I) repeats the analysis of Figure 1(D-F) using a convection velocity of 800 km/s. In 1981-82, when modulation was most likely produced by many disturbances between 1 AU and the boundary, assuming a velocity of 800 km/s significantly improves the agreement between profiles for the relativistic particles at 1 AU and at Pioneer 10. In 1982-84, however, when modulation was dominated by a single event, the data are better organized by a velocity of 400 km/s. The accuracy of the measurements does not allow similar conclusions to be drawn for lower energy particles. For 30-70 MeV protons, agreement is improved in 1983-84 for a velocity of 800 km/s, but, as noted above, changes in the gradient after 1983 make such a conclusion questionable.

An alternative model for explaining outward propagation of the recovery involves 3-dimensional propagation of particles in the heliosphere, leading to the filling in of the inner heliosphere from regions off the ecliptic plane (e.g., Van Allen, 1979). In this model, the radial gradient in the ecliptic could become negative, whereas a negative radial gradient would be inconsistent with the model of Forman and Jones. We find, however, that radial gradients were positive at all times (McKibben et al., 1985b, cf. also Fillius and Axford, 1985).

Our observations of the outward propagation of the recovery from maximum solar modulation are consistent with either the model of Forman and Jones (1985), or with propagation from regions off the ecliptic plane to the inner heliosphere. A definitive observational test to discriminate between the two models must await further explorations by spacecraft off the ecliptic plane.

ACKNOWLEDGEMENTS: This work was supported in part by NASA/Ames Contract NAS 2-11126 and by NASA Contract NAS5-28442.

REFERENCES:

Cooper, J.F., and Simpson, J.A., 1979, Proc. 16th ICRC, Kyoto, Japan, 16, 176.

Fillius, W., and Axford, I., 1985, J. Geophys. Res., 90, 517.

Forman, M.A., and Jones, F.C., 1985, Bull. Am. Phys. Soc., 30, 779.

Garcia-Munoz, M., Mason, G.M., and Simpson, J.A., 1977, Ap. J., 217, 859.

Lockwood, J.A., and Webber, W.R., 1984, J. Geophys. Res., 89, 17.

McDonald, F.B., Lal, N., Trainor, J.H., Van Hollebeke, M.A.I., and Webber, W.R., 1981, Ap. J. (Letters), 249, L71.

McKibben, R.B., Pyle, K.R., and Simpson, J.A., 1982, Ap. J. (Letters), 254, L23.

_____, 1985a, Ap. J. (Letters), 289, L35.

_____, 1985b, Proc. 19th ICRC, La Jolla, Ca., U.S.A., Paper SH4.7-5.

Perko, J.S., and Fisk, L.A., 1983, J. Geophys. Res., 88, 9033.

Pyle, K.R., and Simpson, J.A., 1985, Proc. 19th ICRC, La Jolla, Ca., U.S.A., Paper SH 4.7-9.

Simpson, J.A., Bastian, T.S., Chenette, D.L., McKibben, R.B., and Pyle, K.R., 1980, J. Geophys. Res., 85, 5731.

Van Allen, J.A., 1979, Geophys. Res. Lett., 6, 566.

Van Allen, J.A., and Randall, B.A., 1985, J. Geophys. Res., 90, 1399.

Venkatesan, D., Decker, R.B., Krimigis, S.M. and Van Allen, J.A., 1985, J. Geophys. Res., 90, 2905.

THE LARGE-SCALE MODULATION OF COSMIC RAYS IN MID-1982: ITS DEPENDENCE ON HELIOSPHERIC LONGITUDE AND RADIUS.

K. R. Pyle and J. A. Simpson

Enrico Fermi Institute, The University of Chicago,
Chicago, Illinois 60637 (USA)

ABSTRACT. Near solar maximum, a series of large radial solar wind shocks in June and July 1982 provided a unique opportunity to study the solar modulation of galactic cosmic rays with an array of spacecraft widely separated both in heliocentric radius and longitude. By eliminating hysteresis effects we can begin to separate radial and azimuthal effects in the outer heliosphere. We have been able to show that, on the large scale, changes in modulation (both the increasing and recovery phases) propagate outwards at close to the solar wind velocity, except for the near-term effects of solar wind shocks, which may propagate at a significantly higher velocity. We show that, in the outer heliosphere, azimuthal effects are small in comparison with radial effects for large-scale modulation at solar maximum.

INTRODUCTION. The radially-propagating shock events of mid-1982 provide an exceptional opportunity to examine the dynamic response of the heliosphere to a large, sudden increase in modulation and to study the modulation onset and recovery mechanism as a function of magnetic rigidity and heliospheric radius and longitude. This large series of solar events has been studied intensively over the past several years, both in its modulation effects (e.g. Lockwood and Webber, 1984) and in the shock acceleration of energetic charged nucleons and electrons as far as 28 AU from the sun (Pyle et al. 1984). Observations from a variety of instruments aboard the Pioneer and Voyager spacecraft demonstrate that modulation increases propagate outwards at approximately the solar wind velocity (Pyle et al. 1979; Lockwood and Webber, 1984; McDonald et al. 1981). Fillius and Axford (1985) have reported an outward propagation of recovery from modulation in the 11-year solar cycle, based on a comparison of neutron monitor intensity at 1 AU with Pioneer relativistic cosmic ray measurements. The outward progression of recovery could be due to off-ecliptic fluxes or, as in the model of Perko and Fisk (1983), due to the longer intervals between shocks during the declining phase of solar activity. In a companion paper at this Conference (McKibben et al. 1985) we also discuss the large-scale propagation of solar modulation, showing that both modulation increases and decreases propagate outwards.

In this paper we examine the 1982 large-scale modulation event and its recovery, using a counting rate responding to CNO-Fe nuclei in the approximate energy range 200-1000 MeV/n, measured by identical instruments on Pioneers 10 and 11. We show that for both the onset and recovery of this large modulation event the dominant effect is one of outward propagation at approximately the solar wind velocity, and is relatively independent of heliospheric longitude.

INSTRUMENTATION AND TRAJECTORY. It is well-established that during relatively rapid changes in modulation there is a hysteresis effect whose magnitude is dependent on magnetic rigidity (Simpson 1963; Cooper and

Simpson 1979). Therefore, to eliminate this rigidity-dependent effect, we have used the F2 counting rate from the two identical Fission Cells developed to measure the intense fluxes of protons during the Pioneer 10 and 11 encounters with Jupiter, and later, Pioneer 11 with Saturn. In interplanetary space these counting rates are sensitive to a variety of galactic cosmic ray species, (H-He 1%, C-Ne 14%, Na-V 28%, and Cr-Ni 56%) (see Simpson et al., 1974 and especially McKibben,1983 for a detailed discussion of the Fission Cell response). The energy interval for response is ∿200-1000 MeV/n (∿1-3 GV rigidity). These counting rates provide relatively good statistics and permit a fairly precise measure of modulation changes. The overall elemental response is expected to be insensitive to any long-term instrumental drifts.

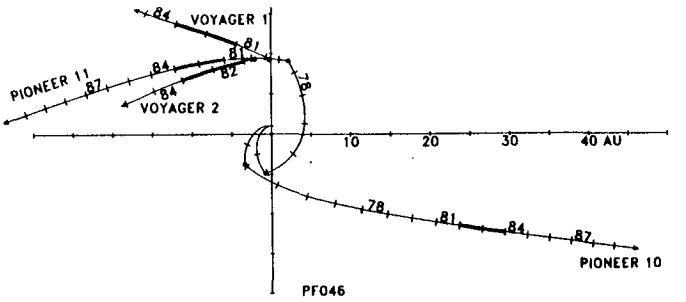

--- FIGURE 1 ---

For comparison we have used the Voyager 1 and 2 counting rates for nucleons >75 MeV (Stone et al., 1977), kindly made available by the Voyager CRS experimenters.

In Figure 1 we have plotted the trajectories of Pioneers 10/11 and Voyagers 1/2, projected onto the ecliptic plane. Pioneer 10, alone among the 4 spacecraft, is moving away from the solar apex, in the direction of the heliospheric tail. The time interval studied here, 1982-3, is indicated by the heavy lines along the trajectories.

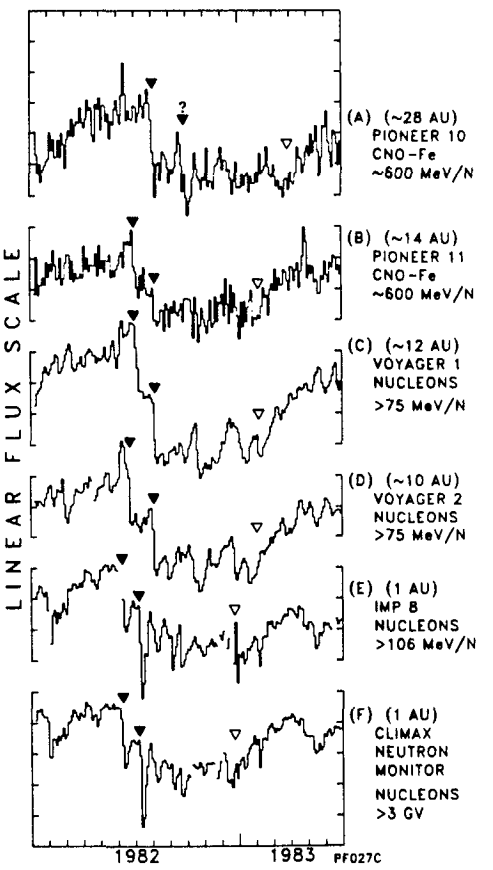

--- FIGURE 2 ---

OBSERVATIONS. In Figure 2 we have plotted 3-day averages of counting rates, showing the behavior of the event at various radii and longitudes in the heliosphere. The two large Forbush decreases seen at 1 AU in mid-1982 (Fig. 1 E,F) are the result of intense solar activity early in June and early in July, 1982. The first of these is apparently caused by the large solar wind shock associated with a flare occurring on 3 June, on the back side of the sun as seen from the earth (Pyle et al. 1984). The longitude of this flare placed it almost directly "under" Pioneer 10. The second decrease (in July), originated with a large solar flare event visible from Earth. In the Figure we have indicated (filled triangles) the outward progression of the modulation. The outward propagation of the recovery is indicated by the open

triangles. At 1 AU the two intensity decreases are distinct in time and superimposed on a general downward trend of flux (Fig. 1E,F). The two decreases are similarly resolvable at 10-14 AU (Fig. 1B,C,D). However, at Pioneer 10 (Fig. 1A) the modulation increased over a ten-day period, and remained more or less constant for a six-month period before a relatively sharp onset of recovery (open triangle). At Pioneer 10 the second shock has no significant effect on the overall intensity level (filled triangle with "?").

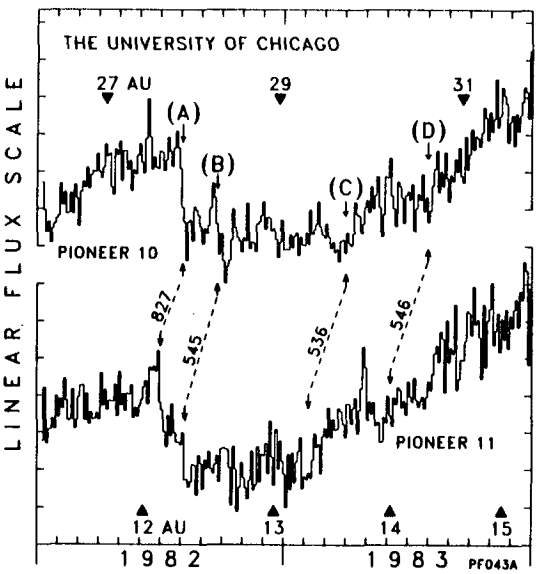

--- FIGURE 3 ---

It is clear from Figure 2 that both the initial Forbush decreases as well as the subsequent rise from the depressed flux levels (open triangles) propagate outwards. Calculation of an accurate value for the radial velocity of the increase, based on this Figure, is difficult owing to the possibility of hysteresis between many of the counting rates shown. To accurately determine the outward velocities we have isolated the two identical CNO-Fe 3-day averaged counting rates from Pioneer 10 and Pioneer 11, between which there are no significant energy hysteresis effects, and plotted them on an expanded scale in Figure 3. The dashed arrows indicate the time shifts necessary to best align the four intensity changes labelled A-D. The triangles show the distance of the two spacecraft from the sun. The initial modulation increase (event (A)) is nearly azimuthally symmetric: we find that the modulation increase propagates outward with approximately the same velocity towards Pioneer 11 and Pioneer 10. However, event (B)'s transit velocity from Earth to Pioneer-11 is approximately 700 Km/sec, but from Pioneer 11 to Pioneer 10 only 545 Km/sec, indicating either a) a large deceleration or b) a significantly higher velocity towards Pioneer 11 (700 Km/sec) than towards Pioneer 10 (600 Km/sec earth-Pioneer 10).

Events (C) and (D) are intensity recoveries where the propagation velocities are near the solar wind velocity, indicating a very small, if any, azimuthal dependence. Near each dashed line in Figure 3 we have indicated the calculated propagation velocity for the feature, assuming azimuthal symmetry. In Figure 4 the Bartels solar rotation averages of the CNO-Fe counting rates for Pioneer 10 and 11 are plotted against each other. In panel (A) the data, covering mid-1982 to mid-1983, are plotted with no time-shifting; in panel (B)

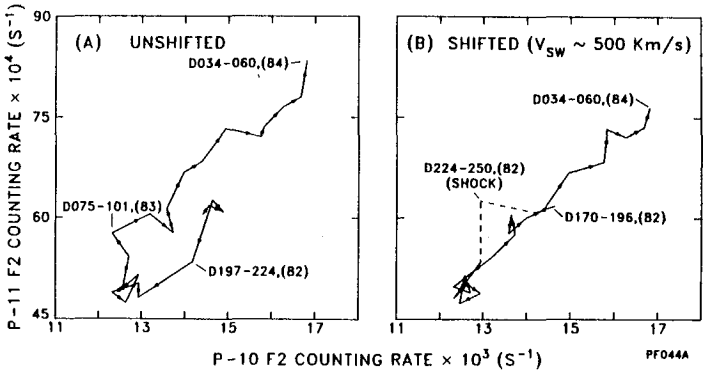

--- FIGURE 4 ---

the Pioneer-11 data have been shifted two solar rotations, equivalent to a solar wind velocity of ~500 Km/sec. This time-shift has placed all of the data points on the same regression line except the one corresponding to the large modulation increase associated with the high-velocity, radial shock. Thus, the assumptions of a) azimuthal symmetry and b) outward propagation at near the solar wind velocity result in a near-perfect alignment of the data at the two spacecraft, differing by ~16 AU in heliospheric radius and by nearly 180 degrees in longitude.

SUMMARY AND CONCLUSIONS. In order to determine the outward velocity of the onset and recovery from modulation of galactic cosmic rays in the heliosphere it is essential to eliminate all magnetic rigidity dependent effects so that rigidity-dependent hysteresis in the heliosphere does not lead to erroneous conclusions.

We have, therefore, selected sets of nucleon-intensity data whose magnetic rigidity ranges are close to each other. The solar-flare generated series of radially-propagating shocks which passed outward through the heliosphere in 1982 provide a unique test of the dynamical processes resulting in large-scale heliospheric modulation.

We have shown that major increases and decreases in solar modulation are primarily radially dependent and not strongly azimuthally dependent.

Not only is the increase in solar modulation an outward propagating effect, as has been shown earlier (e.g. Lockwood and Webber, 1984; Fillius and Axford, 1985) but the recovery from the 1982-3 enhanced modulation period also propagates outward at the approximate solar wind velocity.

ACKNOWLEDGEMENTS. We thank R. Vogt, Principal Investigator on the Voyager CRS experiments, E. Stone, and A. Cummings for making available the Voyager >75 MeV/n nucleon counting rates. This work was supported in part by NASA/Ames Contract NAS 2-11126, by NASA Contract NAS5-28442, and by NSF Grant ATM 84-12382.

REFERENCES:

Cooper, J.F., and Simpson, J.A., 1979, Proc. 16th ICRC, Kyoto, 12, 176.

Fillius, W., and Axford, I., 1985, J. Geophys. Res., 90, 517.

Lockwood, J.A., and Webber, W.R., 1984, J. Geophys. Res., 89, 17.

McDonald, F.B., Lal, N., Trainor, J.H., Van Hollebeke, M.A.I., and Webber, W.R., 1981, Ap. J. (letters), 249, L71.

McKibben, B., 1983, Enrico Fermi Institute Preprint no. 83-21, The University of Chicago.

McKibben, R.B., Pyle, K.R., and Simpson, J.A., 1985, Proc. 19th ICRC, La Jolla, Paper SH4.7-7.

Perko, J.S., and Fisk, L.A., 1983, J. Geophys. Res., 88, 9033.

Pyle, K.R., Simpson, J.A., Mihalov, J.D., and Wolfe, J.H., Proc. 16th ICRC, Kyoto, 5, 345.

Pyle, K.R., Simpson, J.A., Barnes, A., and Mihalov, J.D., 1984, Astrophys. J. (letters), 282, L107.

Simpson, J.A., 1963, Pont. Acad. Sci. Scripta Varia, (Vatican) 25, 363.

Simpson, J.A., Hamilton, D.C., McKibben, R.B., Mogro-Campero, A., Pyle, K.R., and Tuzzolino, A.J., 1974, J. Geophys. Res., 79, 3522.

Stone, E.C., Vogt, R.E., McDonald, F.B., Teegarden, B.J., Trainor, J.H., Jokipii, J.R., and Webber, W.R., 1977, Sp. Sci. Revs., 21, 355.

SH 4.7-10

NONSTATIONARY MODULATION OF GALACTIC COSMIC RAYS IN A NONLINEAR MODEL

V.KH.BABAYAN, M.B.BAGDASARIAN

Yerevan Physics Institute, Markarian st. 2
375036, Yerevan, Armenia, USSR

L.I.DORMAN

Institute of Terrestrial Magnetism,
Ionosphere and Radio Wave Propagation
Moscow Region, Troitsk, USSR

ABSTRACT

An automodel equation for the solar wind velocity is obtained in the self-consistent model. The solution of the convection-diffusion equation is obtained for the density of galactic cosmic rays at a definite dependence of the diffusion coefficient and solar wind velocity on the rigidity and distance.

In studying the propagation of galactic cosmic rays (GCR) in the interplanetary space, properties of the solar wind are considered, independent of the CR intensity. Though it should be noted that the influence of GCR on the supersonic solar wind is comparable with that of other factors (galactic magnetic field etc.).

Then, while investigating the GCR modulations by the solar wind, one should take into account the fact that with the variation of the GCR intensity in time and space, the influence of GCR on the solar wind varies, which in its turn results in the variation of the solar wind velocity. That is, the self-consistent problem should be solved.

In the spherically symmetrical case nonstationary equations of hydrodynamics for the solar wind with account

of the GCR influence have the form

$$\frac{\partial u}{\partial t} + u\frac{\partial u}{\partial r} + \frac{1}{\gamma}\left(\frac{\partial c^2}{\partial r} + c^2\frac{\partial}{\partial r}\ln\rho\right) + \frac{1}{\rho}\frac{\partial P}{\partial r} = 0$$

$$\frac{\partial}{\partial t}(\ln\rho) + u\frac{\partial}{\partial r}(\ln\rho) + \frac{\partial u}{\partial r} + \frac{2u}{r} = 0 \qquad (1)$$

$$\frac{\partial c^2}{\partial t} + u\frac{\partial c^2}{\partial r} + (\gamma-1)c^2\left(\frac{\partial u}{\partial r} + \frac{2u}{r}\right) = 0$$

where u, ρ are the velocity and the density of the solar wind, c^2 is the sound velocity, γ is the polytropic index, r is the heliocentric distance, and P is the GCR pressure equal to $P = \frac{1}{3}\int_0^\infty N(r,R,t)\,p v\,dR$ (here N is the concentration of particles with the rigidity R ; p, v are the momentum and the velocity of GCR particles, respectively).

The variation of the spectrum N is determined by the character of GCR modulation in the interplanetary space, i.e. it is defined in the end by the velocity of solar wind and diffusion coefficient via nonstationary equation of diffusion with account of convection and GCR energy variation /1,2/

$$\frac{\partial N}{\partial t} = \vec{\nabla}(\varkappa\nabla N) + (\vec{u}\,\vec{\nabla})N - (\vec{\nabla}\,\vec{u})\frac{R}{3}\frac{\partial N}{\partial R}. \qquad (2)$$

Let us introduce as in /3/ new dimensionless dependent variables x and y by means of relations $u = x\frac{r}{t}$, $c^2 = y\frac{r^2}{t^2}$ and dimensionless independent variables $\ln t$ and $\ln r$, then the system (1) will have the form

$$\dot{x} - x + x^2 + x' + \frac{1}{\gamma}\left[y' + 2y + y(\ln\rho)'\right] + yp' = 0$$

$$(\ln\rho)^{\cdot} + x(\ln\rho)' + x' + 3x = 0 \qquad (3)$$

$$\dot{y} + xy' + 2(x-1)y + (\gamma-1)y(x' + 3x) = 0$$

where, in calculating the last term in the first equation, it is approximately assumed $(\gamma - 1) \approx 1$.

Let us assume that x and y are the function of one independent variable $z = r t^{-a_1}$, where a - const. Let us require that r and t do not enter explicitly in (2), then the density should have the form $\rho = t^{a_2}\xi(z)$. Since $\partial/\partial(\ln t) = -a_1 \alpha/\alpha(\ln z)$; $\partial/\partial \ln z = \alpha/d\ln z$ the system (3) will take the form

$$
\begin{aligned}
&x'(x-a_1) + x^2 - x + \frac{1}{\gamma}\left(2y + y' + y(\ln\xi)'\right) + y\rho' = 0 \\
&(\ln\xi)'(x-a_1) + a_2 + x' + 3x = 0 \\
&y/y'(x-a_1) + (\gamma-1)x' + [2(\gamma-1)+(\gamma+1)]x - 2 = 0
\end{aligned}
\tag{4}
$$

where the dash means $\partial/\partial \ln z$.

Eliminating $d(\ln\xi)$ from the first two equations of the system, one may rewrite (4) as

$$
\frac{d\ln z}{dx} = \frac{(a_1-x)\dfrac{d\ln y}{dx} - (\gamma-1)}{(3\gamma-1)x - 2} =
$$

$$
= \frac{(a_1-x)^2 - y}{y\left[\dfrac{2(a_1-1)+a_2}{\gamma} + 3x + F(a_1-x)\right] - x(1-x)(a_1-x)} \tag{5}
$$

where it is assumed $F = dp/d\ln z$

As it is seen, the problem of integration of the initial set of equations in partial derivatives of the first order is reduced to the integration of a first order ordinary differential equation of the form

$$
\frac{dy}{dx} = y\,\frac{F_1(x,y)}{F_2(x,y)}
$$

and to two quadratures.

To define N one should solve eq.(2) which in the spherically symmetric case in dimensionless variables has the form

$$\frac{\partial N}{\partial \tau} - b x \frac{\partial^2 N}{\partial \rho^2} + \left(a u - \frac{2 x b}{\rho} - b \frac{\partial x}{\partial \rho}\right)\frac{\partial N}{\partial \rho} - \frac{2}{3}\frac{a u}{\rho}\frac{dN}{d\rho} - \frac{1}{3} a \xi \frac{\partial N}{\partial \xi} = 0 \quad (6)$$

here $\rho = r/r_0$, $\xi = R/R_0$, $\tau = t/T$, $a = T/r_0$, $b = T/r_0^2$ where r_0 is the dimension of the modulating volume, R_0 is the minimum rigidity of particles, T is the time which the solar wind spends to reach the boundary of the modulating volume.

In order to obtain the analytical solution of eq.(6), one should choose the dependence of the diffusion coefficient and the solar wind velocity in the form

$$x = x_0 \rho^{2(1-\alpha)} \xi^{2\beta}; \qquad u = u_0 \rho^{-2-\frac{3\alpha}{\beta}}$$

where α and β are the arbitrary constants.

Let us search for a solution with boundary conditions

$$N(\rho, \xi, \tau)/_{\rho=0} < \infty; \qquad N(\rho, \xi, \tau)/_{\rho=1} = K \xi^{-\gamma}$$

Passing to the variable $z = \rho^{\alpha} \xi^{-\beta}$ and using the separation of the variables $N(z, \tau) = \varphi(\tau)\psi(z)$ we have from (6)

$$\frac{\partial \varphi}{\partial \tau} = -K^2 \varphi, \qquad \varphi = c e^{-K^2 \tau}$$

$$z \frac{\partial^2 \psi}{\partial z^2} + \left(\frac{3}{\alpha} - 1\right)\frac{\partial \psi}{\partial z} + \frac{K^2}{\alpha^2 b x_0}\psi = 0 \quad (7)$$

where K^2 is the separation constant.

The solution of eq.(7) is

$$\psi = c_1 z^{\nu} J_{\nu}\left(\sqrt{1/\alpha^2 b x_0}\, K z\right) + c_2 z^{\nu} Y_{\nu}\left(\sqrt{1/\alpha^2 b x}\, K z\right) \quad (8)$$

where J_{ν} and Y_{ν} are the Bessel functions of type 1 and 2, and $\nu = 1 - \frac{3}{2\alpha}$. After satisfying the boundary conditions we have

$$N = \frac{2}{[Y_{n+1}(\mu_n)]^2} \sum_{l=1}^{\infty} z^{-n} e^{\alpha \sqrt{b x_0}\,(1-\tau)} J(\mu_e z)\left(\int_0^1 z_n(\mu_e \eta)\eta^{\frac{\gamma}{\beta}+n+1} d\eta\right)$$

REFERENCES

/1/ Parker E.N., Planet and Space Sci., 1965, 13, 9.
/2/ Dolginov A.Z., Toptigin I.N., Izv.AN SSSR, ser.fiz., 1967, 31, 1269.
/3/ Stanjukovich K.P. Unsteady Motions of Continuum. Moskva, Nauka, 1970, 90 p.
/4/ Kamke E. Handbook of Ordinary Differential Equations. Moskva, Nauka, 1976, 401 p.

DIMENSIONS OF THE SOLAR WIND CAVITY AND OF THE REGION OF INTERPLANETARY COSMIC RAY MODULATION

Dorman I.V.
Institute of History of Science and Technology of the USSR Academy of Sciences. Moscow I03OI2, Staropansky per.I/5, USSR

Abstract. We discuss the problem of determining effective dimensions of the region of global galactic cosmic ray modulation from the data on II-year CR variations and the data on the parameters of the solar activity and the solar wind.

I. Effects limiting solar wind propagation. CR propagation is limited to the following effects: I) Pressure of interstellar medium (according to the estimates /I/ this gives $r_{sw} \sim$ IOOO A.U. for the boundary between helio-magnetosphere and solar wind); 2) Pressure of the galactic magnetic field $H_G \sim 3\ IO^{-6}$ G (this gives $r_{sw} \sim$ IOO A.U. in the direction perpendicular to the field /2/); 3) Deceleration both by CR and due to charge exchange of interstellar neutral hydrogen (according to nonlinear theory of modulation /3, 4, 5/ this gives $r_{sw} \sim$ 50-IOO A.U. depending on the CR energy density in interstellar space and on the interstellar hydrogen concentration in the vicinity of the Sun). We should emphasize here that we do not know the effects capable of limiting solar wind to $r_0 \sim$ IO-20 a.e. Meanwhile, investigating the correlation between CR intensity variations and solar activity variations, many researchers concluded earlier that the dimensions of the modulation region are extremely small ($r_M \approx$ IO-20 A.U. and even $r_M \approx$ 2-3 A.U.). Moreover, many papers have recently appeared which suggest, as before, that $r_M \approx$ IO-20 A.U. Let us try to explain the reason for such a difference and to understand whether the solar wind dimensions can generally coincide with the effective solar wind dimensions, i.e. $r_{sw} \approx r_M$.

2. Estimation of effective dimensions of the interplanetary CR modulation region and investigation of the structure of this region; time and energy hystereses. This estimate can be obtained from calculation of the delay of the observed galactic CR modulation with respect to the processes on the Sun (time hysteresis). Indeed, as shown in /2/, the hysteresis between the total number W of solar spots on the solar disk and the intensity variations of the CR neutron component (observed on the stations Ottawa - the geomagnetic cutoff rigidity R=I.2 GV, Chicago - I.8 GV, Climax - 3.2 GV, and Huankayo - I3.5 GV) is explained well by the convective diffusion model of global galactic CR modulation with an account of the delay $\Delta t \sim r/u$ (u is the mean velocity of the solar wind /2,6/) of the electromagnetic conditions in interplanetary space at a distance r from the Sun with respect to the corresponding processes on the Sun. From the comparison between calculations and observations it follows that I) For particles with a rigidity of several

GV the radius of the modulation region $r_M \sim$ 100 A.U.; 2) the effective free path for scattering $\Lambda \backsim R$, where R is particle rigidity (in the region where R exceeds several GV), it decreases as $\Lambda \backsim W^{-1/3}$ with an increase of the solar activity; 3) For CR with high rigidities (tens of GV) r_M decreases approximately as $r_M \backsim R_{ef}^{-1}$, where R_{ef} is the effective rigidity of primaty CR registered by a given device; 4) At very small rigidities the delay in the recovery of CR intensity exceeds the theoretical value as the solar wind activity weakens. This indicates the presence, besides the convective-diffusion modulation region (with $r_M \sim$ 100 A.U.), also of a "buffer" layer between solar wind and interstellar medium in which the wind velocity is close to zero but there exists an interplanetary magnetic field amplified due to a permanent pumping by the solar wind. In this layer there is no convective CR outflow, but the delay in the recovery of CR intensity inside the modulation region increases due to a comparatively slow diffusion of low-energy particles. The estimation of the thickness of this diffusion layer gives $L_D \sim$ 100 A.U. (the influence of this layer on particles of high rigidities can be neglected due to relatively small magnetic fields there). It was shown in /6/ that in the buffer layer particles can be accelerated to comparatively small energies, which can explain the appearance of an anomalous CR component. Note that at small distances CR are scattered by magnetic inhomogeneities of solar wind, whereas at large distances the main role in CR scattering and their convective outflow must be played by large solar wind perturbations of the type of shock waves.

We believe that r_M is close to r_{sw} only for particles of rather small rigidities. At large r_M distant regions of heliosphere will not modulate particles with rigidities of tens of GV because the azimuthal component of the interplanetary magnetic field decreases with distance ($\backsim r^{-1}$); this fact leads to a decrease of R (corrolary 3).

Corrolaries 3 and 4 discussed above lead to the energy hysteresis which has been thoroughly investigated in recent years.

3. The shift of helio-latitude of active regions within a cycle of solar activity and the dimension of the modulation region. In many papers attempts have been made to explain time hystere is by the shift of the effective helio-latitude of solar activity from higher to lower values in the course of an II-year cycle (see, for example, /7-9/). In this case the hysteresis disappears in a first approximation, and so the authors have concluded that the modulation region is very small. In our opinion, such a conclusion is to a great extent groundless. A more accurate account of the helio-latitude shift by means of the HL-index /IO/ shows that hysteresis disappears only for an effective angular flux width $\theta \approx$ 5-IO°. But in this case there is a sharp contradiction between the observed /II/ and the calculated

annual variations. The results are in agreement only for $\theta \sim 30\text{-}50°$, but in this case the time hysteresis does not disappear and leads to the results discussed in 3.

4. Short-time variations of solar activity and the dimension of the effective modulation region. The study of the socalled "stepwise" variations in the solar activity and their manifestations in cosmic ray variations /I2/ has led to the conclusion that the corresponding delay in CR with respect to the processes on the Sun makes up I-2 months, which gives $r_M \sim 7\text{-}10$ A.U. But as shown in /I3/, during short-time variations of solar activity only a small part of the modulation region nearest to the Sun takes part in the modulation, and the smaller the characteristic period of solar activity variations, the smaller part of the modulation region is involved in the formation of a corresponding CR variation.

5. Anisotropic diffusion model and the dimension of the modulation region. More accurate calculations of the CR intensity modulation in the framework of the anisotropic diffusion model with an account of polarity reversal of the total magnetic field of the Sun also give large dimensions of the modulation region ($r_M \sim 50\text{-}100$ A.U.) (see e.g. /I4/).

6. Measurements in space and the dimension of the modulation region. The recent measurements of long-term CR variations and their radial gradient (on a cosmic apparatus (CA) Pioneer IO and II, and on Voyager I and 2) give at least $r_M > 65$ A.U. /I5/, and according to /I6/, /I7/, the calculations which made use of the same data and took into account the CA measurements near the Earch as well as the ground-based neutron monitor measurements (for elimination of CR time variations) give $r_M \sim 100$ a.e.

Conclusions: I. Dimensions of the effective modulation region r_M for low-energy (less than several GeV) particles are close to the solar wind dimensions r_{sw}, where $r_M \sim r_{sw} \sim 100$ a.e. 2. As the particle rigidity R increases, the value of r_M decreases, so that in this case r_M can be much smaller than r_{sw}. The value of r_M also decreases with a decrease of the characteristic period of CR variation (it reaches the maximum value only for long-term variations, such as II- and 22-year ones). 4. The region of effective modulation and solar wind is surrounded by a buffer layer which causes the delay in the recovery of CR intensity. 5. The energy hysteresis is caused by two factors: the dependence of r_M on R and the presence of a buffer layer (the time of diffusion through this layer essentially increases as the particle energy decreases).

REFERENCES

I. Parker E.N. 1963, Interplan. dynamic.proc, New York - London.

2. Dorman I.V., Dorman L.I., I967, J.Geoph-Res., 72, I5I3.

3. Dorman I.V., Dorman L.I., I968. Geomagnetism and aeronomy, 8, 8I7, I008.

4. Dorman I.V., Dorman L.I., I969, Izv. AN SSR, ser. fiz., 33, I908.

5. Babayan V.Kh., Dorman L.I., I979. Proc. I6-th ICRC, Kyoto, v.3, II7, I23.

6. Dorman I.V., Dorman L.I., I967, Izv. ANSSSR , ser.fiz., 31, I239, I273.

7. Quenby J.J., I965. Proc. 6-th ICRC London, v.I, 3.

8. Kudo S., Wada M., I968. Report of Ionosph. and Sp.Res. in Japan, 22, I37.

9. Stozhkov Yu.I., Charakhchyan T.N., I969, Geomagnetism i aeronomy, 9, 803.

I0. Gushina R.T., Dorman I.V., Dorman L.I., Pimenov I.A., I970, Izv. AN SSSR, ser.fiz., 34, 2426, 2434.

II. Dorman L.I., Luzov A.A., Manrukova V.P., I967, DAN SSSR, I72, 839, Izv. AN SSSR, ser. fiz., 3I, I368.

I2. Charkhchyan A.N., Charkhchyan T.N., I967. Izv. AN SSSR, ser.fiz., 3I, I3I3.

I3. Dorman L.I., I967. Cosmic rays.N 8, 305.

I4. Alaniya M.B., Dorman L.I., I98I. "Spatial distribution of the density and flux of galactic cosmic rays". Tbilisi.

I5. Mc Kibben R.B., Ryle K.R., Simpson Y.A., I982, Astroph. J. 254, 23-27.

I6. Webber W.R., Lockwood J.A., I98I, J. Geophys.Res., 86, II458-II462.

I7. Lockwood J.A., Webber W.R., I984, Astroph. J., 279, N I, Pt. I, I5I-I56.

DRIFT AND FORBUSH DECREASES

H. Moraal and M.S. Mulder

PU-CSIR Cosmic Ray Research Unit,
Department of Physics,
Potchefstroom University for CHE,
Potchefstroom, 2520.
South Africa.

ABSTRACT

Evidence is presented that the drift effect on the modulation of galactic cosmic rays can be seen on Forbush decreases observed by the Deep River and Hermanus neutron monitors.

1. Introduction

Since the description of drift effects on the modulation of galactic cosmic rays (Jokipii, Levy, and Hubbard, 1977) its significance has been controversial. Lee and Fisk (1981) argued that the topology of, and fluctuations in the Interplanetary Magnetic Field (IMF) might render drift effects quite ineffective. Jones (1983) remarked that observable drift effects seem hard to find. Current drift models (e.g. those of Jokipii and Thomas; 1981, and Potgieter and Moraal; 1985) however are now in agreement that there should be a small effect on near-Earth observations. In addition, Potgieter and Moraal also showed that despite small observable effects, the dynamics of the modulation in consecutive solar cycles (IMF directions reversed), may be drastically different. These authors also summarised a score of independent observations reflecting drift effects.

Figure 1 shows that after a blast wave has passed Earth, the drift velocity field in the 1970 to 1980 IMF configuration should cause a Forbush decrease to reset faster than during the 1959 to 1969 configuration. In this paper we investigate this hypothesis with data from the Deep River and Hermanus neutron monitors.

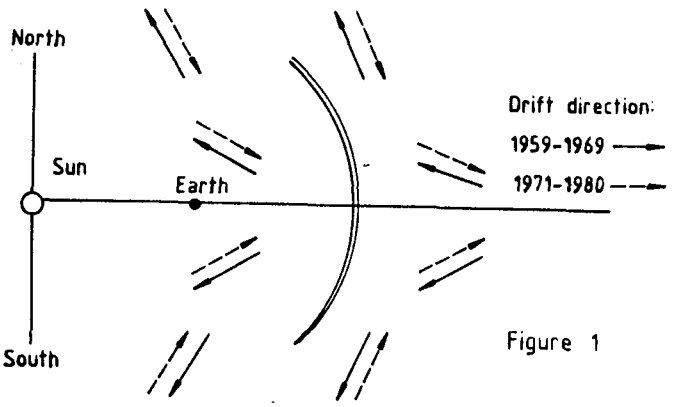

Figure 1

2. Data Analysis and Results

The Table lists the Forbush decreases selected from the Deep River (cutoff rigidity P_c = 1,0 GV) and Hermanus (P_c = 4,7 GV) neutron monitors. The

time of onset is given as a two digit number for the year, a three digit number for the day, and a two digit number for the hour. The selection criteria for the 109 Hermanus decreases were rather loose. This means that about 15% of them are contaminated by other decreases in the onset phase, reset phase, or both. For Deep Rivier even more decreases were included for a total of 131, but the 85 marked with an asterisk are clear, uncontaminated decreases that reach a clear minimum within 12 hours of onset time.

Figure 2a shows the averages of these decreases for Hermanus. The solid curve is for the period 1959 to 1969 and the dashed one for the period 1971 to 1980. The drift effect predicted from figure 1 is clearly visible. Note that the sharp peaks at onset time (hour 48) and diurnal variations are due to subjectivity of selection of the hour of onset: One is inclined to select a high counting rate at onset time, and this automatically favours the peak of the diurnal variation. The drift effect is even more clearly visible on Figure 2b, which shows the five hour running average of the ratio of 1971-1980 decreases relative to 1959-1969 decreases. Figures 3a and 3b repeat this analysis for all 131 Deep River decreases, while Figures 4a and 4b are for the 85 uncontaminated Deep River decreases only.

Hermanus

5900916	6.6	6905907	6.5
5902618	6.5	6908312	8.7
5904516	7.4	6910212	5.3
5909918	5.1	6911710	9.0
5911320	5.2	7127823	4.8
5913122	12.2	7135118	7.0
5916212	7.0	7204906	5.5
5923124	9.0	7215113	5.8
5929214	6.0	7217114	3.7
5933706	5.7	7230516	8.3
6009110	7.8	7312714	4.5
6010614	5.6	7313415	5.4
6012116	10.4	7318917	3.5
6014314	7.0	7321213	4.3
6019620	10.6	7402516	2.7
6022712	6.1	7406424	3.5
6028009	5.9	7501513	3.7
6110614	4.7	7508515	3.0
6114122	5.5	7511012	3.9
6120712	5.9	7513916	4.1
6127320	4.5	7518909	3.0
6201018	4.1	7522516	2.9
6203604	5.6	7529118	2.5
6214714	4.7	7530817	3.7
6223316	3.8	7532609	3.6
6227304	6.5	7605121	2.0
6228106	6.1	7611802	2.5
6306916	4.1	7612411	3.2
6310820	5.8	7623619	2.4
6318514	4.1	7633904	2.3
6323312	3.8	7702911	3.0
6326506	7.2	7709712	3.3
6330212	6.6	7800318	5.3
6425414	3.5	7802914	4.8
6502102	4.6	7806816	7.0
6510911	3.8	7810012	7.4
6516621	3.8	7812105	16.4
6519924	4.7	7815312	7.5
6522721	3.3	7819409	5.7
6527919	3.7	7831601	4.6
6626608	6.5	7835512	5.1
6625810	8.9	7900613	5.0
6629913	4.5	7903412	3.8
6701305	6.5	7906304	3.5
6703822	5.5	7908712	8.2
6714515	7.4	7909501	7.4
6730218	4.7	7911506	7.1
6802620	5.4	7915719	6.2
6807016	5.0	7918711	7.7
6816218	6.1	7921309	4.4
6816823	4.4	7927916	5.4
6819205	5.8	7931505	5.5
6832108	7.7	8003701	6.0
6834012	6.2	8007912	4.8
6902613	5.1		

Deep River

5900919	6.5 *	6608212	6.5 *	7720918	3.7 *
5902621	9.1	6615122	4.3	7726420	10.4 *
5904510	9.1	6618918	5.1 *	7734704	4.0 *
5909917	5.4 *	6624208	8.4	7800320	6.4
5911320	6.4 *	6626619	6.1 *	7810017	9.2
5913121	16.0 *	6628818	5.0 *	7812106	16.5 *
5916208	6.6	6629905	3.9 *	7815311	8.4 *
5919813	21.4	6632117	4.1 *	7823021	5.3 *
5923203	9.6 *	6634716	5.3	7831604	5.0 *
5924621	8.4 *	6701312	5.8 *	7834802	6.7
5926123	9.5	6704623	5.2 *	7804520	20.2 *
5933704	9.2	6712119	6.2	7908712	7.9
6009110	12.7 *	6714519	9.0 *	7909503	7.4
6010722	4.8 *	6730218	5.6	7915718	7.6 *
6012124	14.3	6732602	3.8 *	7918722	8.5 *
6014321	7.2	6802623	4.7	7924106	10.1 *
6014924	6.6	6809622	4.8	7927918	5.6 *
6017923	9.6 *	6811702	3.3 *	7904206	9.6
6019619	7.9 *	6814202	2.9	8003703	6.3 *
6022714	6.6 *	6830221	12.6	8006606	2.5 *
6028005	8.8 *	6901419	3.6 *	8007916	5.7 *
6104624	5.1	6904119	3.7 *		
6110407	6.6 *	6908219	13.6 *		
6114103	4.8 *	6910301	5.0 *		
6120719	9.9 *	7110419	4.4 *		
6127319	8.4 *	7113716	5.2 *		
6130115	5.5	7127823	4.6 *		
6133517	7.6 *	7135116	7.2 *		
6201004	4.5 *	7206619	4.4		
6203520	6.6	7211401	5.0 *		
6207922	3.9 *	7213619	5.8 *		
6209924	5.3 *	7215119	5.7 *		
6211104	6.3 *	7216909	5.9 *		
6227303	5.5	7221721	22.8 *		
6306917	4.0 *	7230518	10.3 *		
6308123	3.5	7235718	3.5 *		
6310903	2.5	7225714	4.9 *		
6312222	5.7	7229219	4.5		
6314720	4.1	7301921	4.1 *		
6325918	10.3 *	7321213	4.5 *		
6326517	9.2 *	7406418	3.1		
6330214	7.8	7412705	6.1 *		
6332020	3.4 *	7428718	5.8 *		
6402820	3.2 *	7501522	3.4		
6425020	2.5 *	7511012	4.0		
6426520	3.0 *	7518909	2.6 *		
6432023	2.4	7506514	5.2		
6502016	3.0	7508520	3.9 *		
6510918	3.2	7522517	2.7 *		
6516619	3.9 *	7612322	5.2 *		
6519317	2.8	7604720	3.1 *		
6520002	2.3 *	7702919	3.9 *		
6522719	2.5 *	7709716	3.4		
6530812	2.9 *	7717017	3.9		
6602815	2.8 *	7717903	3.4		

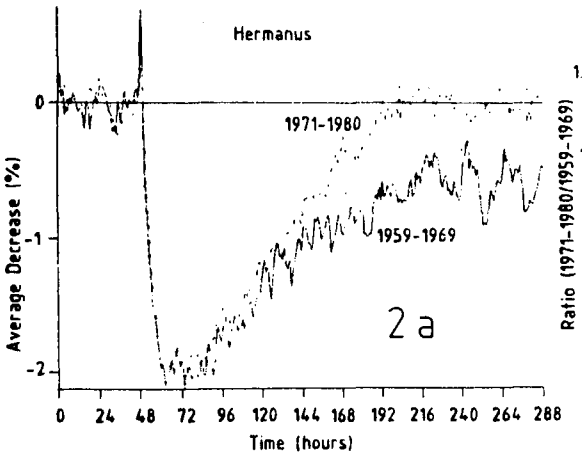

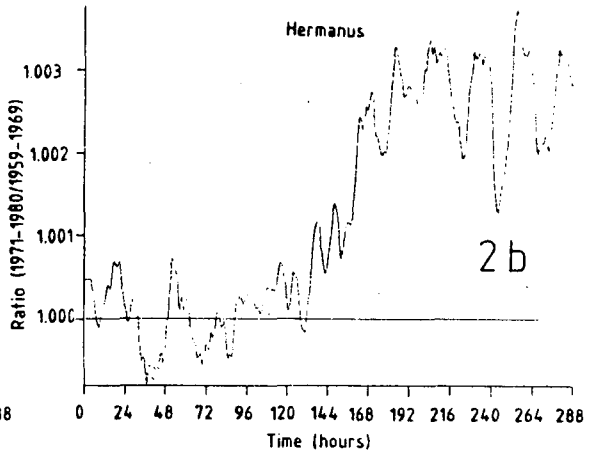

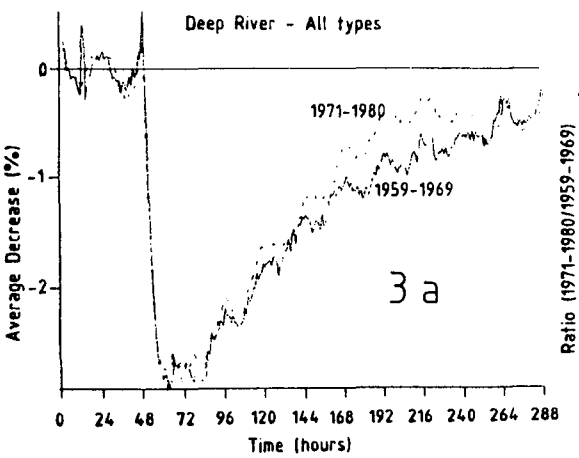

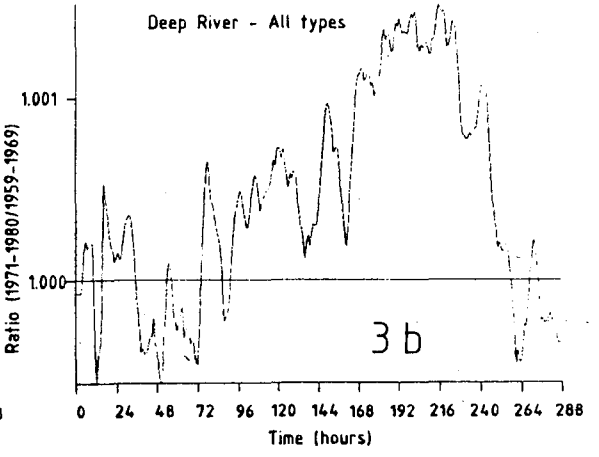

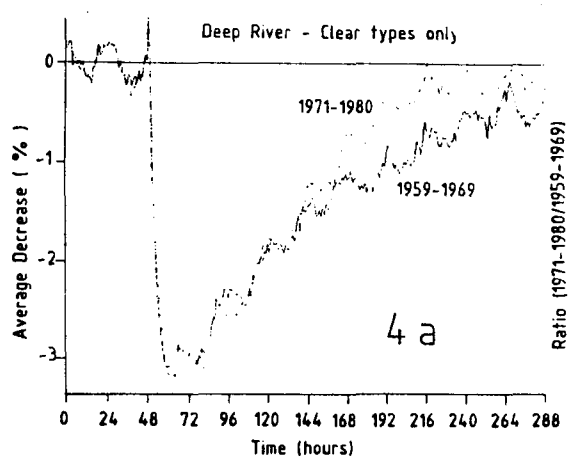

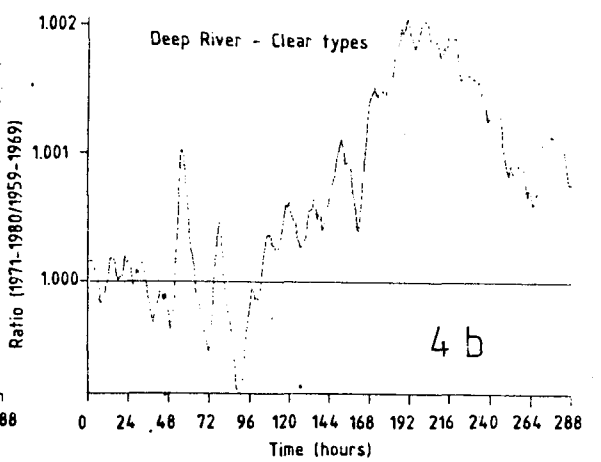

In all cases the effect builds up at approximately the same rate towards maximum at hour 192 (6 days after onset), but on Deep River (Figure 3b) it starts to disappear at about hour 240 (8 days after onset). The Deep River effect is also about a factor two smaller than on Hermanus. Figure 4b shows however that when the contaminated decreases are omitted the effect on Deep River increases somewhat in magnitude and becomes more persistent.

3. Interpretation and Significance

If $\langle \underline{v}_d \rangle$ denotes the omnidirectional drift velocity and U the differential cosmic ray density, then the divergence of the drift flux is

$$\underline{\nabla}.(\langle \underline{v}_d \rangle U) = \langle \underline{v}_d \rangle . \underline{\nabla} U,$$

because $\underline{\nabla}.\langle \underline{v}_d \rangle = 0$. Now $\langle \underline{v}_d \rangle \propto P$ (rigidity) and Potgieter (1984) has shown from his numerical drift model calculations that $\langle \underline{v}_d \rangle . \underline{\nabla} U$ is a rapidly increasing function of P. This qualitatively explains why the Hermanus effect may be larger than the one on Deep River. Quantitative comparison with observations requires that the calculations of Potgieter must be weighted over the response functions of the respective neutron monitors. Such steady state drift calculations can however not explain why the Hermanus effect is more persistent than the Deep River one.

To test the significance of these results, the following tests were performed:

(a) The three largest decreases (5919813, 722172, 7804520 for Deep River and 5913122, 7812105 for Hermanus) were omitted to see whether these had an undesirable weighting effect. This caused no change in the results.
(b) The Hermanus calculations were repeated separately for decreases greater and smaller than the median. Both sets showed the effect, but it was much more significant on the large decreases.
(c) The chronological order of the Hermanus decreases was scrambled randomnly. In this case the effect completely disappeared.

From these tests we think that the drift effect is real and significant. We are presently extending the analysis to additional low, mid, and high latitude neutron monitors to confirm this and to establish a rigidity depence of the effect.

References

Jokipii, J.R., Levy, E.H., and Hubbard, W.G.: 1977, Ap. J., 213, 861.
Jokipii, J.R., and Thomas, B.: 1981, Ap. J., 243, 1115.
Jones, F.C.; 1983, Rev. Geophys. Space Phys., 21, 318.
Lee, M.A., and Fisk, L.: 1981, Ap. J., 248, 836.
Potgieter, M.S.: 1984, Ph.D.-thesis, Potchefstroom University.
Potgieter, M.S., and Moraal, H.: 1985, Ap. J., 294, (July 15 issue).

ANOMALOUS SHORT-TERM INCREASES IN THE GALACTIC COSMIC RAY INTENSITY: ARE THEY RELATED TO INTERPLANETARY MAGNETIC CLOUD-LIKE STRUCTURES ?

N. IUCCI, M. PARISI, C. SIGNORINI, M. STORINI and G. VILLORESI
Istituto di Fisica dello Spazio Interplanetario del C. N. R.
Dipartimento di Fisica - Università "La Sapienza"
Piazzale Aldo Moro, 2 - 00185 ROMA, ITALY

Thirty-one short-term increases (time duration < 24 hours and amplitude up to 5%) in the galactic cosmic ray intensity, occurring inside Forbush decreases events, have been identified over the period 1966 - 1977. These increases are highly anisotropic and occur after the compression region following the shock; the interplanetary medium /1/ is characterized by intense (≥ 10 nT) and higly fluctuating magnetic field $\vec{B}$, high velocity, low density and temperature (flare ejecta piston ?) as it can be seen in the examples given in Figures 1, 2, 3 and in the average behaviours of Figure 4. These $\vec{B}$-fluctuations seem to be ordered variations /2/ which could be representative of magnetic clouds /3/; this structure is particularly evident for the 7 cases given in the Table for which the data were always present and $\lambda_3 < 0.5\,\lambda_2$ and $\lambda_3/\lambda_2 \leqslant \lambda_2/3\lambda_1$ (for the definition of λ_1 see /2/); the average behaviour of these events is given in Figure 5. Also the large cosmic ray increase occurring on 17-18 September 1979, already analyzed by other authors /4, 5/, belongs to this category of events as it is shown in Figures 6, 7. In Figure 8 we show the time variations of $\vec{B}$ in the plane (X', Y') of maximum variance and in the plane (X', Z'), Z' being the minimum variance direction.

The analysis of these events is still in progress; the study of further events occurring during 1978 - 1979 and analytical refinement are necessary to understand the origin of the cosmic ray increases observed inside these magnetic clouds.

MAGNETIC CLOUD					ISOTROPIC C. R. INCREASE		
Start		Duration			Start		Amplitude
D - M - Y	H	(h)	λ_3/λ_2	λ_2/λ_1	D - M	H	(%)
23-09-66	21-22	18	.17	.50	24-09	00-01	1.5
13-12-66	20-21	26	.07	.48	14-12	02-03	2.3
13-01-67	19-20	36	.07	.56	13-01	19-20	1.0
29-07-67	20-21	10	.12	.34	29-07	21-22	1.5
24-03-69	17-18	20	.07	.35	24-03	23-24	1.3
09-11-69	04-05	14	.06	.62	09-11	04-05	2.1
15-05-72	20-21	12	.15	.49	16-11	01-02	0.6

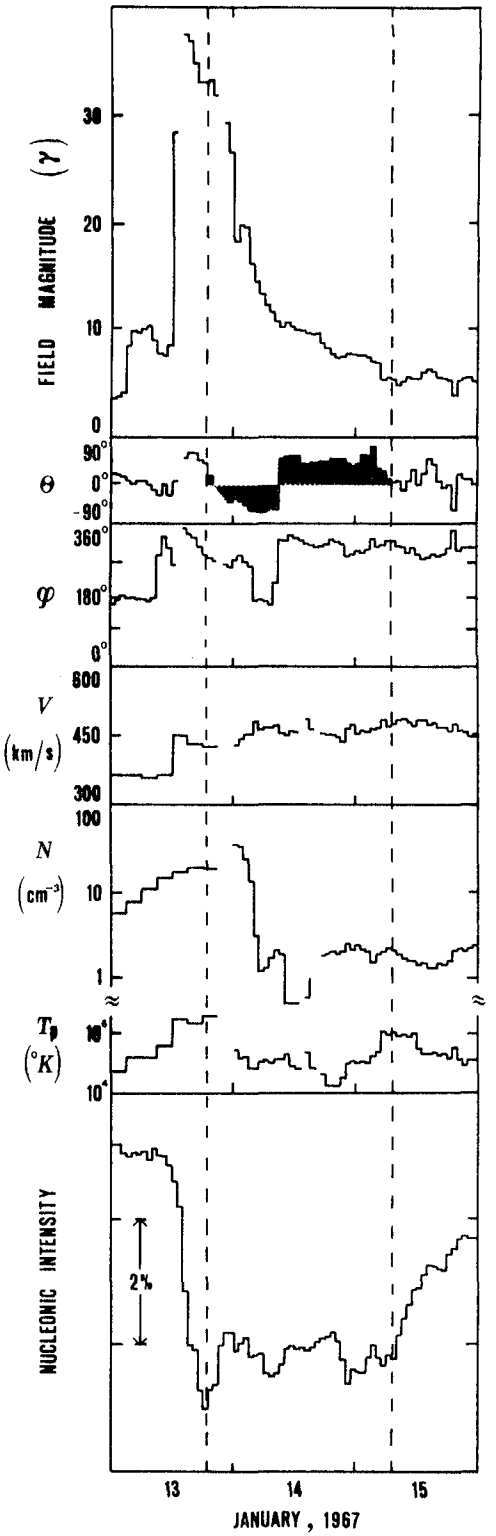

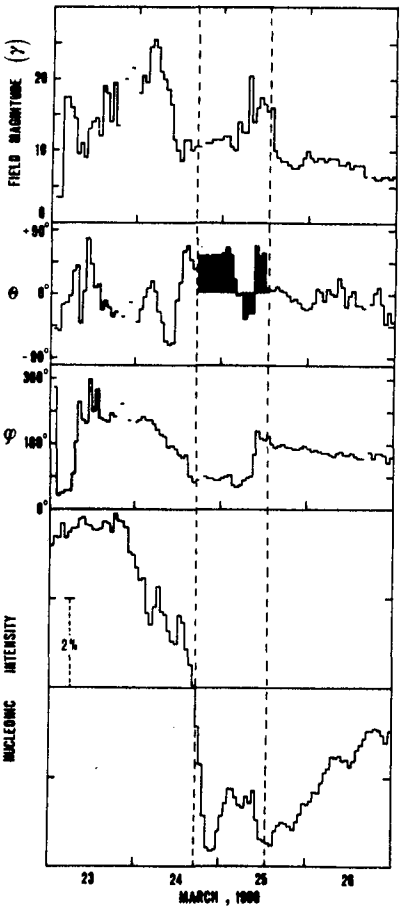

Figure 2 - (see Fig. 1)

Figure 1: Magnetic field, flow parameters and isotropic (average NM-64 intensity of Alert, Deep River, Goose Bay, Inuvik, Kerguelen, Kiel, McMurdo) nucleonic intensity associated with the magnetic cloud which is between the two vertical broken lines.

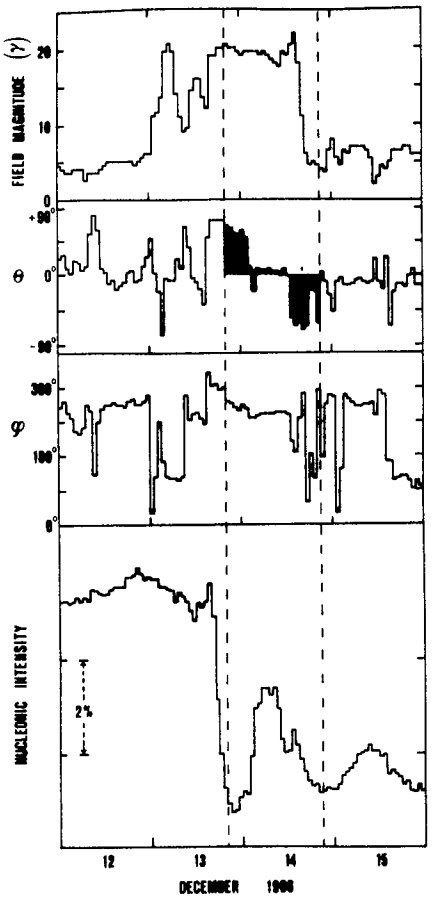

Figure 3 - (see Fig. 1)

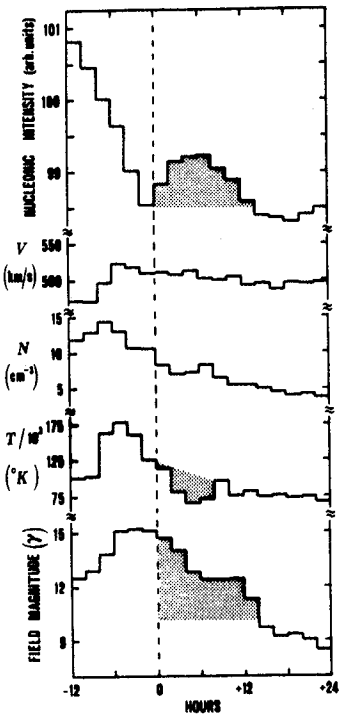

Figure 4

Figure 4: Superposed epoch analysis of interplanetary parameters and average (see the caption of Fig. 1) nucleonic intensity for 31 cosmic ray increases. The epoch time (zero hour) is the first hour of the increase.

Figure 5: a) The same as in Fig. 4 for 7 cosmic ray increases for which it was possible to identify the magnetic cloud structure.
b) The time durations of the 7 magnetic clouds relative to the epoch time are marked by horizontal bars.

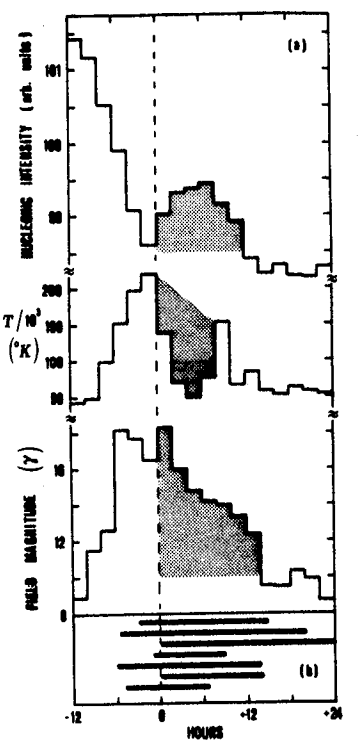

Figure 5

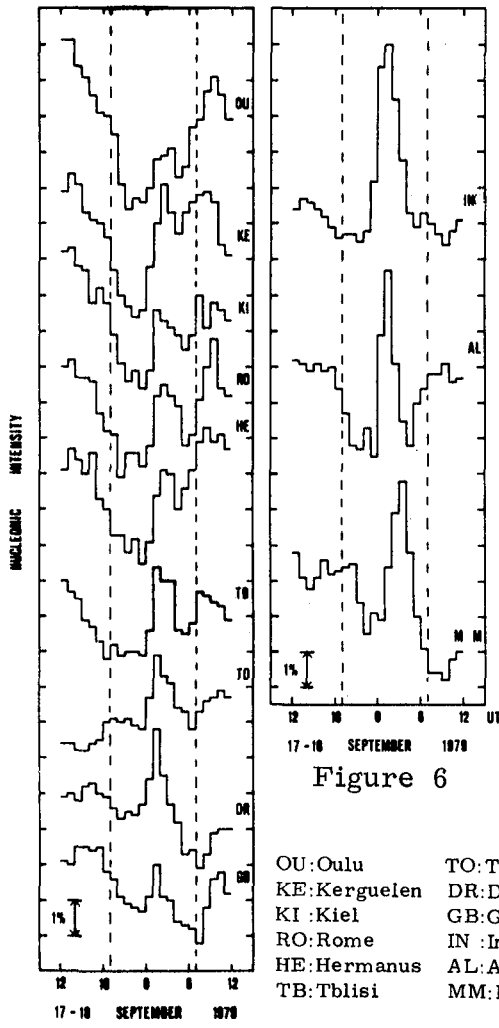

Figure 6

OU:Oulu TO:Tokio
KE:Kerguelen DR:D. River
KI :Kiel GB:G. Bay
RO:Rome IN :Inuvik
HE:Hermanus AL:Alert
TB:Tblisi MM:McMurdo

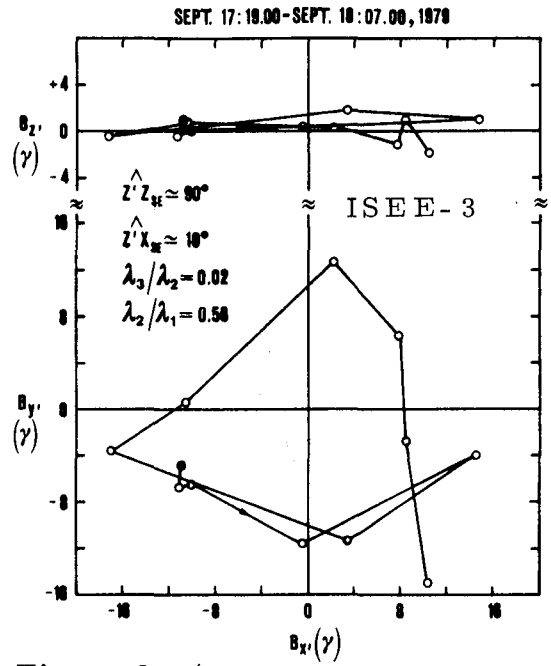

Figure 8 - (see the Text)

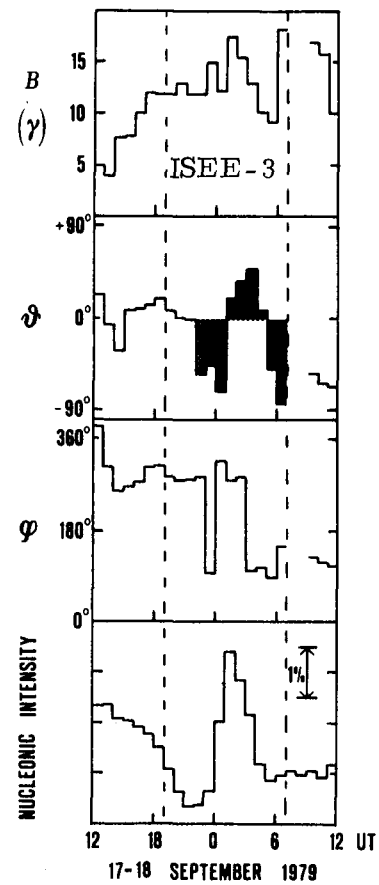

Figure 7 - (see Fig. 1)

References

1) J. H. King: "Interplanetary Medium Data Book", NSSDC/WDC-A-R & S 77-04 (1977), 79-08 (1979).
2) G. L. Siscoe and R. W. Swey: J. Geophys. Res. 77, 1321, 1972.
3) L. W. Klein and L. F. Burlaga: J. Geophys. Res. 87, 613, 1982.
4) S. P. Agrawal and D. Venkatesan: J. Geophys. Res. 87, 9201, 1982.
5) D. Venkatesan et al.: J. Geophys. Res. 86, 4836, 1981.

THE FLARE ORIGIN OF FORBUSH DECREASES NOT ASSOCIATED WITH SOLAR FLARES ON THE VISIBLE HEMISPHERE OF THE SUN

N.IUCCI, M.PARISI, C.SIGNORINI, M.STORINI and G.VILLORESI
Istituto di Fisica dello Spazio Interplanetario del CNR
Dipartimento di Fisica - Universita' "La Sapienza"
Piazzale Aldo Moro, 2 - 00185 ROMA, ITALY

1. Introduction. Previous investigations (e.g. /1/) have shown that Forbush decreases (Fds) are produced by the propagation into the interplanetary space of a strong perturbation originating from a solar flare (Sf) accompanied by Type IV radioemission. As the front of the perturbation propagates into the interplanetary space, the region in which the galactic cosmic rays are modulated (Fd-modulated region) rotates westward with the Sun and is generally included between two boundary streams /2/; therefore the Fds not associated with observed Type IV Sfs (N.Ass.Fds) are likely to be produced by Type IV Sfs occurred on the Sun's backside: these events can be observed when the Earth crosses the corotating Western boundary of the modulated region. The main purpose of this paper is to support our empirical Fd-model by studying the origin of N.Ass.Fds and the corotation of the boundary streams.

2. Data analysis. It is very likely that the strong active regions (SAR) producing great flare-associated Fds during their passage on the visible hemisphere of the Sun can flare up further Type IV Sfs when they are located on the Sun's backside; a N.Ass.Fd should be observed when the Western edge of a modulated region produced by the flares from one of these active zones encounters the Earth. We think that this is the case for the majority of N.Ass.Fds. In order to test this statement we plotted in Figure 1 the distribution of the onset-times of all (~140) N.Ass.Fds (amplitude $\geq$ 1.5% in the polar nucleonic intensity over the period 1957-1979 /1,3,4/) with respect to the central meridian passage (CMP) of 120 SAR /5/ producing large Fds (amplitude $\geq$ 3% for Type IV Sfs located between E90-W45 and $\geq$ 1.5% for W45-W90 /1/). We notice that, over a random distribution, large peaks come out between -4 and +2 days from the 27-day recurrences of the CMP of SAR ; i.e. these N.Ass.Fds are found to begin some days before the magnetic field line connected with the SAR crosses the Earth. The peak at +27 days appears to be the most pronounced as expected, while the peak amplitude at the CMP of SAR is reduced by the occurrence of large Fds, produced by Type IV Sfs in the Eastern quadrant, which mask the contemporary presence of N.Ass.Fds. Moreover we found that ~60% of the ~140 N.Ass.Fds are related with the CMP of SAR or its +27-day recurrence; on the other hand 58% of the 120 SAR analyzed are related to a N.Ass.Fd occurring near the +27-day CMP recurrence, while for 23% of them the possible N.Ass.Fds are masked by the occurrence of flare-associated Fds.

In conclusion it seems that the majority of N.Ass.Fds ($\geq$ 60%) are produced by intense Type IV Sf activity from long-living SAR; therefore we may expect that most of the remaining N.Ass. Fds could be produced by energetic Type IV Sfs occurring on the Sun's backside in active regions not included in SAR.
Figure 2 shows a Bartels display of CMP dates of SAR (•) together with their 27-day recurrences (o); the arrows indicate the N.Ass.Fd onset-times. The time interval between the +27-day recurrence of CMP of SAR and the beginning of N.Ass.Fds may be explained by two effects: the heliolongitude distance between the active region and the solar source of the Western stream and the speed of the Western stream itself. The Table shows that, as an average, the more the N.Ass.Fd onset-time (t_1) precedes the CMP or its +27-day recurrence (t_o), the more the solar wind speed at the Fd-onset is found to increase. This result may account for about a half of the broadening of the recurrent peaks; therefore the solar source of the Western stream seems to be located, from case to case, between ~40° and ~75° in the West of the active region which is, as expected, the half longitudinal extension of the Fd-modulated region.

$t_1 - t_o$ (days)	V (km/s)	Number of Events
−4 ÷ −2	570	13
−2 ÷ 0	465	17
0 ÷ +2	380	10

The corotation with the Sun of the Fd-modulated region is better shown if the boundary streams are found to recur. The interplanetary data /6/ are used to investigate the recurrence of these perturbations. Periods of enhanced magnetic field intensity (B $\geq$ 10nT), not associable either with interaction regions between high-speed streams ejected from coronal holes and the ambient solar wind, or with interplanetary perturbations produced by energetic Type IV Sfs in the visible hemisphere of the Sun, have been identified. The average behaviour of the interplanetary magnetic field intensity B and proton density N for 160 of those perturbations are shown in Figure 3 together with the average behaviour of B and N about $\pm$ 27 days (b) and $\pm$ 54 days (c). The day of the sharp increase in B was chosen as epoch-time. The results show that there is a high probability that these interplanetary structures corotate with the Sun, being the lifetime $\geq$ 2 solar rotations.

3. Conclusions. The parent active regions of most N.Ass.Fds are found to be the ones showing an intense Type IV Sf activity during their passage on the visible hemisphere of the Sun, namely those which are most likely able to produce Type IV Sfs also on the Sun's backside. Type IV Sfs emitted at different times by the same active region will depress the cosmic ray intensity in the same portion of the interplanetary space corotating with the Sun; therefore the Fd-effect will be observed also in the interplanetary regions which were not swept by the front of the perturbation, as it should happen for the N.Ass.-Fds. These results give a further support to the experimental

Fd-model developed by our group (e.g./2/).

References.

/1/ N.IUCCI et al.: Nuovo Cimento 2C, 1, 1979.
/2/ N.IUCCI et al.: Nuovo Cimento 7C, 467, 1984.
/3/ J.F.STELJES: "Cosmic ray NM-64 data" AECL-Canada 1965-1972.
/4/ M.D.WILSON and M.BERCOVITCH: "Cosmic ray NM-64 data" AECL-Canada 1973-1979.
/5/ H.V.DODSON and E.R.HEDEMAN: WDC-A(Boulder) Reports UAG-14, 1971, UAG-52, 1975 and UAG-80, 1981.
/6/ J.H.KING: "Interplanetary Medium Data Book", NSSDC/WDC-A-R & S 77-04 (1977), 79-08 (1979) and 83-01 (1983).

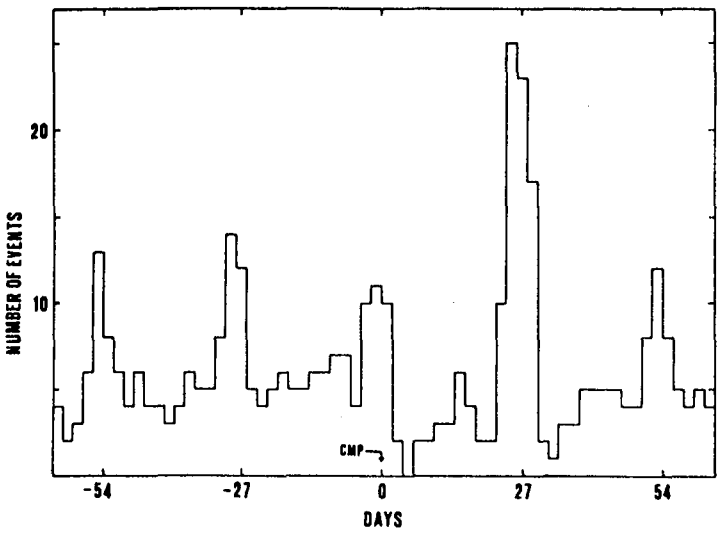

Figure 1: Distribution of the onset times of the N.Ass.Fds with respect to the Central Meridian Passage (CMP) of the active regions producing energetic Type IV Sfs and associated with great Fds (see the Text).

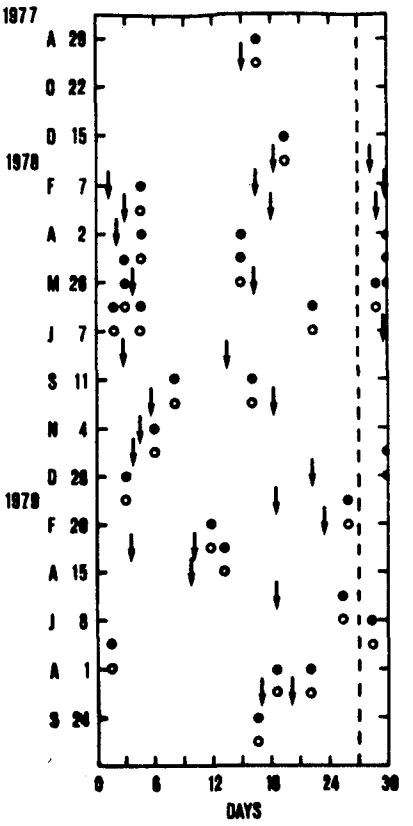

Figure 2: Bartels display of CMP dates of SAR (●) together with their 27-day recurrences (○); the arrows indicate the N.Ass.Fd onset-times.

Figure 3: (a)- Superposed epoch analysis of the interplanetary magnetic field magnitude and proton density for 160 interplanetary perturbations during 10 days centered about the time t_o of the sharp increase in B which is chosen as epoch time; (b)- the same as in (a) using as epoch time: $t_o \pm 27$ days; (c)- the same as in (a) using as epoch time: $t_o \pm 54$ days.

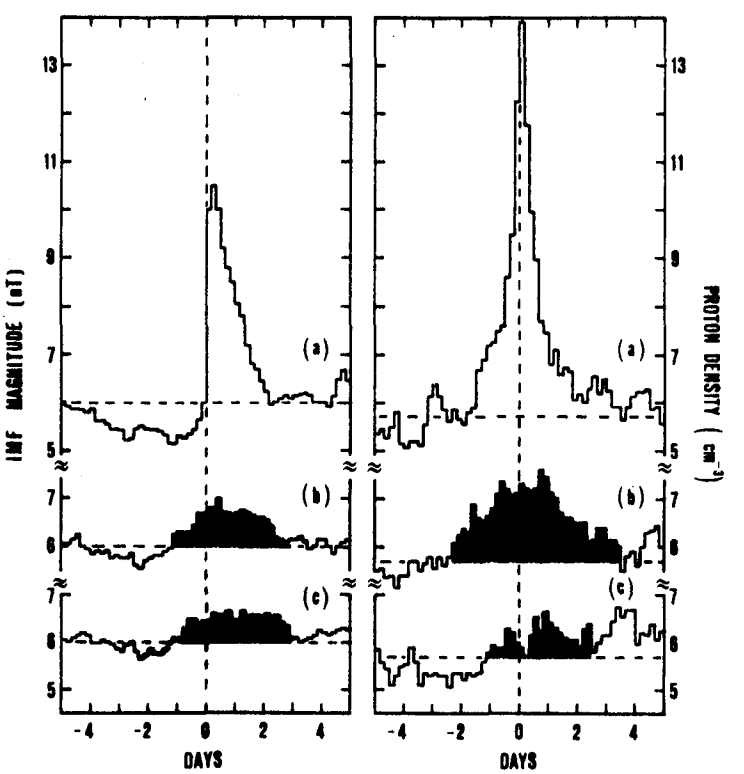

LONGITUDINAL DEPENDENCE OF THE INTERPLANETARY PERTURBATION PRODUCED BY ENERGETIC TYPE IV SOLAR FLARES AND OF THE ASSOCIATED COSMIC RAY MODULATION

N.IUCCI, M.PARISI, M.STORINI, G.VILLORESI and S.PINTER (*)
Istituto di Fisica dello Spazio Interplanetario del CNR
Dipartimento di Fisica - Universita' "La Sapienza"
Piazzale Aldo Moro,2 - 00185 ROMA, ITALY

(*) Geophysical Institute - Slovak Academy of Sciences
947 01 HURBANOVO, CZECHOSLOVAKIA

1. Introduction. One of the most significant features of the flare-associated Forbush decreases (Fds) in the galactic cosmic ray (c.r.) intensity is the so-called East-West asymmetry /1-5/ : the solar flares (Sfs) observed in the Eastern or central region of the solar disk exhibit a higher probability to cause large Fds than the Sfs occurring in the Western portion of the disk. In particular IUCCI et al./5,6/ showed that the interplanetary perturbations generated by Type IV Sfs depress the c.r. intensity in a vast spiral cone-like region (modulated region) which extends along the interplanetary magnetic field from the neighbourhood of the active region to the advancing perturbation, and that, immediately after the flare-generated perturbation, the maximum c.r. modulation is observed between 0° and 40° W (see Figures 4 and 13 in IUCCI et al./5/) of the meridian plane crossing the flare site at time of flare (flare's meridian plane). This asymmetric c.r. modulation could be due to a longitudinal asymmetry in the interplanetary perturbation producing Fds, as suggested by AKASOFU and YOSHIDA /2/ . This expected asymmetry seems to be, at a first glance, in contradiction with the results obtained by PINTER /7/ on the base of multiple spacecraft plasma and magnetic field observations, which indicate that the flare-generated shock waves expand on a broad front which is not spherical but nearly symmetrical with respect to the flare's meridian plane . In fact, if a flare-generated shock wave, displayed symmetrically with respect to the flare's meridian plane, is the only agent responsible for Fds we could hardly explain the observed East-West asymmetry of the modulated region.

IUCCI et al. /8,6/ showed that the front edge perturbation "strength" made up by the shock and magnetic blob effects, is well correlated (correlation coeff. 0.96) with the observed Fd-amplitude. Therefore if the shock is almost symmetrical about the flare longitude, the asymmetry of the Fd-modulated region is likely to be due to the magnetic perturbation following the shock which should be displayed asymmetrically in longitude, as suggested by HAURWITZ et al/9/.

BARNDEN/10/ found that the descending phase of some Fds exhibits a clear two-step structure which is located inside

the associated interplanetary disturbance.The magnetic field intensity and solar wind plasma parameters indicate that the first step begins with the shock passage at the Earth/10,6/; the second step occurs generally near a discontinuity loca - ted inside the magnetic blob and followed by the flare ejec- ta or driver gas, this second decrease can be often connect- ed to the entry of the Earth into a region with loop-like magnetic field configuration (e.g./11/ and ref. therein).

The main purpose of the present paper is to verify ex- perimentally that an asymmetric perturbation (magnetic blob and discontinuities) following the shock is indeed respon- sible for the longitudinal asymmetry of the c.r. modulation; this will be done by studying statistically the separate contributions of the shock front and the following magnetic perturbation on the amplitude of the first and second step of Fds as a function of the associated Sf longitude.

2.The influence of shock and magnetic perturbation following the shock on the Fd-amplitude at 1 AU. An example of a two- step Fd time behaviour and associated parameters of the in- terplanetary medium is given in Figure 1.

First of all we analyzed,over the period 1964-1982, the total Fd-amplitudes as a function of the heliolongitude of the associated Sfs. Figure 2 shows that the total Fd-ampli- tude depends on the longitudinal position of the parent fla- re on the Sun; this result shows in particular that the max- imum Fd-amplitude is observed when the flare is located $\sim 20^{\circ}$ East of the central meridian of the solar disk, in other wo- rds when the Earth enters the Fd-modulated region at $\sim 20^{\circ}$ We- st of the flare's meridian plane.

We next analyzed the relation between the amplitude of the first step of Fds and the longitudinal position of the parent Sfs. Figure 3 shows that, as an average, the highest amplitudes are observed near the flare's meridian plane, in agreement with the results obtained by PINTER /7/.
By means of the envelope curves of Figures 2 and 3 we can determine the large-scale characteristics of the two-step Fds; the polar diagram given in Figure 4 represents the he- liolongitude dependence, relative to the flare longitude, of the total amplitude together with the amplitudes of the first and second steps of Fds. The asymmetric second step of Fds may be due to the longitudinal asymmetry of the magn- etic perturbation following the shock /9,2/ : the magnetic field compression produced by a nearly symmetric shock, sus- tained by the driver gas and expanding into the Archimedean interplanetary magnetic field, will be more pronounced some- where in the West of the flare's meridian plane, but not too far from this plane on which the shock exhibits the highest velocities. This asymmetry is shown in Figure 5 where the parameter $< B >.\Delta t$ of the magnetic blob following the shock is plotted against the heliolongitude of the parent Type IV Sf, where Δt is the time duration and $< B >$ the average fi- eld magnitude during the blob .

3. Relation between the Fd-amplitude and the associated interplanetary perturbation. IUCCI et al./8,6/ found that when the observed interplanetary perturbation is produced by a Type IV Sf the Fd-amplitude is well correlated with an empiric perturbation parameter which is the sum of two parameters: the shock "strength" P_s and the magnetic blob "strength" P_b. If we assume that the magnetic blob "strength" is representative of the magnetic perturbation following the shock, the two parameters will correspond to the two effects reported above and therefore they can be separately correlated with each of the two steps of Fds. On the other hand a shock plus a magnetic blob were recently proved /12/ to form a suitable semipermeable obstacle to particle motion in order to produce the observed Fds. We investigated first the correlation between the total Fd-amplitude and the total perturbation parameter P_o defined as:

$$P_o = P_s + A \cdot P_b = V_L + (V_1 - V_o) + 40[(N_1 - N_o)/N_o + (B_1 - B_o)/B_o] + A(\langle B \rangle \Delta t),$$

where V_L is the local shock velocity (not considered in IUCCI et al. /8,6/) in km/s computed by using the flux conservation equation: $V_L = (V_1 N_1 - V_o N_o) / (N_1 - N_o)$; indexes 0 and 1 refer to the pre- and post-shock values respectively. The coefficient $A = 1/3600$ km.s^{-2}.nT^{-1} was estimated by making $\langle P_s \rangle = A \cdot \langle P_b \rangle$ as indicated by the similar average amplitudes of the two steps of Fds (see Figure 3). For 21 two-step Fds an accurate estimate of P_s and P_b was possible; in Figure 6 the correlation plot between P_o and the total Fd-amplitude confirms the results obtained by IUCCI et al./8,6/ (correlation coefficient 0.96); moreover the first step of the decrease is rather well correlated with the shock parameter P_s (correlation coeff. 0.88) as shown in Figure 7, this lower correlation may be attributed to the lower accuracy in the estimate of the first-step amplitudes.

References

/1/ S.YOSHIDA and S.I.AKASOFU: Plan.Sp.Sci. 13,435,1965.
/2/ S.I.AKASOFU and S.YOSHIDA: Plan.Sp.Sci. 15,39,1967.
/3/ Z.SVESTKA: Bull.Astr.Czech. 18,55,1967
/4/ S.GOPASYUK and L.KRIVSKY: Bull.Astr.Czech. 18,125,1967.
/5/ N.IUCCI et al.: Nuovo Cimento 2C, 1 , 1979 .
/6/ N.IUCCI et al.: Nuovo Cimento 7C, 467, 1984.
/7/ S.PINTER: Space Sci. Rev. 32, 145 , 1982 .
/8/ N.IUCCI et al.: Proc. 17th Int. C.R. Conf. 10,151,1981.
/9/ M.W.HAURWITZ et al.: J. Geophys. Res. 70, 2977 , 1965 .
/10/ L.R.BARNDEN: "Proc. 13th Int. C.R. Conf. 2,1277,1973.
/11/ R.D.ZWICKL et al: "Proc. SOLAR WIND FIVE", 711,1983.
/12/ B.T.THOMAS and R.GALL: J. Geophys. Res. 89, 2991,1984.

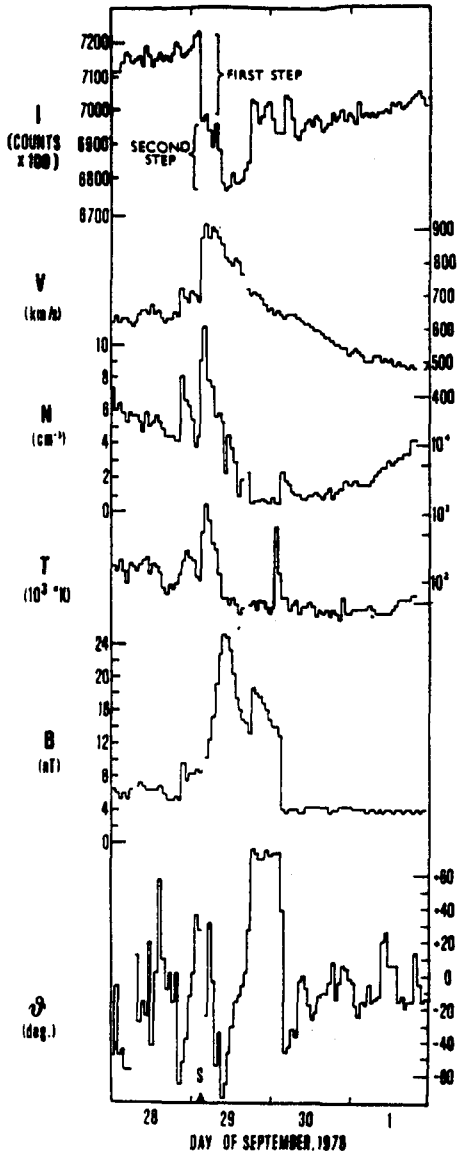

Figure 1

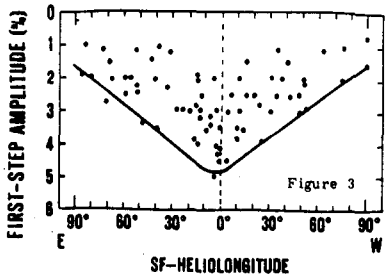

Figure 3

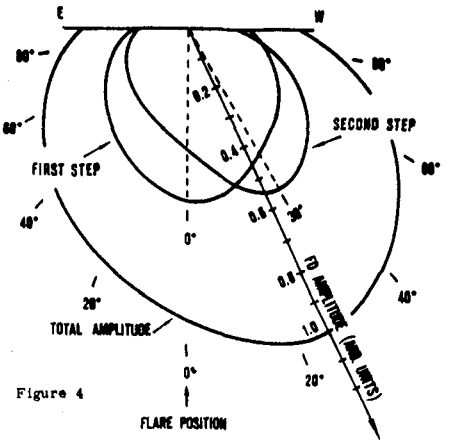

Figure 4

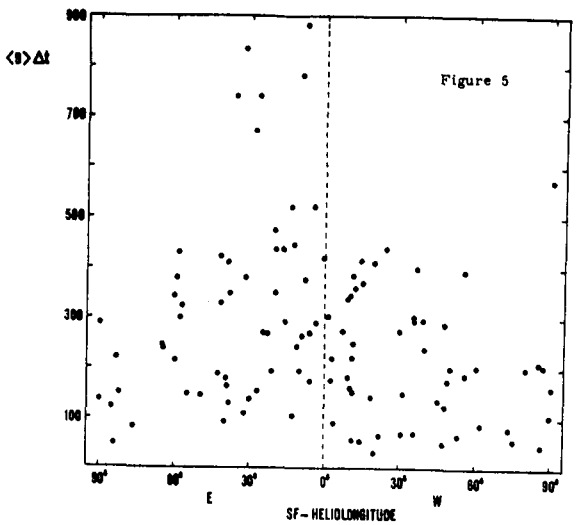

Figure 5

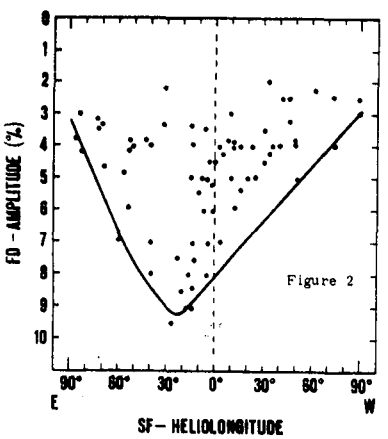

Figure 2

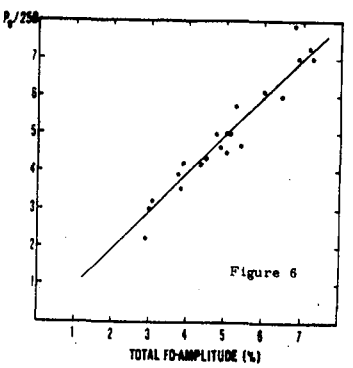

Figure 6

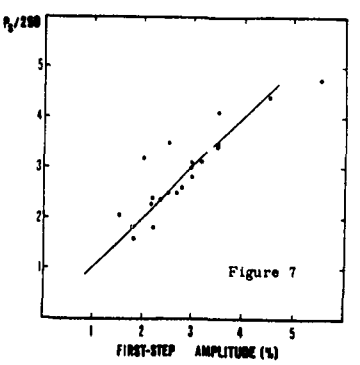

Figure 7

SH 5. 1-6

RIGIDITY SPECTRUM OF FORBUSH DECREASE

S. Sakakibara, K. Munakata and K. Nagashima
Cosmic Ray Research Laboratory, Faculty of Science,
Nagoya University, Nagoya 464 Japan

ABSTRACT

Using data from neutron monitors and muon telescopes at surface and underground stations(Nagoya, 0 m.w.e.; Misato, 34 m.w.e.; Sakashita, 80 m.w.e.), we obtain the average rigidity spectrum of Forbush decreases(Fds) during the period of 1978-1982. Thirty eight Fd-events are classified into two groups "Hard Fd" and "Soft Fd" according to size of Fd at Sakashita station. It is found that a spectral form of fractional-power type($P^{-\gamma_1}(P+P_C)^{-\gamma_2}$) is more suitable for the present purpose than that of power-exponential type or of power type with an upper limiting rigidity. The best fitted spectrum of fractional-power type is expressed by $\gamma_1=0.37$, $\gamma_2=0.89$ and $P_C=10$GV for Hard Fd and $\gamma_1=0.77$, $\gamma_2=1.02$ and $P_C=14$GV for Soft Fd.

1. Introduction. Rigidity spectrum of Forbush decrease(Fd) has been studied by many authors, using neutron monitor data(e.g. Lockwood, 1971; Iucci et al., 1979; Lumme et al., 1983; Fenton et al., 1983), or by adding a small amount of underground muon data to those in the above(e.g. Thambyahpillai et al., 1965; Andreis-Sandrucci et al., 1968; Mishima et al., 1973; Suda et al., 1977; Krymsky et al., 1979; Wada et al., 1979; Sakakibara et al., 1979; Wada and Suda, 1980). These studies have been made by assuming apriori a definite form of the spectrum and have tried to determine parameters involved in the spectral form. In the present paper, we make a comparative study of the spectral forms of Fd, using plenty of data in wide range of primary cosmic ray rigidity. For the muon telescope data, we use the response function given by Murakami et al.(1979,1981). For the neutron monitor data, we choose the response function given by Nagashima(1980) for the maximum solar activity out of three functions(Lockwood and Webber,1967; Aleksanyan et al.,1981; Mori and Nagashima,1984), based on a comparative study of response functions(S.Sakakibara et al.,1984; S.Mori and K.Nagashima,1984).

2. Rigidity spectrum of Forbush decrease. Data used for the present analysis are those of 8 neutron monitors(median primary rigidity P_m=21 ∿ 35GV), 17 muon telescopes at Nagoya(P_m=60 ∿ 119GV), 9 underground muon telescopes at Misato(P_m=145 ∿ 209GV) and 3 underground muon telescopes at Sakashita(P_m=330 ∿ 567GV) during the period of Feb. 1978 - Feb. 1983. Fourty five Fds greater than 2% in depression for neutron intensity at Alert station were selected, but because of missing data of muon components, 38 Fds were finally adopted.

Fig.1 shows the rigidity dependence of the development of Fd on daily basis, obtained by superposing those 38 Fds at the epoch which 0-day includes the occurence time of SC. As can be seen in this figure, the depression at Sakashita is about 0.15% on the average and statiscally significant, but individual Fd at the station is not always statiscally significant and, in some cases, shows some increase. Taking this fact into account, we classify the Fds into two groups "Hard"(23 events) and "Soft"(15 events) according to size of Fd of Sakashita vertical component.

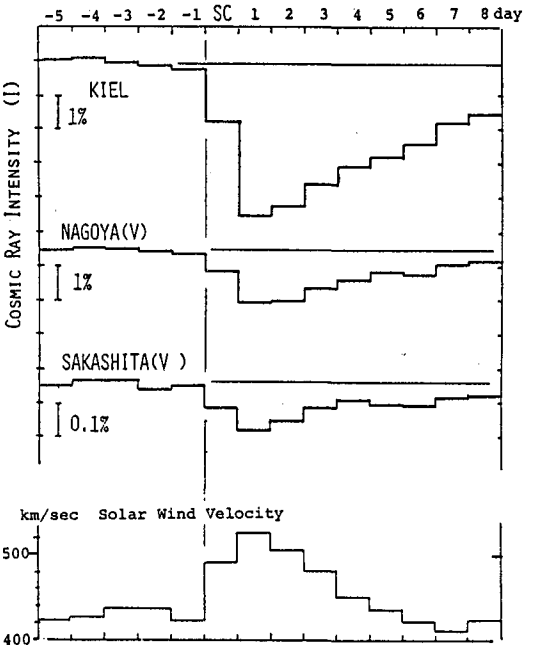

Fig.1 Averaged daily development of 38 Forbush decreases, superposed at the epoch day including SC, and that of the corresponding solar wind velocities.

The magnitude(ΔI) of each Fd is defined by the difference between daily mean intensities on +1 day and -3 day(cf. Fig.1). The boundary of two groups is set at the magnitude(ΔI=0.05%) of Sakashita vertical component, which corresponds to the statistical error for the component.

We made a comparative study of the rigidity spectrum of Fd, using the following three types of the spectrum.

PW : Power type

$$\Delta I \propto \begin{cases} P^{-\gamma} & \text{for } P \leqslant P_u \\ 0 & \text{for } P > P_u \end{cases}$$

PE : Power-Exponential type

$$\Delta I \propto P^{-\gamma} \exp(-P/P_o)$$

FP : Fractional-Power type

$$\Delta I \propto P^{-\gamma_1}(P+P_c)^{-\gamma_2} \qquad \ldots\ldots (1)$$

Corresponding to the parameters involved in Eq.(1), the expected values ΔI_{exp}'s for muon components and neutron monitors are calculated, respectively, from the differential coupling coefficients by Fujimoto et al. (1984) and from those by Mori and Nagashima(1984). By the least squares method, we found that FP-type spectrum in Eq.(1) can produce the expected values ΔI_{exp}'s most compatible with the observations. To demonstrate the coincidence between the observation and ΔI_{exp}'s, we use a diagram whose ordinate represents the observed magnitude of Fd and whose abscissa expresses the corresponding magnitude ΔI_{exp} calculated by using a rigidity spectrum of Fd. We call this the correlation diagram of Fd. If ΔI_{exp} is calculated by using the spectrum determined from the observed data by the least squares method, we call the diagram the best fitted correlation diagram of Fd. In this case, all points on the graph must lie on a line inclined by 45° from the abscissa. Such diagrams of Hard and Soft Fd's are shown in Fig.2, for the FP-type spectrum. It is noted that, in case of Soft Fd, the least squares method was applied to those data excluding those of Sakashita station.

The rigidity dependence of Fd's can be expressed more plainly if we use an effective primary rigidity(P_E) for Fd, which is defined as the median rigidity of a function obtained by multiplying the response function by the best fitted rigidity spectrum of the Fd. Fig.3 shows the P_E-dependence of Hard and Soft Fd's. The average magnitudes $\langle\Delta I\rangle$'s can line up systematically on this graph.

In Table I, we show the best fitted parameters of three types of the

rigidity spectrum.

Table I. The best fitted parameters for three types of the rigidity spectrum.

Spectral type / Group	FP $P^{-\gamma_1}(P+P_C)^{\gamma_2}$			PE $P^{-\gamma}\exp(-P/P_o)$		PW $P^{-\gamma}$, $(P \leq P_u)$	
	γ_1	γ_2	P_C(GV)	γ	P_o(GV)	γ	P_u(GV)
Hard Fd	0.37	0.89	10	0.90	471	0.98	400
Soft Fd	0.77	1.02	14	1.17	145	1.26	100

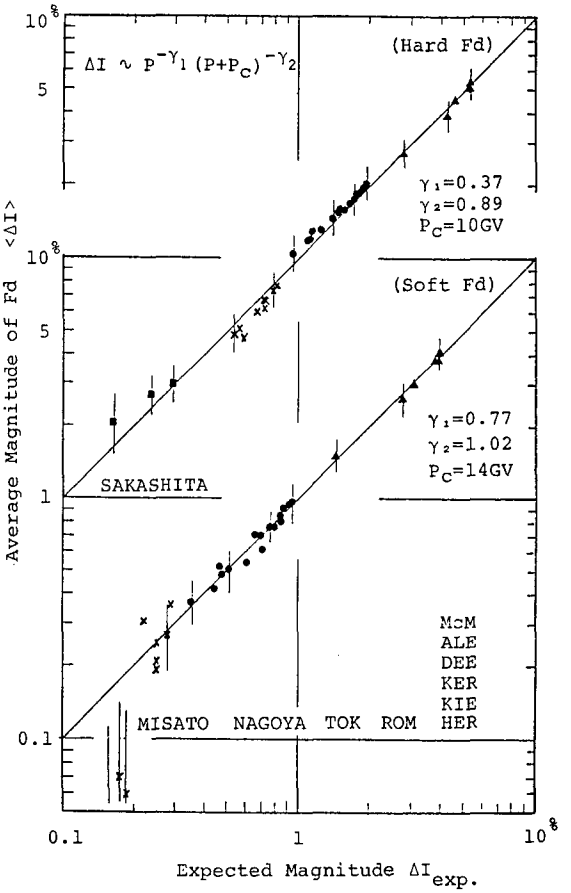

Fig.2 The best fitted correlation diagram of Hard and Soft Fds. ΔI_{exp} is calculated by using the fractional-power type spectrum with parameter shown in the figure, and in case of neutron monitors the NAGASHIMA-response function is selected for the calculation.

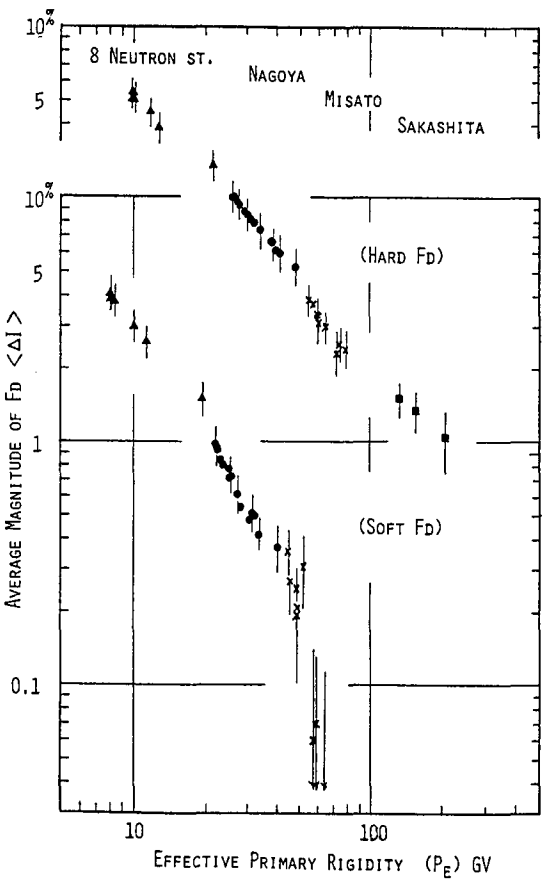

Fig.3 P_E -dependence of average magnitude <ΔI> of Hard and Soft Fds. The effective primary rigidity P_E for Fd defined in the text is calculated under the same conditions as in Fig.2. Errors are derived from the dispersion of individual Fds.

3. Conclusion. It is concluded that the FP-type spectrum is more suitable than PE-type or PW-type to express the observed rigidity dependence of Forbush decrease. However, in case of the Soft Fd, one cannot select the best spectral form out of the three types, by reason of the insufficient accuracy of the observed data in the higher rigidity range.

4. Acknowlegement. The authors are very grateful to Prof. S.Mori and his colleagues, Shinshu University, for providing their data from Misato underground station and also to Dr. M.Wada, Director of WDC-C2, Itabashi, Tokyo, for supplying us neutron monitor data. The authors wish to express their sincere thanks to Prof. I.Kondo, Tokyo University, for his helpful suggestion and discussion.

References

Aleksanyan,T.M., V.M.Beduazhevosky, Ya.L.Bloch, L.I.Dorman, N.S.Kaminar and F.A.Starkov (1981). Proc. 17th Int. Cosmic Ray Conf., (Paris), 3, 225.

Andreis-Sandrucci,L., G.Cini-Castagnoli and M.A.Dodero (1968). Annales de Geophysique, T.24, fasc.3, p.889.

Fenton,A.G., K.B.Fenton and J.E.Humble (1983). Proc. 18th Int. Cosmic Ray Conf., (Bangalore), 10, 164.

Fujimoto,K., A.Inoue, K.Murakami and K.Nagashima (1984). Rep. of Cosmic Ray Research Laboratory, Nagoya Univ., No.9.

Iucci,N., M.Parisi, M.Storini, G.Villoresi and N.L.Zangrilli (1979). Nuovo Cimento, 2C, 411.

Krymsky,G.F., P.A.Krivoshapkin, V.V.Klimenko, A.I.Kuzmin, S.I.Prokopjev, G.V.Skripin, N.P.Chirkov, G.V.Shafer and Yu.G.Shafer (1979). Proc. 16th Int. Cosmic Ray Conf., (Kyoto), 3, 395.

Lockwood,J.H. and W.P.Webber (1967). J.G.R., 72, 3395.

Lockwood,J.A. (1971). Space Sci. Reviews 12, 658.

Lumme,M., M.Nieminen, J.Feltonen, J.J.Torsti, E.Vainikka and E.Valtonen (1983). Proc. 18th Int. Cosmic Ray Conf., (Bangalore), 3, 237.

Mishima,Y., K.Murakami, M.Wada and Y.Miyazaki (1973). Proc. 13th Int. Cosmic Ray Conf., (Denver), 2, 1289.

Mori,S. and K.Nagashima (1984). Proc. Intern. Symp. Cosmic Ray Mod. in the Heliosphere, Morioka, Japan, p.219.

Murakami,K., S.Sagisaka, A.Inoue, Y.Mishima and K.Nagashima (1979). Nuovo Cimento, 2C, 635.

Murakami,K., S.Sagisaka, Y.Mishima, A.Inoue and K.Nagashima (1981). Rep. of Cosmic Ray Research Laboratory, Nagoya Univ., No.6.

Nagashima,K. (1980). personal communication.

Sakakibara,S., H.Ueno, K.Fujimoto, Z.Fujii and K.Nagashima (1979). Proc. 16th Int. Cosmic Ray Conf., (Kyoto), 3, 407.

Sakakibara,S., K.Munakata and K.Nagashima (1984). Proc. Intern. Symp. on Cosmic Ray Modulation in the Helioshpere, Morioka, Japan, p.212.

Thambyahpillai,T. and J.C.Dutt (1965). Proc. 9th Int. Cosmic Ray Conf., (London), 1, 257.

Suda,T., Y.Mishima, K.Murakami and M.Wada (1977). Proc. 15th Int. Cosmic Ray Conf., (Plovdiv), 3, 312.

Wada,M., S.Mori, K.Nagashima, S.Sakakibara and S.Yasue (1979). Proc. 16th Int. Cosmic Ray Conf., (Kyoto), 3, 390.

Wada,M. and T.Suda (1980). Sci. Papers I.P.C.R., 74, 1.

SPECTRAL ANALYSIS OF THE FORBUSH DECREASE OF JULY 13, 1982

E. Vainikka, J.J. Torsti, E. Valtonen, M. Lumme,
M. Nieminen, J. Peltonen, and H. Arvela

Department of Physical Sciences, University of Turku, and
Wihuri Physical Laboratory, University of Turku
SF-20500 Turku, Finland

ABSTRACT

The maximum entropy method has been applied in the spectral analysis of high-energy cosmic-ray intensity during the large Forbush event of July 13, 1982. An oscillation with period of about 2 hours and amplitude of 1 - 3 % was found to be present during the decrease phase. This oscillation can be related to a similar periodicity in the magnetospheric field. However, the variation was not observed at all neutron monitor stations.

In the beginning of the recovery phase, the intensity oscillated with a period of about 10 hours and amplitude of $\lesssim 3$ %.

1. INTRODUCTION

One of the largest Forbush decreases (FDs) was observed on July 13, 1982. It was caused by a solar flare of type 3B on July 12 at 0916 UT at position 11 N, 37 E. The arrival of the shock front was indicated by a sudden commencement (SSC) at 1618 UT on July 13. The magnetic disturbance generated the largest geomagnetic storm ever observed in Finland. At Nurmijärvi Geomagnetic Observatory (60.5 N, 24.7 E), the horizontal component of the geomagnetic field reduced 20 % within a few hours, and returned to its predecrease level in 12 hours.

The decrease of high-energy cosmic rays began at about 1620 UT on July 13, and the recovery phase lasted several days. The amplitude of the decrease was of the order of 20 % as measured by the Turku double neutron monitor and other high-latitude monitors.

In order to find out possible periodicities in the cosmic-ray intensity during this FD, we applied the Maximum Entropy Method (MEM), proposed by Burg in 1967, in analyzing data from nine neutron monitor stations. The advantage of MEM is that it leads to much better resolution than the conventional Blackman-Tukey method. It also gives more realistic power spectral estimates, especially for short data records.

2. DATA AND METHOD OF ANALYSIS

The neutron monitor data used in our analysis are displayed in Figure 1. Before the frequency analysis, long-term trends (period > 12 hours) were removed by using the moving average method.

The power spectral density, P(f), was estimated from the equation

$$P(f) = \Delta t \, P_{M+1} \left| 1 + \sum_{k=1}^{M} \alpha_{Mk} \exp(-2\pi i f k \Delta t) \right|^{-2},$$

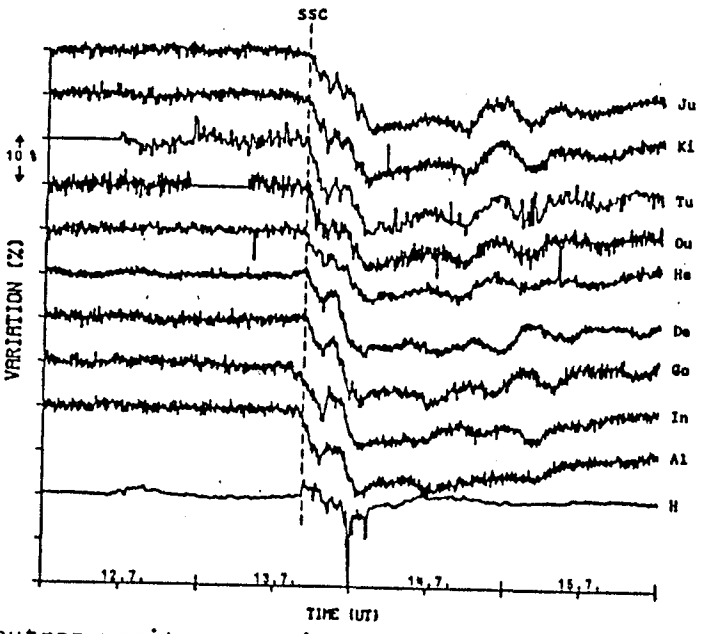

Fig. 1. Neutron monitor counting rates on July 12-15, 1982, at nime stations (see table 1 for the abbreviations). The lowest curve shows the horizontal component of the geomagnetic field as measured at Nurmijärvi station in Finland.

where f is the frequency, Δt is the time interval between the data points, and M is the length of the prediction error filter. The constant P_{M+1} and the coefficients α_{Mk} were determined from the matrix equation

$$\begin{pmatrix} \phi_o & \phi_1 & \cdots & \phi_n \\ \phi_1 & \phi_o & \cdots & \phi_{n-1} \\ \cdot & \cdot & \cdots & \cdot \\ \cdot & \cdot & \cdots & \cdot \\ \phi_n & \phi_{n-1} & \cdots & \phi_o \end{pmatrix} \begin{pmatrix} 1 \\ \alpha_{M1} \\ \cdot \\ \cdot \\ \alpha_{MM} \end{pmatrix} = \begin{pmatrix} P_{M+1} \\ 0 \\ \cdot \\ \cdot \\ 0 \end{pmatrix}$$

where ϕ_l (l=0,...,n) is the autocorrelation with time lag $n\Delta t$ (for details of the method, see e.g. Ulrych and Bishop 1975). The time interval Δt was 5 or 15 min, and M was determined in the standard way ($M \leq N/3$, N = number of data points).

3. RESULTS AND DISCUSSION

3.1. Decrease phase. The decrease phase started at about 1620 UT. However, at Inuvik the onset time was about 1430 UT. The explanation is that the asymptotic directions of Inuvik rotate with the Earth so that at 1430 UT Inuvik receives particles from the direction of the interplanetary magnetic field-line. But these particles were strongly scattered by the arriving shock front, and thus their intensity decreased earlier.

The only significant variation in the frequency range $3 \cdot 10^{-5}$ - 10^{-3} Hz occurred with periods between 112 and 126 min (Table 1). The amplitude was largest at the mountain station Jungfraujoch (≈ 3 %, as reported also by Debrunner et al. 1983). At Finnish stations (Turku and Oulu), the amplitude was $\lesssim 2$ %. An analysis of the neutron-multiplicity data of the

Table 1. The most significant periods in the cosmic-ray intensity at various neutron monitor stations.

Station		R_c^{vert} (GV)	Period (min) Decrease phase	Recovery phase
Jungfraujoch	(Ju)	4.5	118	716
Kiel	(Ki)	2.3	115	706
Turku	(Tu)	1.1	115	706
Oulu	(Ou)	0.8	112	788
Hermanus	(He)	4.6	-	430
Deep River	(De)	1.1	-	640
Goose Bay	(Go)	0.6	-	596
Inuvik	(In)	0.2	126	540
Alert	(Al)	0.0	(119)	702

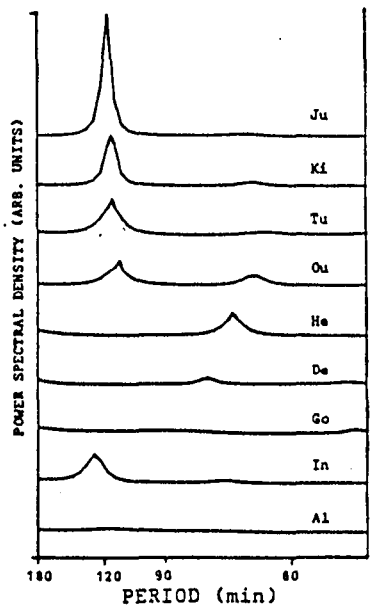

Fig. 2. Power spectral densities of the cosmic-ray intensity observed at various stations during the decrease phase.

Turku neutron monitor showed that this variation was no more present at multiplicities ≥4 corresponding to median primary rigidities ≤35 GV.

The power spectral densities are shown in Figure 2. It is noteworthy that the 2-hour periodicity was practically absent at Hermanus Deep River, and Goose Bay. Further, the period 119 min of Alert is not statistically significant.

In Figure 3, the power spectral density is presented in more details around the 2-hour peak. The superiority of MEM to the conventional Blackman-Tukey method is evident.

The origin of these oscillations is clearly in the strong variation of the magnetospheric field as can be seen in Figure 4, where the observations of the satellite GOES-2 are reproduced.

3.2. Recovery phase. In the beginning of the recovery phase, rather strong oscillations were observed at all stations. The only remarkable variations occurred with a period of about 10 hours and amplitude of 3 % (Table 1 and Figure 5). A similar periodicity was found by Chirkov et al. (1983) as they analyzed data from several stations. This periodicity could be explained by the activity of the Sun. Another possibility could be successive reflections of galactic cosmic rays on

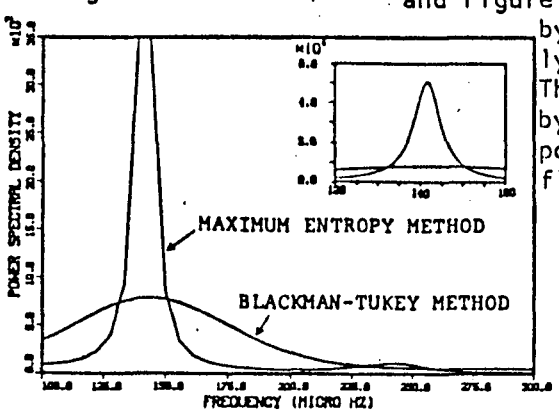

Fig. 3. Power spectral density of the cosmic-ray intensity observed at Jungfraujoch during the decrease phase. The small figure shows the density around the 2-hour peak.

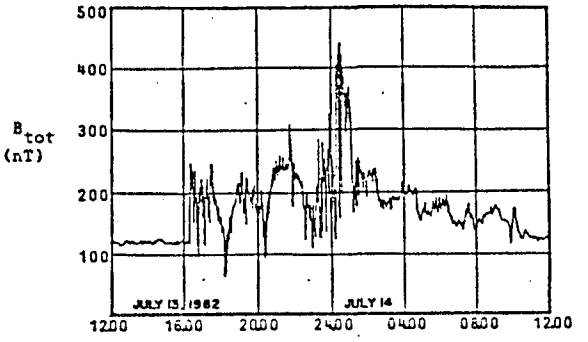

Fig. 4. The total magnetic field as measured by the satellite GOES-2 (from Parsignault et al. 1983).

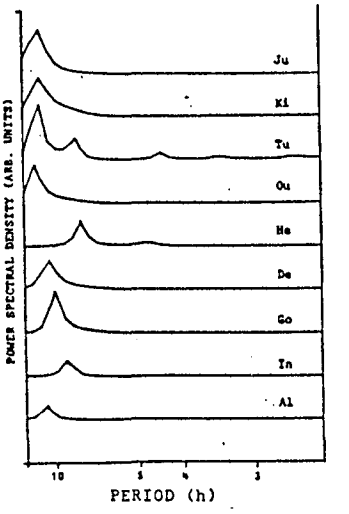

Fig. 5. Power spectral densities during the recovery phase.

the shock front.

Inspection of Figure 1 reveals some phase shifts of a few hours in the 10-hour variation (e.g. Deep River and Goose Bay vs. European stations). This feature is understood in terms of differences in the asymptotic directions of the stations.

4. CONCLUSIONS

The unusual periodicity of 2 hours during the decrease phase of the FD of July 13, 1982, is a direct consequence of strong oscillations in the magnetospheric field. The mechanism of the interactions between the solar wind and the Earth's magnetosphere leading to these oscillations requires further studies.

5. ACKNOWLEDGEMENTS

We are grateful to the following persons for providing us the neutron monitor data: G. Sebor (Jungfraujoch), K. Röhrs (Kiel), H. Kananen (Oulu), P. Stoker (Hermanus), and M. Bercovitch (Deep River, Goose Bay, Inuvik, and Alert). We also thank C. Suchsdorff for the magnetometer data of Nurmijärvi Geophysical Observatory.

REFERENCES

Chirkov, N.P., Filippov, A.T., and Yanchukovsky, V.L., Proc. 18th Int. Cosmic Ray Conf. 3, 245 (1983)

Debrunner, H., Flückiger, E., Gollïez, A., Neuenschwander, H., Schubnell, M., and Sebor, G., Proc. 18th Int. Cosmic Ray Conf. 3, 257 (1983)

Parsignault, D.R., Feynman, J., and Rothwell, P., Proc. 18th Int. Cosmic Ray Conf. 10, 266 (1983)

Ulrych, T.J. and Bishop, T.N., Rev. Geophys. Space Phys. 13, 183 (1975)

TRANSIENT COSMIC RAY INCREASE ASSOCIATED WITH A GEOMAGNETIC STORM

S. Kudo and M. Wada
Cosmic Ray Laboratory, Institute of Physical and Chemical Research
7-13 Kaga-1, Itabashi, Tokyo 173, Japan

P. Tanskanen
Department of Physics, University of Oulu
Linnanmaa, SF-90570, Oulu 57, Finland

and
M. Kodama
Department of Physics, Yamanashi Medical College
Tamaho, Nakakoma, Yamanashi 409-38, Japan

ABSTRACT

On the basis of worldwide network data of cosmic ray nucleonic component, the transient cosmic ray increase due to the depression of cosmic ray cutoff rigidity during a severe geomagnetic storm has been investigated in terms of the longitudinal dependence. Multiple correlation analysis among isotropic and diurnal terms of cosmic ray intensity variations and Dst term of the geomagnetic field is applied to each of various station's data. It is shown that the amplitude of the transient cosmic ray increase associated with Dst depends on the local time of the station, and that its maximum phase is found in the evening sector. This fact is consistent with the theoretical estimation based on the azimuthally asymmetric ring current model for the magnetic DS field.

1. Introduction. The depression of cosmic ray cutoff rigidities and the alteration of the asymptotic direction of approach of cosmic rays during geomagnetic storms have been widely investigated by several authors throuth analysis of cosmic ray data or using trajectory-tracing technique (Yoshida et al., 1968; Debrunner et al., 1979; Flückiger et al., 1981). A particular interest is paid to the longitudinal or local time asymmetry of the cutoff rigidity depression or the storm-time cosmic ray increase, in connection with the asymmetric ring current which causes disturbed daily variation of geomagnetic field (Cummings, 1966; Kudo et al., 1984).

In this paper the storm-time cosmic ray increase for mountain stations is analyzed using 28 severe geomagnetic storm events occurred in 1966-1978. In this way the multiple correlation analysis is applied among isotropic and diurnal components of cosmic ray intensity and geomagnetic Dst term, and then the cosmic ray modulation term due to other origins except the lowering of cutoff rigidity is composed. The amplitude is obtained as a function of longitude of the stations.

2. Method of Analysis. The first step of the analysis is to separate the storm-time increase from other kinds of cosmic ray variations during geomagnetic storms. In the previous paper (Tanskanen et al. 1983) we reported that the observed cosmic ray variation during severe geomagnetic storms, CR(t), is reasonably separated into three components, i.e., the diurnal and the isotropic components A(t) and Iso(t), and the Dst depen-

dent component, Dst(t).

$$CR(t)=A(t)+c\cdot Iso(t)+d\cdot Dst(t)$$
$$where \quad A(t)=a\cdot cos\omega t+b\cdot sin\omega t \qquad \omega=2\pi/24hr$$

The isotropic component Iso(t) is an average of neutron monitor data from Thule and McMurdo to analyze the data from the sea-level stations. An average of Thule and Alert is used to analyze the data from the mountain stations since they are all distributed in the northern hemisphere. The coefficients a,b,c and d are obtained by the multiple correlation analysis based on one hour values covering three days centered at the Dst minimum day. The composed cosmic ray intenstiy, CR'(t), is defined by using some of the coefficients as follows.

$$CR'(t)=A(t)+c\cdot Iso(t)$$

The storm-time increase, STI, in unit of %/100nT is determined subtracting CR'(t) from CR(t). Some examples are shown in Figure 1.

3. Local Time Asymmetry of the Storm-Time Increase. The local time dependence of STI is analyzed by using the cosmic ray data from a number of stations distributed over a whole range of longitude on the earth. In the previous paper (S.Kudo et al., 1984), the sea-level stations below 5GV cutoff rigidity are used. After excluding the rigidity dependence of STI we obtained the local time asymmetry of STI from about 30 stations.

The phase and amplitude of the local time asymmetry of the storm time increase are obtained for six events. The histograms of the frequecy distribution of phases of the six events show that the asymmetry is located in the evening sector in the interval of several hours close to the Dst minimum time. The amplitude of the asymmetry averaged over the six events is kept almost constant at 1%/100nT for the same interval of time.

In Figure 2 the observed storm-time increases of the six events are illustrated together with the theoretical expectations. The black circles are the average values of observed STI of the stations with 4 GV cutoff rigidity, and the arrows denote the amplitudes of the asymmetry. The white circles are the theoretical estimations of the average storm time increase for Kiel, Jungfraujoch and Rome, which are obtained from the theoretical curve for the rigidity dependence of the storm-time increase (Kondo,1961). The theoretical values of the amplitude of asymmetry are estimated by using the result of Flückiger et al.'s work (1981), in which they calculated the depression of cutoff regidity based on a partial ring current model. It is seen that the observed values of STI are comparable with the theoretical expectations in magnitude.

4. Analysis on Mountain Stations. The local time dependence of STI on mountain stations is analyzed by using 28 events which occur in various UT hours. The method adopted for the sea-level stations is not applicable for mountain stations because they have various altitudes and the number of stations are limited. In this paper 28 events listed in Table 1 are used.

A typical example is shown in Figure 3, where STI in unit of %/100nT are plotted against UT of the Dst minimum time. Three hour average values of STI centered at the Dst minimum time are used in the present analysis.

The conversion of unit from % to %/100nT is made by multipling STI(%) by $100/\Delta Dst$, where Δ Dst is the difference of Dst between its flat level and the average over three hours around the Dst minimum time. The large increase near 18h LT(the arrow) show the local time asymmetry of STI. The other European mountain stations with between 4 and 5 GV cutoff rigidity, Lomnicky-Stit, Zugspitze, Pic-du-Midi, have the same tendency in the local time dependence. On the other hand the mountain stations with higher or lower cutoff rigidities, for example Mt.Norikura(11.4 GV) and Climax(3.0 GV), do not show such an evident asymmetry of the storm-time increase. The STI of Rome is also plotted in Figure 3. The phase of the asymmetry is close to 18h LT.

5. Discussion and Summary. We have obtained the local time asymmetry of the storm-time increase from the worldwide neutron monitor data. In section 2 the method for analyzing the data from a number of sea-level stations with cutoff rigidity lower than 5 GV has been shown briefly. The amplitudes of the asymmetry are consistent with the theoretical expectations, and the phases are located in the evening sector. In section 3 another method has been used to analyze the data from mountain stations or individual stations. The two methods are mutually connected with an equation between LT, UT and the longitude of stations, $LT=UT+(longitude/15degrees)$. It is evident that the data from European mountain stations show the local time asymmetry in the storm-time increase, and that the observed amplitude of asymmetry of Jungfraujoch and Rome are consistent with the theoretical expectations shown in Figure 2. We are making further analysis of the data from individual stations.

6. Acknowledgements. The authors express their sincere thanks to all the stations for sending neutron monitor data to WDC-C2. The present analysis is made on these invaluable data.

References

Cummings, W.D., "Asymmetric ring currents and the low-latitude disturbance daily variation", J.Geophys.Res., 71. 4495(1966).

Dubrunner, H., and E.Flückiger, H.von Mandach and M. Arens, "Determination of the ring current radii from cosmic ray neutron monitor data for the 17 December 1971 magnetic storm", Planet.Space Sci., 27, 577(1979).

Flückiger, E.O., D.F.Smart and M.A.Shea, "On the effect of magnetospheric current systems on cosmic ray cutoff rigidities", Proc.17th ICRC, 4, 244(1981).

Kondo, I., "On cosmic ray intensity increase during geomagnetic storm", Rep.Ionos.Space Res. Japan, 15, 319(1961).

Kudo,S., M.Wada, P.Tanskanen, H.Kananen and H.Komori, "Local time asymmetry of the storm-time increases in cosmic rays", Proc.Int.Symp. Cosmic Ray, Morioka, 204(1984).

Sugiura, M., and D.J.Poros, "Hourly values of equatorial Dst", NASA-GSFC Publications and Solar geophysical data.

P.Tanskanen, H.Knanen, S.kudo, M.Wada and H.Komori, "Cosmic ray increases during severe geomagnetic storms", Proc.18th ICRC, 3, 217(1983).

Yoshida, S., S.-I. Akasofu and P.C. Kendall, "Ring current Effects on Cosmic Rays", J.Geophys.Res., 73, 3377(1968).

EVENT NUMBER	DATE YEAR	MONTH	DAY	Dst MINIMUM UT(hour)	nT
1	1966	3	14	6	-132
2	1966	5	26	23	-112
3	1966	8	30	24	-111
4	1966	9	4	3	-229
5	1967	1	14	6	-176
6	1967	2	16	14	-120
7	1967	5	26	4	-418
8	1967	6	6	3	-172
9	1968	4	5	23	- 95
10	1969	2	2	24	-175
11	1969	3	24	2	-240
12	1969	9	30	3	-132
13	1970	3	8	23	-268
14	1970	12	14	10	-142
15	1971	12	17	21	-167
16	1972	6	18	4	-190
17	1972	8	9	12	-154
18	1972	9	14	6	-146
19	1973	4	1	23	-188
20	1974	9	15	20	-149
21	1974	10	13	15	-105
22	1975	11	9	19	-114
23	1976	1	10	24	-164
24	1976	3	26	9	-229
25	1976	4	1	9	-221
26	1978	7	4	17	-114
27	1978	8	28	10	-242
28	1978	9	29	11	-241

Table 1 List of severe geomagnetic storms from 1966 to 1978.

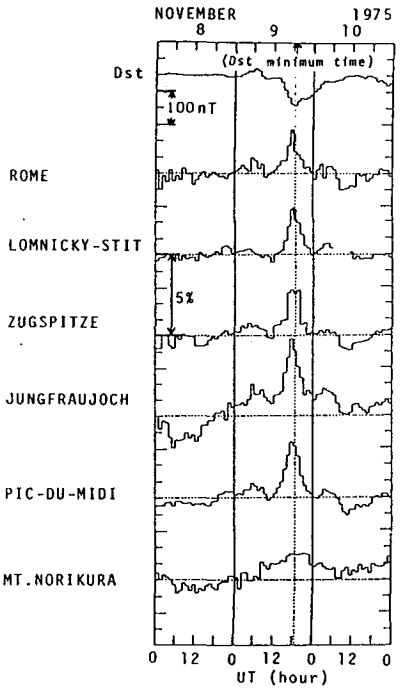

Fig. 1 The storm time increase (STI) for some stations during the geomagnetic storm in November 9, 1975. The topmost curve is the time variation of the geomagnetic Dst(t) (Sugiura).

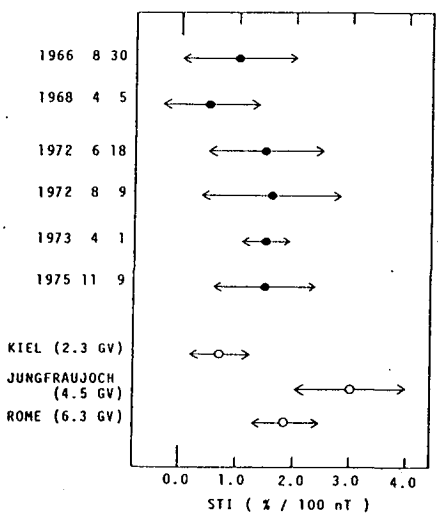

Fig. 2 The observed storm time increase of six events and the theoretical expectations for Kiel, Jungfraujoch and Rome.

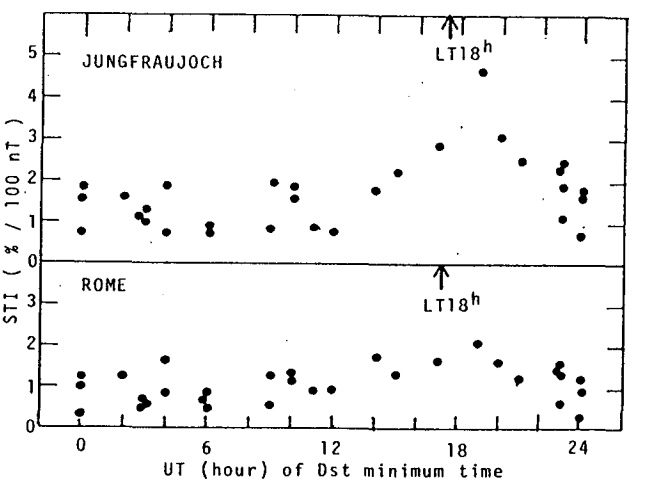

Fig. 3 The local time dependence of the storm time increase for Jungfraujoch and Rome obtained from 28 events listed in Table 1.

GALACTIC COSMIC RAY CURRENTS AND MAGNETIC FIELD IRREGULARITY DEGREE IN HIGH-SPEED SOLAR WIND STREAMS

A.I.Kuzmin

Yakutsk State University, 677007 Yakutsk, USSR

I.S.Samsonov, Z.N.Samsonova

Institute of Cosmophysical Research & Aeronomy
Lenin Ave., 31, 677891 Yakutsk, USSR

ABSTRACT

Currents of galactic cosmic rays (GCR) obtained by global survey method are analyzed. The cases of almost total disappearance of GCR currents are compared with the results of direct measurements of the solar wind parameters. The conclusion is made on a restricted application of the convective-diffusive mechanism of the GCR modulation by the solar wind during the occurence of stationary and regular magnetic fields in the interplanetary medium.

1. Introduction. The cases of almost total disappearance of the GCR currents in a body of the recurrent high-speed streams of the solar wind during three rotations of the Sun for 1974 were indicated in [1] . Here we consider in detail the above phenomenon using the results of direct measurements of the solar wind and interplanetary magnetic field parameters [2] .

2. Results. We used hourly values of the GCR currents obtained by the global survey method [3] on neutron monitor world net data.

As it is known [4] 1973-1974 were characterized by the existence near the Earth of very wide and stable high-speed streams of the solar wind from polar coronal holes. In January - March 1974 the two-sector structure of IMF with noticeably predominance of the negative sector were observed. At this time there were no significant flare origin disturbances of the wind. The GCR intensity was close to the almost unmodulated level which is characteristic for the solar activity minimum in 1976 and it then began to decrease probably due to the solar activity increase.

In the Figure the solar wind speed V , strength H and signs of IMF, intensity I and diurnal values of the GCR currents $\vec{z}_1$ for one rotation of the Sun for 1974 are shown. The $\vec{z}_1$ are shown as arrows the direction and length of which coincide with the direction and value of currents in the solar-earth coordinate system (scale is at the top). The Earth's position with respect to the neutral IMF sheet during one rotation of the Sun is schematically shown. The

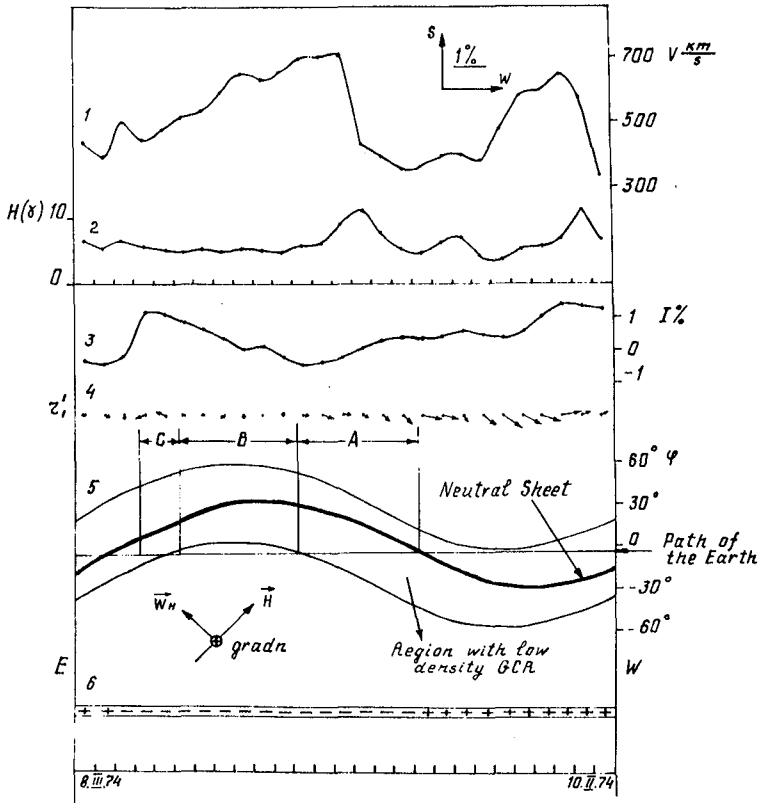

The parameters of the solar wind, IMF and GCR for February 10 and March 8, 1974.
1 - solar wind speed, 2 - IMF strength, 3 - isotropic GCR intensity, 4 - GCR currents in the solar-earth coordinate system, 5 - a scheme of a modulation region of GCR in the solar wind high-speed streams, 6 - the signs of IMF

Earth's heliolatitude corresponds to the analyzed period. The maximum heliolatitude of the neutral sheet was observed to be +30° [5] and it corresponds to the largest removal of the Earth's orbit by 0.5 AU in the meridional plane. In the first narrow high-speed stream the Earth is within the modulation region and the currents behave themselves usually. Therefore we consider here the behaviour of the GCR currents only in the second, wider streams. The velocity of the solar wind stream up to values $\sim$ 700 km/s the IMF strength increases up to 10 γ and the GCR intensity insignificantly ($\sim$ 1%) decreases.

According to the behaviour of the GCR currents the whole considered period can be divided into three parts (Figure, A, B, C). During period A when the Earth enters the high-speed stream an is in the region of the decreased GCR density, the currents have the usual azimuthal direction and the value according to the convective-diffusion mechanism. In 3 days after the IMF disturbance the GCR currents almost completely

disappear (their value is within the accuracy of hourly measurements $\sim$ 0.1%, direction is unstable) (period B). This period lasts $\sim$6 days to its end the intensity is insignificantly re-recovered.

During period C$\sim$3 days before the arrival of the next sector boundary the GCR currents (significant in value) are eastward from the Earth-Sun line nearly perpendicular to IMF force line (about 5-6 hours LT in terms of the GCR anisotropy).

Similar behaviour of the GCR currents which is characteristic for each A,B,C periods was observed at passage of the same high-speed stream in two preceding rotations of the Sun [1].

3. Discussion. In [6] it was established that in the body of recurrent high-speed streams emitted from the coronal holes the IMF irregularity degree $F = D_{\perp}/D_{\parallel}$ is almost zero. Therefore on such streams the GCR modulation takes place only in a narrow region located from both sides of the neutral IMF surface. Based on such conceptions we try to understand the observed behaviour of GCR currents in recurrent high- speed streams.

As it is known [3] the GCR current can be presented as follows: $\vec{W} = \vec{W}_c + \vec{W}_d + \vec{W}_H$,

where $\vec{W}_c$ is the current caused by convection of particles by the solar wind, $\vec{W}_d$ is diffusive stream, $\vec{W}_H$ is diffusion caused by perpendicular density gradient known as the Hall's current.

In part A, in the region with the decreased density the GCR currents are due to convection and diffusion according to the above expression. In region B which is mostly remoted from the neutral sheet in equatorial and meridional planes the Earth falls into the regular and stationary IMF where there are no any scattering centers. In such a field by [7] the convection and the diffusion are absent and the Hall's current [3] appears only when there are density gradients. In the case of the regular field the GCR density gradients will exist at the distance of only one Larmor radius from the boundary of region with decreased density (in our case $\rho \approx 0.04$ AU). As it is seen from the Figure in the region B the GCR density gradient and therefore the Hall's current will not be observed.

In region C the approach of the next sector boundary or of the neutral sheet will be manifested as the Hall's current occurence on a scheme shown in the bottom of the Figure. And the current of the aligned diffusion in this region will be absent while the next sector boundary will arrive since IMF force lines connect the Earth with the west undisturbed hemisphere of the Sun.

For a totally regular field we can write [3] :

$$\vec{W}_H = \left[\frac{\vec{H}}{H} \times \nabla_{\perp} I\right].$$

If the value of GCR currents in region C is known one can

estimate the value of the GCR density gradient perpendicular to ecliptic plane ($\nabla_\perp I \approx 8\%/AU$).

On the other hand, if the stream is stationary then a radial density gradient at the next disturbance of GCR intensity estimated on $\frac{\partial I}{\partial t} = -\nabla_z I V$ is $\nabla_z I \approx 4\%/AU$. Both obtained values of gradients do not contradict each other if to take into account the flattening of the GCR modulation region to the neutral sheet.

4. Conclusion. From the above one can conclude the following:

a) In recurrent solar wind high-speed streams from polar coronal holes observed in 1973-1974 the IMF inhomogeneities causing GCR modulation are located only in a relatively narrow region near the neutral sheet. In some favourable cases (January - March 1974) when this sheet is located far enouth, the Earth can get into the region of IMF with superhigh regularity degree where the GCR modulation is practically absent.

b) In such fields the GCR currents (anisotropy) are absent since neither convection nor diffusion of particles exist. At approach of the neutral sheet the Hall's current can occur because of occurence of perpendicular density gradients.

References.

1. Samsonov, I.S. et al., (1981), Proc.17-th ICRC, Paris, 3, 310.
2. King, I.H., (1977), Interplanetary Medium Data Book, Greenbelt.
3. Krymsky, G.F. i dr., (1981), Kosmicheskie luchi i solnechnyi veter, Novosibirsk, Nauka.
4. Kovalenko, V.A., (1983), Solnechnyi veter, Moskwa, Nauka.
5. Samsonov, I.S. et al., (1979), Proc.16-th ICRC, Kyoto, 3, 481.
6. Korzhov, N.P., (1982), Karty polyarnostei globalnogo magnitnogo polya Solntsa i konfiguratsiya mezhplanetnogo tokovogo sloya v 1971-1978. Irkutsk.
7. Stern, D., (1964), Planet.Space Sci., 12, 973.

STUDY OF DOMINATING PARAMETERS OF HIGH SPEED SOLAR PLASMA STREAMS IN RELATION TO COSMIC RAY AND GEOMAGNETIC STORMS

B.L. Mishra
Govt. Engineering College,
Rewa (M.P.)486001, India.

and

S.P. Agrawal
Physics Department (Vikram Space Physics Centre)
A.P.S. University, Rewa (M.P.)486003, India.

ABSTRACT

The high speed solar wind streams observed near earth are generally associated with the solar features, such as solar flares and coronal holes. Past studies of these streams from the two sources have revealed distinctly different effects on cosmic ray intensity, whereas the effect is similar for geomagnetic disturbances. Moreover, the effect of the magnitude of the high speed streams (V) and its rate of increase (dv/dt) has also been a subject of investigation to understand their relative contribution in producing geomagnetic disturbances. From the analysis of some of the fast streams presented here, it is difficult to predict, which one of the two (V, dv/dt) is more effective in producing geo-magnetic disturbances. Further, in most of the cases, no substential decrease in cosmic ray intensity is observed.

1. Introduction. The high speed solar wind streams are now known to be associated with energetic solar flares during the period of high solar activity, and with large area solar coronal holes during the declining phase of solar activity. Their distinctly different effects on short-term cosmic ray intensity decreases has been recently pointed out (Venkatesan et.al. 1982). Lindblad and Lundstedt (1981, 1983) have compiled the list of high speed solar wind streams for the period 1964-78. Reference is also made in the same reports, that geo-magnetic activity is more closely associated with a large positive time derivative (dv/dt) than with large velocity. Moreover, it has been reported that geo-magnetic activity maximises earlier than solar wind velocity at the earth. (Ballif et.al. 1969; Sawyer and Haurwitz, 1976). However, from a critical review of literature, it is not possible to make a positive statement that dv/dt is better associated with geo-magnetic activity than with V. In this paper, we have considered some of those streams which show a very smooth and sharp rise in velocity, to find out the

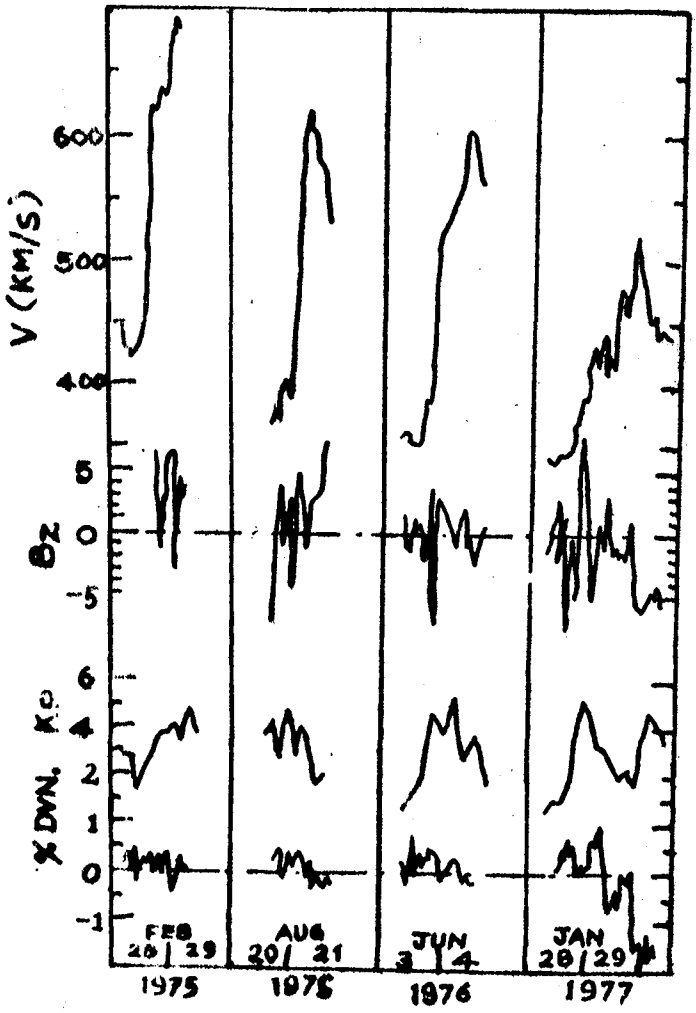

Fig.1 Shows the time intensity plot for three fast rise, high speed solar wind stream events selected from the catalogue published by Lindblad and Lundstedt (1983; see text for details) during the interval 1975-78; in all 25 events were selected. The fourth event (Jan. 28-30, 1977) represents a slow V but smooth rise in solar wind speed with relatively low value of maximum velocity. The Bz component of the interplanetary magnetic field as well as the Kp indices, and the percent deviation of cosmic ray intensity (Deep River neutron monitor) are also shown for each event.

effect of dv/dt and V on geo-magnetic disturbance index Kp, and cosmic ray intensity.

2. Selection of events. For the selection of events, we have made use of the catalogue published by Lindblad and Lundstedt (1983) andthe Interplanetary Medium Data Book, Supp. 1 (No.79-08; Dec. 1979). Moreover, the following conditions were imposed on the solar wind speed profile.

1. The initial velocity of the solar wind, before the start of the event, should be below or around 400 kms/sec.

2. Only that portion of the stream is considered for calculating dv/dt, during which the velocity monotonically increases.

3. The peak value of the solar wind stream is taken within 24-hours of the last hour of the dv/dt. For each event we have selected the maximum value of the 3-hourly Kp-indices for the duration of dv/dt, as well as the maximum value of 3-hourly Kp-indices during the 6-hours on either side of the hour of maximum V. Based on this selection criteria,

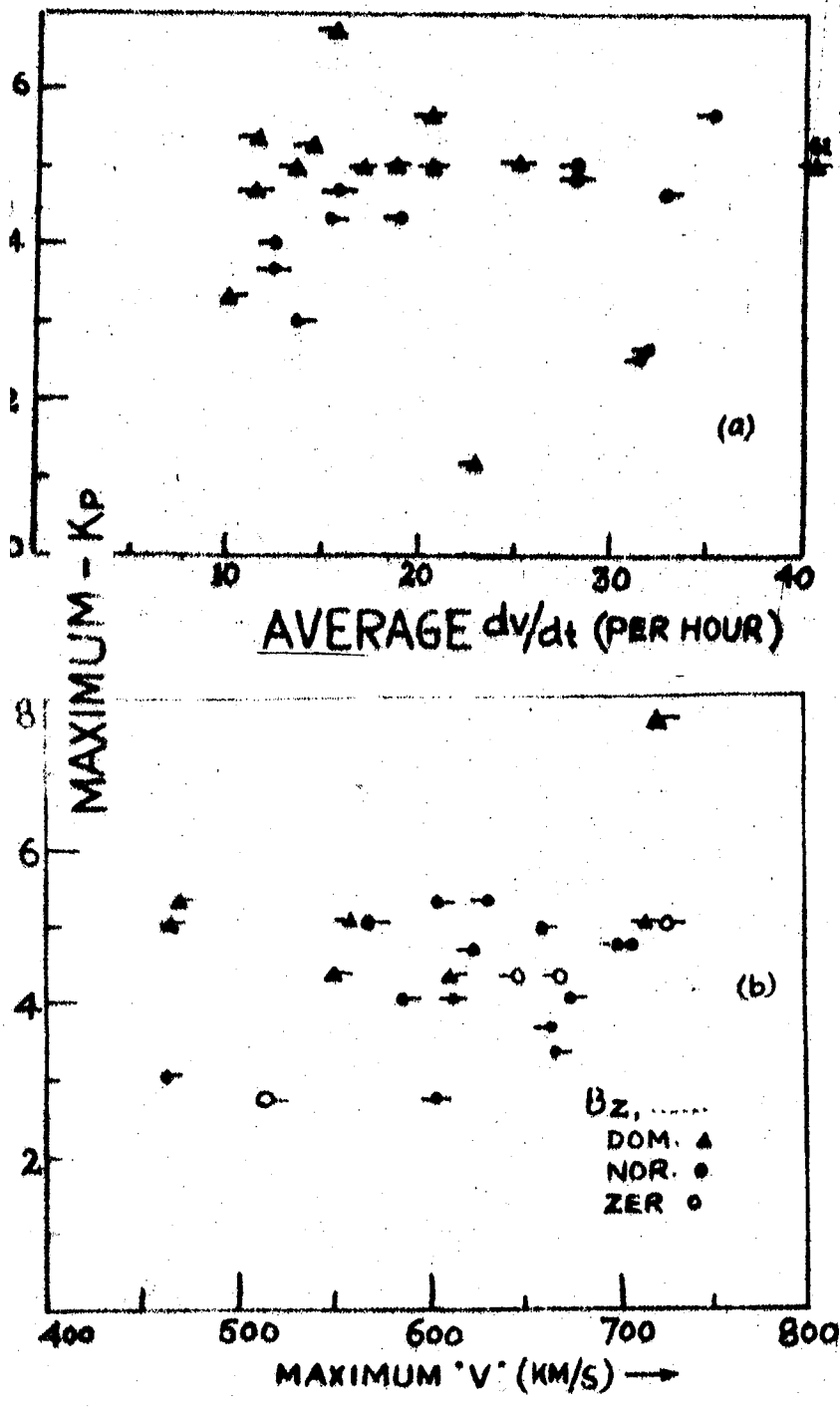

Fig. 2(a) Shows the crossplot between the average dv/dt & Kp-maximum for 25 high speed solar wind stream events. The magnitude of the negative excursion of Bz is represented by different symbols, and the length of the horizontal bars give the estimate of the duration of dv/dt. The position of the bar on right/left depicts the Kp max. being in the start/end of the dv/dt interval.

(b) Shows Kp max. plotted against the peak magnitude of solar wind speed(V) symbols have the same meaning as in fig 2(a). The position of the bar on right/left depicts the time of Kp max. being before/after within six-hours on either side of peak value of V.

we have identified 25 high speed stream events to investigate the effect of dv/dt and maximum-V, on Kp.

3. Analysis and results. Out of 25 high speed streams selected, three representative cases of high dv/dt and large V are depicted in figure 1. In the same figure we have also shown an event of low dv/dt and V, but associated

with highly negative values of Bz. It may be noted that all the three high dv/dt and "V" cases are associated with different conditions of other parameters (Bz, Kp and % deviation of cosmic ray intensity at Alert). From the first 3 cases depicted in figure 1, it can be inferred that Kp is high only when Bz is negative, and is affected equally both during dv/dt and V. This statement is further justified from the plot showing the case of low value of dv/dt and low V, where again for highly negative value of Bz, we find a moderate to high values of Kp. Any significant change in the cosmic ray intensity during the interval of high dv/dt and high V is not observed. On the contrary, a small decrease is associated with the last case of low V and dv/dt, which may be due to other causes.

In figure 2 and 3, we have shown all the 25 cases, correlating the observed maximum value of Kp with the value of dv/dt and V separately. The difference in the magnitude of Bz is also represented in the figure by plotting the value by different symbols. Moreover, the duration of dv/dt is represented by the length of the horizontal bars. The occurrence of maximum value of Kp at the start, middle or end of dv/dt is also represented. Similarly, in the case of V, the occurrence of maximum Kp, before or after the time of maximum V is also depicted.

From both the plots, it is clear that the maximum value of Kp is usually high for all the events (i.e. for maximum V and for average dv/dt), and does not show any significant relationship either with V or dv/dt. This is seen even when we divide the events for various categories of Bz. However, in most of the cases, Kp approaches maximum value either at the end of dv/dt interval, or just before V reaches to maximum values. We have also noticed that the maximum V and dv/dt are loosely correlated with each other, and that could be the reason why maximum Kp is seen in both the cases. Therefore, from the analysis presented here, we conclude that the value of Kp is generally high both during maximum V and high dv/dt and has no preferrence to occur during the interval of dv/dt.

4. References.

Ballif, J.R.; Jones, D.E. and Coleman, P.J., 1969. J.Geophy. Res. 74 p. 2289.

Lindblad, B.A.; Lundstedt, H., 1981. Solar Physics 74 p. 197.

Lindblad, B.A.; Lundstedt, H; 1983. Solar Physics 88 p. 377.

Sawyer, C. and Haurwitz, M.; 1976, J. Geophy. Res. 81 p. 2435.

Venkatesan, D. Shukla, A.K. and Agrawal, S.P. 1982 Solar Physics, 81, p. 375.

SH 5.I- I2

INFLUENCE OF MAGNETIC CLOUDS ON COSMIC RAY INTENSITY VARIATIONS

Badruddin, R.S.Yadav and N.R.Yadav
Space Science Group, Dept. of Phys., A.M.U. Aligarh (India).

S.P.Agrawal
Dept. of Phys., A.P.S. Univ., Rewa (M.P.).

ABSTRACT

Neutron monitor data has been analysed to study the nature of galactic cosmic ray transient modulation associated with three types of interplanetary magnetic clouds -clouds associated with shocks, stream interfaces and cold magnetic enhancements.

I. Introduction. It is well known that interplanetary magnetic field is of basic importance in the modulation of galactic cosmic rays. Most of the earlier studies of transient cosmic ray intensity modulations in relation to IMF are confined to the field strength, irrespective of the origin of change in it and other associated properties (Barouch & Burlaga, I975; Duggal et al., I983). Recently 46 magnetic clouds were identified in the interplanetary data obtained near the earth between I967-78 and classified into three classes - shock associated clouds, a stream interface and a cold magnetic enhancement. The Max. field strength is found to be approximately the same and the temperatures are low in all the three types of clouds. The physical characteristics of the magnetic clouds and their role of occurrence suggest that many or all the clouds might be related to coronal mass ejections(Klein and Burlaga, I982).

Newkirk et al. (I98I) have suggested that the interplanetary manifestation of coronal mass transients(ejection) may play an important role in galactic cosmic ray modulation and Burlaga(I983) has observed that the detailed studies of the relations between magnetic clouds and cosmic rays have not been made, but they are worth taking.

In view of the known characteristics of magnetic clouds in relation to magnetic and plasma properties for different classes of clouds and their association with CMEs, it seems important to investigate, in detail, the cosmic ray intensity variations in relation to these clouds of different classes.

2. Analysis. Three types of clouds mentioned above are observed to be moving high magnetic field structures in the interplanetary space. In earlier studies of transient cosmic ray modulations related to interplanetary magnetic field intensity enhancements, most of them are confined to their relationships irrespective of the origin of their enhancement and their other physical properties. We have performed the superposed epoch analysis, using Deep River super neutron monitor data and the date of the cloud observation at the earth as the epoch day, for three classes of clouds seperately. Some individual events have also been studied for more

specific investigations. The various interplanetary parameters associated with these clouds are then used to study the time profile and other characteristics of large amplitude transient decreases(Fd-type) in cosmic ray intensity, which are generally associated with shock associated clouds.

3. Magnetic clouds and Cosmic ray intensity Variations. Im Fig. I, We have shown the superposed epoch plots of cosmic ray intensity data from Deep River for three classes of clouds. It is found that the decrease in cosmic ray intensity, with the clouds preceded by a shock, is higher in comparision to the decreases observed inassociation with other two types of clouds and the decrease starts earlier than the arrival of the clouds. The recovery is complete nearly ina week time. The decrease in cosmic ray intensity associated with the cloud followed by a stream interface is much smaller than the one mentioned above. The decrease time is also elevated and the onset of the decrease takes place on the arrival of the cloud. The decrease observed in association with the clouds associated with cold magnetic enhancement is still smaller in amplitude and duration, but the decrease in cosmic ray intensity starts when the clouds arrives at the earth.

4. Magnetic clouds following shocks and cosmic ray intensity variation. We have plotted the cosmic ray intensity data in relation to some individual shock associated clouds(Fig.2). Whenever the shock arrival time is not available we have used the sudden commencement of geomanetic storms(SSC) data, since SSC can be regarded as the geomagnetic signature of the arrival time of the interplanetary shocks. We can see from Fig.2 that ,in general, the Forbush-type decrease starts at time of arrival of the shock wave at the earth. However, there are a few cases when no appreciable decrease in cosmic ray intensity is observed, with the shock associated clouds. suggestions have been made in the past that the Forbush-type decrease is caused by the entry of the earth into a loop or tongue of IMF field lines that are fresly ejected from the sun. Cosmic ray density in such loops was considered to be depressed because these field lines do not reach boundary regions of the the heliosphere and also because particles are cooled as the loop expands. We found(Fig.I&2) that in case of shock associated clouds decrease in cosmic ray intensity starts, at the earth ,not at the arrival of the cloud, but at the arrival of the shock that precedes the cloud by few hours. It is difficult to follow the exact time history of the events in detail, because cosmic ray profiles vary significantly with the longitude and latitude of the observing stations. However, it is likely, that the magnetic regime that comtaimed the lowest density of galactic cosmic rays was a portion of the magnetic cloud. These results are in agreement with the view expressed by Palmer et al.(I978).

5. Physical Properties of shock associated magnetic clouds and associated cosmic ray variations.

We have seen that the transient modulation of cosmic ray

intensity is related,ingeneral,to the clouds of all the three classes.However,the time profile and amplitude of cosmic ray modulation for three types of clouds is different.Forbush-type transient modulation is related,generally,with the cloud preceded by a shock.We have thus used the cloud and shock parameters to further study the various features of associated modulation.

Fig.3 shows the relation between the duration of the cloud near the earth and the total time taken for a forbush decrease to recover to pre-decrease level from the start of the event.It seems that the total duration of the forbush decrease increases as the cloud duration increases.However, as shown in Fig.4,the time taken by the decrease from the onset time to reach the minimum value of intensity does not depend on the duration of the cloud.But the recovery time of these decreases seems dependent on the duration of the clouds (Fig.5),it is larger for larger duration clouds.Though our results show the above mentioned behaviour,still there is needto have more data to varify this result conclusively.The observed duration of the cloud will depend upon the size and/or speed of the cloud.Since the clouds are observed to be expanding to distances of at least 4AU,they are more likely to be important at larger distances as far as the recovery time is concerned.From the study of cosmic ray intensity at IAU,6.97AU,& I5.9IAU and the findings that a magnetised plasma cloud moved outward and that the recovery time at these distances were,respectively- 6, 22,and I50 days,it may be possible that some of the cloud move to such large distances;they might also be expanding while moving to such distances.It has beenmentioned by Lockwood and Webber(I977)that the modulation regions associated with Forbush decreases were propagating several astronomical units beyond earth.

6.Amplitude of decrease and its relation to the speed of shock associated clouds. We have also studied the amplitude of decrease in relation to maximum solar wind velocity increase observed in association with these shock associated clouds(Fig.6).In general the increase im amplitude is larger when the cloud speed is larger.

References.

Barouch,E.and Burlaga,L.F.(I975),J.Geophys.Res.,80,449.
Burlaga,L.F.,(I983),Proc. I8th ICRC,I2,2I.
Duggal,S.P.,Pomerantz,M.A.,Schaefer,R.K.and Tsao,C.H.,(I983), J.Geophys.Res.,88, 2973 .
Klein,L.W.and Burlaga,L.F.,(I982),J.Geophys.Res.,87,6I3.
Lockwood,J.A.and Webber,W.R.,(I977),J.Geophys.Res.,82,I906.
Newkirk,G.Jr.,Hundhausen,A.J.and Pizzo,V.,(I98I),J.Geophys. Res.,86,5387.
Nishida,A.,(I982),J.Geophys.Res.,87,6003.
Palmer,I.D.,Allum,F.R.and Singer;S.,(I978),J.Geophys.Res; 83, 75.

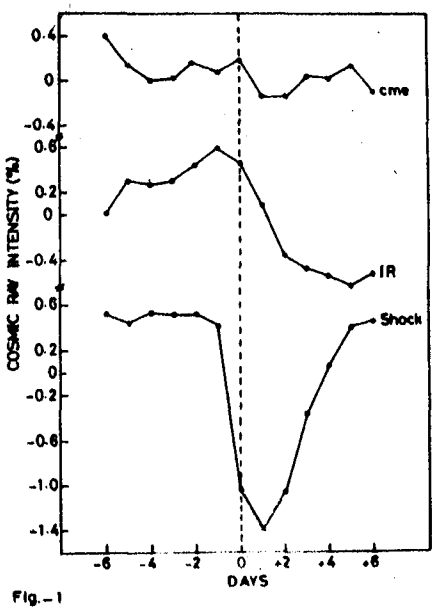

Fig.-1

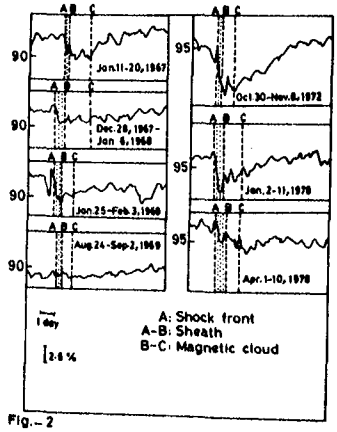

Fig.-2

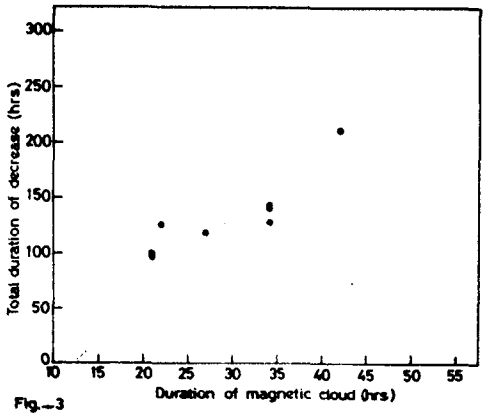

Fig.-3

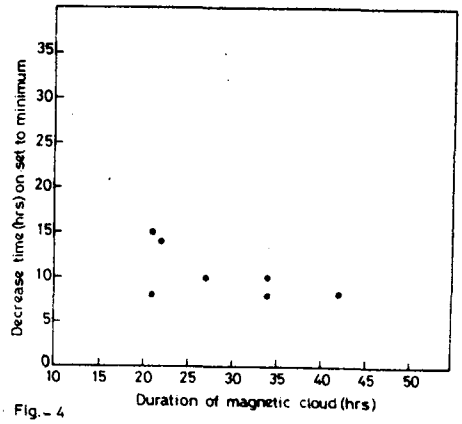

Fig.-4

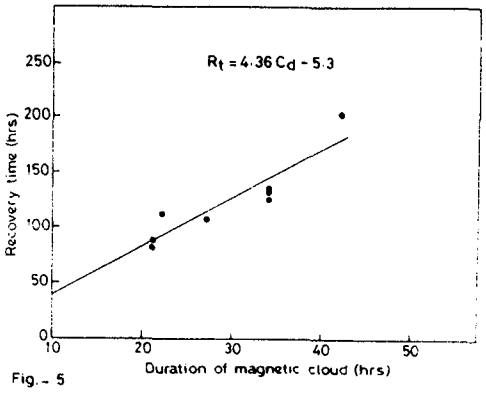

Fig.-5

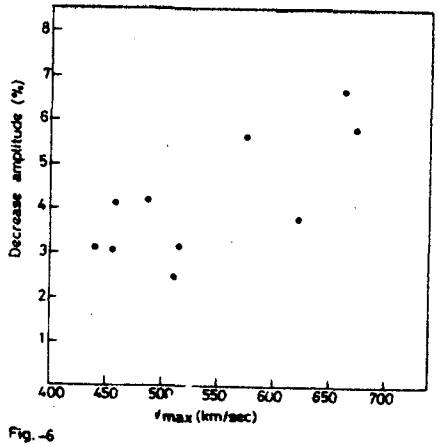

Fig.-6

SH 5.1-13

The Solar Wind Effect on Cosmic Rays and the Solar Activity

Fujimoto,K., Kojima,H.* and Murakami,K.

Cosmic Ray Reserch Laboratory, Nagoya University,
Chikusa-ku, Nagoya 464, Japan

*School of Hygiene, Fujita Gakuen Health University,
Toyoake, Aichi 470-11, Japan

ABSTRACT

The relation of cosmic ray intensity to solar wind velocity is investigated, using neutron monitor data from Kiel and Deep River. The analysis shows that the regression coefficient of the average intensity for a time interval to the corresponding average velocity is negative and that the absolute effect increases monotonously with the interval of averaging, τ, that is, from -0.5% per 100km s^{-1} for τ=1 day to $\sim$-1.1% per 100km s^{-1} for τ=27 days. For τ>27 days the coefficient becomes almost constant independently of the value of τ. The analysis also shows that this τ-dependence of the regression coefficient is varying with the solar activity.

1. Introduction

The relation of cosmic ray intensity to solar wind velocity has been studied by several authors. Duggal et al. (1977) pointed out the effect of high speed wind upon cosmic ray intensity, using neutron monitor data. Iucci et al. (1979) showed the coefficient to be -0.5% per 100km s^{-1}, applying Chree epoch method to neutron monitor data for the period from 1964 to 1974. Munakata et al. (1979) showed that there is a significant correlation between cosmic ray intensity and solar wind velocity. Fujimoto et al. (1983) pointed out that the solar wind effect depends on the solar activity ; its regression coefficient is about -0.8% per 100 km s^{-1} in the maximum activity and -0.2% per 100km s^{-1} in the minimum and the average value over a solar cycle is the same as the coefficient obtained by Iucci et al. (1979).

In the above-mentioned analysis, they used daily mean values for cosmic ray intensity and solar wind velocity. In the present paper, we tried to confirm whether the regression coefficient is determined irrespectively of the time interval of averaging, τ, or not. Cosmic ray intensity is varying sometimes in relation with the solar rotation, while the dominant periodicity in solar wind velocity is of 13.5 days. Then, the regression coefficient was examined for the averaging time interval from τ=1 day to 91 days, covering the wide range around 27 or 13.5 days.

2. Analysis and Result

Data used for the present analysis are daily mean values of neutron intensity at Kiel (1965-78) and Deep River (1965-76). These values (I,s) are measured from their one-year running average level to eliminate the long term variation, they are divided by a time interval τ, and a time series of τ-day averages $\langle I\rangle_{\tau,i}$ (i=1,2,....n) are arranged. Then, the correlations between cosmic ray intensity $\langle I\rangle_{\tau,i}$ and the corresponding averages $\langle V\rangle_{\tau,i}$ of solar wind velocity are caluculated for various values of τ. Fig. 1 shows the τ-dependence of the regression coefficient (β_τ) of $\langle I\rangle_{\tau,i}$ to $\langle V\rangle_{\tau,i}$. It is clearly seen in the figure that the absolute value of β_τ increases monotonously with τ and becomes almost constant for τ>27 days. The numerical values of β_τ and of the correlation coefficient r_τ are listed in Table 1, in which the error for β_τ is of significance level of 67 %.

Next, data at Kiel are divided into two groups corresponding to the solar activity, that is, a group for the period of the solar maximum (1966-72) and another for the period of the minimum (1973-77). For both the groups the τ-dependence of β_τ are analyzed. Fig. 2 shows the result and one can see that the critical time interval τ_c beyond which β_τ becomes constant is different from each other between both the periods of the solar maximum and the minimum.

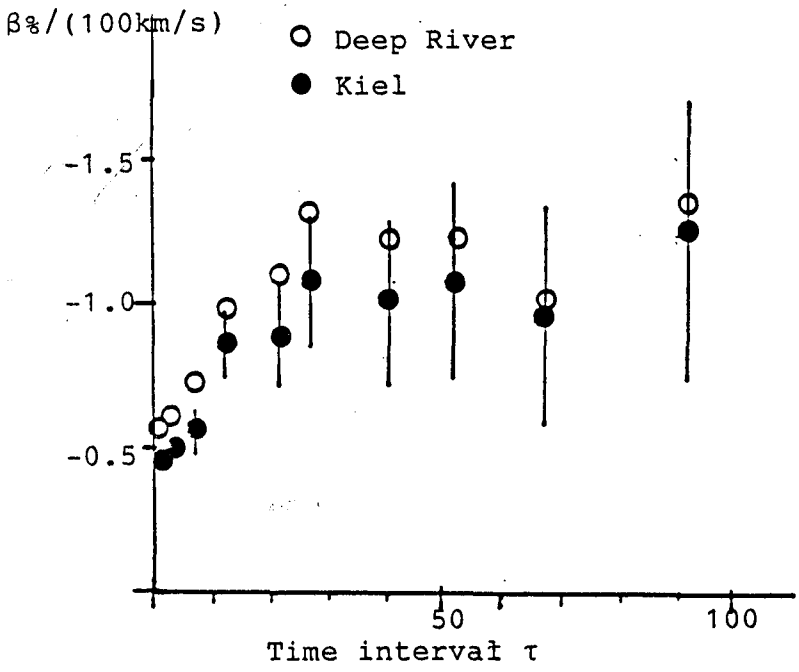

Fig. 1
The regression coefficients as a function of the time interval τ

Table 1 τ-dependence of the regression coefficient (β%/(100km/s)) and of the correlation coefficient (r) of neutron intensity to solar wind velocity, for Kiel (1966-1977) and Deep River (1966-June 1976). n expresses the number of independent data.

	KIEL			DEEP RIVER		
τ (days)	n	β_τ	r_τ	n	β_τ	r_τ
1	3585	-0.45±0.024	-0.29	2687	-0.57±0.031	-0.33
3	1226	-0.49±0.044	-0.30	925	-0.61±0.056	-0.33
7	545	-0.56±0.081	-0.28	406	-0.72±0.10	-0.32
13	301	-0.86±0.13	-0.35	223	-0.98±0.17	-0.35
21	184	-0.88±0.20	-0.31	136	-1.10±0.27	-0.33
27	145	-1.07±0.25	-0.33	107	-1.30±0.34	-0.34
41	97	-1.00±0.31	-0.31	73	-1.20±0.45	-0.30
51	78	-1.07±0.38	-0.30	59	-1.21±0.53	-0.29
67	60	-0.95±0.41	-0.29	45	-0.98±0.56	-0.26
91	45	-1.22±0.49	-0.35	34	-1.33±0.68	-0.32

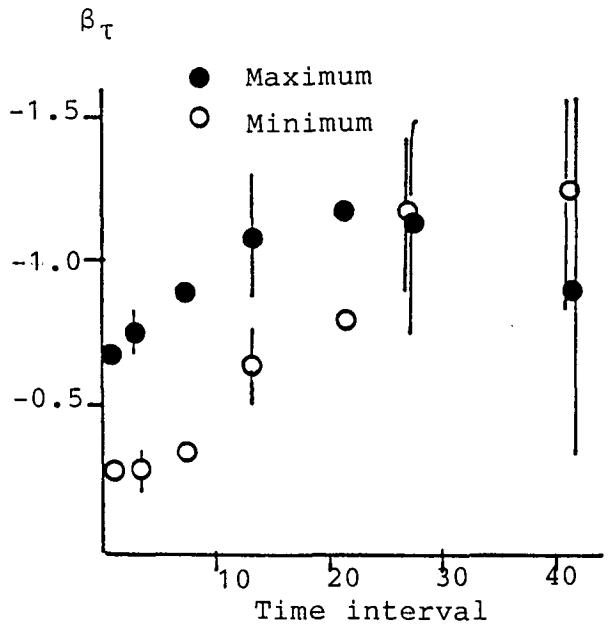

Fig. 2
The regression coefficient (β_τ) as a function of the time interval τ.
Solid circle is β_τ in the maximum period (1966-72) and open circle is β_τ in in the minimum (1973-77).

3. Discussion and Conclusion

As can be seen in Fig. 1, the absolute value of the regression coefficient of neutron intensity to solar wind ve-

locity increases with τ and becomes almost constant for $\tau > 27$ days. As the conclusion, at first, we like to emphasize that the regression coefficient has the τ-dependence; the coefficient β_{27} is twice as large as β_1 in magnitude.

The τ-dependence of the correlation can be interpreted when we suppose that the variation of cosmic ray intensity at the earth is reflecting the integrated effect of electromagnetic condition over the interplanetary space within a distance r_c ($=V \cdot \tau_c$) from the earth. The variations of cosmic ray intensity with periods shorter than T_c ($=k \cdot \tau_c$) give little contribution to the variation of $\langle I \rangle_\tau$, while the variations with periods longer than T_c contribute to the intensity variation, where k is a constant close to unity. Therefore the effect β is expected to increase with τ up to τ_c, and the effect does not vary so much with τ beyond τ_c.

Second, as seen in Fig. 2, the τ-dependence of the correlation varies with the solar activity. The critical time interval τ_c is shorter than 27 days in the solar maximum and is fairly shorter than the critical interval in the solar minimum.

Why the regression coefficient depends so much upon the solar activity has been left as a question which we shall solve, since we pointed out that dependence in Bangalore Conference. In the previous paper we showed that the coefficient varies over a wide range from -0.2 % per 100km s^{-1} at the solar minimum to -0.8 % per 100km s^{-1} at the solar maximum. Fig. 2 also shows the same dependence. If such a wide variation of the coefficient could be explained by particle diffusion coefficient varied with the solar activity, it would be necessary to consider the diffusion coefficient varying by a factor 2 between the solar minimum and maximum. Such a big change of the diffusion coefficient, however, can not be accepted in the comprehension of the eleven-year cosmic ray intensity variation. Therefore, it will be necessary to connect the solar wind effect β with the above-mentioned change of τ_c through the solar cycle.

Acknowledgment

We express thanks to prof. Nagashima for his variable discussion and suggestions.

References

Duggal, SP. and Pomerantz, MA.,
15th ICRC, Plovdiv, 4, 370 (1977)
Iucci, N., Parisi, M., Storisi, M. and Villoresi, G.,
16th ICRC, Kyoto, 3, 491, 496 (1979)
Munakata, Y. and Nagashima, K.,
16th ICRC, Kyoto, 4, 530 (1979)
Fujimoto, K., Kojima, H. and Murakami, K.,
18th ICRC, Bangalore, 3, 267 (1983)

A RELATION BETWEEN THE SHORT TIME VARIATIONS OF COSMIC RAYS AND GEOMAGNETIC FIELD CHANGE

Takasuke SAKAI and Masahito KATO

Physical Science Laboratories,
College of Industrial Technology, Nihon University,
Shin-ei, Narashino-shi, 275, Japan

ABSTRACT

First, we report an event of ~37min. periodicity in cosmic ray intensity observed at Akeno(38°47'N, 138°30'E, 900m above s.l., cutoff 10.4 GV) during 1300~1900 UT on April 25th, 1984, just a day before Forbush decrease of April 26th. This event seemed to be followed by the periodic variations of the geomagnetic field observed at Kakioka(36°23'N, 140°18'E). The regression coefficient between them was obtained ~-0.07%/10nT.

Second, we show that in general the power spectral density of cosmic rays in the frequency of 10^{-4}~10^{-3}Hz correlates positively with the fluctuations of geomagnetic field(Dst field) around ~1.2×10^{-4}Hz. From the analysis of 47 days data(April 14th to June 13th, 1984), the regression curve was obtained as $y=0.275x^{0.343}$ with the correlation coefficient of 0.48, where x and y mean Fourer components of Dst field summed over 1.04 ~1.39×10^{-4}Hz and cosmic ray power spectral density averaged over 10^{-4}~10^{-3}Hz respectively.

1.Introduction. Dhanju and Sarabhai(1967, 1969) first discussed the cosmic ray power spectrum. They showed that the general frequency dependence of the power spectra in the frequency range of 10^{-6}~10^{-3}Hz and also several periodicity in 1.67~8 $\times 10^{-3}$Hz. But Fujii et al(1975) argued against their result obtained in 10^{-4}~10^{-3}Hz. Theoretically, Owens and Jokipii(1972,1974), Toptygin and Vasilijev(1977) discussed the power spectra in the relation to the random magnetic field in the interplanetary space or in the magnetosheath. However, the validity of their model are limitted to the frequency range less than~10^{-5}Hz.

On the other hand, the existence of short time variations of cosmic rays(10^{-4}~10^{-3}Hz) are reported by several authors by the exhibition of the enhancement in the power spectra after subtracting the poisson noise level or clear vissible oscillations in cosmic ray counting rates(Slade,1972; Kodama et al.,1975; Kozlov et al., 1975; Attolini et al.,1979; Debrunner et al., 1983). However, no clear relation to some other interplanetary or geomagnetic field parameters(e.g., Kp, Dst etc.) has been found.

In this paper, at first, we briefly report the periodic variations of cosmic ray intensity of ~37min. period observed on April 25th, 1984, which seems anticorrelated well to the geomagnetic field change observed at Kakioka(Sakai et al., 1985).

The above event may suggest that the cosmic ray power spectral density around 10^{-4}~10^{-3}Hz are affected by the fluctuations of geomagnetic field, especially Dst field around the same frequency. Thus, we analysed both data of 47days and found that the level of cosmic ray power spectral density in the frequency range of 10^{-4}~10^{-3}Hz are related to the Dst field around 10^{-4}Hz with the correlation coefficient of 0.48.

2. Results. We show 3 minute data of cosmic rays, together with the H-component of the geomagnetic field observed at Kakioka from the time of 1200 to 1900 UT on April 25th in Fig.1. In the figure, errors of the cosmic ray are derived from counting rates.

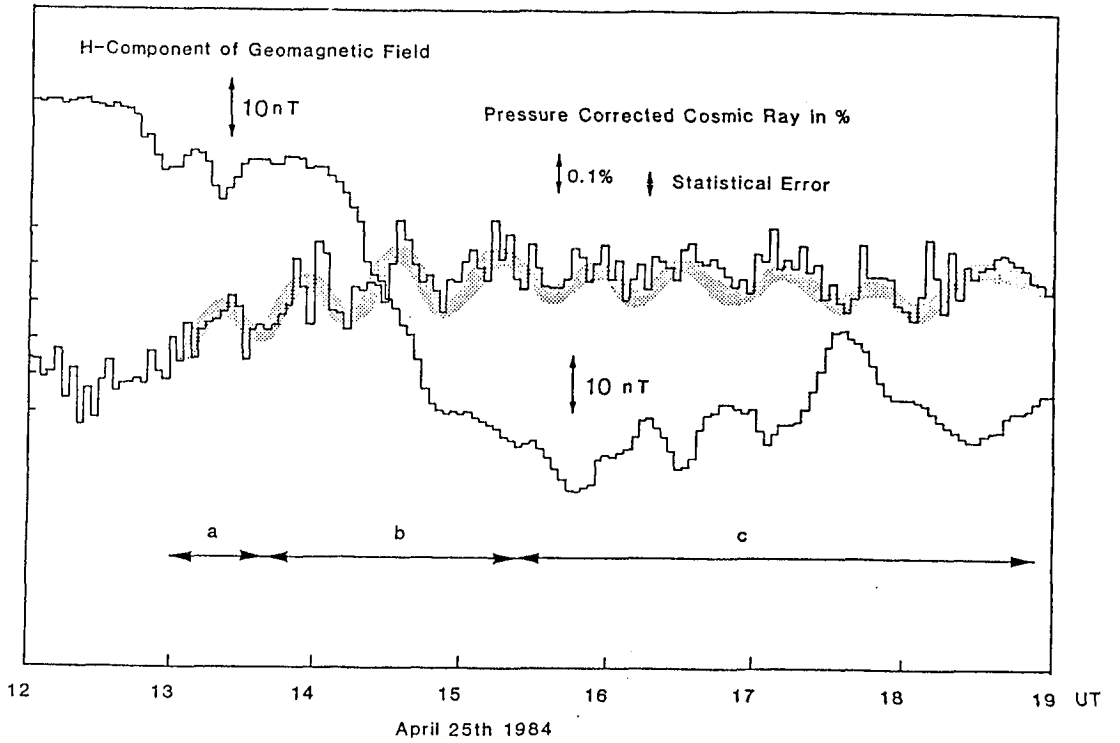

Figure 1. The cosmic ray data of 3 minute value are plotted together with the H-component of the geomanetic field observed at Kakioka from the time period of 1200 UT to 1900 UT on April 25th. The clear oscillations of the cosmic ray counting rates (dotted screen) are seen in anti-correlation with the H-component.

It is clear from the figure that, as shown by a wavy dotted screen, the counting rate of cosmic rays oscillates in anti-correlation with the change of the H-component, especially in the intervals indicated with a letter a and c in the figure. During the time of 1600 ~1700 UT, the oscillating part of the geomagnetic field has an amplitude of ~10nT in p-p(peak-to-peak). At the same time, the counting rates of cosmic rays change ~0.07% in p-p, almost out of phase with the change of the H-component.

From this, we can estimate changing ratio (hereafter refferd to as geomagnetic coefficient) of cosmic rays to the H-component at -0.07%/10nT. More detail discussion are seen in Ref.10.

Also, we can estimate a value of the geomagnetic coefficient following Obayashi(1961) by supposing that the cosmic ray counting rates may be changed by the change of cut off rigidities due to Dst field. The obtained geomagnetic coefficient was -0.3%/10nT. This may be consistent with the observed value if we consider that we don't know about Dst field shorter than 1-hour data. Thus, it seems reasonable that the observed oscillations in cosmic ray counting rates with the period of ~37 min. are mainly due to the change of geomagnetic field.

Further, if we suppose that the above good relationship between cosmic ray intensity and geomagnetic field (probably Dst field) in the frequency range of 10^{-4}~10^{-3}Hz in general exist for not only special days, but also all days, we come to an idea that the power spectral density in the frequency of 10^{-4}~10^{-3}Hz may closely related to the fluctuation of Dst field around the same frequency range. We analysed the data of 47 days through April 14th to June 13th, 1984. The power spectral density of cosmic rays are calculated by using 1-min. data on each day. On the other hand, the data of Dst field, which is available for us, are unfortunately 1-hour data only. 24 data points for a day are too short to get a significant power spectral density around ~10^{-4}Hz. Hence we Fourier analysed 1-day Dst field after running average of 5 hours and computed the components corresponding to the frequency of 1.04 ~1.39 x 10^{-4}Hz. Fig.2 shows a correlation between the cosmic ray power spectral density averaged

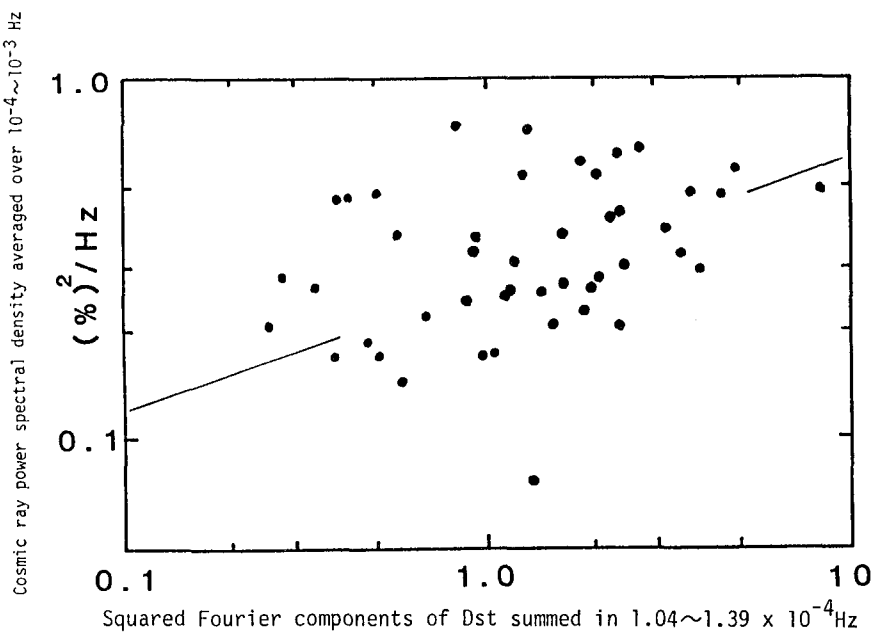

Figure 2. Cosmic ray power spectral density averaged over 10^{-4}~10^{-3} Hz (=y) v.s. squared Fourier components of Dst summed over 1.04~1.39 x 10^{-4} Hz (=x) are shown. The days of analysis are from April 14th to June 13th, 1984. The regression curve is expressed by $y = 0.275\ x^{0.343}$ with the correlation coefficient of 0.48.

over 10^{-4} -10^{-3}Hz (=y) and the Fourier components summed in the frequency of 1.04 -1.39 x10^{-4}Hz (=x). The relation is expressed by the power law of $y=0.275x^{0.343}$ with the correlation coefficient of 0.48.

3. Conclusions.

1) ~37 minutes periodical oscilations with amplitude of ~0.1% in p-p was observed during the time of 1300 to 1900 UT on April 25th, 1984. This oscilation seems to have good correlation with the geomagnetic field change at Kakioka. The geomagnetic coefficient is ~0.07%/10nT, consistent with the theoretically estimated value. Hence we conclude that the oscilation occured by the change in cut off rigidities due to Dst field.

2) From the fact of 1), we can expect that the power spectral density of cosmic rays in the frequency range of 10^{-4}-10^{-3}Hz is partly caused by the fluctuation of Dst field. Hence we examined the relation between the power density of cosmic rays and the fluctuations of Dst field around 10^{-4}-10^{-3}Hz by using 1 minute data and 1 hr data respectivery. The regression curve is expressed by $y=0.275x^{0.343}$ with the correlation coefficient of 0.48.

3) From 2), the power spectral density of cosmic rays in the frequency range of 10^{-4}-10^{-3}Hz may be one of good indicators of the fluctuations of Dst field at the same frequency.

4) More reliable conclusion about the correlation will be obtained by increasing day of analysis and also by using other stations.

4. Acknowlegements. The authors wish to thank to Prof. Kamata, Prof. Tanahashi and also their colleagues for facilitating the apparatus at Akeno observatory.

5. References.

1. Debrunner, H., et al., *18th Intern. Cosmic Ray Conf. Bangalore*, **3**, 257, 1983.
2. Dhanju, M.S. and V. A. Sarabhai, *Phys. Rev. Lett.*, **19**, 252, 1967.
3. Dhanju, M.S. and V. A. Sarabhai, *11th Intern. Cosmic Ray conf. Budapest*, **2**, 237, 1969.
4. Fujii et al., *13th Intern. Cosmic Ray Conf. Denver*, **2**, 783, 1973.
5. Kato, M., T. Sakai, and M. Wada, *16th Intern. Cosmic Ray Conf. Kyoto*, **5**, 1, 1979.
6. Kodama, M., et al., *13th Intern. Cosmic Ray Conf. Denver*, **3**, 803, 1973.
7. Kozlov, V. I. and N. P. Chirkov, *14th Intern. Cosmic Ray Conf. Munchen*, **3**, 1129, 1975.
8. Obayashi, T., *J. Geomag. Geoelectr.*, **13**, 26, 1961.
9. Slade, D. V., *12th Intern. Cosmic Ray Conf. Hobart*, **3**, 876, 1971.
10. Sakai, T., and M. Kato, *J. Geomag. Geoelectr.*, **37**, 61, 1985.

SH 5.1-15

ANOMALOUS LOW LEVEL OF COSMIC RAY INTENSITY DECREASES OBSERVED DURING 1980

A.K.Jain, P.K.Pandey and S.P.Agrawal
Physics Department(Vikram Space Physics Centre)
A.P.S.University, Rewa (M.P.) 486003, India

ABSTRACT

Past studies have revealed solar cycle changes in the sunspot activity, as well as in many other solar parameters, such as, solar flares and solar coronal holes. These solar features in turn produce the observed cyclic variations in the interplanetary plasma and fields. Both the cosmic ray intensity as well as the intensity of geomagnetic disturbances are affected by the interplanetary changes and produce 11/22 years periodicity. During the period of high solar activity, solar flares are more abundent, and are expected to produce large Forbush type cosmic ray decreases as well as intense geomagnetic disturbances. An anomalous situation has been noticed during the year 1980 (period of high sunspot activity), when both the geomagnetic disturbance index Ap, as well as the magnitude and number of Forbush decreases are small. Such an anomaly occurs, inspite of the fact that both the sunspot numbers and the energetic solar flares are almost maximum during the present solar cycle. Further investigations reveal that the observed solar flares in 1980 are also situated in favourable longitudes, and hence the cause for such an observed anomalous low values of Ap and the cosmic ray decreases, is presently not understood.

1. Introduction.

The long term variation in the solar activity is generally represented by sunspot numbers, which shows a recurrent tendency with a period of eleven years. Many other associated solar parameters, such as solar flares, coronal holes, also show 11/22 year cyclic variations (see e.g. review, Rao, 1972). Intense solar flares generally produce high speed solar wind streams, which in turn produce geomagnetic disturbances as well as significant decreases in cosmic ray intensity (see, e.g. review, Lockwood, 1971; Agrawal and Singh, 1976). It is therefore, expected that more number of Forbush decreases with larger magnitudes should be observed during the period of high solar

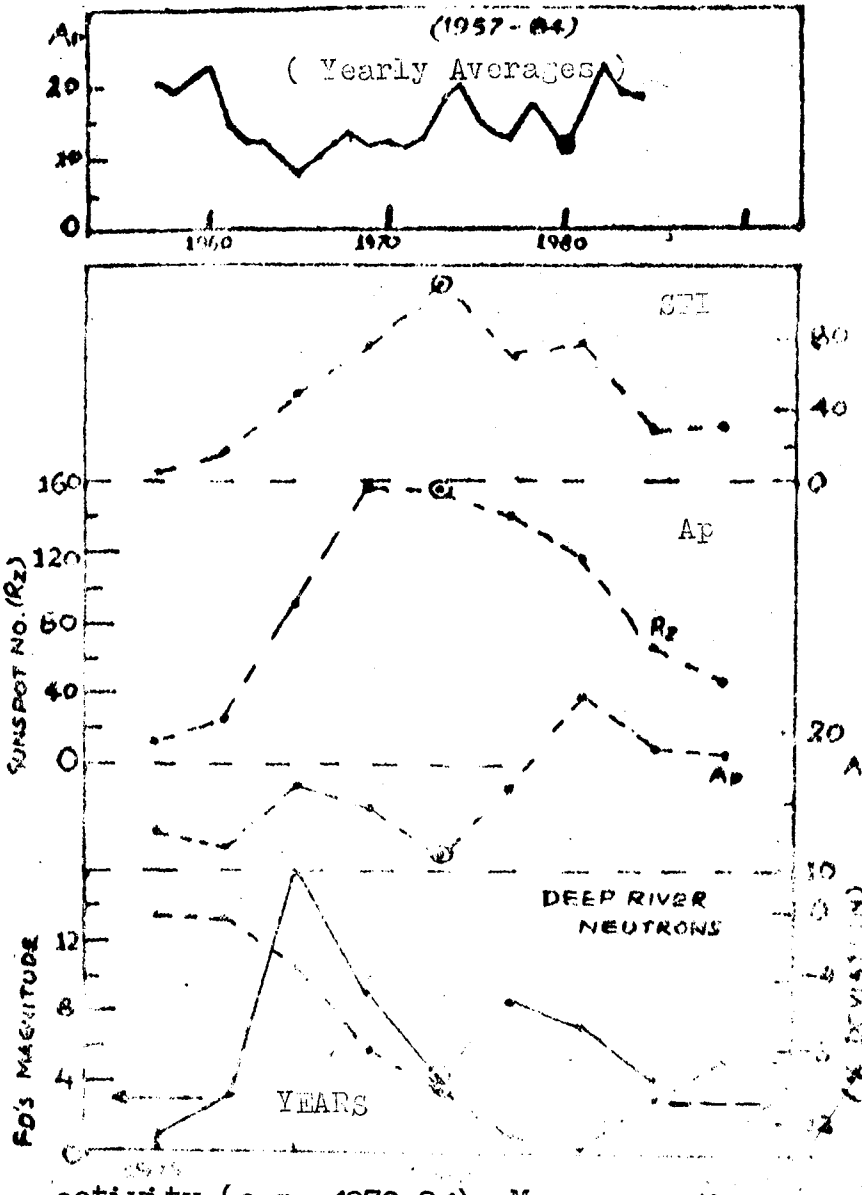

Fig. 1 (top) shows the yearly average variation of the geomagnetic disturbance index Ap, for the years 1957-84. The values for the year 1980 is encircled in this plot as well as in other plots of this figure to clearly identify the anomaly. (bottom) The yearly average values of the solar flare index (see text for details for the computation of SFI), The sunspot number, the Ap index, the Forbush decrease index (see text for details), and the cosmic ray intensity deviation from its max. value observed during Sept.-Nov. 1976, are also shown in the fig. for the years 1976-84. In some cases, the average values for 1984 are derived from 8-10 months data.

activity (e.g. 1979-81). Moreover, the geomagnetic disturbance index Ap should also be high during such periods. In this context, an anomalous situation is observed during the year 1980, when both the Ap index, as well as the number and magnitude of Forbush decreases are quite low. In this paper, we investigate this anomaly to understand, why larger number of energetic solar flares observed in the year 1980 are in-effective in producing geomagnetic disturbances as well as Forbush decreases.

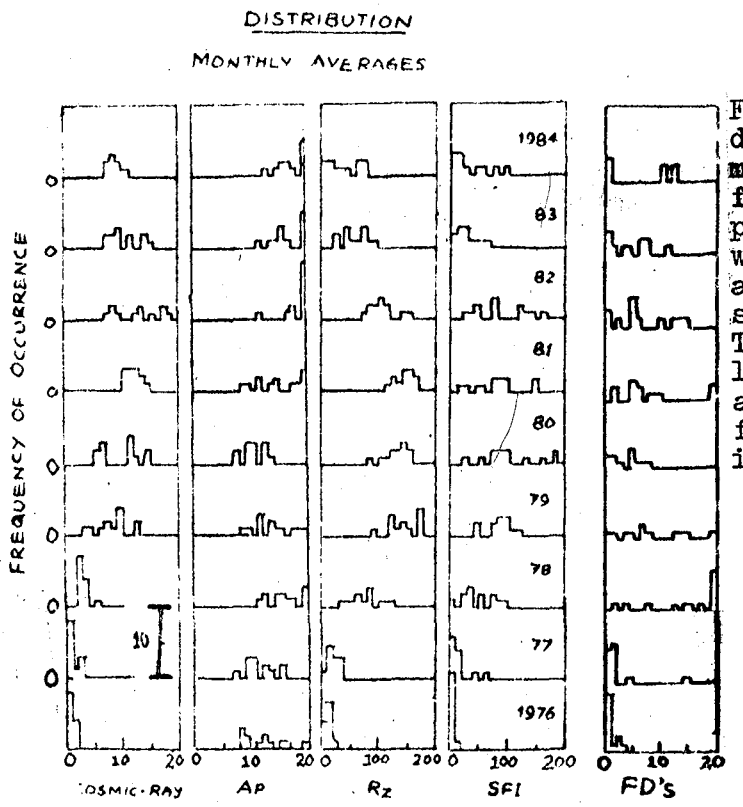

Fig.2 Shows the distribution of monthly averages for all the five parameters for which the yearly averages are shown in figure I. The anomalous low value of Fd's and of Ap index, for the year 1980, is clearly evident.

2. Computation of solar flare and Forbush decrease index.

In another paper (SH 4.4-12) we have described the computation of the solar flare index (S.F.I.) from the list of observed energetic solar flares of importance ≥ 1, published in prompt reports of solar Geophysical Data. Briefly, SFI has been computed by giving weight to the importance of the solar flare by its numerical value, and also by considering weights for the brightness of the flare. Similarly, the Forbush decrease index has been computed for each month, by numerically adding the magnitude of all the Forbush decreases observed in that month. A decrease in cosmic ray intensity is considered only when its magnitude is $\geq 1.5\%$, and the decrease is clearly seen in at-least two high latitude neutron monitor stations. The derived Fd's index has been denoted as Fd's Σmagnitude, and has been used in the diagrams presented later in this paper.

3. Results and Discussion.

The long-term va riation of the geomagnetic disturbance index Ap for the years 1957-84 is plotted in figure 1 (top portion of the figure). We note that the yearly average value of Ap index is quite low during the year 1980. The plot

also shows the minimum value of Ap observed during 1965, the year of minimum solar activity. Other solar and geophysical parameters are plotted in the bottom part of figure 1. Both, the sunspot numbers, as well as the solar flare indices are at their peak value during the year 1980, whereas the Ap index is at its minimum value. We also note that the long term cosmic ray intensity decrease shows a smooth decline starting in 1977 with a minimum in 1982. However, the Forbush decrease index shows a very low value in 1980 as compared to the adjacent values. Thus the low values of Ap and Fd's are quiet anomalous, particularly when one observes the large excess of energetic solar flares represented by SFI. To further analyse the distribution of the five parameters represented in figure 1 on yearly basis, we have generated a frequency histogram for each year, and for each parameter, using their monthly values. Such a distribution is plotted in figure 2, for the years 1976-84. Thus, even on a monthly average basis the anomaly of the low values of Ap index, as well as of the Fd's is apparent. To ascertain that the low values of Ap index and of Fd's during 1980, is not due to any large asymmetry in the longitudnal distribution of the solar flares, we have plotted in figure 3, the frequency histrogram for all the solar flares of importance $\geqslant 1$. From the figure, it is seen that there is no deficiency in the number of solar flares in the longitude region 60° East to 30° West for the year 1980, as compared to the years 1979 and 1981. Such an observation, therefore, rules out the possibility, that the solar flares during 1980 are unfavourably placed to be geo-effective. From the results presented here, we therefore note that even-though we have demonstrated the anomaly in terms of low geo-effectiveness of the energetic solar flares during 1980, however, we have not been able to identify the cause for such an anomaly. It is expected that other characteristics of the cosmic ray time variation might be able to provide some clue to understand the reported anomaly.

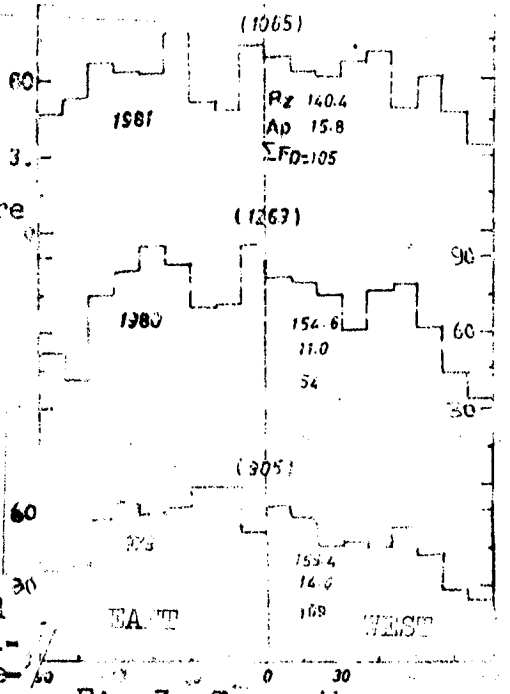

Fig.3 Shows the frequency distribution with heliolongitude of the individual solar flares of importance $\geqslant 1$, for the years 1979,80 & 81. The yearly average values of Rz, Ap and Fd index (Σ Fd) are also mentioned in the fig. alongwith the total number of solar flares for each year.

4. References.

Agrawal, S.P. and Singh, R.L., 1976, Ind.J.Radio & Sp.Phy.5 p.330.
Lockwood, J.A., 1971, Space Sci. Rev. 12 p.658.
Rao, U.R., 1972, Space Sci. Rev. 12 p.719.

SH 5.1-16

OBSERVATIONS OF COSMIC-RAY MODULATIONS IN THE FALL 1984

Torsti, J.J., Nieminen, M., Valtonen, E., Arvela, H., Lumme, M., Peltonen, J., and Vainikka, E

Wihuri Physical Laboratory, University of Turku, and Department of Physical Sciences, University of Turku, SF-20500 Turku, Finland

ABSTRACT

Modulation of cosmic-ray energy spectrum was studied by using the Turku double neutron monitor. The multiplicity region of detected neutrons produced by cosmic ray hadrons in the monitor was divided into seven categories corresponding to mean energies 0.1, 0.3, 1.0, 3.2, 8.6, 21, and 94 GeV of hadrons at sea level. Based on 24-hour frequencies, a statistical analysis showed that modulation of the intensity in all categories occurred during several periods in the fall 1984. The magnitude of the variation was a few per cent.

1. Introduction. The Turku double neutron monitor enables studies of modulation of energy spectrum of cosmic-ray hadrons. The accuracy of the modulated spectrum, particularly at high energies, is dependent on the duration of the disturbance. Measurements at high energies can be made reliably only in such cases when the disturbance continues for a few days.

In this work, cosmic-ray modulation in the time scale of several days is studied. In order to eliminate the daily variation, 24-hour frequencies of neutron multiplicities were used as the basic data. In order to cover a wide energy range, counting rates of multiplicities from 1 to 200 were analysed.

The present preliminary analysis concerns measurements accomplished during the period from September 1, 1984 to January 8, 1985. No drastic variation of cosmic-ray intensity, such as large Forbush decreases or proton flares, occurred during this period.

2. Cusum plots. The analysis is based on cumulative-sum of observed freguencies in neutron monitor. The entire multiplicity range was divided into seven categories as shown in table 1. The average daily counting rates, f_{ave}, are also given in the table. The median hadron energies represent estimates based on a Monte Carlo model of hadron cascades in the atmosphere and in the monitor /2/.

The daily counting rates in categories 5-7 are so small that the statistical error is more than 1 %. Therefore, it is quite difficult to see from the simple frequency versus time plot whether there exists systematic variation in the course of time. In purpose to separate the real modulation from statistical fluctuations, we use cumulative-sum curves of relative frequencies:

Table 1. Daily counting rates, f_{ave}, and median energies of cosmic-ray hadrons in the Turku double neutron monitor

category	neutron multiplicities	f_{ave} (events/day)	median hadron energy (GeV) at sea level	in free space
1	1	786 700	0.1	16
2	2-4	400 300	0.3	24
3	5-8	88 800	1.0	70
4	9-16	16 900	3.2	160
5	17-24	2 890	8.6	310
6	25-48	864	21	540
7	49-200	304	94	1100

$$F_K = \sum_{k=1}^{K} \frac{f_k - f_{ave}}{f_{ave}} \quad \text{for all days } K = 1,\ldots,122 \ ,$$

where f_k represents the pressure-corrected observed frequency for day k. The cusum curves for six multiplicity categories are given in fig. 1.

It is seen that the cusum curves show certain similarities. Changes in the slopes of the curves occur approximately at the same time. The absolute magnitude of the variation tends to increase with increasing multiplicity. Noteworthy is that the curve of the highest category (49-200) shows systematic variation.

3. Periods of constant counting rates. The statistical cusum test reveales which changes in the cusum plots are significant /1/. The risk level of 5 % was used. In the case of the September data, the cusum test showed that multiplicity categories 2, 3, and 4 had two significant changes. The first occurred on the 5th and the second on the 12th of September. In category 1, no statistically significiant changes were found.

Between October 2nd - January 8th, the significance test revealed 4-11 slope changes. The smallest number of changes was obtained in category 7. The poor statistics is a more probable explanation for the small number than physical reasons.

Based on the results obtained from categories 2-4, we conclude that during the following nine periods the daily frequencies do not show significiant changes, i.e., the counting rates can be considered at least roughly constant:

I: September 1-5
II: September 6-12
III: September 13-23
IV: October 2-5
V: October 6-12
VI: October 13 - November 1
VII: November 2-22
VIII: November 23 - December 31
IX: January 1-8

These intervals are shown in fig. 1 by dotted lines.

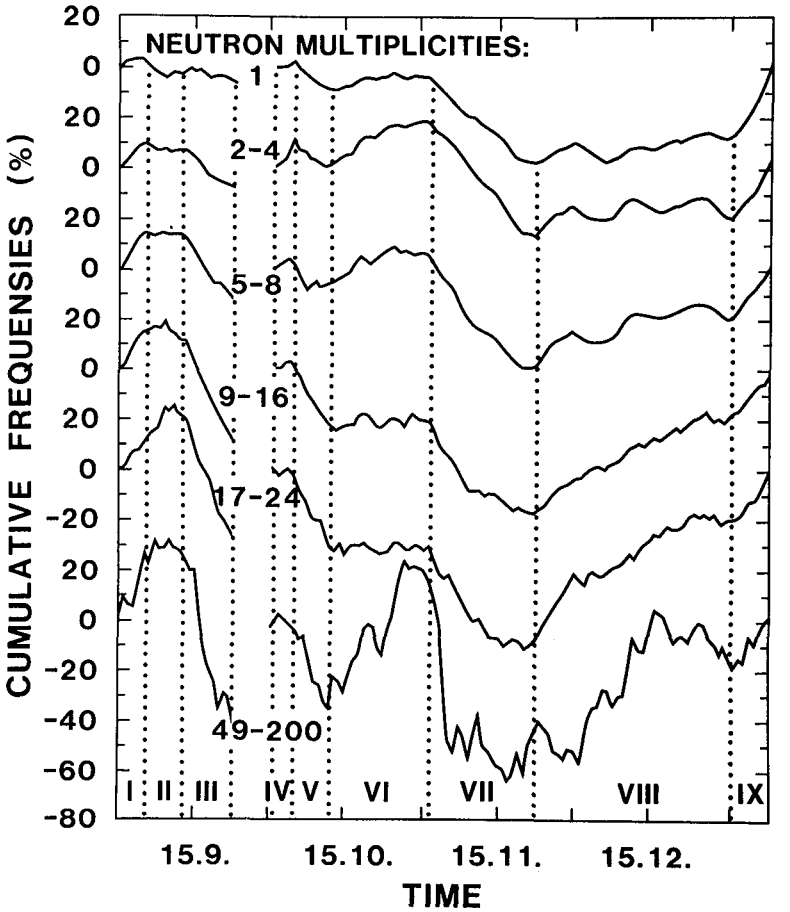

Fig. 1. Cusum curves for various multiplicity categories.

For each interval I-IX we calculated the average intensities. In fig. 2 the deviations of these averages from overall mean intensities are given as a function of the median sea-level energy corresponding to various multiplicity categories.

4. Discussion. An interesting result of this analysis is the fact that the relative intensity deviation does not approach zero as the median energy increases from 0.1 GeV to 100 GeV. It is a contradiction with the generally accepted form of modulations, $\Delta f/f = AE^{-\gamma}$ with $\gamma > 0$.

On the contrary to this general view, e.g. during period I the deviation shows quite a smooth increase up to 3 GeV above which the deviation remains clearly positive up to the highest energy. During period III the negative deviation becomes stronger as the energy increases from 0.1 GeV to 10 GeV. The deviation is -2.4 % at 21 GeV and -6.3 % at 98 GeV. A similar behaviour is seen during the period V.

The deviations from the mean intensity are more or less constant during VII and IX. They are between -1.5 % and -2.6 % and between 2.4 % and 3.1 %, during period V.

Periods II, IV, VI, and VIII represent cases where the energy spectra do not deviate to any noteworthy degree from the mean spectrum.

According to our estimation, the highest multiplicity category cor-

SH 5,1-16

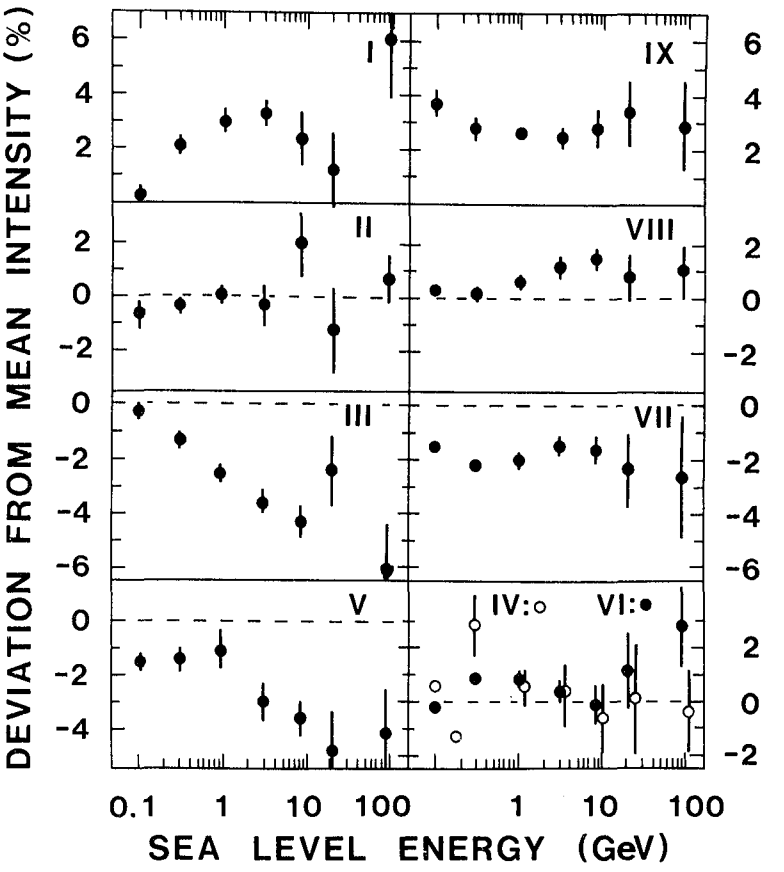

Fig. 2. Deviations of the daily counting frequencies from the mean frequencies during periods I-IX.

responds to primary radiation with median energy of 1100 GeV in free space. In all cases in which the energy spectrum deviates systematically from the mean (I, II, V, VII, and IX), the deviations in the highest category are towards the same direction as in all other categories corresponding to lower median energies. In addition, the estimated standard deviation of these points is smaller than the deviation of the points from the mean intensity. Quite unexpected is the result that in the cases where spectrum modulation is present, no clear indication is seen for decrease of the modulation amplitude in high-energy region.

5. Conclusions. According to the present results the long-term variation of cosmic radiation extends at least upto energies of several hundreds of GeV in free space. There are indications that the relative deviation, $\Delta f/f$, is of the order of a few percent in the energy range above 100 GeV. In some cases, the amplitude of the modulation shows systematic increase in the energy range 15-300 GeV in free space.

References:

/1/ Caulcutt, R., Statistics in Research and Development, Chapman and Hall, London, 1983.
/2/ Lumme, M., et al., J. Phys. G, 10, 683-694, 1984.

FREQUENCY SPECTRA OF SHORT-PERIOD VARIATIONS OF COSMIC RAY

Antonova V.P., Zusmanovich A.G.

Institute of Ionosphere of AN KazSSR,
480068, Alma-Ata, USSR.

ABSTRACT. Frequency spectra for different periods of solar activity were calculated by 5-minutes data of neutron super-monitor of the Institute of Ionosphere of AN KazSSR (altitude 3340 m, cut-off rigidity is 6,7 GV, counting rate is about $4.5 \cdot 10$ per hour). It was shown that shifting of the spectrum power from low-frequency range to high-frequency range takes place from minimum to maximum of the solar activity. It was reliably distinguished the peak with 160-minutes period coincided with the period of the Sun's atmosphere oscillation and some types of geomagnetic pulsation by the method of accumulation of the frequency spectra. It was conducted the comparison of cosmic ray spectra with spectra of geomagnetic field for the same point of the registration and at the same period.

The short-period cosmic rays variations origins from different nonstationary processes in the interplanetary space, magnetosphere and atmosphere of the Earth and these variations may be used for the study of the such processes. The high-altitude neutron monitor of the Institute of Ionosphere of AN KazSSR permits to investigate the spectrum of cosmic ray fluctuations up to $1.7 \cdot 10^{-3}$ Hz. In this paper the spectral density of cosmic ray fluctuations in the range of 10^{-5}--$5 \cdot 10^{-4}$ Hz was calculated by the method of Blacman and Tukey /1/, using 15-minute data of this monitor for the time period from 1974 to 1983. The all data were corrected for the barometric pressure. The solar activity cycle was devided to the four periods: 1-1974-1976-the solar activity minimum, 2-1977-1978-solar activity increase, 3-1979-1980 -activity maximum and 4-1981-1983-activity decrease. The calculation of the spectral density was carried out on the week-interval data with the filtrating of the low-frequency band. It was obtained that at solar activity minima the main power of the spectral density concentrated in the low-frequency range. When the solar activity increased, the spectral power shifts to the high-frequency range. In Fig.1 are shown the summary power spectra $\tilde{G}_{xx}(f)$ for the period mentioned above; a-1st period, b-2nd period, c-3rd period and

d-4th period.The unifirm distribution of the spectral density at the all frequency interval at solar maximum and the presence of large power at low frequency range at solar minimum are observed.

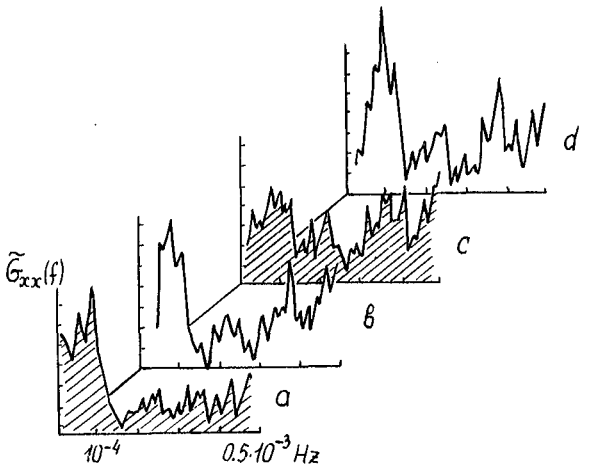

Figure 1.

It was shown earlier that the peak at frequency near 10^{-4} Hz (the period of 160 minutes) is presented in the frequency spectrum of the cosmic ray intensity,but ones was instable and observed irregular.The study of this peak is rather intresting becouse of the stable pulsations of the solar atmosphere /3,4/ and geomagnetic pulsations /5/ were observed at the same frequency.In this paper we calculated the summary power spectrum by the data for 1981-1983 (during the quiet periods) and this spectrum $\tilde{G}_{xx}(f)$ is shown in Fig.2.It is seems the peak at 160 minutes predominates in the summary spectrum.It should be noted that the period of this isolate peak equal to 160 minutes precisely in summary spectrum while it drifted around this period in separate frequency spectra.The amplitude of this peak,standing out against a background of intensity fluctuations, exceedes the 95-% significance level,which denoted the dotted line in fig.2.

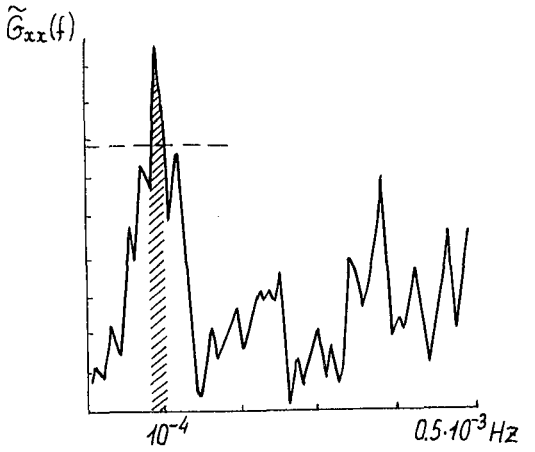

Figure 2.

It was compared the frequency spectra of cosmic ray intensity and the spectra of the geomagnetic field (H-component),registered in Alma-Ata also.The summary spectra of geomagnetic data are shown in Fig.3,for the same intervals of the solar activity cycle as in Fig.1.The main power in these spectra concetrated at low-frequency range and there no statistically significant peaks which could influenced on the cosmic ray fluctuations.There are no the statisti-

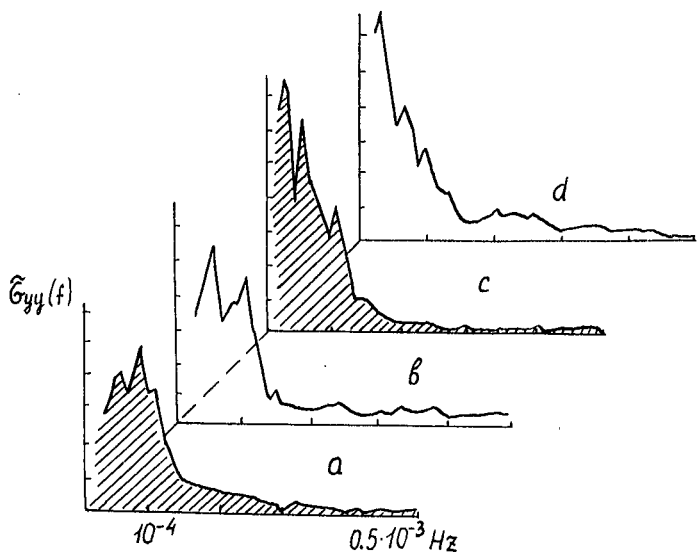

Figure 3.

cal significant values of the spectral density in the coherence spectra of cosmic ray intensity and quiet geomagnetic data for the all investigated periods from 1974 to 1983.

RESULTS. The frequency spectra of the cosmic ray intensity and H-component of the geomagnetic field were studied in the frequency range (10^{-5}-$5 \cdot 10^{-4}$)Hz for period 1974-1983.We can draw a following conclusions from obtained results:

1.The main power of the spectral density in the cosmic ray frequency spectra shifted from low-frequency range to high-frequency range when the solar activity increased.

2.The distinctive peak with the period of 160 minutes observed in the summary frequency spectrum of the cosmic ray intensity.

3.There is no relation between the cosmic ray fluctuations and fluctuations of the geomagnetic field during quiet periods.

REFERENCES.

1.Blackman R.B.,Tukey J.W. The measurement of power spectra. Dover pub.,N.Y.,1958.
2.Antonova V.P.,Zusmanovich A.G. Proc.17th ICRC,Paris,1981, 4,193.
3.Severny A.B.,Kotov V.A.,Tsap T.T. Nature,1976,256,87.
4.Kotov V.A.,Severny A.B.,Tsap T.T. Izv.Krimean Astrophys. Observ.,1983,66,3.
5.Vladimirsky B.M.,Bobova V.P.,Bondarenko N.M.,Veretennikova V.K. Izv.Krimean Astrophys.Observ.,1983,68,75.

SH 5.1-18

STUDY OF COSMIC RAY SCINTILLATIONS FROM 5-MINUTE DATA OF THE SCINTILLATOR TELESCOPE "IZMIRAN" AND WORLD-WIDE NEYWORK STATIONS

O.V.Gulinsky, L.I.Dorman, I.Ya.Libin, R.E.Prilutsky, K.F.Yudakhin

Institute of Terrestrial Magnetism, Ionosphere and Radio Wave propagation, USSR Academy of Sciences, I42092 Troitsk, Moscow Region, USSR

During cosmic ray propagation in interplanetary space there appear characteristic cosmic-ray intensity scientillations /I/ which are due to charged particle scattering on random inhomogeneities of the interplanetary magretic field (IMF). Particles of rather low energies which are sensitive not only to IMF inhomogeneities, but also to the fine structure of approaching shock fronts, undergo the largest scintillations. Nonetheless, the high-energy (more than several Gev) cosmic ray scintillations, which are registered in the most sensitive way be ground-based devices used for recording cosmic radiation, are similarly informative. From the physical point of view this is also connected with the fact that a particle with a large Larmor radius ($R = cp/eH \gg R_C$, R_C is the correlation radius of a random magnetic field) "sses" a wide spectrum of IMF inhomogeneities, whereas when interacting with the high-frequency part of the magnetic inhomogeneity spectrum, low-energy particles bring information about a comparatively narrow region of the IMF turbulence spectrum.

The smallness of scintillation amplitude in the high-energy range is compensated by the fact that measurements in this energy range are made by ground-based devices with a significant statistics and a high accuracy /2/.

The power spectra of cosmic ray scintillations on the Earth during some intervals from I977 to I982 (for quiet periods, for solar flares and Forbush decreases due to power shock waves, Fig. I) have been calculated from five-minute, one- and two-hour values of the cosmic-ray intensity measured by the scintillator supertelescope IZMIRAN and in stations of the world-wide network (Moscow, Utrecht, Kerguelen, Apatity, Tixie Bay, Norikura). The spectra were estimated by the methods of spectral analysis and by autoregressive methods which mutually control each other /3/ and make it possible not only to analyze scintillation powers at distinguished frequencies, but also to determine the behavior of spectrum slopes in some frequency ranges.

Il the power-law spectrum of cosmic ray scintillations is described by the power function $P(f) \sim A \cdot f^{-\delta}$, then using the ratio of the spectrum values in different frequency ranges $f < 8 \cdot 10^{-5}$ Hz and $10^{-5} \leq f \leq 10^{-4}$ Hz (for neutron monitors and scintillator telescopes of the world-wide net of

stations), one can evaluate the product H_0V (in the assumption that the IMF spectrum remains unchanged in the entire frequency range):

$$300 H_0 \cdot V = \frac{2\pi}{\cos\psi}\left[\frac{n-1}{n+3}\cdot\frac{A_1}{A_2}\cdot f^{\gamma_2-\gamma_1+2}\right]^{1/2}\cdot\left[\frac{\int_{R_c} R^{-2}W(R)dR}{\int_{R_c} W(R)dR}\right]^{-1/2}$$

The IMF scintillation spectrum is determined as

$$B(f) = \left(\frac{2}{n+3}\right)^{-1}\frac{4\pi V_{11}^2}{(2\pi)^4(V_\perp\cdot\delta)^2}\cdot f^2\cdot P(f)$$

where H_0 is the mean IMF strength, V is the solar wind velocity, n is the index of pitch-angular distribution, W(R) are coupling coefficients of the devices.

Mean estimations of the indices of the slopes of CR scintillation power spectra for different devices in the stations Moscow, Utrecht, Kerguelen, Lomnicky Stit, Vostok, Baksan, Apatity in quiet periods give the following results: for frequencies $f < 3\cdot10^{-6}$ Hz the spectral index γ lies in the interval $1.45 \leq \gamma \leq 1.75$, for frequencies $4\cdot10^{-6} \leq f \leq 10^{-4}$ the index lies within $1.95 \leq \gamma \leq 3.35$ and, finally, for frequencies $f > 3\ 10^{-4}$ Hz $1.55 \leq \gamma \leq 2.10$ (the latter is due to the competition between the CR scintillation power and the noise power $P(f)/n_0^2 = 2/n_0$). The calculations of the power spectra ($B\cdot f^{-\nu}$) of IMF fluctuations give the values of ν of the order of 1.8 ± 0.1, which agrees well both with the results of field experiments and of ref./4/ (the relation between the spectral indices of IMF, ν and CR, γ, has the form $\gamma = \nu + 2$ in the frequency range $4\cdot10^{-6} \leq f \leq 10^{-4}$ and $\gamma = \nu$ for frequencies $f \leq 3\ 10^{-6}$Hz). Figure 2 presents the power spectra for CR scintillations averaged over the investigated stations for different periods of the maximum (curve 1) and the minimum (curves 2,3) of solar activity. For all the frequencies the power values coincide well with the theoretically calculated values /4/ (for $H_0 = 5\cdot10^{-5}$ Gs and $v = 5\cdot10^7$ cm·s^{-1}) both in the absolute values (in the high-frequency range they differ by a factor of 1.2-1.5 and in the low-frequency range by a factor of 1.5-2) and in the behaviour of the spectra: the values of the indices coincide with an accuracy to 10 %.

There exist also other possibilities for studying the CR scintillation spectrum: one can not only estimate the power spectrum of IMF fluctuations, but also establish a one-to-one correspondence with the level of perturbation in interplanetary medium of both distinguished scintillations at certain frequencies and the spectrum as a whole - the slope of the CR scintillation spectrum in the range $f < 10^{-4}$Hz increases gradually up to the maximum value several hours before the perturbation of interplanetary medium comes to the Earth. Figure 3 shows the behaviour of the index of the po-

wer spectrum of CR scintillations for the events in September 1977 from the data of the Utrecht and Kerguelen stations. It is seen from the figure that at least 18 hours before perturbation the spectral index in the range $10^{-5} \leq f \leq 10^{-4}$ Hz starts increasing whereas the quantity A (if the spectrum is given in the form $A \cdot f^{-\gamma}$) decreases. That CR go ahead of perturbation can be easily explained: CR feel inhomogeneities at a distance of their free path for scattering (about $10^{12} - 10^{13}$ cm) and their velocity is a thousand times larger than the velocity of propagation of perturbation. Hence, CR bring information practically instantaneously, whereas perturbation travels to the Earth long hours. Therefore, the distances between perturbations approaching the Earth can be essentially different: recording particles of different energies, one can observe inhomogeneities at distances up to several AU.

REFERENCES

1. L.I. Dorman., I.Ya. Libin - Space Sci.Rev., 1984, 39, 91-152.
2. L.I. Dorman., I.Ya. Libin, Ya.L. Blokh - Scintillation method for cosmic ray scintillation studies - M., Nauka, 1979.
3. O.V. Gulinsky., L.I. Dorman., R.E. Prilutsky. Proc. of the Conference,
4. L.I. Dorman., M.E. Katz, M. Steglik et al. - Izv. AN SSSR ser. fiz. 1983, 47, N9, 1986.

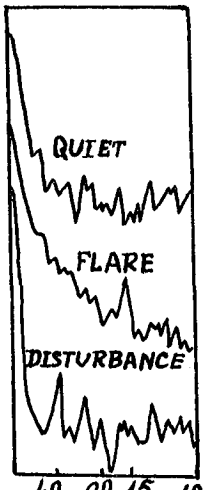

Fig. 1

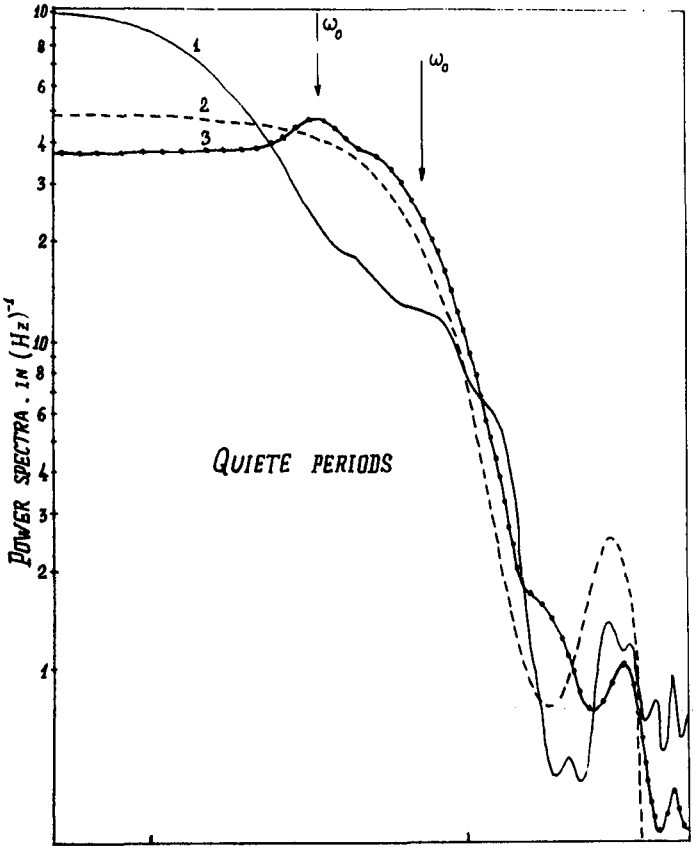
POWER SPECTRA . IN (Hz)⁻¹
QUIETE PERIODS
ω₀
ω₀
1
2
3
FREQUENCY, in K

FIG. 2

FIG. 3

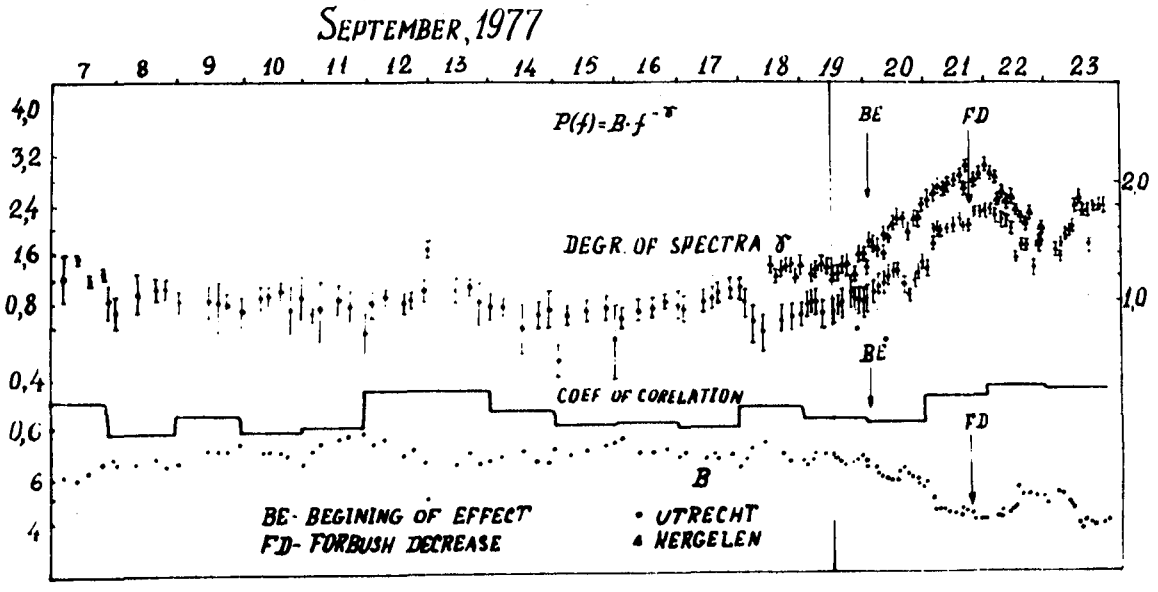
SEPTEMBER, 1977
P(f)=B·f^-γ
DEGR. OF SPECTRA γ
COEF OF CORELATION
B
BE
FD
BE- BEGINING OF EFFECT
FD- FORBUSH DECREASE
• UTRECHT
▲ NERGELEN

SH 5.1-20

THE THEORETICAL AND EXPERIMENTAL INVESTIGATION OF COSMIC RAY FORBUSH-EFFECTS

Alania M.V., Bakradze T.S., Bochorishvili T.V.
Bochikashvili D.P., Despotashvili M.A., Nachkebia N.A.

The Institute of Geophysics, Georgian Academy of Science, Z.Rukhadze str. 1, 380093, Tbilisi

ABSTRACT

The theoretical results of analysis of the expected spatial distributions of density, gradients and anisotropy of cosmic rays, obtained on the basis of the numerical solution of anisotropic diffusion equation in the presence of the disturbances of shock wave type in the interplanetary space are presented. The theoretical calculations on the definition of the energy spectrum and anisotropy of galactic cosmic rays during Forbush - effect are compared with the experimental data.

The theoretical model. Cosmic ray Forbush-effects have a complex structure and nature /1,2/. They differ from each other both by power and by energy spectrum indices et al. However, there exist the indications such as the recurrence and sporadicity of Forbush-effect origin, the character of shock wave development causing Forbush-effects, the change of energy spectrum index in time et al. by with the definite classification of Forbush-effects can be carried out /3-4/.

In this paper the study of cosmic ray Forbush-effects on the basis of the processes occurring in the interplanetary space in the presence of the disturbance passage limited by the heliolongitudes, but having no boundary in the radial direction is carried out i.e. the type of recurrent Forbush--effect is considered.

The anisotropic diffusion equation/5/ is taken as modeling of the electromagnetic conditions occurring in the interplanetary space under the following assumptions: a) solar wind velosity u and the diffusion coefficient $\varkappa$ of cosmic rays in the disturbed region changes nearly twice in comparison with the environment, b) the disturbed region is given in a cone form for which the helioequator is a symmetry plane, i.e. along the trajectory of the Earth the heliolatitudinal gradient $\partial n/\partial\theta = 0$, c) it is considered that, since the disturbed region across the heliolatitude is limited in the range of several a.u., and in the radial direction the process is stationary, the stationary approximation is quite true, i.e. $\partial n/\partial t = 0$. Hence, the anisotropic diffusion equation has the following form:

$$\nabla_i(\varkappa_{ik}\nabla_k n) - \nabla_i(n \cdot u_i) + \frac{1}{3R^2}\cdot\frac{\partial}{\partial R}(R^3 n)\cdot\nabla_i u_i = 0 \qquad (1)$$

where n and R -the density and the rigidity of cosmic ray particles, and u_i the solar wind velocity. Taking into

account the above assumptions for solar wind velocity u and the diffusion coefficient $\partial\ell$: $u=u_0(1+d_1\tau)$ (see Fig. 1a) and $\partial\ell=\partial\ell_0(1-d_2\tau)$ (see Fig.1b), where $d_1=3,4$; $d_2=1,75$; and $\tau=\frac{1}{\pi^2}[arcty(2(\varphi-30))-arcty((\varphi-70)/7)]$.

The equation (1) is solved by net method under the following boundary conditions:

$$\frac{\partial n}{\partial \tau}+\alpha n+\beta\frac{\partial n}{\partial R}\Big|_{\tau=0}=0\,,\quad n\Big|_{R=450}=1\,,\quad n\Big|_{\tau=\tau_0}=1\,,\quad n\Big|_{\varphi=0}=n\Big|_{\varphi=\pi}\,,$$

where $\alpha=(3/2)d$, $\beta=d\cdot R/3$ and $d=u\tau_0/\partial\ell$.

The expected change depending on the heliolongitude during Forbush-effect for two rigidities $R=10$ GV and $R=20$ GV is presented in Fig. 2, It is seen , that the change of solar wind velocity u and the diffusion coefficient $\partial\ell$ (see Fig.1a,b) induce a gradual decrease and restoration of cosmic ray intensity that is characteristic of the recurrent Forbush-effects.

For the case, when the approximation is given by $\frac{\delta D}{D}(R)\sim R^{-\gamma}$, the energy spectrum index of Forbush-effect is equal $\gamma=1,06$.

The expected change of socmic ray anisotropy before, during and after the cosmic ray Forbush-effect duration for the rigidity $R=10$ GV is presented in Fig. 3, It is seen that after strong disturbances of anisotropy vectors near the minimum of Forbush-effect the monotone restoration to the initial position is observed.

The experimental data. The change of intensity of cosmic ray neutron (1) and muon component at a level 0 and 7 m.w.e. (2) and (3) in Tbilisi station for the period February 14-17,1978 is presented in Fig.4a. The change of the energy spectrum of this Forbush-effect in time has been studied by two independent methods. The first one is a well-known spectrographic method /5/ and the second one - the method of the coupling coefficients, presented by the Japanese authors /6/. The analysis by the spectrographic method has been carried out by the intensity of cosmic ray neutron and hard μ-meson components at Tbilisi station and by method of the coupling coefficients - by the data of Tbilisi station and the world network. The changes of the energy spectrum index γ , obtained by the spectrographic method (the dashed curve) and by the coupling coefficients (the solid curve) are presented in Fig. 4b. It is seen that the results obtained by both methods show the same temporal changes, however, the values of the energy spectrum index obtained by the spectrographic method are systematically higher than the values obtained by the method of the coupling coefficients. In the Fig.4c the changes of DSt variation of the Earth's magnetic field (dashed) and the cutoff rigidity threshold ΔR_c (solid) are presented.

Discussion and Conclusion. The obtained result is explained easily. The fact is that the change of the cutoff rigidity threshold ΔR is not taken into account in the process of calculating the energy spectrum index by the me-

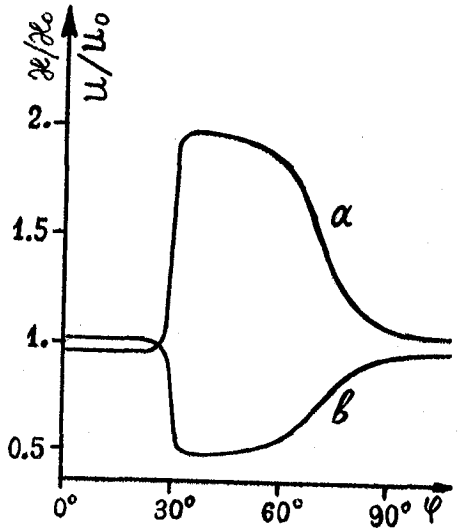

Fig. I

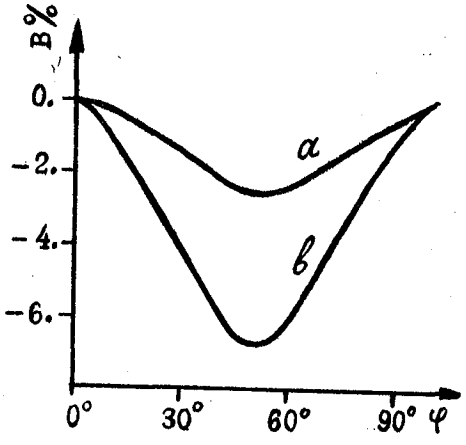

Fig. 2

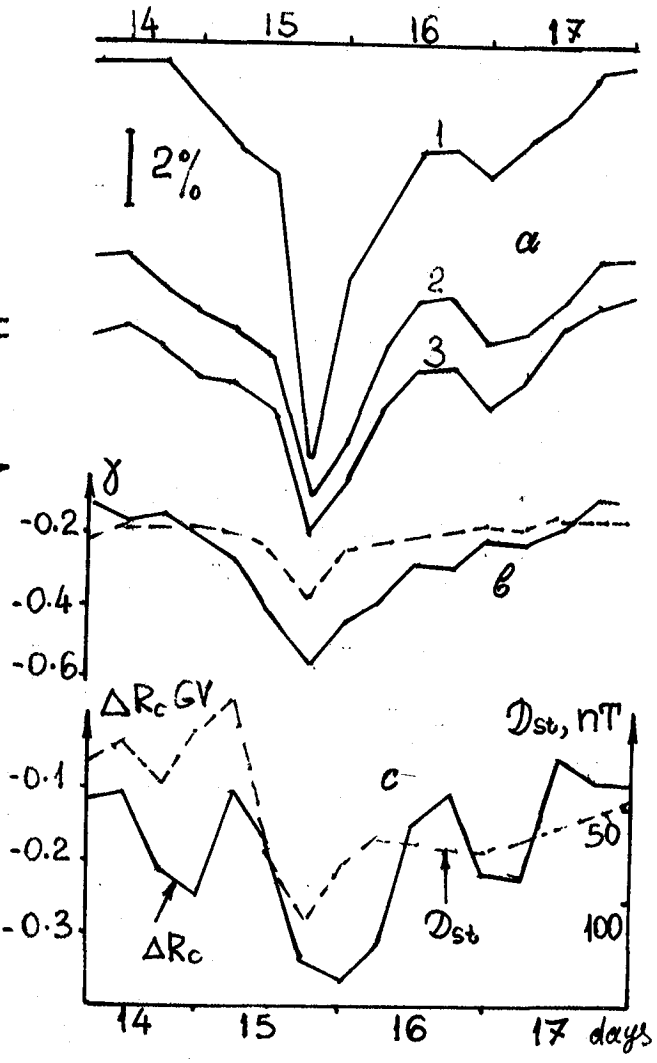

Fig. 4

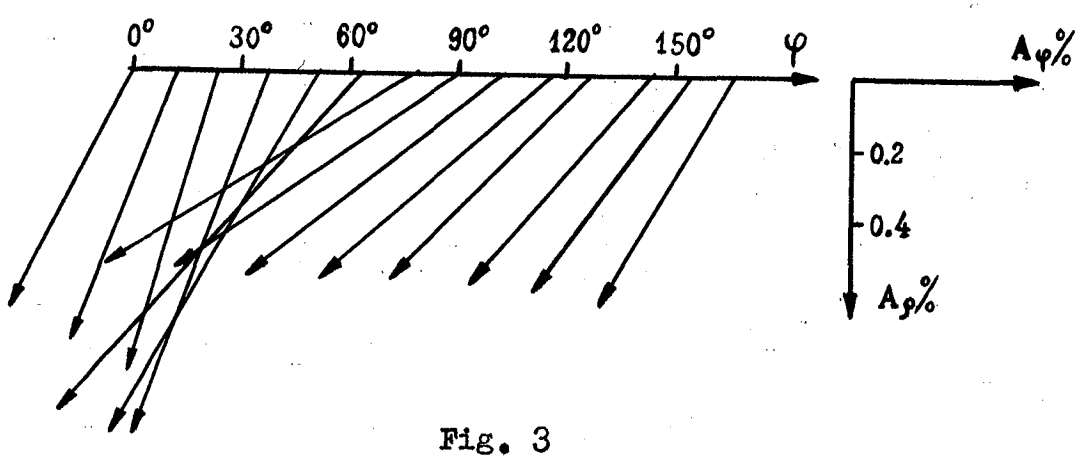

Fig. 3

thod of the coupling coefficients /6/, and is taken into account in the spectrographic method.

For the period considered the change of ΔR_c is observed, in particular, its decrease and therefore the amplitude absolute value of cosmic ray intensity decrease is diminished, i.e. the energy spectrum calculated by the coupling coefficients method will be more rigid, that is really observed.

The rigid energy spectrum before reaching the minimum of Forbush-effect must be connected with the predominant carring out of cosmic ray particles of relatively low energies with the high-velocity flux of the chromospheric flare /8/. In addition, the energy spectrum of magnetic inhomogeneity power of the medium frequencies which can induce cosmic ray particle modulation predominantly of relatively low energies can be increased in front of the magnetic cushion of the shock wave and in the cushion itself. Apparently, the geometric factor, the size of the compressed cavity in the front part of the shock wave plays an important role.

REFERNCES

I. Dorman L.I. "Variatsee Cosmicheskikh Luchei I Issledovanie Cosmosa". AN SSSR, M.I963.
2. Krimski G.F. "Modulatsia Cosmicheskikh Luchei V Mejplanetnom Prostranstve". "Nauka". M.I969.
3. Shah G.N. et al., Proc. I6th ICRC, Kyoto, Japan 3, 423, I979.
4. Alania M.V., Bochikashvili D.P. I8th ICRC, Bangalore, India, L.p. Vol.IO, I68, I983.
5. Dorman L.I. "Astrofizicheskie Aspecti Cosmicheskikh Luchei". "Nauka". M.6, I975.
6. Yasue S. et al., Coupling Coefficients of Cosmic Ray Daily Variations for Neutron Monitor Stations. Nagoya, Japan, I982.
7. Solar-Geophysical Data, Febr. I978, numb. 505, part I.
8. Alania M.V. Autoreferat of Doct. Dissertation, Kiev, I98I.

SH 5.1-21

PECULIARITIES OF GALACTIC COSMIC RAY (GCR) ANISOTROPY VARIATION IN CONNECTION WITH THE RECURRENT AND SPORADIC FORBUSH EFFECTS

B.D. Naskidashvili, N.A.Nachkebia, G.L.Tsereteli, L.Kh.Shatashvili

The Institute of Geophisics, Georgian Academy of Sciences, Z.Rukhadze str. I, 380093, Tbilisi, USSR

ABSTRACT

It has been establised, that the beginning of the change of vector of Solar-diurnal anisotropy of Galactic Cosmic Rays(GCR) preceeds the beginning of Forbush-decrease(FD), which is due to the disturbed region (DR) of Solar wind existing time of which is $\tau \gtrsim 8$ days. The meridional gradient $\nabla_\theta n$ of density during the reccurent FD is valued.

I. Anisotropy of GCR due to the long lived DR ofsolar wind

As is known, the sporadic Forbush decreases (SFD) are caused by thepowerful solar flares on the day-side of the solar disc. If the flare occurs near the central meridian of the Sun, then in this case DR of the Interplanetory me - dium, at the starting point of SFD will have the spatial sizes of order of one a.u. Considerable small size of DR of Solar wind, causing SFD, attaches some definite character on the behaviour of solar-diurnal anisotropy vector of GCR.

The typical case of behaviour of the anisotropy vec - tor, according to the data of Kiel(FRG) during the SFD (06. 09.1982) is given (on fig.Ia). Before the beginning of SFD, vector of anisotropy is not changed, while after the SFD the vector turns to the direction of the Sun. The behaviour of vector of the GCR anisotropy has essentialy distinctive feature during such FD-s, which aren't necessarily connected with the flares on the Sun, arising not far from the central meridian, but are due to the high-velocity flow of Solar wind existing in the interplanetory medium in the course of time $\tau \gtrsim T/4$ (T -is the period of Solar rotation). In such cases, it is easy to notice, that at the starting point of FD the DR of the SW occupies the space area with the sizes of $L \gtrsim 4$ a.u. The corresponding model configuration lines of forces of IMF is presented (in Fig.1b). The passage of the Earth through the inhanced regions of IMF corresponds to the beginning of FD. In front of this region, as it is seen in (Fig.1b) is the nondisturbed region of the Solar wind, however access of GCR into this region is complicated due to the compressing of the lines of forces of IMF at far distances, where the GCR particles come from, mainly directed across the IMF lines of forces. The latter means, that

in this region of SW, similar to the charged particles trap, the diffusional flow of GCR must be greatly decreased. Hence, the GCR anisotropy in this non-dirturbed region of SW will be mainly due to the convectional flow of GCR, which is due to cause the turning of the anisotropy vector to the direction of the Sun. FD on 28.01.1978 serves as a good example of this case. Before the beginning of the FD in the course of 20 days, not a single Solar powerful flare with importance $\geqslant 2$ was observed. Consequently, FD must be due to the long-lived DR of SW. As it is seen from Fig. 1c. the anisotropy vector of GCR , for 8 days earlier before the beginning of FD, is essentialy turning to the direction of the Sun, but after the beginning of FD- tends to orientate to the direction of IMF. The latter is connected with that fact, that after the front passage through the DR, the Earth comes out of the "trap" region and the recovery of GCR intensity occurs due to the diffusional flow across the IMF lines of forces, which at far distances are spread, contributing to the free penetration of the GCR particles from the far distances of the Sun, where the GCR density is large.

2. The meridional gradient of GCR during the recurrent Forbush decreases.

In paper /I/ the classification of FDs is presented and in paper /2/ it is shown that the spectrum of the recurrent FDs is more rigid, than the one of the sporadic FDs. In the given paper the meridional gradient of CR during the recurrent FD is valued /3/.

The data of the world network of station of CR neutron component are analysed as well as the data of the SW, of the IMF, according to /4/ and of Solar activity (Solar Geophysical Data, NOAA). The considering of the FDs with the amplitude $\geqslant 1\%$ is mainly made according to the data of the high-latitudinal stations of CR. Superposition of effects, due to flaring and non-flaring flows complicates the view of recurrent FDs. If the recurrend FD is not preceeded by the chromosperic flare and FD is not created by interactional high-velocity flows of SW, then during the FD the IMF sign must not change. Therefore we've analysed only those FD-s, during which the IMF sign is not changed. Data for the period 1971-1978, when the polarity of the general magnetic field of the Sun was not changed, have been taken for the analysis.

After such selection 47 cases of FD were left. 22 cases out of them were arisen at a time, when IMF sign was negative (towards the Sun). In 25 cases, FDs were arisen at a time, when the IMF sign was positive (from the Sun). Each of these groups we divided into 2 subgroups, according to the IMF sign before and during FD, i.e. while dividing into subgroups, it was taken into account, whether the IMF signs coincided with each-other or not before and during the FD. Thus, we've obtained 4 groups of cases of FDs.

In DR of the SW the CR density is less than out of it, therefore the azimuthal gradient $\nabla_\varphi n$ of CR density

changes its direction near the minimum of recurrent FDs, i.e. in the minimum of recurrent FDs it can be admitted that $\nabla_\varphi n = 0$. Therefore, the meridional gradient $\nabla_\theta n$ will cause the CR additional flow of the Hall type, directed perpendicular to the IMF and $\nabla_\theta n$ /5/.

The observed CR anisotropy A near the minimum of the recurrent FDs can be presented as the sum of $A = A_\circ + A_\perp$, when $A_\circ$ -is a general anisotropy connected with the convectional -diffusional transforming in the high-velocity plasma flow, $A_\perp$ - is the constituent, due to the appearance of $\nabla_\theta n$. The value of $A_\circ$ was calculated by data averaging after the minimum of FDs.

In Fig.2a,b, where effective regions of CR modulation are denoted by the circles, the orbit of the Earth-by dashes, the neutral layer of IMF - by the solid line, the origination of the anisotropy under the influence of $\nabla_\theta n$, during those recurrent FDs, when the IMF is directed from the Sun, is shown schematically. The calculated values $A_\perp$ and values of IMF are also given (in the right part of Fig.2a, b) in the minimum of FDs. It is seen, that in case of 2a (I7 cases of FDs are averaged) the vector $A_\perp$ is really directed perpendicular to the IMF. In case 2b(8 cases of FDs are averaged) the vector $A_\perp$ is turned relatively towards $A_\perp$ corresponding to the case 2a almost by 180° as it was to be expected

In Fig. 3a,b the same as in Fig.2 , is presented only for those recurrent FDs during which IMF is directed to the Sun. In case 3a-I8 cases of FDs are averaged, but in 3b- 4 ones of FDs.

For the more exact definition of $A_\perp$, we've examined those FD-s, which correspond to the cases presented in Fig. 2a,b. The anysotropy A in the minimum FD has the form: In case 2a $A_1 = A_\circ + A_\perp$; In case 2b $A_2 = A_\circ - A_\perp$ Hence, $A_\perp = (A_1 - A_2)/2 = (0,12+0,06)\%$.

According to /5/ $A_\perp = \Lambda[\nabla_\theta n \times \kappa]$, where Λ is the transport path of CR; κ -unit vector along the lines of force of IMF.

In paper /5/ the following is shown

$$\Lambda = (1-F)\rho \qquad \rho = R/(45B)$$

where ρ -is the Larmor radius in a.u. F - degree of irregularity of IMF. R-rigidity (in Gv) B-value of IMF (in nTl). Then $\nabla_\theta n = 45 A_\perp B (1-F)^{-1} R^{-1}$, where $\nabla_\theta n$ is expressed in %/a.u. $A_\perp$ -in %, If $F = 0,1 \div 0,3$ then with R=I0 GV, from the experimental data we obtained, that during the recurrent FD-s meridional gradient of CR density on the Earth orbit is $\nabla_\theta n = (3 \div 4)\%/a.u.$

REFERENCES:

I. Shah G.N., Kaul C.L., Razdan H.Proc.I6th ICRC , v.3, Kyoto, I979, p.423.

2. Nachkebia N.A., Shatashvili L.Kh. I8th ICRC, Bangalore, Late Papers, v.I0, p.I52.

3. Nachkebia N.A., Shatashvili L.Kh., Geomagnetism i aeronomia, t.XXV, №2, I89.
4. King J.H. IMDB, NSSDC, WDCA, I977, I979.
5. Samsonov D.S., Krimsky G.F., Samsonova Z.N., Chirkov N.P. V kn.: "Issledovania po Kosmofisike i aeronomii.Iakytsk: SOAN, SSSR, I975, I72.

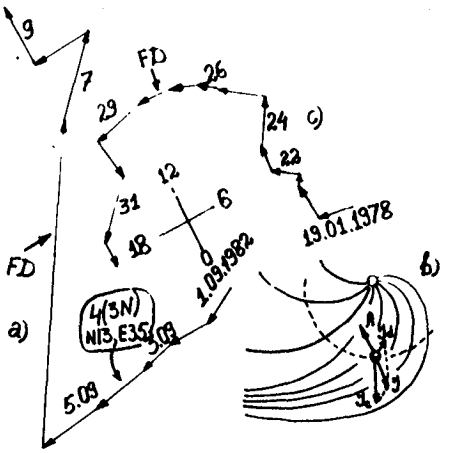

Fig.I

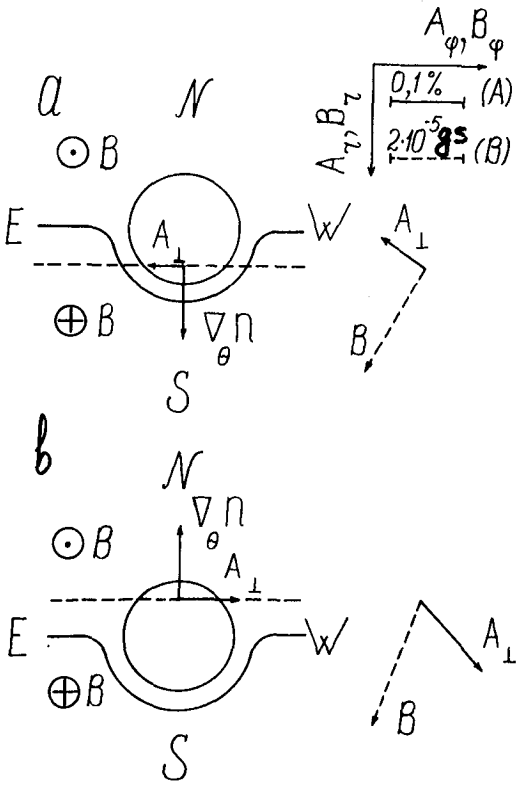

Fig.2

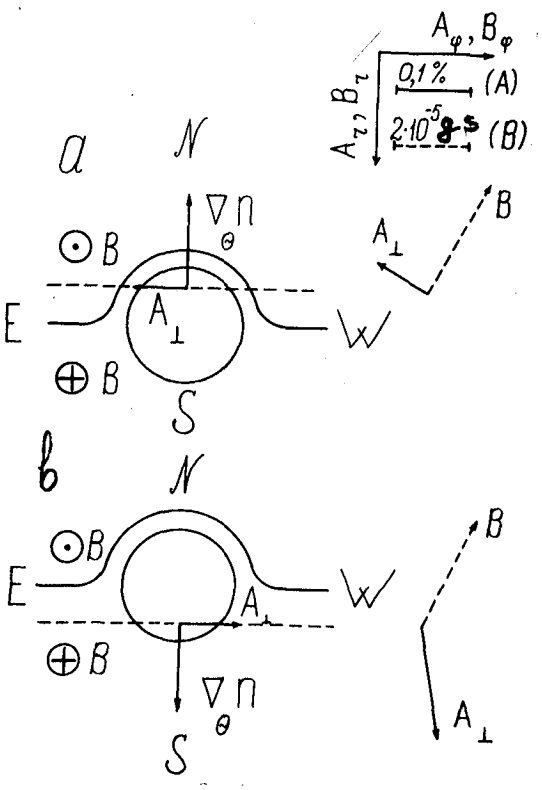

Fig.3

COSMIC RAY MODULATION BY HIGH-SPEED SOLAR WIND FLUXES

Dorman L.I., Kaminer N.S.
Institute of Terrestrial Magnetism, Ionosphere and Radio Wave Propagation, USSR Academy of Sciences, I42092 Troitsk, Moscow Region, USSR

Kuz'micheva A.E., Mymrina N.V.
Uralsk Pedagogical Institute, Uralsk, USSR

Abstract. Cosmic ray intensity variations connected with recurrent high-speed fluxes (HSF) of solar wind are investigated. The increase of intensity before the Earth gets into a HSF, north-south anisotropy and diurnal variation of cosmic rays inside a HSF as well as the characteristics of Forbush decreases are considered.

I. Introduction. Recurrent high-speed fluxes of solar wind connected with coronal holes change essentially the cosmic ray density distribution in interplanetary medium. When such fluxes cross the Earth, different types of cosmic ray (CR) variations are observed. The characteristics of these CR variations may essentially differ from those observed when CR pass sporadic HSF of flare origin.

Below we consider a number of CR variations connected with recurrent HSF observed in I973-I974.

2. Intensity increase before Forbush effect. I2 fluxes of velocities $U \gtrsim 600$-800 km/s were considered, which were accompanied by Forbush effects. The data on the CR neutron component obtained on the Deep River station were used. After the low-frequency trend and the diurnal CR variation were eliminated by the method of superposition of epochs the CR variation was found before the Earth got into a HSF. It is seen from Fig.I that before Forbush effect CR intensity increases with amplitude by about 0.4 %.

3. N-S anisotropy of CR. The N-S anisotropy was investigated from the CR neutron component data obtained in the stations of Thule and Mc Murdo. I8 HSF with a positive IMF direction and I8 HSF with a negative IMF direction were picked. All of them were divided into three groups depending on their speed: I-$v \leq 600$ km/s, II - $v = 600$-700 km/s, III - $v > 700$ km/s.

The results of determining N-S anisotropy by the method of superposition of epochs are presented in Fig.2. The N-S anisotropy is seen to exist in the back part of a HSF (5%) and to be absent in the front part of a HSF. Such a peculiar behaviour of N-S anisotropy is qualitatively explained by

a non-radial plasma outflow from the coronal hole - the flux is divergent. The sign of N-S anisotropy becomes inverse as the IMF direction changes. This means that N-S anisotropy results from the Hall effect. This conclusion is confirmed by the behaviour of the B_z-component of IMF at different IMF directions. The amplitude of N-S anisotropy does not depend on the HSF speed.

4. Diurnal CR variation. The behaviour of the diurnal CR variation was investigated from the data on the neutron component for 58 HSF. It turned out that the amplitudes of first and second harmonics are larger inside a HSF than in a quiet solar wind, that the phase of first harmonic shifts towards earlier hours, and the phase of second harmonic towards later hours (Fig.3). This difference increases with an increasing HSF speed. The characteristics of diurnal CR variation do not depend on the field direction in HSF.

5. Forbush effects of recurrent HSF. The analysis of data on the CR neutron component for 62 HSF has shown that if the HSF width $\Delta t \gtrsim 3$ days, a Forbush decrease is practically absent. Inside each HSF there exists a good correlation ($r \sim -.7$) between plasma velocity and CR intensity decrease. The amplitude of Forbush effect A_F increases with an increase of the HSF velocity (about a 5-% increase for an increase of v by 100 km/s). The shape of Forbush decreases and their amplitude do not depend on the IMF direction. The energy spectra of Forbush decreases for HSF of different velocities have been determined. It turned out that as the HSF velocity increases, the spectral index γ monotonously decreases: from $\gamma = 0.7$ for $v \leq 600$ km/s to $\gamma = 0.5$ for $v > 700$ km/s.

All these results, as well as the results of analogous papers by other authors make it possible to conclude that the main parameter of recurrent HSF which determines the characteristics of various CR variations is their velocity.

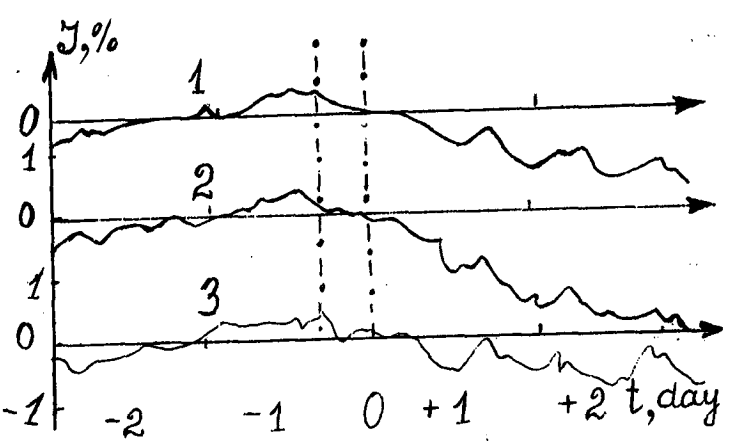

Fig.I. CR intensity increase before side-end of SHF calculated by superposition of epochs from 12 events. Curve 2-effect due to particles coming from transition region. Curve 3-effect due to particles coming from other directions. Curve I-effect averaged over all directions.

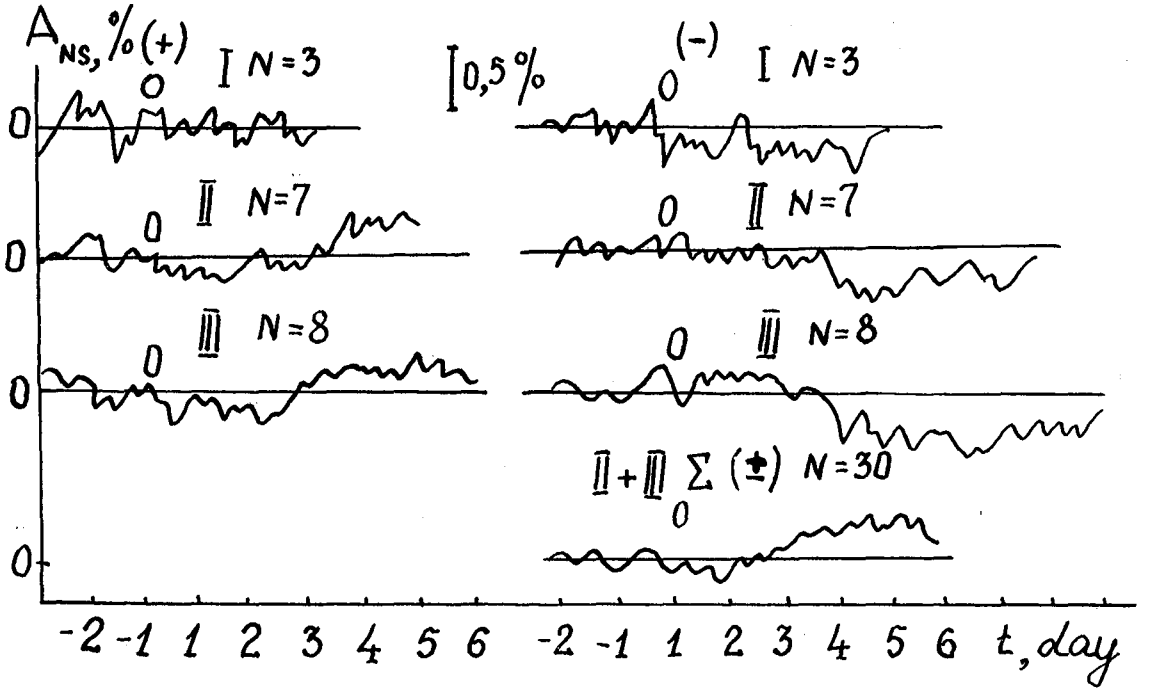

Fig.2. N-S anisotropy of CR inside a HSF. On the left - for the positive IMF direction, on the right - for the negative IMF direction. I - for HSF with $v \leq 600$ km/s, II - for HSF with $v = 600$-700 km/s, III- for HSF with $v > 700$ km/s. At the bottom is the sum curve for the II-nd and III-d groups of HSF.

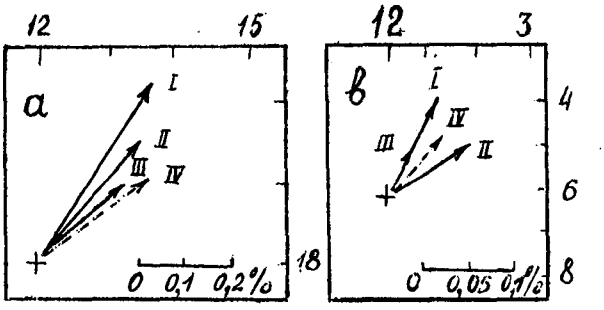

Fig.3. Vectors of a diurnal (a) and semidiurnal (b) CR variations: I - in the front part of HSF, II - in the middle part of HSF, III - in the back part of HSF, IV - in a quiet solar wind

SH 5.1-23

SOLAR ACTIVITY BEYOND THE DISK AND VARIATIONS OF THE COSMIC RAY GRADIENT

Belov A.V., Dorman L.I., Eroshenko E.A., Ishkov V.N., Oleneva V.A.

Institute of Terrestrial Magnetism, Ionosphere and Radio Wave Propagation, USSR Academy of Sciences, 142092 Troitsk, Moscow Region, USSR

Part of galactic cosmic rays (CR) observed near the Earth and on the Earth come from beyond-disk regions of circumsolar space. But CR of those energies which undergo substantial modulation cover too large a path (we mean a transport free pathr) across the lines of force of the interplanetary magnetic field (IMF) in order they could provide an effective transfer of information about beyond-disk solar activity. And if it is still possible, the most probable channel for tranferring such information must be a neutral layer of heliomagnetosphere in which the transverse CR transport is facilitated by their drift in an inhomogeneous magnetic field /I,2/

For charged particles of sufficiently high energy the thickness of the neutral layer is negligibly small as compared with the gyroradius of particles, ρ . In a plane neutral layer the driving centres of such particles will shift along the line (which can be called a drift trajectory) determined by the relation

$$\Delta\varphi = \varphi - \varphi_0 = \int_{r}^{r_0} \frac{u}{\Omega} \frac{dr}{r^2} \qquad (I)$$

Here r and φ are heliocentric radius and heliolongitude, r_0 and φ_0 are coordinates of the observation point, u is solar wind velocity, Ω is angular velocity of synodic rotation of the Sun. The drift trajectories (Fig.I), contrary to the field lines to which they are perpendicular, are almost azimuthal near the Sun and approach the radial direction beyond the Earth's orbit. If u and Ω do not depend on the coordinates, it follows from (I) that $r/r_0 = \left(1+\Delta\varphi \frac{\Omega r_0}{u}\right)^{-1}$. The direction of particle motion along the drift trajectories will be determined by polarity of the total magnetic field of the Sun. So, in the seventies, in the special region of "one-way" particle motion near the neutral layer, protons and other positively charged particles had mostly to shift from the Sun to overstep the Earth's orbit. At that time the drift trajectories could bring to the Earth the information of Forbush decreases which occurred in the opposite to us side of cir-

cumsolar space and were caused by powerful beyond-disk flares.

A simple diffusion model for an expected CR variation in a neutral layer near the Earth gives /3/

$$\delta(x_\delta)=\int_0^{x_\delta}\frac{\delta(x)}{v_d\tau}\exp\left(\frac{x-x_\delta}{v_d\tau}\right)dx \qquad (2)$$

where x is the distance measured along the trajectory, $\delta(x)$ is variation of CR concentration at different points of the trajectory, v_d is effective drift velocity, τ is the mean time necessary for a particle to shift by one gyroradius across the field. High values of $\delta(x_\delta)$ (for example, >1 %) should hardly be expected even for large beyond-disk decreases. However, since the main effect must be concentrated on one gyroradius from the neutral layer, sufficiently large variations of the CR gradients are possible here. The CR gradient variations and consequent anisotropy variations are just the response to beyond-disk events which one may hope to discover by observing CR near the Earth.

The CR gradient near the Earth can be obtained by using the data on the CR concentration and anisotropy along with the data on the velocity of solar wind and IMF /4,5/.

If $\vec{A}$ is the CR anisotropy vector, $\vec{A}_c$ is its convective part, and $\vec{g}$ is the gradient of the logarithm of CR concentration, then in the convective-diffusion anisotropy model /6/ $\vec{A}-\vec{A}_c=-\Lambda\vec{g}$. In the local right-handed coordinate system in which the x-axis is directed along the solar wind velocity and the y-axis lies in the plane of IMF line, the matrix of transport free paths is

$$\Lambda=\rho\begin{pmatrix}\frac{C^2+KS^2}{\sqrt{K}} & CS\frac{1-K}{\sqrt{K}} & -S\sqrt{1-K}\\ SC\frac{1-K}{\sqrt{K}} & \frac{S^2+KC^2}{\sqrt{K}} & C\sqrt{1-K}\\ S\sqrt{1-K} & -C\sqrt{1-K} & \sqrt{K}\end{pmatrix}$$

Here ρ is gyroradius of particles in the total magnetic field /4/, k is the transverse-to-longitudinal diffusion coefficients ratio, $S=\sin\Psi$, $c=\cos\Psi$, Ψ is the angle between $\vec{A}_c$ and the IMF strength vector. It can be shown that the inverse Λ matrix has the following simple form

$$\Lambda^{-1}=\frac{1}{\rho}\begin{pmatrix}\sqrt{K} & 0 & S\sqrt{1-K}\\ 0 & \sqrt{K} & -C\sqrt{1-K}\\ -S\sqrt{1-K} & C\sqrt{1-K} & \sqrt{K}\end{pmatrix}$$

This matrix is convenient in the determination of $\vec{g}$ /5/.

The active regions whose appearance from behind the eastern disk or disappearance behind the western one was accompanied by active phenomena were distinguished with the help of (7). Thus, the periods with a high probability of powerful flares in the invisible side of the Sun were chosen. One of such periods is shown in Fig.2. We can see there substantial variations of the CR gradient and especially its heliolatitudinal component g_z. A considerable part of such variations is observed in a close vicinity of the neutral layer. It is of importance that variations of the CR gradient are not at all always accompanied by considerable variations of IMF and solar wind velocity at the point of observation. And although the observed variations of anisotropy and CR gradient should not necesserily be associated just with beyond-disk events, the experimental data, along with the above estimates and qualitative considerations give grounds for further search for the evidence in favour of beyond-disk solar activity in the behaviour of galactic CR near the Earth.

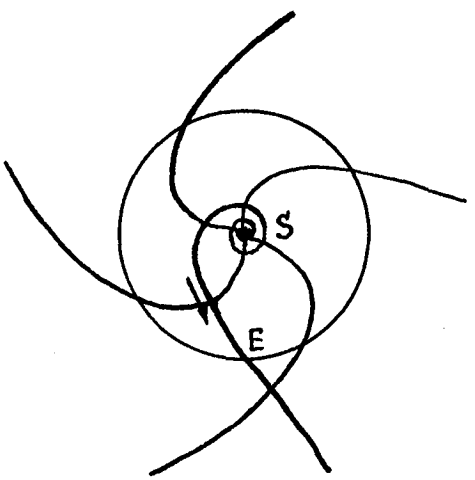

Fig.I. The drift trajectory passing near the Earth. It is calculated by formula (I). Arrow indicates the proton drift direction in the seventies.

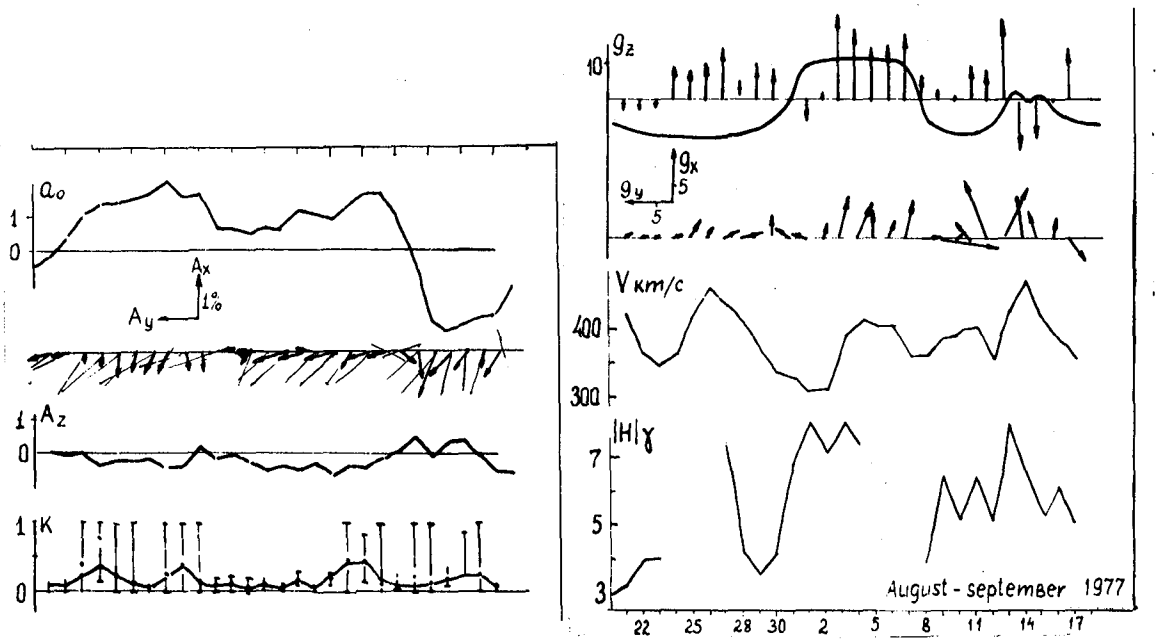

Fig.2. Example of the behaviour of the characteristics of cosmic rays and interplanetary medium in August-September, I977.

a_o - variation of concentration of CR with a rigidity of IO GV.

A_x, A_y, A_z - components of the first harmonic of CR anisotropy. The position of IMF line is shown along with A_x, A_y.

g, g_x, g_y, g_z - gradient and its components for CR with a rigidity of IO GV. The hypothetic configuration of the neutral layer of heliomagnetosphere is shown along with g_z.

K is the degree of anisotropy of CR diffusion (O k I). The directly calculated values of K are shown by points, the smoothed ones - by a solid line.

u - solar wind velocity

H - IMF strength /8/.

REFERENCES

I. Levy E.H. Proc.I6-th ICRC,v.3, p.47, I979.
2. Jokipii J.R., Levy E.H., Hubbard W.B.,Astroph.J.,2I3,86I, I977.
3. Belov A.V., Ishkov V.N. YI Symp. CAPG (Theses of the report) Sochi, November, I984.
4. Belov A.V. et al., Izv.AN SSSR,ser.fiz.,42,IOI3,I978.
5. Belov A.V. et al., Izv.AN SSSR,ser.fiz.,48, , I984.
6. Krymsky G.F. Thesis, I973, FIAN, Moscow.
7. Cataloque of solar proton events in I970-I979, M., IZMIRAN I982.
8. King J.H., Interplanetary Magnetic Field Book,NSSDC 79-08.

COUPLING FUNCTIONS FOR LEAD AND LEAD-FREE NEUTRON MONITORS FROM THE LATITUDINAL MEASUREMENTS PERFORMED IN 1982 IN THE RESEARCH STATION "ACADEMICIAN KURCHATOV"

Alekanyan T.M., Dorman L.I., Yanke V.G.
Institute of Terrestrial Magnetism, Ionosphere and Radio Wave Propagation, USSR Academy of Sciences, 142092 Troitsk, Moscow Region, USSR

Korotkov V.K.
SVKNII, Magadan, USSR

Abstract. The latitudinal behaviour of intensities and multiplicities was registered by the neutron monitor 2 NM and the lead-free neutron monitor 3 SND (slow-neutron detector) in the equator-Kaliningrad line in the Atlantic Ocean. Coupling coefficients for 3 SND show the sensitivity of this detector to primary particles of cosmic rays of energies on the average lower than for 2 NM. As multiplicities increase, the coupling coefficients shift towards higher energies.

The data of latitudinal expeditions have given information on the planetary CR distribution, but mainly from the results of measurements of the summary intensity registered by the neutron monitor, e.g./1,2/. But the available results for measurements of multiplicities are contradictory /3,4/, although it is obvious that large multiplicities must be connected on the average with high energies of primary particles with the exception of a first multiplicity, where the influence of the muon component can be observed. It is also reasonable to specify the known results /5,6/ for the lead-free neutron monitor NMD (Neutron maderated detector) and to compare them with the data for the standard neutron monitor NM-64.

The approximation of the dependence of the recorded intensity I on the geomagnetic cutoff rigidity R has the form /I-6/

$$I = I_o \left[1 - exp\left(-\alpha R^{-\kappa}\right)\right] . \qquad (I)$$

It appears impossible to determine simultaneously three parameters, I_o, α, k in (I) by the method of least squares because of divergency of the iteration process. Therefore, one usually determines the parameter I_o from expedition measurements and then calculates and k by solving the system of equations $\ln\ln[I_o/(I_o-I)] = \ln\alpha - k\ln R$, where I are experimental data. But this method turns out invalid for multiplicities because a statistical accuracy of measurements rapidly decreases, as multiplicity increases, and because in many cases the data of measurements in polar zones are absent. Besides, we cannot

use part of the data, for which $I \gg I_0$ because of statistical difference.

The aim of this papaer is the development of the method of simultaneous calculation of all the parameters in (I) and practical application of this method.

The planetary distribution of CR was measured by the detectors on the research ship "Academician Kurchatov" from 6 to 22 of April, I982 in the Atlantic Ocean in the northern hemisphere. The standard two-counter neutron monitor 2 NM and the three-counter lead-free neutron monitor 3 NMD were used for measurements. Correction due to atmospheric pressure variation was made similarly to /7/. The correction due to variations of extraterrestrial origin was introduced according to the Kiel station; the dependence of the amplitude of variations on the geomagnetic cutoff rigidity was also determined by analogy with /7/. The geomagnetic cutoff rigidities were calculated according to /8/. The results of latitudinal measurements are shown in Fig.I.

The successive approximation method /9/ is proposed for finding the parameters of the approximation (I). The expansion of (I) in a Taylor series with an accuracy to first-order terms at the point of the initial approximation of paramaters has the form

$$I=\left[I_0\left(1-e^{-\alpha R^{-\kappa}}\right)\right]_0+\left(1-e^{-\alpha R^{-\kappa}}\right)_0\Delta I_0+\left(I_0 R^{-\kappa} e^{-\alpha R^{-\kappa}}\right)_0\Delta\alpha+\left(I_0\alpha R^{-\kappa}e^{-\alpha R^{-\kappa}}\ln R\right)_0\Delta\kappa, \quad (2)$$

where the expressions in brackets are taken at the point of the initial approximation $I_0=I_0^{(0)}$, $\alpha=\alpha^{(0)}$, $k=k^{(0)}$. Then one minimizes the sum of the squares of the differences of the calculated values of I according to (2) and experimental values of I

$$S=\Sigma\left(q\Delta I_0+I_0\tau\Delta\alpha-I_0\alpha\tau\ln\tau\Delta\kappa-I_0 q-I\right)=min \quad (3)$$

where $q=1-exp(-\alpha R^{-\kappa})$, $\tau=R^{-\kappa}exp(-\alpha R^{-\kappa})$. The condition of the minimum (3) $\partial S/\partial I_0=0$, $\partial S/\partial\alpha=0$, $\partial S/\partial\kappa=0$ gives the system of equations

$$\begin{cases}\Delta I_0\Sigma q^2+I_0\Delta\alpha\Sigma q\tau-I_0\alpha\Delta\kappa\Sigma q\tau\ln R=\Sigma q\left(I-I_0 q\right)\\ \Delta I_0\Sigma q\tau+I_0\Delta\alpha\Sigma\tau^2-I_0\alpha\Delta\kappa\Sigma\tau^2\ln R=\Sigma\tau\left(I-I_0 q\right)\\ \Delta I_0\Sigma q\tau\ln\tau+I_0\Delta\alpha\Sigma\tau^2\ln R-I_0\alpha\Delta\kappa\Sigma\left(\tau\ln R\right)^2=\Sigma\tau\left(I-I_0 q\right)\ln R\end{cases} \quad (4)$$

the solution of which $\Delta I_0, \Delta\alpha, \Delta k$ determines the following approximation of the parameters $I_0^{(1)}=I_0^{(0)}+\Delta I_0$, $\alpha^{(1)}=\alpha^{(0)}+\Delta\alpha$, $\kappa^{(1)}=\kappa^{(0)}+\Delta\kappa$. This cycle of operations is repeated for subsequent approximations until stable values of the parameters I_0, α, k are obtained. The results of the calculations are shown in Fig.I (solid curve) for all the recording channels: total intensity of the neutron monitor 2 NM, multiplicities m=I-5, $\geq$ 6 and a lead-free monitor. The successive approximation method proved

convergent only for multiplicities m ⩾ 6, which is explained by a low statistical accuracy of measurement of higher multiplicities. For comparison the calculated curves in Fig.2 are normalized for R=0. The polar coupling coefficients calculated in line with /I-3/ as $W(R)=\alpha k R^{-k-1}\exp(-\alpha R^{-k})$ are shown in Fig.3. The table presents the parameters I_0, α, k, as well as the maximal values of the coupling coefficients W_{max} and the corresponding values of the rigidities R_{max}

	I_0	α	k	R_{max}, GV	W_{max}, %/GV
2NM	42930	8.318	0.866	4.76	4.55
3NMD	59076	6.550	0.800	3.80	4.99
m=I	28592	7.I55	0.808	4.2I	4.58
m=2	448I.8	I0.255	0.95I	5.43	5.99
m=3	I055.5	I3.483	0.978	6.96	3.76
m=4	325.63	20.298	I.060	9.I5	3.23
m=5	63.56	42.83	I.29I	II.77	3.30

The measurements give the form of multiplicity distribution

$$I_m = C\exp(-\varkappa m^{\delta}), \qquad (5)$$

where I_m is the number of cases of recording of multiplicity m; $C, \varkappa, \delta$ are the distribution parameters. In a particular case of the use of multiplicities I,2,4 it is easy to obtain explicit expressions for determining the parameters

$$\delta=\ln[\ln(I_2/I_4)/\ln(I_1/I_2)]/\ln 2,\quad \varkappa=\ln(I_1/I_2)/(2^{\delta}-1),\quad C=I_1 e^{\varkappa}. \qquad (6)$$

From Fig.4 it follows that these parameters are functionally connected with one another, in this case $\varkappa=(1{,}87\pm0{,}01)\delta^{1{,}226\pm0{,}008}$, $C=(5{,}77\pm0{,}04)\cdot10^4\exp(0{,}81\pm0{,}01)\varkappa$. This means that a change in the cutoff rigidity leads to an interdependent change in the multiplicity distribution parameters. The dependence of these parameters on the geomagnetic cutoff rigidity is shown in Fig. 5. If $\delta(R)$ is represented by a straigt line according to Fig. 4, $\varkappa(R)$ and C(R) are represented according to (6), then it is easily verified that the expression is not transformed into (I), i.e. $\delta(R)$ has a more complicated form. It can be obtained if (I) is substituted into (6) and then (6) into (5). The $\delta(R)$ thus obtained is illustrated in Fig.5 by a dashed line.

The main results: I. Coupling coefficients shift towards higher rigidities as multiplicity increases; 2. The lead-free monitor NMD is sensitive to lower energies than NM-64. 3. The multiplicity distribution parameters are functionally connected. 4. All the parameters of (I) are determined by the successive approximation method.

REFERENCES : I. E.A.Andreev et al. Cosmic rays, I974,NI4,p.34
2.T.M.Alekcanjan et al.,Proc.I7 ICRC,Paris,I98I,v.4,p.266.
3.T.M.Alekcanjay et al.Proc.I6 ICRC.Kioto,I979,v,4,p.3I5.

4. T.M.Alekcanjan et al. Cosmic Rays,I978,NI8,p.72.
5. T.M.Alekcanjan et al.ProcI6 ICRC,Kioto,I979,v.4,p.32I.
6. L.I.Dorman et al.Proc.I6 ICRC,Kioto,I979,v.4,p.325.
7. M.Kadama and A.Inaue.Yare Scientific Reports,Japan,I970, Ser.A.N O.9,p.I.
8. M.A.Shea and D.T.Smart. J.Geophys.Res.I967,v.22,N O7,p.202I
9. B.P.Demidovich et al.Numerical methods of analysis. Fizmatgiz, I962.

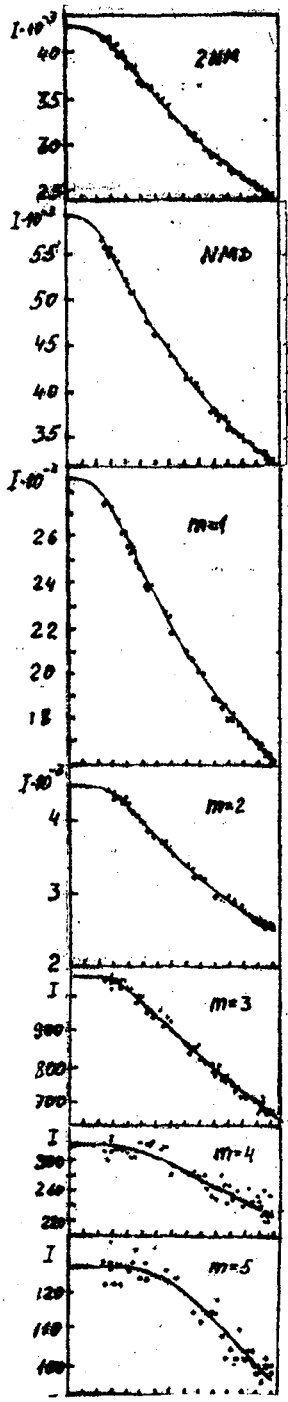

Fig.1

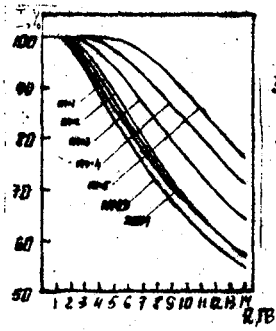

Fig.2

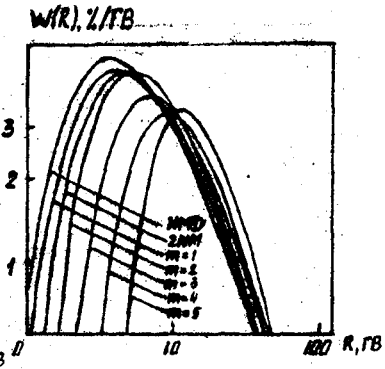

Fig.3

Fig.4

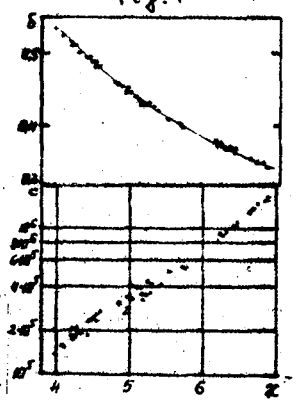

Fig.5

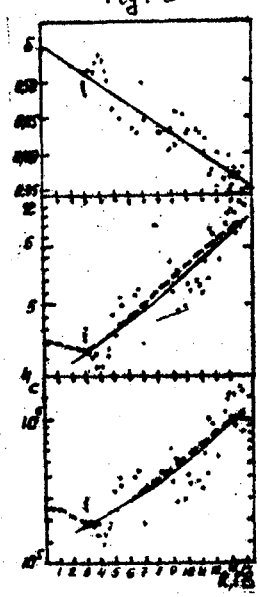

ON THE SOLAR CYCLE VARIATION IN THE BAROMETER COEFFICIENTS OF HIGH LATITUDE NEUTRON MONITORS

M. Kusunose and N. Ogita*

Department of Physics, Kochi University,
Akebono-cho 2-chome, Kochi 780, Japan

* The Institute of Physical and Chemical Research,
Hirosawa, Wako-shi, Saitama 351-01, Japan

ABSTRACT

Evaluation of barometer coefficients of neutron monitors located at high latitudes has been performed by using the results of the spherical harmonic analysis based on the records from around twenty stations for twelve years from January 1966 to December 1977. The average of data at eight stations, where continuous records are available for twelve years, show that the absolute value of barometer coefficient is in positive correlation with the cosmic ray neutron intensity. The variation rate of the barometer coefficient to the cosmic ray neutron intensity is influenced by the changes in the cutoff rigidity and in the primary spectrum.

1. Introduction

Many authors[1] have indicated an eleven year change of the barometer coefficients of the cosmic ray neutron monitors. Since there was no unique technique for determing the coefficient, the results obtained by different authors may be different. We developed a systematic method to examine the barometer coefficient[2-4] and clarified the solar cycle variation of the barometer coefficient more precisely.

To evaluate the barometer coefficient of neutron monitor, it is necessary to separate strictly the cosmic ray intensity variation induced by the primary cosmic ray variation from the one caused by the atmospheric pressure variation. For this purpose, we used the results obtained by the spherical harmonic analysis[5] which is performed on the basis of the neutron monitor records from around twenty stations at high latitudes where the cutoff rigidities Rc's are below 2.3 GV.

2. Residual barometer coefficient

The difference ΔI_p between the pressure corrected neutron monitor data I_p (percentage value) and the estimated neutron intensity $\overline{Y}$ calculated from the spherical harmonic analysis is expressed as

$$\Delta I_p = I_p - \overline{Y}.$$

This subtraction enables to eliminate the effect of the intensity variation of the primary cosmic rays outside the magnetosphere. The

residual barometer coefficient $\Delta\beta$ is obtained as a linear regression coefficient by the statistical analysis of correlation be tween the pressure p and the diffrednce ΔI_p . Results of $\Delta\beta$ for the period, from 1966 to 1977 are presented in the reference(4). The corrected pressure coefficient β_{cor} is derived according to the equation

$$\beta_{cor} = \beta_o + \Delta\beta,$$

where β_o is the reported barometer coefficient from each station.

3. Solar cycle variation of the barometer coefficient

Figure 1 shows the year-to-year variation of cosmic ray intensity $\bar{I}$ and barometer coefficient $\bar{\beta}$. where $\bar{I}$ and $\bar{\beta}$ are the averages of yearly mean data of eight stations (Alert, Deep River, Goose Bay, Inuvik, Kerguelen, Kiel, Oulu and Sanae) where the continuous data are available through twelve years from 1966 to 1977. Mean intensity of neutron component $\bar{I}$ is normalized to 100 percent at the point of the year 1966. C_0 is the yearly mean value of the isotropic component of spherical harmonic coefficients and normalized to the value of 1966, but plotted 4% higher level, and Rz, the sunspot number which is an index of solar activity is plotted inversely.

In order to investigate the solar modulation of barometer coefficient, we analyzed the relation between the barometer coefficient and the cosmic ray intensity. Figure 2 shows the relation between the barometer coefficient $\bar{\beta}$ and the cosmic ray intensity $\bar{I}$. The linear regression coefficient throughout the whole period is $\alpha_\gamma = (1.83 \pm 0.24) \times 10^{-3}$ mmHg with a correlation coefficient, r=0.92.

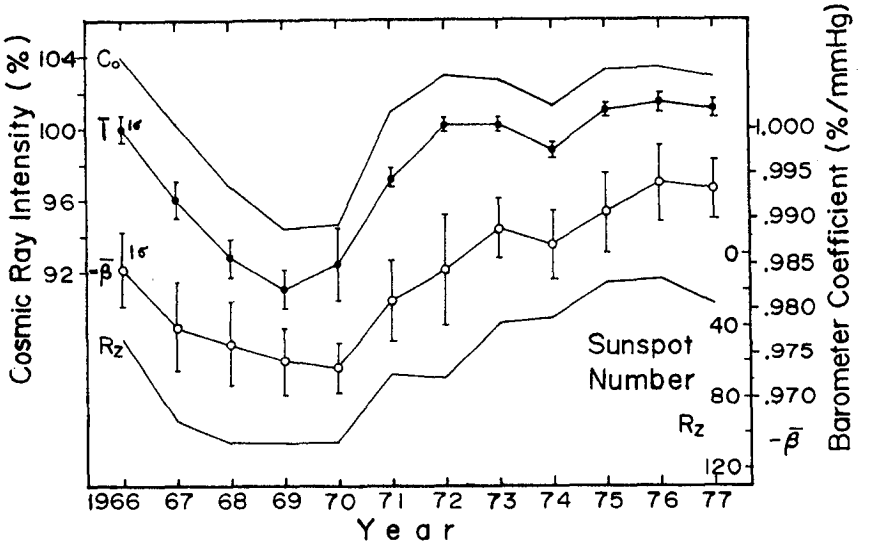

Fig.1. The yearly variation of C_0: the isotropic component of the spherical harmonic coefficients. $\bar{I}$: cosmic ray neutron intensity and $\bar{\beta}$ barometer coefficient, they all are averages of eight stations and error bars indicate the scatter of individual station, and Rz: the sunspot number.

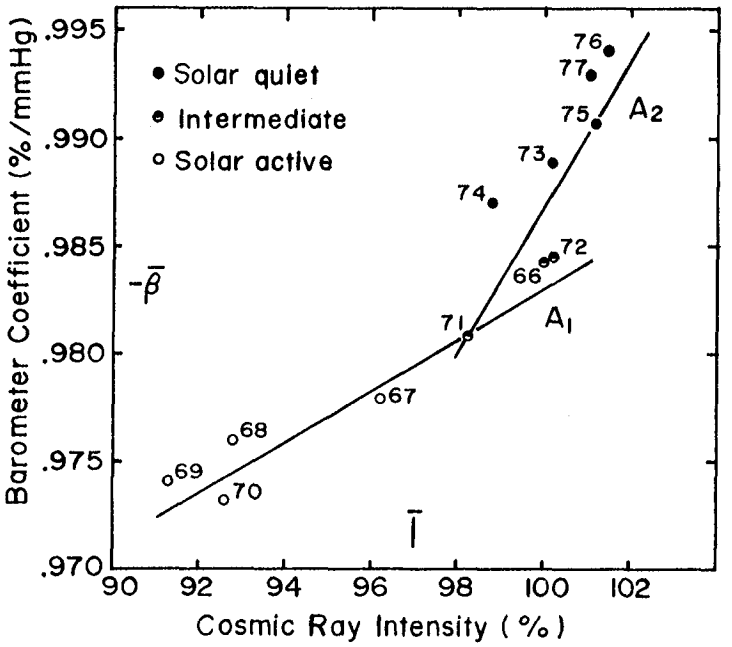

Fig.2. Relation between the barometer coefficient and cosmic ray intensity variations. Lines A_1 and A_2 represent the linear regression line between the barometer coefficient and the cosmic ray intensity in the solar active and the solar quiet period respectively.

4. Relation between the barometer coefficient and the cosmic ray primary spectrum variation

In a previous paper,[4] it was reported that the variation rate of the barometer coefficient to the cosmic ray intensity is larger in the solar quiet period than in the solar active period. About the quantitative relation between the barometer coefficient variation and primary cosmic ray rigidity spectrum, an analysis is performed. The present report is concerned with the numerical calculation to clarify the relation between the barometer coefficient and the cosmic ray primary spectrum variation.

We calculated the variation rate of the barometer coefficent α_γ which is defined as $\alpha_\gamma=\delta\beta/\delta I$. The ratio $\delta J/J_o$ represents the variation of the primary cosmic radiation. For a primary variational spectrum, we assumed as

$$\frac{\delta J(R)}{J_o(R)} = \begin{cases} AR^{-\gamma} & for \quad R \leqq Ru \\ 0 & for \quad R > Ru \end{cases}$$

The calculations[6,8] were performed for several different values of power γ, where A=constant and Ru = 40GV are assumed. The curve in Fig.3 represents the distribution of α_γ, where γ = 1.7 is assumed. It is clearly illustrated by the changes in the cutoff rigidity and in the primary spectrum. As for the computation of α_γ when the solar activity is high, it is necessary to estimate the rigidity dependence of barometer coefficient.

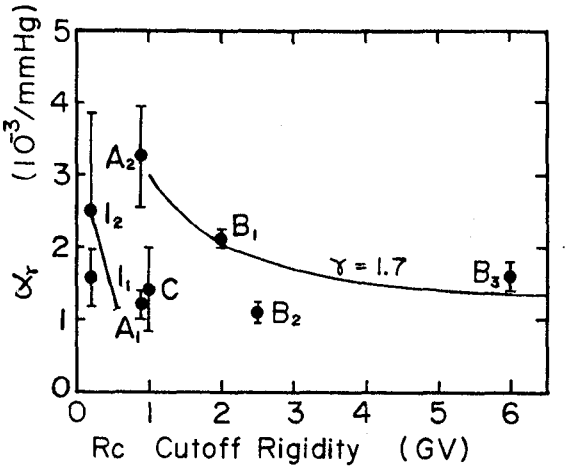

Fig.3. Distribution of α_γ is plotted in absolute value. The abscissa is the cutoff rigidity, where the neutron monitor is located, or the mean rigidity at several stations. Curve represents the distribution of α_γ, which is the result of numerical calculation[8], where γ=1.7 is assumed. A_1 and A_2 (Averages of eight high latitude stations)[4]; I_1 and I_2 (Inuvik)[7]; B_1, B_2 and B_3 (Averages of several stations)[9]; C(Deep River)[10].

6. Acknowledgments

We are indebted to the investigators of the cosmic ray stations for supplying us valuable data through the World Data Center C2 for Cosmic Rays Tokyo by the courtesy of Dr. M. Wada. We are grateful to the staffs of the Division of Electronic Computers of the Institute of Physical and Chemical Research. Numerical calculations were performed mainly on a FACOM 270-30 computer.

References

1) For instance, J. L. Kamphouse, (1968), J. Geophys. Res., **68**, 5608; W. K. Griffiths *et al.*, (1968), Canad. J. Phys., **46**, S1041; M. V. Alaniya *et al.*, (1970), Acta Phys. Acad. Scient. Hungaricae, **29**, Suppl. 2, 605; and the references therein.
2) Ogita, N. *et al.*, (1973), *Proc. 13th Int. Cosmic Ray Conf., Denver*, 2, 831.
3) Kusunose, M. *et al.*, (1981), *Proc. 17th Int. Cosmic Ray Conf., Paris*, **10**, 281.
4) Kusunose, M., (1984), J. Phys. Soc. Japan, **53**, 4488.
5) Yoshida, S. *et al.*, (1971), J. Geopys. Res., **76**, 1.
6) Belov, A. V. and L. I. Dorman, (1979), *Proc. 16th Int. Cosmic Ray Conf., Kyoto*, **4**, 310.
7) Kusunose, M., (1984), Mem. Fac. Sci., Kochi Univ., **6**, Ser. B, 15.
8) Kusunose, M., (1984), Mem. Fac. Sci., Kochi Univ., **6**, Ser. B, 21.
9) Bachelet *et al.*, (1971), Nuovo Cimento, **11 B**, 1.
10) Carmichael *et al.*, (1972), *Proc. 12th Int. Cosmic Ray Conf., Hobart*, 3, 887.

ATMOSPHERIC EFFECTS ON THE UNDERGROUND MUON INTENSITY

A.G.Fenton, K.B.Fenton, J.E.Humble and G.B.Hyland
Physics Department, University of Tasmania
Box 252C, G.P.O., Hobart, Tasmania, Australia, 7001

1. Introduction. We have previously reported that the barometric pressure coefficient observed for muons at Poatina (vertical absorber depth 357 hg cm^{-2}) appears to be appreciably higher than would be expected from atmospheric absorption alone, e.g., Lyons et al. (1981). We have explored the possibility that the effect is due to an upper atmospheric temperature effect arising from an inverse correlation of surface pressure with stratospheric temperature, but we have been unable wholly to account for the observations by this means. In paper SH 4.4-4 presented to this Conference we refer to a new proportional telescope which has been operating at Poatina since about the beginning of 1983 and which has a long term stability suitable for studying variations of atmospheric origin.

2. New Results. Data from the proportional counter telescope for February to December 1983 have been analysed to obtain the total barometric coefficient, the result being -0.042 ± 0.004 % mb^{-1}. This is in agreement with the value obtained for the years 1972-76 with the smaller GM counter telescopes, namely -0.047 ± 0.002 % mb^{-1} (Lyons et al., 1981). These values are to be compared with the coefficient to be expected on the basis of atmospheric absorption, -0.007 % mb^{-1}.

We plan to carry out a more detailed investigation using upper atmospheric data in conjunction with the muon data obtained with the new telescope, taking advantage of its long term stability to compare directly the results obtained in winter and summer, as well as from year to year.

3. Acknowledgements. We wish to thank the Hydro-Electric Commission of Tasmania and its staff for the excellent facilities provided at Poatina. This work is supported in part by the Australian Research Grants Scheme.

Reference.

Lyons,P.R.A., Fenton,A.G. and Fenton,K.B., (1981), 17th ICRC, Paris, Conference Papers 4, 300.

SH 6.1-5

ALTITUDE VARIATIONS OF COSMIC-RAY SOFT AND HARD COMPONENTS OBSERVED BY AIRBORNE DETECTORS

K.Takahashi, A.Inoue, M.Wada, K.Nishi
The Institute Of Physical and Chemical Research
7-13 Kaga-1, Itabashi, Tokyo 173, Japan

K.Murakami
Cosmic Ray Reseach Laboratory, Nagoya University
Furo-cho, Chikusa-ku, Nagoya 464, Japan

ABSTRACT

The altitude variations of cosmic-ray total and hard components were measured upto 12,000 m on voard a jet liner over Japan island on December ,1981. Observed results together with soft component arepresented conparing with the model calculations through the atmosphere by applying the hardronic cascade.

1. Introduction

Since last two air-borne experiments(1979,1981), the altitude and latitude variation of various components of cosmic rays have been analyzed from various points of view (1),(2). In the analyses, we showed that our results did not contradict with Rossi's (3). And the model calculations through the atmosphere by applying the hadronic cascades were compared with the observed results (4),(5).

We used telescopes composed of two plastic scintillators of thickness of 3 cm ,of which geometric factor was 96 cm^2sr(6).

2. Altitude variation of vertical intesity of hard component

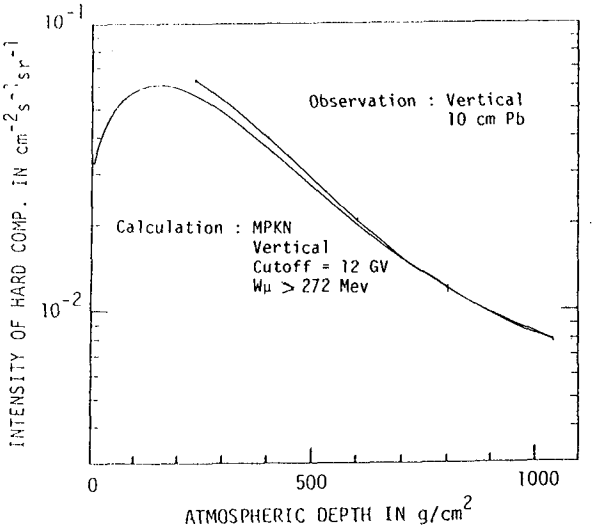

Fig. 1. The observed and calculated integral growth curves of hard components. The calculated curve shows the total of intensities of muons, pions, kaons, and protons. The observation curve is obtained by means of the weighted best fit of the data in 1981.

In Fig. 1 are included the altitude variations of hard component for vertical. The obserbation curve is obtained by means of the weighted best fit of the 41 data points with regard to 4 level flights at the depths of 221, 243, 560, and 1038 g/cm^2, including the ascending and the

descending.

The calculation curve represents the total of intensities of muons, pions, kaons, and protons with threshold energies of 273, 315, 751, and 1260 MeV respectively, at cutoff rigidity of 12 GV.

At the smaller atmospheric depth, it seems that the slight discrepancy exists between the observed and the calculated curve because the observation curve contains some components with high energy other than the calclated four components.

3. Analysis of the total, hard and soft components

In Fig. 2, curve(T) represents the total component measured without lead absorber. The observed total component contains the electronic component of electrons and photons other than the calculated total(H') of muons, pions, kaons,and protons without lead absorber. Curve(H) is the obserbed hard component capable of penetrating 10 cm lead absorber. Curve(S) represents the soft component which are stopped by 10 cm lead, that is to say (S) is the difference between (T) and (H).

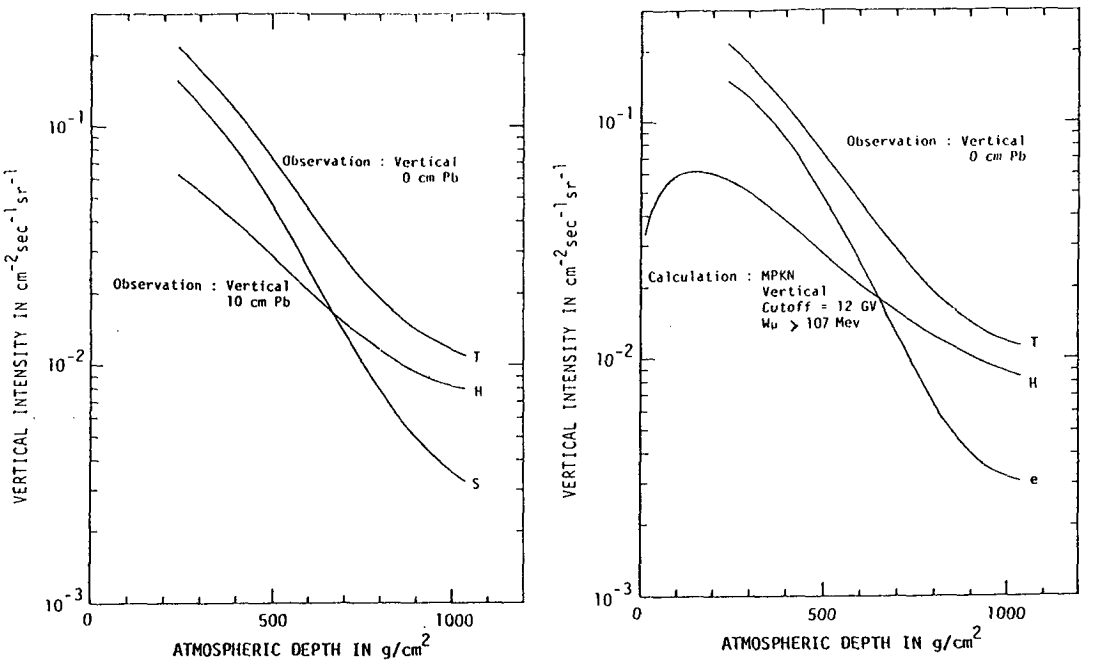

Fig. 2. The vertical intensities of the observed total component(T), of the observed hardcomponent(H), of the soft component(S), of the calculated total like in Fig. 1 (H'), of the (T)-(H') component(e) as a function of atmospheric depth.

We obtained the attenuation curves against the thickness of lead absorber at different altitudes for the vertical component (1979) (1). It is shown in the report that the curves are steeper for smaller thickness than 10 cm of lead and flatter for large thickness. It seems that this is due to the existance of electrons which are easily absorbable.

From what descrived above, we may say that the difference between (T) and (H'), namely (e) represents the electronic component. The energy of electrons are greater than nearly 10 MeV.

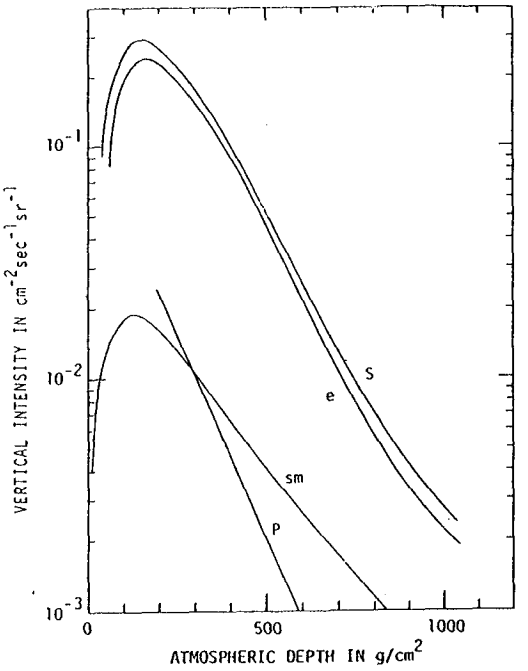

Fig. 3. Analysis of the soft component by B.Rossi. The curves represent vertical intensities as a function of atmospheric depth for slow mesons with momenta smaller than $3 \cdot 10^8$ eV/c (sm), proton (or other charged N-rays) with momenta between $4 \cdot 10^8$ eV/c and 10^9 eV/c (p), electrons of practically all energies above 10^7 eV (e).

Fig. 3 shows analysis of the soft component by B.Rossi (3). At small depth, there are enhancements of (s) and (e) by Rossi compared with ours. It may be caused by a enhancement of low energy electron at high latitude greater than 45°.

At atmospheric depth of 600 g/cm^2, the attenustion meanfree pathes for (s) and (e) by Rossi and us are nearly equal to 140 g/cm^2.

As mentioned above, it seems that the total,hard,soft,and electronic components are able to be explained by means of combining the observed result with the calculated one.

Reference

(1). Takahashi, K. (1979) Conf. Papers 16th ICPC, 4, 342.
(2). Takahashi, K. et al. (1983) Conf. Papers 18th ICRC, 10, 218.
(3). Rossi,B. (1948) Rev. Mod. Phys., 20, 537-583.
(4). Murakami, K. et al. (1979) Nuovo Cimento 2C, 635.
(5). Murakami, K. et al. (1981) Rep. CRRL, Cosmic-Ray Res. Lab. Nagoya Univ. No. 6.
(6). Takeuch, H. (1982) Sci. Papers IPCR, 75, 1.

ADDITIONAL FLUX OF PARTICLES AND ALBEDO-ELECTRONS IN UPPER ATMOSPHERE

Aitbaev F.B., Dyuisembaev B.M., Kolomeets E.V.
Kazakh State University, Timiryazeva St. 46,
Alma-Ata 480121,USSR

The paper presents the results of Monte Carlo simulation of albedo flux from the dense layers of the Earth"s atmosphere and the dependence of angular distribution on the rigidity of geomagnetic cut off and additional flux of particles at the depth in the atmosphere 15-20 g/sm^2.

Figure 1 shows the results of Monte Carlo simulation of albedo-electron fluxes from the dense layers of atmosphere. Influence of geomagnetic field on the propagation of charged particles was not taken into account. One can see that the albedo-electrons at energies more than 10 MeV show anisotropic angular distribution: fluxes of albedo-electrons at zenith angles close to horizon is $\sim$6 times greater than that directed vertically up. The ratio for the albedo-electrons at energies >100 MeV is $\sim$10. Integral energy spectrum within the range 10-100 MeV can not be described by power law function. It results from the fact that electrons produced by products of decay of pions directly contributes importantly to upward albedo. Averaged over zenith angle flux of albedo-electrons at geomagnetic equator at energies more than 10 MeV equals to 120 m^{-2} s^{-1} $ster^{-1}$, at energies more than 30 MeV - 80 m^{-2} s^{-1} $ster^{-1}$, at energies > 100 MeV - 40 m^{-2} s^{-1} $ster^{-1}$.

Analysis of absorption curves of total ionising component obtained during balloon flights at latitude R_c =6,7 GV showed deformation of the depth dependence of cosmic ray intensity in the upper atmosphere (< 90 g/sm^2) after inversion of total solar magnetic field. Deformation of the form of the absorption curves (Table 1) one can explain by appearance additional flux of low energy particles.

Excluding variations produced by solar activity we reveal expected fluxes of abovementioned particles. Figure 2 shows dependence of additional flux on the depth for 1975. One can see that the curve of absorption has maximum at the depth 19-20 g/sm^2 and then drops sharply and at the depth 70 g/sm^2 its value is close to zero. Maximum of additional flux was observed in 1975-1976 at solar activity minimum. Effect was maximal at 15 g/sm^2 depth and was equal to 13%. Effect takes place in 1982-1983 that is after inversion of total solar magnetic field in 1979-1980 (Aitbaev et al., 1983) but its value is 2,3 times smaller than that in 1975.

Let's consider possible nature of the observed flux of low energy particles. First, it can be produced by meteorological effects. Analysis of the variations of barometrical pressure at the various depths in the atmosphere showed that the observed deformation of the form of the absorption curve was not produced by the variation of barometrical pressure.

Analysis of temperature variations at various depthes showed no anomalous change of temperature in the upper atmosphere and as a result no corresponding redistribution of air mass. Secondly, it can be produced by geomagnetic effects. Calculation of the variation of the rigidity cut off due to drift of balloon in the atmosphere over Alma-Ata revealed that maximal variation of counting rate produced by the factor did not exceed 0.3%. Analysis of the data on the variation of rigidity during magnetic storms in Alma-Ata region did not show possibility to attribute the observed flux of particles to the variation of cut off rigidity during magnetic storms. Third it can be produced by arrival to Alma-Ata of singly ionized atoms of < CNO > group. Calculations showed that the flux of the atoms allowed to explain additional flux of singly ionized atoms above 20 particles/ $m^{-2} s^{-1} ster^{-1}$. In order to discover the flux it is necessary to perform experiment,but experiment of the kind

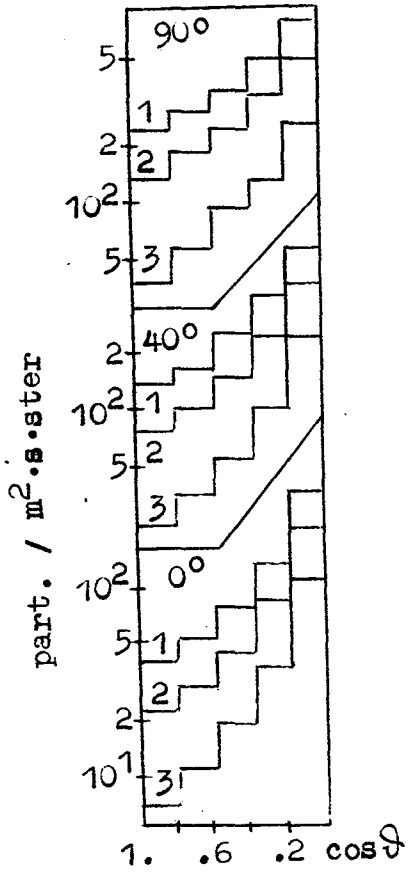

Figure 1. Dependence of electron albedo intensity at energies 10, 30, 100 MeV (histograms 1, 2, 3, correspondingly) at various geomagnetic latitudes on zenith angle.

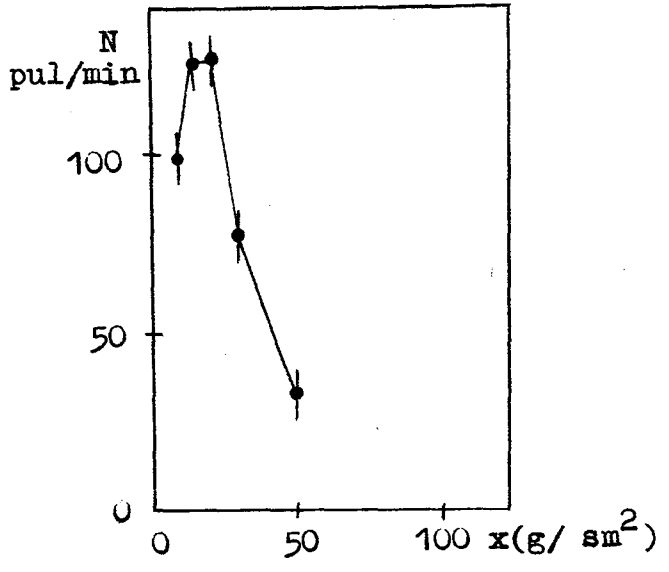

Figure 2. Absorption curve of additional flux of low energy particles (The data on of single counters obtained over Alma-Ata in 1975).

has not been made at the boundary of atmosphere.

Table 1. Annual means of counting rate of single counter calibrated to the maximum of absorption curve

Year	Depth in the atmosphere (g/sm^2)				
	10	15	21,5	30	50
1966	0,5487	0.6234	0.6890	0.7911	0.9309
1967	0.5586	0.6143	0.6920	0,7949	0.9282
1969	0.5420	0.6166	0.6799	0.7877	0.9271
1975	0.6200	0.6936	0.7730	0.8436	0.9497
1976	0.6182	0.6850	0.7655	0.8371	0.9465
1977	0.6191	0,6935	0,7725	0,8430	0.9442
1978	0.6098	0.6844	0.7593	0.8344	0.9460
1979	0.5831	0.6498	0.7324	0.8159	0.9355

R E F E R E N C E

Aitbaev F.B., Dyuisembaev B.M., Erkhov V.I., Likhoded V.A., Stekol'nikov N.V. Proc. 18th ICRC, 1983, v.10,p. 18-21.

OBSERVATION OF ENERGY SPECTRUM OF ELECTRON ALBEDO IN LOW LATITUDE REGION AT HYDERABAD, INDIA.

Verma S.D. and Bhatnagar S.P.
Department of Physics, Gujarat University
Ahmedabad 380 009, INDIA

ABSTRACT

We present the preliminary results of the measurement of the energy spectrum of low energy (5-24 MeV) albedo electrons, moving upward as well as downwards, at about 37 km (~ 4 mb) altitude, over Hyderabad, India, in low latitude region. The flux and energy spectrum was observed by a bi-directional, multidetector charged particle telescope which was flown in a high altitude balloon on 8th December 1984. Results based on a quick look data acquisition and analysis system are presented here.

1. Introduction: The pioneer work of measurement of the flux and energy spectrum of electron and proton albedo was done at high altitude region over Palestine, Texas (Verma 1967) at high energies (20-1000 MeV). In low latitude region the flux of these albedo is expected to be somewhat less (Bhatnagar and Verma, 1983; Kothari and Verma, 1983) but larger at lower energies (5-40 MeV). In the present experiment measurements of low energy (5-24 MeV) Splash and Re-entrant albedo electron spectrum over Hyderabad at 4 mb altitude are reported. Details of the experimental set up and balloon flight are given by Verma et al (1985), for completeness a brief description is given in the next section.

2. Experimental Set-up: A multi detector charged particle telescope (Verma et al 1985) capable of observing simultaneously upward and downward moving singly charge particle (e,μ,p) was used. This telescope is shown in Fig.1. All particles incident on the telescope from above as well as below, and stopping in the central NaI (Tl) total energy detector C were selected for the present work. The arrival direction of the stopping particles was broadly known with the help of two sets of

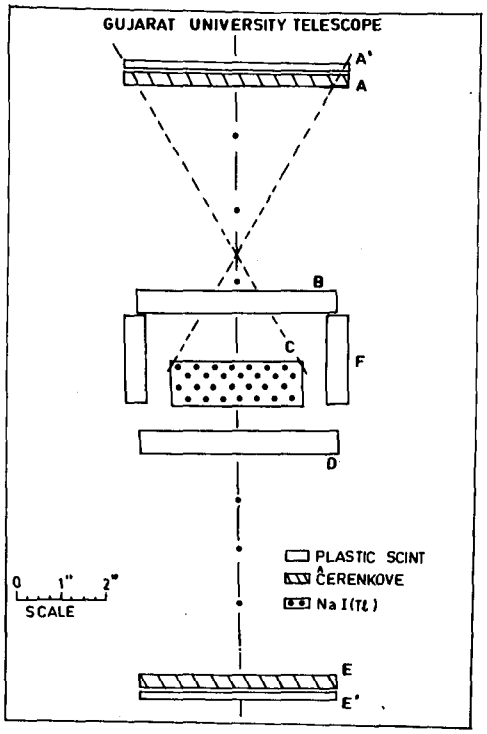

Fig.1

plastic scintillator detectors A B and D E in a combination such as AB C $\overline{DE}$ for downward and $\overline{AB}$ C DE for upward arriving particles. Cerenkov detectors A' and E' were used to identify relativistic electron among stopping singly charged particles. Pulses from total energy detector C and dE/dX detectors B and D were pulse height analysed event by event.

3. Energy Calibration: Various thin plastic detectors were tested using cosmic ray muons present at ground level. The total energy detector C was calibrated with γ-ray sources (e.g. Cs^{137} and Co^{60}) and mono-energetic electron beam of ~ 8 MeV of Microtron of the Department of Physics, Poona University, Poona, India. Cosmic Ray muons and gamma ray sources were also used to test, calibrate and for constant monitoring and preflight check out of various detectors of charged particle telescope. A linear pulse generator was used to test linearity and stability of B, C, D detectors, its electronics and corresponding A/D convertors. Thus all the three P.H.A.'s were calibrated as well as checked for continuous operation for several weeks.

Whole system of CPT and flight electronics was taken through a temperature cycle in completely operating condition and it was found to have practically no drift of muon peak between 15°C and 25°C. Various data matrices were recorded and printed out time to time by quick look system. During these tests and long duration tests singles and coincidence rates, as well as peaks of muon P.H. distributions were monitored which were observed to be quite stable.

4. Data Analysis and Results: A typical two-dimensional pulse height distribution for downward incident is shown in Fig.2. In this the

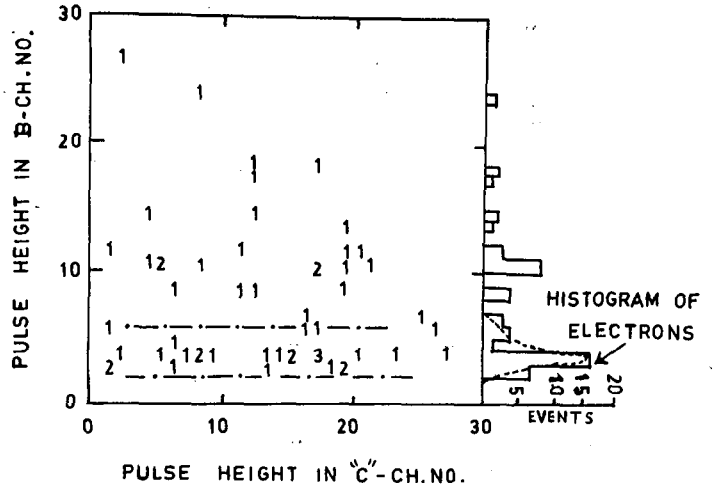

Fig. 2

channel number proportional to the energy deposited in thin detector B' is plotted vs channel number corresponding to energy observed in total energy detector C . Lines in the figure indicates expected track for stopping electrons. Histogram shows a clear peak for electrons. Energy observed in C is converted to the incident energy of the electrons. The events shown in the figure are part of sample of data recorded by quick look display and analysis system (Verma et al 1985). Using the event rate recorded, the geometrical factor (~ 13 cm^2 ster.) of the charged particle telescope and the two-dimensional matrix of stopping electrons shown in Fig.2 the flux and the energy spectrum of down moving low energy electrons were obtained. In the Fig.3 circles represent the flux and the spectrum of re-entrant albedo electronsat balloon altitude of ~ 4 mb in low latitude region, over Hyderabad, India, observed on 8th December 1984. Similarly squares represents the energy spectrum of splash albedo electrons.

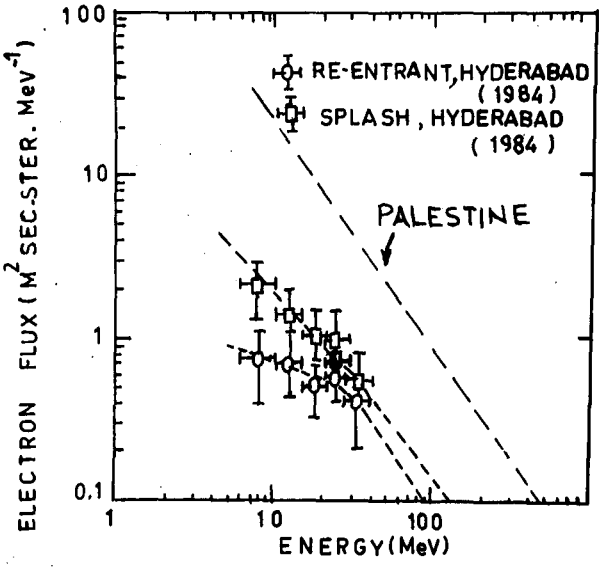

Fig.3

Lines shown in the figure are spectra observed over Palestine, Texas (Verma 1967).

5. Acknowledgement: Authors are thankful to ISRO for providing funds under Respond Program to fabricate Balloon payload and to carry out experiment in a high altitude balloon from Hyderabad. We are also thankful to UGC for providing funds for basic facilities and laboratory equipment to design, test and calibrate space science experiments. Thanks are also due to Dr. V.N. Bhoraskar and his senior and junior colleagues for providing mono energetic electron beam for energy calibration at Department of Physics, Poona University, Poona, India (1981). Thanks are due to Dr. P. Shea (Air Force Geophysical Lab., U.S.A.) for providing NaI(Tl) crystal, and Shri Vikram Shah for help (Metro, Kalol, India) in fabrication work. Thanks are also due to Dr. (Mrs.) Vijaya Sinha for discussions and reading the manuscript.

References

Bhatnagar S P & Verma S D, 17th ICRC, L, p. 266, (1981).

Bhatnagar S P & Verma S D , 18th ICRC, Bangalore, 3, p. 501, (1983).

Kothari S K & Verma S D, 18th ICRC, Bangalore, 3, p. 483, (1983).

Verma S D, Jr. Geop. Res. 72, 915, (1967).

Verma S D, Jr. Radio & Sp. Phys., 6, 171, (1977).

Verma S D, Bhatnagar S P & Kothari S K, 19th ICRC (HE-7), La Jolla, USA, (1985).

PROTON ALBEDO SPECTRUM OBSERVATION IN LOW LATITUDE REGION, AT HYDERABAD, INDIA

Verma S.D. and Kothari S.K.
Department of Physics, Gujarat University
Ahmedabad 380 009, INDIA

Abstract

The flux and the energy spectrum of low energy (30-100 MeV) proton albedos, have been observed for the first time in a low latitude region, over Hyderabad, India. The preliminary results, based on the quick look data acquisition and display system are presented. A charged particle telescope, capable of distinguishing singly charged particles such as electrons, muons, protons in low energy region, records the data of both upward as well as downward moving particles. Thus spectra of splash and re-entrant albedo protons have been recorded simultaneously in a high altitude Balloon Flight carried out on 8th December, 1985, over Hyderabad, India. Balloon floated at an altitude of ≈ 37 km (4 mb).

1. Introduction: The presence of low energy charged particles (albedo) among cosmic rays below the geomagnetic cut-off rigidity, have been predicted by Treiman (1953). However, systematic measurement of the flux and the energy spectrum of the albedos has been made by Verma (1967) at high altitudes, over Palestine, Texas. Large number of these are electrons, while protons are less in intensity. These measurements of proton albedos have been extended to high energies over same location upto thousands of MeV by Pennypacker et al (1973). It is expected that the spectrum of these albedo protons has a negative exponent. It is also expected, as shown by Kothari and Verma (1983) that the spectrum of albedos will be similar in low latitude regions such as Hyderabad, India. The flux however is higher at low energies. Next section describes briefly an experiment in which low energy proton albedo spectrum has been measured in low latitude region over Hyderabad, India.

2. Experiment: The flux and energy spectrum of upward moving splash albedo and downward moving re-entrant albedo protons have been first time

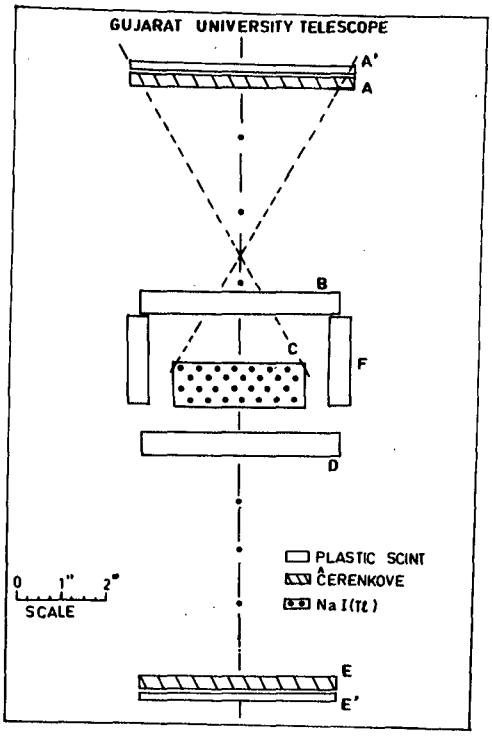

Fig.1

observed in 30-100 MeV energy interval in low latitude region at an altitude ≃ 37 km (≃ 4 mb), above Hyderabad, India. A bi-directional charged particle telescope, described in detail by Verma et.al. (1985), consisting of a total energy NaI(Tl) crystal detector, plastic scintillator and Lucite Cerenkov counters, was used for these observations. This telescope is shown in Fig.1. It has geometric factor ≃ 13 cm^2 Ster. It is capable of separating relativistic electrons from slow moving protons and muons, stopping in NaI(Tl) crystal detector 'C'. All charged particles, incident from upward and downward directions on the telescope and stopping in the NaI(Tl) total energy detector 'C', were selected for the present work. For the downward incident particles plastic scintillator 'B' was used as energy loss detector and D, F were used as anticoincidence counters. Similarly for upward moving particles scintillator 'D' was used as energy loss detector and B, F were used as anti-coincidence counters.

3. Calibration: Pulse amplitudes of B, C and D detectors are digitised by A/D convertors and recorded event by event (Verma et.al. 1985). The energy calibration of these detectors is done using ground level cosmic ray muons. These muons pass through the telescope and are registered as penetrating events. Their energy loss in B, C and D is well known from standard particle data book (Berger and Seltzer, 1966).

4. Data Analysis and Results: The proton flux measurement has been done for the energy range approximately 30 MeV to 105 MeV, both for upward and downward moving protons. A two-dimensional pulse height distribution for particles stopping in energy detector 'C' is shown in Fig.2, for upward

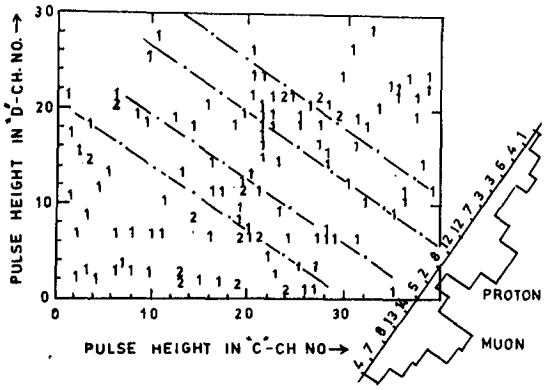

Fig.2

moving particles. The events shown in the Figures are taken during float altitude from quick look data analysis system. The histogram obtained by integrating along the track clearly gives protons and muons peaks both for upward and downward moving particles.

The flux observed for 4 different energy intervals is plotted in Fig.3 for upward moving particles. Triangles represent the flux for present observation of the re-entrant and splash albedo protons at balloon altitude of 4 mb in low latitude region over Hyderabad, India. The squares show the spectrum observed for Palestine, Texas, USA. The flux at Hyderabad, India, is lower for both re-entrant and splash albedo protons than at Palestine, Texas, as expected. The spectrum has a negative slope on a log-log graph, similar to that observed over Texas. The spectra of re-entrant albedo protons (Fig.3a) agree well with calculated spectrum. However, the flux and spectrum of splash albedo protons is somewhat higher than the calculated spectrum (Fig.3b). Data analysis with improved statistics to see if this trend persists, is under way.

Fig.3 *a*

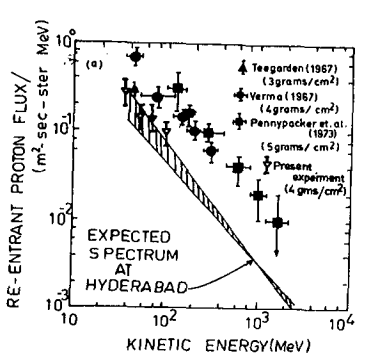

Acknowledgement: Authors are thankful to I.S.R.O. for providing funds to fabricate balloon from Hyderabad. We are also thankful to U.G.C., India, for providing funds for basic facilities and laboratory equipment to design, test and calibrate space science experiments. Thanks are also due to Dr. V.N. Bhoraskar and his senior and junior colleagues for providing

mono-energetic electron beam for energy calibration at Department of Physics, Poona University, Poona, India (1981). Thanks are due to Dr. P. Shea (Air Force Geophysical Laboratory, U.S.A. for providing NaI(Tl) crystal, and Shri Vikram Shah (Metro, Kalol, India) for help in fabrication work. Thanks are also due to Dr. (Mrs.) Vijaya Sinha for discussing and reading the manuscript.

References:

Berger M.J. and Seltzer S.M. NASA Report, NASA SP-3036 (1966).

Bhatnagar S P and Verma S D, 17th ICRC SH.9, 1124, L, p.266 (1981).

Bhatnagar S P and Verma S D, 18th ICRC 3, p.501 (1983).

Kothari S K & Verma S D, 18th ICRC, Bangalore, India (1983)

Pennypacker C.R., Smoot G.F., Buffington A., Muller R.A., and Smith L.H., Jr. Geophys. Res.78, 1515 (1973).

Treimen S.B., The Cosmic Ray Albedo, Phys.Rev., 91, 457 (1953).

Verma S D, Jr. Geophy. Res. 72, 915 (1967).

Verma S D, Jr. Radio & Sp. Phys., 6, 171 (1977).

Verma S D, Bhatnagar S P & Kothari S K, 19th ICRC HE-7, to be held in San Diego, California, USA, in August (1985).

Fig 3.b

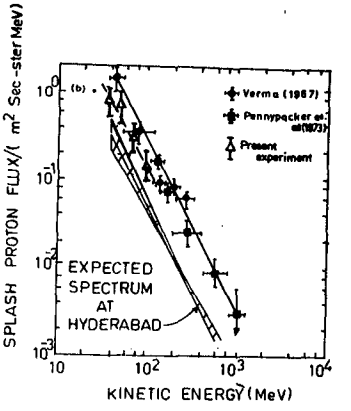

THE INFLUENS OF QUIET ASYMMETRIC MAGNETOSPHERE ON THE CUTOFF RIGIDITIES OF THE MAIN CONE

Tyasto M.I., O.A.Danilova
LOIZMIRAN, 2 line, Leningrad 199053
U S S R

1. Introduction. Some earlier studies (1-4) show that cutoff rigidities of cosmic-ray particles in the model magnetospheric fields of internal and external sources have daily variations caused by asymmetry of the magnetic field due to the currents induced at the magnetopause and tail currents.

The purpose of this paper is to examine cutoff rigidities of the charged particles coming down at the middle latitudes. The mathematical model that is used to specify the geomagnetic field for this investigation is due to Tsyganenko and Usmanov (5). This model of the magnetospheric field is based on the merged IMP-HEOS experimental data set and includes all known at the present time current systems of the magnetosphere: magnetopause, ring, magnetotail currents. Being based upon experimental data, this model implicitly takes into account the magnetic effect of field-aligned currents. Moreover this model includes the effects of changes in the tilt angle of the geodipole to the Sun-Earth line (Ψ) within the limits from -35° up to $+35^{\circ}$ according to annual and daily variations. A separate account of the contribution from different magnetospheric current systems has made it possible to track the Kp - dependence of their main physical parameters.

2. Methods. The suitable methods of trajectory calculations are to be described by Shea and Smart in (6). The trajectory-tracing of cosmic-ray particles is performed by the Gill modification (7) of the Runge-Kutta iteration method applied to the equation for charged particle motion

in a magnetic field:

$$\ddot{\bar{r}} = \frac{em}{c} \dot{\bar{r}} \times \bar{B}$$

The trajectory calculations has been performed for the particles with rigidities ranging from 750 Gv to the first forbidden trajectory with the step size of 0.01 Gv at the cosmic-ray stations Moscow, Irkutsk and Noricura in the superquiet conditions (Kp=0). A trajectory has been considered as forbidden if either 30 000 steps were not enough for a particle to pass beyond the sphere of the radius equal to 25 Earths radii or it returned to the Earth. The last allowed trajectory corresponding to main cone cutoff (1-2) was taken as the threshold rigidity.

3. Results and discussion. Cutoff rigidities were obtained for three Earths orbital positions (summer and winter solstice and equinox). Displaying the results of calculations one can see (Fig. 1) that the duirnal variation of the cutoff rigidities at the stations Irkutsk and Noricura have rather regular character with the maximum corresponding to the morning hours (9^h-12^h) and minimum in the evening (20^h-22^h). The time of the maxumum and minimum don't change appreciably throughout the year but the curve for the station Noricura has an additional maximum at the 18^h on the 22 of december. Diurnal variations for the station Moscow do not have such regular character. As the Fig. 1 shows the cutoff rigidity daily oscillation amplitude is greater for stations with lower cutoff rigidities. For example, the amplitude is 0.15 Gv and 0.02 Gv at the station Moscow and Noricura respectively. One can observe a certain variation of the differences between the maximum and minimum values of cutoff rigidities when the angle Ψ changes. These differences are maximal in summer and amount to 5%, 1.5%, 0.25% of the mean cutoff rigidity value for the stations Moscow, Irkutsk and Noricura respectively. The amplitude of the cutoff rigidity decreases by almost one half of that

quantity at the equinox. The latter result agrees with the Fig.4 of (8) showing that the cutoff rigidity daily variation (which is defind in (8) in the same manner as in the present study according to the last allowed trajectory) observed at the high-latitude station College (Alaska) is greater in summer than in winter or at the equinox.

4. Conclusions. Thus even in the superquiet periods (Kp= 0) the magnetosphere asymmetry causes the daily variations of cutoff rigidities at the middle-latitude stations which are expected to bring the greatest contribution to the observed daily variation of the cosmic- ray neutron intensity about 0.25% at the sea level station Irkutsk and 0.2% at the mount station Noricura.

References

1. Flückiger O.E. et al, (1981), On the effect of magnetospheric current systems on cosmic-ray cutoff rigidities., 17 Int. Cosmic Ray Confer., Paris, v.4, p.244-247

2. Flückiger O.E., (1982), Effects of asymmetric magnetosphere currents on cosmic radiation., AFGL - TR -82-0177

3. Smart D.F., et al, (1969), The daily variation of trajectory-derived high-latitude cutoff rigidities in a model magnetosphere., J. Geophis. Res., v.74,p.4731

4. Gall R., et al, (1971), The daily variation., Space Res., v.11

5. Tsyganenko N.A., A.V.Usmanov, (1982), Determination of the magnetospheric current system parameters and development of experimental geomagnetic field models based on data from IMP and HEOS satellites., Planet. Space Sci., v.30, p.985-998

6. Shea M.A., et al, (1976), Summary of cutoff rigidities calculated with the IGRF model for various epochs., ERP, NO 561, AFCRL-TR- 76-0115

7. Gill S., (1951), A process for the step-by-step integration of differential equations in automatic digital compu-

ting mashine., Proc. Cambridge Phil. Soc., v.47,p.47-96

8. Bravo S., (1981), The tilt effect on cutoff., Geophis. Internat., v.20-2, p.121-128

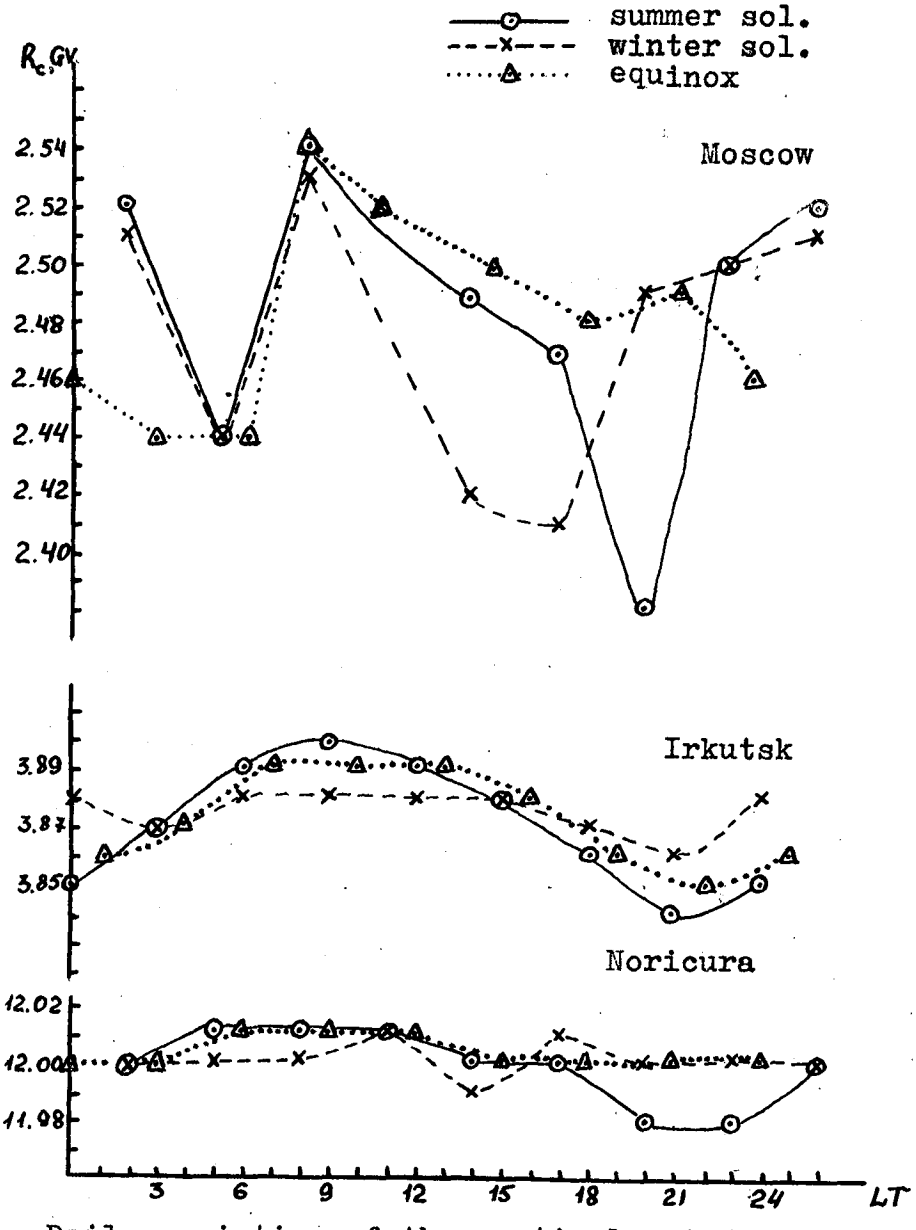

Fig.1. Daily variation of the vertical cutoff rigidities in the magnetospheric field according to the model of Tsyganenko-Usmanov (5).

RE-EVALUATION OF COSMIC RAY CUTOFF TERMINOLOGY

D. J. Cooke[1], J. E. Humble[2], M. A. Shea[3], D. F. Smart[3], N. Lund[4], I. L. Rasmussen[4], B. Byrnak[4], P. Goret[5], N. Petrou[5]

ABSTRACT

The study of cosmic ray access to locations inside the geomagnetic field has evolved in a manner that has led to some misunderstanding and misapplication of the terminology originally developed to describe particle access. This paper presents what is believed to be a useful set of definitions for cosmic ray cutoff terminology for use in theoretical and experimental cosmic ray studies.

1. Introduction. Early work on cosmic ray motion in axially symmetric representations of the field (Stormer, 1930; Lemaitre and Vallarta (1936a, b) was limited to analytic considerations. More recent studies, which rely on digital computer calculations of charged particle trajectories in high order mathematical representations of the field (Shea et al., 1965) emphasize the study of access to locations within the geomagnetic field as a function of particle rigidity, in contrast to the earlier studies which examined the broader directional access picture. The terms used in the early work to refer to the access regions were carried over into the numerical computations, although often in an imprecise way. Whereas the early theoretical workers viewed access conditions in what may be called a "direction picture", describing the directions from which particles of a specified rigidity could or could not arrive, the later computer calculations have usually used a "rigidity picture" in which accessibility is considered as a function of particle rigidity in a single arrival direction. The use of the old geometrical terms, appropriate to the direction picture, has caused considerable confusion in rigidity picture studies.

A re-examination of the characteristics of the access regions distinguished by Stormer and by Lemaitre and Vallarta, together with a comparison between the properties of these analytically distinguished regions and those detected by the digital computer method has resulted in definitions which, it is hoped, will meet present needs.

2. Definitions. The definitions required may conveniently be subdivided by viewpoint, as indicated in Table 1. The list is not exhaustive, but seeks to portray the most useful quantities in each situation.

1. Physics Dept., University of Utah, Salt Lake City, Utah 84112, USA
2. Physics Dept., University of Tasmania, Hobart, Tasmania, Australia 7001
3. Air Force Geophysics Laboratory, Hanscom AFB, Bedford, MA 01731, USA
4. Danish Space Research Inst., Lundtoftevej 7, DK-2800, Lyngby, Denmark
5. Sect. d'Astrophys., Centre d'Etudes Nucl. de Saclay, Saclay, France

TABLE 1.

Summary of terms used in cutoff calculations. Quantities describing phenomena which are equivalent in both pictures are listed on the same line.

Direction Picture	Rigidity Picture
	Cutoff Rigidity
Allowed Cone	
Main Cone	Main Cutoff Rigidity
	First Discontinuity Rigidity
Shadow Cone	Shadow Cutoff Rigidity
Penumbra	Penumbra
Penumbral Band	Penumbral Band
	Primary Band
Stormer Cone	Stormer Cutoff Rigidity
Forbidden Cone	
	Upper Cutoff Rigidity
	Lower Cutoff Rigidity
	Horizon Limited Rigidity
	Effective Cutoff Rigidity
	Estimated Cutoff Rigidity

2.1. Directional Definitions. The following definitions appear to be appropriate for use with the directional picture. Each definition is for charged particles of a single specified rigidity value arriving at a particular point in the geomagnetic field.

Allowed Cone: The solid angle containing the directions of arrival of all trajectories which do not intersect the earth and which cannot possess sections asymptotic to bound periodic orbits (because the rigidity is too high to permit such sections to exist in the directions of arrival concerned).

Main Cone: The boundary of the allowed cone. The main cone is constituted in part by trajectories which are asymptotic to the simplest bound periodic orbits and in part by trajectories which graze the surface of the earth. (For this purpose the surface of the earth is generally taken to be at the top of the effective atmosphere.)

Forbidden Cone: The solid angle region within which all directions of arrival correspond to trajectories which, in the absence of the solid earth, would be permanently bound in the geomagnetic field. Access in these directions from outside the field is, therefore, impossible.

Stormer Cone: The boundary of the forbidden cone. In an axially symmetric field the surface forms a right circular cone.

Shadow Cone: The solid angle containing all directions of particle arrival which are excluded due to short range earth intersections of the approaching trajectories while loops within the local field line bundle are being traversed.

Penumbra: The solid angle region contained between the main cone and the Stormer cone. In general the penumbra contains a complex structure of allowed and forbidden bands of arrival directions.

Penumbral Band: A contiguous set of directions of arrival within the penumbra, the members of which are either all allowed or all forbidden.

2.2. Rigidity Picture Definitions. The following definitions are proposed as being applicable to the rigidity picture. Each definition refers to particles arriving at a particular site within the geomagnetic field from a specified direction.

Cutoff Rigidity: The location of a transition, in rigidity space, from allowed to forbidden trajectories, as rigidity is decreased. Unless otherwise defined, the value normally quoted in representing the results of computer calculations is, for practical reasons, the rigidity of the allowed member of the appropriate juxtaposed allowed/forbidden pair of trajectories computed as part of a spaced series of traces. Sometimes the term is employed to refer to the location of a notional transition from one region to another, for example at the Stormer cone, where an allowed trajectory may not perhaps exist at all.

Main Cutoff Rigidity, R_M: The rigidity value at which the direction concerned is a generator of the main cone as defined in the "direction picture". The associated trajectory is either one which is asymptotic to the simplest bound periodic orbit, or (owing to the presence of the solid Earth) is one which is tangential to the earth's surface.

First discontinuity rigidity, R_1: The rigidity associated with the first discontinuity in asymptotic longitude as the trajectory calculations are performed for successively lower rigidities, starting with some value within the allowed cone. The value of R_1 is approximately equal to the main cutoff as defined above.

Shadow Cutoff Rigidity, R_{SH}: The rigidity value at which the edge of the shadow cone lies in the direction concerned.

Penumbra: The rigidity range lying between the main and the Stormer cutoff rigidities.

Penumbral band: A continuous set of rigidity values within the penumbra, all members of which have the same general access characteristics, either all allowed or all forbidden.

Primary Band: The stable forbidden penumbral band which is associated with the earth intersection of a low point in the loop which lies at the last equatorial crossing before the trajectory (or its virtual extension in the assumed absence of the earth) takes on the characteristic guiding centre motion down the local field line bundle.

Stormer Cutoff Rigidity, R_S: The rigidity value for which the Stormer cone lies in the given direction. In a dipole field (and perhaps also in the real geomagnetic field) access for particles of all rigidity values lower than the Stormer cutoff rigidity is forbidden from outside the field. In a dipole approximation to the geomagnetic field, one form of the Stormer Equation gives the Stormer cutoff rigidity, in GV, as:

$$R_S = M \cos^4\lambda \,/\, \{ r^2 [1 + (1 - \cos^3\lambda \cos A \sin Z)^{1/2}]^2 \}$$

where M is the dipole moment and has a normalized value of 59.6 when r is expressed in units of earth radii, λ is the magnetic latitude, r is the distance from the dipole in earth radii, A is the azimuthal angle measured clockwise from the geomagnetic east direction (for positive particles), and Z is the angle from the local magnetic zenith direction.

Upper Cutoff Rigidity, R_U: The rigidity value of the highest detected allowed/forbidden transition among a set of computed trajectories. The upper cutoff rigidity can correspond to the main cutoff if and only if no trajectories asymptotic to bound periodic orbits lie at rigidities higher than this value. This can be identified from the nature of the trajectory associated with the main cutoff.

Lower Cutoff Rigidity, R_L: The lowest detected cutoff value (i.e., the rigidity value of the lowest allowed/forbidden transition observed in a set of computer calculations). If no penumbra exists, R_L will equal R_U.

Horizon Limited Rigidity, R_H: The rigidity value of the most rigid allowed trajectory found in a set of computer calculations performed for a below horizon direction at a location above the surface of the earth.

Effective Cutoff Rigidity, R_C: The total effect of the penumbral structure in a given direction may be represented usefully, for many purposes, by the "effective cutoff rigidity" - a single numeric value which specifies the equivalent total accessible cosmic radiation within the penumbra in a specific direction. "Effective cutoffs" may be either linear averages of the allowed rigidity intervals in the penumbra or functions weighted for the cosmic ray spectrum and/or detector response.

Estimated Cutoff Rigidity, R_{est}: A value obtained by using an empirically normalized equation to approximate the cosmic ray cutoff variation in the location of a particular point within a magnetic field in order to estimate a cutoff value pertaining to the point. This value can be found by use of a variety of interpolation techniques, one of which is application of the Stormer equation given above. Because the Stormer equation characterises the spatial variation of the cutoff rigidity, with appropriate normalization it may be used to obtain useful estimates of the various cosmic ray cutoff rigidities over intervals of latitude, longitude, zenith and azimuth, for example. In practice, estimates of the value of any cutoff can be obtained from adjacent calculated values to a reasonable accuracy by employing this method.

3. Discussion and Conclusion. Not all the cutoffs defined in the previous section exist for every location and direction. It should be borne in mind that, because the definitions have deliberately been kept usefully general, the application of the terms may require more detailed qualification in some individual circumstances. In addition, there is no doubt that other physically meaningful quantities exist. It is believed, however, that the cutoff concepts described in this paper presently have the greatest significance, and that the use of these definitions should alleviate most of the existing confusion and satisfy the current requirements of investigators involved in cosmic ray access studies.

4. Acknowledgements. DJC acknowledges support from the U.S. Air Force Geophysics Laboratory, under contract # F 19628-81-K0020.

References

Lemaitre, G., and M. S. Vallarta, "On the geomagnetic analysis of cosmic radiation", Phys. Rev., 49, 719-726, 1936a.

Lemaitre, G., and M. S. Vallarta, "On the allowed cone of cosmic radiation", Phys. Rev., 50, 493-504, 1936b.

Shea, M. A., D. F. Smart, and K. G. McCracken, "A study of vertical cutoff rigidities using sixth degree simulations of the geomagnetic field", J. Geophys. Res., 70, 4117-4130, 1965.

Stormer, C., "Periodische Elektronenbahnen im Felde Lines Elementarmagneton und ihre Anwendung auf Bruches Modellverauche und auf Eschenhagnes Elementarwellen des Erdmagnetismus", Astrophys., 1, 237-274, 1930.

THE USE OF THE McILWAIN L-PARAMETER TO ESTIMATE COSMIC RAY VERTICAL CUTOFF RIGIDITIES FOR DIFFERENT EPOCHS OF THE GEOMAGNETIC FIELD

M.A. Shea and D.F. Smart
Air Force Geophysics Laboratory
Hanscom AFB, Bedford, Massachusetts 01731, U.S.A.

L.C. Gentile
Physics Research Division, Emmanuel College
400 The Fenway, Boston, Massachusetts 02115, U.S.A.

ABSTRACT

A useful relationship employing the McIlwain L-parameter to estimate vertical cutoff rigidities has been derived for the twenty-five year period 1955-1980.

1. Introduction. It is intuitively pleasing to utilize the dipolar geometry inherent in the McIlwain L-parameter to order cosmic ray cutoff rigidities. However, in some areas of the world, secular changes in the geomagnetic field between 1955 and 1980 have been large enough to produce significant differences in both the vertical cutoff rigidities and in the L-value for a specified position. In this paper we show that these changes are complimentary, and it is possible to derive a relationship between the L-value and vertical cutoff rigidity that can be used for the twenty-five year period, 1955-1980.

2. Background. The trajectory-tracing process is generally recognized as the most accurate method for calculating cosmic ray cutoff rigidities. Since cutoff rigidities are a function of latitude, longitude, altitude, zenith angle, azimuthal angle, and field model, using the trajectory-tracing method for a large number of positions and directions is impractical. For this reason, cosmic radiation data from many experiments are often ordered by the cutoff rigidity values in the vertical direction.

One method of estimating vertical cutoff rigitities was suggested by Smart and Shea (1967) who derived three equations for the relationship between the McIlwain L-parameter (McIlwain, 1961) and (1) the upper calculated cutoff, (2) the lower calculated cutoff and (3) the effective cutoff rigidities.* These three equations were derived using cutoff rigidities calculated for the Finch and Leaton (1957) field for Epoch 1955.0 and the Jensen and Cain (1962) field for Epoch 1960. The equations thus derived for the upper calculated cutoff, the lower calculated cutoff and the effective cutoff rigidities were essentially the same for both field models.

At the time of this original work, cosmic ray physicists did not recognize that the secular changes in the geomagnetic field were sufficiently large over a relatively small time period (on the order of 25 years) to significantly affect the detection, at the surface of the earth, of galactic cosmic radiation above 1 GV. It was not until Shea (1971) suggested

* In the paper of Smart and Shea (1967), these rigidity values were called main cone cutoff, Stormer cone cutoff and effective cutoff, respectively. Since new terminology for cosmic ray cutoffs has been agreed upon by scientists working in this area (Cooke et al., 1985) we will use these newer terms throughout this paper.

that the decrease in vertical cutoff rigidity at Huancayo over a 20-year period might possibly be observed as an increase in the background radiation measured by a stable neutron monitor at this location (since verified by Cooper and Simpson, 1979), that it became apparent that the secular changes in the geomagnetic field might be sufficiently large in some areas of the world that changes in cutoff rigidities, and consequently measured changes in cosmic radiation, would occur.

In view of the changes in the main geomagnetic field and the related changes in the calculated cutoff rigidities, we feel it is necessary to re-examine the use of the McIlwain L-parameter to estimate cosmic ray vertical cutoff rigidities for the 25-year period 1955-1980.

3. Method. The world grid of vertical cutoff rigidities calculated each 5° in latitude and 15° in longitude for Epochs 1955, 1965 and 1980 (Shea et al., 1968; Shea and Smart, 1975, 1983) and the McIlwain L-values (McIlwain, 1961) calculated for these same locations comprised the basic data sets used for this analysis. All calculations were made for an altitude of 20 km above the surface of the earth as defined by the international reference ellipsoid. Both the vertical cutoff rigidities and the McIlwain L-values were calculated using the geomagnetic field coefficients for the appropriate Epoch (i.e., 1955, 1965 and 1980).

Expressing the cosmic ray cutoffs by an equation of the form $R=KL^{\gamma}$ where R is the cutoff rigidity, L is the McIlwain L-value, K is a constant and γ is an exponent, K and γ were evaluated by a least-squares fit of the (1) upper calculated cutoff rigidity, (2) effective cutoff rigidity and (3) lower calculated cutoff rigidity. Each of the equations derived for each Epoch, together with the RMS error for each set of calculations, is given in Table 1. It is important to note that vertical cutoff rigidities < 0.20 GV were omitted from these calculations. Since the cosmic ray equator and the equator defined by the minimum L-value do not coincide, all grid points within a band ±5 degrees of either equator (or between the two equators) were also omitted. Figure 1 illustrates the locations of each of these equators for Epoch 1980.

Table 1. Equations to estimate cutoff rigidities for various Epochs

Epoch	R_U =	R_C =	R_L =
1955	$16.727\ L^{-2.0054}$ RMS = 6.28 %	$16.192\ L^{-2.0177}$ RMS = 5.48 %	$14.992\ L^{-1.9986}$ RMS = 6.61 %
1965	$16.722\ L^{-2.0212}$ RMS = 6.70 %	$16.222\ L^{-2.0418}$ RMS = 5.52 %	$14.942\ L^{-2.0296}$ RMS = 6.98 %
1980	$16.717\ L^{-2.0206}$ RMS = 7.06 %	$16.222\ L^{-2.0441}$ RMS = 5.74 %	$14.823\ L^{-2.0311}$ RMS = 7.27 %
Composite 1955-1980	$16.762\ L^{-2.0174}$ RMS = 6.67 %	$16.237\ L^{-2.0353}$ RMS = 5.64 %	$14.912\ L^{-2.0185}$ RMS = 7.19 %

4. Discussion. From an inspection of the equations in Table 1 it is evident that the constants K and γ for each of the three vertical cutoff rigidities are essentially independent of Epoch. The root mean square values are also similar, with the slightly larger RMS values for 1980 attributed to the evolution of the magnetic field and an increasing divergence between the cosmic ray equator and the minimum L equator. The area between these two equators has increased approximately 10 percent between 1955 and 1980.

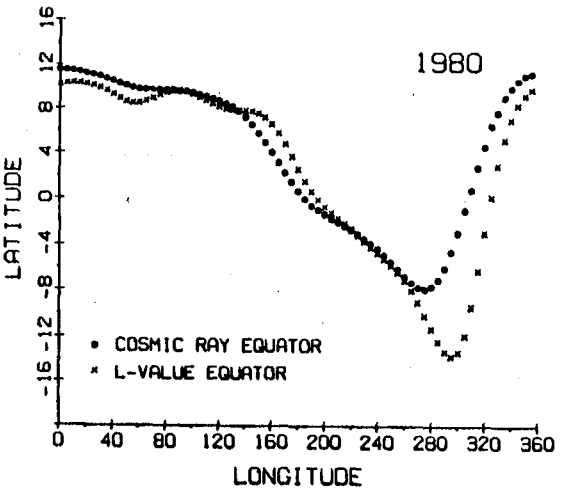

Figure 1. Geographic location of the cosmic ray equator and the minimum L equator for 1980.

Since these equations were almost identical we combined the data for all three Epochs in an effort to determine a suitable equation for the upper calculated cutoff, the effective cutoff and the lower calculated cutoff for the entire 25-year period from 1955 to 1980. Again all locations with cutoffs less than 0.20 GV were omitted from the analysis. Since the location of the cosmic ray equator changed between 1955 and 1980 (Shea et al., 1983), and different equatorial grid locations had been removed for each Epoch, we removed all locations within ±5° of any of the three equators (i.e., if a particular location had been removed for the analysis for one Epoch, it was removed from all three data sets for the composite analysis). Again the constants K and γ were determined by the method of least squares. The results for this composite set of over 1875 data

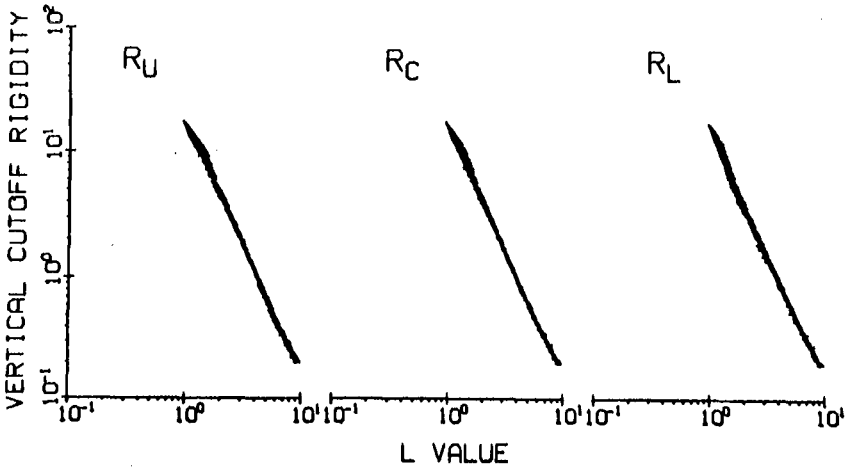

Figure 2. The upper calculated vertical cutoff rigidity (R_U), effective vertical cutoff rigidity (R_C), and lower calculated vertical cutoff rigidity (R_L), plotted as a function of the McIlwain L-value. The data set is a composite of the world grid locations for 1955, 1965 and 1980.

points are graphically illustrated in Figure 2; the equations are given in the bottom line of Table 1. From these results we feel that it is possible to use these three equations to estimate the upper, effective and lower cutoff rigidities for the entire period 1955 to 1980 provided the L-values are calculated using the field model for the same time period that the cutoffs are needed.

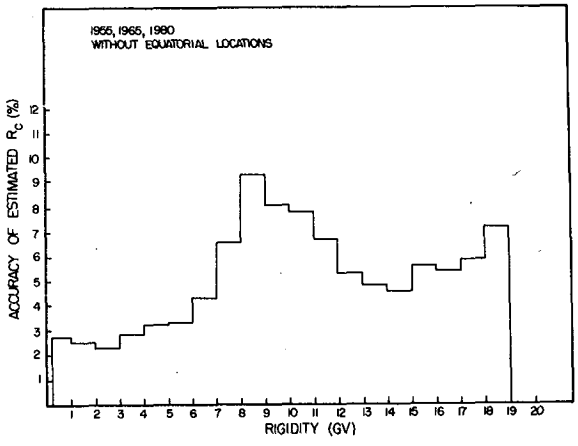

Figure 3: Accuracy of estimated vertical cutoff rigidity.

Figure 3 illustrates the accuracy that can be expected for an estimate of the effective vertical cutoff rigidity as a function of rigidity. These data were obtained by calculating for each location the percentage difference (in rigidity) between the cutoff rigidity value determined by the trajectory-tracing procedure and the value estimated by using the L-value approximation equation. These individual percentages were then averaged as a function of intervals of estimated cutoff rigidity.

5. Conclusion. From this analysis we conclude that the McIlwain L-parameter can be used to estimate upper calculated, effective, and lower calculated vertical cutoff rigidities for the period 1955 to 1980.

Acknowledgments. We gratefully acknowledge the computational assistance of A.A. Bathurst. LCG acknowledges support from the U.S. Air Force Geophysics Laboratory under contract No. F19628-82-K-0039.

References

Cooke, D.J., J.E. Humble, M.A. Shea, D.F. Smart, N. Lund, I.L. Rasmussen, B. Byrnak, P. Goret, and N. Petrou, Paper No. SH 6.1-11, 19th International Cosmic Ray Conference, these proceedings, 1985.

Cooper, J.F., and J.A. Simpson, 16th International Cosmic Ray Conference, Conference Papers, 12, 176, 1979.

Finch, H.P., and B.R. Leaton, Monthly Notices Roy. Astron. Soc., Geophys. Suppl., 7, 314, 1957.

Jensen, D.C., and J.C. Cain, J. Geophys. Res., 67, 3568, 1962.

McIlwain, C.E., J. Geophys. Res., 66, 3681, 1961.

Shea, M.A., 12th International Conference on Cosmic Rays, Hobart, Conference Papers (University of Tasmania), 3, 859, 1971.

Shea, M.A., and D.F. Smart, 14th International Cosmic Ray Conference, Conference Papers, 4, 1298, 1975.

Shea, M.A., and D.F. Smart, 18th International Cosmic Ray Conference, Conference Papers, 3, 415, 1983.

Shea, M.A., D.F. Smart, and John R. McCall, Can. J. Phys., 46, S1098, 1968.

Shea, M.A., D.F. Smart and L.C. Gentile, 18th International Cosmic Ray Conference, Conference Papers, 3, 423, 1983.

Smart, D.F., and M.A. Shea, J. Geophys. Res., 72, 3447, 1967.

ESTIMATING THE CHANGE IN ASYMPTOTIC DIRECTION DUE TO SECULAR CHANGES IN THE GEOMAGNETIC FIELD

E. O. Fluckiger
Physikalisches Institut, Universitat Bern, Sidlerstrasse 5,
CH-3012 Bern, Switzerland

D. F. Smart and M. A. Shea
Air Force Geophysics Laboratory, Hanscom Air Force Base,
Bedford, Massachusetts 01731, U.S.A.

L. C. Gentile and A. A. Bathurst
Emmanuel College, 400 The Fenway, Boston, MA, 02115, U.S.A.

ABSTRACT

The concept of geomagnetic optics, as described by the asymptotic directions of approach, is extremely useful in the analysis of cosmic radiation data. However, when changes in cutoff occur as a result of evolution in the geomagnetic field, there are corresponding changes in the asymptotic cones of acceptance. We introduce here a method of estimating the change in the asymptotic direction of approach for vertically incident cosmic ray particles from a reference set of directions at a specific epoch by considering the change in the geomagnetic cutoff.

1. Introduction. Cosmic ray particles must travel along specific allowed trajectories through the geomagnetic field to reach a location on or near the earth. In order to relate cosmic ray intensity variations observed at different cosmic ray stations to the cosmic ray flux in space the concept of asymptotic directions of approach was developed (see McCracken et al., 1968, for a review). By application of the asymptotic directions of approach the user need not be concerned about the specific details of the allowed cosmic ray trajectories and can relate any specific cosmic ray particle with a unique direction in space. For a cosmic ray particle with rigidity R, arriving at a specific location (characterized by the geographic latitude Λ and the geographic longitude Φ) from a direction of incidence (described by the zenith angle θ and the azimuthal angle ϕ) the asymptotic direction of approach is given by the unit vector $\underline{A}(R,\Lambda,\Phi,\theta,\phi)$ pointing in the reverse direction to the particle's velocity vector prior to the particle's entry into the geomagnetic field. For the purposes of this paper and for a specific location the vector $\underline{A}$ is specified for vertical incidence in terms of the geocentric coordinate system as asymptotic latitude, $\lambda(R) = \lambda(R,R_1(\Lambda,\Phi), \theta = 0°)$ and asymptotic longitude, $\psi(R) = \psi(R,R_1(\Lambda,\Phi), \theta = 0°)$ where R_1 is the rigidity corresponding to the first discontinuity in asymptotic longitude as defined below.

The allowed rigidity spectrum of cosmic ray particles arriving from a specific direction at any location in the geomagnetic field contains distinct fiducial marks: R_1, the rigidity associated with the first discontinuity in asymptotic longitude occurring as the trajectory calculations are progressing down through the rigidity spectrum, and R_U, the rigidity at and above which the trajectory calculations yield allowed

orbits. The rigidity value R_l is always greater than or equal to R_U if both are determined by employing the same uniform discrete (usually 0.01 GV) rigidity intervals in the trajectory calculations. R_l is, in general, a value extremely close to the main cone cutoff rigidity as defined by Lemaitre and Vallarta (1936). A change in the geomagnetic field has an almost equivalent effect on both the rigidity corresponding to the first discontinuity and the vertical upper cutoff, and results in a similar effect on the vertical effective cutoff rigidity (Fluckiger et al., 1983a, 1983b).

Fluckiger et al., (1983b) have shown that geomagnetic disturbances reduce the cutoff rigidity in a predictable manner dependent on the strength and longitudinal structure of the magnetic perturbation and the longitudinal difference between the magnetic perturbation and the observing location. Furthermore, the change in asymptotic longitude (down to the first discontinuity) also behaves in a similarly predictable manner. Therefore the asymptotic directions of approach during perturbed geomagnetic conditions can be deduced with considerable accuracy from the asymptotic directions computed using the quiescent geomagnetic field if the associated change in cutoff rigidity is known. In this paper we extend these concepts to include the time evolution of the geomagnetic field on the asymptotic direction of approach for cosmic ray particles arriving at a particular location.

2. Method. We will define the terms $\delta\lambda^*(R)$ and $\delta\psi^*(R)$ as $\delta\lambda^*(R) = \lambda'(R) - \lambda(R-\delta R_l)$, and $\delta\psi^*(R) = \psi'(R) - \psi(R-\delta R_l)$, where $\delta R_l = R_l' - R_l$, and the primed values indicate the evolved geomagnetic field and the unprimed values indicate the reference geomagnetic field. When these values are plotted as a function of rigidity, it has been found that there are practically no changes for $\delta\lambda^*$ down to the rigidity value of R_l'. Therefore, we may set $\delta\lambda^* = 0°$ (Fluckiger et al., 1983b). For $\delta\psi^*$ only small residual changes on the order of several degrees are found down to rigidities approaching the value of R_l. For any particular location and for rigidities up to several GV above the main cutoff the following expressions can be used to describe the correlation between the asymptotic directions in an evolved geomagnetic field and the asymptotic directions in a reference geomagnetic field:

$$\lambda'(R) \approx \lambda(R - \delta R_l), \text{ and } \psi'(R) \approx \psi(R - \delta R_l) + C \cdot \delta R_l,$$

where C is a measure of the residual change $\delta\psi^*$. This procedure is valid only for rigidities larger than R_l or R_l', respectively.

At rigidities below R_l no similar relation has been found, although coherent clusters of trajectories may be distorted uniformly by magnetic changes. It has been shown that the main features of allowed and forbidden regions in the penumbra are conserved to a certain extent in a perturbed geomagnetic field (Fluckiger et al., 1979, 1982). However, the asymptotic longitudes of the allowed trajectories of the fine detailed structure in the cosmic ray penumbra continue to be quasi-random.

3. Application. We have applied this procedure by comparing the asymptotic directions calculated for the International Geomagnetic Reference Field Epoch 1965.0 with those calculated for epoch 1980.0 for cosmic ray stations and world grid locations. To illustrate this application, we

the evolved values. We would expect a close comparison between the asymptotic directions above the first discontinuity (R_1) such that $\psi(R_1^*) + \Delta R \approx \psi'(R_1^{*'}) + \Delta R$ where ΔR represents an arbitrary rigidity value above R_1^* and $R_1^{*'}$. Here ψ denotes the asymptotic longitude in the reference field and ψ' the asymptotic longitude in the evolved field. R^* and $R^{*'}$ are approximations to the rigidity value of the first discontinuity obtained by examining the gradient in the change of the asymptotic direction with rigidity as the first discontinuity is approached from rigidity values above the main cutoff. The values selected to approximate the first discontinuity in asymptotic direction, R_1^* and $R_1^{*'}$ were the rigidity values where the gradient in asymptotic direction was greater than 1000° per GV and increased by more than 1.5 times in the next 0.01 GV increment. Examination of these results and comparison with other calculations have shown that this approximation is close to and slightly greater than the rigidity of the first discontinuity calculated using very small rigidity intervals.

For the examples given in the following tables, the increment of rigidity added to the approximation of the first discontinuity value was the change in rigidity of the first discontinuity between the reference field and the evolved field. This value was used because it was sure to be in the set of continuous asymptotic directions above the main cutoff in both data sets. In Table 1 we illustrate the results for cosmic ray stations at locations where the geomagnetic cutoff is decreasing with time. In Table 2 we show results for cosmic ray stations at locations where the cosmic ray cutoff is increasing with time. An inspection of the asymptotic longitudes given in the second and third columns from the right in these tables indicates that the asymptotic longitudes for the specified rigidity values are quite similar.

4. Conclusions. We have illustrated that the asymptotic directions for an evolved geomagnetic field for rigidity values above the R_1 value (the first discontinuity in asymptotic direction progressing down through the rigidity scale) can be obtained from a "known" reference set of asymptotic directions if the change in cutoff is known.

5. Acknowledgments. A. A. Bathurst and L. C. Gentile acknowledge support from the U. S. Air Force Geophysics Laboratory under Contract No. F19628-82-K-0039.

References.

Fluckiger, E., H. Debrunner, D.F. Smart, and M.A. Shea, 16th International Cosmic Ray Conference, Conference Papers, 4, 273, 1979.

Fluckiger, E., AFGL-TR-82-0177, 1982.

Fluckiger, E.O., D.F. Smart, and M.A. Shea, J. Geophys. Res., 88, 6961, 1983a.

Fluckiger, E.O., D.F. Smart, and M.A. Shea, 18th International Cosmic Ray Conference, Conference Papers, 3, 431, 1983b.

Lemaitre, G., and M.S. Vallarta, Phys. Rev., 50, 493, 1936.

McCracken, K.G., U.R. Rao, B.C. Fowler, M.A. Shea, and D.F. Smart, Cosmic Rays, Annals of the IQSY, Vol. 1, Edited by C.M. Minnis, Chapter 14, 198, The MIT Press, Cambridge, Massachusetts, 1968.

TABLE 1.
Changes of Asymptotic Longitude for Cosmic Ray Stations Where the Cutoff is Decreasing.

ψ for 1980 at $R_1^{*'} + |\Delta R| \approx \psi$ for 1965 at $R_1^* + |\Delta R|$, where $\Delta R = (R_1^{*'}$ for 1980) - (R_1^* for 1965)

STATION NAME	GEOGRAPHIC LAT	GEOGRAPHIC LONG	EPOCH 1965 R_U	EPOCH 1965 R_1^*	EPOCH 1965 ψ	EPOCH 1980 R_U'	EPOCH 1980 $R_1^{*'}$	EPOCH 1980 ψ'	ΔR_1^*	1965 RIG	1965 ψ	1980 ψ'	1980 RIG
Ahmedabad	23.01	72.61	15.90	15.92	46	15.77	15.79	51	-0.13	16.05	329	327	15.92
Alma Ata	43.20	76.94	6.92	6.93	36	6.87	6.90	30	-0.03	6.96	358	355	6.93
Brisbane	-27.50	153.01	7.39	7.42	121	7.22	7.26	116	-0.16	7.58	31	30	7.42
Buenos Aires	-34.58	301.50	10.59	10.61	266	10.12	10.15	246	-0.46	11.07	130	124	10.61
Chacaltaya	-16.31	291.85	12.85	12.87	257	12.53	12.54	263	-0.33	13.20	144	144	12.87
Climax	39.37	253.82	3.14	3.24	146	3.12	3.22	153	-0.02	3.26	124	128	3.24
Gulmarg	34.07	74.42	12.33	12.35	44	12.24	12.26	45	-0.09	12.44	336	337	12.35
Hermanus	-34.42	19.22	5.02	5.06	307	4.83	4.86	311	-0.20	5.26	215	214	5.06
Hobart	-42.90	147.33	2.10	2.12	44	2.06	2.08	43	-0.04	2.16	13	11	2.12
Huancayo	-12.05	284.67	13.24	13.25	266	12.91	12.93	253	-0.32	13.57	142	140	13.25
Mexico City	19.33	260.82	9.57	10.24	257	9.27	9.94	250	-0.30	10.54	121	123	10.24
Mildura	-34.23	142.22	4.56	4.59	97	4.43	4.46	87	-0.13	4.72	11	11	4.59
Mt. Wellington	-42.92	147.24	2.03	2.11	49	1.99	2.07	49	-0.04	2.15	14	12	2.11
Palestine	31.75	264.35	4.74	4.90	185	4.69	4.86	194	-0.04	4.94	145	147	4.90
Potchefstroom	-26.70	27.10	7.68	7.72	346	7.49	7.53	337	-0.19	7.91	247	245	7.72
Sydney	-33.60	151.10	5.16	5.19	86	5.06	5.09	84	-0.10	5.29	21	21	5.19
Tbilisi	41.72	44.80	6.96	7.00	357	6.95	6.97	14	-0.03	7.03	322	321	7.00

TABLE 2.
Changes of Asymptotic Longitude for Cosmic Ray Stations Where the Cutoff is Increasing.

ψ for 1980 at $R_1^{*'} + |\Delta R| \approx \psi$ for 1965 at $R_1^* + |\Delta R|$, where $\Delta R = (R_1^{*'}$ for 1980) - (R_1^* for 1965)

STATION NAME	GEOGRAPHIC LAT	GEOGRAPHIC LONG	EPOCH 1965 R_U	EPOCH 1965 R_1^*	EPOCH 1965 ψ	EPOCH 1980 R_U'	EPOCH 1980 $R_1^{*'}$	EPOCH 1980 ψ'	ΔR_1^*	1965 RIG	1965 ψ	1980 ψ'	1980 RIG
Athens	37.97	23.72	8.98	8.99	355	9.06	9.08	340	0.09	9.08	280	275	9.17
Bologna	44.50	11.33	5.41	5.44	297	5.52	5.55	295	0.11	5.55	231	231	5.66
Budapest	47.50	18.90	4.74	4.77	309	4.82	4.83	309	0.06	4.83	254	253	4.89
Calgary	51.08	245.91	1.16	1.22	123	1.17	1.24	125	0.02	1.24	95	94	1.26
Deep River	46.10	282.50	1.13	1.19	170	1.25	1.32	150	0.13	1.32	80	85	1.45
Dourbes	50.10	4.60	3.42	3.44	298	3.57	3.60	294	0.16	3.60	208	215	3.76
Durham	43.10	289.16	1.67	1.69	197	1.84	1.86	179	0.17	1.86	93	103	2.03
Fukushima	37.75	140.48	11.36	11.38	104	11.45	11.47	100	0.09	11.47	40	38	11.56
Irkutsk	52.47	104.03	3.92	3.95	34	3.95	3.98	42	0.03	3.98	359	4	4.01
Jungfraujoch	46.55	7.98	4.81	4.82	300	4.91	4.94	289	0.12	4.94	222	220	5.06
Kerguelen Is.	-49.35	70.22	1.24	1.31	299	1.15	1.31	315	0.00	1.31	299	315	1.31
Kiel	54.33	10.13	2.39	2.50	298	2.59	2.61	307	0.11	2.61	224	226	2.72
Kiev	50.72	30.30	3.74	3.77	335	3.79	3.80	332	0.03	3.80	290	289	3.83
Leeds	53.82	358.45	2.26	2.35	265	2.41	2.48	267	0.13	2.48	191	204	2.61
Lomnicky Stit	49.20	20.22	4.21	4.24	314	4.28	4.31	329	0.07	4.31	256	257	4.38
Magadan	60.11	151.01	2.22	2.33	52	2.34	2.36	45	0.03	2.36	9	6	2.39
Morioka	39.70	141.13	10.47	10.51	122	10.61	10.63	109	0.12	10.63	35	32	10.75
Moscow	55.47	37.32	2.60	2.61	320	2.50	2.62	313	0.01	2.62	302	297	2.63
Mt. Norikura	36.12	137.56	12.02	12.04	09	12.09	12.11	107	0.07	12.11	45	46	12.18
Mt. Washington	44.30	288.70	1.41	1.50	165	1.55	1.66	214	0.16	1.66	89	96	1.82
Mussala	42.18	25.58	6.50	6.51	346	6.56	6.57	343	0.06	6.57	281	280	6.63
Pic du Midi	42.93	0.25	5.58	5.61	294	5.80	5.81	306	0.20	5.81	204	209	6.01
Predigtstuhl	47.70	12.88	4.59	4.60	309	4.68	4.70	299	0.10	4.70	235	232	4.80
Rome	41.90	12.52	6.35	6.37	318	6.50	6.54	324	0.17	6.54	235	236	6.71
Tokyo-Itabashi	35.75	139.72	12.12	12.13	115	12.19	12.21	99	0.08	12.21	45	41	12.29
Yakutsk	62.02	129.72	1.74	1.85	22	1.78	1.87	32	0.02	1.87	352	356	1.89
Zugspitze	47.42	10.98	4.62	4.64	314	4.72	4.75	298	0.11	4.75	230	227	4.86

EMPIRICAL MODEL FOR THE EARTH'S COSMIC RAY SHADOW AT 400 KM: PROHIBITED COSMIC RAY ACCESS

J. E. Humble
Department of Physics, University of Tasmania
Hobart, Tasmania, 7001, Australia

D. F. Smart and M. A. Shea
Air Force Geophysics Laboratory
Hanscom AFB, Bedford, MA., 01731, U.S.A.

ABSTRACT

It is possible to construct a unit sphere of access that describes the cosmic radiation allowed to an earth-orbiting spacecraft. In the upper hemisphere of the allowed portion of the cosmic ray sphere of access, the cosmic ray cutoffs can be ordered by application of Stormer theory in offset dipole coordinates. In the downward hemisphere, in westerly directions, the cosmic radiation is allowed at large zenith angles well below the spacecraft-earth horizon, with particles being able to reach satellites at 400 km altitude from large zenith angles of ~140° at azimuthal directions equatorward of west in both the northern and southern hemispheres. We have found it is possible to model the occluded portion of the cosmic ray sphere of access as a circular projection having a diameter bounded by the satellite-earth horizon. Maintaining tangency at the eastern edge of the spacecraft-earth horizon, this optically occluded area is projected downward (toward the earth) by an angle β which is a function of the magnetic field inclination and cosmic ray arrival direction. This projected plane, corresponding to the forbidden area of cosmic ray access, is bounded by the spacecraft-earth horizon in easterly directions, and is rotated around the vertical axis by an angle α from the eastern direction, where the angle α is a function of the offset dipole latitude of the spacecraft.

1. Introduction. It is of considerable interest to evaluate the primary cosmic ray flux which is able to reach a satellite in earth orbit from any specified direction of arrival. The evaluation requires a knowledge of the geomagnetic cutoffs for all four pi steradins of possible arrival directions at all points along the spacecraft orbit. In practice, in order to keep the computational problem within manageable (and economic) bounds, cutoffs are generally calculated for a selected set of directions at each of a chosen set of representative directions along the orbit (Humble et al., 1979). It is then necessary to interpolate cutoffs for directions intermediate to those for which explicit calculations have been performed for a specific location, and for locations intermediate to those for which calculations have been undertaken for particular directions of particle arrival. For the upper hemisphere of arrival directions Smart and Shea (1977) showed that the cutoffs are reasonably

well ordered, for some locations, by Stormer theory. Humble et al. (1979) pointed out that at least some of the exceptions were due to the intervention of the 'shadow cone'.

Recent interest has focussed on particles arriving at the spacecraft from the lower, earthward facing, hemisphere. We have previously reported finding that primary cosmic rays are able to reach a satellite orbiting at quite low altitudes from zenith angles considerably larger than that of the local earth horizon. For a spacecraft at 400 km these angles are at least 140° at all latitudes we have investigated, and reach 150° at one location (Humble et al., 1983; Humble, 1983). We report here results from some further calculations of this type, and then describe a possible method for modelling the bounds of that portion of the unit sphere of access to which primary particles of any energy are unable to gain access because of the presence of the solid earth.

2. Method. A trajectory tracing technique has been devised to search rigidity/zenith-angle space for accessible arrival directions (Humble et al., 1983). The search proceeds, for a given location and azimuth, in the directions of increasing zenith angle and decreasing rigidity, until no further accessible directions of arrival can be found. A number of searches has been performed using this technique. Each was started at a zenith angle of 100° which is above the local satellite-earth horizon at all altitudes considered (Humble, 1984). It was found that, for zenith angles greater than that of the satellite-earth horizon, primary particles are only able to reach the satellite from generally westerly directions. Such particles experience a $\underline{V} \times \underline{B}$ force having a positive radial component in the final stages of their approach to the satellite. Their trajectories consequently have positive upwards curvature, and the local zenith angle of arrival can be greater than that of the satellite-earth horizon. The range of accessible azimuths increases with altitude, as would be expected.

3. Results at 400 km. A considerable number of trajectories have been calculated for the 400 km altitude. In analyzing these results we have found that it is possible to construct a unit sphere of access which describes the access of primary cosmic ray particles to any given detector. In the relatively simple case of a ground-level location the upper half of this sphere is totally allowed and the lower hemisphere is totally forbidden, due to the presence of the earth. For a satellite in earth orbit the situation is more complicated. All of the upper hemisphere is allowed to cosmic rays of some energy, as is part of the downward hemisphere. The latter may be divided into two parts. One is essentially a continuation of the allowed upper hemisphere - an annulus of allowed directions at zenith angles z_e such that $90° \leq z_e < z_h$, where z_h is the zenith angle of the horizon seen by the spacecraft. The second region lies at $z_e > z_h$, opens to the west, and is due to the $\underline{V} \times \underline{B}$ effect discussed in the previous section. The remainder of the sphere of access represents forbidden directions of arrival. We have found that it is possible to model the forbidden, or occluded, portion of the unit sphere of access, in an empirical manner and to varying degrees of accuracy, by the following technique.

Consider the equatorial plane of the unit sphere surrounding the spacecraft. Project the sphere onto a plane calibrated as a polar plot in zenith (as radius) and azimuth. Rotate the disc corresponding to the equatorial plane of the sphere through an angle β about a magnetic north south axis, until its projection, now an ellipse, on the polar plot has a minor axis which matches the distance between the largest and smallest values of zenith indicated. The rotated plane is then relocated, and subsequently rotated about a vertical axis, such that it is tangent to the satellite-earth horizon at the inner surface of the unit sphere at an angle α from the easterly direction. In our present model α is equal to the offset dipole latitude of the spacecraft. Figure 1 shows examples of the fit between the model curve and the points calculated for particular directions of arrival. The rms difference is about 3°; however, the greatest differences occur at positions where there is the largest deviation between the invariant latitude and the offset dipole latitude contours.

4. Results for Higher Altitudes. In general, it has been found that the largest accessible zenith angle for a given latitude, longitude, and azimuth, would also increase with increasing altitude. More detailed results are given by Humble et al. (1983) and Humble (1983). We have not yet applied the empirical model described in this paper to altitudes of 1000 km and above. Preliminary calculations have, however, been made. As the altitude increases above 1250 km a range of large zenith angles in generally easterly directions begins to become accessible, while smaller (but still below-horizon) zenith angles in the same azimuthal directions remain inaccessible. The higher altitude permits particles approaching the general region of the satellite at low altitudes from the west to pass above the top of the atmosphere more than one gyro-radius beneath the satellite. Such particles will arrive at the satellite from easterly directions at large zenith angles. The following table summarizes the results which have been obtained.

Altitude km	Maximum Zenith Angle
400	150°
600	156°
800	166°
1000	172°
1250	180°

Note that a zenith of 180° for an altitude of 1250 km means that primary cosmic ray nuclei are able to reach a satellite at that altitude from the nadir direction, directly underneath it, for at least one location somewhere on the orbit. This does not, however, mean that all possible directions of arrival are accessible at such a location. Easterly arrival directions at below-horizon zeniths are still forbidden.

References.

Humble, J.E: Proc. Astron.Soc.Australia, 5, 265-267, 1983.

Humble, J.E., D.F.Smart, and M.A.Shea: 16th ICRC, Kyoto, Conference Papers, 4, 303-308, 1979.

Humble, J.E., D.F.Smart, and M.A.Shea: 18th ICRC, Bangalore, Conference Papers, 442-445, 1983.

Humble, J.E., AFGL-TR-84-0258, 1984.

Smart, D.F., and M.A.Shea: 15th ICRC, Plovdiv, Conference Papers, 11, 256-261, 1977.

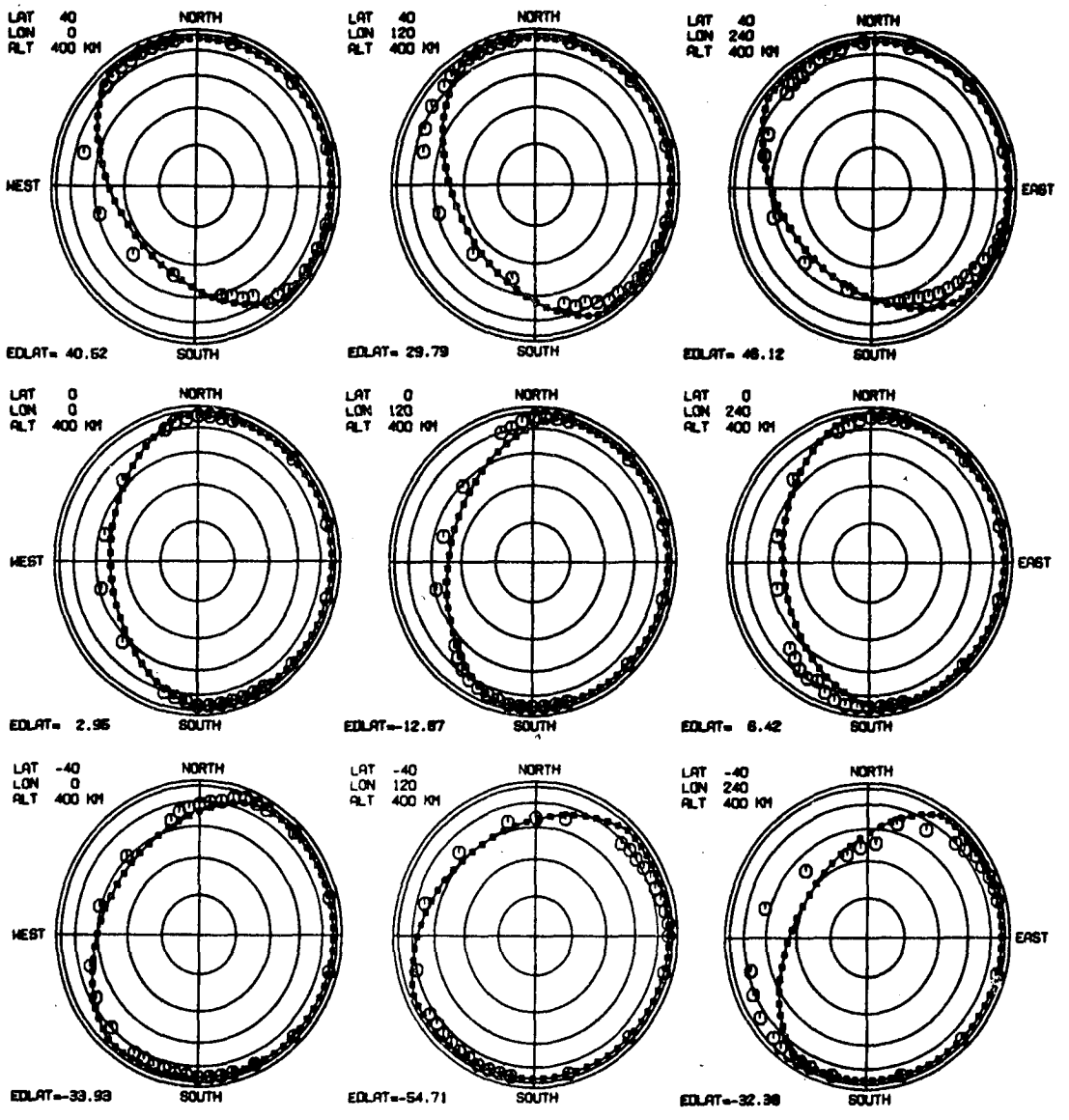

Figure 1. Polar projections of the downward hemisphere beneath an orbiting satellite. The occluded area beneath a satellite to which access is completely forbidden to galactic cosmic radiation of any energy is the area enclosed by the large dots in each projection. In this projection the observer is at the center of the spacecraft. This projection is looking downward from the center of the spacecraft; concentric rings represent 15 degree projections from the spacecraft equator to the nadir. Zero degrees is upward from the top of the spacecraft, 90 degrees is the spacecraft equator, and 180 degrees is in the nadir direction. At the 400 km altitude the local satellite-earth horizon is 109.8° from the zenith. The large open dots in each panel indicate where the maximum accessible zenith directions were determined by the cosmic ray trajectory-tracing method. The line connected with small solid squares indicates the result of applying the model described in this paper.

SH 6.1-15

PENETRATION OF SOLAR PROTONS INTO THE EARTH'S MAGNETOSPHERE ON NOVEMBER 22,1977

E.V.Gorchakov,V.G.Afanasyev,K.G.Afanasyev,P.P.Ignatyev, V.A.Iozenas,M.V.Ternovskaya,G.G.Zenchev

Institute of Nuclear Physics, Moscow State University, Moscow 119899, USSR

ABSTRACT

The low polar-orbiting Cosmos-900 satellite carried a large geometric factor (~0.9 m^2sr) Cerenkov counter which may be used to study the particle anisotropy and spectrum near the proton increase peak in solar cosmic rays. The data obtained supplement the information from the ground-based cosmic ray stations and help understand different temporal behaviour of the increases detected at the stations because the whole set of data has shown that the angular distribution of solar cosmic ray particles in interplanetary space was narrow throughout the observation time, thereby resulting, particularly, in a rapid variation of particle intensity near the poles. The power-law index of the solar cosmic ray integral spectrum varied from -2.4 to -5.2 in the 1-4 GV rigidity range from 10.31 to 11.25 UT on November 22, 1977. The flare-time data from all orbits are indicative of an increased radiation intensity on L=3.5-4.0.

1. Introduction. The solar flare responsible for the Nov.22, 1977 event began at 9.45 UT and reached a maximum at 10.07 UT. The cosmic ray intensity enhancement was detected by the neutron monitors with the cut-off rigidity less than 5 GV and also by the satellite instruments /1-3/. The onset of the cosmic ray intensity enhancement was detected by the neutron monitors at 10.10-10.15 UT and the maximum intensity of the enhancement at 10.35-10.50 UT.

2. Results. The data from three channels of the Cerenkov detector on Cosmos-900 for the interval 8.45-11.50 UT, 22. 11, 1977 are presented in fig.1. Up to 10.30 UT the counting rate corresponds to the latitude behaviour of the cosmic-ray intensity during the quiet period. During the interval 10.30-11.50 UT, while Cosmoc-900 was outside the equatorial region, the intensity enhancement associated with the penetration of cosmic ray into the Earth's magnetosphere was observed. (The peak at 9.35 and 11.12 UT is detected during the passage of the satellite through the Brazil magnetic anomaly). The intensity enhancement was, mainly, due to protons of the solar cosmic rays since the electron contribution for our instrument according to ref. /4/, could not be > 4%. According to the 11th channel detected only particles with $Z \geq 2$, the intensity of these particles during the flare was smaller, at least, by a factor of 200 than the proton intensity. The maximum intensity

of >400 MeV protons was higher by 600 % then the pre-flare level, being equal to $(2.3 \pm 0.5)\ 10^4\ m^{-2}s^{-1}sr^{-1}$.

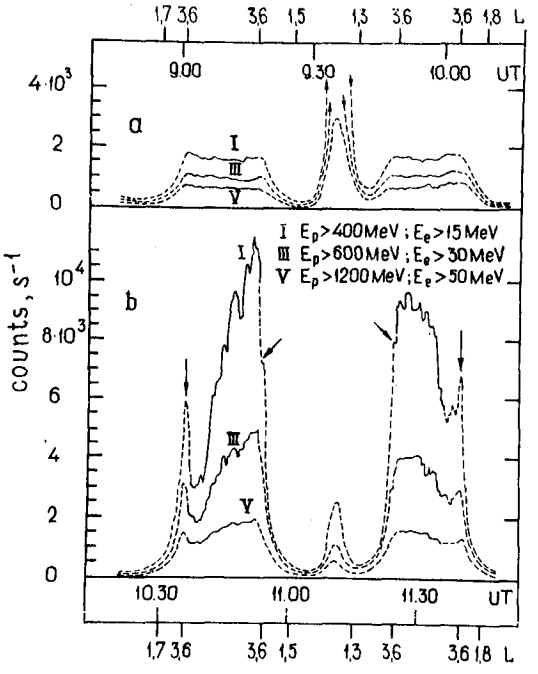

Fig.1. The cosmic ray count rates for three channels:
a) in the quiet time (prior to the flare),
b) during the flare.
The broken curves refer to the satellit passage through the region of action of geomagnetic cut-off.

The intensity distributions are characterized by the peaks and irregularities in the count rates marked by arrows in fig.1b. Note that all these cases were detected on L = 3.6 which proves the spatial behaviour of these variations. Accord to the neutron monitors the latitude distribution is also characterised by irregularities /5/.

It must be noted that this phenomenon is observed on the magnetic shells where the energy of the geomagnetic cut-off is compared with the energy threshold of the instrument.

3. Discussion. The peaks and irregularities in the count rates cannot be attributed to the radiation belts and to the particle precipitation from them /2/. Hence, the peaks on L = 3.6 are connected with the propagation of cosmic rays into the magnetosphere and, possibly, with the albedo particles and, also the quasi-trapping effects.

In our case the flux anisotropy and the longitudinal distribution of the receipt cones are, seemingly, the simplest explanation of the count-rate peculiarities.

On L = 3.6 the receipt cones have a wide longitude distribution and the instrument detects an averaged intensity. In the region adjoining L = 3.6 from the side of high latitudes the longitude distribution of the cones is always narrow and in the case of peaks the sunward particles /6/ are, mainly, detected whose intensity is known to be less then the mean intensity.

From our data it is possible to determine the flux ani-

sotropy during the flare. The angles θ between the axis of the solar proton flux in the interplanetary space and the axis of the asymptotic receipt cone for two points of the satellite trajectory (fig.2) in the high-latitude region of the Northen hemisphere, have been determined from the calculations /6/ including the outer magnetosphere currents. The difference in the intensities detected in these regions can be accounted for by the presence of a positive cosmic-ray flux anisotropy. If the time behaviour of the intensity in the interval 10.38-10.51 UT is neglected (according to the high-latitude neutron monitors the changes in intensity were small in the interval) the antisun-to-sunward ratio of particle fluxes for the above pitch-angles is estimated from our data to be ~6. During the interval 10.15-10.35 UT this ratio is close to 4 according to the neutron-monitor data /7/.

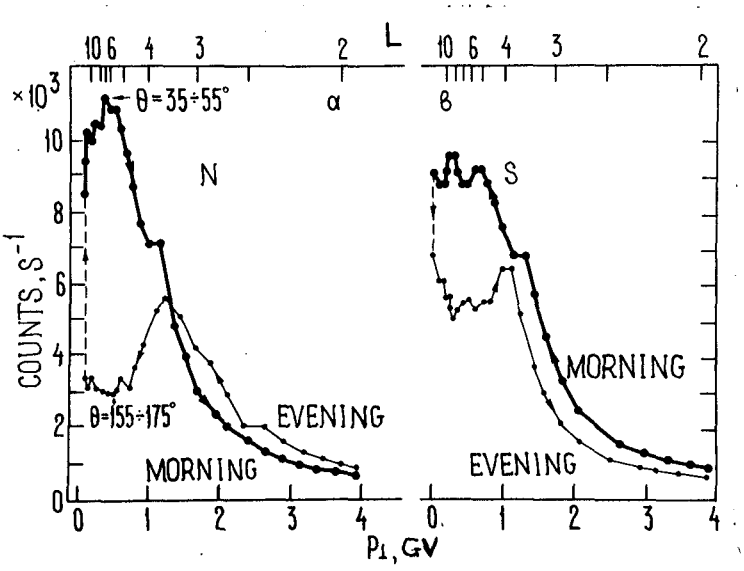

Fig.2a. Counting rate of the first channel versus the vertical rigidity of the geom. cut-off in the flight through the Northern hemisphere during the flare. The arrows mark the time flow. The thin and thick lines correspond to the satellite flight in the evening and morning sides of the Earth. Fig.2b. the same in the Southern hemisphere.

Assuming that in the South hemisphere in the high-latitude region the outer magnetosphere currents exert the same influence upon the asymptotic directions as they do in the Northern hemisphere, we may conclude that the solar cosmic-ray anisotropy decreases with time and maintains a positive sign (at least for high-latitude regions).

The spectra of observed particles within the rigidities 1-4 GV were obtained using the movement of the satellite in space. The calculations shown that in the interval 10.31-10.35 UT the index of the integral spectrum γ was 2.4 and in the intervals (10.54-10.58, 11.21-11.25, 11.40-11.44 UT) γ was on the average 4.1, 4.3 and 4.2, respectively. The slope of the spectra was not always the same, the index γ increased with rigidity, reaching the value 5.2. It follows that at 10.35 UT bulk of 400 MeV protons did

not reach the observing point, and during the next interval the spectrum was equilibrium.

In conclusion we note one more feature of the intensity distribution of the solar cosmic rays, namely the regular small peaks of intensity observed in the first channel every 2 minits throughout the flare observation period. We have failed to connect these variations with the peculiarities of the instrument operation and tentatively attribute them either to the solar or magnetospheric pulsations or to the propagation of particles in the interplanetary space. In the latter case these variations may be connected with the value of free path of particles.

References

1. Solar-Geophysical Data,1978, 405, Part II
2. E.V.Gorchakov et al.,Sov. journal Space Res.,1984, 22, 2, 312
3. M.Gro et al. The book of collected papers in Russian "Cosmic Rays", No. 21, 1980, 70
4. E.A.Devicheva et al.,Proc. of 16th ICRC, Kyoto, 1979,v.5, 170
5. A.G.Fenton et al. Proc. of 16th ICRC, Kyoto, 1979, v. 4, 34
6. M.A.Shea et al. UAG-9, World Data Center A, 68, 1970
7. M. Debrynner et al. Proc. of 18th ICRC, Bangalore, 1983, v. 4, 144

SH 6.I-I6

DYNAMICS OF THE PENETRATION BOUNDARIES OF SOLAR PROTONS DURING A STRONG MAGNETIC STORM

G.A. Glukhov, Yu.P. Kratenko
The Tashkent State University, 700095, Tashkent, USSR

Yu.V. Mineev
Institute of Nuclear Physics, Moscow State University, Moscow II9899, USSR

Abstract. On the basis of the Intercosmos-I9 data, the variations in the equatorial penetration boundary of solar protons with E_p = 0.9-8.0 MeV during a strong magnetic storm of April 3-5, I979 are studied. The dynamics of this boundary is compared with the dynamics of the outer trapping boundary of electrons with E_e = 0.3-0.6 MeV. Alongside with the solar-proton penetration we study the structure of the real magnetic field. The uniqe data on the thin structure of development of a magnetospheric substorm have been obtained for the first time.

In our previous paper /I/ we have analyzed the features of the latitudinal profiles of the SCR protons with E_p = = 0.9-8.0 MeV in the polar regions during a strong magnetic storm of April 3-5, I979 on the basis of the Intercosmos-I9 data (a perigee of ~ 500 km, an apogee of ~ I000 km, a period of ~ I00 min, an inclination of ~ 74°). The present paper is a study of the dynamics of the equatorial penetration boundary (Λ_{peq}) of the SCR protons for this magnetic storm (D_{st}-variation and the AE-index are presented in the lower part of fig.I). The variations in Λ_{peq} are studied alongside with the dynamics of the outer trapping boundaries of electrons with E_e = 0.3-0.6 MeV and E_e = 0.9-I.2 MeV which enables us to investigate the thin structure of development of magnetospheric substorms. Observations of electrons and protons were made by a semiconductor telescope aboard Intercosmos-I9 (IC-I9)/2/.

The outer trapping boundary of electrons was ment to be the threshold sensitivity of the instrument to the particles with a given energy. This definition of the boundary is justified because near the trapping boundary there was a rapid decrease in the particle intensity. Λ_{peq} was determined from the onset of a rapid decrease in intensity.

The dynamics of Λ_{peq} during the event in question is shown in the upper half of fig.I. Data I refer to the day (open circles) and morning (solid circles) sectors MLT and data II, to the evening (open circles) and night (solid circles) sectors. Here is also given the averaged location of Λ_{peq} for protons with $E_p \geq$ I MeV in the day (broken lines I), morning (solid lines I), evening (broken lines II) and night (solid lines II) sectors MLT according to the Cosmos-900 (C-900) and Cosmos-I067) data.

The comparison between the results of observations made on various satellites shows that at the day and night hours MLT the C-900 and C-I067 data, is available, are in good

agreement with the IC-I9 data. At the morning hours MLT on the main phase of the April, 3 magnetic storm at 20-23 UT the IC-I9 data are I-2° higher than the C-900 and C-I067 data, at the maximum D_{st} the IC-I9 data coincide with the C-900 and C-I067 data and at the end of the recovery phase the IC-I9 data coincide or are I° lower than the C-900 and C-I067 data at the pre-noon hours (9.5-II.5) MLT. A strong shift of the evening boundary to lower latitudes down to 55° was observed nearly an hour earlier on the IC-I9 as compared with C-900 and C-I067. According to the IC-I9 data, the evening boundary there shifted to larger latitudes, in conformity with the D_{st}-variation, and again to lower latitudes and the second minimum in the position of this boundary was observed at the maximum of the main phase of the storm. The complex analysis of the main parameters of the magnetosphere disturbance (D_{st}, AE) and the parameters of the interplanetary space (the magnitude and direction of the IMF, the solar wind velocity and density) shown that the strong shift of the evening boundary to lower latitudes is caused by the development of the magnetospheric substorm.

So, the IC-I9 data confirm the conclusion made in ref. /3/ about the prior and leading decrease in Λ_{pec} in the evening sector, that is connected with the asymmetric intrusion of particles of the storm ring current and the magnetic field decrease, yet, this effect is observed on the phase of development of an individual substorm and not of the storm as in ref./3/.

The evening boundary of penetration of solar protons coincides with the night boundary on the recovery phase of the storm.

The IC-data are obtained at later morning and later evening hours MLT which accounts for the differences in the location of the morning and evening boundaries determined from the IC-I9, C-900 and C-I067 data.

The dynamics of the outer trapping boundary of electrons is shown in the middle part of fig.I. A set of curves I is for electrons with E_e = 0.3-0.6 MeV and a set of curves II, for electrons with E_e = 0.9-I.2 MeV. The open circles correspond to the data obtained on the dayside and the solid circles, on the nightside. The position of the trapping boundaries of electrons is seen to be asymmetric in the midday-midnight plane and the asymmetry value depends on energy: the asymmetry decreases with increasing electron energy.

On the dayside the position of the trapping boundaries of electrons depends on rigidity. On the nightside this dependence is much weaker. As the magnetic field increases and decreases during the magnetic storms and substorms, the trapping boundaries shift to higher and lower in variant latitudes, respectively, in which case the trapping boundaries of electrons with different energies come close to each other as the magnetic field decreases and move away from each other as the field increases.

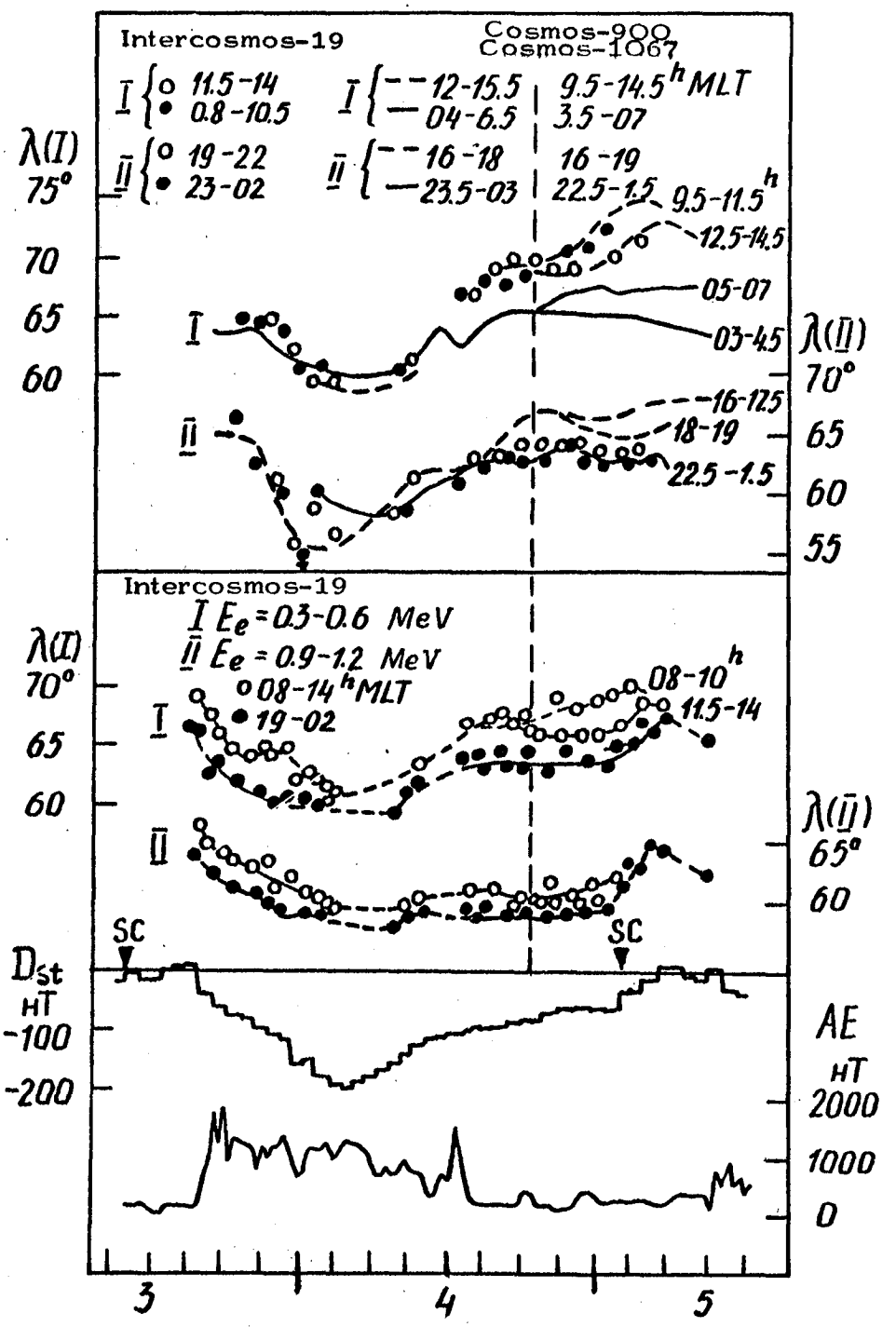

April 1979

Fig.1

The comparison between the dynamics of the equatorial region of penetration of the SCR protons and the outer trapping boundaries of electrons with E_e = 0.3-0.6 MeV and E_e = 0.9-I.2 MeV shown that on the dayside these boundaries behave in a similar manner. On the nighside Λ_{peq} coincides to within I° with the trapping boundary of electrons with E_e = 0.3-0.6 MeV except for the time moments within several minutes before the onset of magnetospheric substorms when the SCR protons are injected into deep L-shells; in this case the proton intensity peaks near the injection boundary and then falls down abruptly towards low latitudes. The intensity maximum can, apparently, be explained by the proton acceleration under the action of the enhanced electric field. Following the injection the SCR protons with E_p = = 0.9-8.0 MeV penetrate deep into the trapping region of electrons with E_e = 0.3-0.6 MeV and during strong magnetospheric substorms, into the trapping region of protons with E_p = 0.9-8.0 MeV.

Because of the violation of the adiabatic conditions of motion, a rapid precipitation of the SCR protons takes place following the injection in the trapping region of electrons with E_e = 0.3-0.6 MeV and also in the quasitrapping region on the dayside. The strong precipitation can also result from the parasitic scattering of the SCR protons on the electromagnetic radiation of the ring current protons.

References

I. Yu.V.Mineev et al. Proc. I8-th Int.Cos.Ray Conf., Bangalore, India, I983, 3, 262-265.
2. Yu.V.Mineev and E.S.Spirkova. Sov.Journal "Vestnik MGU", series 3, I98I, 22, I, 9I-95.
3. L.A.Darchieva et al. Sov. Journal "Geomagnetizm and Aeronomy", I983, 23, 59-64.

SHORT PERTURBATIONS OF COSMIC RAY INTENSITY AND ELECTRIC FIELD IN ATMOSPHERE

Alexeyenko V.V., Chudakov A.E., Sborshikov V.G. and Tizengauzen V.A.
Institute for Nuclear Research of the Academy of Sciences of the USSR, Moscow

Starting from 1975 an experiment was carried out using Baksan E.A.S. array (S = 200 m^2 of scintillators, h = = 1700 m, R = 6,5 GV) /1/ to look at short perturbations in cosmic ray intensity. More than 140 events were recorded up to now, nearly 100 % of them can not be explained by pressure or temperature variations (at the level of observation). The characteristic amplitude of the recorded intensity variations is about 1%, the specific time scale 10 ÷ 20 min and duration up to 5 h. The mentioned "time scale" can be affected by the 4 min read out period in this experiment.

The meteorological nature of observed intensity perturbations was found as most probable from strong association of the phenomenon with precipitations out of cumulonimbus clouds also out of nimbo-stratus clouds. Similar effects were observed by Attolini et all /2/, authors suggested temperature variations as most probable to explain the phenomenon.

In our experiment we installed an electric field meter (from 1982) and included in the read out system (1984) the counting rate of the 6 outside detectors. The latter have 6 x 9 m^2 total area, counting rate 4.10^6 counts/4 min. Though this is only 1/3 of the counting rate of the central part it is useful for speculation concerning energy spectrum of variations because of the difference in the thickness of the roofs, the muon energy threshold or central part being 90 MeV and outside detectors only 20 MeV. 43 events with complete information have been recorded in 1984. In all intensity perturbation cases, if electric field meter was in operation (80 total), a strong electric field ~20 kv/m was recorded. The fig.3 shows the correlation of durations of electric field (t_E) and intensity (t_I) disturbances. The typical examples of records (corrected for pressure) is shown on fig.1 and fig.2. There is no visible correlation between intensity perturbation and pressure or temperature. To explain fig.2 by temperature effect the increase of all the atmospheric temperature should exceed 15°C, which seems most unlikely. The difference of I_{20} and I_{90} responses (fig.1) is quite contrary to the temperature effect hypothesis (soft component contributes 40% to I_{20} and only 7% to I_{90} and temperature coefficient for soft component is smaller than for hard component /3/).

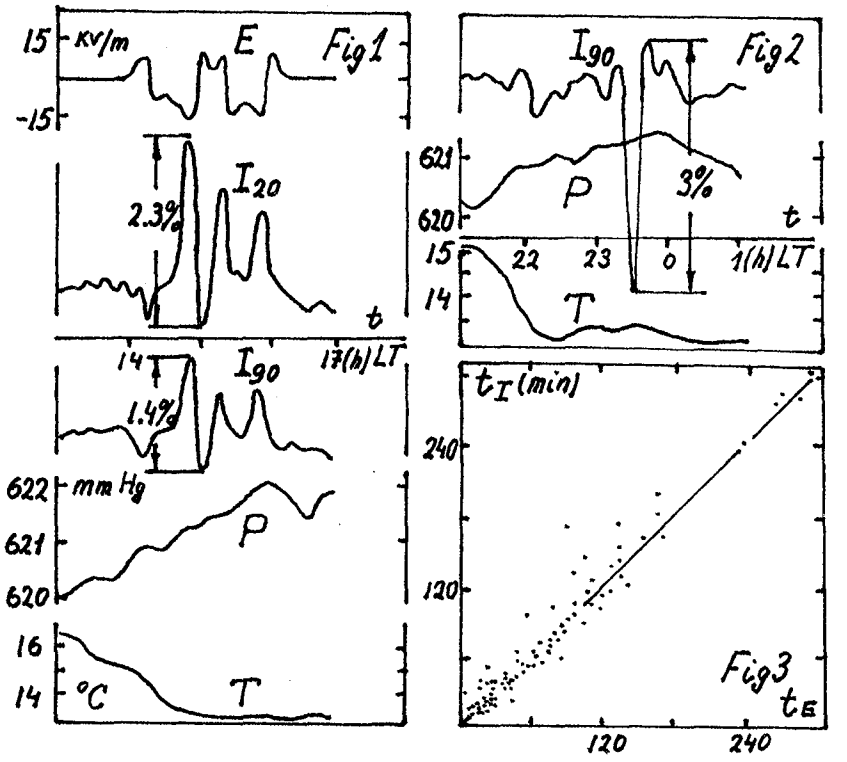

Fig.1. A typical event correlated with rain (13 July 1984) E - electric field. P - atmospheric pressure. T - temperature.

Fig.2. The biggest decrease during a thunderstorm (19--20 June 1983)

Fig.3. The correlation between t_I and t_E

The difficulties in explanation by temperature effect and the obvious connection of short intensity perturbations with electric phenomena (see fig.1,2,3,4,5) make us to examine hypothesis of the influence of electric field on intensity of cosmic rays. The question is not quite new. Many years ago C.T.R.Wilson /8/ suggested the acceleration of electrons by electric field in thunderstorm clouds. The atmospheric electricity effects have been investigated experimentally very long ago /4/, /5/ also /6/ but so far the evidence has been scarce and contradictory.

The main feature of electric field-intensity correlation consists in unambiguous strong connection between both phenomena and, on the other hand, in absence of a strong correlation between E(t) and I(t). More than that, fig.4 and fig.5 show, that there happened to exist events with correlation coefficients R of different sign. There is thought an obvious excess of events with negative R. As a positive direction of electric field was chosen down, so negative R corresponds to the negative charge excess of accelerated (decelarated) particles. Fig.6 shows the

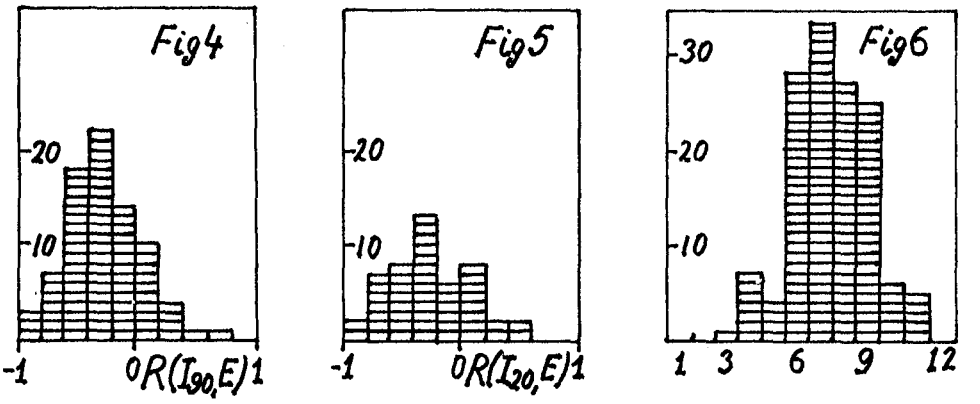

Fig.4. The distribution of correlation coefficients $R(I_{90},E)$

Fig.5. The distribution of correlation coefficients $R(I_{20},E)$

Fig.6. The seasonal distribution of short perturbations of cosmic ray intensity.

absence of events in winter, which is not controversal with the electric field hypothesis.

In principle the electric fields in atmosphere can affect all 3 important c.r.components: electrons, muons and primary protons.

1) e-mechanism due to the excess of negative electrons is presumably a local one because of the short range of electrons, therefore a strong E ↔ I correlation is expected, especially for I_{20}. But experimentally this is not the case - see fig.5 also fig.4. One can think of only small contribution of this mechanism to I_{20} and negligible to I_{90}.

2) μ - mechanism due to the positive excess of muons in the middle atmosphere. Because there is no $\pm$ excess for low energy muons at the level of observation /7/ this mechanism is not local, so the electric field of all atmospheric does affect the I_{20} and I_{90}. This can explain the small and of different signs correlation coefficients R.

3) p-mechanism is located especially high in the atmosphere where the interactions of primary protons with air nuclei give a contribution to the observed muon flux. The change of electric potential at these levels relative to the earth or ionosphere (we believe them to be zero) will change energy of interactions and accordingly the intensity of muon flux. To explain 1% variation in muon intensity the potential at 7 ÷ 15 km should reach 1 GeV or more.

Conclusions. Short perturbations of c.r. intensity were found to be quite common phenomenon. Its meteorological origin and correlation with electric field is established without doubt. The phenomenon probably can be explai-

ned by the electric field if the strength of this field at high altitudes is much bigger than the measured one at surface.

References

1. E.N.Alexeyev, P.Ya.Glemba, A.S.Lidvansky, V.Ya.Markov, N.I.Molchanova, B.B.Tatian, V.A.Tizengauzen and A.E.Chudakov. Proc. 14 ICRC, v.8, p.2996, München (1975)
2. M.R.Attolini, S.Cecchini, M.Galli and J.Guidi. Lettere al Nuov. Cim., 2, N7, p.329 (1971)
3. Dorman L.I. Cosmic ray variations (State Publishing House, Moscow), p.170
4. Shonland B.F.J. Proc.Roy. Soc.A, 130, 37-63 (1930)
5. Shonland B.F.J., Vilfoen J.P.T. Proc. Roy.Soc.A.140, 314 (1933)
6. Clay J., Jongen H.F. and Aart A.J.J. 1952, Physica, 18, 801
7. Singhal K.P.Proc. 18 ICRC, v.7, p.27, Bangalore (1983)
8. Wilson C.T.R. Proc. Camb. Phil. Soc. 22, 534 (1925)

SH 6.1-19

LONG-PERIOD COSMIC RAY VARIATIONS AND THEIR ALTITUDE DEPENDENCE

Belov A.V., Gushchina R.T., Dorman L.I., Sirotina I.V.
Institute of Terrestrial Magnetism, Ionosphere and Radio Wave Propagation, USSR Academy of Sciences, I42092 Troitsk, Moscow Region, USSR

I. The study of long-period variations from the data of ground-based cosmic ray (CR) observations encounters great difficulties. In spite of a large value of an II-year variation, it is more difficult to obtain its spectrum than, say, the spectrum of a solar diurnal variation. Serious obstacles are caused by changes in individual detectors and in the whole world-wide network of CR detectors, by the absence of continuity and uniformity of data series, by various apparatus variations, etc. Therefore, in discrimination and investigation of long-period variations an important and determining point is preparation and preliminary analysis of data.

We have used average monthly data from 28 neutron monitors for the period from IO to 26 years. All the data were preliminarily verified. We made some corrections connected with the change in the efficiency of CR detector and with an incompleteness of some data series. Corrections due to temperature effect were made. We have assumed that the long-period variation δ_i of an individual monitor is caused by an isotropic variation and by first two zonal components of primary CR anisotropy, i.e.

$$\delta_i = a_0 C_0^i(\gamma) + a_1 C_{10}^i(\beta_1) + a_2 C_{20}^i(\beta_2) \qquad (I)$$

where a_0, a_1, a_2 and γ, β_1, β_2 are amplitudes (for a rigidity R= IO GV) and indices of power-law spectrum of the isotropic part and of the zonal components of the primary variation. We have used the acceptance coefficients C_0, C_{IO}, C_{20} calculated in refs. /I,2/ and in the present paper. In average annual data processing the amplitudes a_1 and a_2 did not have a statistically significant difference from zero and variation in each station were determined only by the acceptance coefficient

$$C_0^i(\gamma) = 10^{\gamma} \int_g^{\infty} W(R,g,h) R^{-\gamma} dR, \qquad (2)$$

where g is a cutoff rigidity, h is hight, W(R.g,h) are the coupling coefficients of a given station.

In /3/ it is shown that if one uses the coupling coefficients of the neutron component calculated in /4/ and the approximation

$$W(R,g,h) = \alpha \partial\varepsilon \exp(-\alpha R^{-\partial\varepsilon}) R^{-\partial\varepsilon-1} / (1 - \exp(-\alpha g^{-\partial\varepsilon})),$$

the coefficients α and $\partial\varepsilon$ will be linearly connected with

the depth h in the atmosphere ($\alpha = \alpha_0 + \alpha_1 h$ and $\varkappa = \varkappa_0 + \varkappa_1 h$ for h > 300 mb. For the minimal solar activity $\alpha_0 = 6.25 \pm 0.03$, $\alpha_1 = 0.70 \pm 0.04$, $\varkappa_0 = 1.40 \pm 0.02$, $\varkappa_1 = -0.56 \pm 0.02$.

Figure I presents the behaviour of the isotropic component a_0 of the primary variation of CR (for a rigidity of 5, 10 and 20 GV) and the change in the intensity I_λ of the green coronal line during 1957-1982. Note that the rigidity spectrum of the long-period CR variation is apparently "softer" in the years closest to the maxima of solar activity and "harder" near the minima. The CR modulation depth in a 20-th cycle is much smaller than in a 19-th or a 21-st cycle. This difference is especially large for hard particles. The Table presents the indices γ averaged for years of high solar activity. In the CR spectrum variations a 22-year repeatability is observed. It can possibly be explained by the difference in the level of solar activity in the maxima of three last cycles.

cycle	years	γ
19	58-61	0.6 ± 0.1
20	68-71	1.2 ± 0.1
21	79-82	0.7 ± 0.1

2. The use of acceptance coefficients is not the only way for obtaining the energy spectrum of CR variations from the data of ground-based recorders. The other methods require the knowledge of the altitude dependence of the variation δ of the studied component of secondary CR. It is convenient to characterize the altitude dependence by the quantity $\beta_\delta = \frac{1}{\delta}\frac{\partial \delta}{\partial h}$; it is natural to call this quantity a variational barometric coefficient. The quantity β_δ for the neutron component can be calculated with the use made of the above-mentioned data on the altitude dependence of coupling coefficients and the expression

$$\beta_\delta(g,h) = \left(\int_g^\infty \beta_w(R,g,h) W(R,g,h) \Delta(R)\, dR\right) \Big/ \int_g^\infty W(R,g,h)\Delta(R)\, dR \quad (3)$$

where $\beta_w = \frac{1}{W}\frac{\partial W}{\partial h}$ and $\Delta(R) = \frac{\Delta D}{D}(R)$ is the variation of the primary spectrum of CR. The dependence of β_δ on the cutoff rigidity g and on the variational spectral index γ is shown in Fig.2. The value of the coefficient β_δ can be an indication of the slope of the rigidity spectrum of secondary CR variation. Besides, the calculation of β_δ can be used for reduction of the variations observed at different altitudes to one barometric level and for calculation of variations of the total barometric coefficient for different neutron monitors. With the help of the same data on one can calculate also the partial barometric coefficient $\beta_m = \frac{1}{m}\frac{\partial m}{\partial h}$ (m = m(R,h) is the integral multiplicity of neutron component generation) since $\beta_m = \beta_w + \beta$ where β is the total barometric coefficient. The dependence of β_m on rigidity for h = 600 mb and 1000 mb is shown in Fig.3.

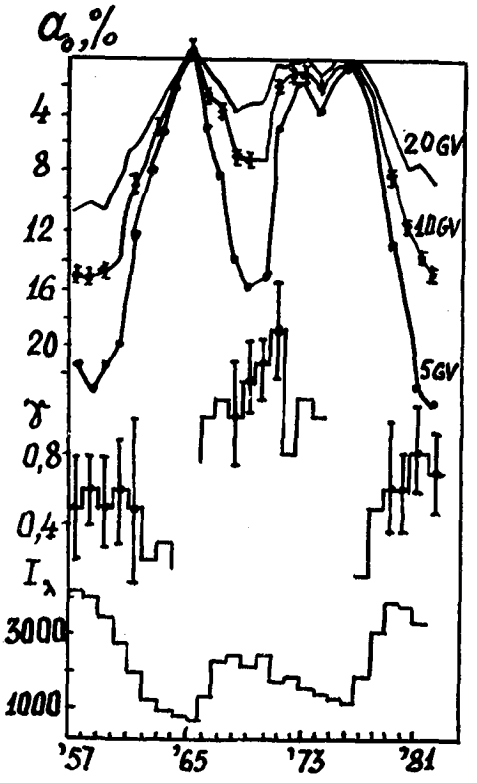

Fig. 1

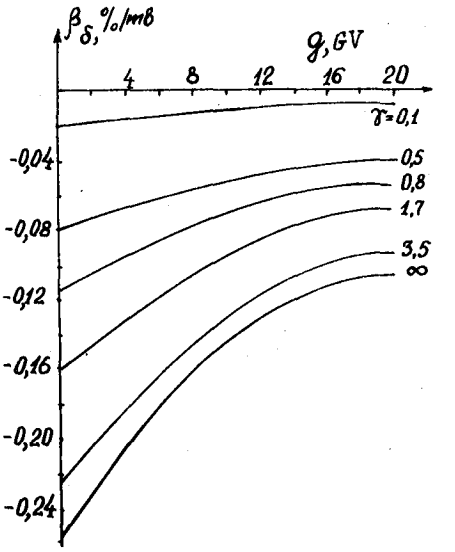

Fig. 2

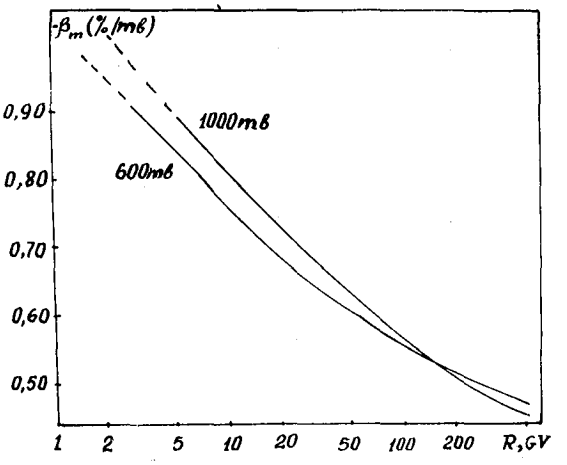

Fig. 3

REFERENCES

1. Yasue S., Mori S., Sakakibara S., Nagashima K. Report of Cos. Ray Res. Lab., 1982, 7, Nagoya, Japan.
2. Belov A.V., Eroshenko E.A. Proc. 17-th ICRC, Paris, v.4, 97, 1981.
3. Dorman L.I., Belov A.V., Yanke V.G. et al. Izv.AN SSSR, ser.fiz., 1982, v.46, 1689.
4. Dorman L.I., Yanke V.G., Proc. 17-the ICRC, Paris, v.4, 326, 1981.
5. Granitsky L.V., Rishe A. Acta Phys. Acad.Sci.Hung., 1970, v.29, Suppl. 2, p. 233.

DIURNAL VARIATIONS OF COSMIC RAY GEOMAGNETIC CUT-OFF THRESHOLD RIGIDITIES

V.M.Dvornikov, V.E.Sdobnov, A.V.Sergeev (SibIZMIR, Irkutsk 33, P.O.Box 4, USSR)

O.A.Danilova, M.I.Tyasto (LO IZMIRAN, Leningrad,V-53)

Abstract. For the period 1 May-30 June 1972, using the method of spectrographic global survey we investigated the rigidity variations Rc of geomagnetic cut-off as a function of local time and the level of geomagnetic disturbance for a number of stations of the world-wide network.
It is shown that geomagnetic cut-off threshold rigidities undergo diurnal variations. The diurnal wave amplitude decreases with increasing threshold rigidity Rc, and the wave maximum occurs at 2-4 hr LT. The amplitude of diurnal variations increases with increasing geomagnetic activity.
The results obtained agree with those from trajectory calculations made for an asymmetric model of the magnetosphere during different geomagnetic fdisturbance conditions.

The study of cosmic ray (CR) intensity variations of magnetospheric origin observable on the ground is of interest for two reasons: first, we cannot study CR variations of interplanetary origin without making adequately allowing for the variations arising in the sphere of action of the magnetic field of the Earth and, second, the variations of magnetospheric origin themselves can be used as an additional source of information on processes occurring inside the magnetosphere at different distances from the Earth.

However, the study of the variations of this class becomes difficult because they are observed simultaneously with CR variations of a significantly larger amplitude which are associated with processes in interplanetary space. In order to separate these two types of variations, a method of spectrographic global survey (SGS) has been developed that makes it possible, using ground-based CR observations at the world-wide network of stations, to obtain information regarding the energy and pitch-angle distribution of primary CR in the interplanetary magnetic field (IMF), on the IMF orientation and on variations of the planetary system of geomagnetic cut-off rigidities (GCR). This method was used in /1/ to obtain information on GCR variations (Δ Rc) for a number of points of the world-wide network during the June 1972 geomagnetic storm; the latitude dependence of the amplitudes of these variations is studied and a quantitative estimation of parameters of current systems of disturbances made. The results obtained are consistent with current views of dynamical processes in the magnetosphere and agree with satellite measurements /2/.

This paper investigates GCR diurnal variations, their dependence on latitude and level of geomagnetic disturbance for the period 1 May - 30 June 1972.

The analysis employed data from 34 world network stations. In order to determine GCR variations at middle and lower-latitude stations it is necessary to have at least two detectors sensitive to these variations, with different coupling coef-

ficients at threshold rigidity. Since many middle and lower-latitude stations lack complexes of detectors required to determine Rc, near-by stations were combined into such complexes and were ascribed equal (averaged) threshold GCR (R c). The

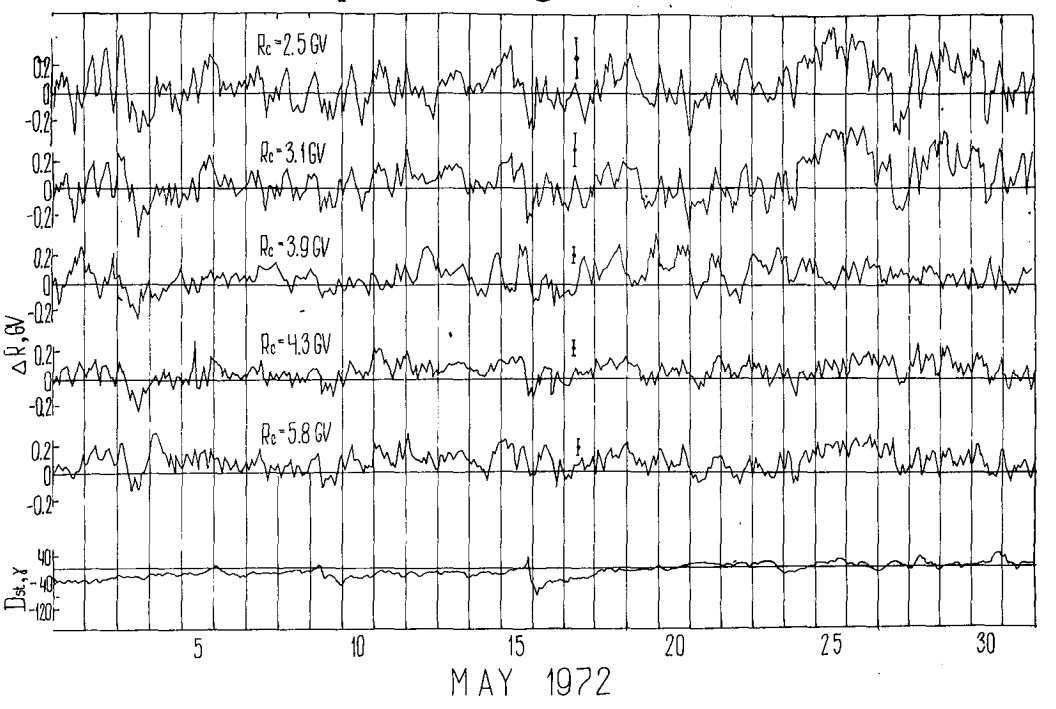

Fig. 1

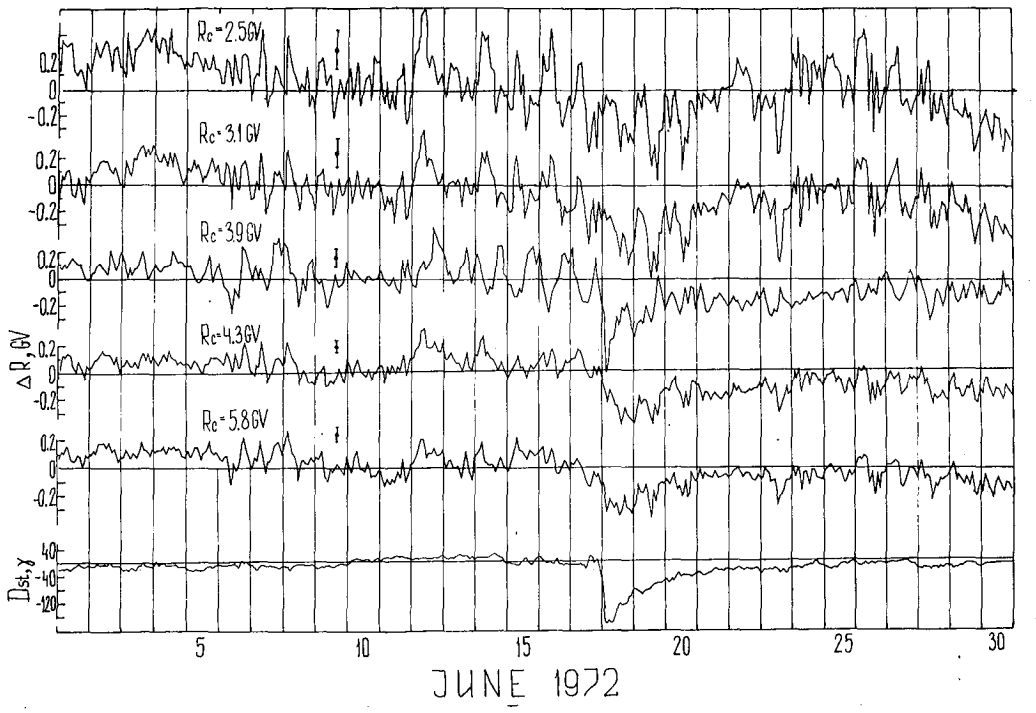

Fig. 2

analysis used observations from five such groups of stations: 1.Kiel and Utrecht ($\bar{R}c$=2.5GV);2.Dourbes and Lindau ($\bar{R}c$=3.1 GV);3.the Sayan spectrograph complex ($\bar{R}c$=3.9GV);4.Hafelekar, Zugspitze, Jungfraujoch ($\bar{R}c$=4.3GV);5.Rome and Pic-du-Midi ($\bar{R}c$=5.8GV). For each group of stations, we determined variations of threshold GCR using data averaged over a two-hour interval.

Figs 1 and 2 show the variations Rc as obtained by the SGS method, of threshold GCR for two months for each of the above groups of CR stations. The period of study includes intervals with both relatively weak geomagnetic activity (Kp $\sim$ 1) and high geomagnetic activity (Kp $\geq$ 3+). The mean Kp-index that defines the geomagnetic activity for the whole period considered is about 2+.

In order to separate the periodic part of the threshold GCR variation, we employed a numerical mathematical filter /3/ which was used to separate oscillations with a period T $\leq$ 24 hr and the filtered-out data were then averaged by the superposed epoch method. The results of the analysis made are presented in Fig. 3 showing the variations of threshold GCR during 24 hr as a function of LT (solid curve). The upper panel of the plots represents the variations of threshold GCR during 24 hr for a period with Kp $\sim$ 2 while the lower panel shows those for the period with Kp $\sim$ 5.

As follows from the plots, the variations of threshold GCR involve a diurnal variation with its maximum occurring at 2-4 hr LT. For the group of stations with $\bar{R}c$=2.5GV, the amplitude of variations in threshold GCR during 24 hr is $\sim$ 0.12GV for a period with Kp $\sim$ 2 and $\sim$ 0.3 GV for a period with Kp $\sim$ 5; for the group of stations with $\bar{R}c$=3.1 GV, these variations are $\sim$ 0.12GV and $\sim$ 0.2GV, respectively, with $\bar{R}c$=3.9GV, $\sim$ 0.1GV and $\sim$ 0.16GV, with $\bar{R}c$=4.3GV - $\sim$ 0.06GV and $\sim$ 0.1GV,with $\bar{R}c$=5.8GV, $\sim$ 0.05GV and $\sim$ 0.08GV.

Thus, the amplitude of the diurnal variation in threshold GCR depends on threshold GCR, decreases with increasing

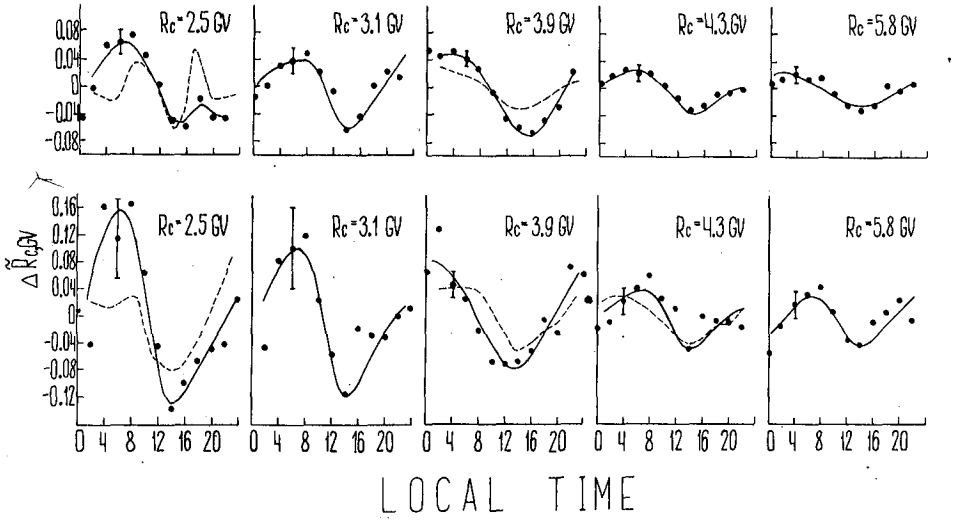

Fig. 3

Rc and increases with an enhancement of geomagnetic activity.

This diurnal variation in threshold GCR can be due to several reasons, in particular to an asymmetry of the magnetosphere as a consequence of its being compressed by the SW.

Since the diurnal wave in the threshold GCR variations was obt ined from CR observations covering a rather long period, this indicates that the asymmetry source for threshold GCR in the magnetosphere is quasi-stationary.

In order to confirm this, we made numerical trajectory calculations of the motion of charged particles in a real geomagnetic field. The real geomagnetic field was specified in the calculations in terms of a model reported by Tsyganenko N.A. et al. /4/, in which a separate description is made of magnetic fields from each current system of the magnetosphere showing a substantially different spatial structure. The parameters of the model depend on the level of geomagnetic activity that is characterized by the Kp-index.

A dotted line in Fig. 3 shows the results from the numerical calculations of the dependence of threshold GCR on LT. The upper panel refers to a quiet period ($Kp \sim 0$) and the lower panel corresponds to the period with $Kp > 3+$. The numerical calculation results confirm the presence of a diurnal wave obtained from experimental data, the dependence of its amplitude on threshold GCR at the observation point and on the level of geomagnetic activity.

Conclusions. It is demonstrated both experimentally and theoretically that diurnal variations of CR threshold GCR do exist at middle and lower latitudes. The diurnal wave amplitude of threshold GCR decreases with increasing threshold GCR and increases with increasing geomagnetic activity. Diurnal wave maximum occurs at 2-4 hr LT. The trajectory calculations of the motion of charged particles in the geomagnetic field showed that the experimentally found diurnal wave in threshold GCR is due to the asymmetry of the magnetosphere because of its being compressed by the SW.

REFERENCES

1. V.M.Dvornikov, V.E.Sdobnov, A.V.Sergeev. 1984, Preprint SibIZMIR SO AN SSSR 25-84.
2. F.W.Berko, L.J.Cahill, T.A.Fritz, J.G.R., 1975, 80, p. 3549-3552.
3. L.I.Dorman, A.A.Luzov. 1967, In: "Kosmicheskie luchi", 8, 285, "Nauka", Moscow.
4. V.A.Sergeev, N.A.Tsyganenko. The Earth's Magnetosphere. 1980, "Nauka", Moscow.

SH- 6.1-22

THE INFLUENCE OF THE EARTH'S MAGNETOSPHERE ON THE HIGH-ENERGY SOLAR PROTONS

G.A.Bazilevskaya
P.N.Lebedev Physical Institute of the Academy of Sciences of the USSR, 117924,Leninsky Prospect,53, Moscow, USSR

V.S.Makhmutov
Industrial Institute of Roudny, 459120,Roudny, USSR

T.N.Charakhchyan
Institute of Nuclear Physics, Moscow State University, 119899,Moscow, USSR

Abstract

The North-South asymmetry in the fluxes of solar protons with the energy ~70-200 MeV in stratosphere at the invariant latitudes 62°-76° is discussed.

1.Introduction. In the earth'S polar regions the intensity of the solar protons with the energy above the critical energy of geomagnetic cutoff is, according to the Liouville theorem, the same as in the interplanetary space. The penumbra in the polar regions is small and the East-West effect is also small /1/. However the geomagnetic cutoff rigidity R_c in polar regions is difficult to calculate because it is not sufficient to include only the internal sources of the geomagnetic field. According to /2/, during the magneto-quiescent periods the real value of R_c can be less by 0.1 GV than the calculated value because of the external sources. During the geomagnetic storms the real value of R_c is still lower.

2.Observations. The stratospheric exploration of the cosmic rays (CR) initiated in the USSR in IGY provides information on the energy spectrum and absolute flux of the solar protons intruding into the earth's atmosphere. The detector consists of two Geiger counters forming the telescope interlaid with the 7 mm thick aluminium filter /3/. The data on the stations of the stratospheric CR observations are listed in the Table. Although the calculated values of R_c are 0.5GV and 0.6 GV at Olenya and Apatity respectively, the lower

Table. Polar stratospheric stations

Station	Geograph.coordinates Latitude	Longitude	Invariant Latitude	R_c,GV /2/	E , MeV
Olenya, (Murm.reg.)	68.95 N	33.05 E	65.7	0.5	125
Apatity, (Murm.reg.)	67.55 N	33.33 E	62.5	0.6	175
Mirny	66.57 S	92.92 E	76.4	0.03	0.48

energy limit of the observed solar protons at these locations is nevertheless always determined by the ionization ab-

sorption in the residual atmosphere and is sometimes as low as 50 MeV. This means that even in the magneto-quiet periods the rigidity of geomagnetic cutoff at Olenya and Apatity is not higher than 0.3 GV.

Since the asymptotic directions of CR arrival in the Murmansk region (Olenya, Apatity) and at Mirny are different /2/, the N-S anisotropy in the stratospheric observations can be expected in case of the pitch-angular anisotropy of the solar cosmic ray (SCR)fluxes in the interplanetary space. This effect is usually observed only near the onset of a proton event. If the SCR intensity at the atmospheric boundary is not isotropic this leads to the discrepancy between the flux values of solar protons obtained with a single counter and a telescope. This effect sometimes happens /4/, but the present paper will deal with the N-S anisotropy which appears after the maximum of a proton event. In such cases the data of a single counter and a telescope coincide as a rule, so the pitch-angular isotropy at the atmospheric boundary takes place.

3.Comparison of the results for the Northern and the Southern hemispheres. During the period of combined measurements in the Southern and the Northern hemispheres, starting from 1963, about 60 solar proton measurements simultaneously within an hour have been performed. From these data we excluded the balloon flights during which the temporal dynamic of intensity was observed and also the data obtained at the onset of events when according to the neutron monitor data the SCR angular anisotropy was observed. In 31 of the remainder 43 flights the results agree within 10% accuracy. In 10 flights the SCR flux was higher in the Northern hemisphere, among them 6 flights manifested discrepancy more than 30%; 2 measurements showed the excess SCR flux at Mirny.

The most remarkable case of the N-S anisotropy is the SCR event of 12.10.81 reported in /5/. During this event 10 flights in the Southern hemisphere and 39 flights in the Murmansk region were carried out. Some energetic spectra measured during this event are presented in Fig.1 together with the Meteor /6/ and IMP-8 /7/ data. The IMP-8 differential spectrum is recalculated by us to the integral spectrum taking into account the intensity of protons with $E \geq 90$ MeV according to the Meteor data. The features of the event in question are: 1/ the anisotropy is not persistent; 2/ when the N-S anisotropy is observed the satellite data agree with the Mirny data, and thus in the Northern hemisphere there is an excess flux of particles. According to Meteor observations in the polar caps there was no any noticeable anisotropy at $E \geq 90$ MeV during this period /6/. We may infer that an excess flux of particles in the Murmansk region has a magnetospheric origin . The surplus flux causes the steepening of proton spectrum at $E < 200$ MeV which can be seen in Murmansk data even without any comparison with simultaneous Mirny data /5/. This excess cannot be accounted for by the bremsst-

rahlung of the auroral electrons because these are not registered with a telescope. A certain contribution of the bremsstrahlung can be admitted only at 03-04 UT and 15-16 UT observations on 13.10.81.

The time behaviour of the anisotropy is shown in Fig.2 It is seen, that the value of the excess flux (if occurs) gradually decreases with time. The spectrum index of the excess flux, γ, is equal to 3-5 and it increases up to $\sim$ 14 during the last flight on 15.10.81. The anisotropy calculated as $\alpha = (I_N - I_S)/(I_N + I_S)$ also becomes stronger to the end of the event. In the bottom of Fig. 2 we give the values of K_p- index /8/. We failed to reveal any correlation between the N-S anisotropy and geomagnetic disturbances.

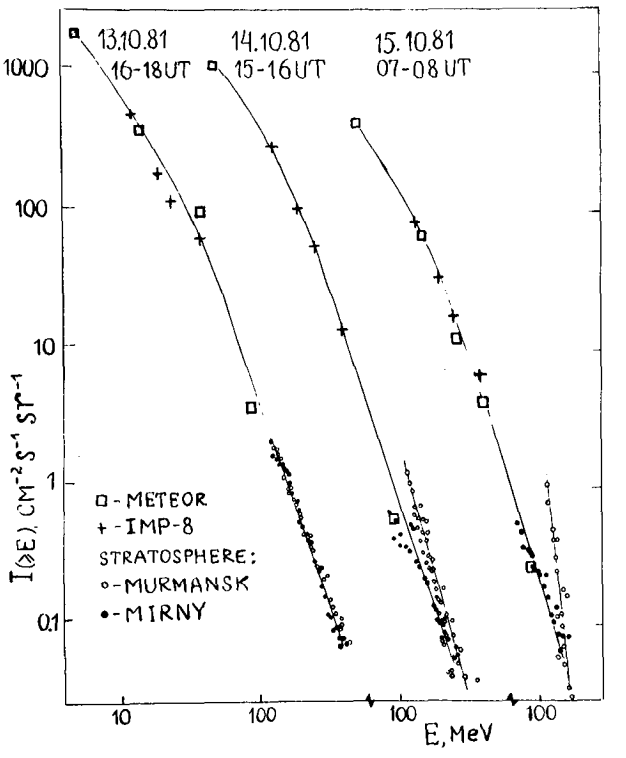

Fig. 1 Examples of energy spectra of solar protons according to stratospheric and satellite data

4.Discussion. The N-S asymmetry in the fluxes of solar protons with E≅70-200 MeV is occasionally observed in the stratosphere. The 700-1000 km height satellite observations in the polar caps /6/ have not confirmed the presence of the anisotropy. The SCR fluxes in the polar caps agree with the Mirny data. The surplus flux of particles in the Murmansk region is not persistent, has a steep energetic spectrum and the maximal energy does not exceed $\sim$ 200 MeV. There is no correlation with the geomagnetic disturbances, but an especially strong anisotropy was observed during the latest phase of the event more than a day after the sudden commencement of the geomagnetic storm marked by a triangle in Fig. 2. Similar effects against a background of the geomagnetic storms were observed in the stratosphere during powerful proton events of the 19-th solar cycle /3/. The spectrum steepening was supposed to be associated with the particles accelerated or localized near the front of the interplanetary shock of flare origin. However the direct

measurements in the interplanetary space have shown that the energy of storm particles is not higher than 30 MeV /9/. Unfortunately no measurements in the Southern hemisphere were made at that time.

The difference between Murmansk and Mirny is that Murmansk is situated on the closed magnetic shell and Mirny on the open one. An important fact is that the effect is limited in the energy range of particles which penetrate mainly through the tail of the magnetosphere /10/. The nonadiabatic processes leading to an additional flux of high-energy protons should play a role here /11/.

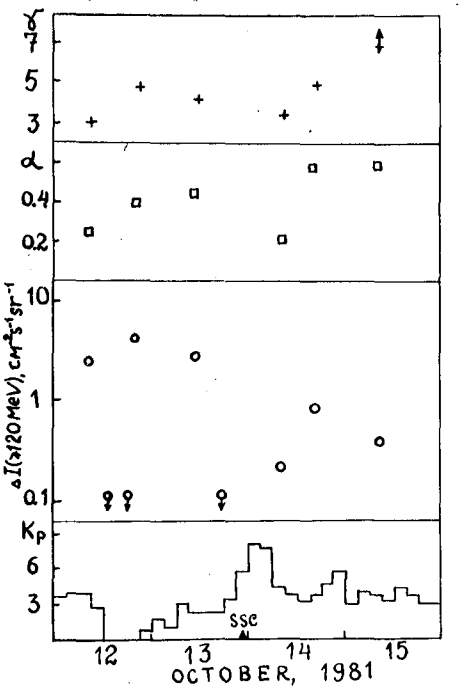

Fig. 2. Time behaviour of an excess flux of particles in Murmansk region.

References.

1. Dorman,L.I.,Smirnov,V.S.,Tyasto,M.I.,(1971),Cosmic Rays in the Earth's Magnetic Field.Moscow, Nauka.
2. Shea, M.A., Smart,D.F.,(1975), AFCRL-TR-0247.
3. Charakhchyan,A.N.,(1964),Uspekhi Fiz. Nauk, v.83,p.35.
4. Borovkov,L.P., et al.,(1982) Izv. Acad. Nauk SSSR, ser.fiz., v.46, p.1709.
5. Bazilevskaya,G.A., et al.,(1983),Proc.18-th ICRC, Bangalore, v.4, p.189.
6. Avdyushin,S.I.,Pereyaslova,N.K.,(1983),Izv. Akad. Nauk SSSR, ser.fiz., v.47, p.1805.
7. Solar-Geophysical Data,(1984),475(II), U.S.Dep.of Commerce, Boulder, USA.
8. Solar-Geophysical Data (1981),448(I), U.S.Dep.of Commerce, Boulder, USA.
9. McDonald, F.B.,(1981),Proc. 17-th ICRC., Paris,v.13, p.189.
10. Gall,R.,Bravo,S.,(1981),J.Geophys.Res.,v.86,p.2467.
11. Il'in,V.D., et al.,(1984),Izv. Acad. Nauk SSSR, ser. fiz., v.48, p.2200.

SH 7.1-1

COSMIC RAY ^{10}Be BIENNIAL DATA AND THEIR RELATIONSHIP TO AURORAE AND SUNSPOTS.

M.R.Attolini, S.Cecchini, Istituto TESRE del CNR, Bologna
G.Cini Castagnoli, Istituto di Fisica Generale, Università di Torino
M.Galli, Dipartimento di Fisica, Università di Bologna
T.Nanni, Istituto FISBAT del CNR, Bologna, Italy

1.Introduction. Studies of Galactic Cosmic Ray (C.R.) variations should give information on three dimensional aspects of the heliospheric magnetic fields and on the Solar wind, which modulate their influx into the Solar System. But in order to decode the information from the C.R. series it is necessary to know the mechanisms through which the modulation is produced; and this problem is not yet solved[1], although it is clear that a balance of effects with sources at different heliospheric latitudes results in the modulated C.R. intensity.

The investigation of the structure of various time series of data, characterized by the imprint of the Solar variability and its comparison with the structure of the C.R. time series may contribute to the phenomenological individuation of the different sources of modulation.

The C.R. data are of two types: a)the direct measurements of the C.R. intensity at ground since their discovery in the last four decades or b)the record of earlier C.R. flux that has been left as cosmogenic isotopes in different reservoirs. In this paper we examine the ^{10}Be series in polar ice from 1900 to 1976 A.D. measured by J.-Beer[2] et al.(1983) in core Dye3, Greenland.

The other time series that we take into consideration are those of the Sunspot (S.S.) number (R_z)[3] of the global geomagnetic activity <aa>[4] and of the Aurorae[5].

The R_z time series is related to the contribution to the C.R. modulation resulting from the solar conditions in the equatorial region; its anticorrelation to the C.R. series is well known (see Figure 1). The Auroral activity is the result of energy transfer from the solar wind to the magnetosphere, when interplanetary shocks and recurrent wind streams with origin at different heliospheric latitudes pass by the Earth. The comparison of the <aa> index and of the aurorae series with the ^{10}Be series may lead us to the determination of a contribution to the ^{10}Be production due to effects with origin at the higher heliospheric latitudes: the effects of the stable polar high speed wind recurrent streams occuring much more frequently during the declining and minimum phases of solar activity and associated with coronal holes. The size of the polar coronal holes and the C.R. intensity from 1965 to 1976 were already found positively correlated by Hundhausen et al.[6] from 1965 to 1976. This correlation is an evidence for the importance of the drift effects or of the

large-scale structure of the magnetic field effects on the C.R. modulation[7]. Therefore we expect an increased C.R. flux associated to an auroral activity independent from R_z. The identification of two types of geomagnetic activity (the transient or Sunspot shaped activity and the stable wind stream activity) has been pointed out by Legrand and Simon[8].

2.The series of Aurorae, <aa> index and Sunspot number R_z. One of the most important historical series belonging to the study of the Solar-Terrestrial relationships is the millennial series of the Aurorae. It is therefore very important to compare the behaviour and structure of this series during recent times with that of the geomagnetic activity <aa> series available from 1868 and with the R_z series available from 1701. The annual average of <aa> is in fact a terrestrial parameter objectively measured, related[9] to the annual average solar wind parameter $|B_z| V^2$. In Figure 2 the time series are shown. The Aurorae from 1721 to 1780 are those collected by Rubenson and reported by Feynman and Silverman[10] (note that they may be not homogenous to those starting in 1780[5]). On the whole the Aurorae appear in phase with R_z except for the intervals before the most important maxima of R_z in which they appear to be also abundant a little before the R_z minima.

In Figure 3 the phase cyclograms of the three series are reported at τ =10y. We notice how similar the topology (i.e. loops, bendings and stretchings) of the three series looks like. Moreover a phase shift between the cyclograms of the Aurorae (or of <aa>) and R_z can be observed. This phase shift is confirmed by the cross-cyclogram performed on the Aurorae and R_z series in the band around τ =11y (Figure 4), which is not stretched along the real axis. The two facts leed to the conclusion that there is a part of the Auroral activity which is not related to R_z and although with similar periodicity is substantially phase shifted. We have therefore computed the series of Aurorae linear-regression-corrected-for R_z, after the second order detrending. The phase cyclogram for τ =11,1y of these residual aurorae, obviously independent from R_z, is given in Figure 5, where we have also given how to find the time of maxima of the series. This cyclogram is very straight, showing that the periodicity is constant in time and equal to 11,1y. This is confirmed by the power spectral density (p.s.d.) analysis of the residual Aurorae, given in Figure 6 (lower graph) in which we give also for comparison the p.s.d. of the series of the total Aurorae (upper graph). Two interesting points must be noticed: a)the psd of total Aurorae shows two lines one at 10.0y and one at 11.1y; after correcting for the equatorial activity the residual Aurorae show only the second line; b)the psd of the residuals shows the peak at 21.6y with its third harmonic at 7y reinforced.The maxima starting from 1877 of the residual aurorae (see Figure 5) happen at about the same time of the recurrent geomagnetic

activity, which has been shown by Legrand and Simon (1981) in Fig.1 of their paper to be mostly due to the polar high speed wind streams.

3.The series of ^{10}Be. The biennial experimental ^{10}Be data were smoothed by the running mean of two data, giving a series of 39 data starting from 1900-1901. The global geomagnetic activity (or the Aurorae see Figure 7a) has been splitted into the two aforementioned series: the stable-wind-stream and the transient-R_z-related activity (Figure 7b) covering the same interval and with the same averaging time of ^{10}Be shifted by 3 years according to the cross cyclogram of ^{10}Be and R_z. The ^{10}Be series has been correlated in a threefold correlation, according to the statistical model: $^{10}Be = k\langle aa\rangle_{trans} + h\langle aa\rangle_{stab}$ The threefold correlation shows a negative coefficient $k=-0,0047$ Be^{10} units/$\langle aa\rangle$ units, ave$[\langle aa\rangle_{trans}]$ =32.06 and a positive coefficient $h=0,0057$, ave$[\langle aa\rangle_{stab}]$ =14.79. With these coefficients the curve of the expected values of ^{10}Be was calculated and it is shown in Figure 7c together with the experimental data. The two curves agree rather well if one takes into account the measurement experimental errors. The errors account for about 20% of the total variance of the series so that only 80% of the variance should be explained from the correlation with $\langle aa\rangle_{trans}$ and $\langle aa\rangle_{stab}$. In our case the total correlation is 62%, covering almost the entire possibility.

4.Conclusions. We have found by statistical analysis that the modulation of ^{10}Be in polar ice may be due to at least two main contributions: one is negative and in phase with the Solar flare activity modulating the cosmic ray flux in Forbush-type decreases and one is positive in phase with the appearence of large wind streams situated at both polar coronal holes. Furthermore from the analysis of Aurorae we have found that the high heliolatitude activity is related to a stable periodicity of 11.1y whereas the low heliolatitude activity contributes to the wondering of the solar cycles.

References

1. Jokipii J.R., (1984), Proc.Int.Symp. on C.R., Morioka,Japan
2. Beer J., Andrée M., Oeschger H., Stauffer B., Balzer R., Bonani G., Stoller C., Suter M., Woelfli and Finkel R., (1983), Radiocarbon 25, 269
3. Waldemayer M., (1961), The Sunspost Activities in the years 1616-1960, Schulthess and CO, Zurich, Switzerland
4. Mayaud P.N., (1973), Iaga Bulletin 33
5. Legrand J.P., private communication (Aurorae 1780-1979)
6. Hundhausen A.J., Sims D.G., Hansen R.T., (1980), Science 207, 761
7. Fisk L.A., (1979), Proc.Conf. Ancient Sun (Pepin, Eddy, Merryl) Geochimica et Cosmochimica Acta suppl. 13 (1979),p.103
8. Legrand J.P. and Simon P.A., (1981), Solar Physics 70, 173,
9. Feynman J., (1983), Reviews of Geophysics and Space Phys. 21, 338
10. Feynman J., Silverman S., Nasa Conf. publication 2098

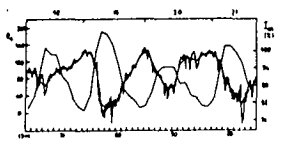

Fig. 1

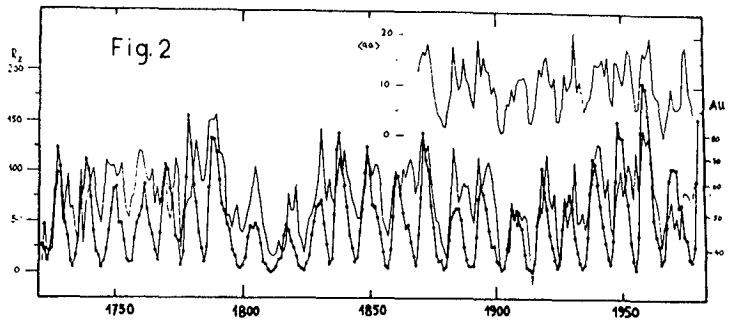

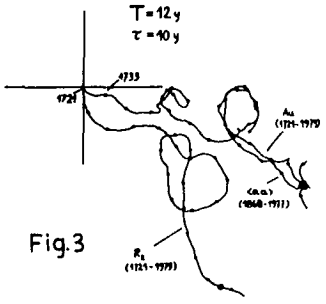

Fig. 3

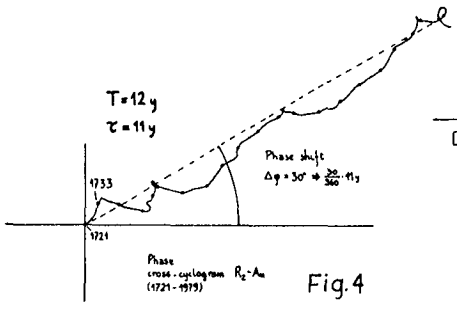

Fig. 4

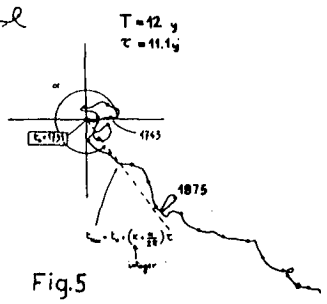

Fig. 5

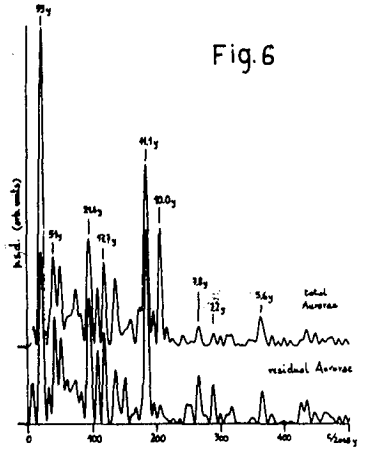

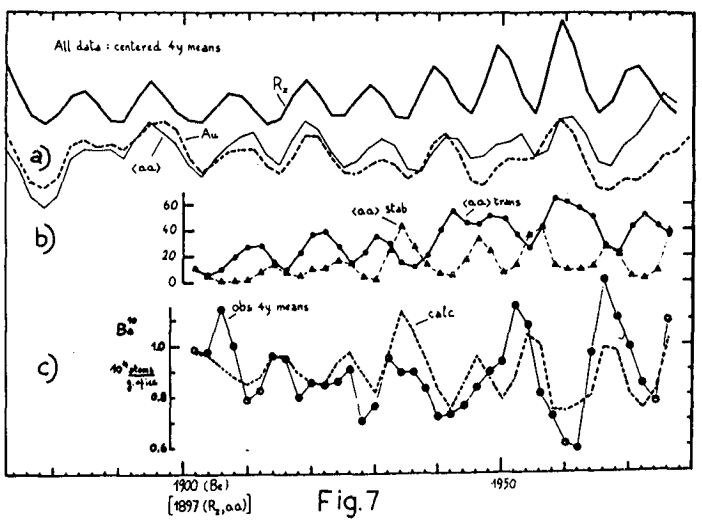

Fig. 7

SOLAR MODULATION OF COSMIC RAY INTENSITY AND SOLAR FLARE EVENTS INFERRED FROM ^{14}C CONTENTS IN DATED TREE RINGS

C. Y. Fan
Department of Physics, University of Arizona, Tucson, AZ 85721, USA

T. M. Chen and S. X. Yun
Archaeological Section, History Department, Peking University
Beijing, China

K. M. Dai
Department of Physics, Nanjing University, Nanjing, China

We have measured the $\Delta^{14}C$ values in 42 rings (from 1824 to 1865 AD) of a white spruce grown in Mackenzie Delta (68°N, 130°W) as our continuing effort of tracing the history of solar modulation of cosmic ray intensity. We also measured the $\Delta^{14}C$ values in 6 rings (from 1940 to 1945 AD), searching for a ^{14}C increase due to two large solar flares that occurred in 1942 and were detected by Forbush. The results will be presented and discussed.

1. Introduction. Carbon-14 nuclei in the atmosphere are produced by cosmic-ray-generated neutrons in $^{14}N(n,p)^{14}C$ reaction. After the production, these nuclei react rapidly with ambient atmosphere to become $^{14}CO_2$ molecules. The concentration of the $^{14}C_2$ molecules is mainly determined by the rate of production and the rate of transfer, first to the troposphere from the stratosphere where most of them are produced, and then from the troposphere to the deep-sea sink reservoir. Since cosmic ray intensity is modulated by interplanetary magnetic fields whose strength depends on the solar activity, it is expected that the concentration is anti-correlated with sunspot numbers. While the long-term change in $\Delta^{14}C$ in tree rings samples, which reflects the variation of the atmospheric ^{14}C concentration, has been studied by many investigators and the correlation established beyond any doubt (e.g., Stuiver and Quay, 1980, and references therein), the question remains as to whether the amplitude of the expected 11-year variation is large enough to be measurable.

There was some indication that $\Delta^{14}C$ values in grains and trees grown at high lattitudes show 11-year periodicity (Baxter and Farmer, 1973). To study the possible latitudinal effect, we searched and, fortunately, obtained two sections of dated white spruce grown near Campbell River in Mackenzie Delta, Canada (68°N, 130°W) from Dr. M. L. Parker of the University of British Columbia; one of the sections contains rings from 1510 to 1972 AD. Initial measurements of 27 samples, covering the period from 1866 to 1925 AD, indicated that the $\Delta^{14}C$ values do exhibit a $10^{o}/_{oo}$ fluctuation, anticorrelated with sunspot numbers. The results were reported at the 18th International Cosmic Ray Conference (Fan et al., 1983a, 1983b). In this paper we shall report $\Delta^{14}C$ in the ring samples from 1824 to 1865 AD. We also measured the $\Delta^{14}C$ in 1940 to 1945 rings, looking for the signature of ^{14}C increase, due to two large solar flares that occurred in 1942 and were reported by Forbush (1946). The results will be discussed.

2. Experiment. The task of the measurements was divided between two institutions; the 1824 to 1865 rings were measured at the Department of History of Peking University, whereas the 1940 to 1945 rings were measured at the

Department of Physics of Nanjing University. The equipment used was similar; a liquid scintillator-photomultiplier tube device, which were carefully intercalibrated. Both systems used two photomultiplier tubes in coincidence to count ^{14}C decay electrons and a pulse height discrimination to reduce cross-talks between the two tubes. There was, however, a slight difference between the two systems. At Peking University, 5-10 cm of lead was used to reduce cosmic-ray-induced background, whereas at Nanjing University, in addition to a lead shield, a plastic scintillator-photomultiplier tube system was used as an anti-coincidence shield. The result of the addition was a reduction of the background from 6 cpm to 2 cpm. An overall precision of both systems was about $4^{o}/_{oo}$, including a pure statistical uncertainty of $\sim 3^{o}/_{oo}$.

For each measurement, about 10 g of wood is needed. Because of the narrowness of the rings, except the 1928 ring, we had to combine two, and sometimes three, rings to obtain a sufficient specimen for one measurement. After being treated with the routine HCℓ-NaOH-HCℓ procedure to remove resin, the samples were converted to CO_2 and then to benzene. For one measurement, 5 cc of synthesized benzene was used. The net count rate for a modern sample was 39 cpm. For each sample, we measured $^{13}C/^{12}C$ for fractionation correction.

3. Results on Modulation of Cosmic Ray Intensity. The experimental results are expressed as $\Delta^{14}C$ values which are the relative deviations of the measured ^{14}C activities from the standard oxilic acid activity of the U.S. National Bureau of Standards, corrected for ages and isotope fractionations. For the sample prior to 1885, the correction for the Suess effect was not needed.

The data points, including 11 previously published values, are plotted in the bottom panel of Fig. 1, along with other published $\Delta^{14}C$ values for comparison. To show the correlation with solar activity, we plotted in the upper panel the sunspot numbers with ordinates inverted. It is seen that, except for the 1922 cycle, with a delay of about five years, the $\Delta^{14}C$ values are anti-correlated with sunspot numbers; the cross-correlation coefficient is ~0.6. At present, we are baffled by the reverse correlation in the 1822 cycle. Also, we feel uneasy about the five-year delay, which is longer than what we had expected. We do not rule out a possible error in the tree ring count.

4. Results on ^{14}C Produced by Solar Protons. Damon et al (1973), in their study of the magnitude of the 11-year radiocarbon cycle, found that the ^{14}C content in the 1943 ring of their Arizona tree sample (32°N, 112°W) is exceptionally high. They attributed this high activity to the ^{14}C production by two large solar flares, on February 28 and March 7 of 1942, detected by Forbush (1946). A similar increase was also observed by Burchuladze et al. (1980). Since our tree section was from Mackenzie Delta, only about 10° from the geomagnetic pole, we expect to observe a larger ^{14}C activity in the tree rings than in the samples of Damon et al.

In Fig. 2 we plotted the six $\Delta^{14}C$ values, together with the measurements by Damon et al. (1973) and that by Stuver and Quay (1980), in the period from 1940 to 1954 AD. The high $\Delta^{14}C$ values in the Mackenzie wood, as compared with that in the Washington wood of Stuiver and Quay and that in the Arizona wood of Damon et al., can be explained by the fact that in the near arctic circle, the air is less contaminated by fossil fuel burning. Disregarding the difference in the

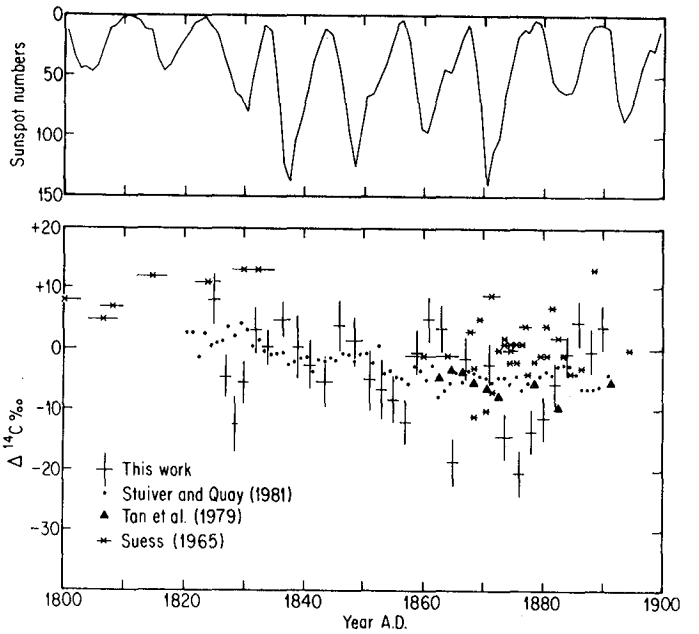

Fig. 1. Upper panel, sunspot numbers; lower panel, $\Delta^{14}C$.

general $\Delta^{14}C$ level, the increase in $\Delta^{14}C$ in the 1943 ring of the Mackenzie wood agrees remarkably well with that in the Arizona wood. The puzzling fact is that the Washington State sample does not show any sign of increase. If one assumes that the increase in $\Delta^{14}C$ in the Mackenzie wood was indeed due to the two flares in 1942, then the magnitude of the flares can be estimated as follows:

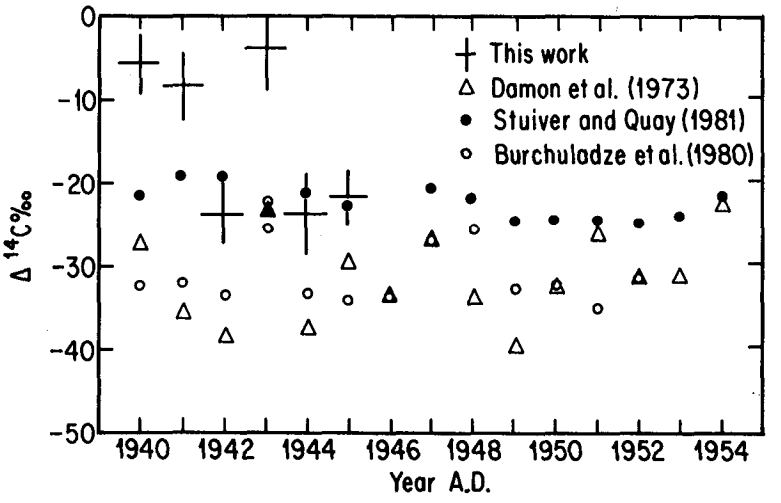

Fig. 2. $\Delta^{14}C$

Ligenfelter and Ramaty (1970) calculated the ^{14}C production rates during the 1953-1954 solar mnimum and the 1957-1958 solar maximum period as 5.0 and 3.5 ^{14}C nuclei/cm^2 sec, respectively, in the 70°-90° geomagnetic latitude range. A 42% increase in the production rate from solar activity maximum to solar activity minimum period. The corresponding periods in the 19th century are 1866 to 1867 and 1870 to 1871. In these two periods, we found that there is a 20°/$_{oo}$ increase in the $\Delta^{14}C$ value. That is, a 40% increase in the production rate in the high latitude region results in a 20°/$_{oo}$ increase in the $\Delta^{14}C$ value. The $\Delta^{14}C$ increase in the 1943 ring of the Mackenzie wood is about 20°/$_{oo}$. Therefore, the ^{14}C increase due to the two flares is equivalent to a 40% increase in the ^{14}C production, or, 1.5 ^{14}C nuclei/cm^2 sec. According to Lingenfelter and Ramaty (1970), the number of ^{14}C nuclei produced by the 1956 solar flare is equivalent to the one-year production by cosmic ray particles. Therefore, the combined effect of the two flares in 1942 is about one-half of that of the 1956 flare. We are continuing our search for larger events.

5. Acknowledgment. Dr. M. L. Parker of the University of British Columbia supplied us with the two sections of dendrochronolgocally calibrated white spruce that made this study possible. This project is partially supported by the subcontract R 277664 from the University of Maryland.

6. References

Baxter, M. S. and J. G. Farmer, Earth Planet. Sci. Lett. 20, 295 (1973).

Burchuladze, A. A. et al., Nature 287, 320 (1980).

Damon, P. E., A. Long and E. I. Wallick, Earth Planet. Sci. Lett. 20, 300 (1973).

Fan, C. Y., T. M. Chen, S. X. Yuu and K. M. Dai, Radiocarbon 25, No. 2, 205 (1983a); 18th ICRC, conference paper, vol. 3, 173 (1983b).

Forbush, S. E., Phys. Rev. 70, 771 (1946).

Lingenfelter, R. E. and R. Ramaty, Radiocarbon Variations and Absolute Chronology, I. U. Olsson, ed. (John Wiley and Sons, 1970), p. 513.

Stuiver, M. and P. D. Quay, Science 207, 11 (1980).

Tans, P. P., et al., Nature 280, (1979).

COSMIC RAY SECULAR VARIATIONS IN TERRESTRIAL RECORDS AND AURORAE

M.R.Attolini, Istituto TESRE del CNR, Bologna
G.Cini Castagnoli and G.Bonino, Istituto di Fisica Generale, Università and Istituto di Cosmogeofisica,CNR,Torino, Italy
M.Galli, Dipartimento di Fisica, Università di Bologna
T.Nanni, Istituto FISBAT del CNR, Bologna

1.Introduction. The rediscovery that the Sun and the Solar wind can undergo important changes on historical time scales[1,2,3] has brought into question the stability of the cyclic behaviour of past time series of Solar and Solar-terrestrial origin. In preceding papers we have found[4,5,6] by Vector Fourier analysis that the solar eleven year cycle is present in the series of ^{10}Be, $\delta^{18}O$, in ice cores and of TL (thermoluminescence) in sea sediments during the last Millennia with a frequency modulation, that we could relate to the Sun behaviour, as tested by comparison with the Sunspot number R_z series[7], in recent times. In a companion paper of this Conference (SH 7.1-1) we have shown that the cyclogram of the series of yearly Aurorae from 1721 to 1979 linear-regression-corrected-for-R_z is straight for the periodicity τ=11,1y, indicating that such periodicity is constant in time corresponding to the only line present in the 11y band. The maxima of this component appear at the same time together with the high speed solar wind streams taking place in coronal holes situated at high heliolatitudes. This connection with a regular solar rithm induced us to search for the possibility that this frequency would be dominant also in the long running (2300 years) scanty record of historical Aurorae recorded at mid and low latitudes in European and oriental countries.

2.Historical Aurorae. The record of Aurorae[8,9] from 686BC to 1731AD is here analysed: unfortunately the Sunspot record is not available before 1700 so we cannot undertake the aforementioned procedure adopted for the yearly Aurorae. However similarities can be tested on the total series: the power spectral density (p.s.d.) of the Hystorical Aurorae has been computed for two subseries one from 687 BC to 1000 AD and the other from 1000 AD to 1731 AD; and compared to the p.s.d. of the Aurorae from 1721 to 1979 (see Figure 1). We may notice that all three p.s.d. show in the 11y band two peaks respectively around 11,1y and 10.0y: before 1000 AD at 10.8y and 9.5y whereas after 1000 AD at 11.4y and 10.5y, the recent p.s.d. at 11.1y and 10.0y. The phase cyclogram (see Figure 2) at τ=11y and T=100, infact shows frequency oscillations of duration of about 2 centuries around two main frequencies one of a little less than 11y (right bending) before 1000 AD and the other a little greater than 11y (left bending) after 1000 AD. The values of the periodicities (11.1y and 9.9y) in the recent Aurorae record could represent a transition similar to the one observable in Figure 2 around

the XI century (1016 AD) and perhaps to another one which could have occurred around the beginning of the Christian era.

3.Comparison of Solar-terrestrial records. The frequency modulation of the eleven year cycle on a 2 century time scale could be associated with the presence in the series of oscillations of the same period. Therefore we have performed the phase cyclogram of the historical Aurorae (Au) series at τ =200y together with those of three other series of data in which the Solar-Terrestrial relationships could be involved: D/H in a South Pole ice core[10], ^{14}C in tree rings[11], Thermoluminescence (TL) in a sea sediment[12], from 500 A.D. up to the present time. They are shown in Figure 3. All of these cyclograms are fairly stretched, indicating that this recurrency is present during this interval in all the four series. However the phases of the four cyclograms are different. The phase shift between Au and ^{14}C is about 180°. This can be interpreted as a consequence of the known fact that increasing Solar activity corresponds to decreasing C.R. intensity and therefore cosmogenic ^{14}C production.
The cyclograms of Au and TL are approximately in phase, this favours the hypotesis that the TL signal is in direct correlation with the Solar activity.
The cyclograms of Au and D/H are out of phase of about 90°. This corresponds to the fact that the global temperature index D/H has its maximum during the ascending phase of the 200y cycle of the Aurorae. These considerations however are not sufficient to assess that the origin of the 200y cycles is definitely of solar and not of terrestrial origin, in particular because the series which shows the strongest amplitude of 200y wave and its constancy in phase is indeed the series of D/H.
Moreover the phase-cyclogram for ^{14}C over the entire la Jolla series for 8400y (see Figure 4) shows that a regular bisecular wave is not always present: trains appear from time to time, the last one starting at about the third century B.C. For comparison the cyclogram at τ =178y is shown in the same Figure. The long periodicities "Suess wiggles" have been extensively discussed by Sonett[13] and the presence of common long periodicities in ^{14}C and TL were previously pointed out by us[14].

4.Conclusions. This analysis shows that a cyclicity of about 200y is present in terrestrial natural phenomena (^{14}C in tree rings, TL series in marine sediment, D/H global temperature index and Aurorae), which could have a common control processbased on Solar-Terrestrial relationships.
If one assumes that the Aurorae record can be used as proxy data of Solar activity then:
a) its anticorrelation with ^{14}C can be interpreted as a consequence of

the well known fact that increasing Solar activity corresponds to decreasing C.R. intensity;
b) its direct correlation with TL favours the hypothesis that Solar activity is responsible for this effect;
c) the global temperature index D/H has its maximum during the ascending phase of the Solar activity.
The analysis of the eleven years cyclicity of the Solar activity through the structure of the Aurorae records seems to suggest that in modern time we are having a transition similar to the one observable in the XI century AD. Moreover there is strong evidence that the eleven year cycle has undergone frequency oscillations on a time scale of two centuries, although it is very difficult to determine the periodicities with high accuracy.

References

1.Eddy J., (1980), In Proc.Conf.Ancient Sun, Geochimica and Cosmochimica Acta suppl.13, p.119
2.Siscoe L., (1980), Rev.of Geophys. and Space Phys. 18, 647
3.Feynman J., (1983), Reviews of Geophys. and Space Phys., 21, 338
4.Cini Castagnoli G., Bonino G., Attolini M.R., Galli M. and Beer J., (1984), Il Nuovo Cimento 7C, 235
5.Attolini M.R., Beer J., Cecchini S., Cini Castagnoli G. and Galli M., (1984), Proc.of Int.Symp. on C.R. modulation in the heliosphere, Morioka, Japan
6.Beer J., Oeschger H., Finkel R.C., Cini Castagnoli G., Bonino G., Attolini M.R. and Galli M., (1984), Proc. 8th Conf. on the Application of Accelerators in Research and Industry, Denton,(Texas), 12-14 nov' 84 in Nuclear Instr.& Methods (In press)
7.Attolini M.R., Galli M., Cini Castagnoli G., (1985), Solar Physics, 95, 391
8.Aurorae records: Stothers, Link, Newton, Dall'Olmo, Keimatsu (kindly provided to us by Dr. F.R.Stephenson)
9.Shove D.J., (1980), Proc.of the SolarTerrestrial Predictions Workshop U.S. Dept.of Comm., Washington DC
10.Benoist J.P., Jouzel J., Lorius C., Merlivat L., Pourchet M., (1982), Annals of Glaciology 3, 17
11.Suess H.E., (1980), Radiocarbon 22, 200
12.Cini Castagnoli G., Bonino G. and Miono S., (1982), Il Nuovo Cimento 5C, 488
13.Sonett C.P., (1984), Reviews of Geophys. and Space Phys., 22, 239
14.Attolini M.R., Bonino G., Cini Castagnoli G. and Galli M., (1983), 18th ICRC, 9, 321

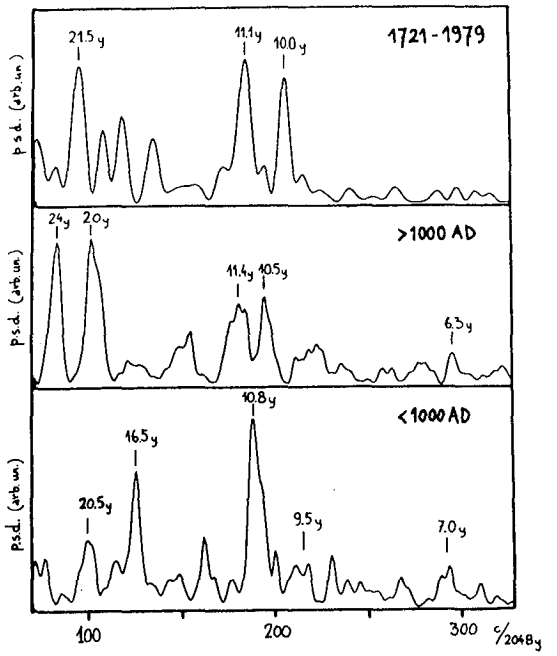

Fig. 1

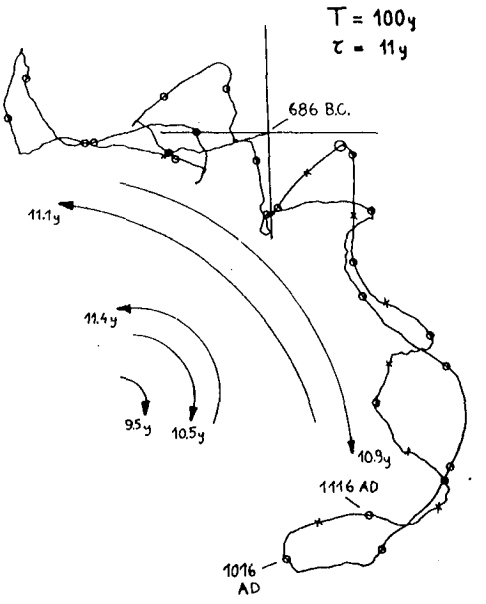

Fig. 2

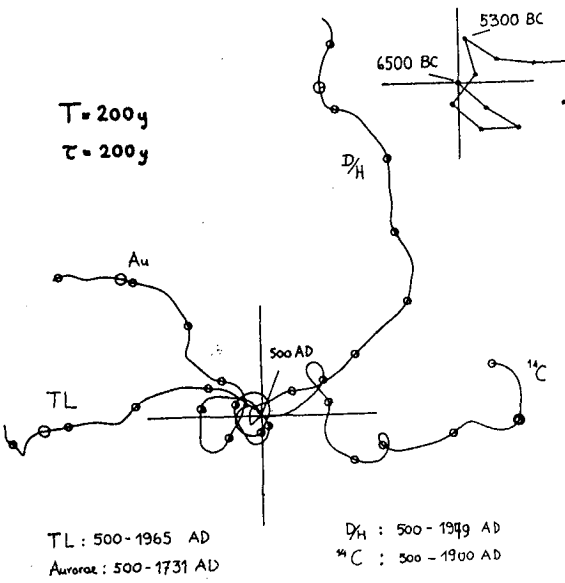

Fig. 3

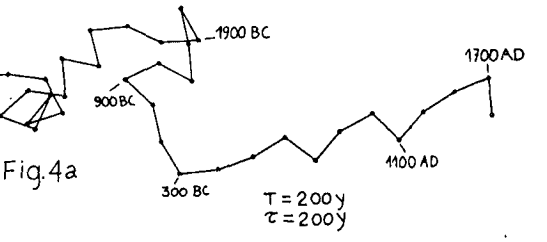

Fig. 4a

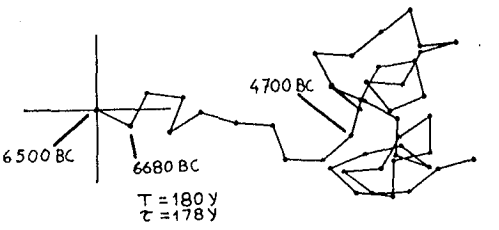

Fig. 4b

WHEN DID THE AVERAGE COSMIC RAY FLUX INCREASE?

K. Nishiizumi, S. V. S. Murty, K. Marti and J. R. Arnold
Department of Chemistry, B-017
University of California, San Diego
La Jolla, CA 92093 (U. S. A.)

Abstract

We developed a new ^{129}I-^{129}Xe method to obtain cosmic ray exposure ages and to study the average cosmic ray flux on a 10^7-10^8 year time-scale. The method is based on secondary neutron reactions on Te in troilite and the subsequent decay of ^{129}I, the reaction product to stable ^{129}Xe. We report the first measurements of ^{129}I and ^{129}Xe in aliquot samples of a Cape York troilite sample.

Introduction

Several investigations were carried out regarding possible variations of cosmic ray intensity in the past. Cosmic ray produced ^{14}C in trees provides one of the most reliable records for the cosmic ray intensity in the past 10^4 years in spite of some uncertainties in the carbon cycle and/or past geomagnetic field variation [eg. 1]. For longer periods ^{10}Be ($t_{1/2} = 1.6 \times 10^6$ years) and/or ^{36}Cl (3.0×10^5 years) concentrations in ice cores or deep sea sediment cores may provide additional information on the cosmic ray flux in the past. However, there are many uncertainties in past climates, in precipitation and sedimentation rates, in geomagnetic fields, because the terrestrial environment is rather complex. On the other hand, the study of cosmogenic radionuclides in extraterrestrial matter provides key information for the history of cosmic rays. Kohl *et al* (1978) found that the average solar cosmic ray (SCR) flux changed relatively little over the last 1-10 million years, based on a study of cosmogenic ^{53}Mn ($t_{1/2} = 3.7 \times 10^6$ years) and ^{26}Al (7.05×10^5 years) in several lunar rocks [2]. The average SCR flux during the last few million years was similar to that measured during the last few decades by detectors on satellites. However, ^{14}C ($t_{1/2}$ = 5740 years) [3] and ^{81}Kr (2.1×10^5 years) [4] activities in lunar samples indicate that the average SCR flux during the last 10^4 - 10^5 years was somewhat higher than the recent average flux. Very useful records on the galactic cosmic ray (GCR) flux were observed in meteoritic detectors. Nishiizumi *et al* (1980) carried out systematic studies on cosmogenic nuclides of various half-lives such as ^{22}Na ($t_{1/2}$ = 2.6 years), ^{81}Kr, ^{26}Al, and ^{53}Mn in chondrites as a test for possible variation of the GCR flux during the last ~10 million years [5]. All sets of nuclides, with the possible exception of ^{26}Al indicate that the averaged GCR flux was constant within ~15%, at least during the last 5 million years. More recently, Moniot *et al* (1983) confirmed this result using ^{10}Be as the monitor [6]. On the other hand, the records of spallation K and Ar observed in iron meteorites reflect ~33% smaller average GCR fluxes on the 10^8-10^9 year timescale [7, 8]. This suggests a cosmic ray flux increase $\leq 2 \times 10^8$ years ago.

^{129}I-^{129}Xe Method:

An investigation for possible intensity changes of GCR flux between 10^7 and 10^8 years is required. The half-life of ^{129}I (1.57×10^7 years) makes this an appropriate nuclide for such a study. The ^{129}I in extraterrestrial materials is produced by cosmic ray secondary neutron reactions on Te, ^{130}Te (n,2n,β) ^{129}I and ^{128}Te (n,γ β)^{129}I, and by high energy spallation reactions on Ba and the Rare Earth elements. Troilite inclusions in iron meteorites are ideal monitors among extraterrestrial materials because of their long cosmic ray exposure ages (10^8 to 10^9 years) their relatively high Te contents (~ ppm) and their low abundances of Ba and Rare Earth elements. The ^{129}I decays to stable ^{129}Xe. ^{129}Xe is not directly produced by cosmic ray secondary neutrons, yielding a fractional isobaric production ratio P (^{129}I)/P(^{129}I + ^{129}Xe) ~1 [9]. The simultaneous determination of cosmogenic ^{129}I and ^{129}Xe in the same troilite phase is the basic concept of the new method of determining ^{129}I-^{129}Xe exposure ages. This exposure age can be obtained without any shielding and target element corrections for a constant exposure geometry. The exposure age T can be calculated from the equation:

$$\frac{\lambda_{129}T - 1 + e^{-\lambda_{129}T}}{1 - e^{-\lambda_{129}T}} = \frac{^{129}Xe_{Te}}{^{129}I_{Te}}$$

where λ^{129} is decay constant of ^{129}I, $^{129}I_{Te}$ is ^{129}I content (atom/sample), and $^{129}Xe_{Te}$ is cosmogenic ^{129}Xe content (atom/sample) produced from Te after subtraction of other components. The comparison of ^{129}I-^{129}Xe exposure ages and with those obtained by methods such as ^{40}K-^{41}K [7], ^{26}Al-^{21}Ne, and ^{36}Cl-^{36}Ar could indicate either a complex exposure history of the meteorite or a change in cosmic ray flux intensity. We developed the experimental techniques and measured both ^{129}I and ^{129}Xe in the same troilite sample of the large Cape York iron meteorite. The ^{129}I measurement was carried out by accelerator mass spectrometry using the University of Rochester MP tandem van de Graaff accelerator [see 10], while the ^{129}Xe measurement was performed by static mass spectrometry.

Discussion:

The Cape York iron meteorite contains $(8.3 \pm 1.3) \times 10^6$ atoms ^{129}I/g troilite and $(2.6 \pm 0.3) \times 10^7$ atoms $^{129}Xe_{Te}$/g troilite. The ^{129}I-^{129}Xe exposure age of Cape York is calculated from the above equation as T = 93 $\pm$18 million years. This is the first determination of a cosmic ray exposure age of Cape York. The inferred Ar production rate P (^{38}Ar) ~ 200 atoms/g Fe x year [11] is one order of magnitude smaller than that corresponding to the most shielded location for which P(^{38}Ar) data are available. This result documents (a) the extremely heavily shielded location of our sample and (b) that secondary cosmic ray neutrons are very useful in unravelling exposure histories and geometries. The Cape York results, however, do not allow an evaluation of the average cosmic ray flux over the 93 million year exposure period, since no other

information on the exposure age is available. Therefore, we are now applying the ^{129}I-^{129}Xe dating method to meteorites for which independent exposure age information is either available, or can be obtained.

Acknowledgements: We thank D. Elmore for his collaboration on the ^{129}I accelerator mass spectrometry. This work was supported by NASA Grants NAG 9-33 and NAG 9-41.

References

1. Suess, H. E. (1980) Radiocarbon 22, 200-209.

2. Kohl, C. P. et al, (1978) Proc. 9th Lunar Planet. Sci. Conf., 2299-2310.

3. Boeckl, R. S., (1972) Earth Planet. Sci. Lett., 16, 269-272.

4. Yaniv, A., et al, (1980) (abstract) Lunar Planet. Sci., XI, 1291-1293.

5. Nishiizumi, K., et al, (1980) Earth Planet. Sci. Lett., 50, 156-170.

6. Moniot, R. K., et al (1983) Geochim. Cosmochim. Acta, 47, 1887-1895.

7. Voshage, H. (1962) Z. Naturforschg. 17a, 422-432.

8. Lavielle, B. et al, (1984) Proc. of Conf. on Isotopic Anomalies in the Solar System, Paris.

9. Marti, K., (1984) Proc. of Workshop on Cosmogenic Nuclides, (Los Alamos, New Mexico).

10. Nishiizumi, K., et al, (1983) Nature, 305, 611-612.

11. Murty, S. V. S. and Marti, K. (1984) Manuscript in preparation.

COSMOGENIC-NUCLIDE PRODUCTION BY PRIMARY COSMIC-RAY PROTONS

Robert C. Reedy
Nuclear Chemistry Group, Mail Stop J514
Los Alamos National Laboratory
Los Alamos, NM 87545, USA

ABSTRACT

The production rates of cosmogenic nuclides were calculated for the primary protons in the galactic and solar cosmic rays. At 1 AU, the long-term average fluxes of solar protons usually produce many more atoms of a cosmogenic nuclide than the primary protons in the GCR, the exceptions being nuclides made only by high-energy reactions (like Be-10). Because the particle fluxes inside meteorites and other large objects in space include many secondary neutrons, the production rates and ratios inside large objects are often very different from those by just the primary GCR protons. Thus it is possible to determine, by examining its cosmogenic nuclides, if a small object, such as found among deep-sea spherules, was small in space or broken from a meteorite. Because heliospherical modulation and other interactions change the GCR particle spectrum, the production of cosmogenic nuclides by the GCR particles outside the heliosphere will be different from that by modulated GCR primaries. Production rates and ratios for cosmogenic nuclides would be able to identify small particles, possibly interstellar in origin, that were exposed to an unmodulated spectrum of GCR particles and to characterize the spectrum of particles to which they were exposed.

1. Introduction. The energetic particles in the cosmic rays are about 90% protons and induce a wide variety of nuclear reactions in extraterrestrial matter (1). Relatively low energy (~10- to 100-MeV) particles are emitted occasionally from the sun--the so-called solar cosmic rays (SCR). The SCR particles are rapidly stopped in matter (within a few centimeters) and produce a high density of product nuclei very near the surface. The high-energy (~1-GeV) galactic cosmic-ray (GCR) particles produce a large cascade of secondary particles, especially neutrons, that penetrate meters into solid matter. The flux of GCR particles in the solar system varies with solar activity and is lowest at periods of maximum solar activity. Most studies of cosmogenic nuclides have been for large objects (the Earth, moon, and meteorites) and for long periods of time (averaged over many solar cycles). Recently, there has been more interest in cosmogenic nuclide production in very small objects (2) and also in the production variations over a solar cycle (3), outside the solar system (4), or for periods of unusual solar activity (5).

2. Primary Cosmic-Rays. The spectrum of solar protons is well approximated by an exponential function in rigidity (6); it has an average spectral shape over the last million years (1) of R_o = 100 MV. Castagnoli and Lal (5) give an equation for the spectral shape of the GCR as a function of a solar modulation parameter (M). For the GCR protons, spectra like those for the last two solar minima (M = 375 MeV) and maxima

(M = 950 MeV) (1,5) were used, as well as one that is similar to the average over a solar cycle (M = 550 MeV). A fourth GCR spectrum was the expression of (5) for no modulation (M = 0), possibly like that of the GCR particles outside the solar system in the local interstellar space (IS). The shape for the expression with M = 0 is very similar to (E + 1050) to the -2.87 power, with E in MeV. Such an unmodulated spectrum could be approached in the solar system during the long periods of essentially no solar activity that occur about every few hundred years (1,5). One estimate of the proton spectrum at the source of GCR particles is a power law in rigidity. At high energies, this rigidity power law was assumed to have the same intensity and shape as that observed in the solar system. As any source GCR-particle spectrum is modified by passage through ~5 g/cm^2 of matter, this pure rigidity power-law spectrum overestimates the proton fluxes at lower energies, especially below ~100 MeV (6). Production rates for seven cosmogenic nuclides were calculated with these proton spectra and with cross sections for proton-induced reactions (see Table I). The production rates of these nuclides observed in meteorites (with typical radii of 10 to 30 cm) are also shown in Table I.

3. Cosmogenic-Nuclide Production Rates. Production by solar protons usually dominates that by primary GCR protons. Only nuclides made mainly by high-energy protons, such as Be-10 and Cl-36, have very low production rates by the low-energy solar protons. These high rates by solar protons only occur very near the surface, and solar-proton production rates become relatively unimportant below depths of a few centimeters (1,6). Only the GCR source spectrum exceeds the solar-proton production rates, mainly because of its high fluxes at lower energies. In most meteorites, production by solar protons is usually not observable because the surface layers are removed by ablation during the meteorite's passage through the Earth's atmosphere. The ratio of the amount of a nuclide readily made by solar protons (for example, Al-26) to that of a high-energy product (such as Be-10) is a good indicator of the object's size when it was irradiated in space. Activities of Al-26 and Be-10 were measured in several groups of small (0.3- to 0.5-mm) spherules collected from sediments on the ocean floor (2). The Al-26/Be-10 ratio and the Al-26 activity were quite high in several of them, which indicate that those spherules probably came from parent bodies less than a few centimeters in diameter. Studies of such small objects would be interesting because they may be different from the forms of solar system matter found in most meteorites.

The production rates of nuclides by GCR protons in interstellar space are high, similar to the rates produced by both primary and secondary GCR particles in meteorites. The relatively low-energy protons normally removed by solar modulation in the inner solar system have produced about the same number of nuclides as are made by secondary neutrons in meteorites. These high production rates, plus the relatively low loss of product nuclides by recoil in small grains (4), mean that one should be able to identify grains that were irradiated in interstellar space. Such grains may have been incorporated in meteorites or could enter the Earth's atmosphere as cosmic dust. The cross sections as a function of energy for making secondary neutrons are similar in shape to those for producing He-3. The He-3 production rate in interstellar space is 4 times that for the average over a solar cycle, and the flux of

protons above 1 GeV in interstellar space is 2.4 times that for the solar-cycle average. Thus, the production rates of cosmogenic nuclides by GCR particles that have not been modulated are higher (by factors up to 3 to 4) than those observed near the Earth during long periods of typical solar activity.

During periods of normal solar variations, the extremes in the activity of the sun and its subsequent modulation of the GCR particles are represented by the solar minimum and maximum used in Table I. The ratio of 2.4 for the He-3 production rates between these extremes is about the variation that would be expected for the production of secondary neutrons. When Evans et al. (3) measured the activities of short-lived radionuclides in a number of meteorites that fell from 1967 to 1978, the activities varied by about a factor of 3. Some of these variations probably were caused by differences in the meteorites' sizes or shapes or in the sample location. However, the calculations reported here show that most of these radioactivity variations are caused by the solar modulation of the GCR-particle flux. The observed radioactivity variations correlated well with other indicators of solar activity (3). Larger variations in nuclide production rates would be expected if the solar activity exceeded one or both of the average extremes used here.

In Table I, the ratio of the GCR production rates typically observed in meteorites to the solar-cycle-averaged rates for primary GCR protons ranged from 2.3 to 8.0. Because the flux of primary protons inside a meteorite is attenuated by nuclear interactions, the ratios of observed activities to those made only by the primary GCR protons should be even larger. These relatively low contributions by the primary particles illustrate the importance of secondary particles in nuclide production in large objects like meteorites. This big difference between nuclide production by primaries only and by the fully developed secondary cascade present in most meteorites indicates that small meteorites without a fully developed cascade could have some unusual production rates or ratios. Studies of such small meteorites also would help us understand the production and transport of secondary particles in meteorites.

4. Conclusions. The calculations and results in Table I show that the production of cosmogenic nuclides can vary considerably with both the size of the extraterrestrial object and the amount of the solar modulation of the primary GCR particles. Very small objects have high production rates by solar protons. Typical meteorites are large enough that the cascade of secondary particles dominates nuclide production. Intermediate-size objects could have some unusual production rates and ratios. Temporal and spatial variations in nuclide production can also result from differing GCR-particle modulation. Variations by factors of 2 to 3 can occur during a normal solar cycle, and even larger deviations can occur when solar modulation is much stronger or weaker than usual.

5. Acknowledgements. This research was supported by NASA work order W-14,084 and done under the auspices of the US DOE. Discussions with J. Evans, H. Völk, R. Jokipii, and M. Forman helped in planning this work.

References
1. Reedy, R. C., et al., (1983), Science 219, 127-135.
2. Raisbeck, G. M., et al., (1983), In Lunar and Planetary Science XIV (Lunar and Planetary Institute, Houston), pp. 622-623.
3. Evans, J. C., et al, (1982), J. Geophys. Res. 87, 5577-5591.
4. Ray, J., and H. J. Völk, (1983), Icarus 54, 406-416.
5. Castagnoli, G., and D. Lal, (1980), Radiocarbon 22, 133-158.
6. Reedy, R. C., and J. R. Arnold, (1972), J. Geophys. Res. 77, 537-555.

TABLE I. Nuclide Production Rates by Primary Cosmic-Ray Protons, Assuming C2-Chondritic Chemistry.

	10^6 years Av SCR	Solar Max. GCR	Solar Av GCR	Solar Min. GCR	Local IS GCR	GCR Source	Typical Meteorite
Parameter	R_o=100	M=950	M=550	M=375	M = 0	$R^{-2.65}$	
Integral Flux[a]	70	1.21	1.80	2.39	4.33	4.33	
Nuclide	(atoms/minute/kg)						
He-3	66.	190.	318.	459.	1258.	4095.	900.
Be-10	4.1	5.0	8.1	11.5	28.6	60.8	22.
Ne-21	395.	11.6	20.8	31.7	117.	1603.	150.
Al-26	344.	3.9	7.5	11.9	56.	1344.	60.
Cl-36	0.9	1.8	3.1	4.5	11.2	20.1	7.
Ar-38	72.	3.3	5.5	8.0	24.4	260.	20.
Mn-53	590.	7.6	13.6	20.8	90.	2177.	105.

[a] In protons/cm^2/s: solar protons for E > 10 MeV, GCR for E > 1 GeV.

COSMIC-RAY EXPOSURE RECORDS AND ORIGINS OF METEORITES

Robert C. Reedy
Nuclear Chemistry Group, Mail Stop J514
Los Alamos National Laboratory
Los Alamos, NM 87545, USA

ABSTRACT

The cosmic-ray records of meteorites can be used to infer much about their origins and recent histories. Some meteorites had simple cosmic-ray exposure histories, while others had complex exposure histories with their cosmogenic products made both before and after a collision in space. The methods used to interpret meteorites' cosmic-ray records, especially identifying simple or complex exposure histories, often are inadequate. Besides spallogenic radionuclides and stable nuclides, measurements of products that have location-sensitive production rates, such as the tracks of heavy cosmic-ray nuclei or neutron-capture nuclides, are very useful in accurately determining a meteorite's history. Samples from different, known locations of a meteorite help in studying the cosmic-ray record. Such extensive sets of meteorite measurements, plus theoretical modeling of complex histories, will improve our ability to predict the production of cosmogenic nuclides in meteorites, to distinguish simple and complex exposure histories, and to better determine exposure ages.

1. Introduction. Meteorites are fragments from a variety of objects in the solar system and can provide important information about these bodies. Well-determined cosmic-ray exposure histories are needed to help to establish the origins of meteorites: where they came from and how they were produced (1,2). In principle, the exposure history of a meteorite should be well determined if sufficient measurements are made of its cosmic-ray record and if the production rates and profiles of the cosmogenic products used to interpret the measurements are known well enough. It is unlikely that many meteorites have had their cosmic-ray exposure histories properly determined. Wetherill (3) noted that complex histories should be common for most likely meteorite-origin scenarios. However, complex histories for meteorites are seldom reported, especially for stony meteorites. Is this discrepancy between the predicted and reported frequencies of meteorite complex histories a problem with the approaches presently used to study the exposure records of meteorites? Inadequacies in the interpretation of the cosmic-ray records of meteorites could mean that exposure ages and other results of meteorite studies, such as cosmic-ray variations, also might not be correct. Systematic experimental and theoretical studies are needed to study how well we have been determining the recent histories of meteorites and to develop better methods for unfolding the cosmic-ray records of meteorites.

2. Cosmic-Ray Exposure Records. Among the ages of a meteorite, the youngest are those determined from the activities or concentrations of cosmogenic products. Exposure ages, the lengths of time that meteorites

have been exposed to cosmic rays, are typically orders of magnitude shorter than their radiometric formation ages and, for some meteorites, their brecciation ages and collisional shock ages (4). The cosmogenic products used to study exposure records of meteorites include stable and radioactive nuclides and tracks of heavy cosmic-ray nuclei. If a meteorite had a simple exposure record, then the concentration of a cosmogenic product and its production rate can be used to determine an exposure age. However, the production rates vary considerably with meteoroid size and shape and with sample location (5), so corrections for the effects of the sample's shielding geometry must be applied. Most methods for estimating shielding corrections, such as the Ne-22/Ne-21 or He-3/Ne-21 ratios, do not yield unique production rates but only narrow the range of possible values (5).

Many meteorites had simple exposure ages. Detailed investigations of the cosmic-ray records of several meteorites, such as the tracks, radionuclides, and spallogenic noble gases in St. Severin (6), show that the cosmogenic products were made only during one exposure geometry. However, most meteorites have not had their exposure records shown to have been simple by such systematic studies. Another clue that a meteorite probably had a simple history is that its exposure age is the same as a number of other meteorites of the same type. However, there are only a few clusters for the exposure ages of meteorites; the exposure ages for most meteorites form a continuous distribution.

The clusters of exposure ages for a given class of meteorites, such as the ~675 Ma (675 million years) cluster for IIIAB irons (7) or the ~6 Ma peak for H-chondrites (8), suggest that these meteorites were all produced by single, major collisional events. If these two clusters really represent individual events, the widths of the peaks, about 15-20% of the age, indicate that the sums of the uncertainties in determining cosmic-ray exposure ages are fairly large. As the measurement uncertainties are much smaller than 15-20%, the spread in the exposure ages for these clusters probably results from interpreting the measurements (although pre-irradiation or gas losses could account for some of the spread). One likely source of this width in the exposure-age peaks is the significant correction for shielding.

Several meteorites clearly had their cosmogenic products made both before and after a major collisional event in space that changed the meteoroid's geometry. The Jilin chondrite was irradiated by a significant flux of cosmic-ray particles for ~10 Ma near the surface of a very large object prior to its ejection ~0.4 Ma ago as an 85-cm-radius sphere (9). Several other meteorites have had complex histories, such as several inferred from the disagreements among exposure ages determined with different radionuclides or stable cosmogenic products. In very large meteorites, such as the Canyon Diablo iron meteorite (10), one part could have been removed by a minor collision without seriously affecting the formation of cosmogenic products in other parts of the meteoroid.

The distinction between simple and complex exposure histories can be difficult in some cases. Some meteorites probably have small amounts of cosmogenic products made prior to the event that produced the object that eventually hit the Earth. In most cases, the amounts of cosmogenic

products made during the meteorite's final exposure geometry overwhelm any previous production. However, if this last exposure stage was short, then possibly the products made during the previous exposure could be detected. As suggested by (9), the high production rates inferred for Ne-21 from meteorites that have undersaturated Al-26 activities (that is, exposure ages of ~1 Ma) could be a consequence of pre-irradiation. A very special case of a complex history is when a foreign clast in a brecciated meteorite has had a previous exposure to the solar wind or cosmic rays prior to incorporation in the meteorite (11).

3. Systematic Experimental Studies. To properly calibrate the predicted production rates and profiles of cosmogenic products in meteorites, extensive sets of measurements are needed. The measurements should be made for samples from different, known locations and also of products with a wide range of production-rate-versus-depth profiles (tracks, high- and low-energy spallation, and neutron capture) and a variety of half-lives (including stable isotopes). For example, the Na-22 and Co-60 activities measured in Jilin (9) serve as a calibration points for cosmogenic nuclides in a meteoroid with a radius of 85 cm. The measurements of cosmogenic products in meteorite cores, such as those from St. Severin (6) and Keyes, also are valuable reference data.

However, few such well-characterized data sets for cosmogenic nuclides in meteorites exist (5). Most meteorites that have been investigated in detail have radii of ~10-40 cm, which are typical of most meteorites. There have not been many extensive studies of smaller meteorites. Laboratory irradiations of small spherical targets are helping to understand the production of cosmogenic nuclides in small meteoroids (12). While Jilin had a radius of 85 cm for its last 0.4 Ma, its initial exposure limits studies of cosmogenic nuclides in large spherical meteoroids mainly to short-lived radionuclides, such as Na-22 and Co-60. More detailed measurements are needed to calibrate the models used to predict the production rates and profiles of cosmogenic nuclides, especially for meteorites that had unusual preatmospheric sizes or shapes.

4. Theoretical Modeling. Calculated size- and depth-dependent production rates can be used to illustrate the use of a meteorite's cosmic-ray record to accurately unfold its exposure history. Most models do a fairly good job of reproducing the profiles of cosmogenic products in typical-sized meteorites, such as St. Severin (6). However, some models have trouble with very large meteoroids, like Jilin (9). Very small meteoroids are hard to model because the cascade of secondary particles, especially neutrons, is not fully developed (5,12) and solar-proton production is important. Improved models are needed for all sizes, shapes, and types (irons and stones) of meteorites.

Some of these model results have been used to study criteria for identifying complex histories. For example, the calculated track production rates and the Ne-22/Ne-21 ratios for meteorites with simple histories cover a small region of all possible values (13). Meteoritic samples with tracks and neon ratios that are outside this region have complex histories. The activities of cosmogenic radionuclides are often used in looking for complex histories, and often these activities versus track

production rates or Ne-22/Ne-21 ratios are used to search for unusual exposure histories. Artificial exposure records derived from calculated production rates and profiles can be used to test the methods used to infer the exposure histories of meteorites. These theoretically constructed records for complex histories will especially help to show which features of a meteorite's cosmic-ray record are best suited for distinguishing complex from simple histories and which types of complex histories are most easily detected. Such theoretical studies would help to find the areas where meteorite measurements or more laboratory simulations or cross sections would be most useful.

5. Conclusions. Many experimental and theoretical studies are needed to improve our ability to unfold the cosmic-ray exposure records of meteorites. More extensive measurements of cosmogenic products in meteorites, especially shielding-sensitive ones like tracks and neutron-capture-produced nuclides, will help to identify meteorites that had complex histories and to yield better exposure ages. Such improved recent histories could aid in identifying the parent bodies for certain meteorites, such as primitive carbonaceous chondrites (possibly from cometary surfaces) or the SNC meteorites (the Shergottites, Nakhlites, and Chassigny, which were possibly ejected from the martian surface). Detailed measurements of cosmogenic products in meteorites could be used to improve the models for predicting the production rates of these products. Theoretical studies of the production systematics of cosmogenic products in meteorites will help to identify areas where additional laboratory or meteorite measurements are needed.

6. Acknowledgements. This research was supported by NASA work order W-14,084 and done under the auspices of the U.S. Department of Energy. K. Marti and S. Regnier contributed to the ideas presented here.

References

1. Wetherill, G. W., (1985), Meteoritics 20, 1-22.
2. Greenberg, R., and C. R. Chapman, (1983), Icarus 55, 455-481.
3. Wetherill, G. W., (1980), Meteoritics 15, 386-387.
4. Bogard, D. D., (1979), In Asteroids, (T. Gehrels, ed.), pp. 558-578.
5. Reedy, R. C., (1985), J. Geophys. Res. 90, C722-C728.
6. Englert, P., and W. Herr, (1980), Earth Planet. Sci. Lett. 47, 361-369.
7. Voshage, H., and H. Feldmann, (1979), Earth Planet. Sci. Lett. 45, 293-308.
8. Crabb, J., and L. Schultz, (1981), Geochim. Cosmochim. Acta 45, 2151-2160.
9. Heusser, G., et al., (1985), Earth Planet. Sci. Lett. 72, 263-272.
10. Heymann, D., et al., (1966), J. Geophys. Res. 71, 619-641.
11. Schultz, L., (1979), Phys. Chem. Earth 11, 39-45.
12. Englert, P., et al., (1984), Nucl. Instrum. & Methods B5, 415-419.
13. Bhandari, N., and M. B. Potdar, (1982), Earth Planet. Sci. Lett. 58, 116-128.

ACCELERATOR EXPERIMENTS ON THE CONTRIBUTION OF SECONDARY PARTICLES TO THE PRODUCTION OF COSMOGENIC NUCLIDES IN METEORITES

P.Dragovitsch and P.Englert
Department of Nuclear Chemistry, University of Köln,
D-5000 Köln 1, FRG

R.Michel
ZfS, University of Hannover, D-3000 Hannover 1, FRG

1. Introduction. Through the interaction of galactic cosmic particle radiation (GCR) a wide variety of cosmogenic nuclides is produced in meteorites. They provide valuable historical information about both the cosmic radiation and the bombarded meteorites. An important way to understand the production mechanisms of cosmogenic nuclides in meteorites is to gather information about the depth and size dependence of the build-up of GCR-secondary particles within meteorites of different sizes and chemical compositions. This can be obtained by analyzing cosmogenic nuclide depth profiles in meteorites [e.g. 1]. However, suitable meteorites are rare and the especially significant short-lived radioactive species have not been measured extensively. Simulation experiments with meteorite models offer an alternative to direct observation providing a data basis to describe the development and action of the secondary cascade induced by the GCR in meteorites.

2. Methods. A series of thick target irradiations of spherical meteorite models with radii (R) of 5, 15 and 25cm with 600 MeV protons, the maximum of the differential GCR proton fluxes, was performed at the CERN-synchrocyclotron [2]. The materials used to simulate the meteorite body were diorite (R=5cm) and gabbro (R=15,25cm), both having a density of $\sim$3g cm^{-3} and an extremely low water content of $\leq 10^{-3}$g/g. Pure elemental foils and simple chemical compounds were exposed to the particle fields along cores drilled perpendicular to each other through the center of the models. A homogeneous 4π isotropic irradiation was achieved combining four independent movements (two translational and two rotational) of the meteorite models in the fixed particle beam. The irradiation parameters for the three simulation experiments are given in table 1.

Table 1: Irradiation parameters of the 600 MeV proton simulation experiments

Model-radius [cm]	Irrad.time [min]	p-Dose [cm^{-2}]	"Exposure age" [10^6y]
5	489.5	4.82×10^{15}	76.0
15	750.0	2.17×10^{14}	3.4
25	763.0	5.99×10^{14}	9.3

3. Results and discussion. The depth-dependent production rates of radionuclides and stable isotopes from the target elements were determined by gamma spectroscopy, low-level counting techniques, accelerator- and conventional mass

spectrometry. The symbols in Figures 1a-e show the experimental production rates of five short-lived radioactive products in units of [10^{-4} atoms $s^{-1}g^{-1}$] as a function of depth within the meteorite models, assuming a primary proton flux of [$1cm^{-2}$ s^{-1}]. Product nuclides and targets are given in the Figures. The limits of uncertainty do not exceed the size of the symbols unless indicated by error bars. Figures 1a-e show only a small fraction of over 90 target-product-pairs obtained or in the process of reduction for each of the meteorite models. This selection especially emphasizes low energy secondary reactions. The extreme examples are the $^{27}Al(n,\alpha)^{24}Na$-reaction and the (n,p)-reaction on ^{54}Fe, mainly responsible for the ^{54}Mn production from iron. The other reactions occur at slightly higher threshold energies such as the $^{59}Co(n,2n)^{58}Co$ reaction, the mainly proton induced $^{27}Al(p,3p4n)^{22}Na$ reaction and the exclusively proton induced reaction $^{56}Fe(p,n)^{56}Co$.

Focussing on the measured data points in Figure 1, it is obvious that the depth profiles of all these low energy products increase from the surface to the center by 20%-30% independent of the radius of the meteorite model. This behavior was expected for the R=15cm and the R=25cm spherical model, but was striking for the R=5cm model, demonstrating that the contribution of GCR-secondaries cannot be neglected in small meteorites.

It is also remarkable that for all of the mainly neutron-produced species, the absolute production rates at the centers of the model meteorites increase with increasing model-radius, as predicted for low-energy secondary products in meteorites by various model calculations [3,4].For the exclusively proton produced $^{56}Co(Fe)$, the center activities for the two large meteorite models are indistinguishable within the limits of uncertainty. Moreover, for the ^{22}Na-production from Al, the highest center activity is found in the R=15cm model, whereas the center activity of the largest sphere is only slightly higher than that of the smallest. Taking into consideration that the production rates of the $^{56}Fe(p,n)^{56}Co$-reaction are more than an order of magnitude lower than those of the others the reversal of the sequence for ^{22}Na may then only be attributed to lower fluxes of charged secondaries above the threshold energy at the center of the largest model.

More precise information about the action of low energy secondary hadrons within the meteorite models can be obtained by calculating the contributions of primary protons to the production of the nuclides. The solid lines in Figure 1 show the calculated primary proton-induced contributions. The calculations consider stopping and absorption of the primaries, their fluxes for given energies and given positions [5] and excitation functions of the individual nuclear reactions[6]. The general tendency for cosmogenic nuclide production by primary protons is a decrease in production rate from the surface to the center. For the small R=5cm sphere the absolute contribution of secondary neutrons increases with increasing

threshold and charge (Z) of the target from the $^{27}Al(n,\alpha)$ over the $^{54}Fe(n,p)$ to the $^{58}Co(n,2n)$ reaction, i.e. the primary contribution becomes less important. For other nuclear reactions in all models a systematic description of the primary and secondary contribution as a simple function of Z of target, threshold energy and model radius cannot be observed. It is necessary to study the nuclear parameters of each individual target-product pair in detail. Nevertheless, the depth profiles presented provide an excellent basis for a quantitative description of primary and secondary particle fields in extended spherical targets under proton bombardment.

A more general point of interest is the question as to whether the 600 MeV simulation experiments performed are suitable to interpret observations in meteorites. There are several obstacles that prevent a direct comparison of the depth profiles in Figure 1 with meteorite data. Short-lived radionuclides have been measured only in a limited number of meteorite falls. Depth profiles of short-lived isotopes in meteorites have not been determined. Table 2 lists a number of meteorites of different preatmospheric sizes for which a few short-lived isotopes were measured [7]. Their production rates are given in the same units as in Figure 1. In view of these limitations the following conclusions can be made: ^{54}Mn and ^{22}Na-production rates follow directly the tendency given in Figure 1: they increase from the smallest to the largest meteorites. Assuming an average Fe-concentration of 25%, the respective production rates in table 2 will have to be multiplied by a factor of 4 to be directly comparable. In case of the ^{54}Mn-production in meteorites, Fe is the major target and the meteorite production rate thus exceeds the one found in the models by a factor of 3-4. The same is valid to a larger extent for the ^{22}Na-production, but here the largest contribution in a meteorite comes from Mg. The slight differences between actual meteorite data and the results of the simulation series presented may be caused by the use of diorite and gabbro to develop the secondary cascade, the density and average Z of which is somewhat lower than that of most meteorite classes; another reason may be found in using 600 MeV protons only.

Though the results of the 600 MeV proton irradiation series look very promising in modeling GCR primary and secondary fluxes in meteorites, further experiments using higher energies and different particles are necessary to more accurately simulate realistic conditions in space.

4. Acknowledgement. This work was partially funded by the DFG.

References: [1] P.Englert and W.Herr (1980), Earth Planet. Sci.Lett. 47 361-369. [2] R.Michel et al. (1984), Lun.Planet. Sci. XV, 542-543. [3] R.Reedy (1985), J.Geophys.Res. 90, C722-C728. [4] T.P.Kohmann and M.L.Bender (1967), in: B.S.P.Shen (ed.) High Energy Nuclear Reactions in Astrophysics, Benjamin, N.Y.. [5] R.Michel and R.Stück (1984),J.Geophys.Res. 89 B673-B684. [6] J.Tobailem, C.-H.de Lassus St. Genies (1975), CEA-N-1466 (1). [7] J.C. Evans et al. (1982), J.Geophys.Res. 87,

5577-5591. [8] N.Bhandari et al. (1980), Nucl.Tracks 4, 213-262. [9] P.Englert (1985), Lun.Planet.Sci. XVI, 215-216. [10] K.Marti et al. (1969), in: P.Millmann (ed.) Meteorite Research, Reidel, 248-266.

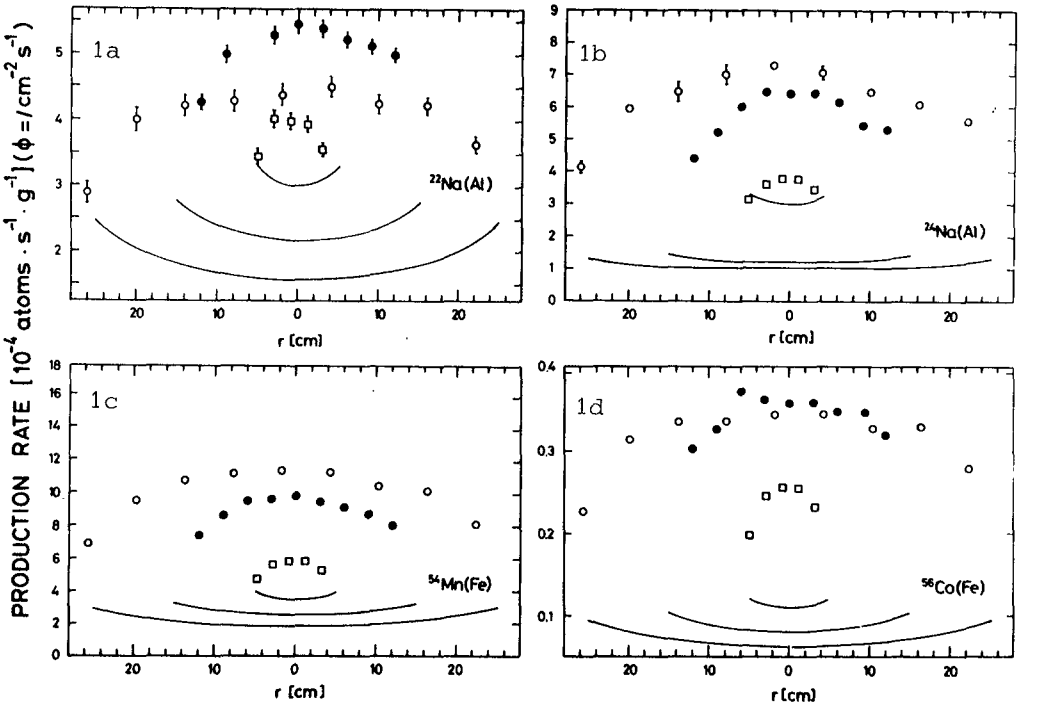

Figures 1a-e: Production rates of short-lived isotopes in meteorite models as a function of depth. A primary proton flux of [1cm^{-2}s^{-1}] is assumed.

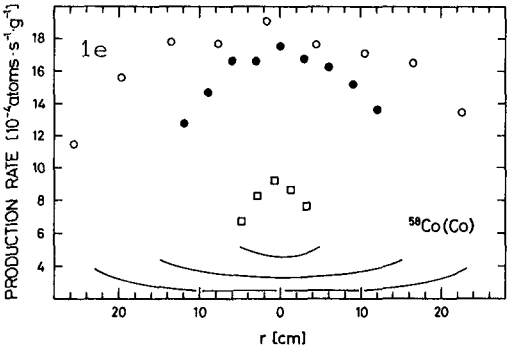

Table 2: Short-lived radionuclides in meteorites of different preatmospheric sizes [7]

Meteorite	Class	Preatm. mass [kg] [8]	Production rates [10^{-4}atoms $s^{-1}g^{-1}$] ^{22}Na	^{54}Mn
Denver	L6	1.35	5.74±0.16	6.50±1.70
Murchison	CM2	>15	6.75±0.25	6.40±0.33
Lost City	H5	<200 [9]	5.67±0.16	5.33±0.25
St.Severin	LL6	372±14	8.41±0.66 [10]	6.75±0.16 [10]
Innisfree	L	350±100	7.92±0.41	6.92±0.33
Dhajala	H3	850±135	9.08±0.16	13.16±0.50
Jilin	H	>3000	9.50±0.41	11.30±1.50

DEPTH AND SIZE EFFECTS ON COSMOGENIC NUCLIDE PRODUCTION IN METEORITES

P. Englert
Department of Nuclear Chemistry, University of Köln,
D-5000 Köln 1, FRG

1. Introduction. The galactic cosmic particle radiation (GCR) can cause changes in condensed extraterrestrial matter in different ways. It can lose energy via ionization processes or induce nuclear reactions which lead to a wide variety of stable and radioactive cosmogenic nuclides. Which process dominates depends on the charge and the energy of the particle radiation and on the nature of the extraterrestrial object exposed to this radiation, i.e. its size, chemical and mineralogical composition. Heavy particles ($Z \geq 20$) incur radiation damage in minerals such as olivine and pyroxene. Light particles predominantly tend to induce nuclear reactions, causing the development of a secondary particle cascade of neutrons, protons, pions and γ-rays and the production of cosmogenic nuclides. Such processes are described in detail by various models [1,2], which predict the depth and size dependent production of cosmogenic nuclides.

The two principal approaches to the study of these effects are simulation experiments and direct observations of meteorites. While the simulation experiments may have advantages with respect to a better understanding of the production processes and the development of secondary hadron cascades in extended matter [3], measurements of depth profiles of cosmogenic nuclides in meteorites fulfill two functions: They are the criterion for the validity of the model calculations and simulation experiment results and they establish an empirical network of cosmogenic nuclide relations, which may help to answer questions about the history of both the GCR and the meteorites. This study focusses on the long-lived cosmogenic nuclides ^{53}Mn, ^{26}Al and ^{10}Be, the light noble gases and cosmic ray tracks (CRT), keeping in mind that many other nuclides determined also bear valuable information.

2. Methods. In order to systematically study depth and size effects of cosmogenic nuclides in meteorites, one has to find objects of known preatmospheric size which survived entry into the earth's atmosphere with only a few cm of ablation losses. In addition, well-documented samples from a core drilled through the meteorite or from otherwise accessible parts must be available for a successful study. Table 1 lists a number of meteorites which fulfill these criteria and of which cosmogenic nuclides and CRT's have been measured extensively. In addition, several other meteorites are reported in the literature, for which a part of these measurements have been done [4,5]. The meteorites are listed in order of increasing preatmospheric radius ranging from 5 cm (77003) to approx. 1m (Jilin)[6]. The coverage of the full range of shielding depths is not always complete, as in

Table 1: Cosmogenic nuclide depth profiles in meteorites

Meteorite	Preatm. radius [cm]	^{53}Mn	^{26}Al	^{10}Be	light rare gases	cosmic ray tracks
ALHA77003	6	[T1]	[T2]	----	[T1]	P
ALHA78084	14	[T3,4]	[T3,4]	[T5]	[T4]	[T4]
Lost City	18	[T6]	[T7]	----	[T8]	[T9]
St. Severin	25	[T10,11]	----	[T12]	[T13]	[T14]
Keyes	25	[T15]	[T16]	P	[T17]	[T18]
Dhurmsala	>30	[T3,19]	[T3,19]	P	[T19]	[T19]
Jilin	85	[T20]	[T20]	[T20]	[T20]	[T20]

Footnotes: P - in preparation. [T1] P.Englert et al. (1982), Lun. Planet. Sci. XIII, 201. [T2] J.C. Evans et al. (1979), Proc. Lun. Planet. Sci. Conf. 10th, 1061. [T3] P.Englert et al. (1982), Fifth Int. Conf. Geochron., Nikko, Japan, 89. [T4] R.Sarafin et. al (1985), Earth Planet. Sci. Lett., to be published. [T5] R.K. Moniot et al. (1982), Nucl. Instr. Meth. 203, 495. [T6] P.Englert (1985), Lun. Planet. Sci. XVI, 215. [T7] P.J. Cressy (1971), J. Geophys. Res. 76, 4072. [T8] D.D. Bogard et al. (1971), J. Geophys. Res. 76, 4076. [T9] J.C. Lorin and P.Pellas (1975), Meteoritics 10, 445. [T10] P.Englert and W.Herr (1980) Earth Planet. Sci. Lett. 47, 361. [T11] S.K. Bhattacharya et al. (1980) Earth Planet. Sci. Lett. 51, 45. [T12] C.Tuniz et al. (1984), Geochim. Cosmochim. Acta 48, 1867. [T13] L.Schultz and P.Signer (1976), Earth Planet. Sci. Lett. 30, 191. [T14] Y.Cantelaube et al. (1969), In: Meteorite Research, (P.Millman, ed.), 705. [T15] P.Englert (1984), Lun. Planet. Sci. XV, 248. [T16] P.J. Cressy (1975), J.Geophys. Res. 80, 1551. [T17] R.J. Wright et al. (1973), J. Geophys. Res. 78, 1308. [T18] J.C. Lorin and G.Poupeau (1978), Meteoritics 13, 410. [T19] J.T. Padia et al. (1984), Meteoritics 19, 288. [T20] Jilin Consortium Study I (1985), Earth Planet. Sci. Lett. 72, 246.

Dhurmsala and Lost City. In the case of 77003, possible contributions of the solar cosmic radiation to the ^{26}Al- and ^{53}Mn production are discussed [7]. Jilin, which underwent a two stage irradiation, provides a model for different irradiation geometries in space, depending on the half life of the cosmogenic nuclide considered [6].

Figure 1 is an example of the kind of multiple two dimensional relations which have been established for depth and size studies of the cosmogenic nuclide production in meteorites. The solid lines compare the semiempirical models for the ^{53}Mn production [1] and the CRT-production [8] in meteorites. The symbols represent same sample measurements of the ^{53}Mn and CRTs in core AIII of St. Severin [9,10]. If several cosmogenic nuclides are determined in one or two samples, this and other relations can be used to derive shielding depths in and preatmospheric sizes of meteorites.

3. Results and Discussion. Table 2 combines results of ^{53}Mn and other cosmogenic nuclides measured predominantly in meteorite falls with high exposure ages (exception: Leedy and

FIGURE 1

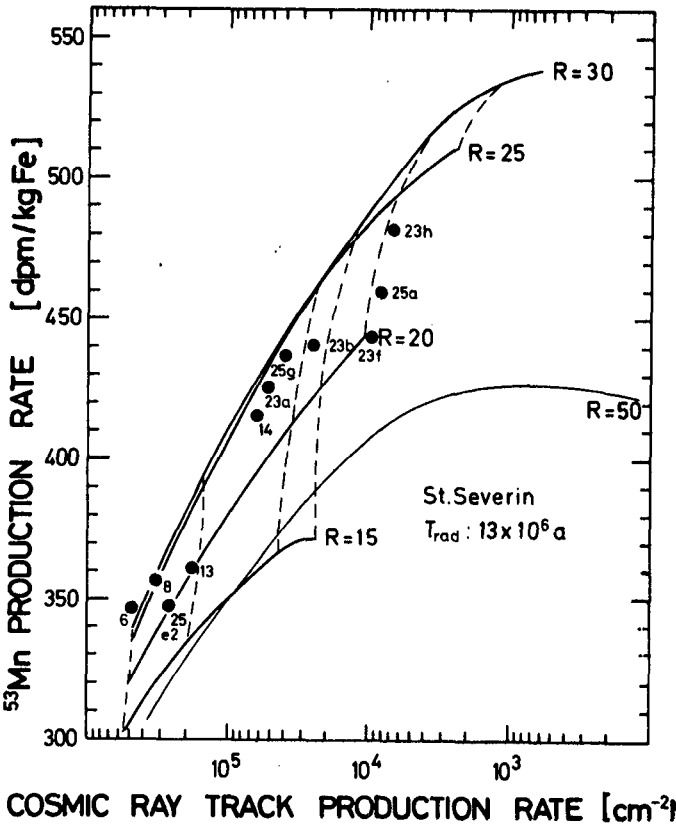

New Concord). All of these meteorites are saturated with respect to the long-lived cosmogenic nuclides. Thus, only depth and size effects or complex irradiation histories can be responsible for the GCR-product signatures.

In general, $^{22}Ne/^{21}Ne$-ratios on the order of 1.1±0.3 indicate well-shielded locations within a meteorite. Thus the majority of the meteorite samples in Table 2 come from shielding depths as they can be found in Dhurmsala [11] and Jilin [10]. This conclusion is in agreement with most of the ^{53}Mn, ^{26}Al and ^{10}Be data.

Preatmospheric mass determinations via CRTs are given for Aztec (18kg) and Hainhotz (260 kg) and were tried for Rangala and Leedy without conclusive results [12]. In the case of Hainhotz, the ^{53}Mn activity of 352±21 dpm/kg Fe confirms the CRT result. Aztec, however, must have been a larger object in space than indicated by the CRT measurements, because of its low $^{22}Ne/^{21}Ne$ ratio and a ^{53}Mn production rate of 339±28 dpm/kg Fe, exceeding that of small bodies if compared with ALHA 77003 and ALHA 78084 [13,14]. Discrepancies between the ^{53}Mn production rates and $^{22}Ne/^{21}Ne$ ratios exist for some meteorites with very long exposure ages, such as H-Ausson, Charsonville, Breitscheid and Yocemento and are probably best explained by complex irradiation histories. [15].

Table 2:

Meteorite	Class	Recov.(a) mass [kg]	$(^{22}Ne/^{21}Ne)_c$	^{21}Ne(b) [$10^{-8}cm^3STPg^{-1}$]	T_{21}(c) [10^6y]	^{53}Mn(d) [dpm/kg Fe]	^{26}Al [dpm/kg]	^{10}Be(h) [dpm/kg]	(i)
Alfianello	L6	228S	1.103	8.40	26.2	490±25	55.5±3.5(f)	--	NNNN
Aztec	L6	2.83	1.103	11.20	35.0	339±28(e)	--	--	YYOO
Breitscheid	H5	1.0	1.075	9.25	27.0	297±18(e)	--	--	YYOO
Charsonville	H6	>27	1.066	22.00	61.2	333±23(e)	--	--	YYOO
Ergheo	L5	20	1.089	7.31	16.3	415±20	57.0±2.5(f)	--	YYNO
Kuyahinya	L5	500S	1.098	11.20	34.2	403±32	57.0±2.5(g)	--	NNNO
Merzö-Madras	L3	27.7S	1.085	9.77	28.0	447±23	55.0±2.3(g)	--	YYNO
Rangala	L6	3.2	1.078	9.14	25.2	485±25	54.2±2.2(d)	--	YYYO
Rose City	H5	>11	1.042	9.42	22.7	464±25	56.0±3.5(f)	--	YYNO
Khairpur	E6	>15	--	--	--	401±24	--	--	OOOO
Leedy	L6	50	1.085	2.34	6.1	410±34	--	--	NNOO
New Concord	L6	226	--	0.90	3.0	174±11	--	--	NNOO
H-Ausson	(H)	(50)	1.101	21.70	72.2	302±20(e)	--	--	YYOO
Ausson	L6	50	1.094	20.20	60.5	356±21	62±5(h)	--	NNNO
Menow	H4	10.5	1.16	4.90	17.5	382±32(k)	60±6(h)	19.6±2.0	YYYY
Selden	LL5	1.56	--	15.50(h)	≧50	359±28(k)	--	19.2±2.8	OYOY
Yocemento	L5	5.92	--	20.10(h)	≧65	256±26(k)	--	17.6±2.2	OYOY
Hainholtz	MES	16.5	--	5.80	19.5	352±21	--	--	ONNO

Footnotes: (a) M.H.Hey (1966), Catalogue of Meteorites. (b) L.Schultz and H.Kruse (1978), Nucl.Track Det. 2, 65. (c) K.Nishiizumi et al. (1980), EarthPlanet.Sci.Lett. 50, 156. (d) this work. (e) W.Herr et al. (1981), Meteoritics 16, 324. (f) I.R.Cameron and Z.Top (1975), Geochim.Cosmochim.Acta 39, 1705. (g) D. Heymann and E.Anders (1967), Geochim.Cosmochim.Acta 33, 653. (h) R.K.Monict et al. (1983), Geochim. Cosmochim.Acta 47, 1887. (i) Two Y confirm that aliquots of the same sample were analyzed for cosmogenic nuclides. (k) preliminary results.

References: [1] T.P.Kohmann and M.L.Bender (1969), in: B.S.P.Shen (ed.), High Energy Nuclear Reactions in Astrophysics, Benjamin, N.Y., 169. [2] R.C.Reedy (1985), J.Geophys.Res. 90, C722. [3] P.Dragovitsch et al. (1985), SH 7.1-8, this conference. [4] T11. [5] P.Englert and R.Sarafin (1984), Meteoritics 19, 223. [6] T20. [7] P.Dragovitsch et al. (1985), Proc.Nucl.Data.Conf. Santa Fe. [8] S.K.Bhattacharya et al. (1973), J.Geophys.Res. 78, 8356. [9] T10. [10] T14. [11] T3,T19. [12] N.Bhandari et al. (1980), Nucl. Tracks 4, 213. [13] T1. [14] T3, T4. [15] T15.

SPALLOGENIC ORIGIN OF NUCLEI IN METEORITES

B.ZANDA[1] AND J.AUDOUZE[1,2]

1 Institut d'Astrophysique du CNRS,
98 bis, boulevard Arago
75014 Paris, FRANCE

2 Laboratoire René Bernas,
91405 Orsay, FRANCE

1. Introduction

The study of the cosmic ray fluxes propagation inside meteorites is a way to improve our knowledge both on these objects (exposure ages, size of irradiated parent bodies, location of samples within these bodies...) and on these fluxes (spectral index, total intensity, time variation...).

In this communication, we present some preliminary results obtained from a model built to evaluate the different interactions between cosmic rays and meteorites. With this model, we are able to compute fluxes as a function of depth inside the meteorite, taking into account energy losses by ionization and spallation reactions which induce both particle destruction and production. This procedure, in which particle fluxes and cross sections are treated independently from each other, differs significantly from the thick target approach (see Kohman & Bender-1967, Trivedi & Goel-1973) based on the measurement of spallation products generated in accelerator experiments.

2. Cosmic rays propagation inside meteorites

The basic equation describing the independent of time variation with depth of the flux Φ_i (cm^{-2} s^{-1} MeV^{-1}) can be written as :

$$\Omega\nabla\ \Phi_i + \sigma\ n\ \Phi_i = Q_i + \frac{\partial(\omega_i\ \Phi_i)}{\partial E} \qquad (1)$$

where . σ is the total destruction cross section of nuclear species i
. n is the number of target nuclei per unit volume,
. Q_i is the production term of secondary particles,
. ω_i is the energy loss of nucleus i due to excitation and ionization of the target medium ($\omega_i = -dE/dx$)
. The streaming factor $\Omega\nabla$ depends on the geometry of the meteorite :
If θ is the propagation angle,

- $\Omega \nabla = \cos\theta \frac{\partial}{\partial x}$ in plane parallel geometry

  x being the depth inside the meteorite
- $\Omega \nabla = \cos\theta \frac{\partial}{\partial r} + \frac{\sin^2\theta}{r} \frac{\partial}{\partial(\cos\theta)}$ in spherical geometry,

  r being the distance from the center.

3. Asymptotical behaviour of the transport equation at high energy

Above 1 GeV N^{-1}, energy losses and secondary particles production become negligible. Therefore, equation (1) reduces to :

$$\Omega \nabla \Phi_i + \sigma n \Phi_i \simeq 0 \qquad (2)$$

The boundary conditions are :

$$\phi(0, \cos\theta) = \Phi_{i,o} \qquad (0<\theta<\frac{\pi}{2}) \text{ in slab geometry}$$

$$\phi(R, \cos\theta) = \Phi_{i,o} \qquad (-\frac{\pi}{2}<\theta<\pi) \text{ in spherical geometry}$$

(we assume here that the incoming cosmic ray flux $\Phi_{i,o}$ is isotropic).

With such conditions, the solutions of equations (2) are :

$$\Phi_{slab}(x,\cos\theta) = \Phi_o \exp(-\frac{\sigma n x}{\cos\theta})$$

$$\Phi_{spherical}(r,\cos\theta) = \Phi_o \exp[-\sigma n(r\cos\theta + \sqrt{R^2-r^2\sin^2\theta})]$$

In figure 1, we compare the integrated flux ϕ over all directions calculated as a function of depth inside a meteorite in the case (i) of a plane parallel shape and (ii) of a spherical shape with R= 40 cm. It can be seen that the flux is always lower if calculated in the plane parallel assumption than in spherical geometry. The error made in treating a spherical 40 cm radius meteorite as an infinite slab would only be of a factor 1.2 at the surface but it would become as high as a factor 8 in the center.

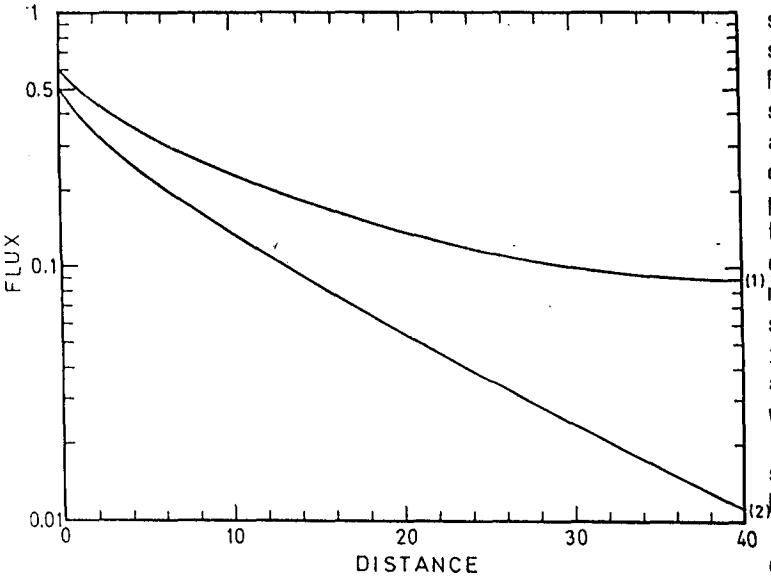

Figure 1

Comparison of depth dependent integrated fluxes (1) in spherical geometry and (2) in slab geometry. Note that the surface flux (1) is higher than (2) because of outgoing particles.

4. Solution of the complete equation including secondary particles production and energy losses

We have adopted the following procedure and assumptions:
(i) the ionization energy loss dE/dx was calculated from the Gloeckler formula (1970),
(ii) the secondary particles production can be written as :

$$Q(E,\cos\theta,r) = \int_E^\infty \sigma(E')\ P(E'\to E)\ \Phi(E',\cos\theta,r)dE'$$

where $P(E'\to E)$ is the probability to produce a secondary particle of energy E from a primary particle of energy E'.

In this preliminary approach, we used $P(E'\to E)= \frac{P}{E'}$,

where P, the average number of outgoing secondaries per spallation reaction is an ajustable parameter of our calculation, and the secondary spectrum is assumed to be flat.

The presence of an integral term in the second member of (1) requires the use of iterative computations.
This can be described as follows :

$$(\Omega\ \nabla + \sigma\ n - \frac{\partial \omega i}{\partial E})\ \phi^{(n)} = \int_E^\infty P\ \frac{\phi^{(n-1)}}{E'}\ dE'.$$

Details of the flux computations will be described in Zanda (1985).

The spallation cross-sections used to deduce nuclei production are derived from Silberberg and Tsao (1972a, 1972b, 1977, 1979).

The energetic particles may have two origins :
(i) the galactic cosmic rays which are modulated by the solar activity (we derived our modulated spectrum out of Proteroe, Ormes and Comstock -1981),
(ii) the solar cosmic ays. Since this solar source consists in particles with E<100 MeV, it only affects the first few centimeters of the meteorite and will not be considered here.

5. Preliminary results

Because of the existing experimental data, we chose to first test our model on the iron meteorite Grant. Computations were made for a meteorite having the same chemical composition and various radius (40 cm, 35 cm and 30 cm) admiting a secondary particle yield per interaction p=0.75. Figure 2 shows a comparison of our results with measurements by Signer and Nier (1960) for Ne21. It can be seen that there is a good agreement between calculation results and experimental datas for a radius of 35 cm which is a little less than the pre-atmospheric radius that these authors derived of their calculation.

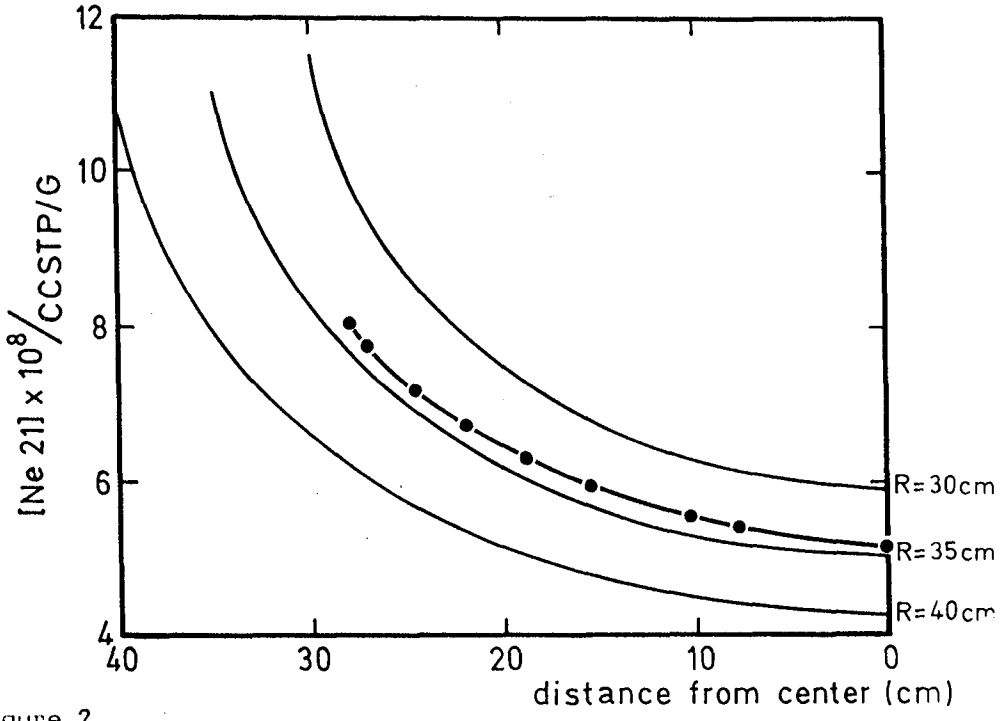

Figure 2
Comparison of computations results for various radius (single curves) and experimental datas from Signer and Nier (dotted curve).

6. Conclusion

The results obtained with the model presented here are sufficiently encouraging to pursue and improve that type of studies, in particular by finding a proper treatment for the outstanding problem of secondary particles production. Unfortunately, taking into account the actual geometry of a meteoritical sample at the time it suffers the bulk of the cosmic ray irradiation will still remind a difficulty.

We wish to thank G. Malinie for helpful discussions throughout the preparation of this paper.

7. References

1. Gloekler, G., (1970), in "Introduction to Experimental Techniques of High Energy Astrophysics" p.1, Ogelman H. and Wayland J.R. Ed. NASA SP-243
2. Kohman, J.P., and Bender, M.L., (1963) in "High Energy Nuclear Reactions in Astrophysics" p.169, B.S.P. Shen Ed. Benjamin, New York
3. Proteroe, R.J., Ormes, J.F. and Comstock, G.M., (1981) Ap.J., 247, p.362
4. Signer, P., and Nier, A.O., (1960), J.G.R., 65, p.2947
5. Silberberg, R., and Tsao, C.H., (1972a&b), Ap.J.Suppl. series, 220, p.315 & p.335
6. Silberberg, R., and Tsao, C.H., (1977), in 15th I.C.R.C., Plovdiv, 2, p.84
7. Trivedi, B.M.P., and Goel, P.S., (1973), J.G.R., 78, p.4845
8. Tsao, C.H., and Silberberg, R., (1979) in 16th I.C.R.C., Kyoto, 2, p.202.

SH 7.1-11

CLUSTERS AND CYCLES IN THE COSMIC RAY AGE DISTRIBUTIONS OF METEORITES

Martin F. Woodard* and K. Marti
University of California, San Diego
La Jolla, California 92093

ABSTRACT

Statistically significant clusters in the cosmic ray exposure age distributions of some groups of iron and stone meteorites are observed, suggesting epochs of enhanced collisions and breakups. Fourier analyses of the age distributions of chondrites reveal no significant periods, nor does the same analysis when applied to iron meteorite clusters.

*Present address: Smithsonian Astrophysical Observatory, Mail Stop 16, 60 Garden Street, Cambridge, Massachusetts 02138.

Introduction. Cosmic ray interactions in meteorites produce a variety of spallation products which depend on the target element abundances, the size and location within a meteorite. Radioactive and stable cosmogenic nuclide pairs with half-lives ranging from a few years to 10^9 years can be used to determine the cosmic ray exposure history of an object. The radioactive nuclides with half-lives short, compared with the time interval of exposure to cosmic rays, are in secular equilibrium and define the production rates. For a constant exposure geometry measured amounts of the stable integrating nuclides coupled with radionuclide measurements are used to obtain the integral time of exposure to cosmic rays. The advantage of this approach is that reliable exposure age information can be obtained in samples reflecting variable degrees of cosmic ray shielding as in large meteorites or in cases of incomplete development of the secondary cascade typically observed in small meteorites. A number of methods were developed for the calculation of production rates and of cosmic ray exposure ages (e.g. Voshage, 1962; Nishiizumi et al., 1980; Marti, 1984; Lavielle et al., 1984). Exposure ages for iron meteorites based on ^{40}K-^{41}K and ^{38}Ar data indicate some clustering of exposure ages for several groups of irons (e.g. Voshage and Feldmann, 1979; Lavielle et al., 1984). Exposure age distributions for chondrites were studied several times (e.g. Wänke, 1966; Crabb and Schultz, 1981). Noble gas data were recently compiled by Schultz and Kruse (1983).

Methods of Analysis. To test the significance of a cluster of M samples within a given group of N (>M) meteorites, we first assign an age span, T, to the group as a whole, based on the rough appearance of the age distribution of the group. We then select a value, W, much shorter than T, similar to the age spread of the candidate cluster. Under the assumption that the N group members are uniformly and randomly distributed over the age interval [0,T], we calculate the probability of finding at least M samples within some subinterval of duration W.

The cluster probabilities were computed by performing Monte Carlo simulations on a vax 11/780 computer. For each trial of the simulation, N pseudo-random numbers were generated on the interval [0,T]. A set of overlapping subintervals, each of duration W, were defined so that their starting

points form a uniform grid in which successive subintervals overlap by 90% so as to cover the interval [0,T]. If at least M of the N random numbers is found in one or more of the subintervals, a "success" is recorded. The estimated occurrence probability for a cluster of M meteorites is the number of successes divided by the total number of trials.

Various tests of the Pseudo-random number generator have been made, including a comparison with a direct calculation of the cluster probability in a limiting case where a simple analytic expression applies.

We have also searched for periodicity in the age distributions of both individual meteorite groups and in the age distributions of clusters. A discrete time series is formed by assigning to each of a set of uniformly-spaced time bins, the number of samples lying within the bin. A Fourier spectrum is then computed for these time series and is examined for outstanding peaks, the significance of a peak in the power spectrum is evaluated by computing the probability of finding a peak at least as high as the real one in the spectrum of a randomly generated age distribution (using a Monte Carlo procedure quite analogous to the above method of establishing cluster probabilities.

Results. A cluster is designated "probable" if its probability of occurrence, by the previously described test, is less than 10% and "very probable" if the probability is less than 1%. Groups of probable and very probable clusters are listed in the table below.

Table List of Significant Exposure Age Clusters and Calculated Probabilities.

Group	N	T (Myr)	Average Age of Cluster (Myr)	M	W	Probability
H Chondrites	95	20	7	45	3	$0/10^5$
Enstatite Achondrites	9	115	60	5	8	$94/10^4$
Irons IA	13	10^3	440	5	50	$20/10^3$
Irons IIA	7	10^3	25	4	50	$111/10^4$
Irons IID	3	10^3	360	3	50	$60/10^4$
Irons IIIA	19	10^3	650	7	50	$2/10^3$
Irons IIIE	6	10^3	475	3	50	$104/10^3$
Irons IVA	13	10^3	375	10	150	$1/10^4$
			400	6	75	$60/10^4$
			400	4	40	198/2000
Irons IVB	5	10^3	875	3	50	$50/10^3$

Column 1 gives the group containing the cluster, columns 2 and 3 give the size of the group, N, and its age span, T. Column 4 gives the estimated age and column 5 the number of samples in the cluster. Columns 6 and 7 give, respectively, the age span, W, of the cluster and the probability of random occurrence (the latter expression displays explicitly both the number of successes and the total number of trials from which the successes were derived). The table does not list all clusters found because some of these overlap in time.

A Fourier analysis of the H chondrite group, using only meteorites with exposure ages between 10 and 40 Myr (i.e., ignoring the big peak at 7 Myr) yielded no significant periods. Similarly, no significant peaks were found in the fourier spectrum of the L chondrites between 0 and 40 Myr. A power spectrum of the age distribution of the iron meteorites (see table) also yielded no significant periods.

Discussion. We regard the clustering as real since probable or very probable clusters occur in most of the major subgroups. The statistical significance assigned to the clusters depended on the assumed test model of a uniform distribution over the stated ranges, T. For instance, for each of the iron groups T = 1000 Myr is roughly the cutoff age for the irons as a whole. A more realistic hypotheses against which to test cluster significance might be to distribute the samples exponentially, to simulate the gradual decrease in the number samples of increasing age.

To obtain some idea of the sensitivity of the results to our assumptions, we have also computed the cluster probabilities by choosing a width W in excess of the apparent age range of the cluster, thereby overestimating the probability, for example, for the iron IIIE subgroup, changing W/T from 5% (corresponding to the result in the table) to 7% increases the probability from ~10% to ~20%, therefore, this cluster must be considered marginal. On the other hand, the probability of the cluster in the IA iron group increases from ~2% to ~9% when the assumed width of the cluster changes from 5% to 8%. The IA cluster and most of the clusters listed in the table are at least probable even when their age ranges are overestimated.

One interpretation of the clusters is that they represent epochs of increased meteorite formation resulting from individual collisions of asteroids or comets. In this case, one would expect to see a cluster of width corresponding to uncertainties in the age values. However, secondary breakups of the original collision products, complex exposure histories, and spatial variations in the cosmic ray flux, can all degrade the sharpness of the clusters. Thus it is important to know whether the actual spread in the ages of samples from a given cluster can be accounted for by any of the above factors.

Multiple collisions with asteroids might produce meteorites over an extended period. One possible example of such an enhancement is the iron IVA cluster at 400 Myr, extending over an age interval W = 150 Myr. The fact that this interval, containing 10 samples is exceptionally long leads us to suspect that two or more clusters are present. Belonging to the aforementioned 10 are 6 samples of average age 400 Myr, which themselves constitute a very probable cluster listed in the table. The remaining four samples do not constitute a cluster by our criterion, however a more sophisticated test might reveal a second cluster.

Conclusions. The record of cosmic ray effects in iron and stone meteorites was studied. Statistically significant clusters in the exposure age distributions of these objects were found, suggesting epochs of enhanced meteorite formation, possibly as the result of collisions and breakups. Significant exposure age clusters are found or confirmed for the following groups of meteorites: H-Chondrites at 7 Myr, enstatite achondrites at 60 Myr, iron group IA at 450 Myr, IIA < 50 Myr, IID at 350 Myr, IIIA at 650 Myr, IIIE at 475 Myr, IVA at 400 Myr and IVB at 875 Myr. A Fourier analysis of the age distributions of both H and L chondrites reveals no significant periods, nor does the same analysis when applied to the age distributions of iron meteorite clusters

Acknowledgements. This research was supported by NASA NAG 9-41.

References.

Crabb, J. and Schultz, L. (1981), Geochim. Cosmochim. Acta 45, 2151-60.

Lavielle, B., Marti, K. and Regnier, S. (1984), Proceedings of Conf. on Isotopic Anomalies in the Solar System, Paris.

Marti, Kurt (1984), Abstract, Workshop on Cosmogenic Nuclides, July, Los Alamos, New Mexico.

Nishiizumi, K., Regnier, S. and Marti, K. (1980), Earth Planet. Sci. Lett. 50, 156-70.

Schultz, L. and Kruse, H. (1983), Helium, Neon and Argon in Meteorites; A Data compilation. Special publication of the Max-Planck-Institute for Chemistry, Mainz.

Voshage, H. (1962), Z. Naturforsch. 17a, 422-32.

Voshage, H. and Feldmann, H. (1979), Earth Planet. Sci. Lett. 45, 293-308.

Wänke, H. (1966), Z. Naturforsch. 21a, 93-110.

THE $^4He/^1H$ RATIOS IN THE CHEMICAL COMPOSITIONS OF SOLAR FLARE PARTICLES AND THE PRIMORDIAL SOLAR NEBULA

Kunitomo Sakurai

Institute of Physics, Kanagawa University
Rokkakubashi, Yokohama 221, Japan

ABSTRACT

Except for the proton component, it is well known that the chemical abundances of solar flare particles are similar to those of galactic cosmic rays at their sources. In order to infer the $^4He/^1H$ ratio in the solar atmosphere, this ratio as observed in the interstellar gases has been taken into account in addition to those which have been obtained of galactic cosmic rays and the stars classified as the early types. Since it is clear that the most of these ratios ever deduced for both of the sun and solar flare particles are lower than those for the interstellar gases, this ratio thus obtained seems to suggest that hydrogens are relatively overabundant in the chemical abundances of the sun and the primordial solar nebula as compared to those of the interstellar gases being currently observed.

1. Introduction

As well known, the relative abundance of the helium atoms in the sun has never been exactly determined spectroscopically because the temperature of the solar photosphere is too low for these atoms to be excited(1). Using the observed data on the chemical composition of solar flare particles and the solar chromosphere, the ratio of heliums to hydrogens in number, being denoted as $^4He/^1H$ in this paper, has thus been estimated so far. This ratio, however, gives a value about equal to 0.0625, which is not coincident with those which have been estimated as 0.091 - 0.11 from the spectroscopic observations of the early type stars. Even now, it can, therefore, be said that the ratio $^4He/^1H$ for the sun has not been determined as yet. For this reason, many people still use the values as estimated for these stars in investigating some problems on solar physics, though they do not seem to be confident of their usage of those values for this ratio.

Recently, the spectroscopic data on the ratio $^4He/^1H$ have been accumulated from the investigations on the chemical compositions of the interstellar gases and the planetary nebulae(2). In this paper, this ratio in the sun will be reexamined by taking into account these data.

2. The Relative Abundance of Helium Atoms in the Solar Atmosphere and Solar Flare Particles

It is thought that the chemical composition of solar flare particles may give us an important clue to understand the acceleration mechanism of these particles in solar flares. This composition has, therefore, been repeatedly observed by means of balloons, rockets and satellites since the late 1950's. At present, it is known that this composition tends to become systematically overabundant for the heavy nuclei with the increase of their charge numbers(3, 4). It has, however, been shown that the relative abundance of hydrogen atoms is somehow variable, but the ratio $^4He/^1H$ is given to be 0.063 ± 0.015 (1).

Since it is known that the ratio of helium to the medium nuclei (C,N,O) in number is almost constant from one observation to another, the variability on the ratio $^4He/^1H$ seems to have been caused by that of the hydrogen atoms in solar flare particle events. However, it should be noted that this ratio as given above is much less than that which is currently applied to the study of the solar interiour and atmosphere. Furthermore, this ratio is not coincident with those which have been determined from the spectroscopic observations on the interstellar gases and the planetary nebulae(2). Really speaking, the former is also much less than the latters.

In order to compare these ratios from each other, they are shown in Fig. 1 as a function of the logarythmic value

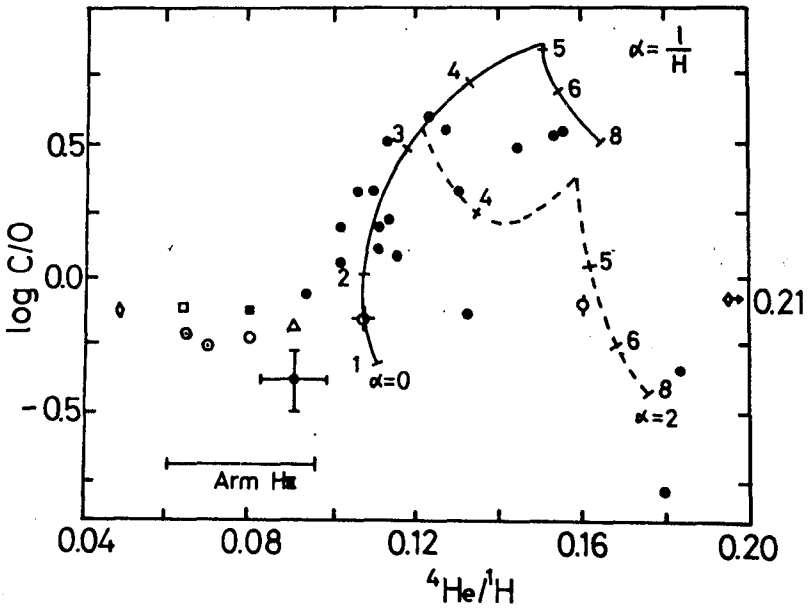

Fig. 1 Relation between the ratios C/O and $^4He/^1H$ for the interstellar gases, the solar atmosphere, solar flare particles and galactic cosmic rays(see text for the detail).

of the ratio C/O(2). In this figure, black circles(1) show the spectroscopic data on the interstellar gases and the planetary nebulae. White circles with and without dot inside (5, 6), black squares(7) and triangle(8) all indicate the data from the spectroscopic observations on the solar atmosphere by different authors. Two diamonds have been obtained from the chemical composition of galactic cosmic rays(9). The left-end one indicates the value for the high-energy galactic cosmic rays, which is still less than that for solar flare particles which is indicated by white square.

It is clear from Fig. 1 that the ratio C/O remains almost constant for all the values of the solar atmosphere and solar flare particles, whereas the ratio $^4He/^1H$ widely ranges from 0.06 to 0.095. In this figure, there are two curves for the relation between the ratios of C/O and $^4He/^1H$ which are given as a function of the stellar masses. Black and dashed curves, respectively, correspond to different values of the mixing length, l, in the convective layers of the stars of different masses, where H denotes the scale height of these layers. The numbers on these curves give the masses of the stars in the unit of the solar mass.

Since the ratio $^4He/^1H$ for the sun is highly deviated from these two curves, the relative abundance of hydrogen atoms may be overabundant to the sun as compared with other sunlike stars. If this is to be the case, the accretion of hydrogen gases may have happened very effectively during the early phase of the formation of the primordial solar nebula. Thus the excess of hydrogens seems to have resulted in the relative abundances of the present solar atmosphere.

3. Conclusion

The $^4He/^1H$ ratios in the chemical compositions of solar flare particles and the solar photosphere have been shown to be always less than those which are observed on the interstellar gases and the planetary nebulae. This tendency is also found on the chemical composition of the primordial solar nebula. These results suggest that the primordial solar nebula might have already been overabundant of hydrogen atoms in the initial stage of its evolution.

It is noted that this overabundance of hydrogen atoms in the chemical composition of the present solar atmosphere seems favorable to fix the case for the missing solar neutrinos, which is now thought as the one of the most difficult problems in astrophysical research(10).

References

(1) e.g., K. Sakurai (1974) Physics of Solar Cosmic Rays, Univ. of Tokyo Press, Tokyo.

(2) M. Peimbert, A. Serrano and S. Torres-Peimbert, (1984) Science 224, 345.

(3) A. Mogro-Campero and J.A. Simpson (1972) Ap. J. 171,L 5 and 173, L 35.
(4) J.-P. Meyer (1985) Ap. J. Suppl. Ser. 57, 151 and 173.
(5) E. Anders and M. Ebihara (1982) Geochim. Cosmochim. Acta 46, 2363.
(6) A.G.W. Cameron (1982) Essays in Nuclear Astrophysics, p. 22 (eds. C.A. Barnes et al.) Cambridge Univ. Press., Cambridge.
(7) J.E. Ross and L.H. Aller (1976) Science 191, 1223.
(8) L. Goldberg, E. Müller and L.H. Aller (1960) Ap. J. Suppl. 5, 1.
(9) J.A. Simpson (1983) Ann. Rev. Nuclear Part. Sci. 33, 323.
(10) K. Sakurai (1984) Space Sci. Rev. 38, 243.

HIGH PRECISE MEASUREMENTS OF COSMOGENIC RADIOCARBON ABUNDANCE BY COMPLEX OF SCINTILLATION EQUIPMENTS

[1]G.E.Kocharov, [2]R.Ya.Metskvarishvili, [2]S.L.Tsereteli

1. Ioffe Physico-Technical Institute
Academy of Sciences of the USSR, Leningrad
194021, U S S R

2. Tbilisi State University, Tbilisi 380028
U S S R

The main characteristics of scintillation equipments which enable the measurements of radiocarbon content with high accuracy of 0.2-0.3% have been considered. The complex of scintillation devices has been operating very well for the last 15 years and has allowed to investigate the temporal variation of solar activity and intensity of cosmic rays for the last 300 years.

Studies of various astrophysical, geophysical and ecological phenomena by way of investigation of radiocarbon activity in dendrocronologically dated samples have been under way since 1965 [1].

Two types of detectors are used at present for the measurement of the ^{14}C concentration in dendrochronologically dated tree-rings: proportional and liquid scintillation counters. We prefer the liquid scintillation counter because it allows to use tens of gram of carbon in relatively small volume, which is important for high precise measurements of astrophysical samples. Firstly single-channel equipment with a stabilization of the photomultiplier and amplifiers was developed and used [2-3] . For stabilization the special light impulse generator with stable amplitude was developed. Counting rate of onefold standard was 48.33 imp.per min. at a background 6.5 imp.per min. Precision of radiocarbon measurements was of 0.3-0.4%.But use of an electron lamp 6G-14 B as a light impulse generator had several defects: a necessity of stabilization of light impulse amplitude, short life time

of the electron lamp,increased background of the scintillation equipments and so on.That is why light impulse generator using light diode KL 102B has been developed,which is smaller,more simple and has longer life in comparison with device with electron lamp.

Block-diagram of developed two-channel scintillation equipments is shown in Fig.1.

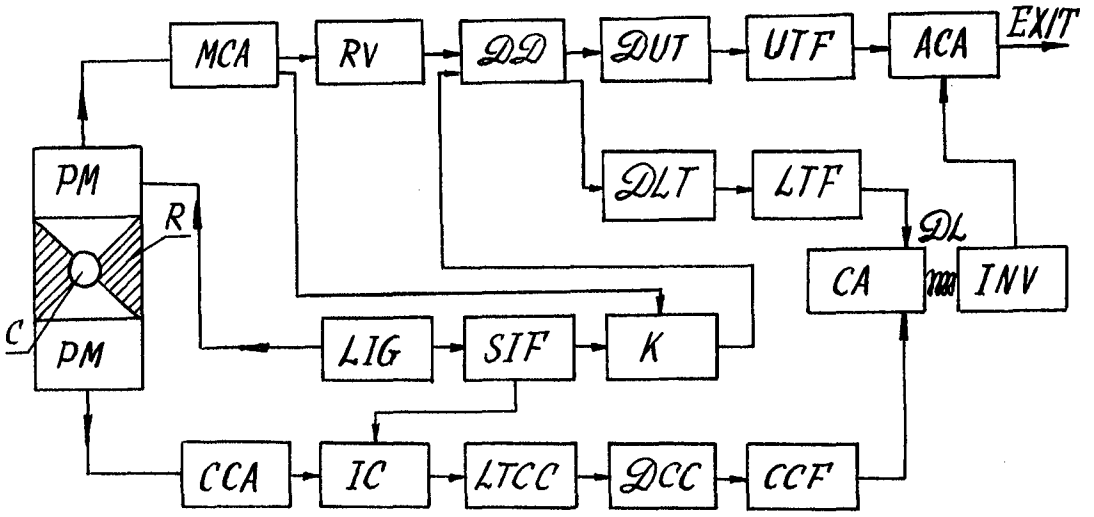

Fig.1. Block-diagram of two-channel scintillation equipment. C-cuvette with investigated sample,R-reflector,PM-photomultiplier,MCA-main channel amplifier,CCA-coincidence channel amplifier,LTG-light impulse generator,SIF-synchronous impulse former,RV-reference voltage,K-key,IC-intermediate cascade,DD-differential discriminator,LTCC-lower threshold of coincidence channel,DCC-discriminator of coincidence channel,DUT-discriminator of upper threshold,DLT-discriminator of lower threshold,UTF-upper threshold former,LTF--lower threshold former,CCF-coincidence channel former, CA-coincidence assembly, DL-delay line,INV-invertor, ACA-anticoincidence assembly.

Stabilization is made by light impulses of the diode KL 102B which is triggered by signals of electric impulses generator with a stable amplitide and definite frequency 1700 Hz.Generator operates the key which forbids a passing of the stabilization impulses.

Light impulses passing through photomultiplier and main amplifier form a voltage in the scheme of reference voltage which is proportional to the value of stabilization impulse and operate the thresholds of differential discriminators. With the variation of amplification coefficient of PM and amplifier the thresholds of discriminators are automatically changed into necessary direction and prevent the system from destabilization.

To study temporal variation of radiocarbon abundance in the samples with high precision it is necessary to make longcontinued measurements. To increase the number of measured samples five two-channel scintillation equipments were made (Table).

Table.

Volume ml	Counting rate of the background N_b imp./min	Counting rate of the standard N_{st} imp/min	$\frac{N_{st}}{\sqrt{N_b}}$	Detection efficiency ε, %
6	4.77	39.42	18	58
10	5.48	55.98	24	53
13	7.75	82.42	30	58
15	9.59	92.48	30	58
21	9.25	146.90	48	64

Different values of cuvettes allow to use the samples with different masses of carbon without dilution.

To investigate time variation of ^{14}C abundance in the Earth's atmosphere dendrochronologically dated annual rings of the trees of different species and from different regions of the Earth were used. Dated samples were transformed to a benzene in a chemical way.

Activity of investigated sample relative to the standard is calculated by the following formulae:

$$\delta^{14}C\,(‰) = \frac{N_s - N_{st}}{N_{st}} \cdot 1000.$$

where N_s and N_{st} - are counting rates of the sample and standard accordingly.

For fractionation correction we measured $^{13}C/^{12}C$ in the samples.

$$\delta^{13}C = \left[\frac{R_s - R_{st}}{R_{st}}\right] \cdot 1000\%$$

R_s and R_{st} are the ratios of $^{13}C/^{12}C$ in the sample and standard accordingly.

Radiocarbon activity with taking into account fractionation correction is calculated by the formulae:

$$\Delta^{14}C = \delta^{14}C - (2\delta^{13}C + 50)(1 + \frac{\delta^{14}C}{1000})\text{‰}.$$

Obtained results on time variation of cosmic rays are discussed in paper SH 7.1-15 presented at this conference.

References.

1. Konstantinov B.P., Kocharov G.E., 1965. Dokl. AN SSSR, v. 165, p. 63.
2. Metskvarishvili R.Ya. et al. 1971, Radiocarbon, Vilnus, p. 129.
3. Metskvarishvili R.Ya., Dergachev V.A., ibid., p. 131.
4. Metskvarishvili R.Ya., 1974. Proc. All-Union Conference on the problem "Astrophysical phenomena and radiocarbon", Tbilisi University Press, p. 27.

RADIOCARBON CONTENT IN THE ANNUAL TREE RINGS DURING LAST 150 YEARS AND TIME VARIATION OF COSMIC RAYS

G.E.Kocharov[1], R.Ya.Metskvarishvili[2], S.L.Tsereteli[2].

1. Ioffe Physico-Technical Institute
Academy of Sciences of the USSR
Leningrad,194021,USSR
2. Tbilisi State University,Tbilisi,380028
U S S R

The results of high accuracy measurements of radiocarbon abundance in precisely dated tree rings in the interval 1800-1950 yrs have been discussed. Radiocarbon content caused by solar activity is established.Using obtained data the temporal dependence of cosmic rays is constructed.

Using the complex of scintillation equipments [1] temporal variations of radiocarbon content in the Earth's atmosphere have been obtained for the time interval 1800 to 1950 year. Accuracy of radiocarbon measurements in tree rings was 0,2-0,3%. For fractionation correction we measured $^{13}C/^{12}C$ by mass-spectrometer MI-1201 with the accuracy 0.03%.

To reveal the cyclic components in the radiocarbon abundance temporal dependence we used two possibilities: method of spectral analysis and Burg's method. Spectral analysis method can be used both for long and short temporal rows and allow to treat experimental data row with the gaps. Burg's method is used for short rows and allows to reveal a periodicity which is comparative with a length of the row.

Now we consider the concrete results for the period 1850-1940 years. Both using methods allow to establish in the radiocarbon row 11-years periodicity which can be connected with the well-known solar cycle. To reveal the nature of connection between the solar activity and the radiocarbon abundance we use correlative analysis: between $\Delta^{14}C$ and Wolf numbers W(t) not only for all the interval (1850-1940 yrs) but for single solar cycles too. Analysis shows negative correlation with a time shift about 4-5 yrs.

Negative correlation means that the main source of radiocarbon abundance variation is solar modulation of cosmic ray intensity. Based on this fact the time-variation of cosmic ray intensity in the past has been obtained.

The scheme is the following. One adopts a model for the carbon-exchange reservoir and establishes its dynamic parameters. Then one converts the radiocarbon content of tree-rings into the rate Q(t) of radiocarbon formation in the Earth's atmosphere in the time-interval of interest. And finally one transforms Q(t) into the galactic cosmic-ray flux.

We used the five-reservoir model, incorporating the atmosphere A, the biosphere B, humus H, the ocean surface layer S and the deep ocean O (for details see [2,3]).

Within the rigidity range $0.5 \leq R \leq 50$ GV, which contributes about 95% to Q(t), the variations of the primary spectrum D(R,t) caused by solar modulation are described by an exponential function of the type [3] :

$$\mathcal{D}(R,t) = \mathcal{D}(R,0)e^{-K(t)/R} \qquad (1)$$

where D(R,0) represents the interstellar cosmic-ray specrum and K(t) is a modulation parameter. Dorman [4] has obtained an expression relating the atmosphere ^{14}C formation rate to the variations in the primary cosmic-ray spectrum:

$$\frac{\delta Q(t)}{Q_o} = \frac{Q(t)-Q_o}{Q_o} = \int_0^\infty \frac{\delta \mathcal{D}(R,t)}{\mathcal{D}(R,0)} W(R)\,dR \qquad (2)$$

where W(R) serves as the planetary coupling factor for the rate of radiocarbon formation by cosmic rays.

In view of the normalization condition

$$\int_0^\infty W(R)\,dR = 1$$

and the relation

$$\frac{\delta \mathcal{D}(R,t)}{\mathcal{D}(R,0)} = \frac{\mathcal{D}(R,t)}{\mathcal{D}(R,0)} - 1 = e^{-K/R} - 1$$

one may put E_q (2) in the form

$$\frac{\delta Q(t)}{Q_o} = \int_0^\infty e^{-K/R} W(R)\,dR - 1 \qquad (3)$$

Using Dorman's values [4] of W(R) one readily obtains the expression [5]

$$\kappa(t) = 0.028 \left| \frac{\delta Q(t)}{Q_0} \right|^{1.29} \qquad (4)$$

Normalization is taken here at minimum solar activity (maximum radiocarbon formation rate).

If the primary cosmic-ray spectrum confirms to a power law with respect to total energy the intensity variation in the rigidity range (R_1, R_2) at the Earth's orbit will be:

$$\frac{\delta I}{I_0} = \frac{I - I_0}{I_0} = \int_{R_1}^{R_2} E^{-\gamma}(R) e^{-\kappa/R} dR \Big/ \int_{R_1}^{R_2} E^{-\gamma}(R)\, dR - 1 \qquad (5)$$

where $\gamma \simeq 2.6$ is the spectral index, $E(R) = e\sqrt{R^2 + \frac{m_0 c^2}{e}}$ is the total energy of a proton (m_0, e are the proton mass and charge; c is the speed of light).

Figure 1 shows the cosmic-ray intensity variation we have obtained in this way within the rigidity interval

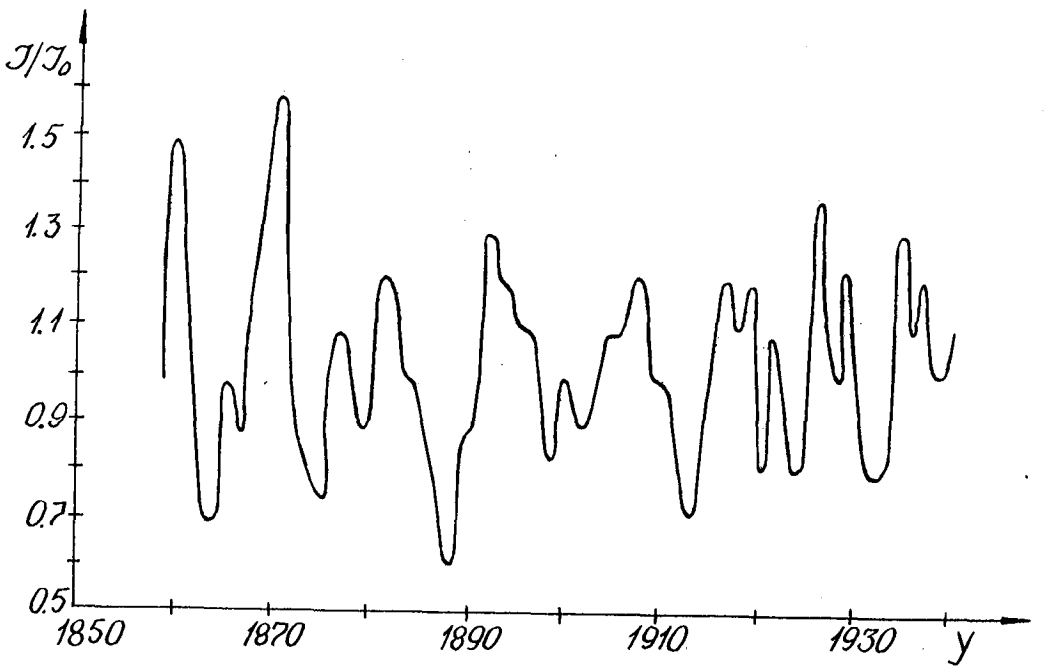

Fig.1. Intensity variations of galactic cosmic rays within the rigidity range $0.5 \leq R \leq 50$ GeV

$0.5 \leq R \leq 50$ GV. 11-year periodicity is clear seen in all considered time-interval. Amplitude of variation is in good agreement with the direct experimental data obtained during two last cycles of solar activity.

References.

1. Kocharov G.E. et al.,1985, paper SH 7.-14 presented at 19-th ICRC, San-Diego,USA.
2. Kocharov G.E. et al. 1983,Pis'ma Astronom.Zh. v.9,p.206.
3. Lockwood J.A.,Webber W.R.,1967, J.Geophys.Res.,v.72, p.5977.
4. Dorman L.I. in Proc.: 6-th All-Union Conf. on Astrophysical Phenomena and Radiocarbon, Tbilisi Univ.Press, USSR,1978,p.49.
5. Dergachev V.A.,Kocharov G.E.,Tleugaliev S.Kh.,1979, Proc. 16-th ICRC,Kyoto, p.142.

COSMOGENIC Mn-53 IN METEORITES

Alexeev, V.A. and Lavrukhina, A.K.

V I.Vernadsky Institute of Geochemistry and Analytical Chemistry, USSR Academy of Sciences, Moscow, USSR

The distributions of the Mn-53 contents in 106 nonantarctic and 112 antarctic chondrites were analysed. A correlation analysis of these distributions showed that the correlation coefficient is a maximum ($r_{max}=0.75\pm0.03$) when the histogram for antarctic chondrites is displaced by 40 ± 8 dpm $kg^{-1}Fe$ towards lower Mn-53 contents.

The distribution of Mn-53 saturated contents in nonantarctic ordinary chondrites was investigated as a function of their radiation age (T). It is found that the Mn-53 average content is higher by (21+9)% in H-chondrites with radiation age $T \leq 12$ Myr than in those with $T > 12$ Myr. This effect can be attributed to the fact that a considerable proportion of H-chondrites with $T \leq 12$ Myr originates from a comet or from the objects of Chiron like, with the orbits more inclined to the ecliptic plane and/or more extended, which caused their irradiation by cosmic rays of higher intensity. The greater proportion of such chondrites in the antarctic meteorites might cause the aforementioned higher Mn-53 content in the meteorites from Antarctica.

Studies of long-lived cosmogenic radionuclide Mn-53 ($t_{1/2}=3.7$ Myr) in meteorites can supply evidence on both the cosmic-ray intensity variation and the radiation history of these cosmic bodies. The direct counting of Mn-53 presents difficulties because of the soft K-radiation; also rather large amounts of precious material would be needed. Millard /1/ pointed out the possibility of converting Mn-53 into the γ-emitting Mn-54 by a neutron capture. The large cross- section affords much greater sensitivity for the determination of Mn-53.

We studied the different procedures on the Mn isolation from the meteoritic metal, found the optimal conditions of the irradiation, and determined the Mn-53 content in the iron meteorites and in the metal of chondrites. About 1 g of meteoritic metal along with the Mn carrier (5 mg) were dissolved in HNO_3. Pre- and post-irradiation chemical procedures were mainly similar to those reported by Imamura et al. /2/. The manganese was isolated by ion exchange procedures and

then in the form MnO_2 was irradiated 1156 hours in the researh reactor. Results of our measurements were published in /3,4/. This paper presents an analysis of data reported in the literature and authorss data on the Mn-53 content in ordinary chondrites.

The distributions of the Mn-53 contents in 106 nonantarctic and 112 antarctic chondrites were analysed (see Fig.1). A correlation analysis of these distributions showed that the correlation coefficient is a maximum ($r_{max}=0.75\pm0.03$), when the histogram for antarctic chondrites is displaced by 40 ± 8 dpm kg^{-1}Fe towards lower Mn-53 contents (Fig.2). That is, the Mn-53 content in antarctic chondrites is higher, on the average, than in nonantarctic chondrites, in spite of higher earth age of the antarctic meteorites.

This fact can be explaned by several reasons: (a) antarctic meteorites have higher radiation ages; (b) antarctic meteorites were irradiated in space by cosmic rays of higher intensity due to, possibly, a higher extent or a larger inclination to the ecliptic plane of the orbits of these meteorites /5/.

The distribution of Mn-53 saturated contents in nonantarctic ordinary chondrites was investigated as a function of their radiation age. The equation:

$$A_{sat}=A_{meas}/(1-e^{-T.\ln 2/t}),$$

was used to calculate the saturated content of Mn-53 (A_{sat}). Here A_{meas} is measured content of Mn-53, t is half-life of Mn-53, and T is radiation age of meteorite. The radiation age of chondrites was determined from the cosmogenic ^{21}Ne content and its production rate (P_{21}). The P_{21} values were calculated according to relation proposed by Nishiizumi et al. /6/. The noble gas data are from the compilation by Schultz and Kruse /7/. When more than one analysis was available for a given meteorite, the average of the exposure ages was used. Ne-21 and Ne-22 concentrations were corrected for a trapped component, using a solar isotopic composition for the solar-gas bearing meteorites and atmospheric ratios for the rest of the analyses /8,9/.

The results for 56 H-chondrite are shown in Fig.3. It is found that the Mn-53 average content is higher by $(21\pm9)\%$ in H-chondrites with radiation age $T \leq 12$ Myr years than in those with $T > 12$ Myr. A similar excess, though less pronounced, we observed for L- and LL-chondrites too. The analysis showed that this excess takes place both for the falls and for the finds, and is not due to the difference in meteorite mass distribution in different age groups. A similar, but less pronounced effect is noticed also for Al-26. The higher Mn-53 and Al-26 saturated contents in chondrites of low radiation age, especially in H-chondrites, can be attributed to the fact that a considerable proportion of

meteorites with $T \leq 12$ Myr originates from a comet or from the objects of Chiron like, with the orbits more inclined to the ecliptic plane and/or more extended /10,11/, which caused their irradiation by cosmic rays of higher intensity. The greater proportion of such chondrites in the antarctic meteorites might cause the aforementioned higher Mn-53 content in the meteorites from Antarctica.

These data can supply the additional information for study of variations of galactic cosmic-rays intensity during the last ~ 10 Myr.

References

1.Millard, H.T., Jr. Science, 1965, 147, 503.
2.Imamura, M., Matsuda, H., Horie, K., and Honda, M. Earth Planet. Sci. Lett., 1969, 6, 165.
3.Alexeev, V.A., Malishev, V.V., and Lavrukhina, A.K. Lunar Planet. Sci. XIII, 1982, 5.
4.Lavrukhina, A.K., Alexeev, V.A., and Malishev, V.V. Isotopenpraxis, 1980, 16,9, 301.
5.Ustinova, G.K. and Lavrukhina, A.K. Geochimia, 1983, 4, 483 (in Russian).
6.Nishiizumi, K., Regnier, S., and Marti, K. Earth Planet. Sci. Lett., 1980, 50, 1, 156.
7.Schultz, L. and Kruse, H. Helium, neon, and argon in meteorites. A data compilation. Max-Planck-Institut für Chemie, Mainz, 1983.
8.Crabb, J. and Schultz, L. Geochim. Cosmochim. Acta, 1981, 45, 11, 2151.
9.Wasson, J.T. Meteorites. Classification and properties. Springer, N.Y., 1974, 317 p.
10Lavrukhina, A.K. Acta Geophys. Polonica, 1973, XXI, 185.
11Wood, Ch.A. and Mendell, W.W. Lunar Planet. Sci. XIII, 1983, 877.

Figure captions

Fig.1. Distributions of Mn-53 content in 112 antarctic (dashed line, the histrogram is hatched) and 106 nonantarctic (solid line) ordinary chondrites.

Fig.2. Correlation coefficient (r) of the distributions of Mn-53 contents in antarctic and nonantarctic chondrites as function of the histogram displacement (δ). Displacement of the antarctic chondrites histogram towards lower Mn-53 contents corresponds to the positive values of δ. The equation of the parabola was derived by the least sguares method and is of the form:

$$r=(71\pm4).10^{-2}+(22\pm3).10^{-4}\delta-(27\pm3).10^{-6}\delta^2$$

Analysis of this eguation showed that the maximum of the r ($r_{max}=0.75$) corresponds to the $\delta = 40\pm8$dpm·kg^{-1} Fe.

Fig.3. Distributions of Mn-53 saturated contents as a function of radiation age in 56 nonantarctic H-chondrites. Hatched areas correspond to the average Mn-53 contents ($N \pm \sigma_{\bar{N}}$) for $T \leq 12$ and $T > 12$ Myr. The open circles stand for the finds, and the full for the falls.

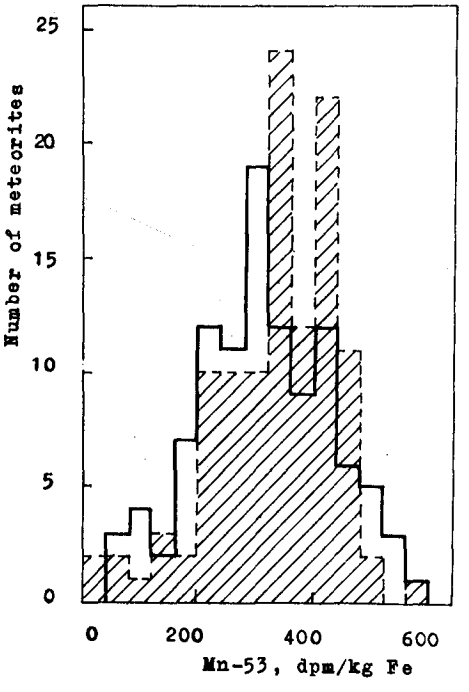

Fig. 1

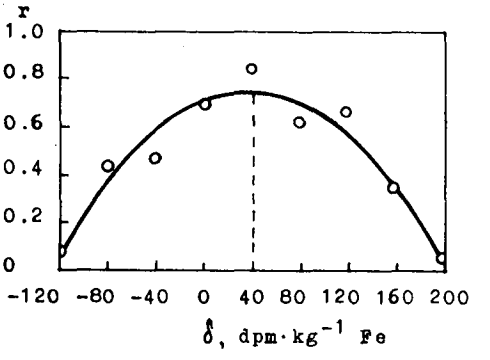

Fig. 2

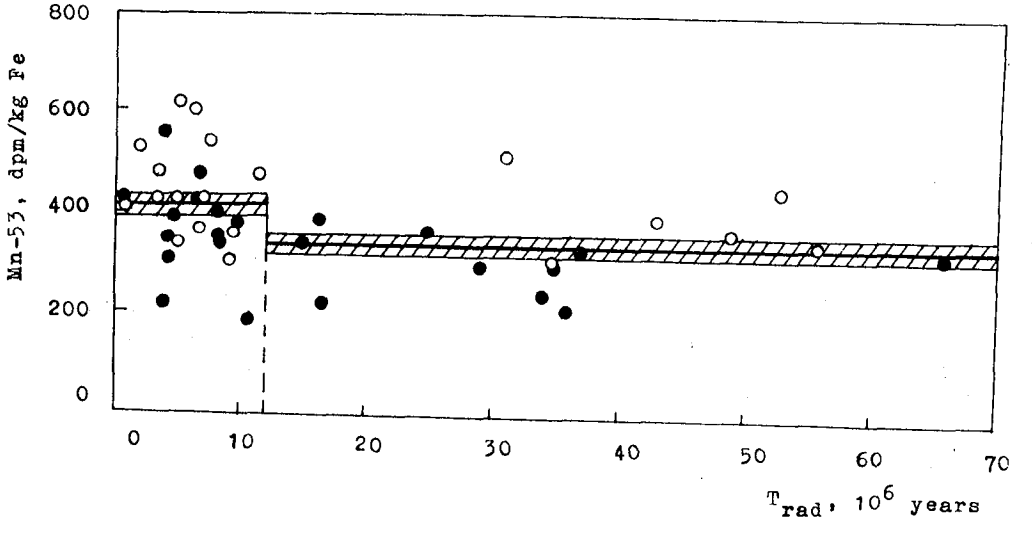

Fig. 3

RESULTS OF ULTRA-LOW LEVEL ^{71}Ge COUNTING FOR APPLICATION IN THE "GALLEX"-SOLAR NEUTRINO EXPERIMENT AT THE GRAN SASSO UNDERGROUND PHYSICS LABORATORY

Hampel, W., Heusser, G., Hübner, M., Kiko, J.
Kirsten, T., Schneider, K. and Schlotz, R.
Max-Planck-Institut für Kernphysik, Postfach 103980
D-6900 Heidelberg, Federal Republic of Germany

ABSTRACT

It has been experimentally verified that the Ultra-Low-Level Counting System for the "Gallex"-solar neutrino experiment is capable to measure the expected solar ν-flux to $\pm$12% during two years of operation.

1. Introduction. More than a decade after Davis implemented his Chlorine detector, experimental solar neutrino spectroscopy is still in a state of infancy and lacks behind existing technical possibilities. The only available experimental result, a deficit of solar ^{8}B-neutrinos as measured with the Cl-detector, has caused serious doubts on the appropriateness of our understanding of stellar structure and evolution. Urgently required is the detection of the pp-neutrinos from the principal fusion reaction $p+p \rightarrow d+e^{+}+\nu_e$. Their flux is largely model independent and directly related to the solar luminosity. The extremely low energy of pp-neutrinos (maximum 420 keV) limits the choice of potential radiochemical detector materials. The Gallium detector, based on $^{71}Ga(\nu_e,e^{-})^{71}Ge$ is by far the most promising pp-neutrino detector. The newly formed "Gallex-collaboration" (1) intends to perform a solar neutrino experiment based on this reaction at the Gran Sasso Underground Physics Laboratory (Italy) (2). The major goals of this experiment are:

- to provide the first experimental proof that the sun is producing its energy by nuclear fusion.
- to limit or identify neutrino mass differences through eventual ν_e-disappearance between sun and detector via neutrino oscillations. The parameter range accessible in this way is many orders of magni-

tude below that for other ν-oscillation experiments.

- to identify the cause of the "solar neutrino puzzle" posed by the Chlorine solar neutrino experiment (3).

2. Outline of experiment components

(1) Underground laboratory

Cosmic ray-induced (p,n) reactions produce ^{71}Ge from ^{71}Ga just as solar neutrino capture. The overburden required to suppress the cosmic ray-induced ^{71}Ge production rate to $\leq$2% of the expected neutrino induced production rate is 3100 m.w.e. (corresponding to a muon flux of $I_\mu = 21\ m^{-2}d^{-1}$). The generous space available in the Gran Sasso underground laboratory is shielded by 3200-3500 m.w.e., hence sufficient for the experiment. Background reactions will also be monitored by $^{69}Ga\ (p,n)^{69}Ge$. This reaction has an even larger yield than $^{71}Ga(p,n)^{71}Ge$, whereas pp-neutrinos do not produce ^{69}Ge.

(2) Target

The high costs of Gallium force us to choose the smallest target size which is still sufficient to produce a $\pm$10% result within 4 years of measurements (this assumes the standard solar model neutrino flux). Given the achieved conditions (see below), this corresponds to 30 t of Ga (converted into 8m $GaCl_3$ solution). The required radiochemical purity of this solution has been demonstrated to be achievable even in the multiton scale. Ga acquisition is pending.

(3) Ge extraction system

The quantitative and reproducible extraction of Ge (as volatile $GeCl_4$) from $GaCl_3$ solution and its conversion into GeH_4 (Germane) to be used as counting gas has been developed and tested in the earlier BNL MPI 1.3 t Ga pilot experiment (4).

(4) Counting system

^{71}Ge ($T_{1/2}$=11.43 d) decays by K (88%) L (10.3%), and M(1.7%) electron capture. Auger-electrons and stopped X-rays are counted in GeH_4/Xe gas mixtures in miniaturized proportional counters made of ultrapure materials. Up to 8 counters can be accommodated in the well of a well type NaI pair spectrometer. Apart from its anticoincidence mode, it serves in the coincidence mode to

identify ^{69}Ge decays ($T_{1/2}$=1.6 d; EC; EC+γ; and $e^+ \overset{e^-}{\rightarrow} 2\gamma$). The NaI crystal is surrounded by plastic scintillator anticoincidence shields and passive Fe/Pb shields. The data from all active components (proportional counters, NaI halves, plastic scintillators) are fed into the PDP/LSI computer both for on line evaluation and for storage on magnetic tape ("Mulia" system) (4).

3. Results of Ultra-Low Level Background Reduction

In the proposed configuration of the Gallex experiment one expects per run an average of 7 ^{71}Ge decays during the first month after extraction according to the standard solar model. From this it follows that background rates of order $\lesssim$ 1 c/10 days must be achieved. Apart from the measures described above, this goal is in particular approached by a complete pulse shape analysis using a transient digitizer to reject background, mainly from Compton electrons and from electronic noise.

The energy deposition from Auger electrons and X-rays emitted in the ^{71}Ge electron capture decay results in a spectrum with 2 peaks: the L peak at $\sim$1.2 keV and the K peak at $\sim$10.4 keV. Counting efficiencies ε are determined using active ^{71}Ge in prototype counters. Thus, the acceptance fields of 95% are defined in an energy-pulse form parameter plot for K- and L peak (Fig.1). The pulse form is most efficiently parameterized as $G \cdot I = S(T)/S(t_{max}) \cdot \frac{1}{T} \int_0^T S(t)dt/S(t_{max})$ where S(t) is the pulse height at time t after pulse onset, t_{max} is the time at which S(t) is maximal, and T is an empirically selected parameter, here T=160 nanoseconds. In this way, background pulses simulated by Compton electrons from a ^{60}Co source are rejected with an efficiency of 96.3% (L peak) and 99.9% (K peak).

The values previously achieved with many counters (ε_L=25%, b=0.2 cpd; ε_K=38%, b=0.08 cpd) would allow to determine a solar neutrino rate of 90 SNU with a standard error of 14% in a two year experiment (50 extractions). 90 SNU is the rate compatible with the Cl detector result interpreted in terms of astrophysical causes ("consistent" model). Meanwhile, improvements have been made and background rates measured with some counters are about a factor of two lower than the values listed above. Fig.2 displays the results of a 51.5 day background measurement obtained with one of the best counters. Here b_K=0.04 cpd, b_L=0.08 cpd. This would allow to measure 90 SNU with a 30 t Ga detector during two years of operation

to ± 12%, as compared to ±10% if the background were zero. Additional advances have been recently made with an improved counter design. Its dead volume is reduced to 5% by directly evaporating the Al-cathode onto the quartz tube and directly sealing the tungsten anode wire into the quartz ends. With this counter type we obtain an overall efficiency of 74% (ε_K=46%, ε_L=28%).

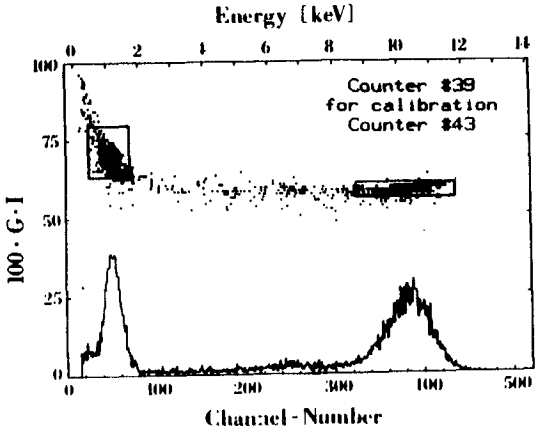

Fig.1: ^{71}Ge spectrum and 95% acceptance fields for genuine ^{71}Ge decays. The pulse shape parameter G·I is defined in the text.

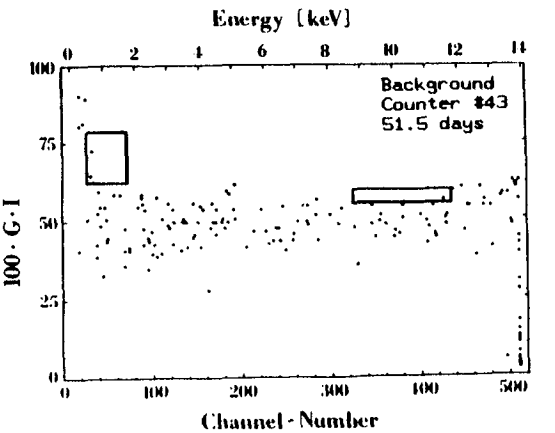

Fig.2: Result of 51.5 days of background counting of counter #43 applying pulse shape analysis with the MULIA system. Acceptance windows for K and L peak are indicated.

References

(1) Members of the collaboration: T. Kirsten (spokesman), W. Hampel, G. Eymann, G. Heusser, J. Kiko, E. Pernicka, B. Povh, M. Schneller, K. Schneider, H. Völk (HEIDELBERG) - K. Ebert, E. Henrich, R.Schlotz (KARLSRUHE) - R.L. Mößbauer (MÜNCHEN) - I. Dostrovsky (REHOVOT) - M. Cribier, G. Dupont, B. Pichard, J. Rich, M. Spiro, D. Vignaud (SACLAY) - G. Berthomieu, E. Schatzman (NICE) - E. Fiorini,E.Bellotti, O. Cremonesci, C. Liguori, S. Ragazzi, L. Zanotti (MILANO) - L. Paoluzzi, S. D'Angelo, R. Bernabei, R. Santonico (ROMA).

(2) A. Zichichi, AIP Conf.Proc. 96, 52 (1983).

(3) J. Rowley, B. Cleveland, R. Davis, AIP Conf.Proc. 126, 1 (1985).

(4) W. Hampel, AIP Conf.Proc. 126, 162 (1985).

CORRELATION BETWEEN SOLAR"NEUTRINO FLUX" AND OTHER SOLAR PHENOMENA

SIDDHESHWAR LAL,
DEPARTMENT OF PHYSICS,
UNIVERSITY OF INDORE,
INDORE - 452001.

A.SUBRAMANIAN,
TATA INSTITUTE OF FUNDAMENTAL RESEARCH,
BOMBAY-400005.

1.Introduction.

We have made a study of the solar neutrino data obtained by Davis et al (1) with a tank of CCl_4 located 4800 mwe underground and shown in Fig.1 for the period 1970-83.These observations are on the production rates of Ar^{37}atoms via the reaction $\nu_e+Cl^{37}\rightarrow Ar^{37}+e^-$ in the tank caused presumably by a flux of neutrino's from the Sun.

It is now well known that the combined average rate of production of Ar^{37}obtained as 0.47±.04 atoms/day and depicted in Fig.1 is too low by a factor ≈3 from that expected from thermonuclear chain reactions in the Sun (2).Added to this difficulty in understanding the source of discrepancy between the expected and observed reaction rates are the numerous suggestions that the obtained data exhibit temporal variations (3,4).Recently we have carried out a statistical analysis (5) of the data shown in Fig.1.While one cannot make a strong claim for time variations based on a simple χ^2 test,we have shown that the data represented by run numbers marked 27,71 and the sequence of low values following run no.60 and some others are significantly deviated.In fact there seems to be a correlation of adjacent data points exhibiting a pattern of variation shown in Fig.2 for which the χ^2 test of constancy hypothesis yields a probability of only 0.03% (χ^2=37.5/13d.f.)

In this paper we pursue the idea of possible time variations in the data shown in Fig.1 and attempt to correlate the variations to two other phenomena of solar origin-the sunspot number and the geomagnetic Ap index.

2. CORRELATION STUDIES WITH SUNSPOTS AND GEOMAGNETIC INDICES

Following the early suggestions(4), Basu (6) has found a positive correlation between the solar neutrino data of Davis of et al and monthly average of geomagnetic Ap indices.Sakurai (3) suggested the correlation with

biennial variations in the sunspots.

We have noted a correlation between the geomagnetic Ap index and $|\dot{R}_z|$, the derivative of smoothed sunspot number (7), which is shown in Fig.3, This correlation could merely suggest a common link of solar wind between $|\dot{R}_z|$ and monthly mean Ap index. We also find a fairly good correlation between the production rate of Ar^{37} atoms and $|\dot{R}_z|$ (Fig.4). The significance of this correlation is at a level of 4σ effect. $|\dot{R}_z|$ appears to be a better correlation parameter than the biennial periodicity of the sunspot number as orignially suggested by Sakurai (3). The correlation of Ar^{37} with Ap index is somewhat less significant (3.3σ effect) than with $|\dot{R}_z|$.

3. Conculsions.

A statistical analysis of the data obtained by Davis et al on the solar neutrino flux suggests fluctuations with time within a period of 12 years or so for which the data is currently available. These variations appear to have positive correlation with $|\dot{R}_z|$ (absolute rate of variation of smoothed sunspot number) which in turn has a positive correlation with the geomagnetic Ap index. Thus the solar neutrino flux recorded in the Davis et al experiment seems to have a connection with even a low energy phenomenon occurring on the such as the generation of solar wind. We admit the possibility of isolated large fluctuations like run nos.27 and 71 (Fig.1 and 2) being correlated to large solar flares occurring on the visible disc of the sun as has been suggested by Bazilevskaya et al (3).

We would like to thank Dr.S.P.Agrawal for discussions.

References.

1. R. Davis Jr., D.S.Harmer and K.C.Hoffman, Phys. Rev. Lett, 20, 1205, (1968).
R.Davis Jr., B.Clevland and J.K.Rowley, in "Workshop on Science Underground," A.I.P.Conf.Proc.No.96, Los Alamos, 1982, Published by A.I.P., New York, 1983. We thank Dr.R.Davis Jr. for sending a compilation of the data as of mid 1984 to one of the authors (A.S.).
2. See for e.g., J.N.Bahcall et al, Phys. Rev. Letters, 45, 945 (1980).
3. W.R.Sheldon, Nature, 221, 650 (1969).
P.Raychaudhuri, Ap SP. Sci. 13, 231, (1971).
K.Sakurai, Nature, 279, 146 (1979); 18th Int. Cosmic Ray Conf.: Conference Papers ed., Durgaprasad et al; Vol.4, Paper SP-1, Bangalore, 1983.
G.A.Bazilevskaya et al, JETP Lett, 35, 341 (1982); 18th Int. Cosmic Ray Conf.: Conference Papers ed., N.Durgaprasad et al, Vol.4, Paper SP-4, Bangalore, 1983.
H.J.Haubold and E.Gerth, Astron. Nach. 304, 299 (1983)

4. A.Subramanian,Current Science,48,705(1979)
5. A.Subramanian,Current Science,52,342(1983)
A.Subramanian and Siddheshwar Lal,Preprint TIFR-BC-83-12, Submitted to Current Science.
6. D.Basu,Solar Physics,81,363(1982).
7. Solar-Geophysical Data,Reports Published by U.S.Dept.of Commerce,Boulder,Colarado,U.S.A..

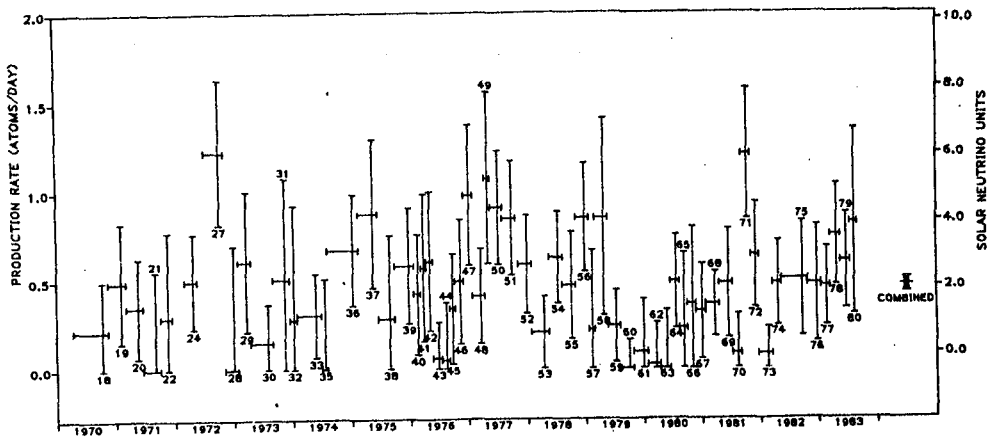

Fig.1 The data of R.Davis Jr. et al (1) on the solar neutrino flux during the period 1970-83.

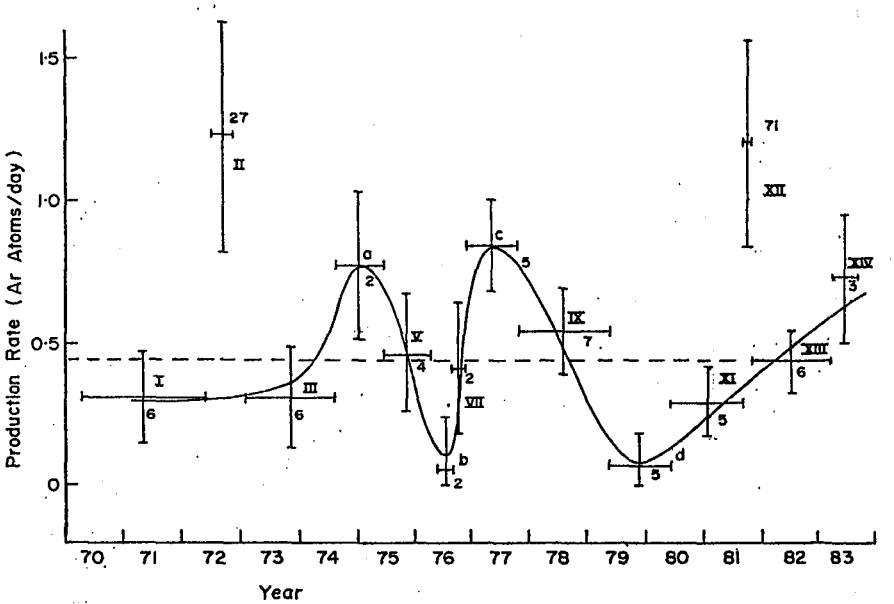

Fig.2 Grouped averages of the solar neutrino flux data given in Fig.1 which exhibit variations in time as suggested by the guiding continuous curve excluding run no.27 and 71. The grouped data points are labelled by Roman number or alphabets. The numbers attached to the groups except II and XII indicate the no.of independent measurements that have gone into the grouping.

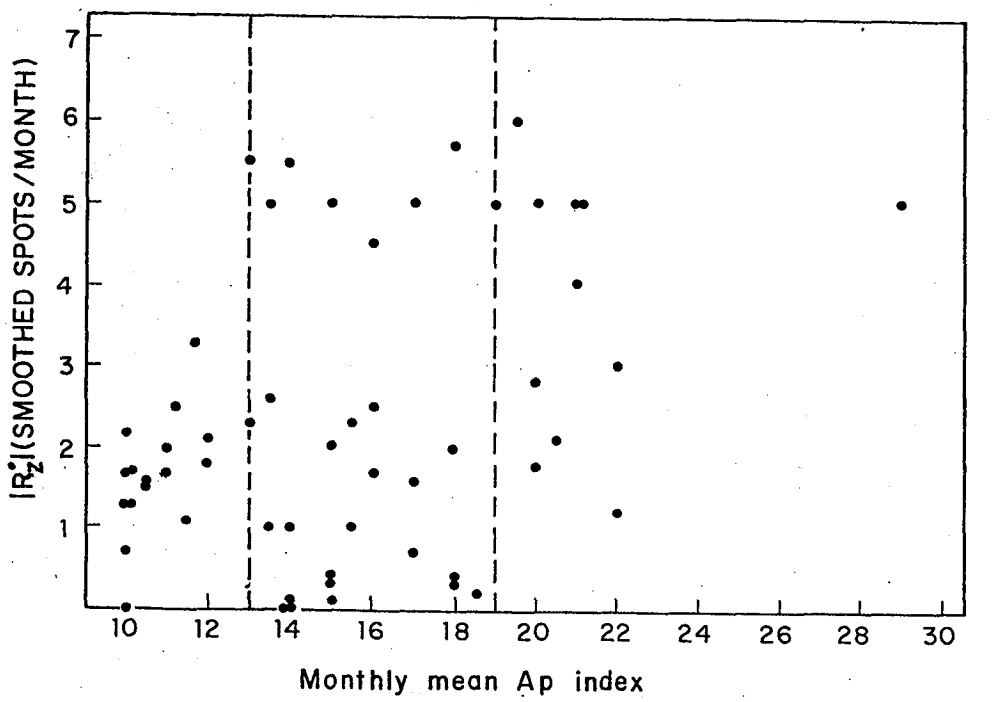

Fig.3 A plot showing the correlation between monthly average geomagnetic Ap index and the absolute derivative $|\dot{R}_Z|$ of smoothed sunspots. Vertical dashed lines separate different regions of the mean Ap.

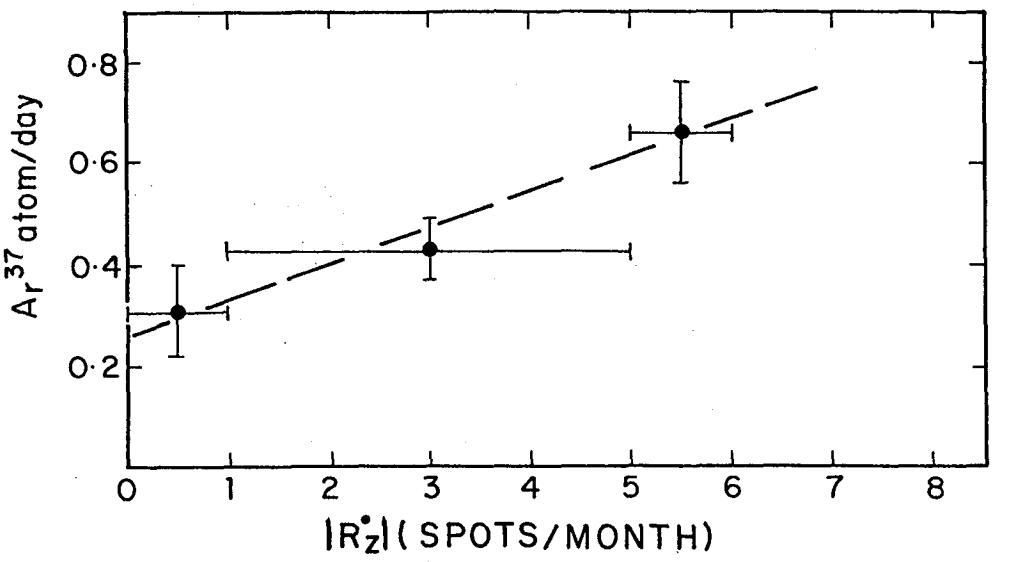

Fig.4 The correlation between Ar^{37} production rate in the Davis et al experiment and $|\dot{R}_Z|$, the absolute derivative of smoothed sunspots.

A POSSIBLE MECHANISM TO CAUSE THE QUASI-BIENNIAL VARIABILITY ON THE SOLAR NEUTRINO FLUX

Kunitomo Sakurai and Mitsuru Hasegawa

Institute of Physics, Kanagawa University
Rokkakubashi, Yokohama 221, Japan

ABSTRACT

It is suggested that the quasi-biennial change in the observed flux of the solar neutrinos is causally related to some non-linear process at the central core of the sun, being associated with the change in the central temperature. This process seems to be responsible for the physical adjustment of the internal structure of the sun. Numerical simulation on this process is able to reproduce the quasi-biennial change in the flux of these neutrinos.

1. Introduction In order to see the rate of the energy production at the central core of the sun, Davis and his associates have been measuring the flux of the solar neutrinos which are mainly produced from the PP III process(1). According to their results, the mean observed flux of these neutrinos for more than ten years is by a factor three or more less than the flux theoretcially expected from the standard model of the sun. At present, this discrepancy between observed and theoretical fluxes is thought as a serious problem in the research fields of astrophysics, being known as the "missing solar neutrinos,"because this has seemingly suggested that the proton-proton chain reactions have been prevented from working well effectively in a manner as predicted from the theoretical treatment for the internal structure of the sun on the basis of the standard model(2).

The observed results by Davis et al. certainly indicate that the proton-proton chain reactions are only ineffectively taking place in the interiour of the sun, but it has recently been suggested that these results further indicate that the rate of these reactions has been varying quasi-biennially with a period of about 26 months(3). Although the sun itself should be considered to be a self-regulating feedback system with respect to the energy generation, such periodic variation just mentioned may have been caused by some non-linear process taking place in association with the proton-proton chain reactions.

2. Quasi-Biennial Change in the Observed Flux of the Solar Neutrinos Davis and his associates have been making the measurement of the neutrino flux from the sun for more than ten years(1). Since the results obtained by them are now available to investigate the efficiency of the proton-proton chain reactions at the cnetral core of the sun and its long-term change if any. Using these results, an analysis has

been done to find out possible periodic change in the observed fluxes of these neutrinos during the last ten years or so(3,4,5).

Since the intervals between two successive measurements of these neutrinos are not equally distributed, but scattered at random, the observed fluxes have been averaged over for four monthly intervals without taking the number of the measurements in each interval into account(3). The analysed

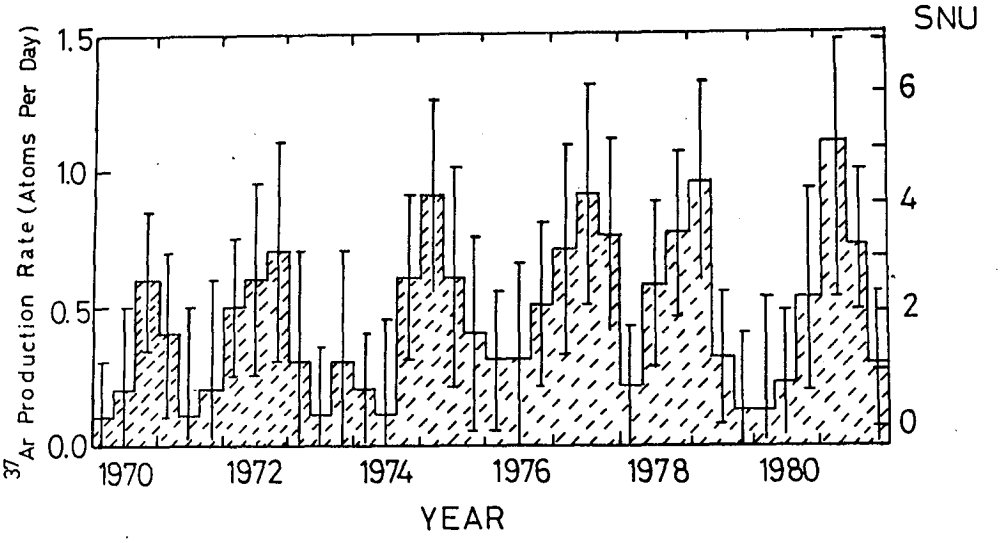

Fig. 1 A "periodic" variation of the four-monthly mean flux of the solar neutrinos produced mainly from the PP III reaction(3).

result is shown in Fig. 1, in which error ranges have been estimated using the error bars appeared in the original data given by Davis and his associates.

The result shown in Fig. 1 clearly indicates that the observed flux of the solar neutrinos had been varying quasi-biennially with a period of about 26 months during the years up to 1981. This seems to mean that the efficiency of the PP III process had been changing quasi-biennially because these neutrinos had been mostly released within three seconds into outer space after produced at the central core of the sun. According to Fig. 1, it seems that the observed background flux of the neutrinos has a tendency to vary throughout the solar activity cycle, since this flux seems to have been highest during the solar maximum. However, this tendency is not so clearly seen when compared with the quasi-biennial change as considered above.

3. Possible Mechanism of the Quasi-Biennial Change In order to explain the quasi-biennial periodicity on the time variation of the neutrino production at the central core of the sun, a non-linear process has been considered as a candidate to control the proton-proton chain reactions, in particular, PP III reaction. Since the efficiency of this reaction is shown to be strongly dependent on the temperature at the central core of the sun, this process seems to be controlled

by this temperature(6). Thus it seems appropriate to assume that this temperature, being denoted by T, is controlled by a non-linear process as following the equation described as

$$\frac{dT(t)}{dt} = [\,\underline{a} - \underline{b}T(t-\tau)\,]T(t),$$

where $\underline{a}$ and $\underline{b}$ are both constant. Time $T(t-\tau)$ is the one which is earlier than t by τ. The above equation, therefore, expresses that the temperature T(t) is regulated by the time $T(t-\tau)$ as dtermined by the time $(t-\tau)$. This has first been considered to apply to biological population and chemical reactions(7).

From the physical point of view, this process indicates that the temperature varies as being controlled by the time being earlier by τ. By taking some numerical values for $\underline{a}$ and $\underline{b}$, the above equation has been numerically simulated to reproduce the periodic change as shown in Fig. 1. One of these numerical simulations is shown in Fig. 2 as an example and this seems to be applicable to explain the quasi-biennial periodicity in the temperature variation at the central core of the sun. Thus, the quasi-biennial periodicity in the neutrino flux from the sun can be well reproduced

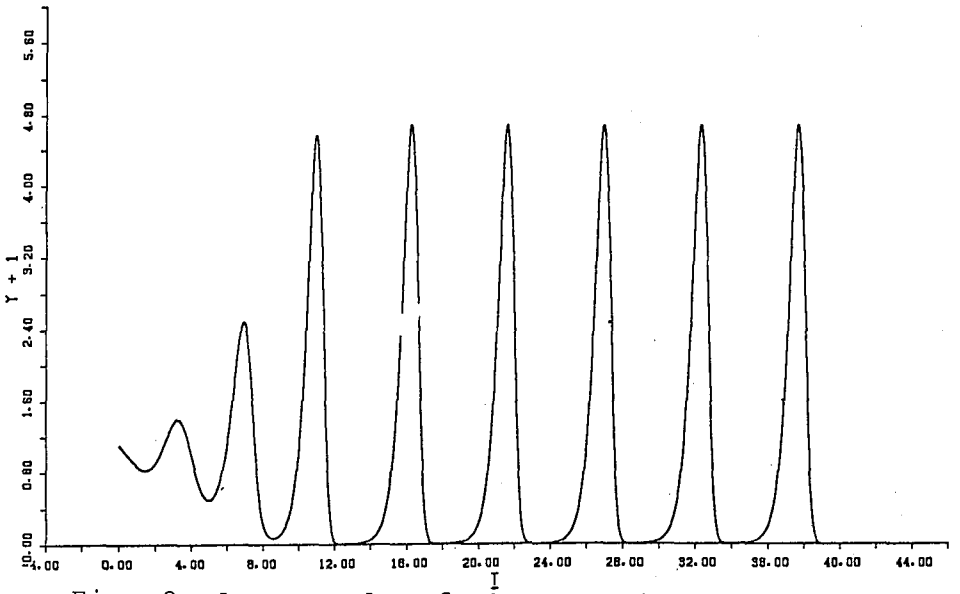

Fig. 2 An example of the numerical simulation for the efficiency of the PP III reaction.

from the non-linear process considered above.

As inferred from from Fig. 2, the occurrence of the periodicity as seen in this figure does not depend seriously on the initial condition which is related to the numerical values of τ, $\underline{a}$ and $\underline{b}$. For this reason, the quasi-biennial change in the efficiency of the PP III reaction as shown in Fig. 1 seems to be almost always excited easily whenever some instability is induced at the central core of the sun, which is associated with the change in the temperature there.

4. Concluding Remarks The quasi-biennial change as seen on the observed flux of the solar neutrinos has been numerically simulated by taking into account the non-linear process as described in this paper, which is associated with the change in the temperature at the central core of the sun. As theoretically deduced earlier, the sun is thought as a self-regulating feedback system with respect to the maintenance of the internal physical processes as related to the proton-proton chain reactions. It should be noted, furthermore, that the temperature and its radial gradient plays the most important role in adjusting the internal structure of the sun(2).

Thus it may be said that, as described in this paper, the non-linear process associated with the change in the central temperature is responsible for the quasi-biennial variation on the efficiency of the PP III reaction.

References

(1) R. Davis, Jr. et al. (1983) Science Underground, AIP Conf. Proc. No. 96, p. 2 (eds. M.M. Nieto et al.) Amer. Inst. Phys., New York.
(2) K. Sakurai (1984) Space Sci. Rev. 38, 243.
(3) K. Sakurai (1979) Nature 278, 146 and (1981) Pub. Astro. Soc. Japan 35, 547.
(4) D. Basu (1983) Solar Phys. 81, 363.
(5) H.J. Haubold (1983) Proc. 18th ICRC, Bangalore 10, 389.
(6) e.g., K. Sakurai (1981) Solar Phys. 74, 35.
(7) W.J. Cunnigham (1954) Proc. Nat. Acad. Sci., Math. 40, 708.

SH 8.1-6

THE CONJECTURE CONCERNING TIME VARIATIONS IN THE SOLAR NEUTRINO FLUX

H.J. Haubold and E. Gerth

Akademie der Wissenschaften der DDR
Zentralinstitut für Astrophysik
DDR - 1502 Potsdam-Babelsberg
German Democratic Republic

1. Introduction.

The most challenging problem in neutrino astronomy in the past two decades has been the solar neutrino problem, i.e., the discrepancy between the predicted rate of detection of neutrinos in the standard solar model of 6...8 SNU and the averaged value 2.1 ± 0.3 SNU actually observed (1SNU ≙ 10^{-36}captures/sec ^{37}Cl atom; cf. 1,2).

In this paper we shortly review the results of our Fourier transformation of the unequally-spaced time series of the recorded ^{37}Ar production rate of the solar neutrino experiment (runs 18-80, 1970-1983). We will determine significance criteria for every period discovered by the harmonic analysis (3,4). We will also perform a Fourier synthesis of certain discovered harmonics and it seems that the solar neutrino flux increases shock like with a period of approximately 8.3 years and after that breacks down. We point to possible connections between the periods found by the harmonic analysis and several observed phenomena on the solar surface.

2. Fourier Analysis of the ^{37}Ar Production Rate Measurements

For the harmonic analysis of the time series of 59 measurements of the ^{37}Ar production rate $f(t)$ (runs 18-80, cf. 1) we consider it as a stochastic process which we can split phenomenologically into two components : $f(t) = \mu(t) + \eta(t)$ where $\mu(t)$ denotes a non-stochastic function of time - the systematically varying component in $f(t)$ -, and $\eta(t)$ denotes the stationary stochastic process - the remainder in $f(t)$. The systematically varying component $\mu(t)$ can be split also into the trend φ which we consider as time independent identified with the mean value over all n = 59 measurements (φ = 0.47 ^{37}Ar atoms per day), and the non-stochastic periodic function $\nu_k(t)$: $\mu(t) = \varphi + \sum_k^n \nu_k(t)$. Further we make the ansatz for $\nu_k(t)$ composed of sinusoidal and cosinusoidal terms : $\nu_k(t) = a_k \cos(2\pi\nu_k t) + b_k \sin(2\pi\nu_k t), k=1,\dots,n$. From the harmonic analysis of $f(t)$ by means of the finite Fourier transformation of unequally-spaced data described in (2,4) we obtain the power spectrum $N_1 = F(\nu) F^*(\nu)$ shown in Fig.1 by multiplying the Fourier transform $F(\nu)$ with its conjugate complex form $F^*(\nu)$. For a detailed discussion of the connection between the power spectrum $N_1(\nu)$ and the related spectral window see (4, 5). In Fig.1 are clearly recognizable the periods π_i = 8.33,

5.26, 2.13, 1.56, 0.83, 0.64, 0.54, and 0.50 (all T's in years, i = 1,...,8). We consider the complementary power quotient, $\lambda\text{-}Q = (\sigma^2 - \sigma^2(2\pi\nu_i))/\sigma^2$, shown in Fig.1 as a function of ν, as the significance criterion for every discovered harmonics of frequency ν_i (σ is the variance of the respective measurement). The higher the complementary power quotient the higher the significance of the considered harmonics. If we compare the power spectrum in Fig.1 obtained for runs 18-80 with earlier results of the Fourier analysis for runs 18-69 (2) and 18-74 (5) we find full consistency.

3. Fourier Synthesis of Certain Harmonics Discovered in the ^{37}Ar Production Rate

All variations in the power spectrum $N_1(\nu)$ shown in Fig.1 with power quotients $\lambda\text{-}Q$ = 0.9500...1.0000 we consider as belonging to the stationary stochastic process $\eta(t)$ which has by definition no significant meaning for the search for periodics in $f(t)$. The periods $T_1 \ldots T_6$ in Fig.1 are characterized by nearly equidistant frequencies and could be attributed to a series of harmonic waves. Taking every frequency of those six periods into consideration we can synthesize it to sinusoidal oscillations of the ^{37}Ar production rate belonging to a fundamental wave with $T_1 = 8.33$ years. For the purpose of smoothing the stochasticly caused function $\eta(t)$ in $f(t)$ we perform a folding of $f(t)$ with Gauss' normal distribution function. If we multiply the Fourier transform of $f(t)$ by the Gauss function the high frequencies will be smoothed out symmetrically to the frequency zero. In the process of the reconstruction (Fourier synthesis) of the time series $f(t)$ all harmonics with low frequencies will have the main contribution and determine the smoothed form of $f(t)$. This procedure applied to the ^{37}Ar production rate $f(t)$ with the fundamental wave T_1 = 8.33 years as shown in Fig.1, and a smoothing constant σ = 3 years^{-1} led to Fig.2. In Fig.2 we see that there occur three shock like rising waves within the fundamental period T_1 = 8.33 years up to a maximum ^{37}Ar production rate and after that a breack down of the ^{37}Ar production rate can be observed. To prove the influence of a curve shown in Fig.2 on the power spectrum given in Fig.1 we performed the Fourier analysis of $x(t)$ in Fig.2 and obtained the power spectrum $N_2(\nu)$ (see Fig.3). The power spectrum $N_2(\nu)$ in Fig.3 reproduces nearly completely all periods found in the harmonic analysis of the ^{37}Ar production rate measured in the solar neutrino experiment (1), T_2 = 4.5, T_3 = 2.34, T_4 = 2.17, T_5 = 1.73, T_6 = 1.49 (all T's in years), and fits into the fundamental period T_1 = 8.33 years the new period T_0 = 11.1 years. We believe that the value of the period T_0 = 11.1 years is connected with the total running period of the experiment of Davis and associates (1).

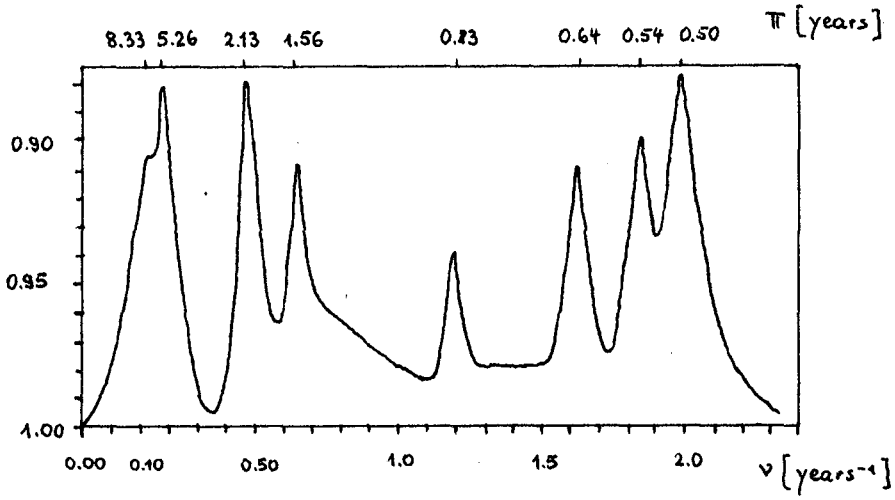

Fig.1

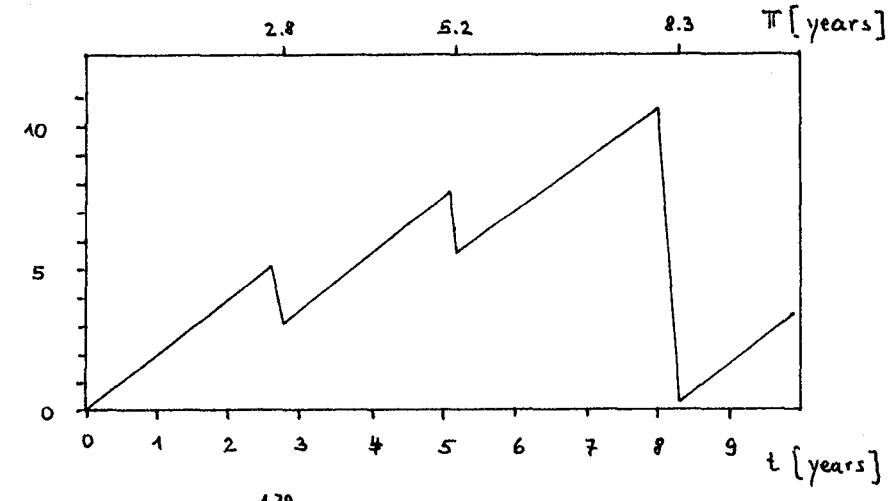

Fig.2

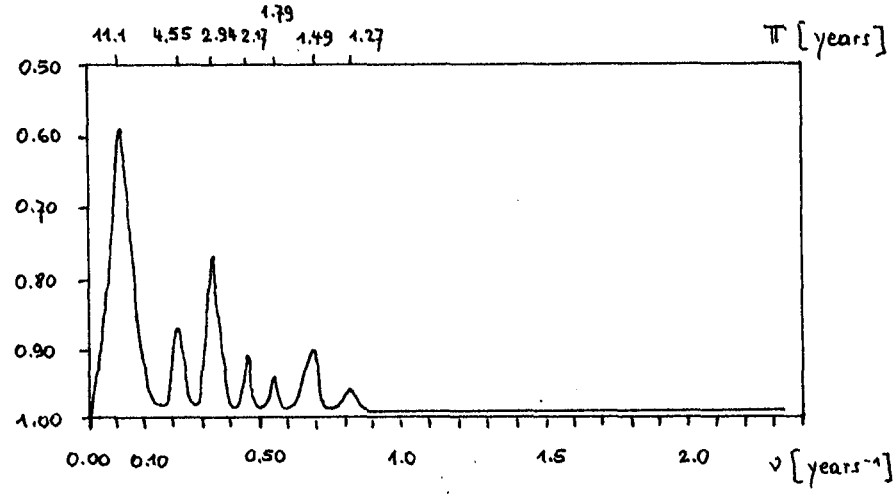

Fig.3

4. Remarks

- One of the eight periods discovered by harmonic analysis, π_3 = 2.13 years, is identical with the quasi-biennial period obtained by Sakurai (6).

- It is interesting to note that Rieger et al. (7) recently published results concerning a 154 day periodicity in the occurence of hard x-ray flares of the Sun. Approximately the same periodicity observed Wolff (8) which he attributes to g-mode oscillations of the Sun. Both periods are rather close to our periods π_7 and π_8.

- In the present understanding of the solar interior only very few is known about physical processes which could lead to variations of the solar neutrino flux with periods in the order of years. However, non standard solar models are still under consideration where gravity mode oscillations are excited (9) and specific stratification of the solar interior exists (10). Such non standard solar models can explain, in principle, short time variations of the solar neutrino flux.

5. Acknowledgements

It is a pleasure for us to express our acknowledgement to Professor Dr. R. Davis, Jr. for his generosity of sending us the solar neutrino data and for many suggestions concerning our results.

References

1. Davis Jr.,R., Cleveland,B.T., and Rowley,J.K., (1984), Conference on the Intersections Between Particle and Nuclear Physics, Steamboat Springs, CO, May 23-30,1984.
2. Haubold,H.J., and Gerth,E., (1983), Astron. Nachr. 304, 299.
3. Haubold,H.J., and Gerth,E., (1983), Proc. 18th ICRC, Bangalore, 10, 389.
4. Haubold,H.J., and Gerth,E., (1985), AIP Conf. Proc., No. 126, 129.
5. Haubold,H.J., and Gerth,E., (1985), submitted for publication to Astron. Nachr., 306.
6. Sakurai,K., (1983), Proc. 18th ICRC, Bangalore, 4, 210.
7. Rieger,E., et al., (1984), Nature, 312, 623.
8. Wolff,C.L., (1983), Ap.J., 264, 667.
9. Kopysov,Yu.S., (1983), Preprint P-0317, Academy of Sciences of the USSR, Institute for Nuclear Research, Moscow.
10. Vandakurov,Yu.V., (1984), Pis'ma v Astron. Zhurnal, 10, 873.

SOLAR NEUTRINO: FLUX, COSMIC RAYS AND THE 11 YEAR SOLAR CYCLE

Probhas Raychaudhuri
Department of Applied Mathematics
Calcutta University, Calcutta-700009, INDIA

A B S T R A C T

It is shown that the results of maximum likelihood treatment of Monte Carlo simulation with constant production rate of 7•6 SNU and 1•8 SNU are consistent with the constant production rate when the tests of hypotheses(e.g. t-test, χ^2-test, Wilcoxon-Mann-Whitney test, run test etc.)has been applied to the two groups of data formed from sunspot minimum range and sunspot maximum range whereas the real data pulsates with the solar activity cycle. It is shown that SN flux-change is in opposite phase to the solar activity cycle and lags behind the latter by about one year. A correlation between SN flux and the cosmic rays has also been suggested.

Raychaudhuri(1,2,3,4,5,6)and Gavrin et al(7)showed that the solar neutrino(SN)flux data is varying with the solar activity cycle. Raychaudhuri (3,4,5,6)showed that the fluxes will be higher in the sunspot minimum range than in the sunspot maximum range. This is supported by the data presented by Rowley et al(8)at the solar neutrino and neutrino astronomy conference held at Lead, South Dakota. Apart from the above variation Raychaudhuri(5,6)showed that there is also a quasibiennial variation from 1970-1975 and 1979-1984. This type of variation is already observed by Gnevyshev(9)and Filisetti(10)in the cosmic ray intensity(proton flare).

In this paper an estimate of the moving average(5 successive run number) data is considered to find the statistical significant variation of SN flux with the solar activity cycle of 11 years by t-test, χ^2-test, Wilcoxon-Mann-Whitney test and run test. To search variation in a convincing manner the above tests of hypotheses have been applied to the data that had been generated by Monte Carlo simulation and background parameters are typical of those in the actual experiment.

SOLAR ACTIVITY CYCLE AND(a)MOVING AVERAGE DATA, (b)MONTE CARLO SIMULATED DATA WITH CONSTANT PRODUCTION RATE(i)7•6 SNU AND(ii)1•8 SNU.

Here we apply the same proceedure as in Raychaudhuri(5,6).

I)Student t-test:-a(i)Moving average data

We form the two groups, the first group comprises sunspot minimum range (about 4•6 years)and the second group i.e., the rest comprises sunspot maximum range. Let us now collect the data from the run number 36 to 58 from August 1974 to February 1979(about 4•6 years)for the first group. If we now set up the null hypothesis $H : m_1 = m_2$ against the alternatives $m_1 > m_2$. The statistics t is given by(here the difference of variance is not significant).

$$t = \sqrt{\nu}\sqrt{\frac{N_1 N_2}{N_1+N_2}}\,\frac{\bar{x}-\bar{y}}{\sqrt{N_1 S_1^2 + N_2 S_2^2}}$$

where $\nu = N_1 + N_2 - 2$. In the above case $N_1=23, N_2=27, \nu=48$ which gives t=4•54. Thus we can conclude that 99•9% of the data pulsates with the solar activity cycle. The standard error of the difference of means is 4•54. Hence the data are inconsistent with the assumption that the two means are equal.

(ii)Yearly average of the moving average data:-Here one group comprises the yearly average data from 1975 to 1978 and the other group comprises rest of the moving average data. We get for 9 d.f. t=2•76. The standard error of the difference of the means is 3•1 which suggests that the

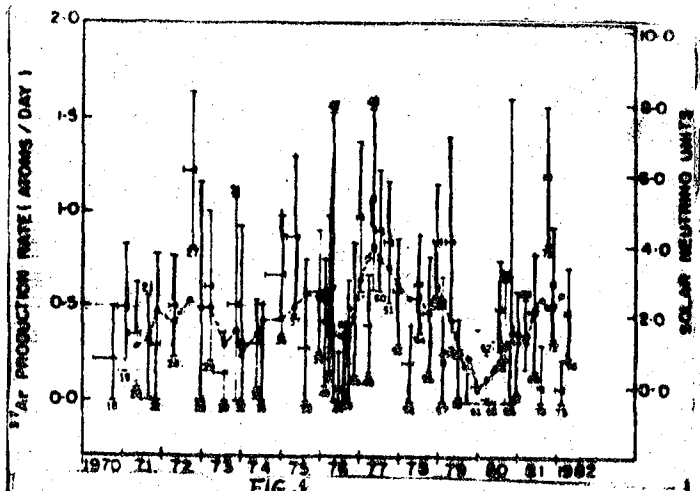

FIG.1

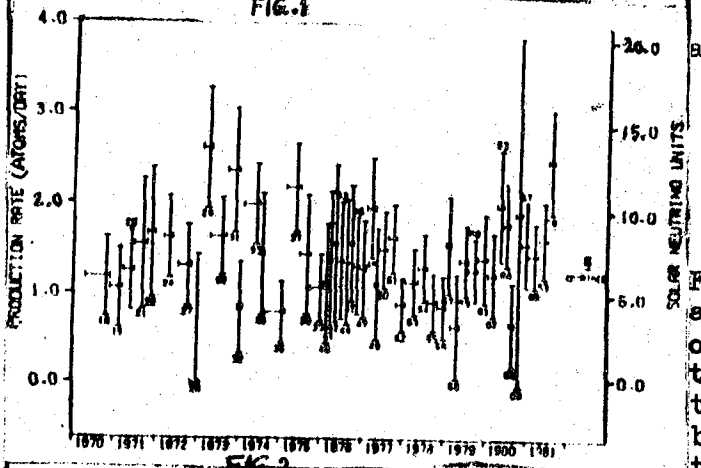

FIG.2

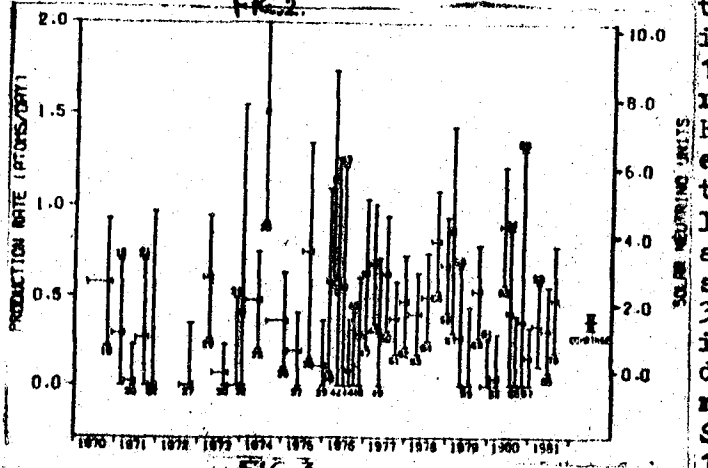

FIG.3

Fig·1.37 Ar production rates observed in the Chlorine SN experiment 1970-1982 and the moving average data(dashed curve)·

Fig·2 and 3·Results of maximum likelihood treatment of Monte Carlo simulations with constant production rate of 7·6 SNU and 1·8 SNU respectively·

means of the two samples are not equal·

b)Monte Carlo simulated data :-i)7·6 SNU andii)1·8 SNU· We form the groups as in moving average data· In the case of 7·6 SNU the difference of variance is significant· We have to use the formula for fro the difference of two means·

$$t = \frac{\bar{x} - \bar{y}}{\left\{\delta_1^2/N_1 + \delta_2^2/N_2\right\}^{1/2}}$$

For d·f· 47, t=1·19· The standard error of the difference of two means is 1·1 ϵ · Hence the two means are equal i·e·, the steady flux is acceptable· In the case of 1·8 SNU the difference of variance is not significant· Hence t= 1·84, d·f· 45· The standard error is found to be 1·8 ϵ · Hence the data are consistent with the assumption that the steady flux is acceptable· Next we take the yearly average of the Monte Carlo simulated data from fig 2 & 3 and form the two groups as in t-test· Here in both cases difference of variance is not significant· In case 7·6 SNU, t=0·43 d·f· 9· In case 1·8 SNU, t=1·01 d·f· 9· Here the standard error is found to be (i)0·53 ϵ and(ii) 1 ϵ respectively· Hence the data are consistent with the assumption that the steady flux is acceptable·

II)χ^2-test:-(i)We form the group as in the t-test· For moving average data σ^2=0·02 and for d·f·49, χ^2=73·19· Thus the hypothesis of steady flux is not acceptable· For the case of 7·6 SNU, σ^2=0·291, χ^2=47·84 d·f·47· again for 1·8 SNU, σ^2=0·10, χ^2=46·83 d·f· 45· Hence the difference of two samples are not significant for the case of 7·6 SNU and 1·8 SNU·

(ii)if we take the yearly average of the moving average data and Monte Carlo simulated data•We form the groups as in t-test•We get σ^2=•01, χ^2= 18•55,d•f• 10 for moving average data•In this case steady SN flux is not acceptable•Again (i) σ^2=•09, χ^2=9•39,d•f• 9 for 7•6 SNU and (ii)σ^2=•05, χ^2=10•48,d•f• 9 for 1•8 SNU•Hence the steady SN flux is acceptable in Monte Carlo simulated data•

(III)Wilcoxon-Mann-Whitney test:-Here we take the yearly average data of moving average data and Monte Carlo simulated data 7•6 SNU and 1•8 SNU and form the two groups as in t-test and χ^2-test•If we set up the null hypothesis H_0 :the distribution of x and y are identical•If a two sided test at 5% is desired for m=4,n=7 we use $3 < U < 25$ as the accepted region•For this test $\alpha = P_{H_0}(U \leq 3 \text{ or } U \geq 25) = •042$•

a)Moving average data:- we write the two sets of data as y: •3552,•4740, •3546,•4007,•3089,•2469,•4707 and x:•5305,•4437,•7482,•5421•Putting these numbers in order and keep track of which numbers came from x and which from y:yyyyyxyyxxx•There are 12 inversions of the y's and the rank of y's is $1+2+3+4+5+7+8 = 30 = 2+\frac{7\times8}{2}$•Since the number of inversion of the y's is not within 3 and 25 ,we reject the null hypothesis,i•e• the constant SN flux is not acceptable•

b)(i)7•6 SNU :-y:1•408,0•993,1•430,1•286,1•277,1•928 and x:1600,1•396, 1•320,1•098•Putting these numbers in order and keep track of which numbers came from x and which came from y: yxyyxxyyxyy•There are 16 inversions of the y's and the rank of y's is $1+3+4+7+8+10+11 = 44$•

(ii)1•8 SNU:-y:1•545,•6001,•165,•805,•537,•307,•378 and x:•3755,•4900, •518,•581•There are 8 inversion of the y's and the rank of y's is 36• Since the number of inversion of the y is within 3 and 25,we accept the null hypothesis i•e•,steady SN flux is acceptable in both the Monte Carlo cases•

(IV)Run test:-In the case of run up and down the total number of runs is approximately normally distributed under the assumption of randomness with mean and variance is given by $E(r) = \frac{1}{3}(2n-1)$ and $V(r) = \frac{1}{(90)}(6n-29)$• For moving average data:- n=50,E(r)=33,V(r)=8•57•In this case there are 21 runs either positive or negative•If we take the critical region to be α =0•20 would yield a K of $33-0•84\sqrt{8•57} = 30•543$•Thus we cannot accept the randomness since $21 < 30•543$•Thus we can suggest that the constant SN flux is not acceptable•For case 7•6 SNU,n=49,E(r)=32•33 and V(r)=8•389•In this case there are 31 runs either positive or negative•For the case 1•8 SNU,n=47,E(r)=0•31 and V(r)=8•03•In this case there are 29 runs is either positive or negative•If ew take the critical region to be $r < K$,a choice of α =0•20 would yield a K of (i)$32•33-0•84\sqrt{8•389} = 29•9$;(ii)$31-0•84\sqrt{803} = 28•62$•Thus we accept the randomness in both the case since(i)$31 > 29•9$ and (ii)$29 > 28•62$•So we can conclude that the Monte Carlo simulated data do not pulsate with the solar activity cycle•

Sunspot cycle and SN flux:- We have taken the yearly average smooth sunspot from solar geophysical data,yearly average of the moving average data from fig•1•and yearly average of the cosmic ray data I with E =0•1-5•8 Gev(11)•We have displayed the data in Table I•

The correlation coefficient between sunspot cycle and ^{37}Ar production data are $r(S,Q_M) = -0•61$,when $\Delta T=-1$,$r(S,Q_M)=-0•49$ when $\Delta T=0$,$r(S,Q_M)= -0•35$ when $\Delta T=-2$ where $\Delta T = T_S - T_{Q_M}$ (in years)•Thus the ^{37}Ar production rate anticorrelates with the sunspot cycle•The correlation coefficient between the galactic cosmic ray intensity and ^{37}Ar production data $r(I_0, Q_M)=0•58$ when $\Delta T=0$,$r(I_0, Q_M)=0•31$ when $\Delta T=-1$,$r(I_0, Q_M)=0•39$ when /

SH 8.1-7

Table 1. Yearly averages of smooth sunspot number(S), Ar production data (Q_M), yearly average of cosmic ray data I_o with E=0.1-5.8 Gev.

	1971	1972	1973	1974	1975	1976	1977	1978	1979	1980	1981
Yearly average Sunspot number (S)	66.6	68.9	38.5	34.4	15.5	12.6	27.5	92.7	155.3	155	140
Moving Average of the yearly Ar production data(Q_M)	.36	.44	.35	.40	.53	.44	.75	.54	.31	.25	.47
I($10^3 m^{-2} s^{-1} st^{-1}$) Galactic cosmic ray intensity	2.01	2.86	2.80	2.71	3.11	3.20	3.29	2.79	1.89	1.24	1.13

$\Delta T=1$. Where $\Delta T = T_{I_o} - T_{Q_M}$ (in years). Thus there is an important correlation between the SN flux in Davis' data and galactic cosmic rays. This shows that the galactic cosmic rays and SN flux undergo the essential changes in the solar acivity cycle from 1970-1982.

From the SN flux data we see that SN flux is higher during the ascending phase(about 2-3 years)and descending phase(about 2-3 years)of the solar cycle avoiding the sunspot maximum time. We call the time 2-3 years before the sunspot maximum as the second minimum time. Thus SN flux is higher in both second minimum time and second maximum time and SN flux is lower in both first minimumand first sunspot maximum stage. In addition to two prominent maximum in the year 1957 and 1960 they(9,10)have found third maximum of smaller amplitude in the cosmic ray intensity but veru clear in 1963. From fig.1 we see that run number 37 is connected with third maximum. This may have some connection with the quasibienniel variation of SN flux found from 1970-1975 and 1979-1984. From the moving average data in fig.1 it appears that SN flux varies with a period of about 2.4 to 2.5 years from 1970-1975.

In conclusion it may be remarked that the present SN data exhibits a high level of statistically significant variation of SN flux with the solar activity cycle. The above results strongly suggests that the solar activity cycle is due to the pulsating character of the nuclear energy generation inside the core of the sun. We suggest that the chlorine SN experiment should be continued to get the data like the sunspot data etc. and this data could be of great importance to our understanding of the sun and cosmic rays.

Acknowledgement:-The author would like to thank Professor R. Davis,Jr. for sending the SN data prior to publication.

References:-

1)P. Raychaudhuri(1976)JINR communications E2-10019,USSR,2)P. Raychaudhuri (1976)Talk given at the International School of Cosmic physics,Erice,Italy 3)P. Raychaudhuri(1981)Spec. Sci. Tech. 4,271. 4)P. Raychaudhuri(1983)Proc. 18th. ICRC, Bangalore 7, 108. 5)P. Raychaudhuri(1984)Solar Phys. 93,397.6)P. Raychaudhuri(1984)Proc. 3rd. Asian Pacific regional meeting of IAU held at Kyoto(to be published)Ap. Sp. Science. 7)V. N. Gavrin et al.(1982)JETP lett 35 608,8)J. K. Rowley et al.(1984)American Institute of Physics conference proceedings(to be published)held at South Dakota,USA.,9)M. N. Gnevyshev (1967)Solar Phys. 1,67.,10)O. Fillisetti et al.(1974)Lett. Nuovo Cimento 11, 29,11)G. A. Bazilevskaya et al.(1983)Proc. 18th. ICRC, Bangalore,4,218.

SH 8.1-8

SOLAR NEUTRINOS, SOLAR FLARES, SOLAR ACTIVITY CYCLE AND THE PROTON DECAY

Probhas Raychaudhuri
Department of Applied Mathematics
Calcutta University, Calcutta-700009, INDIA

A B S T R A C T

It is shown that there may be a correlation between the galactic cosmic rays and the solar neutrino data but it appears that the neutrino flux which may be generated during the large solar cosmic ray events cannot in any way effect the solar neutrino data in Davis experiment. Only initial stage of mixing between the solar core and solar outer layers after the sunspot maximum in the solar activity cycle can explain the higher(run number 27 and 71)of solar neutrino data in Davis experiment. But solar flare induced atmospheric neutrino flux may have effect in the nucleon decay detector on the underground. The neutrino flux from solar cosmic rays may be a useful guide to understand the background of nucleon decay, magnetic monopole search, and the detection of neutrino flux in sea water experiment.

Sheldon(1)indicated that the solar flares and solar active regions are energetic disturbances in the sun and may be associated with the production of neutrinos. The emission of particles from flares and active regions is well known phenomena. Thus any such relation between solar neutrino data and solar cosmic rays is important and may serve as an accurate long range predictor of solar cosmic ray activity properly. Recently Lanzerotti and Raghavan(2) and Raychaudhuri(3)suggested that the production of solar neutrinos by energetic particles involved in solar actvity is not a significant contributor to the solar neutrino flux recorded in the SN experiment(4). Again Raychaudhuri(5) pointed out that the neutrino flux which appears in the SN experiment can in no way connected with the solar surface nuclear reactions as the temperature and density are not suitable for such a rate of neutrino flux observed in the run numbers 27 and 71. We know that the energy release in solar particle flares where relativistic protons can be accelerated are seen typically in the energy range 10^{32}-10^{33} ergs or 10^{35} to 10^{39} Mev in about 5 minutes over an area of 10^{19} cm^2 projected on to the solar surface. Subramanian(6)and Bazilevskaya et al(7)suggested that the neutrino emission process underlying the flare mechanism may contribute to the higher SN flux as observed in Davis experiment. Recently Bazilevskaya et al(8) and Basu(9) have found that there is a significant relationship between SN data and solar particles. It is true that the geomagnetic index Ap is the index of solar particles but it may not have any connection with the SN flux. As mentioned earlier(3) that the surface nuclear reaction which may occur during large solar flare cannot account the flux observed in SN experiment. It is believed that the measurable fluxes of neutrinos could not be produced by solar flare particles interacting in the earth's atmosphere(10). The possible mechanism that may explain incresed ^{37}Ar production from flares and cosmic ray intensity is that the particles with energy mostly less than 1 Gev, produced spallation products in the earth atmosphere(^{15}O , ^{13}N , ^{8}B etc.). The expected yield from ^{15}O , ^{13}N , ^{8}B (which decays into neutrino with energy greater than 1 Mev)are less than 10^{-2} cm^{-2} sec^{-1}. Although ^{8}B decays into high energy neutrino upto 14 Mev

but it cannot contribute an appreciable fraction in the SN data of Davis et al•(4)•Thus the question remains whether the cosmic ray muons, pions and kaons at the time of large solar flare can produce detectable flux of neutrinos in the Davis experiment•We know that (11)in the biggest solar flare which occurs in August 1972 produced proton flux $5•5\times 10^{8}$ cm^{-2} above 100 Mev in about 5 minutes and thus we cannot expect to have neutrino flux as high as 5×10^{6} cm^{-2} sec^{-1} from pions, kaons and muons produced by relativistic protons through cascades in the earth's atmosphere• Thus from our present knowledge we cannot expect that the solar flare can effect the production of ^{37}Ar in the Davis experiment•We present below the solar cosmic ray event(12,13)which produces intense X-ray, γ-ray etc•)with the corresponding run in Davis experiment in Table I to see whether solar flare can contribute any detectable perturbation in the recorded SN flux•

Table I

No• of runs in SN experiment	Solar cosmic ray event connected with flare etc)	No of runs in SN experiment	Solar Cosmic ray event connected with flare etc•
19	24•1•71	67	25•11•80
21	1•9•71		24•12•80
27	4•8•72	68	1•4•81
	7•8•72		4•4•81
30	29•4•73		10•4•81
32	7•7•74		27•4•81
36	23•9•74	69	30•4•81
42	30•4•76		10•5•81
51	19•9•77		6•5•81
	24•9•77	71	7•10•81
52	22•11•77		12•10•81
53	29•4•78	75	12•7•82
55	23•9•78	76	26•11•82
60	20•8•79		7•12•82
	21•8•79		18•12•82
63	7•6•80		16•2•84
66	6•11•80		25•4•84

It is interesting to analyze the possible temporal fluctuation of SN flux with solar cosmic ray variation• If we see the data of fig• 1(14) we see that the run numbers 21,27,29,31,36,39,42,47,49,51,52,54,56,58, 64,71 gives the higher ^{37}Ar production than the average ^{37}Ar production rate• The run numbers 36-58 belong to the sunspot minimum range(5)• According to Bazilevskaya et al (15)only solar cosmic ray events connected with the run numbers 21,27,51,71 can increase the production rate of ^{37}Ar in the SN experiment• But 2 solar cosmic ray events(connected with run numbers 21 and 51) took place on invisible side of the sun and therefore the increases of ^{37}Ar production will be absent• Raychaudhuri(16,17,5)showed that the SN data varies with 11 year solar cycle• He also explained why the SN flux is increased from 1975 to 1978• It is clear from the data(8,15) that there is a correlation between the galactic cosmic rays and the SN data and all of them vary with the 11 year solar cycle• Raychaudhuri(5,16)already explained the

increase of SN data(in run numbers 27 and 71) due to large amount of ^{3}He is mixed periodically in the core after the sunspot maximum·Thus the largest solar flare and highest SN flux occurs synchronously and the solar flare has no direct connection with the SN flux·~~Thus~~ If the solar cosmic ray event has some effect on the SN flux we could have observed it from other solar flare event~~s~~·g· run number 55,since the proton fluence greater than 10 Mev and 30 Mev in run numbers 55,71 are almost the same(18), but it did not happen·The solar flare event cannot explain the higher counts in run numbers 27 and 71 in Davis experiment but it may have effect in the nucleon decay detector and also on the neutrino experiment in the accelerator etc·Thus the solar flare has no direct connection with the SN flux(5)·

Proton decay:- Accurate calculation of low energy neutrino fluxes ($E_\nu \simeq$ 1 Gev)is necessary for the evaluation of the nucleon decay background· Gaisser et al(19)calculated the atmospheric neutrino flux by taking into account the effects of solar modulation that they did not consider the atmospheric neutrino flux from solar cosmic ray events·They consider only that the cosmic ray flux is higher at solar minimum and lower at solar maximum·But it was indicated by Kodama(20)that the unusual increases in cosmic rays and fast type PCA events occur only during the ascending(for about 2 years before sunspot maximum year) and descending phases(for about 2-4 years after sunspot maximum year)of the solar cycle avoiding the sunspot maximum year·The neutrinos are generated in the earth atmosphere by solar protons but because of the diffusion mechanism of protons moving between the sun and earth the whole process is very prolonged in time and difficult to identify against the background of an ordinary atmospheric flux·We have gathered from table I of King(11) that in August 1972 biggest solar flare events produces flux of protons above 200 Mev constitute 83% of the fluxes obtained by integrating over the entire solar cycle· The biggest solar flare which occured in October 1981 is almost the same as powerful as the August 1972 flare·The fluence of proton of 100 Mev—1 Gev constitute above $6{\cdot}6\times10^{8}$ cm^{-2}·We know fluxes of neutrinos around 1 Gev are $3{\cdot}93\times10^{-2}$ cm^{-2} sec^{-1} $sterad^{-1}$ in vertical direction and $6{\cdot}20\times10^{-2}$ cm^{-2} sec^{-1} $sterad^{-1}$ in horizontal direction at ground level from galactic cosmic rays·Again we know that the fluxes of protons around 1 Gev are 10^{-1} cm^{-2} sec^{-1} $sterad^{-1}$ from the best estimates of galactic cosmic rays as we have taken the fluxes of protons at the time of low solar activity·Thus we can~~not~~ expect the ratio between the neutrino flux and proton flux is within 2/5 and 3/5 around 1 Gev·From October 1981 to July 1982 the average fluence of proton greater than 100 Mev constitutes 5×10^{7} cm^{-2} (roughly)·Let us take that the solar flares lasted in such a way which produces significant fluxes of neutrinos·We get the neutrino flux is about $1{\cdot}8$ cm^{-2} sec^{-1} $sterad^{-1}$ and which is about 30 to 35 times higher than the cosmic ray neutrino flux around 300 Mev to 500 Mev· This supports also that the 100 Mev to 1 Gev solar proton flux is atleast an order of magnitude higher than the galactic proton fluxes·Here although neutrino energy is lower than 1 Gev but the fluences are higher so it is possible that the atmpspheric neutrinos from solar cosmic ray affect the underground experiment on nucleon decay·Similarly muon fluxes from solar cosmic rays will also be an order higher than the muon fluxes from galactic cosmic rays in the region from 100 Mev to 1 Gev·As the experiments of KGF,Mont Blanc,IBM,Kamiokande,Soudan I were operated within the range of bigger solar cosmic ray event we suspect that all the nucleon decay events observed by them are due to atmospheric neutrinos from solar cosmic ray

in the large scale experiments conducted at great depths underground since 1965 KGF group(21)recorded several anomalous events some of which are suggestive of decay of new particles or some of nucleon decay. From the above preliminary analysis we suggest that previous events was also perhaps due to theatmospheric neutrinos produced from solar cosmic ray events. So to decide about the nucleon decay properly we need better estimate of neutrino flux from solar cosmic ray events. At present we do not have better estimate of solar cosmic ray proton flux from the 21st solar cycle. So it is necessary to know the better knowledge of solar proton fluxes around Gev. We hope to calculate the neutrino flux from solar cosmic ray event when the full data of solar proton fluxes will be available upto 1984 for the 21st solar cycle from space missions. The solar cosmic ray neutrino flux will be an important step and guide(i)to understand the background for nucleon decay research from atmospheric neutrinos and also (ii)to the neutrino experiment which is operated on the underground, sea water and accelerator.

References:-

1)W. R. Sheldon(1969)Nature 221,650
2)L. J. Lanzerotti and R. S. Raghavan(1981)Nature 293,122.
3)P. Raychaudhuri(1983)Ind. J. Theo. Phys. 31, (in press).
4)R. Davis,Jr., B. Cleveland and J. K. Rowley(1982)AIP conference proceedings 96,1.
5)P. Raychaudhuri(1984)Solar phys. 93,397.
6)A. Subramanian(1983)Current sci. 52,342.
7)G. A. Bazilevskaya et al(1982)JETP lett 35,343.
8)G. A. Bazilevskaya et al.(1983)Proc 18th. ICRC 4,218.
9)D. Basu(1982)Solar Phys. 81,363.
10)K. O'Brien and A. dela Zerda(1984)Am. Nucl. Soc. 46,64.
11)J. H. King(1974)J. Space Craft and Rockets 11,401.
12)M. Pomerantz and S. P. Duggal(1974)Rev. Geophys. &Space Phys. 12,343.
13)S. I. Avdyushin et al.(1982)Bull. Acad. Sci. USSR(phys. Ser)46, 107.
14)P. Raychaudhuri(1985)Proc. 19th. ICRC SH 8.1-7., San Diego, USA.
15)G. A. Bazilevskaya et al(1983)J. Nucl. Phys(submitted).
16)P. Raychaudhuri(1983)P_{ro}c. 18th. ICRC, 7, 108.
17)P. Raychaudhuri(1984)Proc. 3rd. Asian Pacific regional meeting held at Kyoto, Japan, 30th. Sept-6 Oct. (to be published in Astrophys. Sp. Science.
18)R. E. Mcguire et al(1983)Proc. 18th. ICRC 2,66.
19)T. K. Gaisser et al(1983)Phys. Rev. Lett 51,223.
20)M. Kodama(1962)J. Phys. Soc. Japan 17, Suppl. II-A, 594.
21)M. R. Krisnaswami et al.(1981)Phys. lett 106B,339.

SH 8.1-9

NEUTRINO PRODUCTION FROM THE SOLAR ATMOSPHERE

Inazawa, H. and Kobayakawa, K.
The Graduate School of Science and Technology
and College of Liberal Arts, Kobe University
Nada, Kobe 657, JAPAN
Kitamura, T.
Institute for Cosmic Ray Research, University of Tokyo
Midori-cho, Tanashi, Tokyo 188, JAPAN

ABSTRACT

When the high energy primary cosmic rays enter near the solar surface, they pass through a thick matter but having a low density. If the density and path length satisfy an appropriate condition, the primaries collide with the constituents near the solar sphere (almost protons) and produce pions and kaons, most of which decay into $\mu+\nu_\mu$ without successive hadron collisions. Muons also decay into ν_μ and ν_e before reaching the earth. The neutrino flux of which the producer is matter near the solar surface is computed by solving cascade diffusion equations. The calculated differential flux of muon neutrino at 1 TeV is 1×10^{-13} $(\mathrm{GeV\cdot cm^2\cdot s\cdot ster})^{-1}$ which is rather difficult to be observed in the present apparatuses or DUMAND.

1. Introduction. Recently, the production mechanisms of cosmic ray neutrino with high energies are considered other than conventional ones which are decay products of pions and kaons in the primary - air nucleus collisions. One is the neutrino emission from the matter surrounding a source of very high energy cosmic ray protons (1, 2). The other is the neutrinos produced by the collisions of the primary and 3K background radiation (3) and so on. Besides these the following mechanism is treated here. As the high energy primary cosmic rays collide with nulei in terrestrial atmosphere and produce pions and kaons which decay into neutrinos (conventional neutrino), we expect that the primaries can produce high energy neutrinos from the solar atmosphere (we call this neutrino the solar neutrino, hereafter). Though the solar atmosphere takes a part of producer, the solar neutrinos at high energies (nearly equal to or more than 1 TeV) originate from the Sun. In this paper, the flux of the solar neutrino is estimated and its observation is discussed. The flux is so sensitive to the densities near the solar surface that the observation, if possible, gives informations the density which will be helpful for searching the solar models.

2. A Critical density and the density near the solar surface. Firstly, let us introduce a critical density with which produced pions (or kaons) decay into $\mu\nu$ or trigger a succesive collision with same probability. The critical density can be written by

$$\rho_{cr}(i) = m_i Br_i c/N_A E_i \tau_i \sigma_i \ , \qquad (1)$$

where N_A is Avogadro's number, the suffix i means π or K and m, Br, E, τ, σ are the mass, the branching ratio to $\mu\nu$, the energy, the mean life and the inelastic cross section, respectively. For σ_π = 30 mb and σ_K = 20 mb, we have

$$\rho_{cr}(\pi) = (2.11/E_\nu)\ 10^{-6}\ \ g/cm^3\ , \tag{2}$$

$$\rho_{cr}(K) = (2.23/E_\nu)\ 10^{-5}\ \ g/cm^3\ , \tag{3}$$

where the relation of E_i and the neutrino energy E_ν on the average is used and E_ν in the unit of TeV. When the target matter is the terrestial atmosphere, the relation of $z/\rho(z) = H$ (constant), where z is a hight in g/cm^2, holds in the upper part and decay constants defined by $m_i H/c\tau_i$ make the diffusion equations for pions and kaons simple. However the present problem is not the case.

Up to now, the density ρ near the solar surface is seemed not to be well confirmed. But referring to (4, 5), we express ρ for the quiet Sun as an approximate analytical form as follows:

$$\rho = 1.05\times10^{-11}\ (300-h)^{1.78}\ \ g/cm^3 \text{ for } h<100\ , \tag{4}$$

$$\rho = 3.29\times10^{-7}\ \exp(-h/107)\ \ g/cm^3 \text{ for } h>100\ , \tag{5}$$

where h in km is a height measured from the surface of the photosphere, which is $R = 6.96\times10^5$ km distant from the center of the Sun. For $h = 0$, $\rho = 2.7\times10^{-7}$ g/cm^2 which nearly corresponds to $\rho_{cr}(\pi)$ with $E_\nu = 10$ TeV. so the region of $h<0$, i.e. the inside of the photosphere, as well as $h>0$, i.e. the solar atmosphere, should be taken into account.

3. Derivation of the solar neutrino flux. We consider the production of the solar neutrinos at energies $1\sim100$ TeV. The contribution of produced charmed particles is neglisible. The source of muon neutrinos is π (or K) $\longrightarrow \mu\nu_\mu$ and $\mu \longrightarrow e\nu_\mu\nu_e$. On the other hand, electron neutrinos originate only from muon decays. After the diffusion equations for π, K, μ, ν_μ and ν_e are written down, fluxes of ν_μ and ν_e are solved and can be expressed by some multi-integral forms. These forms contain the variable represented by

$$dz = \rho(b,x)\ dx\ , \tag{6}$$

where z and x are path lengths in units of g/cm^2 and of cm, respectively and b means an impact parameter related to the center of the Sun. When b is fixed, the partial flux $f_\nu(E_\nu, z(b))$ can be obtained by multi-integration with respect to other variables including dx. In this procedure, the primary cosmic ray spectrum

$$I_0(E)dE = 1.8E^{-2.7}dE \tag{7}$$

(E in GeV, $I_0(E)$ in $(cm^2\cdot s\cdot sr\cdot GeV)^{-1}$) is used. The energy moments of π and k are taken as (6)

$$F_\pi = 0.0724\ ,\quad F_k = 0.00959\ , \tag{8}$$

and the average mass number is taken as 1.25 by considering the exsistence of He, C and O nuclei.

The partial flux $f_\nu(E_\nu, z(b))$ depends on the integrated path length given by

$$z(b) = \int_{-a}^{a} \rho(h)dx\ \ g/cm^2 \quad \text{with } h = (b^2+x^2)^{1/2}-R\ , \tag{9}$$

where as the origin of co-ordinate x is taken the closest point from the center of the Sun, namely $h = b-R$ at the origin. In eq.(9), since $\rho(h)$ is a steep decreasing function of h, $a \longrightarrow \infty$ may be allowed.

The observed differential flux of the solar neutrino on the earth can be expressed by

$$f_\nu(E_\nu) = \frac{1}{(S\Omega)_E}\int_{b_{min}}^{b_{max}} db \frac{d(S\Omega(b))}{db} f_\nu(E_\nu, z(b)) \quad , \tag{10}$$

where $(S\Omega)_E = 2\pi^2 R_E$, R_E is the radius of the earth and $S\Omega(b)$ is $S\Omega$ having a fixed b with respect to the center of the earth. In eq.(10), b_{max} and b_{min} are determined as follows: b_{min} is given by the condition

$$\rho(b_{min}-R) \approx 15\rho_{cr}(E) \quad . \tag{11}$$

when a primary cosmic ray passes with impact parameter less than b_{min} most produced π and K give rise to a successive collision before decay. As far b_{max}, inserting eq.(5) into eq.(9), one has

$$z(b) \simeq \rho(b-R)(2\pi \times 1.07 \times 10^7 R)^{1/2} \ g/cm^2 \quad . \tag{12}$$

Then b_{max} = R+1000km where $z(b_{max})$ is about 0.1 g/cm^2. In case E = 10 TeV, h corresponding to ρ_{cr}(10 TeV) is about zero, i.e. just the surface of photosphere, $z(R) = 810\ g/cm^2$ and $h_{min} = b_{min} - R$ is about -400km. These numerical values may give us some ideas.

4. Result and discussion. The derivation of the flux concerned with is necessary to carry out complex multi-integrations. In the present report, since the precision of numerical integrations is low, the following numerical values might more or less be modified. However our result say that $f_\nu(E_\nu)$ $(GeV \cdot cm^2 \cdot s \cdot sr)^{-1}$ of $(\nu_\mu + \bar{\nu}_\mu)$ are 1.1×10^{-14}, 3.8×10^{-14} and 2.7×10^{-18} for E_ν = 1, 10 and 100 TeV, respectively. These values are compared with the conventional fluxes through terrestial atmosphere: 2.3×10^{-11}, 7.2×10^{-15} and 1.6×10^{-18} at the vertical direction (7). On the flux of $\nu_e + \bar{\nu}_e$, we have 5.4×10^{-13}, 1.1×10^{-14} and 6.5×10^{-19}, corresponding to conventional ones at the vertical direction: 1.1×10^{-12}, 3.3×10^{-16} and 7.4×10^{-20} (7) for E = 1, 10 and 100 TeV, respectively.

In our case, because most of muons decay into $e\ \nu_\mu\ \nu_e$, the flux of ν_e is enhanced compared with the conventional one. Around E_ν = 10 TeV, our flux is enhanced. The reason is that at these energies the main contribution come from the pass near the solar surface which has an appropriate low density and long pass length. We have the ratio of the solar flux to the conventional ones is from several tens % to comparable order. But the angular resolution of apparatus should be taken into consideration in order to detect the solar neutrino flux. Since DUMAND's minimum detectable flux, as an example, is 10^{-10} $(cm^2 \cdot s)^{-1}$, the solar neutrino treated here is hard to be measured.

The flux of the solar neutrino is so sensitive to its density that the measurement of the flux in future may make clear the density or its change, say due to a violent solar flare, around the surface of the Sun.

References

1. Stenger, V.J., (1984), Astrophys. J. 284, 810.
2. Lee, H. and Bludman, S.A., (1984), preprint UPR-0259T.
3. Hill, C.T. and Schramm, D.N., (1983), Phys. Lett. 131B, 247.
4. Allen, C.W., (1962), 'Astrophysical Quantities' (2nd ed.) The Athlone Press
5. Gibson, E.G., (1978), 'The quiet Sun' translated into Japanese by Sakurai, K., Kodansha.
6. Thompson, M.G., and Whalley, M.R., (1977), J. Phys. G. 3, 97.
7. Mitsui, K. and Minorikawa, Y., (1985), the paper submitted to 19th ICRC.

SH-8.1-10

SOLAR COSMIC RAY BURSTS AND SOLAR NEUTRINO FLUXES

G.A.Bazilevskaya, S.I.Nikolsky, Yu.I.Stozhkov

P.N.Lebedev Physical Institute of the Academy of Sciences of the USSR, 117924, Leninsky Prospect,53, Moscow, USSR

T.N.Charakhchyan

Institute of Nuclear Physics, Moscow State University, 119899, Moscow, USSR

Abstract

The neutrino flux detected in the Cl-Ar experiment /1/ seems to respond to the powerful solar cosmic ray bursts. The ground-based detectors, the balloons and the satellites detect about 50% of the bursts of solar cosmic ray generated on the Sun's visible side. As a rule, such bursts originate from the Western side of the visible solar disk. Since the solar cosmic ray bursts are in opposite phase with the 11-year galactic cosmic ray cycle which also seems to be reflected by neutrino experiment, the neutrino generation in the bursts will flatten the possible 11-year behaviour of the ^{37}Ar production rate, Q, in the Cl-Ar experiment. The detection of solar-flare-generated gamma-quanta with energies above tens of Mev is indicative of the generation of high-energy particles which in turn may produce neutrinos. Thus, the increased Q during the runs, when the flare-generated high energy gamma-quanta have been registered, may be regarded as additional evidence for neutrino generation in the solar flare processes.

Definite evidence for neutrino generation in powerful solar cosmic ray bursts has been obtained by now /2-4/. During the period from 1970 up to the present the mean ^{37}Ar production rate in the Cl-Ar experiment /1/ was $Q=0.47\pm0.04$ ^{37}Ar atoms/day. The highest value of Q were observed during the periods when powerful solar cosmic ray bursts have been registered, namely, the run No 27, $Q=1.23\pm0.41$ ^{37}Ar atoms/day (the bursts of August 4 and 7, 1972) and the run No 71, $Q=1.21\pm0.37$ ^{37}Ar atoms/day (the burst of October 12,1981) /5,6/. A powerful solar cosmic ray burst can hardly be ex-

pected in 1985-1987 because the solar activity will approach its minimum whereas the solar flare events are usually observed near solar maximum.

It should be noted that the solar-flare-generated neutrinos will flatten the 11-year cycle of Q which, according to /2-4/ is in the opposite phase with the solar activity.

The fluctuations of the Q-value from one run to another may be due to the cosmic ray bursts, which have not been detected at the Earth. Fig. 1 a, b shows the heliolongitudinal distribution of the parent flares of solar cosmic ray bursts detected at sea-level since 1942 (35 events) /7/, and in the stratosphere since 1958 (68 events). The strong heliolongitudinal dependence of detection probability of solar cosmic ray bursts gives a $\sim 50\%$ probability of the detection such events with the charged-particle detectors installed on the Earth'surface, on balloons and satellites.

It may be assumed that the detection of high-energy γ-quanta (E_γ is more than several tens of MeV) from π^0-meson decays in solar flares will significantly increase the detection probability of the events occurring on the Eastern side of the visible solar disk. Such events must generate π^+-mesons whose decays will produce ν_e. In their turn the fluxes of such neutrinos may raise the Cl-Ar detector counting rate.

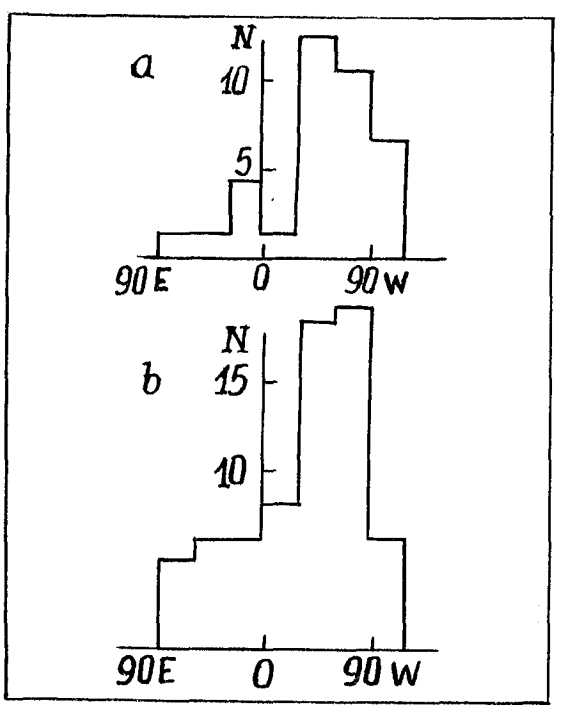

Fig.1. Heliolongitudinal distribution of the parent flares of solar cosmic ray bursts detected at sea-level (a), and in the stratosphere (b).

SH-8.1-10

The Table presents the solar flare events in which the γ-quanta with $E \gtrsim 50$ MeV were detected /8/. Solar neutrons were also detected in these events. It may be asserted quite safely that nuclear reactions, in which π-mesons are produced and then decay, occure in the solar flares presented. The rate of ^{37}Ar production in the Cl-Ar detector during the flare runs proved to be increased (Q_o) compared with the previous (Q_{-2}, Q_{-1}) and subsequent (Q_{+1}, Q_{+2}) runs. The run numbers which are indicated in the brackets and Q-values are taken from /5/. The bottom of the Table presents the mean values of Q for two events.

Table

No	Date of γ-burst	Q_{-2}	Q_{-1}	Q_o	Q_{+1}	Q_{+2}
1	21.06.80	(62) 0.023± 0.231	(63) 0.000± 0.325	(64) 0.488± 0.266	(65) 0.224± 0.425	(66) 0.361± 1.253
2	03.06.82	(73) 0.077± 0.151	(74) 0.478± 0.242	(75) 0.503± 0.327	(76) 0.475± 0.231	(77) 0.461± 0.224
the mean value		0.050± 0.138	0.239± 0.203	0.496± 0.211	0.350± 0.242	0.411± 0.636

The increased values of Q were registered durihg the runs when the high-energy γ-quanta and solar neutrons were observed. The results obtained agree with the conclusion /2-4/ concerning the possible generation of neutrinos in solar cosmic ray bursts.

References

1. Davis,R.,Jr., Evance,J.C.,(1974), VI Leningrad. Mezhdunarodny Seminar, p.91.
2. Bazilevskaya,G.A., Stozhkov,Yu.I., Charakhchyan,T.N., (1982), Pisma ZhETF, v.35, No6,p.273.
3. Bazilevskaya,G.A., Mukhamedzhanov,A.M.-A., Nikolsky, S.I., Stozhkov, Yu.I., Charakhchyan,T.N., (1984), Sov. Nuclear Phys., v.39, No 4, p.856.

4. Bazilevskaya,G.A., Nikolskii,S.I., Stozhkov,Yu.I., Charakhchyan,T.N., Mukhamedzhanov,A.M.-A.,(1983), Proc. 18-th ICRC, Bangalore, v.4, p.218.
5. Cleveland,B.T., Davis,R., Rowely,J.K.,(1984), Proc. of the Second International Symposium on Resonance Ionization Spectroscopy and its Application, England, (in press).
6. Bahcall,J.N., (1985), Highlights in Astrophysics: Concepts and Controvercies, (in press).
7. Cliver,E.W., Kahler,S.W., Shea, M.A., Smart,D.F., (1982), Astrophys. J., v.260, p. 362.
8. Share,G.H., Chupp,E.L., Forrest,D.J., Riger,E.,(1983), Positron-Electron Pairs Astrophys. Workshop, Goddard Space Flight Center, p.15.

THREE DIMENSIONAL CALCULATION OF FLUX OF LOW ENERGY ATMOSPHERIC NEUTRINOS

H. Lee and S.A. Bludman

Department of Physics, University of Pennsylvania,
Philadelphia, PA 19104

Abstract; Results of three-dimensional Monte Carlo calculation of low energy flux of atmospheric neutrinos are presented and compared with earlier one-dimensional calculations [1,2] valid at higher neutrino energies. These low energy neutrinos are the atmospheric background in searching for neutrinos from astrophysical sources. Primary cosmic rays produce the neutrino flux peaking at near E_ν=40 MeV and neutrino intensity peaking near E_ν=100 MeV. Because such neutrinos typically deviate by $20^0 \sim 30^0$ from the primary cosmic ray direction, three-dimensional effects are important for the search of atmospheric neutrinos. Nevertheless, the background of these atmospheric neutrinos is negligible for the detection of solar and supernova neutrinos.

1. Introduction

Recently one-demensional Monte Carlo calculations of cosmic ray production of neutrinos in the Earth's atmosphere, including geomagnetic and solar modulation effects, were reported [1,2]. These calculations agree well with the flux and angular distribution of neutrinos of energy $E_\nu > 200$ MeV observed in underground detectors. But these earlier one-dimensional cascade calculations are inapplicable to neutrinos of lower energy $E_\nu < 50$ MeV important in neutrino astronomy. In fact, we shall see (Fig. 3) that the mean angular deviation between the primary cosmic rays and neutrinos is appreciable even for neutrinos of several hundred MeV. The flux of low-energy atmospheric neutrinos we obtain (Fig. 2) in the present three-dimensional calculation is negligible compared with the known flux of solar or supernova neutrinos, but maybe significant in the case of other sources of astrophysical neutrinos.

The three-dimensional atmospheric neutrino flux is

$$dN_\nu(E_\nu, \theta_\nu, \phi_\nu)/dE_\nu = \int y_\nu \Omega\,(E_p, \theta_p, \phi_p, \lambda)(dN_p/dE_p)\,dE_p\,d\omega_p,$$

where $y_\nu(E_\nu, \theta_\nu, \phi_\nu, E_p, \theta_p)$ is the yield of neutrinos of energy E_ν, zenith angle θ_ν and azimuth angle ϕ_ν by primary cosmic rays of energy E_p and zenith angle ϕ_p. dN_p/dE_p is the primary cosmic ray spectrum, and $\Omega\,(E_p, \theta_p, \phi_p)$ is the geomagnetic cut-off. This geomagnetic cut-off depends on geomagnetic latitude λ and magnetic rigidity $R = pc/e$ where p is the primary cosmic ray's momentum.

2. Calculational details

We modified the Gaisser-Protheroe-Stanev one-dimensional hadron interaction model [5] by assigning to secondary particles the transverse momentum distribution.

$$W(a,x_t)=(a+1)(a+2)x_t(1+x_t)^a.$$

Here $a=2p/<p_p>-3$ for $p>1.5<p_t>$, $a=0$ for $p<1.5<p_t>$, $x_t=p_t/p$ and p is the incident hadron's momentum. At high p, $W\sim p_t\exp(-ap_t)$. The angular deviation of secondary hadrons from the incident hadron direction produced by the above formula affects our results insignificantly.

In our computer program analytic formulae are used for the energy distribution of decay particles. For those energies, a microcanonical ensemble average is taken; total energy is conserved in each individual decay. The secondary directions are, however, assigned according to a canonical ensemble; the total momentum is conserved on average but not in individual decays. Interaction cases are treated similarly. We use energy-independent energy loss rates for charged particles by air ionization in a simple isothermal atmosphere to determine the decay height and energy, and energy-dependent formulae to determine the interaction height and energy. Our results are insensitive to these parameters.

For the comparison with the earlier one-dimensional calculation we calculated the yield function

$$Y_\nu(E_\nu,E^p,\theta_p)\equiv\int y_\nu(E_\nu,\theta_\nu,\phi_\nu,E_p,\theta_p)d\omega_\nu,$$

integrated over appropriate neutrino directions.

3. Results and Conclusions

Fig.1 shows the yield Y_ν of vertically incident protons of several energies E_p, integrated over the downward 2π solid angle of neutrino's directions. Because low-energy neutrinos are made mainly from low-enrgy pions and muons at rest, for all primary cosmic ray energies the peak flux occurs near 40 MeV and the peak intensity near 100 MeV. Because most muons decay at rest and $<E_{\nu_e}>=0.3E_\mu$, $<E_{\nu_\mu}>=0.35E_\mu$, the atmospheric neutrino flux peaks near 40 MeV.

Fig.2 shows the downward neutrino flux produced by vertically incident primaries at high geomagnetic latitude, where

$$dN_\nu/dE_\nu\approx\int Y_\nu\Omega\,(dN_p/dE_p)dE_p.$$

While this expression is not exact for a three-dimensional cascade, it compares simply with the one-dimensional calculations. The near-vertical neutrino flux is also insensitive to zenith angle. Because, if not supressed by geomagnetic cut-off, the primary cosmic rays have a steep power-law spectrum, the main contribution to the low-energy neutrino flux is from primary cosmic rays just above the pion-production threshold energy. The total flux is therefore very sensitive to geomagnetic cut-off [6].

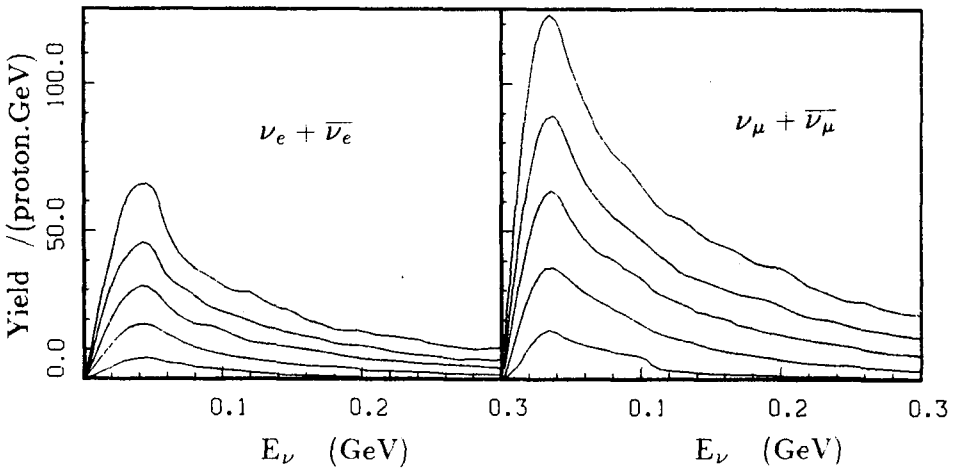

Fig. 1. Integrated neutrino yields from vertically incident protons. 2 5 10 20 50 GeV cases from bottom to top.

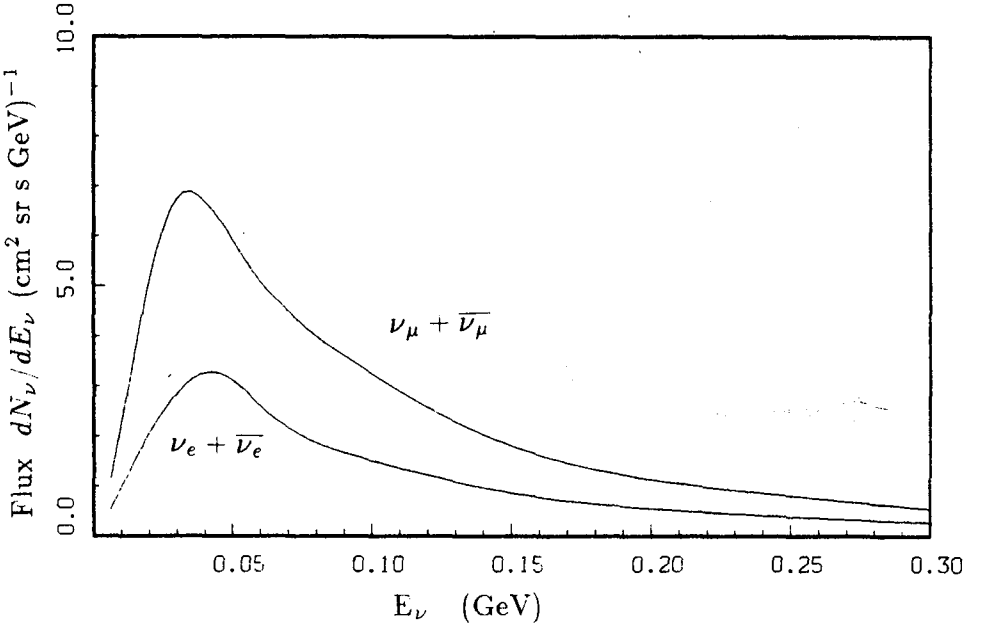

Fig. 2. Calculated downward neutrino flux at high geomagnetic latitude

For neutrinos above E_ν=200 MeV, this three-dimensional calculation agrees with earlier one-dimensional calculations [1,2]. At lower energies (E_ν< 50 MeV), however, we now obtain neutrino fluxes significantly lower than those one-dimensional calculations would give.

This atmospheric neutrino background is totally negligible compared to the solar neutrino flux and the flux of neutrinos expected from supernova at any reasonable distance (< 10^3 Mpc).

Fig.3 shows the average angular deviation of down-going ν_es of energy E_ν produced by vertically incident protons of energy E_p=2, 10, 50 GeV. Other neutrino types have similar spectra. While average angular deviation is $20^0 \sim 30^0$, neutrino direction at neutrino energy below 50 MeV is near isotropic and a long tail of more energetic neutrinos deviating by $5^0 \sim 10^0$ is produced at E_ν> 200 MeV.

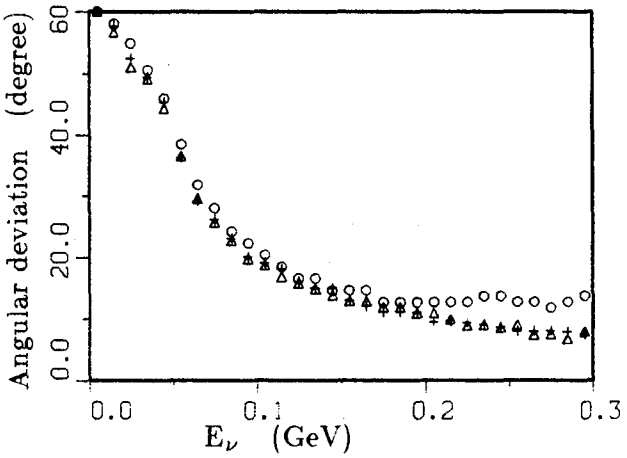

Fig. 3. ν_e angular deviation from primary proton.
2 GeV (○), 10 GeV (△), 50 GeV (+) cases.

Acknowledgements; We thank to T. K. Gaisser and Todor Stanev for useful discussions. This work was supported by U.S. Department of Energy.

References

[1] T. K. Gaisser, Todor Stanev, S. A. Bludman and H. Lee, Phys. Rev. Lett 51, 223(1983) and Fourth Workshop on Grand Unification (FWOGU), U. of Pennsylvania, (Birkhauser, Boston, ed. A. Weldon, P. Langacker, P. J. Steinhardt, p. 87 (1983)).

[2] T. K. Gaisser and Todor Stanev, to appear in Proc. ICOBAN

[3] Private communication with T. K. Gaisser and Todor Stanev, also *see*, T. K. Gaisser and Todor Stanev, to appear in Proc. Neutrino '84 conference, Dortmund, June 1984.

[4] D. J. Cooke, Phys. Rev. Lett. 51, 320 (1983).

[5] T. K. Gaisser, R. J. Protheroe and Todor Stanev, Proc. 18th ICRC (Bangalore) 5, 174 (1983)

[6] H. Lee and S. A. Bludman, exact 3-dimensional expression of neutrino flux and angular dependence is in preparation.

DETECTOR CALIBRATION OF THE INDIAN COSMIC RAY EXPERIMENT (IONS) IN SPACE-SHUTTLE SPACELAB-3

J.S.Yadav, S.Biswas and N.Durgaprasad
Tata Institute of Fundamental Research
Bombay 400005, India.

ABSTRACT

In IONS experiment in Spacelab-3 we intend to study nuclei upto iron in low energy cosmic rays, using CR-39 (DOP) detectors. We have exposed CR-39 (DOP) to He^4, C^{12}, O^{16}, Ne^{20}, Si^{28}, Ar^{40}, Cr^{52} and Fe^{56} accelerated beams from various accelerator facilities available around the world. We have used different beam energies and exposure angles. From these exposures, we have studied the charge resolution and energy resolution for our detector in the region of our interest. We have also studied the effect of pre-annealing and depth on the response of our detector. For isotopic resolution, we have exposed the detector samples to Ne^{20} and Ne^{22} accelerated beams. We have also kept samples of CR-39 (DOP) exposed to different accelerated heavy ions in our detector module to take into account the effect of ambient conditions on detector response during the flight.

1. Introduction. The passive track detectors provide the advantage of high geometrical factor to study low intensity cosmic rays. CR-39 plastic detectors are the most sensitive among passive detectors.[1] However, CR-39 has following disadvantages: (1) Its surface becomes frosty after etching for long time, and (2) It shows track response variation along the depth of detector samples. The first problem makes the multisheet measurements difficult while second problem affects directly track identification and hence the resolution of the detector. Both these problems are very important for cosmic ray studies. These problems are overcome by using long curing cycle and adding 1% dioctyl phthalate in CR-39 monomer (CR-39 [DOP]).

We are using CR-39 (DOP) detectors in our cosmic ray experiment in Space Shuttle Spacelab-3.[2] This plastic (of thickness $\sim 250\mu m$) is prepared by Pershore Moulding Ltd., UK, using 32 hours of curing cycle. We have studied the response of this plastic detector using different heavy ion exposures. In this paper, the results of this study are presented.

2. Experimental Details and Results. Indian cosmic ray experiment in Space Shuttle Spacelab-3 has been designed to perform the measurements of the ionization states, flux and energy spectra of elements from alpha particles to iron ions in the low energy region below 100 MeV/N. We have exposed CR-39 (DOP) samples to different heavy ions in this charge region. The exposure details are given in Table 1.

Table 1 : Exposure Details

Ion Beams	Energies MeV/N	Angle of Exposure
He	1.0, 2.1, 7.5 and 10.5	90^{o}
C	1.75, 3.5, 4.5, 7.0 & 8.8	30^{o} and 60^{o}
N	3.2 and 10.4	-do-
O	1.1, 4.2, 5.4 and 8.8	-do-
Ne^{20}	1.4, 7.3, 8.0 and 9.1	30^{o}, 60^{o} and 90^{o}
Ne^{22}	2.65, 4.6 and 7.5	-do-
Si	6.5	30^{o}
Cr	6.5	10^{o},20^{o},30^{o},45^{o}, 60^{o} and 90^{o}
Ni	6.0	30^{o}
Fe	$\leq$ 300	60^{o}

The exposures to alphas are obtained from Variable Energy Cyclotron (VEC), Calcutta, India. The exposures to iron beam (all energies below 300 MeV/N) are obtained from Berkeley, USA. All other exposures are obtained from Joint Institute for Nuclear Research, Dubna, USSR.

All the exposed samples are etched in 6.25 N NaOH at 70^{o}C simultaneously for different etching times. Different track parameters are measured to obtain the etch rate ratio for different particles of different energies. Different sets of four parameters are used to calculate the actual track length in order to cross check the values so obtained [3]. This method also gives the parameters with the least percentage errors in different etch rate ratio regions. The measured values of etch rate ratio are plotted as a function of dE/dX as well as $(Z_{effective}/\beta)^2$ calculated using different relations for energy loss and range [4,5]. Fig. 1 shows log-log plot between etch rate ratio and dE/dX (from Mukherjee and Nayak relations) [4]. The experimental data from other studies for relativistic ions are also included. It is clear from the figure that in low energy loss region, etch rate ratio is a linear function of energy loss. However, in high energy loss

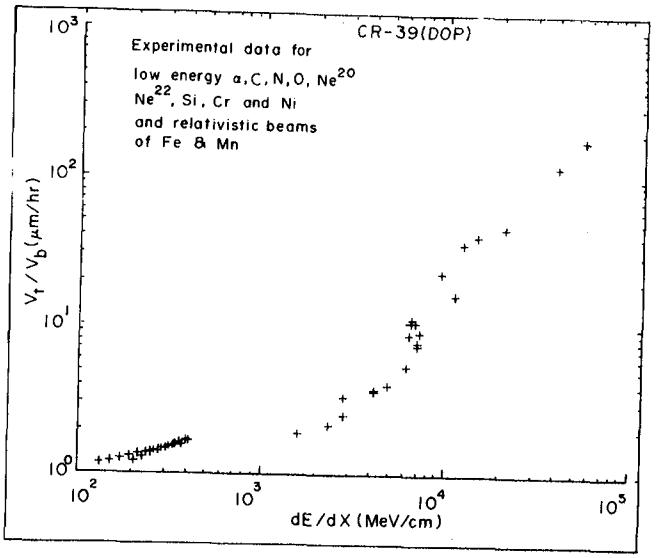

Fig. 1 Track response of CR-39 (DOP)

region, etch rate ratio is a power function of energy loss. A polynomial of the form

$$V_t/V_b = A + b\ (dE/dX) + c\ (dE/dX)^d$$

is fitted to data points (not shown in the figure). From response curve, we have generated curves between Vt/Vb versus residual range for different ions. From these curves, we have studied the charge resolution of CR-39 (DOP) in terms of standard deviation in measurements. The accuracy of the charge resolution turns out to be about 0.2 charge unit.

Isotopic resolution is studied from Ne^{20} and Ne^{22} exposures. The depth dependence of detector response of this plastic is studied from 6.5 MeV/N Cr exposures (range $\sim$ 95 μm). The track length measurements for different exposure angles, on both sides, do not show any difference beyond experimental error. We also do not find any significant effect of annealing on track response of this plastic.

References

1. Cartwright, B.G. et al. (1978), Nucl. Instrum. and Meth., 153, 457.
2. Biswas, S. et al., (1985), these proceedings.
3. Henke, R.P. and Benton, E.V., (1971), Nucl. Instrum. and Meth., 97, 483.
4. Mukherjee, S. and Nayak, A.K. (1979), Nucl. Instrum. and Meth., 159, 421.
5. Benton, E.V. and Henke, R.P. (1969), Nucl. Instrum. and Meth., 67, 343.
6. Thomas, W. et al., (1984), Nucl. Track, 9, 107.
7. Ahlen, S.P. et al., (1981), 17th ICRC, 8, 77.

A SILICON SURFACE BARRIER TELESCOPE FOR SOLAR PARTICLES IDENTIFICATION

J. Sequeiros+, J. Medina

Grupos Científicos CONIE
INTA. Torrejón de Ardoz. (MADRID). SPAIN.
+ and Physics Dpt. Universidad de Alcalá de Henares.

ABSTRACT

The calibration results of a laboratory model of a three silicon surface barrier detector telescope developed to identify energetic solar particles produced in solar flares and low energy cosmic rays in interplanetary space, by the ΔE-E method, are presented.

1. Introduction. During this last decade a number of experiment on board spacecrafts have been gathering information on the composition and energy of solar energetic particles and low energy cosmic rays. The most striking features to be extracted form the data are: a) Charge range $1 \leq Z \leq 28$ b) Energy range $\sim 1 \leq E \leq 50$ MeV/n c) Composition highly variable from event to event, with energy and even with time during a particular event. A detailed review has recently been published by J.P.Meyer (1985).

A International Solar-Terrestrial Physics programme is being studied by NASA, ESA and ISAS for the 90's, in which the European Space Agency is contributing with a multidisciplinary Solar-heliospheric observatory (e.g.SOHO) whose aims include the measurement of energetic particles in Interplanetary Space. The laboratory model of a detector telescope presented here is being realized as a first step towards our eventual participation in such programme.

2. Detector characteristics. The laboratory model of the heavy ion telescope has been designed to separate elements from $_2$He to $_{26}$Fe in the energy range of interest for solar energetic particles and C.R. anomalous component (Fig. 1). The telescope consists of three silicon solid state surface barrier detectors (D1, D2 and D3, Fig. 2) housed in a modular aluminium structure of cilindral symmetry which can easily be modified to hold different detector size and opening angles. The third detector (D3) is set in anticoincidence to reject particles which are not stopped in D2. TABLE I shows the main cha

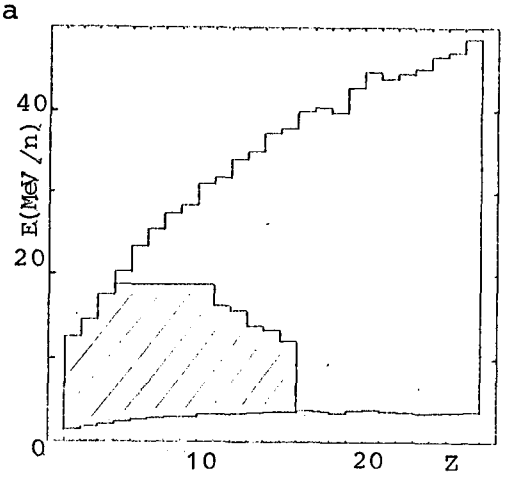

Fig. 1 Energy and charge ranges of the telescope.

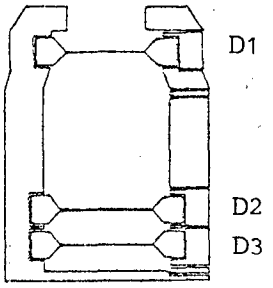

Fig. 2 Schematic cross section of the telescope.

TABLE I
Detector characteristics

	D1	D2	D3
Surface Area (cm^2)	3	4.5	4.5
Thickness (μm)	31	1014	470
Resistivity ($K\Omega cm$)	408	12.5	6.7
Dead Layers ($\mu g/cm^2$)	40.0 Au 40.1 Al	40.1 Au 40.0 Al	40.3 Au 121.0 Al
Alpha Resolution (FWHM in KeV)	36.8	20.8	18.8

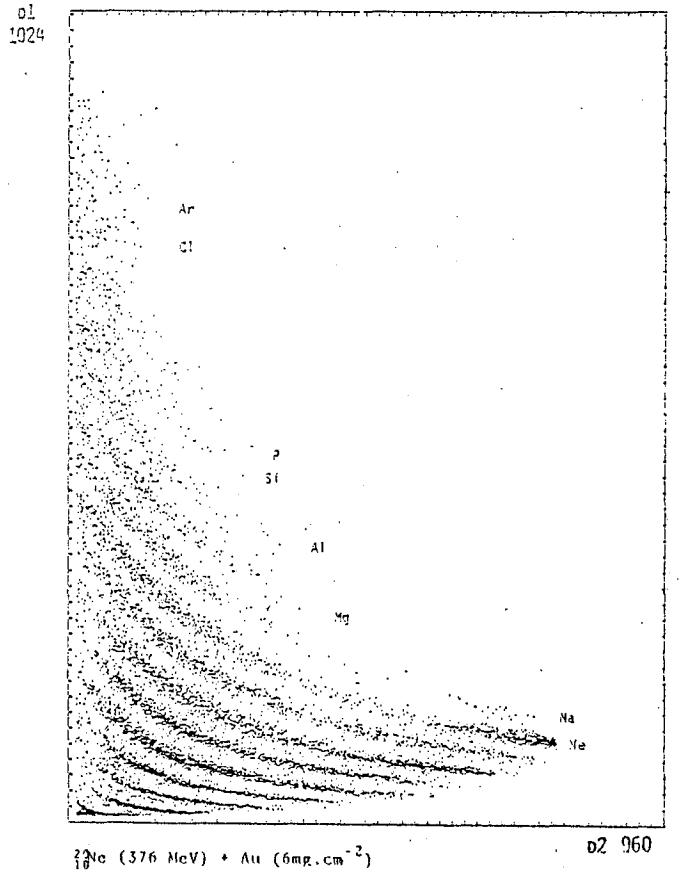

Fig. 3 D1 v.s. D2 matrix of raw data.

racteristics of the detector chosen. All detectors are ORTEC silicon surface barrier totally depleted. Alpha resolutions have been measured with an ^{241}Am source and include the contribution of noise from our electronic system. The geometrical factor of the model telescope has been G=0.4sr.cm^2.

3. Accelerator calibration. Absolute calibration of the telescope was performed in the VICKSI (Van-de-Graaff-Isochron-Cyclotron-Kombination fur Schwere Ionen) accelerator of the Hahn-Meitner-Institut (Berlin,F.R.G.). Two shifts, with beams of ^{20}Ne of 230 and 376 MeV, and ^{197}Au targets of 210 $\mu g.cm^{-2}$ and 6 mg.cm^{-2} and ^{12}C target of 50 $\mu g \cdot cm^{-2}$, were used. The scattered and fragmented ions were detected by the telescope placed at 20 cm from the targets and at θ = 25° (gold targets) and θ = 15° (carbon target) with respect to the beam direction. The angular acceptance of the telescope was about 0.3°. The data were split by a data distributer and collected simultaneously by our ADC's interfaced to a HP 9825 minicomputer and the da

ta adquisition system of the Institute, in order to check the reliability of our system.

4. Results. The resolution of D1 and D2 detectors for ^{20}Ne of 230 MeV elastically scattered in a 210 $\mu g \cdot cm^{-2}$ ^{197}Au target were measured to be 1.7 MeV and 1.9 MeV FWHM which correspond to 7.6% and 0.9% respectivily. Fig. 3 shows a D1 v.s. D2 energy-loss matrix of raw data from ^{20}Ne (E=376MeV) + ^{197}Au (6mg$\cdot cm^{-2}$) which gives and idea of the charge resolution of the detector system in low gain mode.

The charge spectra, over the whole charge and energy ranges produced (shade area in Fig. 1), have been obtained using a particle identifier algorithm described by Seamster et al. (2). This algorithm is based on integrating Bragg curves using the Bethe-Bloch equation and assuming

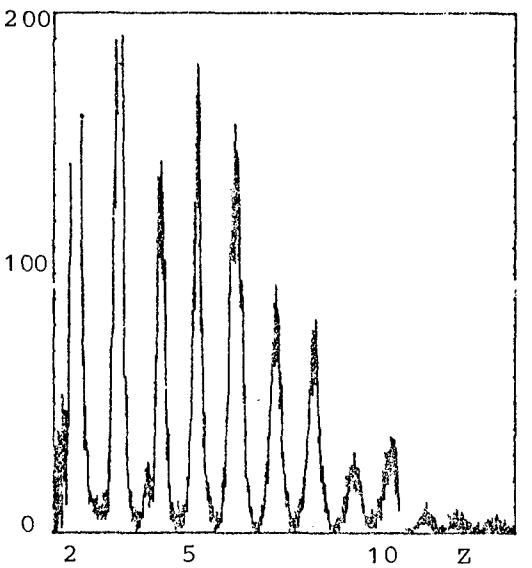

Fig. 4 Charge spectrum from de data of Fig. 3.

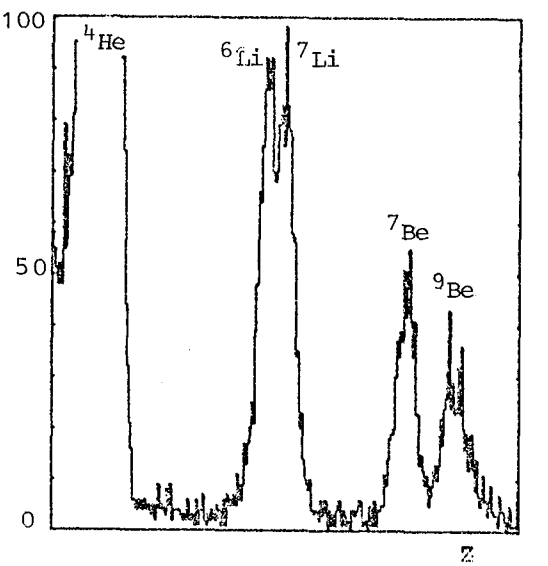

Fig. 5 Charge spectrum of ^{20}Ne (376MeV)+^{12}C(50μg cm^{-2}) in high gain mode.

M(amu)=2Z. For each event, by an iterative calculation, a particle identification parameter $PI=(1/2\,MZ^2)^{1/3}$ has been obtained. Fig. 4 shows the charge spectrum obtained from the data of Fig. 3. In Fig. 5 the low charge spectrum of the reaction products of ^{20}Ne (376 MeV) + ^{12}C(50 $\mu g \cdot cm^{-2}$) in high gain mode, is shown. No corrections have been performed on the data. The bias voltages were in creased 25% for detectors D1 and D3 and 50% for detector D2 above the depletion voltages, in order to reduce the contribution of plasma recombination to pulse hight defect.

5. Conclusions. From the results shown in Fig. 4 and 5 three conclusions can be made: a) The detector system described and tested is capable of good charge resolution from He to Al

although beyond Ne the statistic is very poor b) In the high gain mode, isotopic resolution has been acheived for $^{6}Li/^{7}Li$ and $^{7}Be/^{9}Be$ c) The much higher yield of ^{4}He over ^{3}He and of ^{9}Be over ^{10}Be in this type of nuclear reactions prevent from obtaining experimental evidence of those isotopes, although we believe that, at least $^{3}He/^{4}He$, can be resolved under other more favorable conditions (i.e. solar ^{3}He-rich events).

6. Acknowledgements. This work is being supported by the Comision Asesora de Investigación Científica y Técnica (CAICYT, grant 3433/79).

We are also grateful to Dr. V. Domingo and Mr. J. Henrion of the Space Science Dpt. of the European Space Agency, and Dr. H. Homeyer and Mr. J. Ucker of the Hahn-Meitner-Institut (Berlin, F.R.G.) for their advice and help.

References

1. Meyer, J.P. (1985) Ap.J.Suppl., 57,151
2. Seamster, A.G., et al. (1977) Nucl.Inst. and Meth., 145,583

A BI-DIRECTIONAL CHARGED PARTICLE TELESCOPE TO OBSERVE FLUX, ENERGY SPECTRUM AND ANGULAR DISTRIBUTION OF RELATIVISTIC AND NON-RELATIVISTIC PARTICLES

S.D. Verma, S.P. Bhatnagar & S.K. Kothari
Department of Physics, Gujarat University
Ahmedabad 380 009, INDIA

1. INTRODUCTION

A Charged Particle Telescope[1] (CPT) was designed, fabricated and calibrated to make the following observations[2,3]:

(i) Discrimination between various singly charged particles e.g. electrons, muons and protons, in about 5-100 MeV energy range.
(ii) Measurement of the flux and the energy of the charged particles incident on telescope from two opposite directions and stopping in the Telescope, thus obtaining flux and energy spectrum of downward and upward moving charged particles.
(iii)Measurement of broad angular distribution of selected particles as a function of azimuthal angle.

This telescope can be used to study low energy electron, muon and proton energy spectra. The experiment was flown in a high altitude balloon from Hyderabad, India, in December 1984. This same equipment is also useful in ground level electron, muon spectrum study.

2. EXPERIMENT

The Charged Particle Telescope contains a stack of Plastic Scintillators, inorganic scintillator and Cerenkov detectors. The telescope is described below.

The total energy detector consisted of a 1" thick NaI(Tl) crystal of 3" diameter. The total energy of particles was observed for those stopping in the crystal. Pulse height analysis was done for stopping as well as for penetrating particles. To distinguish various singly charged particles, dE/dX vs E technique has been used, aided by a Lucite (plastic) Cerenkov detector. The capability of charged particle separation by

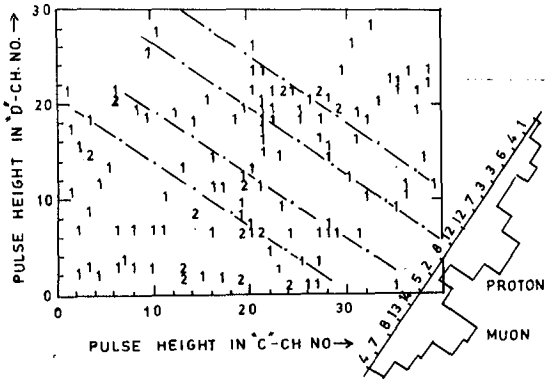

FIG 1

telescope is demonstrated by dE/dx vs. E graph with quick look data shown in Fig. 1. From Fig. 1, it is clear that various charged particles will produce different energy losses in a thin dE/dx detector for a given residual energy E, measured by Total energy detector. Those electrons which stop in total energy detector[4] are all relativistic while the stopping muons and protons are non-relativistic. Therefore, a velocity threshold Cerenkov detector will produce output for a stopping electrons only and other stopping particles will thus be separated. Combination of these two techniques results in an effective separation of electrons, muons and protons in selected energy interval of 5-30 MeV.

The up and down moving particles are distinguished using upper and lower dE/dx counters as anticoincidence detectors for upward and downward particles respectively.

3. ENERGY CALIBRATION

The energy calibration of various detectors of CPT was done using ground level Cosmic Ray Muons and radioactive Gamma Ray sources (Cs^{137}, Co^{60}). These sources were used for NaI(T1) detector energy calibration. Beta particle source Sr^{90} was used for dE/dx detector testing, energy calibration and monitoring. A 8 MeV monoenergetic electron beam from microtron was used for various detector calibrations and for determining efficiency of Cerenkov

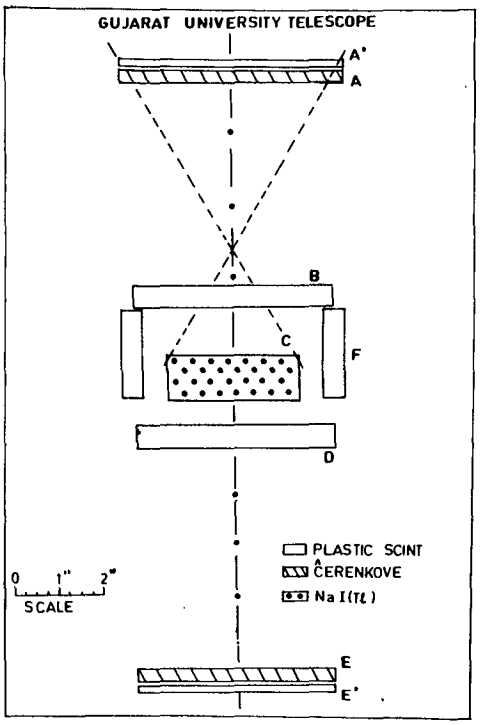

FIG 2

detector.

Fig 3

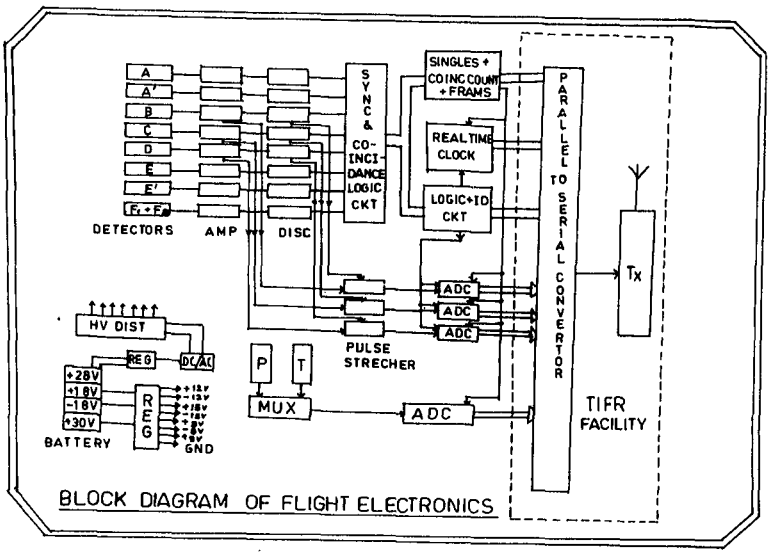

4. TELESCOPE HARDWARE

The Schematics of CPT is shown in Fig.2. The geometry of the telescope is defined by 1/8" thick plastic scintillator A' and 1" thick NaI(Tl) detector C. Geometrical factor of the telescope is 13 cm^2 Ster. Detector A is a Lucite Cerenkov detector, used as velocity threshold discriminator for various stopping particles. The detector B is 1/2" thick plastic scintillator, working as energy loss (dE/dx) detector. Lower detector D is another 1/2" thick plastic scintillator working as anticoincidence detector for downward moving particles. Detectors E and E' are complementary to A and A', creating another telescope for upward particles, with B acting as the anticoincidence detector, D as dE/dx detector. Fig.3 is a block diagram of the Electronic Support subsystem. The Ground Support System is shown in Fig.4. It consists of a microcomputer and a teletype unit. The microcomputer receives clock and data from Bit-synchroniser and analyses the incoming data in real time. The desired information from quick look system can be printed out on teletype on getting a command from keyboard. Telescope assembly can be rotated around its horizontal axis to study angular distribution.

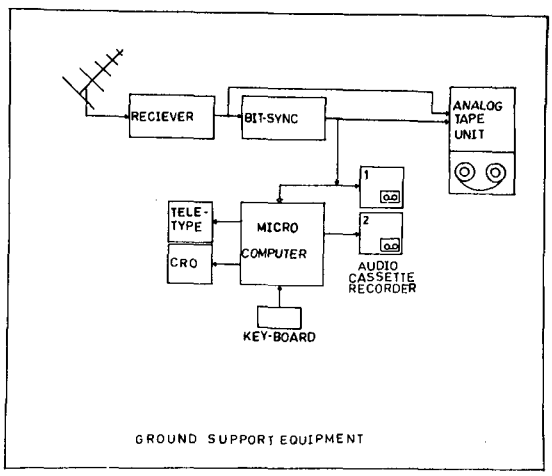

Fig 4

The experiment was tested for several weeks before the flight for various detector characteristics, gain shifts, singles and coincidence count rates, high voltages, discriminator levels etc.

5. BALLOON FLIGHT

On 8th December 1984, this experiment was flown in a high altitude balloon in early morning hours (5.23 a.m. IST) from Hyderabad, India. Balloon ascended to an altitude of 37 km (4 mb) and floated for four hours. Experiment was cut down by telecommand at 12.00 noon and was picked up in a reasonably good shape. Post flight checkout runs indicate experimental condition to be good. Data analysis and results are presented in SH session[5,6].

6. ACKNOWLEDGEMENT

Authors are thankful to Mr. Vikram Shah of Metro Industries for support in fabrication of mechanical systems and to Dr. Peggy Shea of A F G L, Bedford, USA, for providing the NaI(Tl) crystal for this experiment.

Indian Space Research Organisation's financial support under RESPOND Programme is thankfully acknowledged, without which it would not have been possible to conduct this experiment. The important assistance of Dr. V.N. Bhoraskar and his colleagues in calibration of CPT using microtron at University of Poona, India, and the useful discussions with Dr. (Mrs.) V. Sinha are gratefully acknowledged.

References

1. Bhatnagar S.P. & Verma S.D., 17th ICRC, Paris, 1981, Vol. L, p.266.
2. Bhatnagar S.P. & Verma S.D., 18th ICRC, Bangalore, India, 1983, Vol.3, p.501.
3. Kothari S.K. & Verma S.D., 18th ICRC, Bangalore, India, 1983, Vol.3, p.483.
4. V.B. Asgekar et al, Technical Report on Microtron, University of Poona, 1979.
5. Verma S.D. & Bhatnagar S.P., 19th ICRC, La Jolla, USA, (1985) (SH-6).
6. Verma S.D. & Kothari S.K., 19th ICRC, La Jolla, USA, (1985) (SH-6).

PHOTOMETRIC AND SPECTROSCOPIC GAMMA-RAY OBSERVATIONS OF SOLAR TRANSIENT PHENOMENA USING LONG DURATION BALLOONS

Pelling, M.R. and Duttweiler, F.
UCSD/CASS, Code C-011
La Jolla, CA 92093

Lin, R.P., Levedahl, W.K., Primbsch, H., and Curtis, D.W.
UCB/SSL, Berkeley, CA USA

Hurley, K.C.
CESR, Toulouse, FRANCE

ABSTRACT

We describe a program, currently in progress at UCB and collaborating institutions, UCSD and CESR Toulouse to conduct extended duration spectroscopic and photometric observations of solar X-ray phenomena from balloons. High photometric sensitivity to weak hard X-ray bursts is attained using a 600 cm^2 array of phoswich scintillators. High spectral resolution for stronger bursts is available from an array of planar germanium detectors. These instruments are carried in a novel balloon gondola designed for the 15 to 20 day float durations available through using conventional zero-pressure balloons in the radiation controlled (RACOON) mode.

1. Introduction Important new results concerning energetic flare processes have been obtained using a unique instrumental complement combining high spectral resolution and photometric sensitivity in a conventional balloon flight. The excellent spectral resolution available through the use of germanium solid state detectors permitted the discovery of a superhot (3.5×10^7 K) flare emission component (1) and the high photometric sensitivity of a large area phoswich scintillation counter permitted detection of ~25 "μ-flares" with fluxes 10^{-1}–10^{-2} lower than conventionally associated with major flare activity (2). The existance of superhot emission components has since been indirectly confirmed through Fe XXVI measurements (3) and continuum measurements below 30 keV (4). The optical counterpart of μ-flare events were subsequently discovered through analysis of co-ordinated H_α observations (5). The μ-flares have a non-thermal spectral distribution and show evidence for temporal structure faster than ~1 s.

2. Scientific Objectives The general significance of these phenomena is not clear since the superhot component has been directly observed in only one flare and the observed μ-flares were probably the product of a single active region. It is interesting to note; however, that the size/frequency distribution for the μ-flares suggests that their underlying particle population could be significant for heating of the active corona. Thus, it is of great interest to determine how general the acceleration of >20 keV

electrons is for transient processes on the sun. Other interesting questions include: How does the superhot component vary from flare to flare? Indeed, how hot do flare regions get? How are the heating and acceleration mechanisms related?

In order to clarify the role of these hard x-ray processes in overall solar energetic phenomena it is necessary to extend the observations to span a variety of solar activity conditions. The primary requirement for these follow-on studies is to attain a relatively long observing period (comparable to solar rotation period) using instrumentation having high photometric and spectroscopic sensitivity. For this purpose we have modified our original balloon instrument to provide additional sensitivity and to function within the constraints of a long duration balloon flight.

3. Flight Apparatus To attain the above objectives we have enlarged the collecting area of the original payload and adapted it to a unique balloon gondola designed to capitalize on the long float duration available using standard zero-pressure balloons in the radiation controlled (RACOON) mode. A block diagram for the detector system is shown in Figure 1.

Our detector complement consists of an array of four actively shielded high purity cooled planar germanium detectors totaling ~50 cm^2 active area plus three large area NaI(Tl)/CsI(Na) phoswich scintillation counters totaling ~600 cm^2. Cooling for the germanium detector array is provided by a 160 l dewar of liquid nitrogen. The aperture of the germanium array is oriented vertically with an acceptance angle of 40 degrees (full width, zero response). This permits sensitivity to solar transient events for roughly two hours of each day at >33% response. The phoswich scintillation counters have 3 mm thick primary detector elements and are optimized to respond in the 15 to 150 keV energy range. Each phoswich has a crossed slat collimator which defines a pyrimidal angular response with FWHM of 15 degrees.

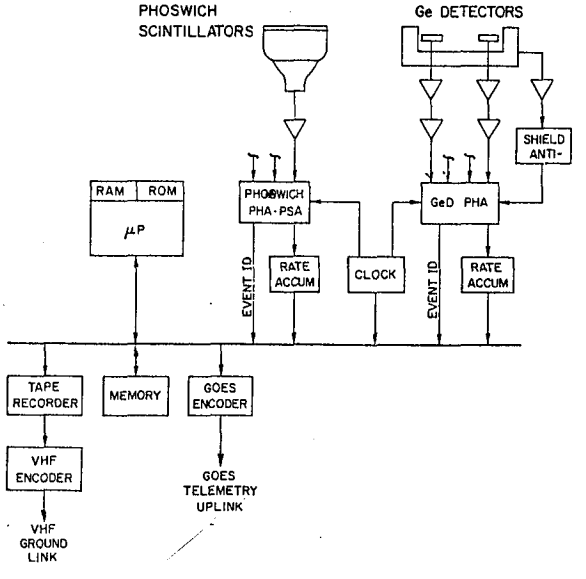

Figure 1 - The μ-processor based data system accommodates a wide dynamic range of detector event rates and prioritizes the data for storage or telemetered output (see text).

The phoswich array is carried in an alt-azimuth gimbal which is slaved to an external aspect sensor platform. The aspect sensor platform is programmed during the day to track the sun in azimuth and elevation with a precision of ~ 1 degree. During night operation or periods when the sun is too low in the sky to permit useful x-ray observations the aspect sensor platform may be reprogrammed to track the local magnetic field. This

operating mode permits observation of non-solar sources via a pre-programmed tracking routine with an accuracy of ~2 degrees. The aspect sensor platform also incorporates a sunrise/sunset sensor to provide daily navigation updates to the tracking routines.

The data generated by these detector systems are processed by an on-board computor and prioritized for output via one or more of three channels as shown in Figure 1. Discrete x-ray event words in which pulse height and timing information are encoded are read directly into a large dynamic random access memory via direct memory access control. This memory is sized to hold the transient events totaling up to 10^6 discrete detected photons. The raw event rates are monitored in parallel with memory storage of the detector data streams by the on-board processor to detect the presence of solar burst events. Data segments which contain such burst events are then tagged for preferential storage and output. When ~50% of the main buffer RAM is filled (~2 hours under background rate conditions) the data are transferred to the on-board tape storage system. This system includes two 3M model HD-75 digital recorders having a total capacity of 136 Mbytes which is sufficient to hold all of the data generated during the nominal 20 day balloon flight. Burst event data from the previous day are read out of the burst memory section each night and transmitted via the Geostationary Orbiting Environmental Satellite (GOES) network at an effective rate of 60 bps. During the day this data channel is used in real time to transmit the integral rates in three broad energy windows as monitored by the the phoswich array. This channel provides a rudimentary data base for studying μ-flare characteristics should the tape recorder data not be recovered. An additional data transmission channel is provided via line-of-sight VHF telemetry to permit high rate monitoring of the payload during the initial float checkout phase of the balloon flight before the payload is committed to a circumnavigation. This channel will also be used to dump the data stored in the on-board tape recorders as a precautionary measure before cutdown and recovery of the payload.

Additional features are provided in the balloon gondola system to support a nominal 15-20 day float duration. Power is provided by an 8 m^2 solar panel array which is deployed after launch and operates in conjuction with a lead acid battery stogage system. The power system is scaled to support an average energy usage of 2500 watt-hours per day. The balloon/gondola system incorporates an auto-ballast system which functions in three stages. Nominal sunset cooling and settling of the balloon will trigger a minimal ballast drop of ~5% of the payload weight. An anomalous altitude change, as might occur over a cold cloud layer, will trigger an additional ballast drop of 10%. In the event of a very large altitude excursion (which might result in the payload descending below the tropopause) a ballast destruct occurs to provide some possibility of restoring the payload to a functional altitude. The primary payload is fully enclosed within an insulation blanket which includes additional thermal ballast to maintain tempertures above 0° C. Additional thermal isolation and heating is provided for the phoswich scintillator array which needs a 20-30 °C operating environment.

4. Long Duration Balloon Operation The RAdiation COtrolled balloON (RACOON) concept offers near ideal conditions for the study of solar phenomena (6, 7). Since essentially continuous exposure is possible for periods within ± 4 hours hours of local noon, one is not limited by the ~40 minutes of earth occulation which occur for a spacecraft instrument in

each 90 minute low earth orbit. The RACOON mode involves the use of a standard zero pressure polyethelyne balloon for multi- day flights without the use of extensive ballasting to maintain float altitude through sunset. The initial float altitude must be chosen such as to ensure that the sunset altitude change does not bring the balloon below the tropopause where the negative temperature gradient would result in loss of the flight. For the present system we require a daytime float altitude of ~3 gm/cm^2 residual depth to conduct x-ray observations. This is adequate to keep the balloon safely above the tropopause at night. Allowing 1 to 2 hours to reattain daytime float altitude we expect ~250 hours of total float duration at 3 gm/cm^2. This should be compared with the nominal maximum float durations of 25-40 hours which are occasionally attained under normal balloon flight conditions.

The balloon is to be launched in January, 1986 from Alice Springs, Australia, where the strong prevailing stratospheric winds will keep the system within ~2 degrees of a constant latitude for the 15-20 day duration of the global circumnavigation. Cutdown is planned for the Eastern coastal region of Australia.

5. Summary We have developed a sophisticated balloon gondola which will provide the first astronomical observations of solar and cosmic phenomena from long duration balloons. We will use the RACOON long duration mode which is ideally suited for observations of the sun. We expect one 20 day balloon flight to yield ~150 hours of solar and ~100 hours of cosmic source observations. We estimate that ~20 flare events strong enough for spectroscopic analysis should be observed in a January, 1986 flight.

6. Acknowledgements The authors wish to acknowledge the valuable asistance provided by the National Scientific Balloon Facility in the design and construction of the payload and planning for the long duration flight operation. We also wish to thank R. Sood and J. Thomas at the University of Melbourne for their assistance in preparations for the Australian lauch and recovery operation. We also wish to acknowledge the generous support of National Science Foundation Grant ATM-8402231, National Aeronautics and Space Administration Grant NAGW-516, and California Space Institute Grant CS30-82.

References

1. Lin, R.P., Schwartz, R.A., Pelling, R.M., and Hurley, K.C. (1981), *Ap.J. (Letters)*, **251**, 109.
2. Lin, R.P., Schwartz, R.A., Kane, S.R., Pelling, R.M., and Hurley, K.C. (1984), *Ap.J.*, **283**, 421.
3. Tanaka, K., Nitta, N., Akita, K., and Watanabe, T. (1983), *Solar Physics*, **86**, 91.
4. Duijveman, A. (1983), *Solar Physics*, **84**, 189.
5. Canfield, R.C. and Metcalf, T.R. (1984), *B.A.A.S.*, **16**, No. 4, 891.
6. Lally, V.E. (1981), *The Radiation Controlled Balloon*, Preprint, National Center for Atmospheric Research.
7. White, R.S. (1983), *A Plan for Long Duration Scientific Ballooning*, Report of the Long Duration Balloon Flight Study Committee, printed by the National Scientific Balloon Facility, Palestine, Texas.

MONTE CARLO CALIBRATION OF THE SMM GAMMA RAY SPECTROMETER FOR HIGH ENERGY GAMMA RAYS AND NEUTRONS

J. F. Cooper and C. Reppin
Max Planck Institute for Extraterrestrial Physics
D-8046 Garching, F.R.G.

D. J. Forrest and E. L. Chupp
University of New Hampshire, Durham, N.H. 03824, U.S.A.

G. H. Share and R. L. Kinzer
Naval Research Laboratory, Washington, D.C. 20375, U.S.A.

1. Introduction. The Gamma Ray Spectrometer /1/ on the Solar Maximum Mission spacecraft was primarily designed and calibrated for nuclear gamma ray line measurements, but also has a high energy mode which allows the detection of gamma rays at energies above 10 MeV and solar neutrons above 20 MeV. The GRS response has been extrapolated until now for high energy gamma rays from an early design study /2/ employing Monte Carlo calculations. The response to 50-600 MeV solar neutrons was estimated from a simple model which did not consider secondary charged particles escaping into the veto shields /3/. In view of numerous detections by the GRS of solar flares emitting high energy gamma rays /4/, including at least two emitting directly detectable neutrons /3,5,6/, the calibration of the high energy mode in the flight model has been recalculated by the use of more sophisticated Monte Carlo computer codes described in Section 2. New results presented in Section 3 show that the GRS response to gamma rays above 20 MeV and to neutrons above 100 MeV is significantly lower than the earlier estimates.

2. Monte Carlo Simulation of the GRS. The simulation of GRS response in the high energy mode has required several stages of software development: (1) representation of the principal materials and structures, both active and passive, by combinatorial geometry routines, (2) propagation of primary photons, and their secondary interaction products, through the GRS with the Electron-Gamma Shower Code (EGS) /7/, (3) propagation of neutrons and their secondary products with the High Energy Transport Code (HETC) /8/ and with EGS, (4) calculation of charged particle scintillation efficiencies /9/, and (5) the final selection of events satisfying pulse height logic criteria.

The combinatorial geometry routines give an accurate representation of the GRS flight model /1/, consisting of seven (7.6-cm x 7.6-cm) NaI detectors in an upper array and a large (24.2-cm x 7.6-cm) CsI detector, located 18 cm below the upper array. These detectors are surrounded by an array of plastic and CsI veto shields to reject charged particle events.

In the calculations the flight model is represented by fifty active scintillator or passive structure elements. These volume elements are defined in terms of intersections or unions of solid cylinders, cylindrical shells, hemispherical shells, and planar boundaries, in order to represent the upper NaI and lower CsI detector crystals, photomultiplier tube assemblies between the upper and lower detectors, the plastic and CsI shields, and the principal supporting structures, including the metal housings for the active detectors and shields. A significant improvement over the previous study /2/ is in the treatment of empty interstitial spaces between the material volumes. Tracking of Monte Carlo particles through all of these volumes and boundaries is accomplished with common geometry routines in EGS and HETC.

The compatibility of the tracking routines is particularly useful for the simulation of neutron interactions, which produce secondary products requiring two-stage tracking, first by HETC for nucleons and pions, and then by EGS for secondary gamma rays from pion decay or the de-excitation of nuclei excited by collisions. Interactions of nucleons and pions with target nuclei, and the residual excitation energy emitted as gamma rays, are simulated with the two-stage intranuclear-cascade and nuclear evaporation routines in HETC. A low energy cutoff of 15 MeV is used for the propagation of nucleons and pions in HETC, although the intranuclear cascade model, decomposing interactions with nuclei into individual collisions with the constituent nucleons, is not valid for collision energies below 100 MeV. EGS uses cross sections derived from analytical formulae or experimental data to simulate the interactions of gamma rays above 100 KeV and electrons above 500 KeV. Cumulative errors due to Monte Carlo statistics and the accuracy of the interaction cross sections used in both HETC and EGS are about 10-20 percent.

The present calculations use only a rough approximation procedure for energy deposition in the detectors by secondary neutrons produced at energies below 15 MeV. The neutron response calculations have been run for two cases: (1) the low energy neutrons produced below 15 MeV deposit their full energy locally via nuclear recoil or inelastic interactions, or (2) these neutrons escape from the GRS without any further interaction. The final neutron responses are the average of the results from these two cases, significantly different for 50-100 MeV neutrons but much less so for higher energies.

The pulse height logic criteria for gamma ray or neutron events in the high energy mode are the following: (1) 10-100 MeV electron-equivalent energy deposited in either the upper NaI detector assembly or the lower CsI detector, or in both, (2) no deposits greater than about 3 MeV in the annular CsI side shields, and (3) no deposits greater than about 500 KeV in either the

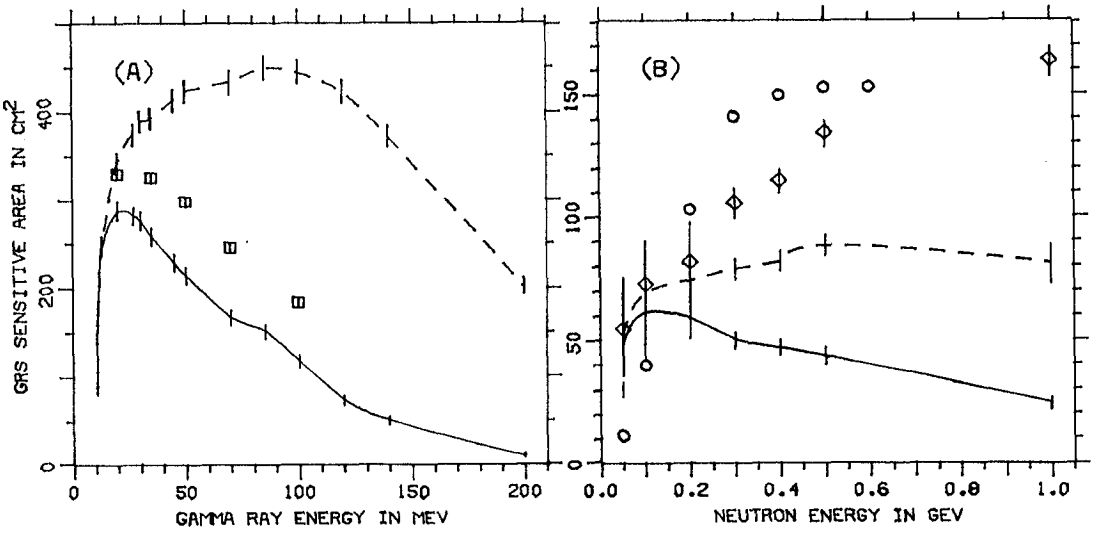

Figure 1: (A) 10-140 MeV gamma ray response. (B) 50-1000 MeV neutron response. Nominal high energy matrix response with (solid curves) and without (dashed curves) shield veto. Gamma ray response from /2/ with corrections for the GRS flight model (boxes). Neutron response without shield veto and 100-MeV cutoff from present work (diamonds) and /3/ (circles).

front or back plastic shields. Energy deposits in the upper and lower detector arrays are pulse-height analysed separately with four channels below 100 MeV, while deposits above 100 MeV in either array are not recorded due to preset electronics limitations. The four channels correspond to electron-equivalent energy deposits of 10-25, 25-40, 40-65, and 65-100 MeV. The GRS event logic also records a two-dimensional high energy matrix which includes "mixed" events triggering both the upper and lower detectors, as the result of secondary charged particle and photon showers, and depositing total energies up to 140 MeV. The total energy deposited in the matrix gives at least a minimum measure of the incident particle's energy, while the fraction of mixed events allows some discrimination between gamma rays and neutrons.

3. High Energy Gamma Ray and Neutron Response. Calculated results for the total GRS responses to gamma rays and neutrons as functions of incidence energy are shown respectively in Figures 1(A) and 1(B). The incident photons or neutrons are perpendicularly incident onto the front surface of the GRS, as would be the case for radiation of solar origin. The GRS response to high energy gamma rays from off-axis sources has also been calculated and used for in-orbit calibration and cosmic burst studies, the response being nearly constant up to 30 degrees off-axis at all energies and falling off by up to a factor of three at 90 degrees and 20 MeV.

The high energy matrix response for solar gamma rays, shown by the solid curve in Figure 1(A), is heavily attenuated above 15 MeV by the vetoing of events which produce shower electrons escaping through the active shields, where these electrons trigger the side and bottom shields at about the same rates. The new responses are ten percent below the earlier ones /2/ at 20 MeV, but the differences increase to thirty percent at higher energies. These differences arise from the use of different instrument models and shield veto criteria which produce increasingly divergent results above 20 MeV.

The strong forward showering of secondary photons and electrons produces a characteristic response in the GRS to solar gamma rays above 20 MeV, where these events contribute mixed events to the high energy matrix. At increasing energies the mixed events increase in significance but are also associated with high veto rates and low total response. The calculated ratios of mixed and total matrix events are 0.01, 0.2, 0.6, and 0.4 at 30, 70, 140, and 200 MeV respectively, decreasing above 140 MeV due to matrix energy limits.

In Figure 1(B) the solid curve shows the large cumulative effect on the neutron response from shield vetoes and the 100-MeV cutoff, without which the present and earlier /3/ calculations converge above 500 MeV. The relative significance of shield vetoing alone is illustrated by the increasing difference between the solid and dashed curves at higher energy. The large error bars for the response to neutrons at 50-100 MeV arise from the low energy neutron approximation discussed in Section 2. The neutron response is characterized by a relatively negligible fraction (less than 0.03) of mixed events, arising from the physical separation of the upper and lower GRS detectors, and from the relatively isotropic scattering of neutron interaction products.

4. Discussion. The new Monte Carlo calibration gives a significant improvement of the earlier results /2/ for higher energy gamma rays producing mixed events, the difference between the two calculations at 20 MeV being relatively negligible. Since average gamma ray energies in the high energy GRS flares /4/ were less than 25 MeV in the impulsive phase, the integral fluences for those flares do not require revision. Analyses of flares emitting higher energy gamma rays from pion decay /10/ are highly dependent

on the measured fraction of mixed matrix events and require the new calibration.

Aside from residual uncertainties regarding the newly calculated GRS response to solar neutrons below a few hundred MeV, the important effects of shield vetoing, the 100-MeV high energy mode cutoff, and details of the secondary interaction product distributions, have otherwise been accurately modeled for the first time. The earlier estimates /3/ of GRS response to neutrons, derived from simple cross section arguments without consideration of these effects, greatly exceed the new ones at neutron energies above 100 MeV. At 20-100 MeV the earlier estimates should be used, since neutron cross sections in the new HETC calculations have probably been overestimated at those energies. The total matrix responses of the GRS with shield vetoing to neutrons at 50, 100, 200, 300, 400, 500, and 1000 MeV are then 11, 40, 59, 50, 47, 44, and 24 cm^2 respectively, and the corresponding ratios of the new and old responses are 1.0, 1.0, 0.57, 0.36, 0.31, and 0.28 up to 500 MeV.

The in-flight GRS data provide some confirmation that the current calibration of the high energy mode is reasonably accurate. In-flight calibration data have confirmed the stability of energy deposit thresholds for the shields, although thresholds at 10 MeV and above for the high energy matrix are still uncertain by a few MeV. The gamma ray calibration has been checked at 30-200 MeV by measurements of atmospheric gamma rays, as the GRS points toward the earth's horizon during the night portion of its orbit, which agree within 20-30 percent with comparable SAS-2 data /11/. For a check of the neutron response, delayed neutrons from the June 21, 1980 solar flare /3/ provide a relatively "clean" neutron source, uncontaminated by high energy gamma rays emitted only in the initial impulsive phase. These neutrons produced a very small fraction of mixed events in the high energy matrix after background subtraction /6/, thereby confirming the predicted response from these calculations.

5. Acknowledgements. This work was supported partially by contracts 010K017-ZA/WS/WRK 0275:4 at the Max Planck Institute, NAS 5-23761 at the University of New Hampshire, and by NASA contract S.70926A at NRL.

References

1. Forrest, D. J., et al.: 1980, Solar Physics, 65, 15.
2. Kinzer, R. L., et al.: 1977, Monte Carlo Simulation of the SMM Gamma Ray Detector, unpublished report, Naval Research Laboratory, Washington, D.C.
3. Chupp, E. L., et al.: 1982, Ap. J. Lett., 265, L95.
4. Rieger, E., et al.: 1983, 18th Int. Cosmic Ray Conf. Papers, Bangalore, 10, 338.
5. Chupp, E. L., et al.: 1983, 18th Int. Cosmic Ray Conf. Papers, Bangalore, 10, 334.
6. Chupp, E. L., et al.: 1985, this conference, Paper SH 1.4-1.
7. Ford, R. L., and W. R. Nelson: 1978, The EGS Code System, Stanford Linear Accelerator Center Rep. 210, Stanford University, Palo Alto, Ca.
8. Chandler, K. C., and T. W. Armstrong: 1972, Operating Instructions for the High Energy Nucleon-Meson Transport Code HETC, Oak Ridge National Laboratory Rep. 4744, Oak Ridge, Tenn.
9. Birks, J. B.: 1964, The Theory and Practice of Scintillation Counting, Pergammon Press, Oxford.
10. Forrest, D. J., et al.: 1985, this conference, Paper SH 1.4-7.
11. Thompson, D. T., et al.: 1981, J. Geophys. Res., 86, 1265.

COMPARISONS OF MONTHLY MEAN COSMIC RAY COUNTING RATES OBSERVED FROM WORLDWIDE NETWORK OF NEUTRON MONITORS

Jai Young Ryu and Masami Wada*

Department of Physics, Kunsan National University,
Miryoung-Dong,Kunsan-city, Chullapuk-Do,511 Korea

* Cosmic Ray Laboratory,Institute of Physical and Chemical Research,
7-13 Kaga-1, Itabashi-Ku, Yokyo 173, Japan

ABSTRACT

In order to examine the stability of neutron monitor observation, each of the monthly average counting rates of a neutron monitors is correlated to those of Kiel neutron monitor. The regression coefficients thus obtained are compared with the coupling coefficients of isotropic intensity variation. The results of the comparisons for five year periods during 1963 to 1982, and for whole period are given. The variation spectrum with a single power law with an exponent of -0.75 upto 50 GV is not so unsatisfactory one. More than one half of the stations show correlations with the coefficient greater than 0.9. Some stations have shifted the level of mean counting rates by changing the instrumental characteristics which can be adjusted.

INTRODUCTION

The relation between the long lived Forbush decreases and the 11 year variation has long been interested (see for example, Lockwood and Webber, 1984; Burlaga et al. 1984). In order to examine whether the neutron monitor counting rates are satisfactorily stable for periods of months to tens of months to be used to inspect the variations mentioned above, the present paper is given (Ryu and Wada, 1983). After some trials, Kiel has been selected as the main key station of neutron monitor data. Correlations of monthly averages between each of 65 stations and Kiel for 5 year periods during 1963 and 1982 are studied statistically. The years 1963-67 and 1973-77 are of the sunspot minimum periods, and those of 1968-72 and 1978-82 are nearly during the sunspot maximum years. All of the stations have more than five years continual data which are refered to WDC-C2.

ANALYSIS AND RESULTS

The correlation diagrams are prepared for any pairs of stations. Form inspections of these diagrams, we can classify them into three groups as a, b, and c. Group a shows close correlation of which the coefficients are greater than 0.9. There are 37 stations in the group a out of 65. For example, the diagrams between Thule and Kiel are given in Fig.1, and for Kerguellen and Kiel in Fig.2. The scales of both axes are of natural logarithms, so that the variational amounts are approximated in the values relative to the counting rates of each point. As seen in the figures, the standard deviation of the scatter about the regression line is extimated to be around 0.5 percent at the best condition.

Using the results of correlation, the regression coefficients are plotted in Fig.3 against the coupling coefficients of isotropic varistion normalized to that of Kiel. The coupling coefficients are derived from the variation spectrum of primary cosmic rays of a single power law with an exponent

-0.75 upto 50 GV (Yasue et al. 1982). From Fig.3, it can be seen the correlations are rather well, though there are some scatters in points. Most remarkable scatter is seen for the figure of 1968-72, the sunspot maximum period. There seems some tendency of downward shift of southern stations. The spread of decreases seen in plot of whole period in Fig.2 (left hand side) is also noticable aspect. We have examined whether this trend is statistically significant or not. After variaous test, we found no clear conclusion to prove the situation given above. That means the existence of limitation of the data stability.

Group b contains stations which have rather low correlation coefficients. Those stations are mostly situated in lower latitudes, and the amounts of variation are relatively small, which result lower coefficients. There are continuities from the stations whose coefficients are higher than 0.9. Some stations reveal hysteresis, but there is no systematic trend of hysteresis.

Group c diagrams in Fig.4 show significant level changes of the mean counting rates. They may mostly arise from artificial instrumental changes such as the number of counters. There are 15 stations in this group. We are trying to get the amounts of level changes for those stations by using reasonable method.

CONCLUSION

The monthly average counting rates of most of the existing neutron monitors are examined from a point of view of the stability of operation. More than a half of the stations treated show satisfactory operations. If the artificial level changes are adjusted, we can use practically all of the stations, except small number of stations whose data are significantly deviate with time. The standard deviation of the residual variation is around 0.5 percent in the best condition, which makes some limitation of the analysis. It can be improved if one uses multiple number of stations for such variations spanning months to tens of months period.

REFERENCES

Burlaga,L.F. et al. (1984), J. Geophys. Res. in press.

Lockwood,J.A. and W.R.Webber (1984), J. Geophys. Res. 89, 17.

Ryu,J.Y. and M.Wada (1983), Conf. Papers 18th ICCR,3,511.

Yasue,S. et al. (1982), Rep. CRRL. No. 7, Cosmic-Ray Res. Lab. Nagoya Univ. Nagoya, Japan.

FIGURE CAPTIONS

Fig.1. Correlation diagrams of monthly average neutron monitor counting rates between Thule and Kiel for 5 year periods and for all the period (left hand side).

Fig.2. The same as Fig.1, but for Kerguellen and Kiel.

Fig.3. The correlation diagrams of the regression coefficient against the coupling coefficient normalized to that of Kiel.

Fig.4. The same as Fig.1, but for the stations which show level changes due to artificial change in the operational condition.

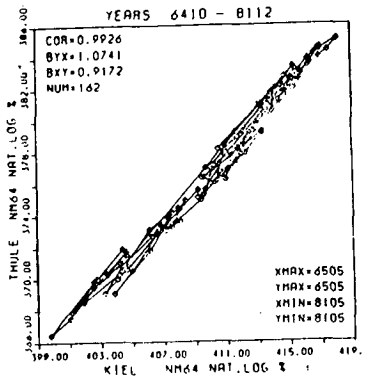

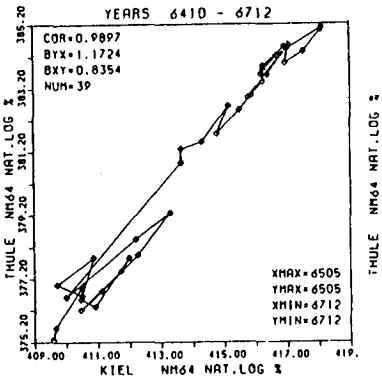

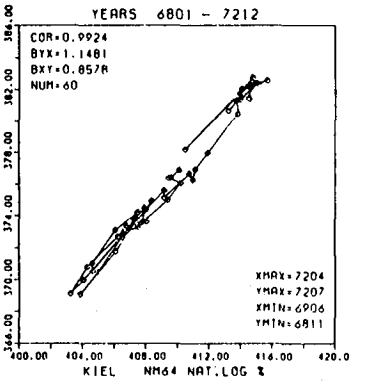

Fig.1. Thule-Kiel

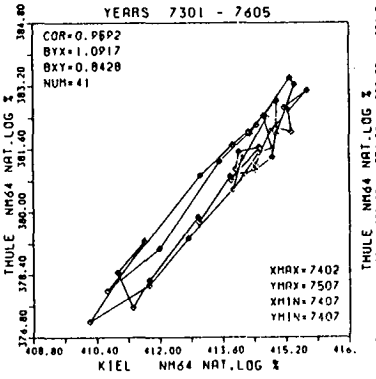

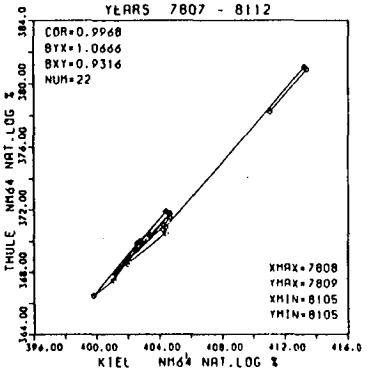

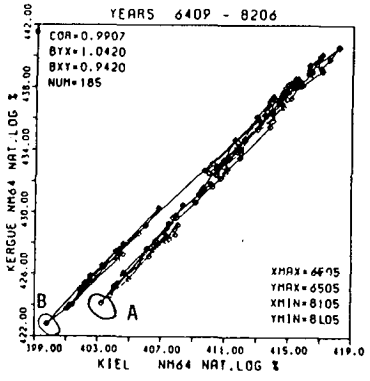

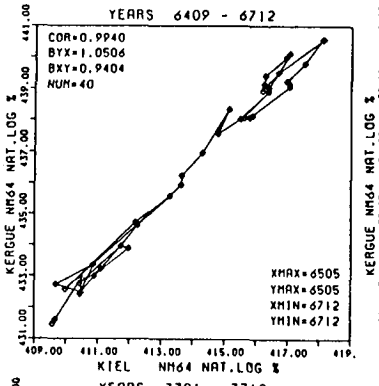

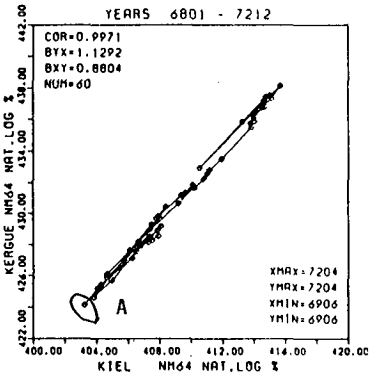

Fig 2. Kerguellen-Kiel
A and B correspond
with each other.

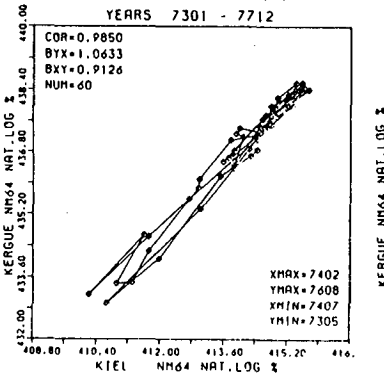

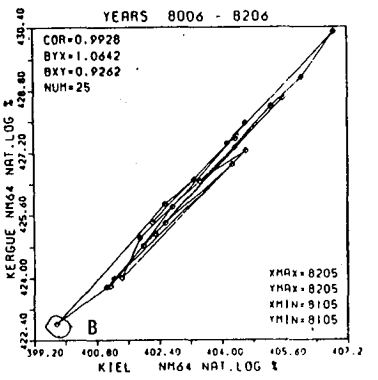

SH 9.1-7

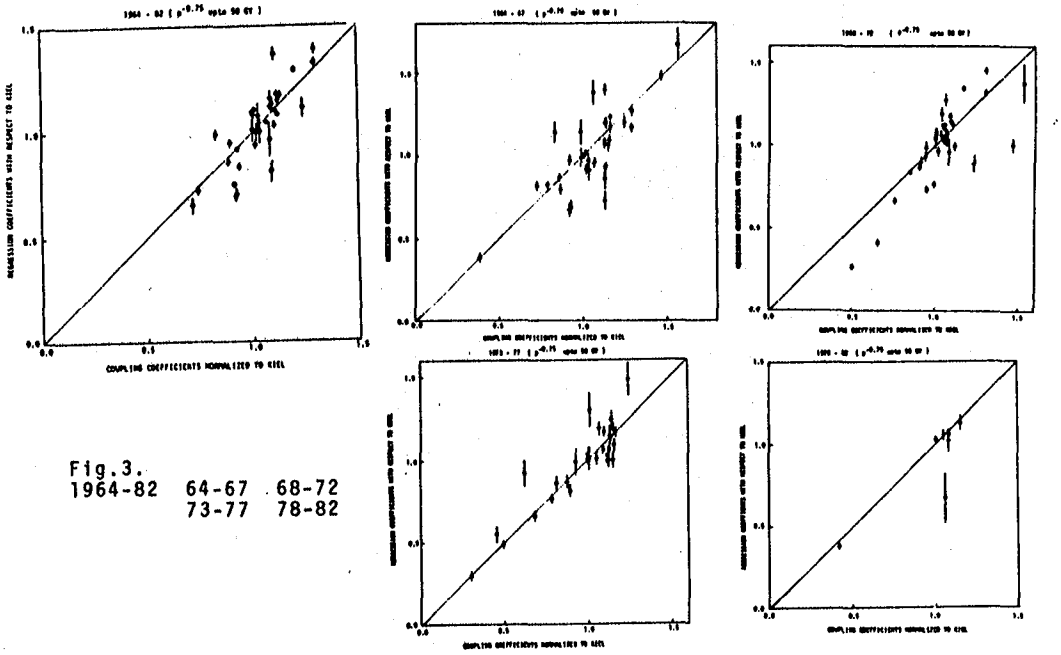

Fig.3.
1964-82 64-67 68-72
73-77 78-82

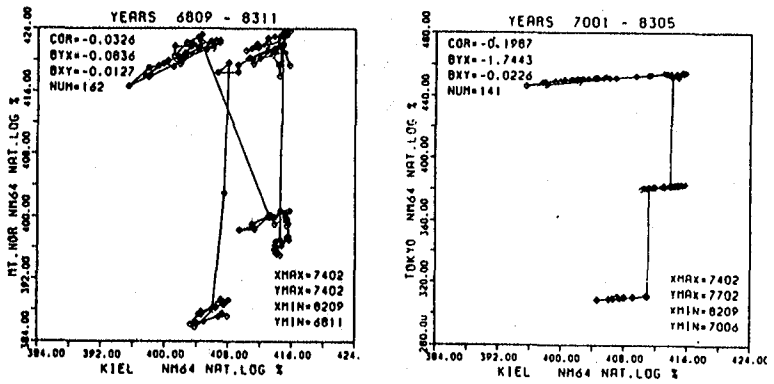

Fig.4.

RECORDING SYSTEM FOR THE SOLAR NEUTRON MONITORING AT MT. NORIKURA

Yu Shao Hua
Institute of Space Physics, Academia Sinica,
P.O. Box 5112, Beijing, China

M. Kusunose, H. Sasaki, N. Ohmori
Department of Physics, Kochi University,
Akebono-cho 2-chome, Kochi 780, Japan

K. Takahashi, and M. Wada
Cosmic Ray Laboratory, Institute of Physical and Chemical Research,
Kaga 1-chome, Itabashi-ku, Tokyo 173, Japan

ABSTRACT

In order to monitor the solar neutron events, a new recording system will be installed at Mt. Norikura Cosmic Ray Observatory. The recording system is composed of a pulse counter with clock and a microcomputer with minifloppy disk. The counter and the microcomputer are connected through the General Purpose Interface Bus line. The one-minute total count of neutron monitor is recorded on the minifloppy disk.

1. Introduction

Direct observations of the solar neutrons associated with solar flares were made at the earth, on June 21, 1980 and June 3, 1982 by the Gamma-Ray Spectrometer (GRS) on board the Solar Maximum Mission satellite (SMM).[1,2] It was reported that, on June 3, 1982, the solar neutrons were also detected by the ground-based neutron monitors at Jungfraujoch,[2,3] Lomnicky Stit,[4] and Rome.[5,6] From the analysis of the Rome NM-64 data, Iucci *et al.*[6] analyzed that the solar energetic neutron events could be detected by ground-based stations particularly when they were located at mountain altitudes and low latitudes.

Here, we present a plan to record the output of neutron monitor at Mt.Norikura (4-NM-64, altitude=2770m, cutoff=11.36GV) and, if possible, simultaneously at Tokyo (36-NM-64, altitude=20m, cutoff=11.61GV).

2. Recording hardware system

This system is contrived to record the total counts from the neutron monitor in every minute. Figure 1 shows the arrangement for recordings of the neutron monitor counts. The counter/clock is operated through the IEEE-488 standard digital interface bus for programable instrumentation (or General Purpose Interface Bus, GPIB). The control of GPIB and the data acquisition is operated by an ordinary microcomputer.[7]

The interface between microcomputer and GPIB is made by using an LSI (TMS9914, Texas Instruments), and 4 MHz clock pulse is supplied from the microcomputer. The control of the counter/clock is operated through an interface LSI (SM8530B, Nippon Precision Circuits).

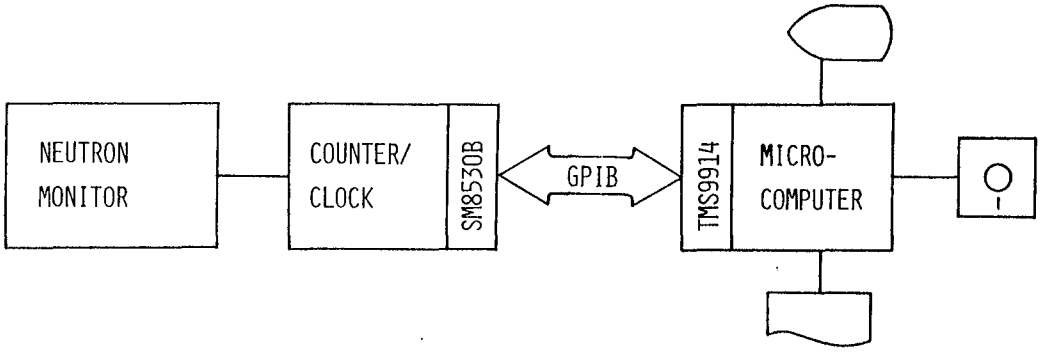

Fig.1. Blockdiagram of the recording system for the solar neutron monitoring.

3. Recording software system

The microcomputer is operated under the operating system of CP/M (Control Program for Microprocessors, Digital Research). The LSI TMS9914 that we used contains all of the logic necessary to interface TALK, LISTEN and CONTROL in accordance with GPIB. For the microcomputer, the control of GPIB means the read-and-write process to the various registers in the TMS9914. All programs which control the TMS9914, the floppy disk and the printer, are written in C language (C compiler by BD Software).

Figure 2 shows the flow chart of the operating program of the recording system. The counting rates of the neutron monitor in every one minute is transfered from the counter/clock to the memory of microcomputer, and written on the minifloppy disk in every ten minutes. Year, month, day, hour and minute are written at the beginning of the hour. The exchange of floppy disk can be operated between the ten minute recording. One block of data is composed of an hour data, which requires 128 bytes each. A sheet of floppy disk (in this case) can be operated for three months. The records on the floppy disk are transfered to a magnetic tape, and the data will be analyzed by using electronic computers.

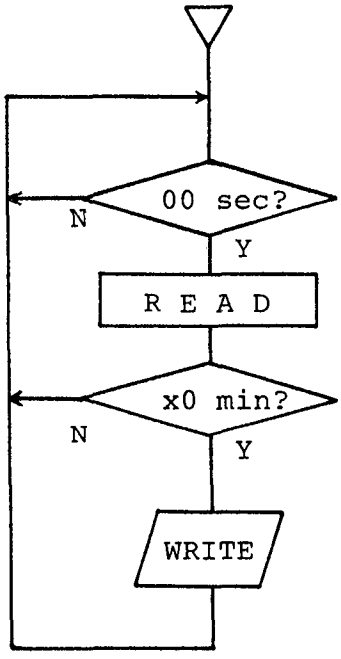

Fig.2. Flowchart of operating program.

Table 1. Distribution of neutron monitors.

Station	Jungfraujoch	Rome	Mt. Norikura	Tokyo
Monitor	IGY	12-NM-64	4-NM-64	36-NM-64
Latitude	46.55° N	41.91° N	36.11° N	35.75° N
Longitude	7.98° E	12.50° E	137.55° E	139.75° E
Altitude	3550 m	60 m	2770 m	20 m
Cutoff rigidity	4.48 GV	6.32 GV	11.36 GV	11.61 GV
Counting rates (Nov. 1977)	6.0×10^5 /hr	3.0×10^5 /hr	5.5×10^5 /hr	9.4×10^5 /hr

4. Discussion and Summary

As is seen in Table 1, Mt. Norikura station is located at an advantageous place, namely, mountain altitude, relatively low latitude, and different longitude from European stations. It is preferable that one minute record at Tokyo neutron monitor should be operated simultaneously to study the response and yield function for the solar neutron.

The features of the the recording system for the solar neutron monitoring are summarized as follows:

1) Using of the general purpose interface bus (GPIB) to facilitate the automatic data handling and also the alteration of the recording system.

2) By the adoptation of an ordinary microcomputer and the control and operation software in C language, it is easy to change operation system afterwards.

3) One minute count data from the neutron monitor are recorded on the minifloppy disk, which can endure for a long time record (in this case, three months).

5. Acknowledgments

One of the authors (YSH) had stayed for about three months at the Cosmic Ray Laboratory, Institute of Physical and Chemical Research and at the Department of Physics, Faculty of Science, Kochi University, and engaged in the development of the recording system of the solar neutron event. The authors are grateful to Mr. K. Kondo who is a student of Kochi University, for writing the control program mentioned in the text.

References

1) Chupp, E. L. *et al.*, (1982), Astrophys. J. (Letters), **263**, L95.
2) Chupp, E. L. *et al.*, (1983), *Proc. 18th Int. Cosmic Ray Conf., Bangalore*, **10**, 334.
3) Debrunner, H. *et al.*, (1983), *Proc. 18th Int. Cosmic Ray Conf., Bangalore*, **4**, 75.

4) Kocharov, G. E., (1983), Invited talks, *8th E. C. R. Symp., Bologna*, Tecnoprint, 51.
5) Iucci, N. *et al.*, (1984), Detection of solar neutrons by ground-based neutron monitors, Preprint.
6) Iucci, N. *et al.*, (1984), *Proc. Int. Symp. on Moduration in the Heliosphere, Morioka*, 429.
7) Kusunose, M. *et al.*, (1984), Mem. Fac. Sci., Kochi Univ., Ser. B, **5**, 19.

SH 9.1-9

BURST SIZE DISTRIBUTIONS IN THE DIGITIZED DATA OF THE ION CHAMBERS AT MT.NORIKURA AND SEA LEVEL STATIONS

M. Kusunose, M. Wada*, S. Kudo*, and L. S. Chuang**

Department of Physics, Kochi University,
Akebono-cho 2-chome, Kochi 780, Japan
* Cosmic Ray Laboratory, Institue of Physical and Chemical Research,
Kaga 1-chome, Itabashi-ku, Tokyo 173, Japan
** Department of Physics, The Chinese University of Hong Kong,
Shatin, New Territories, Hong Kong

ABSTRACT

A practical and simple method for burst rejection was applied to the digitized data of cosmic ray ion chambers at Mt. Norikura, Tokyo and Kochi. As a result of burst rejection, the burst size-frequency distributions in the digitized data at mountain altitude and sea-level ion chambers were obtained. The results show that there are no significant differences between the digital and analog data processing in the burst rejection.

1. Introduction

Cosmic ray ion chambers have been used for the continuous observation since the early days of cosmic ray studies. Five sets of Nishina-type ion chambers were built during the period from 1935 to 1941.[1,2] Continuous recording by those Nishina-type ion chambers had been started at Tokyo in 1948, Mt. Norikura in 1955, Hong Kong in 1970 and Kochi in 1979. At present, the digital recording systems for cosmic ray ion chambers[3,4] are in operation (see Table 1).

The burst distribution in ion chamber records is recognized from an abrupt change in charge up voltage. It is generated from a bremsstrahlung of muon or some nuclear interaction in lead absorber which covers the chamber to avoid undesirable radiation around the apparatus. Since the size of a burst sometimes exceeds total voltage variation in an hour, it should be rejected to reduce fluctuations. In this paper, we discuss on the burst rejection and the burst size distribution in the digitized data at Mt. Norikura, Tokyo and Kochi.

Table 1. List of Nishina type ion chambers in Japan

Station	Mt. Norikura	Tokyo	Kochi
Cutoff rigidity (GV)	11.36	11.50	12.88
Altitude (m)	2770	20	30
Atmospheric depth (g/cm^2)	740	1030	1030
Nishina type ion chamber	No.1	No.5	No.4
Argon gas pressure (kg/cm^2)	39	30	39
Electrometer output range (V)	30	10	10
Thickness of roof (g/cm^2)	20	10	120
Thickness of lead shield (cm)	10	10	10

2. Method of burst rejection

There is no *a priori* way of rejecting the burst data, since smaller bursts can not be distinguished from ordinary statistical fluctuations. As a method of burst rejection, Wada *et al.*[4] proposed to chose the threshold from the distribution, so that the average is not change.

Kusunose *et al.*[5] presented a practical method to separate bursts from the ordinary cosmic ray data on the assumption that the frequency of burst number per hour follows the Poisson distribution. We reduced the procedure of burst rejection, where the principle is the same as the previous method. The threshold of burst rejection is taken as $k_n\sigma_n$ (n=1,2,...), where σ_n are standard deviations and k_n are constants, which are determined so that the frequency of burst obeys the Poisson distribution. In the previous report, n was taken up to 10, now we reduce it to 3.

χ^2-test of the Poisson distribution was applied to the distribution of the burst frequency per hour. The results show fairly good fitness to the Poisson distribution except for a few cases. The distributions of one minute values as differences from averages of respective hours are shown in Fig.1. Curves A's are the distribution of one minute values due to ionization current of cosmic rays detected in the chamber, and B's are the distribution of the rejected burst values. As shown in the figures, both curves are separated each other reasonably.

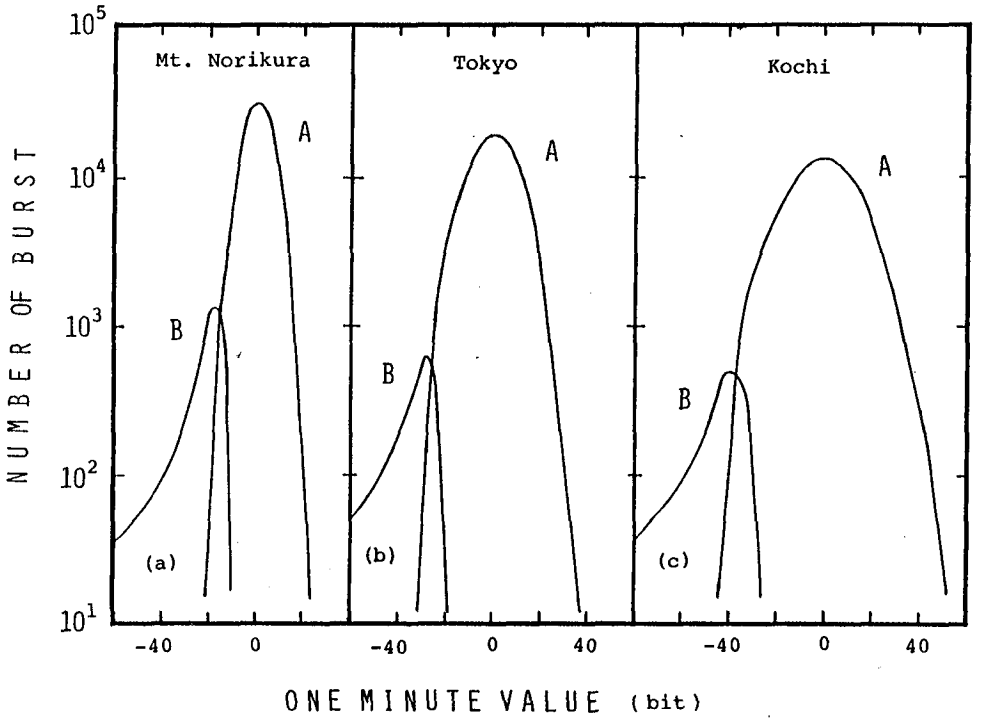

Fig. 1. Distribution of one minute values as deviation from the averages of respective hours at the period from May 24, 1980 to May 9, 1981.

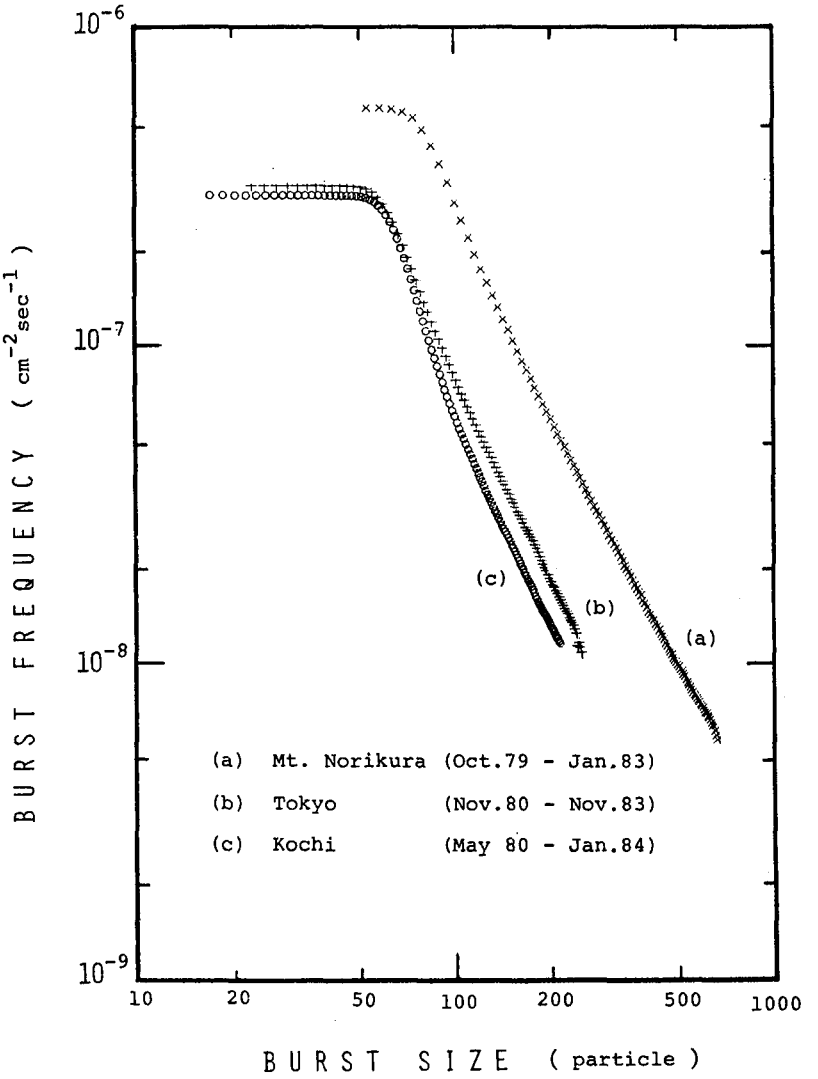

Fig. 2. Burst size-frequency distribution.

3. Burst size distribution

The integral size-frequency distributions of bursts thus obtained are shown in Fig. 2, where (a), (b) and (c) are those of Mt. Norikura, Tokyo and Kochi ion chamber respectively. In the figure, the burst size is represented in unit of particle that means the number of incident charged particles in a ion chamber. The frequencies of the bursts are indicated in the number of bursts divided by the time of total duration and by the horizontal cross-sectional area of the chamber.

The frequencies of the bursts at a point where the burst size is 200 particles, are shown as, 6.0×10^{-8} cm^{-2}sec^{-1} at Mt. Norikura, 1.83×10^{-8} at Tokyo, and 1.35×10^{-8} at Kochi. The burst frequency at Mt. Norikura is 3.3 times that of Tokyo. According to Kameda and Wada[6], it means that considerable parts of the total bursts at sea level are those induced by N-components. The ratio of Tokyo to Kochi is found as 1.3. It will be

explained by the difference in the cutoff rigidities and the thickness of roof materials.

The burst frequency spectrum can be expressed partly by the form of power function as $S^{-\gamma}$, where S is the burst size in unit of particle. We calculated the power γ in the range of burst size from 150 to 220 particles by the least square method. The results are $\gamma=2.07\pm0.01$ at Mt. Norikura, $\gamma=2.09\pm0.01$ at Tokyo, and $\gamma=2.09\pm0.01$ at Kochi. There is no significant difference among them.

4. Summary

In summary, we separated one minute data of cosmic ray ion chamber into the ordinary cosmic ray data and the burst data by the statistical way under the assumption that the number of bursts in one hour follow the Poisson distribution. The merit of this method is capable of testing the appropriateness of burst rejection by application of χ^2-test on the Poisson distribution.

As a result of the burst rejection, the distributions of burst size-frequencies were obtained. The differences of burst size spectrum bwteen Mt. Norikura and sea level ion chambers are generally in coincidence with the results of Kameda and Wada.

5. Acknowledgments

The observations at Mt. Norikura were made in cooperation with the staffs of the Norikura Cosmic Ray Station (by Prof. I. Kondo) of the Institute for Cosmic Ray research, University of Tokyo. The compilation of the data of Tokyo-Itabashi was performed by Mrs. K. Imai. Computer works were performed by using M-380, M-140F, and F270-30.

References

1) Ishii,C, (1944), Bull. I. P. C. R. (in Japanese), **23**, 535.
2) Miyazaki, Y., (1954), J. Sci. Res. Inst., **48**, 80.
3) Chung, L. S. *et al.*, (1981), *Proc. 17th Int. Cosmic Ray Conf., Paris*, **8**, 154.
4) Wada, M. *et al.*, (1982), Nucl. Instr. Meth., **200**, 457.
5) Kusunose, M. *et al.*, (1984), Mem. Fac. Sci., Kochi Univ., Ser. B, **5**, 15.
6) Kameda, T. and M. Wada, (1952), Prog. Theor. Phys., **7**, 1.

SENSITIVITY OF SINGLE AND MULTIPLE COSMIC RAY NEUTRONS TO THE SURROUNDING MEDIUM IN A LEAD-FREE MONITOR

Dorman I.V., Dorman L.I., Libin I.Ya.
Institute of Terrestrial Magnetism, Ionosphere and Radio Wave Propagation, USSR Academy of Sciences, I42092 Troitsk, Moscow Region, USSR

Korotkov V.K.
SVKNII, Magadan, USSR

In I98I-I985 the neutron component of cosmic rays was recorded, the effect of cosmic ray multiplication in lead being disregarded /I-2/. The recording device consisted of neutron counters placed in a polyethylene retarder (polyethylene tubes with wall thickness of 2 cm). The device registered neutrons formed directly on the surface or not deep underground; the intensity of neutrons depended on the chemical composition of the substance.

The neutron component was measured by a lead-free monitor in an expedition in the Moscow Canal, Belomor-Baltic Canal and in the Atlantic Ocean. Figure I presents the time variation of 5-minute data of the intensity obtained in the Belomor-Baltic Canal and in the Atlantic Ocean relative to the mean value in the open sea (in %, Fig.I b). The intensity is seen to increase considerably when cosmic rays pass through locks and ports. In different locks the amplitudes of the effect are different which is due to the difference in the depth, in the geometry of the locks, and in the chemical composition of the shore substance.

The observed intensity increases due to recording of additional neutrons formed in nuclear interactions in the shore substance. These neutrons leave the nucleus at the evaporation stage, and the larger the mass number of the nucleus, the more the amount of evaporating neutrons for a given energy of an incident particle. Thus, it seems possible to use the method of recording multiplicities for the determination of substance composition since these neutrons can be considered as multiple. The possibility of their recording is much smaller than in local-generation detectors because of a large distance from the place of their formation to the place of recording. For this reason the counting level for multiplicity $k = 2$ is not high relative to the total count and is negligibly small for higher multiplicities. Nonetheless, since the increase in the count is just due to multiple neutrons, it is reasonable to record multiplicities.

Besides the total intensity, the multiplicities were al-

so recorded in the Belomor-Baltic Canal. Along with intensity variations δI, Fig.I demonstrates the $\delta I_{\geq 2}$ time dependence of δI, which is the multiple neutron intensity variation for multiplicity $k = 2$ and the mean multiplicity k for the time of passing through the Canal (from 5-minute data). The results of these measurements show a synchronous variation in the level of count of I and $I_{\geq 2}$. But if the increase of the intensity I in locks makes up on the average 20-30 %, for multiplicities $k \geq 2$ the increase reaches 2000-3000 %. This difference confirms the fact that the intensity increase in locks is due to recording of neutrons formed in interactions between cosmic rays and lock-wall or shore substance nuclei. (In the open see this effect is relatively small - the rate of counting of $I_{\geq 2}$ is about 3 pulses per 5 minutes). Thus, the data on the multiplicities are many times more sensitive to the influence of the environment than the data on the total intensity, the rate of counting multiple neutrons formed in CR - air interactions being negligibly small. Standard deviations in locks for δI and $\delta I_{\geq 2}$ make up 2 and 300 %, which in the relative units make up about 8 and II %, respectively. Therefore, in spite of the small rate of $I_{\geq 2}$ count, the accuracy in determining the variation $\delta I_{\geq 2}$ is comparable with the accuracy of determining the intensity variations. Thus, the information on the surrounding medium is more complete if neutrons are recorded by both methods. Because of its smallness, the mean multiplicity does not react to the surrounding medium since statistic fluctuations overlap possible variations.

The influence of the chemical composition of the surrounding medium on multiplicity distribution is of considerable interest. Within the statistical error of measurements the multiplicity distribution for a lead-free neutron monitor is exponential, $I_K \sim \exp(\lambda_K)$ (Fig.2), the parameter λ depending on the position of the neutron monitor; in locks with rocky shores (Fig.2, curve I) $\lambda = 3.70 \pm 0.08$; in locks with ordinary ground (curve 2) $\lambda = 4.00 \pm 0.10$; between locks with a distance to the shores of 4-8 m, $\lambda = 4.11 \pm 0.11$ (curve 3); in the open see $\lambda = 7.0 \pm 0.6$ (curve 4). In locks with rocky shores (Fig.I, locks N 6-9) λ decreases, in locks with ordinary groung such a decrease is not observed. In the open see the intensity $I_{\geq 2}$ makes up only 0.I % of the total intensity which is responsible for a corresponding maximum value of λ. (It should be noted that the riverside effect on the intensity makes up I0-20 % if the distance to the banks is I0-I5 m. As the distance increases to I00 m, the riverside effect vanishes and the data on the intensity correspond to those obtained in the open see).

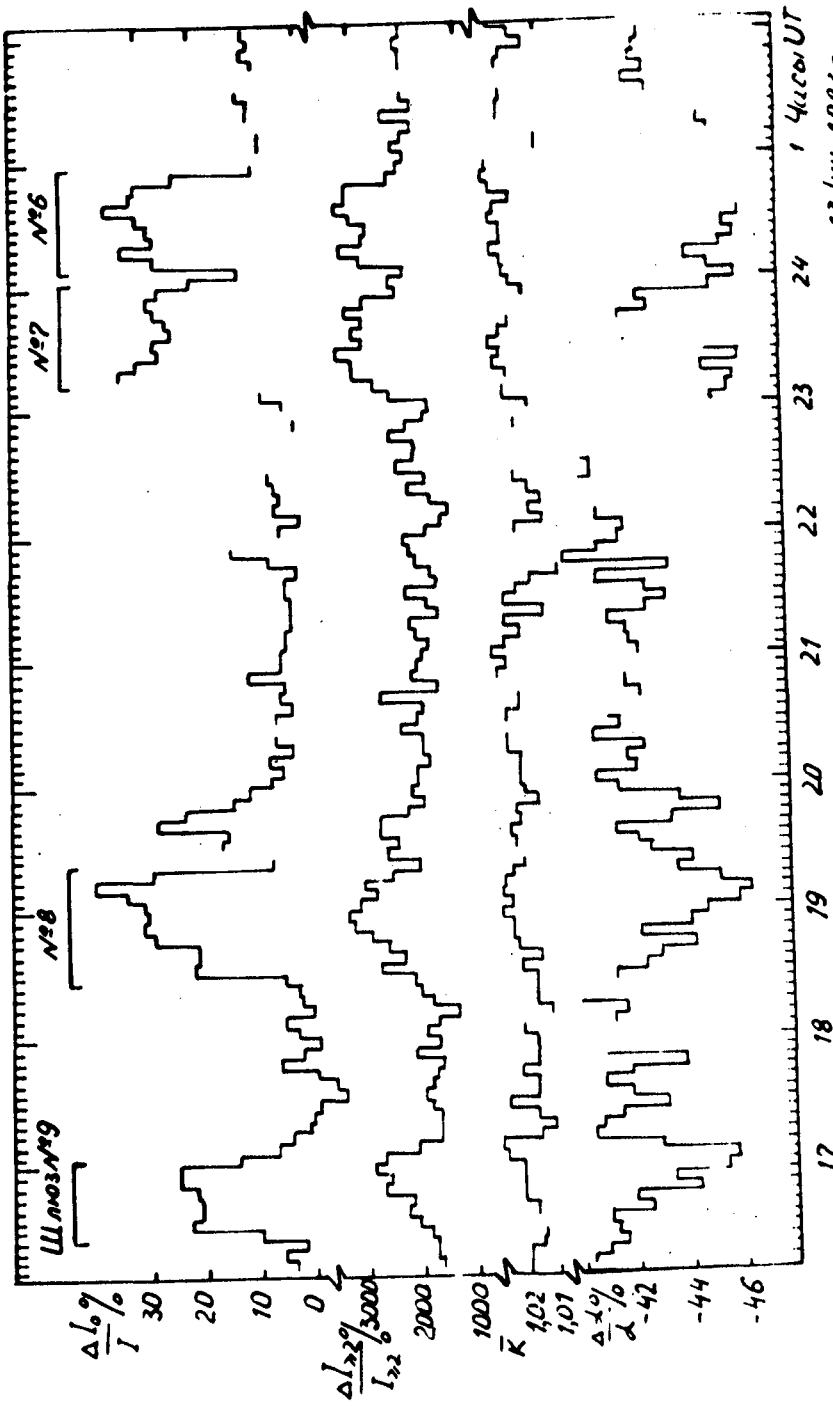

Fig. 1

REFERENCES

I. Dorman L.I. Cosmic Ray Variations. M.: Gostekhteoretizdat, I957, p.492.

2. Babayan V.Kh., Mashkov Yu.E., Ptuskin V.S. in: Cosmic Rays. M.: Nauka, I983, p.66.

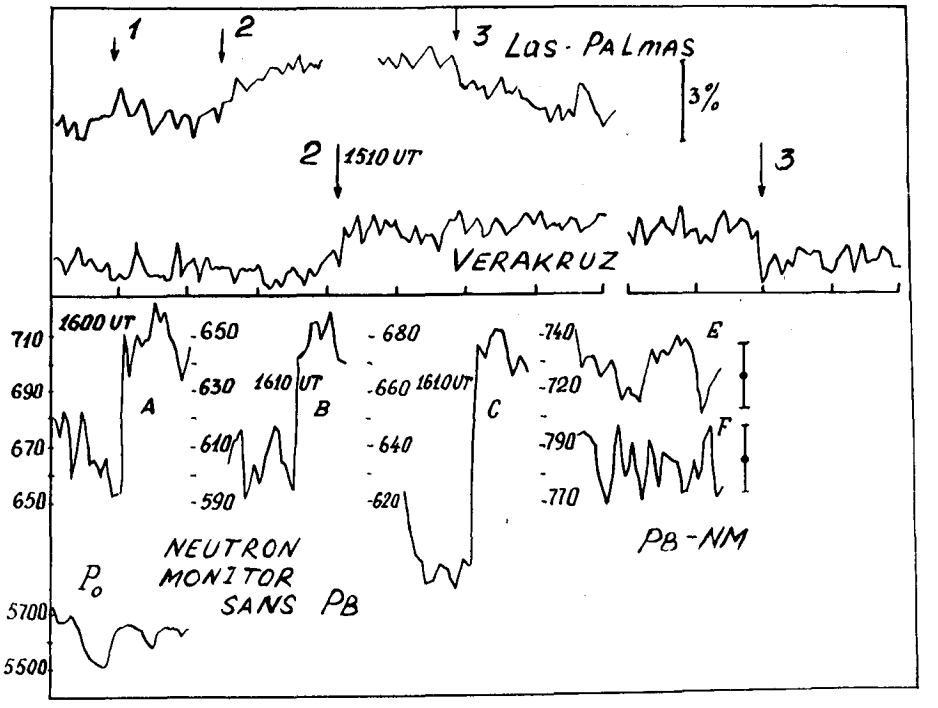
1
2
3
LAS-PALMAS
3%
2
1510 UT
3
VERAKRUZ
1600 UT
1610 UT
1610 UT
A
B
C
E
F
710
690
670
650
650
630
610
590
680
660
640
620
740
720
790
710
NEUTRON
MONITOR
SANS PB
PB-NM
Po
5700
5500

Fig. 2

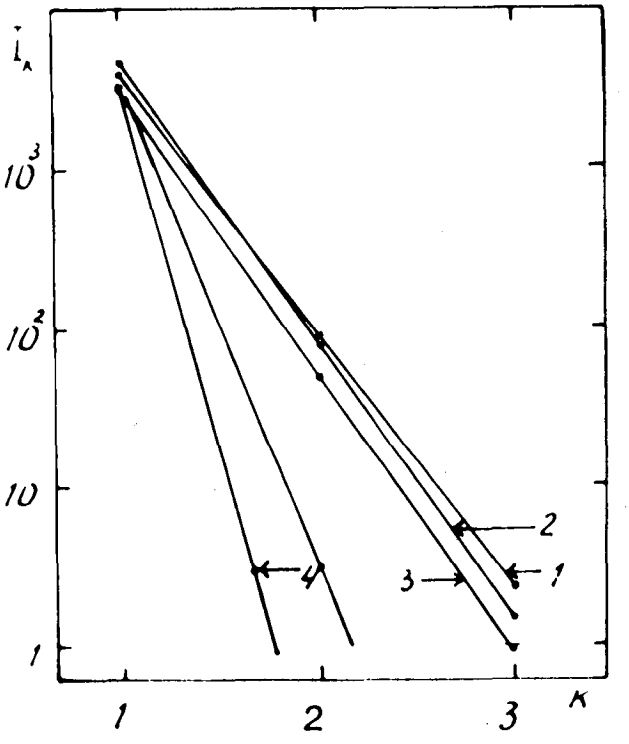
I_A
10^3
10^2
10
1
1
2
3
K
2
1
3
4

Fig. 3

SH 9.1-11

PLASTIC SCINTILLATORS IN COINCIDENCE FOR THE STUDY OF MULTI-PARTICLE PRODUCTION OF SEA LEVEL COSMIC RAYS IN DENSE MEDIUM

L.S. Chuang and K.W. Chan
Department of Physics, The Chinese University of Hong Kong
Hong Kong

M. Wada
Cosmic Ray Laboratory, The Institute of Physical and Chemical Research
Tokyo, Japan

1. Introduction. Cosmic-ray particles at sea level penetrate a thick layer of dense medium without appreciable interaction. These penetrating particles are identified with muons(1). The only appreciable interaction of muons are by knock-on processes(2). A muon may have single, double or any number of knock-on with atoms of the material so that one, two, three or more particles will come out from the medium in which the knock-on processes occur. The probability of multi-particle production is expected to decrease with the increase of multiplicity.

The present report presents measurements of the single, double, and triple particles generated in a dense medium (Fe and Al) by the sea level cosmic rays at 22.42 N. Lat. and 114.20 E. Long. (Hong Kong) using a detector composed of two plastic scintillators connected in coincidence.

2. Experimental. The detector consists of two units, each of which comprises a plastic scintillator, 1 m^2 x 5 cm, and an RCA-8055 (ϕ = 12.7 cm) photomultiplier tube installed in a light-tight iron case as shown in Fig. 1. A block diagram of the counting system is also shown in Fig. 1. The whole system is installed in a room where the room temperature is kept within 20 ± 1°C.

By adjusting the high voltages and the amplifier-gains, differential pulse height spectra for each of the detector systems, as shown by curve (A) in Fig. 2, were brought to nearly matching. Then, setting the high voltages and the amplifier-gains at the optimum values and the SCA discriminator of the upper detector fully open, coincidence measurements of the signals from the upper and the lower detectors were made by varying the SCA discriminator level of the lower detector with the channel width 0.1 V. A suitable resolving time of the coincidence unit was chosen to be 0.5 μs so that the accidental coincidence counts were always negligibly small (i.e. less than 0.01 cpm against a counting rate of about 1000 cpm in each of the two detectors.

Keeping the two detector surfaces 11.7 cm apart and having the dense medium, Fe or Al slabs, of varying thicknesses placed between the detectors, the coincidence pulse height spectra were measured for each of the varying conditions (Fig. 2; curves (B)).

With Fe-absorber, the peak positions for triple-particle spectra are clearly appearing in the multi-particle spectra, e.g. at discriminator level 2.48 in Fig. 3(B). The corresponding peak area, however, can hardly be determinable due to poor counting statistics. Existence of triple-particle is further confirmed by the nearly equidistances of the triple-particle peak position from that of the double-particle (ΔL = 0.76) and the double-particle peak position from that of the single-particle (ΔL = 0.72). (Fig. 2(B) and 3(B))

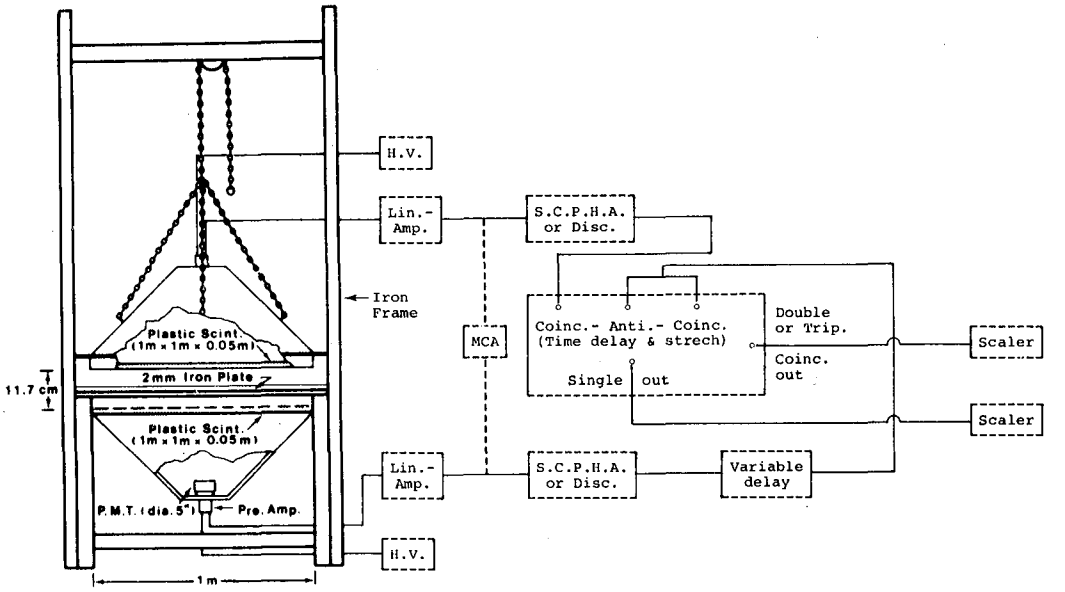

Fig. 1 The detector and the counting system.

The same procedures as above were applied in the measurements using Al-absorber of thicknesses 1.28 - 5.29 cm. None of the four absorption curves obtained gave good linearity to be able to obtain the absorption coefficient. Inspection by superpositions of the spectra for the four different absorber thicknesses with the single-particle spectrum reveals the poor absorption power of Al-absorber - little evidence of absorption or with irregularities, if any, in the multi-particle free portion and also in the portion where multi-particle contribute. This is thought to be due to very poor absorptivity and thus poor productivity for multi-particle of Al-absorber in the present experimental conditions.

3. Data analysis and Results. Each of the five pulse height spectra resulting from coincidence measurements, Fig. 2(B), is expected to be a result of superpositions of the multi-particle pulse height spectra over the single-particle spectrum.

To obtain the multi-particle spectra, the single particle spectrum (This spectrum too is superposed with multi-particle spectra due to the 0.4 cm thick Fe medium making up the surfaces of the detector housings) which has been corrected for absorption in the absorber is used for subtraction from the experimental spectrum which is placed with an absorber. An exponential form of absorption is adopted with reference to the nature of absorption of charged particles in passing through matter. In the lower pulse heights region, i.e. where the discriminator levels are smaller than that for the peak point of the spectrum, effect of multi-particle is absent. In this region, we have $\ln(I_o(L)/I(L)) = \mu(L - L_o)$ (where $I_o(L)$ and $I(L)$ are the coincidence counting rates of the single-particle, with pulse height L, before and after passing through the absorber, and μ is a linear absorption coefficient of the absorber for the sea level cosmic-ray particles. L_o is a threshold discriminator level which is a constant of the system). From the plots of $\ln(I_o(L)/I(L))$ versus $(L - L_o)$ for the various absorber thicknesses, e.g. Fig. 3(A), the

slopes μs are obtained with an average value 0.15 ± 0.06. Once μ is known, the multi-particle spectra can be determined from $I(L) - I_o \exp(-\mu(L-L_o)) = I_2(L) + I_3(L) + \ldots$ (where $I_2(L)$, $I_3(L)$ ..., are the double-triple-, and the successive higher order multi-particle spectrum, respectively.)

Defining the peak area (K) as a product of the peak value and the FWHM of the peak, we obtain an average value of (K_d/K_s) as 0.07 ± 0.01 for Fe-absorber (where the subscripts d and s denote for double-particle and single-particle, respectively) which is identical to say that the probability of double-particle production in Fe-absorber of thicknesses ranging 0.65 - 4.97 cm is 0.07 ± 0.01.

To the single-particle spectrum, a Gaussian curve is fit to the single-particle portion. The difference between the experimental curve and this hypothetical curve is considered as due to the multi-particle spectra. A remarkable double-particle peak with a value 0.07 for K_d/K_s is also obtained.

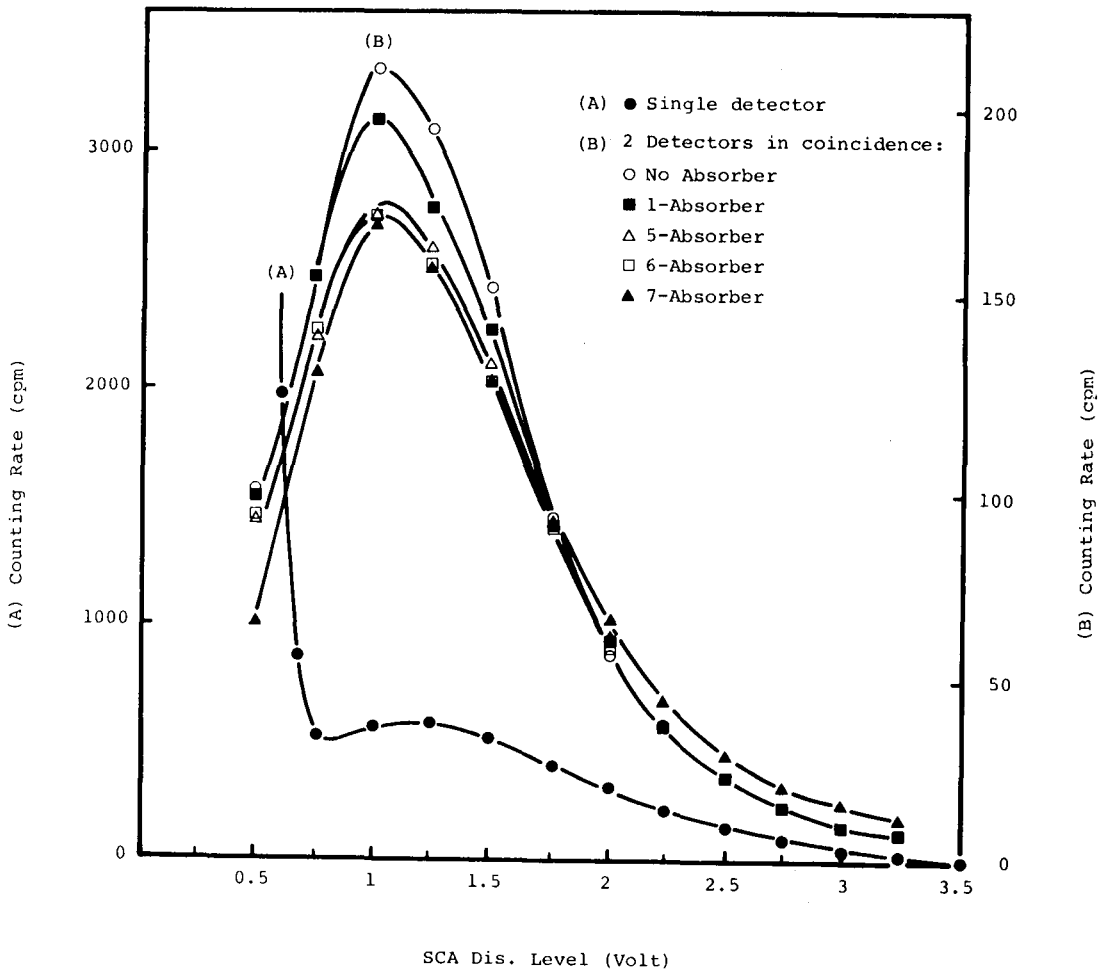

Fig. 2 Pulse height spectra: (A) taken with single detector (B) taken with upper and lower detector in coincidence (Dis. levels: upper fully open; lower varied from 0.5 to 3.25 with channel width 0.1 V).

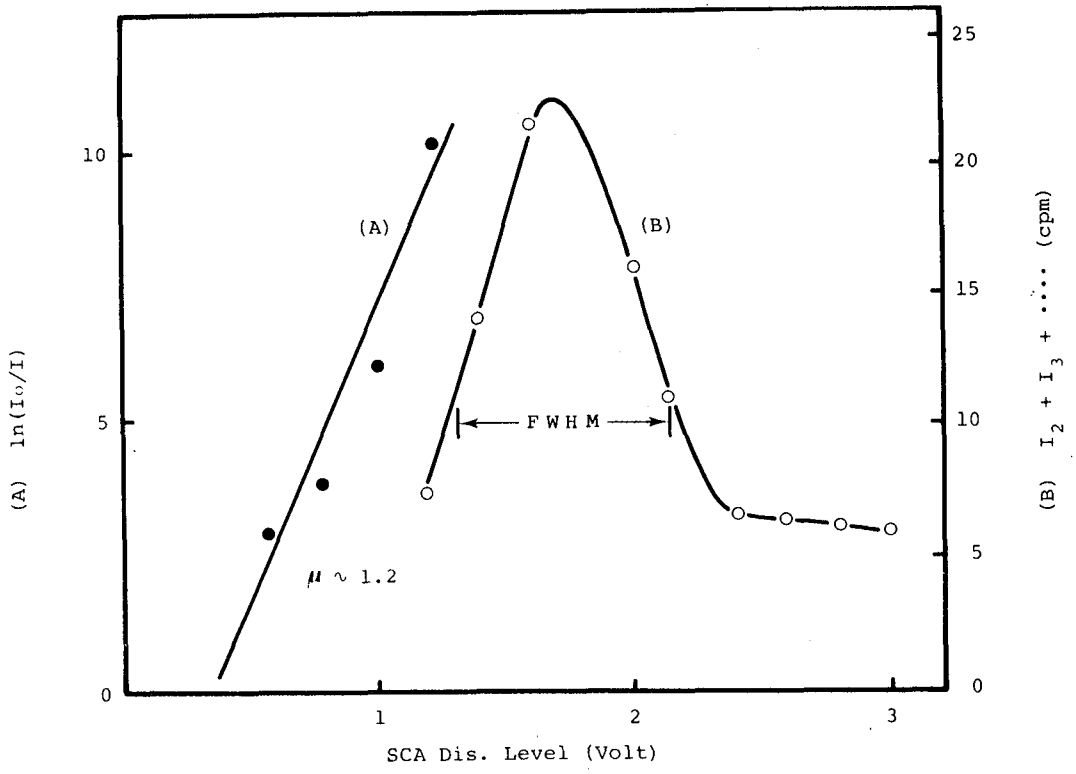

Fig. 3 (A) Absorption curve for single-particle in Fe.
(B) Double-particle peak and triple-particle component seen at Dis. level 2.3 - 3.0.

4. Discussion. The average value 0.07 ± 0.01 for the probability of double-particle production per muon (i.e. one knock-on process) in Fe-absorber of thicknesses 0.4 to 4.97 cm, which is negligibly small as compared to the range of sea level muons in Fe-absorber (e.g. 71 cm of Fe for muon with momentum 1000 MeV/c(3)) seems reasonable from the following comparisons with theoretical information: Taking the value 0.07 per g cm^{-2} to be the probability of double-particle production (one knock-on process) in Fe medium the agreement with the theoretical calculation of 0.14 per g cm^{-2} in Fe medium(4) for muons with the average momentum of sea level muons, 3500 MeV/c(5), is rather good. Present result for the average value of energy transfer per knock-on is estimated to be about 29 MeV with the rate of energy loss in Fe medium by 3500 MeV/c muons taken as 2 MeV per g cm^{-2}(3). While, the calculated maximum transferable energy per knock-on is 545 MeV.

References

1. Hayakawa, S., Cosmic Ray Physics, Interscience, John Wiley & Sons, New York, 318 (1969).
2. Bhabha, H.J., Proc. Roy. Soc. A154, 195(1936).
3. Rossi, B. and Greisen, K., Rev. Mod. Phys. 13, 240(1941).
4. Hayakawa, S., (1969), Cosmic Ray Physics, Interscience, John Wiley & Sons, New York, 412.
5. Kocharian, N.M., et al., J. Exp. Theor. Phys. USSR, 30, 243(1956). Janossy, L., Cosmic Rays, 2nd Ed., Oxford at the Clarendon Press, 172(1950).

SONTRAC: A Solar Neutron Track Chamber Detector

Glenn M. Frye, Jr., Thomas L. Jenkins, Alan Owens
Physics Dept., Case Western Reserve University
Cleveland, Ohio 44106, U.S.A.

1. Introduction. The recent detection on the SMM satellite of high energy neutrons emitted during large solar flares (1) has provided renewed incentive to design a neutron detector which has the sensitivity, energy resolution, and time resolution to measure the neutron time and energy spectra with sufficient precision to improve our understanding of the basic flare processes. Over the past two decades a variety of neutron detectors has been flown on satellites and high altitude balloons to measure the atmospheric neutron intensity above 10 MeV and to search for solar neutrons. Most of these detectors have relied on n-p scattering as the basic detection process. In this paper we describe the SONTRAC (Solar Neutron Track Chamber) detector, a new type of neutron detector which utilizes n-p scattering and has a sensitivity 1-3 orders of magnitude greater than previous instruments in the 20-200 MeV range. The energy resolution is 1% for neutron kinetic energy, $T_n > 50$ MeV. When used with a coded aperture mask at 50 m (as would be possible on the space station) an angular resolution of ~ 4 arc sec could be achieved, thereby locating the sites of high energy nuclear interactions with an angular precision comparable to the existing x-ray experiments on SMM.

The scintillation chamber has been investigated as a track chamber for high energy physics, either by using arrays of scintillating optical fibers or by optical imaging of particle trajectories in a block of scintillator. Recently square plastic scintillation fibers 0.2 and 0.1 mm in size have been developed (2), which makes it possible to construct a block of plastic scintillator composed of alternate layers of x and y oriented fibers in which the range and direction of proton recoils from n-p scattering can be determined with a spatial resolution of approximately 0.1 mm. The 4π geometry and high spatial resolution make possible the enhanced detection efficiency and energy resolution over existing techniques.

2. Detection Efficiency and Energy Resolution. Neutrons interact in plastic scintillator either by elastically scattering from hydrogen or by interacting with carbon (n-C). The n-p events (Fig. 1) are the most useful. If the source is a point source and its direction is known, measurement of the energy and direction of the recoil proton in a single scattering is sufficient to determine the incident neutron energy. For a double scattering event where the energies and directions of both recoil protons are measured, the energy and direction of the incident neutron are uniquely determined. Thus double scattering events can be used to measure the neutron intensity from an extended source such as the secondary neutrons produced in the atmosphere

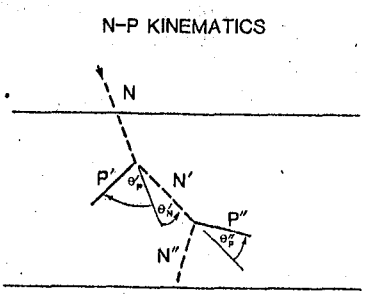

SINGLE SCATTER:

$$T_N = T_p' / \cos^2\Theta_p' = T_p' / \sin^2\Theta_N'$$
$$\Theta_p' + \Theta_N' = \pi/2$$

DOUBLE SCATTER:

$$T_N' = T_p'' / \cos^2\Theta_p''$$
$$T_N = T_p' + T_N'$$
$$\vec{P}_N = \vec{P}_p' + \vec{P}_N'$$

Fig. 1. The kinematics for n-p scattering.

by the primary cosmic radiation. When a localized source such as the Sun is observed, the background is greatly reduced by restricting the accepted events to a cone about the solar direction. The interpretation of single and double tracks in plastic scintillator is complicated by (n,p) and (n,d) reactions in carbon. Fig. 2 shows the effective cross sections for $^{12}C(n,p)$ + $^{12}C(n,d)$ for proton kinetic energies T > 10 and 15 MeV. Above 90 MeV the inelastic carbon cross section is an upper bound. The effective n-p scattering cross sections for the same threshold were calculated using the angular distribution parameterization of Rindi et al (3). Below 50 MeV n-p scattering predominates and single scattering can be used. Above 50 MeV, where the sum of the effective carbon cross section is larger than the effective n-p cross section, the kinematic criterion that $\Theta'_p + \Theta'_n = 90^o$ identifies the double scattering events in which the first proton is from an n-p scatter. Above about 200 MeV most of the interactions will result in the emission of several particles from carbon which can be used to infer the neutron energy. SONTRAC's performance therefore is characterized by three interaction modes. The energy ranges over which these modes are applicable overlap, thereby providing a check of internal consistency.

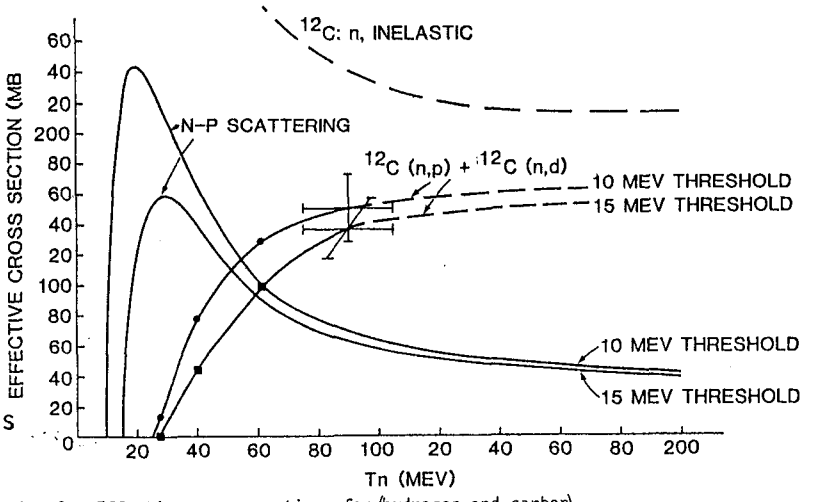

Fig. 2. Effective cross sections for (hydrogen and carbon).

A. Single Scattering Mode. The detection efficiency in the single scattering mode is shown in Fig. 3 for an infinite slab of CH of various thicknesses where the neutron direction is normal to the slab and the proton track stops within the slab. The curves reflect the initial rise above the threshhold energy, the decrease in the n-p cross section with energy, and an increase in slope above 100 MeV as tracks are increasingly lost out the bottom. The corrections for loss of tracks out the sides of a finite size detector are small. For a cube 60 cm on a side, the efficiency is reduced by 2.7% at 100 MeV and 9.5% at 200 MeV. The high efficiency in the 15-40 MeV region where n-C contamination is low makes the single

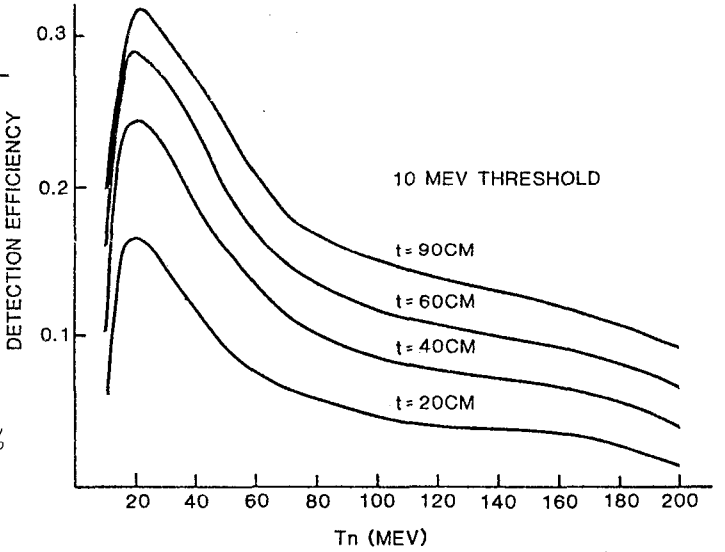

Fig. 3. Calculated detection efficiency as a function of neutron energy for an infinite slab of CH in the single scattering mode.

scattering mode particularly useful in determining the low energy portion of the solar neutron spectrum. This is especially important for small flares as the flux is reduced by neutron decay; e.g. 93% of the 20 MeV neutrons decay over the 1 AU flight path. Above 50 MeV the effective cross section for $^{12}C(n,p) + {}^{12}C(n,d)$ is greater than for n-p scattering. For a given neutron kinetic energy the protons observed at a particular angle have a distribution in energy extending from the maximum permitted by the reaction kinematics down to the threshold energy. In practice the deconvolution of the carbon protons will be less precise than that of the proton recoils where the width of the energy point spread function is due primarily to the instrumental energy resolution.

B. Double Scattering Mode. The detection efficiency for the double n-p scatters can be found by folding the single scattering results with the n-p angular distribution. The efficiency for a 60 cm thick infinite slab is 2% or greater over most of the 25-100 MeV range and > 1% for $T_n < 200$ MeV. This is two orders of magnitude greater than previous double scattering detectors where the energy and direction of both recoils were determined. Of comparable importance is the use of the 90^o criterion to identify the first scattering as n-p. The neutron energy is given by $T_n = T_p/\sin^2\theta_n'$ and the uncertainty by $\Delta T_n/T_n = [(\Delta T_p'/T_p')^2 + (2\cot\theta_n'\Delta\theta_n')^2]^{\frac{1}{2}}$. The second term is small because $\Delta\theta \sim 10^{-3}$. For $T_n > 50$ MeV, the predominate contribution to ΔT_p comes from the straggling in the proton range; therefore $\Delta T_p/T_p < 1\%$. The second proton may result from n-C rather than n-p without affecting the above analysis for solar neutrons. However if the source direction is unknown, the contamination of n-C protons will introduce an additional contribution to ΔT_n. The energy and directional resolution can be determined by a Monte Carlo simulation or by an accelerator calibration of the instrument.

C. Calorimeter Mode. At 100 MeV the n-C inelastic cross section is a factor of three greater than the n-p cross section, increasing to a factor of six at 300 MeV. Although some of this energy escapes in secondary neutrons or γ's and the various possible reactions have different Q values, a measurement of the ionization of the secondaries and/or their ranges can yield the incident solar neutron spectrum.

3. Response to Solar Flare Neutrons. The energy spectrum of the solar flare of June 3, 1982 has been determined over the range 20-1000 MeV in three separate observations (4,5,6). The neutron fluence for 20-200 MeV was 500 cm^{-2}. A 60 cm cubic SONTRAC detector would detect 5×10^4 events spread over half an hour. During the same interval the atmospheric background could contribute $\sim 10^2$ events within 5^o of the sun. Thus a flare with neutron emission 10^{-3} of the June 3, 1982 event would be detectable at the 5σ level. Also of interest in the study of solar flares is the time correlation between neutron emission and the time structure of flare emitted electromagnetic radiation. The timing uncertainty is given by $\Delta t = (\Delta T_n/T_n)\,\tau\,(\gamma+1)^{-1}(\gamma^2-1)^{-\frac{1}{2}}$, where γ is the Lorentz factor and $\tau = 500s$ is the light transit time over 1 AU. For $T_n = 100$ MeV, $\Delta t = 3s$. This resolution is sufficient to resolve the 1 min time structure seen on some flares (4).

4. Location of Emission Region. The coded aperture mask technique has recently been applied to the imaging of high energy electromagnetic radiation. The complications introduced by a finite mask thickness and

only partial absorption in the mask have been considered in a similar context for high energy γ-ray astronomy (7), Because SONTRAC locates the neutron in the detector to an accuracy of 0.1 mm, the method is also applicable to the imaging of neutrons with an angular resolution determined by the pinhole geometry, as long as the mask cell size is large compared to the spatial resolution of the detector. For a cell size of 1 mm and a mask-detector separation of 50 m, the angular resolution is 4". At 50 MeV 10 cm of Fe gives 90% absorption. The mask vignetting angle of 0.6^{0} is greater than the angular width of the Sun; thus the entire solar disk can be imaged with comparable resolution.

5. Discussion. SONTRAC has the sensitivity and energy resolution to measure the temporal neutron energy spectrum from solar flares over a dynamic range of 10^3. This capability will make possible precision neutron measurements on a large number of flares during the next solar maximum. Determination of the neutron spectra for many flares will provide information on the statistics of ion acceleration, the acceleration time, the ion energy, the He content of the ions, the time dependence of the ion spectra, and possible beaming of the accelerated ions.

Observations of solar neutrons are best done from a satellite, since the long observing time makes it possible to detect a large number of flares in a low background environment. SONTRAC meets the criteria recommended for the neutron detector in the High Energy Cluster on the Advanced Solar Observatory (8). In the past it has not been practical to observe large flares from balloons because the flight times were at most of a few days duration and predictions of the flare time of occurrence were not reliable enough to give a reasonable probability of observation. Recently the RACOON technique has made it possible to obtain flights of several weeks duration (9). It has been found during the present solar cycle that large flares exhibit a 154 day periodicity (10) The combination of longer flight duration and cyclic flare occurrence make balloon observations of solar flare neutrons feasible. Flare observations from balloons have an advantage over satellites in that the 12 hr/day observation window is long compared to the flare duration. Therefore most flares will be observed in their entirety even though the neutrons are delayed in their arrival at the earth relative to the E-M radiation.

References

1. Chupp, E.L., et al, (1982), Ap. J. Ltts 263, L95.
2. Binns, W.R., et al, (1983), Nuc. Instr. Meth. 216, 475.
3. Rindi, A., et al, (1970), UCRL-20295.
4. Chupp, E.L., et al, (1983), 18th Int. Conf. CRP 4, 374, Bangalore.
5. Debrunner, H., et al, (1983), 18th Int. Conf. CRP 4, 75, Bangalore.
6. Evenson, P., et al, (1983), Ap. J. 274, 875.
7. Carter, J.N., et al, (1982), M.N.R.A.S. 198, 33.
8. Walker, A.B.C., et al, (1984), The Adv. Solar Obs. Exe. Sum. NASA GPO 1984-746-070/179.
9. Koga, R., et al, (1985) This Conference, Paper SH 1.4-6.
10. Reiger, E., et al, (1984), Nature 312, 623.

THE NEUTRON MODERATED DETECTOR AND GROUNDBASED COSMIC RAY MODULATION STUDIES

P.H. Stoker and B.C. Raubenheimer
PU-CSIR Cosmic Ray Research Unit
Department of Physics
Potchefstroom University for CHE
POTCHEFSTROOM 2520
South Africa

ABSTRACT

Over the past years several reports have appeared on modulation studies with the neutron monitor without lead. Some of these studies cast doubt on the reliability of this detector. We report here on the stability of the neutron moderated detector (NMD) at Sanae, Antarctic. The barometric coefficient of the 4NMD for epoch 1976 appears not to differ statistically from the 0.73%/mb of the 3NM64. The monthly averaged hourly counting rate of our 4NMD and 3NM64 correlates very well (correlation coefficient: 98%) over the years from 1974-1984, with the 4NMD showing a 8% larger longterm modulation effect than the 3NM64, indicating a difference in sensitivities of the two detectors. From this difference in sensitivities spectra of ground level solar proton events and modulation functions of Forbush decreases were deduced.

1. Introduction. A neutron counter surrounded by a low Z moderator records at ground level secondaries produced by primary cosmic rays with primary energies down to ~ 1 GeV. The counting rate may be increased significantly when high Z materials are also part of the neutron monitor geometry because of the much larger rate of neutron production by cosmic rays in the heavier materials (Simpson and Uretz, 1953).

It was shown by Mischke et al. (1973) that the neutron moderated detector (NMD), consisting of BP28 Chalk River neutron counters surrounded by paraffin wax but without lead, is more sensitive to low rigidity (~ 1 GV) primary cosmic rays than the NM64 super neutron monitor. They reported on differential response functions deduced from aircraft latitude surveys at 30 000 feet pressure altitude for both the NMD and NM64 and on the altitude dependence of the counting rates of these two detectors at different cutoff rigidities. They have also shown that the fractional variations in counting rates of these two detectors are different during ground level solar proton events and that the hardness of the relativistic solar protons as described by the spectral rigidity function may be deduced from the relative increases in counting rates above the cosmic ray background.

In this paper we report on the performance of the 4NMD in comparison with the 3NM64 at Sanae, Antarctica (72°S 02°W). Zhu and Kawasaki (1983) occasionally observed fluctuations in the counting rate of a neutron monitor without lead in comparison with the counting rate of the Tokyo super neutron monitor. When raining the counting rate of the neutron monitor without lead was decreased, while the cause of many other fluctuations in counting rate could not be traced. Similar problems were experienced by other investigators. We found on the contrary that changes in counting rates of the 4NMD and 3NM64 correlate well with each other and that the relative changes in counting rates of the two detectors may be related to temporal variations in the low rigidity portion (~ 1 GV) of the primary cosmic ray spectrum (Stoker et al., 1979). Simpson (1951) reported that local production in materials

of high atomic weight and slowing down of neutrons in hydrogenous materials were the principle sources of erroneous results with the neutron moderate detector. At Sanae the local environment is hydrogenous throughout the year and the snow fall amounting to 2 meters annually does not effect the counting rate. The station is situated on a ice shelf.

2. Experimental details. In Figure 1 curves a, b and c are representing the sensitivity of neutron counters surrounded by paraffin wax of thicknesses 1.25 cm, 7.5 cm and 12.5 cm respectively as a function of neutron energy (Hess et al., 1959). Also shown is the sensitivity as a function of neutron energy (curve d) for a NM64 neutron monitor (Hatton, 1971). It appears that the contribution to the counting rate by environmentally produced low energy neutrons may be reduced by surrounding a neutron counter with a relatively thick layer of paraffin wax.

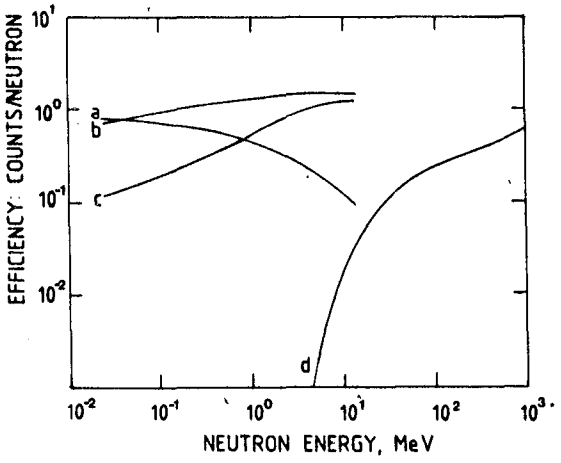

Figure 1

The 4NMD at Sanae consists of 4 BP28 Chalk River neutron counters, each of which is, together with its polyethylene cylinder, inside a paraffin wax cylinder with a wall thickness of 7.5 cm. These 4 paraffin wax cylinders with their neutron counters are enclosed in a rectangular aluminium container, having cavity walls filled up with paraffin wax of 5 cm thickness. This container is temperature controlled. The 3NM64 neutron monitor is enclosed in a similar temperature controlled container. Each container is inside a small wooden hut with heat insulated walls, about 3 meters above snow level and some 100 meters away from the station and its invironment.

3. Intercomparison of changes in counting rates. Since the fractional changes in pressure corrected counting rates of the two detectors differ during temporal variations of cosmic rays, 1976 was selected for intercomparing barometric pressure dependent changes in counting rates. During this period of minimum solar activity, temporal variations in counting rates due to cosmic rays may be neglected comparing to barometric pressure effects. Daily averaged hourly counting rates and barometric pressures were considered.

A linear regression fitting between the pressure uncorrected counting rates of the 4NMD and the 3NM64 yielded a gradient $m = (9.68 \pm 0.035) \times 10^{-2}$ with a correlation coefficient of 0.999. With the average ratio of the counting rates = 0.09670 it follows that the ratio of the barometric coefficients of the 4NMD to the 3NM64 is

$$\frac{\beta(4NMD)}{\beta(3NM64} = 1.0008 \pm 0.0035$$

This implies an identical pressure dependence for both detectors. In order to confirm this result, a linear regression analysis was also carried out on the ratio of the counting rates of the 4NMD and the 3NM64 as a function of the barometric pressure.

With

$$\ell n \frac{N(4NMD)}{N(3NM64)} = \ell n \left[\frac{N(4NMD)}{N(3NM64)}\right]_o + \Delta\beta(p-p_o)$$

we found $\Delta\beta = -(3 \pm 2).10^{-5}$/mb. with a correlation coefficient of r = -0.33. Since $\Delta\beta = \beta(4NMD) - \beta(3NM64)$, it means that the ratio of the barometric coefficients

$$\frac{\beta(4NMD)}{\beta(3NM64)} = 0.997 \pm 0.003$$

if one accepts that $\beta(3NM64) = 0.0073$/mb.

When the linear regression method for successive differences of Lapointe and Rose (1962) was used, the same value for the ratio of the barometric coefficients was obtained, but the correlation coefficient, r, was as small as - 0.05. The small correlation coefficients obtained by both linear regression methods confirm that the barometric coefficients of both detectors are the same.

In Figure 2 are shown the monthly averaged pressure corrected counting rates of the 4NMD and of the 3NM64 for the period from March 1974 through to December 1984. Different symbols have been used in the plot for different years. A linear regression analysis gives for the longterm variation of the 4NMD relative to the 3NM64 a ratio of 0.108 ± 0.002, with a correlation coefficent of 0.985.

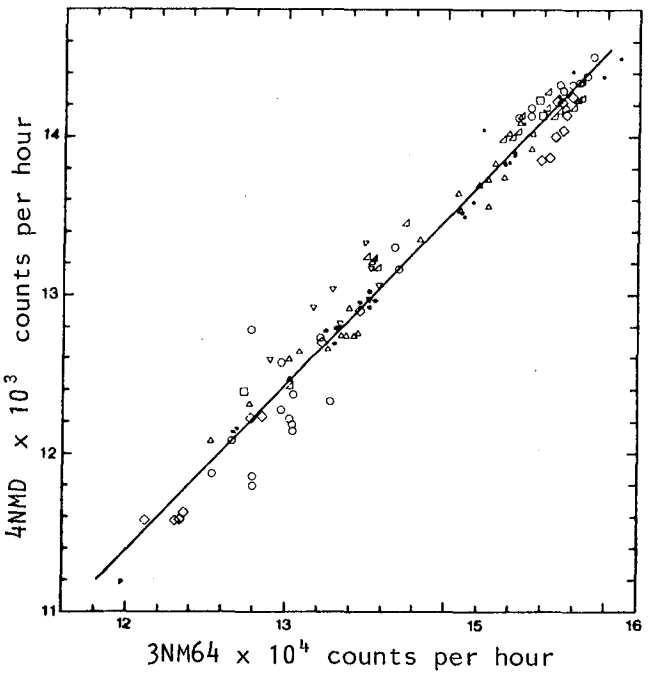

Figure 2

4. Discussion and conclusions. The results show a highly correlated variation of the counting rates of the 4NMD and the 3NM64, both due to pressure variations and to temporal variations in the primary cosmic ray intensity. No statistically significant difference in the pressure dependence of the two detectors could be established.

The 4NMD shows an 8% larger variation in counting rate than the 3NM64 on long term modulation. This relative larger variation in fractional counting rate of the 4NMD was expected from the larger latitude dependence of the 1NMD compared to the 1NM64 (Mischke et al., 1973). Also the larger variations of the counting rate of the 4NMD relative to the 3NM64 for Forbush decreases and ground level solar proton events (Stoker et al., 1979) show a larger sensitivity of the 4NMD relative to the 3NM64 for primary cosmic rays of rigidity $\gtrsim$ 1 GV.

Mischke et al. (1973) reported a barometric coefficient of (0.76 ± 0.02)%/mb for the 1NMD, which was then in operation at Sanae, with the same nominal shielding by paraffin wax than the present 4NMD. This coefficient may be compared with the barometric coefficient of the 3NM64, which is 0.73%/mb. The pressure dependence of the 4NMD may be different from the 1NMD, because the inner tubes of the 4NMD are shielded from the environment by the outer tubes, since environmentally produced neutrons do contribute significantly to the counting rate of a neutron moderated detector (Simpson, 1951).

Zhu and Kawasaki (1983) reported a barometric coefficient of (0.593 ± 0.013)%/mb for their 6 BP28 neutron counters with only the 2 cm polyethylene cylinder, compared with 0.667%/mb for the Tokyo super neutron monitor. This difference in pressure dependence reported by Zhu and Kawasaki may also be due to environmental effects.

The scattering of the points in Figure 2 should be due to variations in the rigidity spectrum of primary cosmic rays. Variation in the rigidity dependence of the modulation function for galactic cosmic rays may be deduced from the relative variation in the counting rates of the two detectors, provided that the specific yield function of each detector at ground level is known.

References

Hatton, C.J., Progress in Elementary Particle and Cosmic Ray Physics 10, 5. Horth-Holland Publ. Co. 1971.

Hess, W.N., Paterson, H.W., Wallace, R. and Chupp, E.L., Phys. Rev. 116, 445, 1959.

Lapointe, S.M., and Rose, O.C., Canadian J. Phys. 40, 687, 1962.

Mischke, C.F.W., Stoker, P.H., and J. Duvenage, 13th I.C.R.C. Conf. Papers 2, 1570, 1973.

Simpson, J.A., Phys. Rev. 83, 1175, 1951.

Simpson, J.A., Fonger, W. and Treiman, S.B., Phys. Rev. 90, 934, 1953.

Simpson, J.A., and Uretz, R.B., Physical Rev. 90, 44, 1953.

Stoker, P.H., Potgieter, M.S. and Venter, A.J., 16th I.C.R.C. Conf. Papers, 4, 358, 1979.

Zhu, B.Y. and Kawasaki, S., 18th I.C.R.C. Conf. Papers 3, 507, 1983.

NEW MATSUSHIRO UNDERGROUND COSMIC RAY STATION (220 M.W.E. IN DEPTH)

Mori, S., S. Yasue, S. Sagisaka, K. Chino, S. Akahane, T. Higuchi, M. Ozaki and M. Ichinose*

Department of Physics, Faculty of Science and Faculty of Liberal Arts*, Shinshu University, Matsumoto 390, Japan

ABSTRACT

A new underground cosmic ray station has been opened at Matsushiro, Japan and multi-directional (17 directional channels) muon telescope has been installed at an effective vertical depth of 220 m.w.e. The counting-rates are; 8.7×10^4/hr for the wide-vertical component and 2.0×10^4/hr for the vertical component. The continuous observation has been performed since March 22, 1984. Some details of the telescope and preliminary analyzed results of the data are presented.

1. Introduction

More than a dozen of the underground cosmic ray stations have been actively operated, and invaluable data have been accumulated. Based on those data, a great deal of investigation has been performed on the cosmic ray modulation in the heliosphere, cooperated with small air shower measurements (e.g., Nagashima and Mori, 1976). Complete pictures of the modulation have not yet been established in the rigidity range of $10^{11}\sim10^{14}$ eV, therefore more accumulation of the data of high counting-rates with multi-directional channels would be mostly acknowledged.

2. Underground Site and Muon Telescope

Matsushiro is located in Nagano-city, Nagano Pref., Japan and ∿40 km northeast of our Cosmic-Ray Lab. of Shinshu University in Matsumoto-city. A new station is very close to our elder one (∿4 km in distance) (Yasue et al., 1981; also in this issue). Locality of the present station is; 36.53°N and 138.02°E in geographic coordinate and 360 m in altitude. Fig. 1(a) shows the contour map of the underground site and Fig. 1(b) illustrates one of the cross-sections along the line AB in Fig. 1(a).

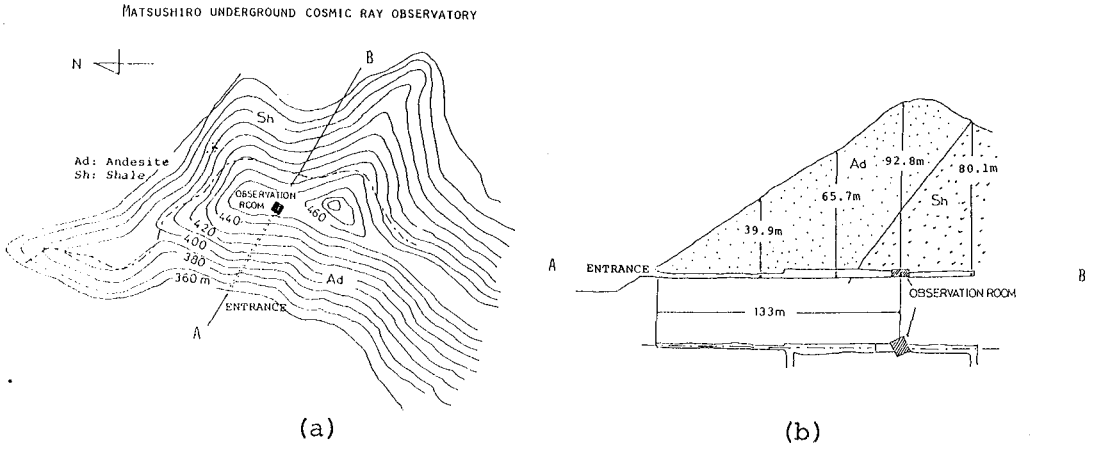

Fig. 1 (a) Contour map of tunnel area and (b) Cross-section along AB

The vertical rock depth is 92.8 m, and the rocks overburden are mostly andesite (Ad) and shale (Sh), its average density ≅2.65 g/cm^3, therefore ≅240 m.w.e. The depth is somewhat different in each direction, and the effective vertical depth is estimated at ∿220 m.w.e.

The temperature inside the tunnel is 14∿15°C, almost constant throughout the year (precise temperature variations on the daily and seasonal bases have not yet been measured). Both observation room (10×10 m^2 in area) and recording room have been heated up to ∿19°C, and the humidity has been kept as $\lesssim$50%.

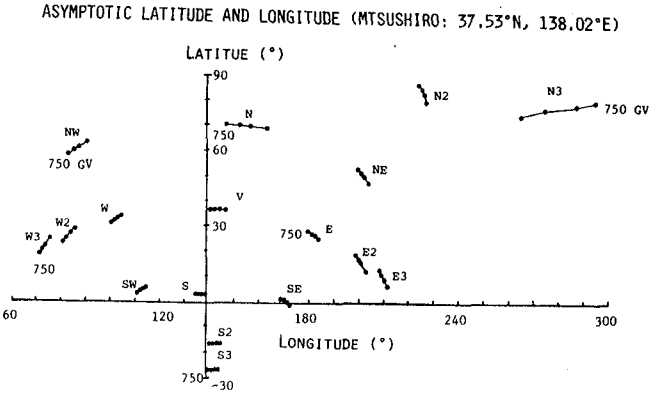

Fig. 2 Asymptotic orbit for 13 comp.'s.

Fig. 2 shows the asymptotic directions for 17 component telescopes calculated for the rigidities of 750, 450, 350 and 250 GV (Inoue, personal communication).

The median primary rigidity is estimated at ∿600 GV, using the response function given by Murakami et al. (1981). The corresponding Lamore radius for 6 nT of the IMF strength is ∿2 AU.

The muon telescope consists of 50 plastic scintillation detectors in all, as shown in Fig. 3, arranged in two layers spaced by 150 cm. The detectors are exactly the same as those of our elder Matsushiro station (Yasue et al., 1981); each having 1×1 m^2 in area, 4 plastic scintillators (50×50×10 cm^3), and viewed with double photomultipliers (5" in diameter), as shown in Fig. 4, to obtain good S/N ratio and high detection efficiency.

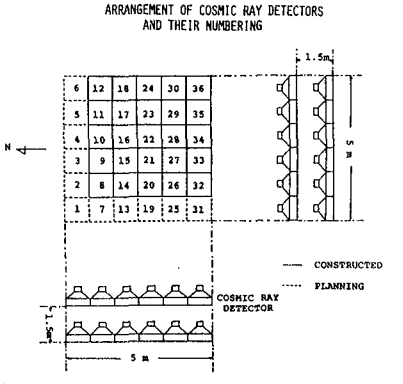

Fig. 3 Arrangement of detectors

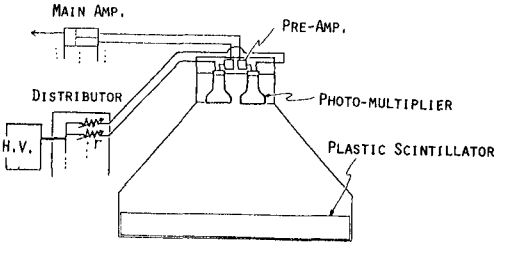

Fig. 4 Cosmic ray detector

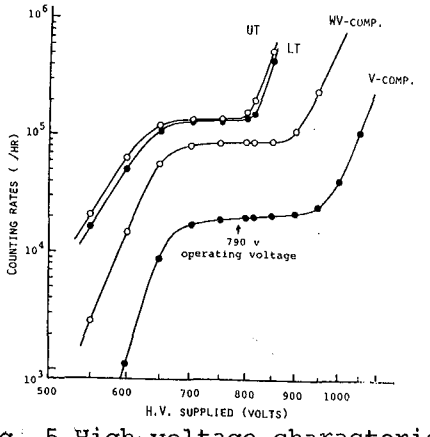

Fig. 5 High-voltage characteristic

Based on this arrangement, 17 component telescopes are constructed by taking an appropriate 2-fold coincidence between the detectors in upper and lower trays. In Fig. 5, high-voltage characteristics of some telescopes are plotted of real counts vs. high-voltage supplied for the upper (US) and the lower (LS) trays, the wide-vertical component (WT; 2-fold coincidence between US and LS) and the vertical component (V). The continuous observation has been performed since March 22, 1984 and the hourly counts have been recorded. In the followings, some preliminary analyzed results of the data are presented.

3. Data and Their Analysis

3.1 Atmospheric effect

Barometric pressure effect was examined; one for a short time-period of 6 days when transient large atmospheric pressure change was observed in a range of ∿30 mb and the other for a long time-period of abour 6 months (Mar.∿Oct., 1984). Single correlation between the pressure and the counting-rate was taken. Barometric coefficients were obtained as; $\beta \cong -0.01\%$/mb for the former short-period and $\alpha \cong -0.04\%$/mb for the latter long-period. These are in good agreement with our previous results and can be well explained by taking accounts of the upper atmospheric temperature effect (Sagisaka et al., 1983).

3.2 Cosmic ray north-south asymmetry (N-S asymmetry)

Among 17 component telescopes, some telescopes (e.g., N, N2, ...) view rather northern latitude, while some (e.g., S, S2, ...) view rather southern latitude or equatorial plane, as shown in Fig. 2. Using the daily mean values of these directional intensities ($\sim 60\times10^4$/day), N-S asymmetry was evaluated daily as

$$\Delta = (N+N2+N3+NE+NW) - (S+S2S3+SE+SW)^*$$

where * indicates the normalized counts between these two groups (Mori and Nagashima, 1979). Also IMF-sense dependence of this N-S asymmetry was examined by referring to Toward (T)- and Away (A)-sense given by Stanford group (Solar-Geophysical Data, NOAA, 1985). Fig. 6 shows the correlation between derived N-S asymmetries of the present station and Misato (34 m.w.e. in depth). Table 1 gives the numerical values on T and A of these two stations for the period Mar.22∿Oct. 31, 1984. From this result, some indication may be noted that even such high rigidity particles (∿600 GV) observed at 220 m.w.e. underground station, are influenced by the IMF-sense.

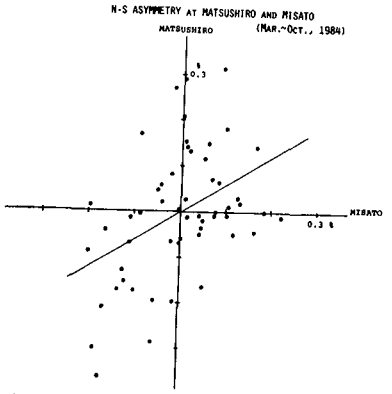

Fig. 6 Correlation between Matsushiro and Misato.

Station	T(%)	A(%)
Matsushiro	0.02	-0.05
Misato	0.066	-0.060

Table 1 N-S asymmetries on T and A

3.3 Daily intensity variation

The hourly data (without corrected for barometric effect) were harmonically analyzed in solar (SO), sidereal (SI) and anti-sidereal (AS)

time for full one-year (Apr. 1984 Mar. 1985). Fig. 7 shows one of month-to-month variations of SO(1st) for V-comp. The monthly vectors move counterclockwise systematically, indicating the at deep undergrouns station SI(1st) may be more significant in the 1st harmonics. Fig. 8 illustrates some of the harmonics for 13 component telescopes (V, N, S, E, W, NE, NW, SE, SW, N2, S2, E2 and W2); Si(1st) in (a), AS(1st) in (b) and SO(2nd) in (c). In the figure, errors are derived from counting-rates. We may note that from their directional dependence, almost of them are significant.

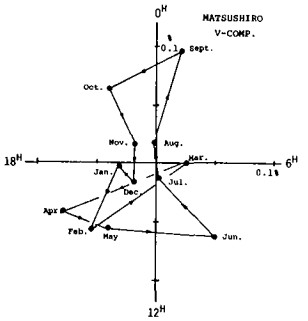

Fig. 7 Monthly movement of SO(1st) for V-comp.

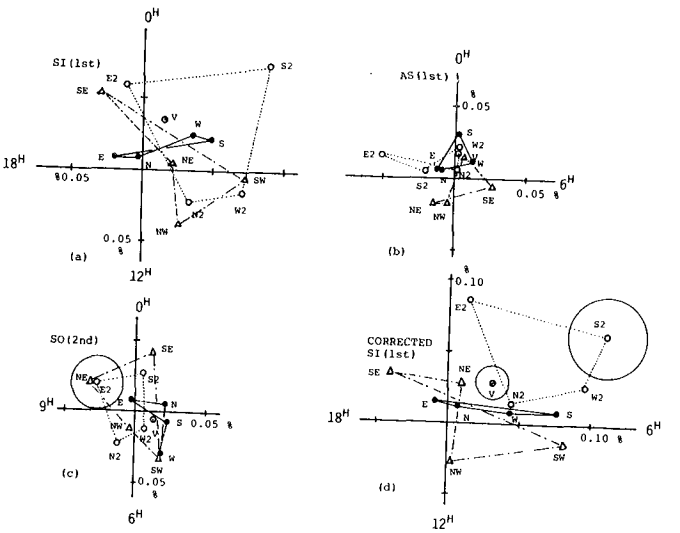

Fig. 8 Harmonics of; (a) SI(1st), (b) AS(1st), (c) SO(2nd) and (d) corrected SI(1st)

In a case, where SO(2nd) is observed significantly, as developed by Nagashima et al. (1983), space anisotropy of 2nd order responsible for the observed SO(2nd) produces the spurious SI(1st) and AS(1st) having equal amplitude and due phase. As in Fig. 8 (b), AS(1st) may be significant. Based on Nagashima correction (1983), the observed SI(1st) should be, at least, corrected for the above spurious SI(1st) by utilizing the observed AS(1st). Fig. 8 (d) shows the corrected SI(1st) thus derived. We may summarize that 1) these results are consistent with those so far reported; almost of them lie in the direction 3~5 hr LST. And 2) some of SI(1st)'s, e.g., S2-comp. is rather larger (~0.13% in ampltude) than others, which is consistent with that of Ueno et al. (1984) at Sakashita.

4. Acknowledgement

The authors express their aapreciation to Prof. K. Nagashima for his kind discussion.

References

Mori, S. and K. Nagashima, (1979), Plant. Space Sci., 27, 34.
Murakami, K. et al., (1981), Rep. CR-Lab., Nagoya Univ., No. 6.
Nagashima, K. and S. Mori, (1976), Int. CR-Symp. (Tokyo), p326.
Nagashima, K. et al., (1983), Nuovo Cimento, 6C, 550.
Sagisaka, S. et al, (1983), 18th ICRC (Bangalore), 10, 237.
Ueno, H. et al., (1984), Int. CR-Symp. (Morioka), p349.
Yasue, S. et al., (1981), 17th ICRC (Paris), 4, 304.
Yasue, S. et al., (1985) in this issue (SH 4.4-9).

A SUGGESTED STANDARDIZED FORMAT FOR COSMIC RAY GROUND-LEVEL EVENT DATA

M. A. Shea and D. F. Smart
Air Force Geophysics Laboratory
Hanscom AFB, Bedford, Massachusetts, 01731, U.S.A.

M. Wada and A. Inoue
Institute of Physical and Chemical Research
7-13, Kaga-1, Itabashi, Tokyo 173, Japan

ABSTRACT

A standardized format is suggested for the archival and exchange of neutron monitor data obtained during solar-flare-initiated ground-level cosmic ray events. Using the data for the 7 May 1978 ground-level event, we have developed a format that incorporates hourly data preceding and following the event and small-time interval data immediately before and during the event. Provision has been made for the inclusion of uncorrected and corrected data as well as the atmospheric pressure. The cosmic ray intensity data are then reduced to a standard counting rate of counts per second facilitating the graphing and comparison of these data for various analyses.

1. Introduction. Thirty-four relativistic solar proton events have been detected by ground-based neutron monitors since 1955. These events are intensely studied not only for the physics of the flare process, but also for information on relativistic solar particle propagation in the interplanetary medium and entry into the magnetosphere. The first ground-level cosmic ray event detected by neutron monitors on February 23, 1956, was so unexpected and unique that many scientific papers were written on the measurements at just one station. However, the events of May and November 1960 illustrated the necessity of utilizing data from the world-wide neutron monitor network to study interplanetary and magnetospheric propagation characteristics.

Unfortunately one of the most time-consuming tasks in the analysis of multi-station ground-level event data is the collection and assembly of these data into a common useable format since most cosmic ray stations use their own unique data collection system regarding time intervals, scaling factors, and normalization factors. Since the rapid and efficient exchange of data relating to solar-flare-initiated ground-level events would be practical and beneficial to the community, we have developed a format that includes the parameters that cosmic ray scientists use in the analysis of these relatively unusual events, and suggest that this format be adopted as a standard for the archival and exchange of these data.

2. Method. To develop a useful format we first identified the data we felt were essential for the analysis of any ground-level cosmic ray event that utilizes the data from the world-wide neutron monitor network. These included sufficient data to establish a pre-event level, small time increments during the rising and maximum portion of the event, and both uncorrected and corrected data to permit use of the two-attenuation

method of correcting the solar flare particle spectrum for atmospheric effects (McCracken, 1962). Using neutron monitor data from 32 stations for the ground-level cosmic ray event of 7 May 1978, we proceeded to identify the data we felt should be included as follows:

6 May 1978:	0000-2400 UT	Hourly data (uncorrected data)
7 May 1978:	0000-0200 UT	(corrected data)
		(barometric pressures)
7 May 1978:	0200-0700 UT	Small time interval data
		(uncorrected data)
		(corrected data)
		(barometric pressures)
7 May 1978:	0700-2400 UT	Hourly data (same as above)

The hourly data for the day preceding the event would permit consideration of any unusual daily variations that might be present for some stations. The small time interval data, which are station specific, would give information on the rate of rise and maximum intensity, as well as a portion of the decay of the event. The hourly data for the remainder of 7 May would cover the complete decay of the event for all stations. In order to be able to compare cosmic ray intensities both throughout the event and between stations, we adopted a standard counting rate in units of counts per second. This necessitated utilizing multiplication factors and/or normalization factors for each individual station. However, the advantange of this procedure is that odd time intervals, such as changes from hourly to five-minute or one-minute data, can be easily compared. The following format was adopted:

Columns 1 - 10:	Station identification (alphanumeric)
Columns 11 - 19:	Year, month and day (3I3)
Columns 20 - 23:	Number of minutes in this time interval (I4)
Columns 24 - 33:	Time interval included (I5, 1H-, I4)
Columns 34 - 50:	Uncorrected counting rate; counts per second (6X,F11.2)
Columns 51 - 57:	Barometric pressure (F7.1)
Columns 58 - 68:	Corrected counting rate; counts per second (F11.2)
Columns 69 - 75:	Percentage increase (F7.1) normalized to some pre-event level.

Table 1 illustrates a portion of the data for Leeds, UK. The intensity for the hour immediately preceding the increase (i.e., 0200-0300 UT) was selected as the pre-event level. Figure 1 illustrates the cosmic ray intensity increase for this same station. Notice that this method allows inclusion of "odd" time intervals such as the 3-minute value obtained prior to the activation of the flare alarm rapid time recorder.

3. Discussion. In compiling these data into a standard format it became evident that much of the data we wanted to include was not available from the data that had been exchanged among various investigators. The following data were most commonly found to be missing: all data for the day prior to the event, uncorrected data throughout the event, and data multiplication and/or normalization factors. Data given for different time intervals without any notation as to changes in multiplication and/or normalization factors were extremely difficult to include. In the case of Hermanus, hourly data were given for four sections of the

Table 1. An example of the ground-level event data, in the proposed standard format, for 0000-0500 UT for the event on 7 May 1978. Only a portion of the complete data set for the Leeds neutron monitor is shown. The time interval of 0200-0300 UT was selected as the pre-event level.

STATION	YY	MM	DD	MIN	TIME SPAN	UNCOR.	PRES.	COR.	% INC.
LEEDS	78	05	07	60	0000-0100	167.97	751.7	170.42	-.1
LEEDS	78	05	07	60	0100-0200	178.19	751.6	170.50	-.1
LEEDS	78	05	07	5	0200-0205	178.67	751.5	170.67	.0
LEEDS	78	05	07	5	0205-0210	175.67	751.5	168.00	-1.5
LEEDS	78	05	07	5	0210-0215	178.33	751.6	170.67	.0
LEEDS	78	05	07	5	0215-0220	178.00	751.6	170.33	-.2
LEEDS	78	05	07	5	0220-0225	178.67	751.6	171.00	.2
LEEDS	78	05	07	5	0225-0230	180.33	751.6	172.67	1.2
LEEDS	78	05	07	5	0230-0235	178.67	751.6	171.00	.2
LEEDS	78	05	07	5	0235-0240	177.67	751.5	170.00	-.4
LEEDS	78	05	07	5	0240-0245	180.00	751.5	172.00	.8
LEEDS	78	05	07	5	0245-0250	179.33	751.5	171.33	.4
LEEDS	78	05	07	5	0250-0255	177.33	751.5	169.67	-.6
LEEDS	78	05	07	5	0255-0300	178.00	751.5	170.33	-.2
LEEDS	78	05	07	5	0300-0305	178.67	751.5	170.67	.0
LEEDS	78	05	07	5	0305-0310	177.67	751.5	170.00	-.4
LEEDS	78	05	07	5	0310-0315	179.67	751.6	172.00	.8
LEEDS	78	05	07	5	0315-0320	176.00	751.6	168.33	-1.4
LEEDS	78	05	07	5	0320-0325	179.00	751.6	171.33	.4
LEEDS	78	05	07	5	0325-0330	179.67	751.6	172.00	.8
LEEDS	78	05	07	5	0330-0335	179.00	751.6	171.33	.4
LEEDS	78	05	07	3	0335-0338	217.22	751.6	207.78	21.8
LEEDS	78	05	07	1	0338-0339	301.67	751.6	288.33	69.0
LEEDS	78	05	07	1	0339-0340	316.67	751.6	303.33	77.8
LEEDS	78	05	07	1	0340-0341	331.67	751.6	316.67	85.6
LEEDS	78	05	07	1	0341-0342	328.33	751.6	315.00	84.6
LEEDS	78	05	07	1	0342-0343	315.00	751.6	301.67	76.8
LEEDS	78	05	07	1	0343-0344	308.33	751.6	295.00	72.9
LEEDS	78	05	07	1	0344-0345	300.00	751.6	286.67	68.0
LEEDS	78	05	07	1	0345-0346	293.33	751.6	280.00	64.1
LEEDS	78	05	07	1	0346-0347	288.33	751.6	276.67	62.1
LEEDS	78	05	07	1	0347-0348	280.00	751.6	268.33	57.2
LEEDS	78	05	07	1	0348-0349	266.67	751.6	255.00	49.4
LEEDS	78	05	07	1	0349-0350	271.67	751.5	260.00	52.4
LEEDS	78	05	07	1	0350-0351	260.00	751.5	248.33	45.5
LEEDS	78	05	07	1	0351-0352	258.33	751.5	246.67	44.6
LEEDS	78	05	07	1	0352-0353	240.00	751.5	230.00	34.8
LEEDS	78	05	07	1	0353-0354	245.00	751.5	235.00	37.7
LEEDS	78	05	07	1	0354-0355	240.00	751.5	230.00	34.8
LEEDS	78	05	07	1	0355-0356	238.33	751.5	228.33	33.8
LEEDS	78	05	07	1	0356-0357	235.00	751.5	225.00	31.9
LEEDS	78	05	07	1	0357-0358	228.33	751.5	218.33	27.9
LEEDS	78	05	07	1	0358-0359	220.00	751.5	210.00	23.1
LEEDS	78	05	07	1	0359-0400	226.67	751.5	216.67	27.0
LEEDS	78	05	07	1	0400-0401	220.00	751.5	210.00	23.1
LEEDS	78	05	07	1	0401-0402	211.67	751.5	201.67	18.2
LEEDS	78	05	07	1	0402-0403	211.67	751.5	201.67	18.2
LEEDS	78	05	07	1	0403-0404	215.00	751.5	205.00	20.1
LEEDS	78	05	07	1	0404-0405	213.33	751.5	203.33	19.2
LEEDS	78	05	07	5	0405-0410	205.67	751.5	196.67	15.3
LEEDS	78	05	07	5	0410-0415	199.00	751.5	190.33	11.5
LEEDS	78	05	07	5	0415-0420	194.33	751.5	186.00	9.0
LEEDS	78	05	07	5	0420-0425	192.67	751.6	184.33	8.0
LEEDS	78	05	07	5	0425-0430	189.00	751.6	181.00	6.1
LEEDS	78	05	07	5	0430-0435	186.33	751.6	178.33	4.5
LEEDS	78	05	07	5	0435-0440	184.00	751.6	176.00	3.1
LEEDS	78	05	07	5	0440-0445	186.00	751.6	178.00	4.3
LEEDS	78	05	07	5	0445-0450	184.33	751.6	176.33	3.3
LEEDS	78	05	07	5	0450-0455	185.33	751.6	177.33	3.9
LEEDS	78	05	07	5	0455-0500	183.00	751.6	175.00	2.6

monitor, but the flare data only included three sections. When the proper normalization factors are obtained, we will be able to include these data in the standard format. Another problem was encountered with small-time interval data corrected for small-time increments, which, when summed over the hour, were not in agreement with the listed hourly data. The use of local time instead of Universal Time without any notation as to the difference between these times also caused some difficulty. Some stations in the Soviet Union listed hourly data in Universal Time and small-time interval data in local time; some also listed hourly time for the hour ending with the indicated time, but small-time interval data were listed at the start of the interval. Consequently we utilized information available from the World Data Center records and from previously published tables to complete, as much as possible, a uniform set of tables for the 32 neutron monitors.

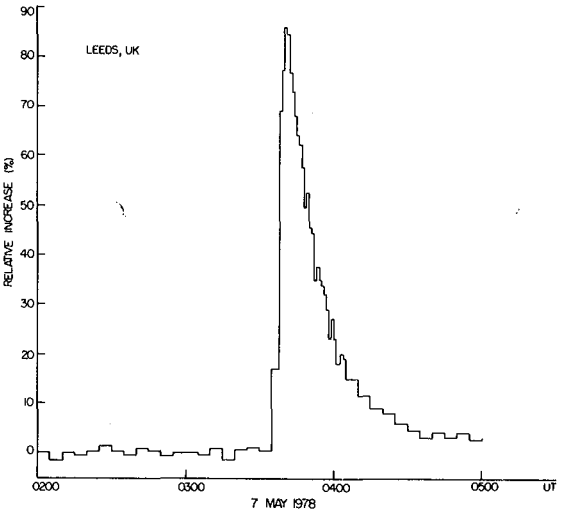

Figure 1. Relative increase recorded by the Leeds, UK neutron monitor for the 7 May 1978 ground-level event.

4. Future Plans. We plan to complete and publish the uniform set of tables for the 7 May 1978 ground-level event, at the same time work is progressing on similar tables for the following events: 21 August 1979, 12 October 1981, 8 December 1982, and 16 February 1984. To complete some of these tables it will be necessary to contact the principal investigator; we would appreciate cooperation in supplying the data requested. We also anticipate compiling similar records for as many of the 34 ground-level events as time (and patience) permits. We are afraid that many of the records for the earlier events, particularly those prior to this solar cycle, may be difficult to obtain. Therefore, we request all cosmic ray physicists who have ground-level event data for either their own or other cosmic ray stations to send the data to any of the authors of this paper and to the World Data Centers for archival in an effort to preserve this historical data set.

Acknowledgments. The computational assistance of M. Nichol and L.C. Gentile are gratefully acknowledged.

References

McCracken, K.G., "The Cosmic Ray Flare Effect; 1. Some New Methods of Analysis", J. Geophys. Res., 67, 423, 1985.

SH 9.1-16

THE READ-OUT SYSTEM OF SPATIAL DISTRIBUTION OF THERMOLUMINESCENCE IN METEORITES

Kiyotaka Ninagawa, Isao Yamamoto and Yasumasa Takano
Okayama University of Science, Okayama Japan
Tomonori Wada and Yoshihiko Yamashita
Okayama University, Japan
Nobuo Takaoka
Yamagata University, Japan

1. Introduction The thermoluminescence [TL] technique used for dating the terrestrial age of the meteorites[1] was based on the TL fading of interior samples. The depth dependence of the TL for Antarctic meteorites with fusion crust was measured[2]. Usually, meteorites were powdered and their TL were measured under a photomultiplier. In this time, we have measured a TL spatial distribution of a cross section of antarctic meteorites by using a read-out system of spatial distribution of TL[3], because a meteorite is inhomogeneous material. Antarctic meteorites MET-78028[L6], ALH-77278[LL3] are used.

2. Methods The system is shown in Fig. 2 of this conference HE 7.1-7. TL data are recorded by video cassette tapes. TL data are able to be analysed repeatedly via image processor. For the case of taking emission spectra of TL, we have changed a camera lens with a filter for a spectroscope. One example of emission spectra is shown in Fig. 1. The sample is powdered

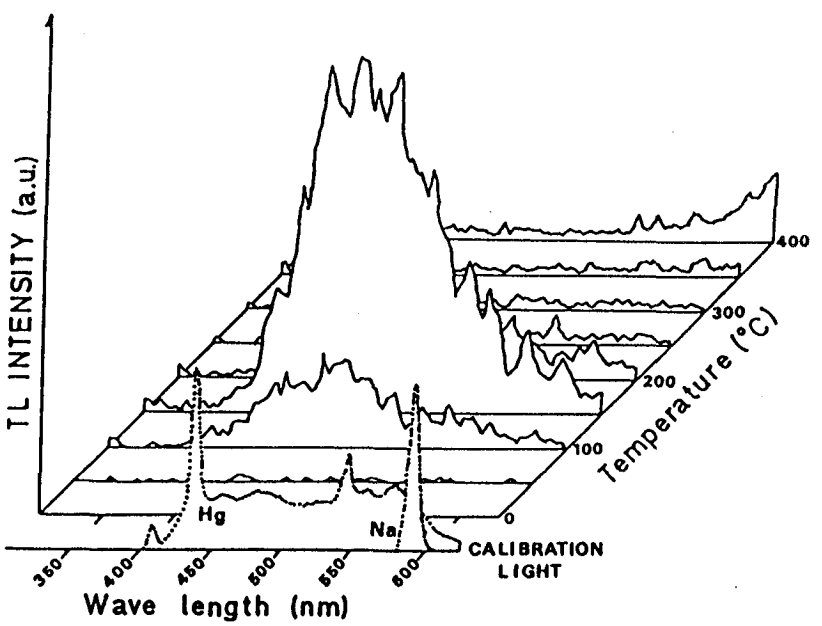

Fig. 1. Emission spectra of TL of MET-78028 at various temperature. For calibration, a Na-lamp and a fluorescent lamp are used.

meteorite MET-78028 irradiated with X-rays ($\sim 10^5$ R). The meteorite TL has a wide spectral band with a maximum at about 450 nm. So in the TL measurement of MET-78028, we have used the band pass filter, Corning 4-96 (blue-green).

3. The spatial distribution of TL for MET-78028 [L6].

Samples of slices of the meteorite are shown in Fig. 2. One slice of a pair was artificially exposed to ^{60}Co 1 kR γ-rays in addition to natural exposure. Using TV-camera system (Ref. 3), a pair of slices and an interior piece of the meteorite were heated (rising rate:2.3 °C/sec) and TL spatial distributions of these sample were recorded onto video cassette tape for about 160 sec ($\sim$5300 frames). Two examples of read out are shown in Fig. 3a, 3b. The Fig. 3a is TL spatial distribution

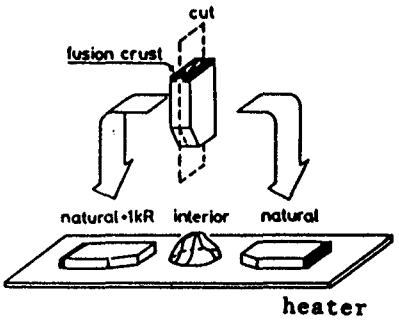

Fig. 2. Cutting and setting.

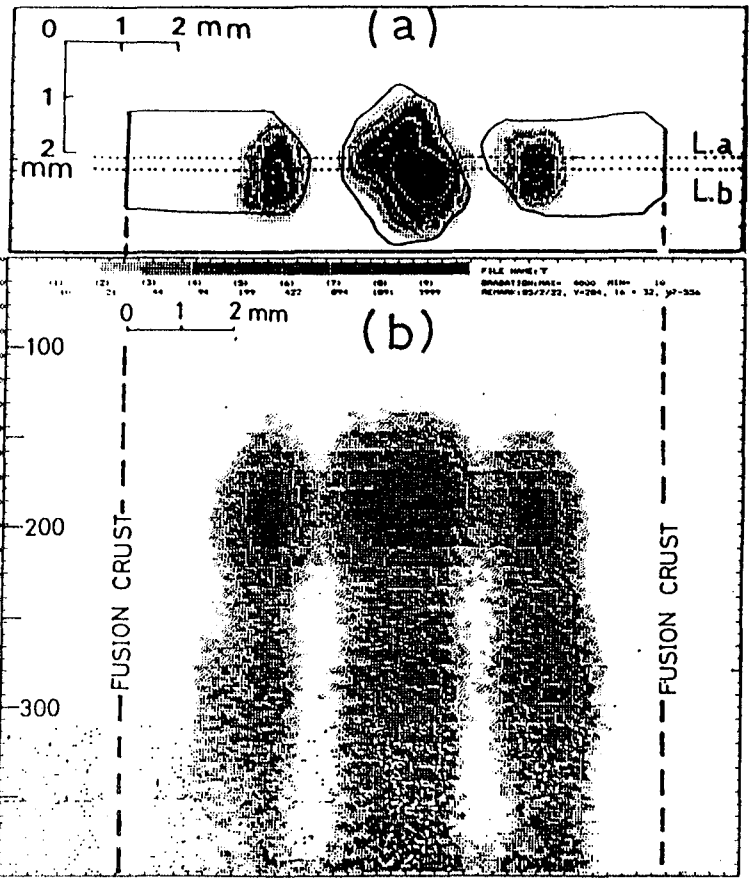

Fig. 3a. TL spatial distribution of slices in pair and of interior one. [MET-78028]

Fig. 3b. Time variation (corresponding to temperature) of TL for the area from line L.a to L.b in Fig. 3a. [MET-78028]

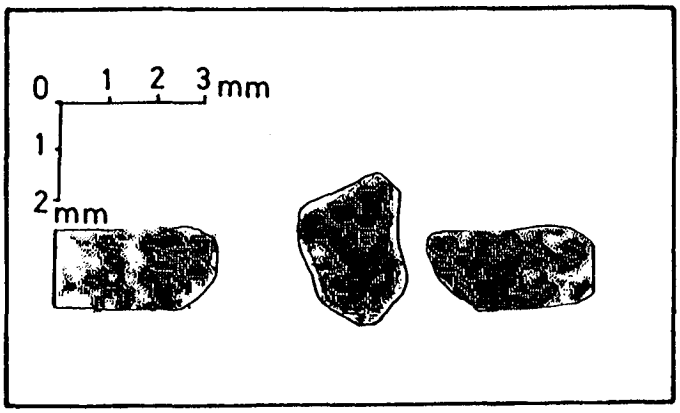

Fig. 4. Spatial distribution of TL sensitivity for antarctic meteorite, MET-78028 (L6). The meteorites were irradiated with 10^5 R X-rays.

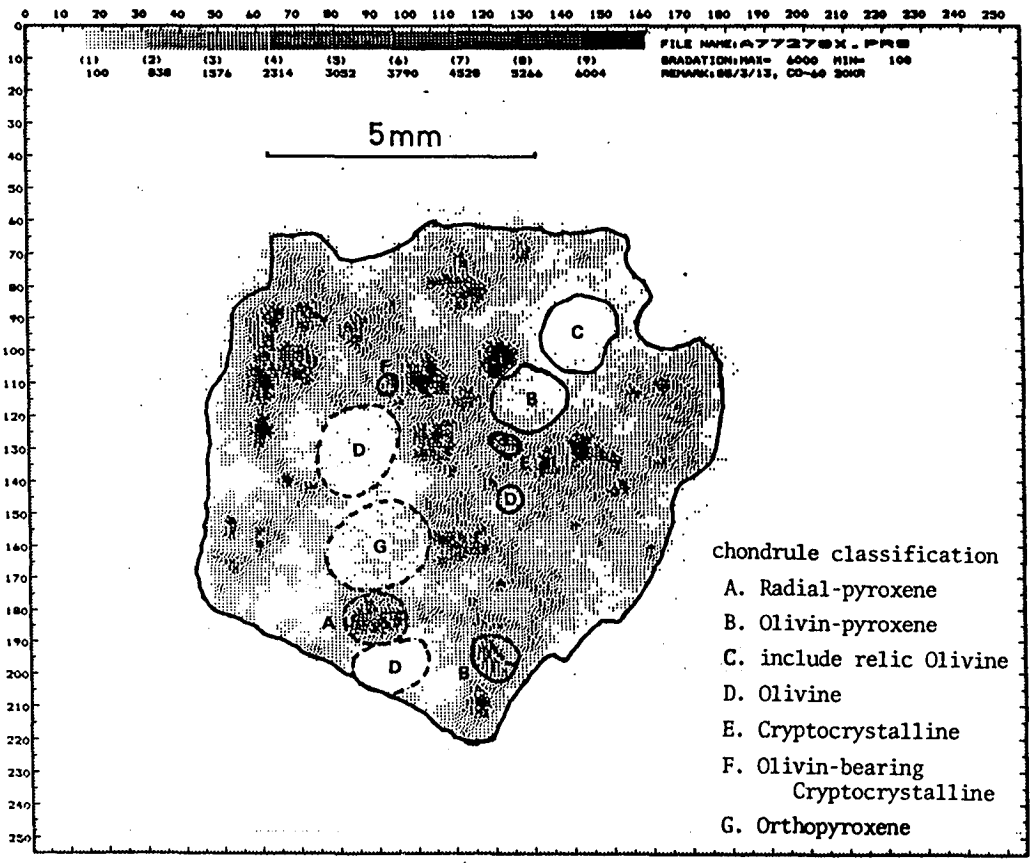

Fig. 5. Spatial distribution of TL sensitivity for antarctic meteorite, chondrite ALH-77278 (LL3). The meteorite was irradiated with 20 kR γ-ray.

of samples. The TL yeild of both slices was not detectable at near fusion crust. The fig. 3b shows the TL variation vs. heating temperature at the area from line L.a to L.b. The TL on the fusion crust side was obtained at higher temperature region.

4. Spatial distributions of TL sensitivity

(A) MET-78028 (L6): After reading out of natural TL, samples corresponding to Fig. 3a were irradiated with X-rays (10^5 R) and were heated. TL spatial distributions of these samples are shown in Fig. 4, which shows spatial distributions of TL sensitivity of these samples. Slices in pair of MET-78028 have low TL sensitivity near fusion crust. Here, the TL sensitivity is represented with logarithmic intensity.

(B) Chondrite, ALH-77278 (LL3): After reading out of natural TL, the sample was irradiated with ^{60}Co γ-rays (20 kR) and was heated. TL spatial distribution is shown in Fig. 5, which shows spatial distribution of TL sensitivity of the sample. Some chondrules have high TL sensitivity and other chondrules have low TL sensitivity or no sensitivity.

5.Conclusions. As shown in Fig. 4 and 5, the TL spatial sensitivity is not uniform, it may occur since meteorites are inhomogeneous material. So, when one searches the terrestrial age of antarctic meteorites or classifies the petrologic type of chondrites by using TL technique, one must investigate thoroughly TL spatial sensitivities. It is not only meteorites but also natural materials on the occation to measure natural TL.

6. Acknowledgements. The authors are greatly indebted to Prof. T.Nagata and Dr. K.Yanai, National Institute of Polar Research for the meteorite samples. They also thank Dr. Y.Ikeda, Ibaragi University for the chonrule classification.

References

1. Sears, D.W. and Durrani, S.A. (1980), Earth Planet. Sci. Lett., 46, 159.
2. Ninagawa, K. et. al., (1983), Lettere al Nuovo Cimento, Serie 2, 38, 33.
3. Yamamoto, I. et. al., (1985), This conference paper, HE 7.1-7.

METHODS AND SOFTWARE FOR COSMIC RAY SCINTILLATION STUDIES

O.V.Gulinsky, L.I. Dorman, R.E.Prilutsky

Institute of Terrestrial Magnetism, Ionosphere and Radio Wawe Propagation, USSR Academy of Sciences, 142092 Troitsk, Moscow Region, USSR

Methods and programs for statistical processing of cosmic ray intensity measured in the world-wide network are proposed.

The main instrument in scintillation studies is the cosmic ray spectrum constructed from the intensity onservation /I/. The problem of psctrum estimation from measured time series has a long-standing history, but the specificities of the phenomenon of interest do not permit the direct use of the classical methods. One of such specificities is that besides the appearance of regular trends, which can in principle be eliminated by different filtration methods, in the periods most interesting from the viewpoint of the physics of processes (for instance, Forbush decreases, solar flares) the statistical characteristics of the process undergo essential reconstruction, i.e. the process besomes nonstationary. In this case the concept of spectrum is not defined, and the methods based on Fourier transform, Blackman-Tusky method) give wrong results. The technique usual in this situation, i.e. discrimination of quasistationary regions, encounters the following difficulties. Such regions, if any, can be very short. When based on a small amount of data, the methods using Fourier transform are known to give inaccurate results, in particular, they do not allow us to separate close frequencies, whereas the second specific feature is just the necessity to separate close frequencies, some of which can be associated with a certain process in solar space. For a better separation of near frequencies in short regions, the so-called autoregressive methods have lately been used for spectrum estimation /2/. These methods suggest introduction of an additional possibility to describe the process by an autoregressive model

$$x_{t+1} = \sum_{i=0}^{p} a_i x_{t-i} + \xi_t, \quad t = 0, 1, \ldots \qquad (I)$$

where ξ_t is the sequence of independent random quantities of a certain unkhown order p. This assumption is based on the fact that a wide class of stationary processes can be described by such a model. The coefficients of regression are in this or that way estimated under this assumption for a certai chosen order p, and then the single-valued analytical estimate of the spectrum is found from these coeffi-

cients. Such an approach, using different algorithms for estimating the coefficients (of the type of Berg, Levinson-Durbin, Pisarenko, and other methods), is also realized in our methods. In some cases it gives satisfactory results. But it cannot be applied to essentially nonstationary processes either.

To eliminate these difficulties we have proposed the following two approaches. One of them suggests the description of a process by an autoregressive model in which the coefficients vary in time

$$x_{t+1} = \sum_{i=0}^{p} a_i(t) x_{t-i} + \xi_t, \quad t = 0, 1, \ldots \tag{2}$$

Each coefficient is represented as a series in a given complete set fo functions $\{\varphi_k(t)\}$

$$a_i(t) = \sum_{k=1}^{N} c_{ik} \varphi_k(t) \tag{3}$$

with the unknown coefficients $\{c_{ik}\}$. As a set of functions one can choose, in particuler, a power series $\{1, t, t^2, \ldots\}$. Then, using the method of least squares, one can calculate the coefficients for the chosen order p of the model and for the number N in the expansion (3). The order p of the model and the number of terms N in the expansion ca be chosen, so to say, in the best possible way.

Such an approach makes it possible to introduce the concept of an instantaneous spectrum for a nonstationary process. At each time moment (estimated from the time series of lenght T) the parameters correspond to an autoregressive model with known constant coefficient $a_i^T = \sum_{k=1}^{N} c_{ik} \varphi_k(t)$

$$x_{t+1} = \sum_{i=0}^{p} a_i^T(t^*) x_{t-i}$$

Such a process will be thought of as stopped at a time moment t (starting at some initial point x_0, it passes through a stationary sequence). This process corresponds to a psectrum which can be calculated analytically from the moment t will be called a t -instantaneous **spectrum** of the nonstationary process (2).

Arranging the sequence of instantaneous spectra with respect to t , one obtains a dynamical picture of reconstruction of a nonstationary process.

The other approach to investigation of a nonstationary process is based on the on-line method for estimating the parameters of the model (2), i.e. on the stochastic approximation method. Let the coefficients $\{a_i^T(t^*)\}$ be time-independent (model (I)), then the algorithm of stochastic

approximation for estimating $\{a_i\}$ for a chosen order p of the model has the form ($\hat{a}$ is the vector of parameter estimation, $\varphi_t = (x_1, \ldots, x)$ is the measured time series):

$$\hat{a}_{t+1} = a_t - \gamma_t \varphi_t \left(x_{t+1} - \sum_{i=0}^{p} \hat{a}_i x_{t-i}\right) \qquad (4)$$

Under certain conditions, if the sequence γ_t tends to zero with an appropriate velocity, one can show (see, for instance, /3/) that as $t \to \infty$, the estimates of $\hat{a}_t$ converge to the vector of the coefficients a of model (I). It is a disadvantage of the method that it needs a large sample, which is hardly to be provided under the described conditions. At the same time, this difficulty can be eliminated if we reject the requirement concerning constancy of the coefficients and pass over to the model (2) without expanding a in the series (3).

In this case, to estimate the coefficients of the model (2), we use the algorithm /4/, in which the sequence γ_t is chosen differently. One can show that under certain conditions on the growth of the coefficients $a_i(t)$ and for a corresponding rate of convergency γ_t to a certain constant, the algorithm (4) will trace the trend of the parameter $a_i(t)$. Under these assumptions one can provide a large sample of data since the series need not necesserily be stationary, and the algorithm works well. The way of constructing an instantaneous spectrum is the same as described above.

The software considered includes all the approaches described above, namely, direct Fourier transform and its modifications, autoregressive and instantaneous spectrum methods. Being used in various combinations, they prove helpful in handling the time series. The methods have been verified in special tests. Some results of investigation of scintillations using these methods are presented in /4/.

REFERENCES

1. Libin I.Ya., Gulinsky O.V. In: Cosmic Rays N 22. M.Nauka, I979, 22.
2. S.M.Kay, S.L.Marple - Proc.of the IEEE - I98I, v.69, N II.
3. Y.Z.Tsypkin, E.D.Avedyan, O.V.Gulinsky, - IEEE TRANS on automatic control, I98I, v. AC-26, N 5.
4. O.V.Gulinsky, L.I.Dorman, I.Ya.Libin et al. - Proc.XIX-th ICRC, San-Diego, USA, I985.

THE INFLUENCES OF THE GALACTIC COSMIC RAY ON THE ATMOSPHERIC OZONE

Ye Zonghai Xue Shunsheng
(Institute of Space Physics, Academia Sinica, P.O.Box 5112, Beijing, China)
Wang Lianying
(Institute of Atmospheric Physics, Academia Sinica, P.O.Box 2718, Beijing, China)

I. Introduction. Warneck [1] and Nicolet et al. [2] first put forward that cosmic ray is a source of NO production in the atmosphere. The Nicolet et al.[3,4,5] proved that each ion pair producted by cosmic ray forms about 1-1.5 NO molecules because of the ionization and the dissociation processes. Because of the reaction between NO and O in the atmosphere NO will dispapear in part, so the change of [NO] will directlly influence [O_3] in the atmosphere. The observational results proved that the solar cosmic ray events will cause the large decrease of[O_3] in the polar stratosphere [6] . Ruderman et al.[7] proved that[O_3] has the law of 11 years variation.

This paper has analysed the relationship between yearly variation of cosmic ray intensity and [O_3], and[O_3] disturbance initiated by Forbush decrease for 1965-1976. The data of cosmic ray intensity were selected from the records of the superneutron monitor at Deep River station and the ionization chamber at Beijing station; [O_3] data were selected from Resolute (74.4°N, 94.6°W), Canada, Bismarck (46.4°N, 100.5°W), America, Kagoshima (31.4°N, 130.4°E), Japan, Kodaikanal (10.1° N, 77.3°E), India. The statistical results show that [O_3] prominently is modulated and disturbed by 11 years variation and Forbush decrease of the galactic cosmic ray.

II. The modulation of 11 years variation of cosmic ray intensity on the ozone. Fig. 1c is the curves of yearly variation of cosmic ray intensity. The solid line is the data of the superneutron monitor at Deep River. The dashed line indicats μ meson component recorded by the ionization chamber at Beijing. It can be seen that there is the maximum of cosmic ray intensity during the solar activity minimum (1964-1965), there is the minimum of cosmic ray intensity during the solar activity maximum (1969-1970). Fig. 1 a,b are the corresponding content of O_3 at four variant latitudes. Used [O_3] data is selected from "Ozone data for the world" published by Canada[8] . The analysis results show that except Resolute Station at high latitude 11 years variation of [O_3] is very evident. The ozone content decreases when cosmic ray intensity increases, The ozone content increases whe cosmic ray intensity decreases. This means the relationship between the ozone variation and cosmic ray intensity variation is the nagetive correlation.

It is seen from fig. 1 that 11 years variation of [O_3] has evident latitude effect. From maximum year of cosmic ray in-

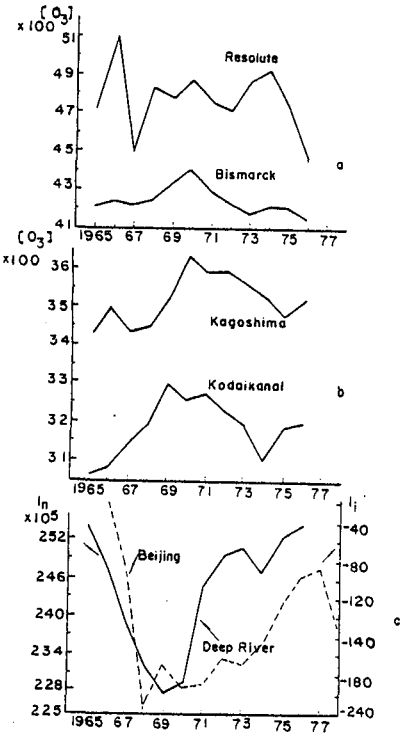

Fig.1 The modulation of 11 years variation of cosmic ray intensity on the ozone

tensity to minimum year $[O_3]$ increased by 7.8% and 5.8% at Kodaikanal and Kagoshima respectively. The increase of $[O_3]$ decreased with the increase of the latitudes, $[O_3]$ only increased by 4.8% at Bismarck. But 11 years variation of $[O_3]$ become indistinct at Resolute in the polar region.

III. The disturbance of Forbush decrease on $[O_3]$. 1. Data analysis. In order to study the disturbance stage of Forbush decrease for variant amplitudes on $[O_3]$, Forbush decrease events are divided >1%, >2%, >3% and >5% four importances based on their amplitudes. The disturbance analysis of the solar flare and Forbush decrease on vorticity arear index (VAI) showed that the disturbances of VAI have evident seasonal property [9]. So the time occurred Forbush decrease is also divided the winter (10-3 months) and the summer (4-9 months). According to the seasons and importances occurred Forbush decrease, their variant combination is analysed. There were 234 Forbush decrease events during 1965-1976. The distribution of various Forbush decrease events as table 1 shown.

Table 1 The distribution of Forbush decrease events

importance / season	>1%	>2%	>3%	>5%
winter	119	49	22	4
summer	115	48	28	4
total	234	97	50	8

The method of the statistical study has used the superposed epoch method. The day of the minimum of Forbush decrease is considered as the zero day. The abscissa denotes the time in days for all of the figures in this section. The ordinate represents the ozone content. The horizontal line refers to the average value of the total absembly of $[O_3]$. The dashed line represents confidence level with probability 0.05 or the degree of confidence 95%. n is the number of Forbush decrease events.

2. Analysis results. The statistical study for all Forbush decrease events shows that the disturbance of Forbush decrease on $[O_3]$ is of statistical significance, and the amplitude of $[O_3]$ disturbance increases with the increase of Forbush decrease amplitude. The disturbance of Forbush decrease on $[O_3]$ increases with the increase of the latitudes. But at

high latitudes, the effect of the solar cosmic ray and precipitating particles on [O_3] will be over Forbush decrease, so that the ozone disturbance produced by Forbush decrease all is covered.

The disturbance of Forbush decrease occurred in the winter on [O_3] is larger and more evident. Usually on the day started Forbush decrease, i.e. about at -1 day, [O_3] begins increase, and there is a larger increase after the fourth day. The amplitudes of [O_3] disturbance increase with the increase of the latitudes of the observational stations. Fig. 2 shows the disturbance of [O_3] for variant latitude regions in the winter. Because the data of [O_3] observed in the winter at Resolute is a few numbers, the change of [O_3] can not be given.

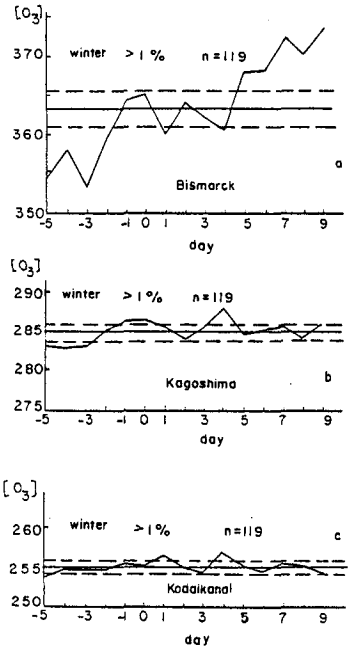

Fig.2 The disturbance of Forbush decrease in the winter on [O_3]

The disturbance Forbush decrease occurred in the witner on [O_3] at same latitude increases with the increase of Forbush decrease amplitudes. If the average value of [O_3] from the third day to the fifth day before the zero day is considered as the undisturbance value of [O_3], that the largest disturbance of >1% Forbush decrease on 0 was about 5.3%. The largest disturbance of >2%, >3% and >5% Forbush decrease events were 5.9%, 6.2% and 10.3% respectively.

The disturbance of Forbush decrease occurred in the summer on [O_3] in low latitudes can also be seen, but its disturbance is very less than in the winter. The disturbance of Forbush decrease on [O_3] all is covered at high latitudes. It always is the decrease tendency after the solar flare, and it lasts several days (see Fig.3).

IV. Conclusions and discussion.

According to the results discribed above, we obtain the following conclusions:

[O_3] is modulated by 11 years variation of cosmic ray intensity. The relationship between the ozone variation and cosmic ray intensity variation is the negative correlation. The 11 years vibration of [O_3] is most evident at the middle and the low la-

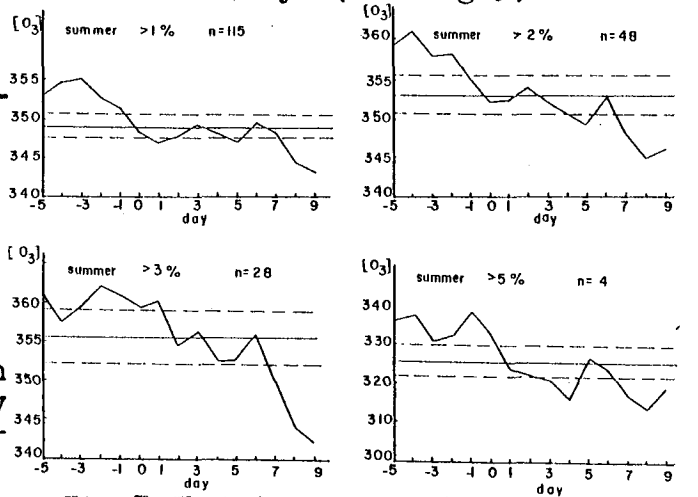

Fig.3 The change of [O_3] during Forbush decrease in the summer at Bismarck.

titudes. The law of this variation is more indistinct at the high latitudes. Because the influences of the solar cosmic ray and precipitating particles on [O_3] are so large that the effect caused by the long period variation of cosmic ray intensity is covered.

The disturbance of Forbush decrease occurred in the winter on [O_3] is very remarkable. The disturbance of [O_3] evidently increases with the rising of the latitudes. Usually [O_3] increases after Forbush decrease started, and lasts several days. The disturbance occurs the maximum after the fourth or the fifth day. The amplitude of [O_3] disturbance also increases with the increase of Forbush decrease amplitude.

The disturbance of Forbush decrease occurred in the summer on [O_3] is very interesting. The effect of Forbush decrease on [O_3] is also evident at the low latitudes, but the disturbance of [O_3] is just opposite to the effect caused by Forbush decrease at the high latitudes. Evidently, this is not produced by Forbush decrease. It is produced by the solar cosmic ray and precipitating particle events. As was shown by Shah [10] , the disturbance of the solar cosmic ray events occurred in the summer on VAI is the most remarkable. We discover that the larger solar cosmic ray events occur in the summer. So the disturbance of the solar cosmic ray events occurred in the summer on [O_3] can also be the most remarkable.

References.

1. Warneck, P. (1972), J. Geophys. Res., Vol. 77, 6589
2. Nicolet, M. et al. (1972), Annals Geophys., Vol. 28, 751
3. Brasseur, G. et al. (1973, Planet. Space sci., vol. 21 939
4. Nicolet, M. (1975), Planet, Space Sci,. Vol. 23, 637
5. Reagan, J. B. (1981), J. Geophys. Res., Vol. 86, 1473
6. Donald, F. H. et al. (1977), Science, Vol. 197, 866
7. Ruderman, M. A. et al. (1975), Planet. Space Sci., Vol. 23, 247
8. Ozone data for the world, environment Canada, atmospheric environment Service 1965-1976
9. Ye Zonghai et al. (1984), Chinese Journal of Space Science, Vol. 4, 198
10. Shah, G. N. (1981), J. Atmos. Terres. Phys, Vol. 43, 147

Using the Information of Cosmic Rays to Predict Influenza Epidemic

Yu Zhen-dong

Hubei Research Institute of Environmental Protection, Wuhan, China

Abstract

Why does influenza become worldwide pandemic at times? This paper suggests some new observations. First, there is a remarkable relationship between influenza pandemics and cosmic ray environment. Second, there is an excellent correlation between influenza pandemics and bright novae and Nova 7 Car. In addition, we propose four indexes to predict future influenza pandemics. Using one of these indexes we successfully predicted the influenza epidemic in 1984.

A. Introduction

Influenza has caused the greatest visitation and the severest natural calamity in this century. Unimaginably about twenty million people died in the influenza pandemic of 1918-1919. Why does influenza become worldwide pandemic at times? For exploring its basic cause, in 1978 R.Ing suggested that except for the pandemic of 1889, the beginning dates of historical influenza pandemic in the 18th and 19th centuries, as well as pandemics and viral antigenic shifts in this century, appear to have occurred in years of high sunspot number.(1) We have different views on this. At the time of suggesting his viewpoint, R.Ing cited seven influenza pandemics in the 18th and 19th centuries, based on the researches by J.R.Mote. But from complete data published by J.R.Mote, there were fifteen main influenza epidemics in the 18th and 19th centuries.(2) Although he employs different terms of "epidemic" and "pandemic", however, this distinction is purely for convenionce as Mote indicated. Because different historical records had different criteria and different detailed extent, it is very difficult to compare epidemical scale one another exactly. The distribution of the beginning dates of fifteen main influenza epidemics in the sunspot cycle is shown in figure 1.

From figure 1 we can see that there are four times in years of high sunspot number(over 80) and five times in years of low sunspot number(below 25). In addition, from researches by W.I.B. Beveridge in 1977, there were seven considerable worldwide influenza pandemics in the 18th and 19th centuries.(3) The beginning dates of these pandemics are also shown in figure 1. We note that there are one time in year of high sunspot number and four times in years of low sunspot number. Therefore, according to the studies by J.R.Mote and researches by W.I.B.Beveridge, we can conclude that in sunspot cycle the phase that correlated to a certain extent with epidemics and pandemics of influenza should be the years of low sunspot number, it was more than the occurred number in high sunspot year.

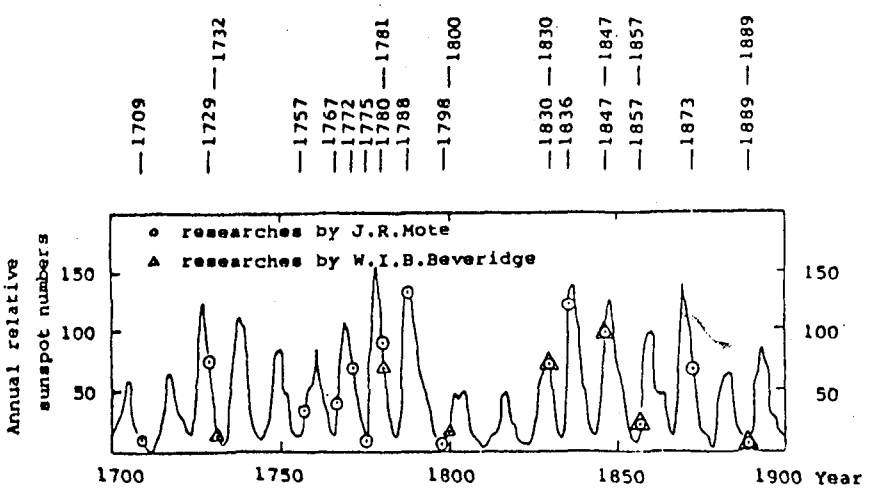

Fig.1 The distribution of the beginning dates of main influenza epidemics in the sunspot cycle in the 18th and 19th centuries

For explaining the mechanisms on how the high sunspot activity can affect influenza pandemics,Ing indicates that people conjecture that the amount of ultraviolet light(UV) incident on the surface of the earth is increased by enhanced solar activity, which might conceivably accelerate the mutation rate of the influenza virus. This speculation cannot, however, explain influenza pandemics occurred in years of low sunspot number. In this paper we try to offer an explanation for this based on cosmic ray researches.

But why have influenza pandemics occurred in some times and why have they not occurred in the others around the periods of low and high sunspot number? Actually, the periods of low and high sunspot number ire merely a favorable conditions and a minor causing factor of influenza pandemic,and the dominant causing factor might be earth's cosmic ray environment.

B. Influenza and the cosmic ray environment

Since the start of systematic and continuous observations of cosmic ray in 1936,the number of ground level enhancement event had been rare in more than forty years. Among them large enhancement events happened only five times.[4] These large Ground Level Solar Cosmic Ray Events (GLEs) occurred on Feb.28,1942; Mar.7,1942; July 25,1946; Nov.19,1949 and Feb.23,1956.According to the researches by V.M.Zhdanov et al.[5] there were five influenza pandemics in the first half of this century. Among them the beginning dates of two pandemics were in 1943 and in 1947. They occurred just after the first three large GLEs respectively. After the large GLE on Nov.19,1949, in 1950-1951 there also occurred a severe influenza epidemic spreading to Europe,Africa, North America, Japan and other places. In Liverpool, the death rate even surpassed that of the pandemic of 1918.[5] So V.M.Zhdanov et al. held that the epidemic time of the fifth influenza pandemic in this century was 1947-Feb.1952. Even more, in 1957, the next year of large GLE on Feb.23, 1956, there occurred a worldwide influenza pandemic too. Among seven influenza pandemics occurred hitherto in this century, it was the second severest pandemic. We note that after five large GLEs occurred in the past forty years or so influenza pandemic invariably broke out in each case. Therefore, very remarkable is the corresponding relationship between influenza pandemic and the large variation in the cosmic ray environment.

These extraordinary events of cosmic ray environment all occurred before influenza pandemics one year or so. To start a new influenza pandemic this interval is reasonable, since it takes time for influenza viruses to mutate or to recombine genes and then for selection of human immunity to form new pandemic strains.

Among three pandemics the severest one was that of 1957. And the GLE on Feb.23,1956 was the largest GLE among all recorded GLEs. It seems as if the scale and harmfulness of influenza epidemic were related to the enhanced amplitude of ground level cosmic rays. But this relationship might not be simply understood as a direct proportion relationship.

The mechanisms on how the cosmic ray environment can affect influenza pandemics cannot be discussed here in detail. We presume it has these main aspects. First, the sudden enhancement of cosmic ray environment could deplete the atmospheric ozone layer and therefore bring the increase of the amount of ultraviolet light incident upon the surface of the earth. Second, the abrupt enhancement of ground level cosmic rays seems to give living things an X-ray. The ionizing radiation resulted from cosmic rays in human and animal body and the enhanced ultraviolet rays could lead to mutation of influenza viruses or gene recombination among different human and animal influenza viruses and therefore bring viral antigenic shifts and form new subtypes of influenza virus. Third, the large variation of cosmic ray environment could lead to corresponding variation of other natural environment elements and therefore bring a more favourable ecological environment for infection and transmission of new subtype of influenza virus.

From these mechanisms, we can understand the reasons that influenza pandemics sometimes occurred in the years of low sunspot number. Because the years of low sunspot number were just the years of high cosmic ray intensity on the earth[6], so the years of low sunspot number were just the years of high ultraviolet intensity incident on the surface of the earth.

C. Influenza and novae

The researches on the relationship between cosmic ray environment and influenza pandemic provide a new way for exploring causes of other influenza pandemics. We might envisage that influenza pandemic can also be aroused by other astronomical phenomena not just the sun, if these phenomena can cause large enhanced effect of cosmic ray environment of life on the earth.

Here we want to raise a new issue i.e. the relationship between the novae and influenza pandemics. From table 1 we notice that there is a very good corresponding relationship between bright novae and the front four influenza pandemics occurred in this century. In this century there have hitherto occurred only eight novae with maximum apparent magnitude(MAM) brighter

than 2.2. And table 1 listed as many as five bright novae. The three others are GK Per with MAM 0.2 in Feb.1901, V476 Cyg with MAM 2.0 in Aug.1920, and V1500 Cyg with MAM 2.2 in Aug.1975. After the occurrence of Nova V1500 Cyg, we have noted that swine influenza virus($H_{sw}1N1$) reappeared in 1976 and the H1N1 subtype resurfaced in 1977 and spread to wide regions of the world. After the occurrence of Nova V476 Cyg, we have also noted that influenza epidemic occurred in many countries, such as UK, Ireland, Belgium, Norway etc., the influenza mortality reached a peak in 1922.[5] As regards the Nova GK Per, we have not had detailed epidemiological data of influenza in 1902, so we donot know whether an influenza epidemic occurred or not in that year. We note that after seven bright novae out of those eight all occurred epidemics or pandemics of influenza. Therefore, the corresponding relation between bright novae and influenza pandemics is also very remarkable.

About the great pandemic of 1918-1919 we think that its beginning was caused by other factor but the Nova V603 Aql took a decisive role for that why the second wave of this pandemic became very different than the first wave in harmfulness and turned to the most spectacular outbreak of any disease for hundreds of years.

Table 1. The contrast between bright novae and the first four influenza pandemics in the 20th century

The beginning dates of influenza pandemics[5]	Bright novae [7]
1918	Nova V603 Aql, maximum apparent magnitude -1.1 on June 10,1918
1926	Nova RR Pic, maximum apparent magnitude 1.2 on June 8,1925
1936	Nova DQ Her, maximum apparent magnitude 1.4 on Dec.22,1934
	Nova CP Lac, maximum apparent magnitude 2.1 on June 20,1936
1943	Nova CP Pup, maximum apparent magnitude 0.2 on Nov.11,1942

Table 2. The contrast between the years of maximum of brightness of Nova η Car and the years of influenza pandemics in the 18th and 19th centuries

The years of epidemics and pandemics of influenza by J.R.Mote[2]	All the years of maximum of brightness of Nova η Car[7]	The years of influenza pandemics by W.I.B.Beveridge[3]
1709-1712		
1729-1733	1729	1732-1733
1757-1762	1752	
1767		
1772		
1775-1776		
1780-1782		1781-1782
1788-1790		
1798-1803	1801	1800-1802
1830-1833	1827	1830-1833
1836-1837		
1847-1850	1843	1847-1848
1857-1858	1856	1857-1858
1873-1875	1871	
1889	1889	1889-1890

As regards the influenza pandemics of 18th and 19th centuries, we found that there existed an interesting relationship between them and Nova η Car. The brightness of η Car was variable. It was sometimes bright and sometimes dark. According to the researches by C.Payne-Gaposchkin,[7] in 18th and 19th centuries its maximum occurred only eight times. Table 2 shows that after every maximum of brightness of Nova η Car there was almost always the influenza pandemic. Especially in the 19th century, their relation was bordering on one to one corresponding relation. It is hardly conceivable for such good correlation. Is it possible that the Nova η Car could bring a very large amount of UV,X- and r-rays incident on the earth when it turned up outburst?

Nova is a violent phenomenon of star explosion. People believe it is one of the sources of cosmic rays. If the nova can really bring the influenza pandemic, then the transmitter of nova information should be its high energy X-,r-rays (nova's X-,r-rays→ the depletion of the atmospheric ozone layer→ the strong increase in the solar UV incident on the surface of the earth → influenza pandemic). Nevertheless, bright nova is a rare astronomical phenomenon. In the past forty years or so there occurred only one bright nova with MAM 2.2. The modern data of cosmic ray intensity variation effect of nova are very few, so it is difficult now to make sound comments on affection extent of bright nova on earth's cosmic ray environment. However, the excellent correlation between influenza pandemics and novae implies strongly that the cosmic ray environment variation of earth should be seriously investigated after the occurrence of nova. Therefore, we suggest that the intensity variation of X-,r-rays and UV will have to be investigeted by various observation means from ground level to satellite altitude when turning up outburst for η Car or when occurring of bright nova in the future.

D. To predict influenza epidemic

According to the excellent correlation in the past, we propose four indexes to predict future influenza pandemics: first, the occurring of the large GLE; second, the occurring of the bright nova; third, the turning up outburst again for η Car; fourth, the large enhancement of life's cosmic ray environment caused by other astronomical phenomena.[8][9][10] When one of these indexes takes place, it would not at all be surprising if a new influenza pandemic should emerge soon after.

We are glad to report that according to the first index we successfully predicted the influenza epidemic in 1984. On Dec.8,1982 there occurred a middle GLE.[11] So the author wrote a report to the China Influenza Centre to predict that influenza epidemic would soon emerge in the world in 1984. As expected, the influenza epidemic has emerged. In the USSR in two months from the second half of January to the first half of March the number of cases of influenza illness reached several millions, about 3-5% of the population were affected during the week of highest activity,[12] in big cities and in the capitals of fifteen Soviet Socialist Republics the incidence reached about 10% of the population. In the same time, widespread influenza illness has been reported also in the USA, many european countries, Japan, Pakistan, Algeria, Morocco, Tonga etc..[13] Therefore, one of the viewpoints of this paper has got a successful verification.

References:

1. Ing R. Solar activity and influenza. Nature 1978; 276:556.
2. Mote JR. Human and swine influenzas. In: Virus and Rickettsial Diseases. Harvard University Press, 1948: 429-516.
3. Beveridge WIB. Influenza,The Last Great Plague. New York: Prodist, 1977: 27-30.
4. Duggal SP. Relativistic solar cosmic rays. Rev Geophys Space Phys 1979; 17:1021-58.
5. Zhdanov VM,et al. Influenza. Moscow, 1958: 408-422. (in Russian)
6. Pomerantz MA, Duggal SP. The sun and cosmic rays. Rev Geophys Space Phys 1974; 12:347.
7. Payne-Gaposchkin C. The Galactic Novae. Amsterdam: North-Holland, 1957: 2-98.
8. Wdowczyk J, Wolfendale AW. Cosmic rays and ancient catastrophes. Nature 1977;268:510-12.
9. Clark DH, McCrea WH, Stephenson FR. Frequency of nearby supernovae and climatic and biological catastrophes. Nature 1977; 265:318-19.
10. Agraval SP, Ananth AG, Bemalkhedkar MM, Kargathra LV, Rao UR. High-energy cosmic ray intensity increase of nonsolar origin and the unusual Forbush decrease of August 1972. J Geophys Research 1974; 79:2269-80.
11. Fenton KB, Fenton AG, Humble JE. Cosmic ray flare increases. Proc 18th Int Cosmic Ray Conf 1983; 4:189.
12. WHO. Wkly Epidem Rec 1984; 59:115.
13. WHO. Wkly Epidem Rec 1984; 59:19-179.

Strong Earthquakes, Novae and Cosmic Ray Environment

Yu Zhen-dong

Hubei Research Institute of Environmental Protection, Wuhan, China

Abstract

This paper suggests some new observations about the relationship between seismic activity and astronomical phenomena. First, after investigating the seismic data (magnitude 7.0 and over) with the method of superposed epochs we find that the world seismicity evidently increased after the occurring of novae with maximum apparent magnitude brighter than 2.2. Second, a great many earthquakes of magnitude 7.0 and over concentrated to occur in the 13th month after the occurring of two largest Ground Level Solar Cosmic Ray Events (GLEs). From these, we put forward explanations of the causes about three high level phenomena of global seismic activity in 1918-1965 and suggest that according to the information of large GLE or bright nova we shall be able to predict the occurring time of global intense seismic activity.

Is seismic activity affected by astronomical phenomena? This paper tries to offer some noticeable results.

A. Seismic data used in this paper

Gutenberg and Richter (1954)[1] edited the catalog of worldwide large earthquakes in 1904-1952. But the number of earthquakes is incomplete for magnitude below 7.9 in 1904-1917. Duda (1965)[2] and Rothe (1969)[3] continued Gutenberg-Richter's classical work. They extended the catalog to 1965. Therefore, this paper discusses world seismicity of magnitude 7.0 and over in 1918-1965.

B. The effect of bright novae on world seismicity of magnitude 7.0 and over

During this period of 1918-1965 there appeared six novae with maximum apparent magnitude brighter than 2.2.[4] For investigating the effect of novae on seismic activity, the method of superposed epochs requires to define the "zero day". This date ought to be the date when nova started explosion. But this date was often uncertain. Because brightness rose very fast for most novae, from starting explosion to maximum brightness the duration was only a few days, we unify to use the date of maximum brightness as the "zero day". It is available to those six except Nova RR Pic.The character for Nova RR Pic was that its risen period sustained for a long time (Payne-Gaposchkin,1957)[4]. Its maximum apparent magnitude was 1.2 on June 8,1925 and before two months, however, it had already reached apparent magnitude 3.0. It probably took a long time from starting explosion (apparent magnitude 12.7),to apparent magnitude 3.0. So for the present we move the date up 3 months from its maximum brightness date, namely March 8,1925, as the "zero day".

From the next day of the "zero day" on,we take every two months as one time-interval and investigate the numbers of worldwide earthquakes in every time-interval.For six novae we obtain the mean value of earthquake number in each time-interval.They are shown in figure 1.

From fig. 1 we note that after the occurrence of bright novae the curve of seismic activity was evidently higher than horizontal line. The increased effect showed successive two waves. In the forty months after the occurrence of bright novae the number of worldwide earthquakes of magnitude 7.0 and over increased eleven or so on average than the mean level before the occurrence of novae. Because there is no third party which can affect the nova and the seismic activity simultaneously, the obvious relationship of them has to be understood as the causation. Therefore, statistical analysis shows that there is an effect that bright novae caused enhanced seismic activity of magnitude 7.0 and over.

Although it is still unclear now about the variation of cosmic-ray environment around Earth after the occurrence of bright novae, yet we can presume that the enhanced seismic activity was caused by nova's x-, r-rays incident upon the earth.

C. The effect of large GLE on world seismicity of magnitude 7.0 and over

Since the start of systematic and continuous observation of cosmic rays,the number of GLE was rare in past forty years or more (Duggal,1979)[5]. Among them large GLE happened only five times and they are shown in table 1 (Dorman,1957)[6]. In table 1 in the years of the occurrence of front three GLEs there also occurred bright novae, their seismic effects were overlapped. The single seismic effect of large GLE cannot be shown. So we discuss the last two events, i.e.two largest GLEs.

From the next day of those two GLE's dates on, we investigate the numbers of worldwide earthquakes of magnitude 7.0 and over in every month and obtain fig.2. From fig.2 we note that in the

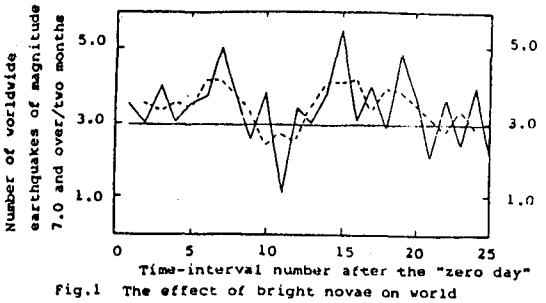

Fig.1 The effect of bright novae on world seismicity of magnitude 7.0 and over six bright novae:V603Aql,V476Cyg,RRPic,DQHer,CPLac,CPPup.
solid line: curve of the average of earthquake numbers
dashed line:curve of three time-intervals running average
The horizontal line of 2.97 is two-monthly average of the number of worldvide earthquakes of magnitude 7.0 and over in six two-years before the "zero days" of six bright novae (before the "zero day" of each bright nova all take two years). It *represents the mean level of seismic* activity when the seismic effect of bright novae did not occur yet.

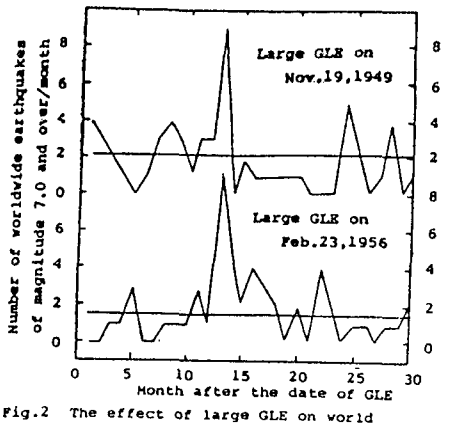

Fig.2 The effect of large GLE on world seismicity of magnitude 7.0 and over
The horizontal lines of 2.17 for upper part and 1.46 for under part represent respectively the monthly mean level of global seismic activity before the occurrence of two GLEs. They are the averages of the numbers of worldvide earthquakes of magnitude 7.0 and over in two years prior to the GLE date.

Table 1 The large GLE data

No.	Date	$\frac{I_{max}}{I}$ *, %	Remarks
1	Feb.28,1942	15.5	average on 15 minutes
2	Mar. 7,1942	15	"
3	Jul.25,1946	22	"
4	Nov.19,1949	57	"
5	Feb.23,1956	200	

* The sea-level enhanced magnitude of cosmic ray hard component at high latitudes (Dorman,1957).

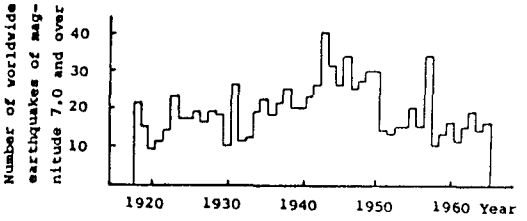

Fig.3 The annual number of worldvide earthquakes of magnitude 7.0 and over in 1918-1965

13th month after the occurrence of the GLE there occurred unusual groups of worldvide large earthquakes. Earthquake number increased extremely obviously. Both of two events were just the same. The risen amplitudes are so high and the peak times are so uniform, thereby fig.2 clearly shows the effect of large GLE on seismic activity of magnitude 7.0 and over. About large GLE in 1949, in increased period (7th-13th month afte the GLE's date) the number of worldvide earthquakes of magnitude 7.0 and over increased eleven than that of mean level prior to the occurring of the GLE. About large GLE in 1956, in increased period (11th-18th month after the GLE's date) the number of worldvide earthquakes of magnitude 7.0 and over increased seventeen than that of mean level prior to the occurring of the GLE.

It can be questioned that whether the enhanced seismic activity would be able to cause by other emission component of those two solar flares on Nov.19,1949 and on Feb.23,1956.Among solar flare emissions, besides solar cosmic rays (SCR) there were also plasma cloud, vissible light,UV, X-rays and radio emission. At the time of the occurring of other large solar flares, except for the large GLE the sudden big increase of these components had been observed many times. But after them the enhanced seismic activity has not been observed. The enhanced seismic activity was only after the large GLE. Therefore we could judge that the enhanced seismic activity was just caused by enhanced high-energy SCR.

D. About causes of three high level phenomena of global seismic activity of magnitude 7.0 and over

1. About the decade of the most earthquake number

From fig.3 we note that the forties were the decade of the most earthquake number. Why was this? It turned out to be that the Earth's cosmic ray environment occurred quite a few enhanced events. In the forties there occurred four times out of five large GLEs described above.At the same time, in 1942 there occurred the Nova CP Pup which is the brightest nova in the last sixty years. Besides, in 1946 there also occurred the recurrent Nova T CrB (Payne-Gaposchkin,1957)[4]. These astronomical phenomena all gave rise to enhanced effects of seismic activity. So the forties became the decade of the most earthquake number.

2. About the year of the most earthquake number and about the years in which earthquake number strikingly increased

From fig.3 we note that in 1943 there occurred the most earthquake number and it unexpectedly was forty. Why was this? It turned out to be that in 1942 there simultaneously occurred two large GLEs and the bright Nova CP Pup. The enhanced periods of seismic activity caused by them were in 1943. So the number of large earthquakes was so high in that year. From fig.3 we note that in some years the earthquake number suddenly increased over ten than their last year. These years were1931, 1943 and 1957. Why was this? The reason for 1943 has explained above. For 1957 it was due to the occurrence of large GLE on Feb.23,1956 which was the largest GLE since the start of systematic and continuous observation of cosmic rays. The enhanced period of seismic activity caused by it was in 1957, so the number of large earthquakes unusually increased than 1956. As regards 1931,because at that time it had not the data of cosmic ray observation, we cannot explain it now.

3. About unusually concentrated periods of earthquakes of magnitude 7.0 and over

The yearly average of the number of worldwide earthquakes of magnitude 7.0 and over was 19.5 in 1918-1965. It corresponded to 3.25 per two months. Nevertheless, in the some periods the seismic activity was unusually high. The number of earthquakes reached over ten in two months and was three times or more of the average. Why was this? In table 2 we listed all of these data in 1918-1965 and put forward explanations of their causes.

The concentrated phenomenon of large earthquakes was more projecting for one month. The monthly average of the number of worldwide earthquakes of magnitude 7.0 and over was 1.6 in 1918-1965. Nevertheless, in the some periods the earthquake number reached unexpectedly 8 or 9 in a month and was five times of the average. In table 3 we listed all of these data in 1918-1965 and put forward explanations of their causes.

Above explanations could already illustrate that the occurring of high level phenomena of global seismic activity of magnitude 7.0 and over was neither accidental nor at random.

Table 2 The explanation of causes on all of the data which the earthquake number of magnitude 7.0 and over reached over ten in two months(61 days) in 1918-1965

No.	Date	Earthquake number M≥7.0	Explanation on causes
1	Jan.27,1931-Mar.28,1931	11	?
2	Oct.10,1938-Dec. 6,1938	11	The Nova CP Lac in 1936; Possible large GLE in Oct.1937?
3	Feb.16,1943-Apr. 9,1943	11	Large GLEs on Feb.28,1942 and on Mar.7,1942; Also existing the effect of the Nova CP Pup in 1942
4	Oct.21,1943-Dec. 1,1943	12	The Nova CP Pup in 1942; Also existing the effect of two large GLEs on Feb.28,1942 and on Mar.7,1942
5	Aug. 2,1946-Sept.30,1946	11	The Nova T CrB in 1946; Large GLE on July 25,1946
6	Jan. 4,1948-Mar. 3,1948	11	The Nova T CrB in 1946; Large GLE on July 25,1946
7	Oct.23,1950-Dec.14,1950	12	Large GLE on Nov.19,1949
8	Mar. 9,1957-Apr.25,1957	15	Large GLE on Feb.23,1956

Table 3 The explanation of causes on all of the data which the earthquake number of magnitude 7.0 and over reached eight in 31 days in 1918-1965

No.	Date	Earthquake number M≥7.0	Explanation on causes	Interval*
1	Nov. 5,1938-Nov.30,1938	8	Possible large GLE in Oct.1937?	
2	Mar. 9,1943-Apr. 9,1943**	8	Large GLEs on Feb.28,1942 and on Mar. 7,1942; Also existing the effect of the Nova CP Pup in 1942	12 months or more
3	Nov. 2,1943-Dec. 1,1943	9	The Nova CP Pup in Nov.1942; Also existing the effect of two large GLEs in 1942	12 months or so
4	Dec. 1,1950-Dec.14,1950	9	Large GLE on Nov.19,1949	12 months or more
5	Mar. 9,1957-Mar.23,1957	9	Large GLE on Feb.23,1956	12 months or more

* The interval between the beginning date of seismic activity increased period and the occurring date of its major cause.

** The interval was 30 days 23 hours between the large earthquakes on Mar.9 and on Apr.9.

E. Discussion

1. We discuss some tentative ideas on mechanisms that cosmic rays affect seismic activity. The cosmic ray particles incident in lithosphere were rare. It was still limited when occurring large GLE. So the effect of the direct action probably is very small for the mechanisms.

Cosmic rays gave rise to atmospheric ionization when they passed though the atmosphere. The ionicity had difference at different atmospheric altitude and at different geomagnetic latitude. From the atmospheric ionization there forms an atmospheric electric-field,we call it *cosmic ray* atmospheric electric-field. Its maximum intensity was at the top of troposphere or at the bottom of stratosphere. When occurring the large GLE the cosmic-ray atmospheric electric-field would intensify. The sudden intensifying of atmospheric electric-field probably was just the factor which led to the occurrence of enhanced seismic activity. Through affecting the telluric electric-field and atmospheric circulation which affected the rate variation of the Earth's rotation it finally led to the occurrence of large earthquakes. The possible *mechanisms are as follows*:

solar cosmic rays or nova's x-,r-rays ⟶ cosmic ray atmospheric electric-field ⇄
⟶ atmospheric circulation ⟶ Earth's rotation ↘
↘ telluric electric-field ⟶ earthquakes

2. About the groups of largeearthquakes in Mar.1943,Dec.1950 and Mar.1957(see table 3),we think they were caused by the corresponding large GLE one year ago.It seems to show that at least for some earthquakes of magnitude 7.0 and over their brewing time was not long,only one year or so.

3. Fig.1 shows the seismic effect of bright novae had successive two waves. We think that it probably was caused by two batches of nova's radiation which reached Earth in different time.The first batch reached Earth in the time which was soon after or simultaneous with the visible light. From fig.1 we estimate that the main current of the second batch reached Earth in the 17th month or so on average after nova started explosion. Aikin et al.(1980)[7] suggested that among supernova radiation caused Earth effects the first batch was prior to the second batch to reach Earth for several months. Maybe nova is similar to supernova.

4. The explosion scale of supernova is more violent than that of nova. If occurring the bright supernova visible to the naked eyes, we could infer that the global seismic activity will soon increase obviously.

5. Since aforesaid change of cosmic ray environment could lead to the increase of world seismicity, we could infer that the background and other variations of cosmic rays should also be able to affect the world seismicity.

6. The occurring of the groups of large earthquakes is not a mystery to us now.Moreover,as a means it could help us to research the changes of cosmic ray environment. That is,it is an "indicator", according to this indicator we can know the enhanced event of cosmic ray environment had already occurred before it. For example, about the groups of worldwide large earthquakes($M \geq 7.0$) in 1931 and in Nov.1938[1] we could infer that in 1930 there probably had occurred the enhanced event of cosmic ray environment and in Oct.1937 there probably had occurred a large GLE.

7. When occurring the large GLE or bright nova in future, according to fig.1,fig.2, and table 3 we shall be able to predict the occurring time of global intense seismic activity.

References

1. Gutenberg,B.,and C.F.Richter(1954). Seismicity of the earth and associated phenomena, Princeton University Press, Princeton, 133-160.
2. Duda,S.J.(1965). Secular seismic energy release in the Circum-Pacific Belt, Tectonophysics 2, 409-452.
3. Rothe,J.P.(1969). The seismicity of the earth 1953-1965, UNESCO, 29-307.
4. Payne-Gaposchkin,C.(1957). The galactic novae, North-Holland, Amsterdam, 2-146.
5. Duggal,S.P.(1979). Relativistic solar cosmic rays, Rev. Geophys. Space Phys. 17, 1021-1058.
6. ДОРМАН(Dorman),Л.И.(1957). Вариации космических лучей, ГОСТЕХИЗДАТ, МОСКВА, 353-395.
7. Aikin,A.C.,S.Chandra,and T.P.Stecher(1980). Supernovae effects on the terrestrial atmosphere, Planet. Space Sci. 28, 639-644.

OBSERVATION OF NUCLEI WITH ENERGIES 8-30 MeV PER NUCLEON IN THE EARTH's MAGNETOSPHERE AT THE ALTITUDES 350 KM

Bobrovskaya V.V., Grigorov N.L., Gordeev Yu.P., Zhuravlev D.A., Nymmik R.A., Podgurskaya A.V., Smolensky L.G., Tretyakova Ch.A., Gordeev I.V., Iyagushin V.I., and Solloviev A.V.

Institute of Nuclear Physics, Moscow State University
Moscow, USSR

ABSTRACT

Observations of the flux of nuclei with an energy of IO MeV per nucleon on the Salyut-7 Station in September I984 are presented. The observed flux is smaller by a factor of 50 than the flux detected in May, I98I.

I. Introduction. We continue investigations of the fluxes of nuclei with energies of 8-30 MeV per nucleon in the orbits of scientific stations (inclination $\sim 50^{\circ}$, height ~ 350 km). The noted nuclei cannot get into these orbits from the interplanetary space because of the insufficient magnetic rigidity. In ref. /I/ the nuclei observed in I973/74 year were interpreted as the particles of the anomalous cosmic ray component which, according to ref. /2/, are the singly-charged atoms. Our preceding experiment performed in May, I98I /3/ speake in favour of the magnetospheric origin of the observed particles, which was first suggested in ref. /4/.

This paper reports the preliminary results of a new experiment made with the improved technique enables one both to measure the flux of nuclei and to fix the registration point in the orbit.

2. Experiment. We used an instrument with 3 stacks of 3.7xI2.5 cm^2 dielectric track detectors. Each stack contained IO sheets CN-85 of I00 mkm thick and was protected against the ultraviolet solar radiation by two layers of aluminized lavsan film I.4 mg/cm^2 in total thickness. During the experiment the 3 mm thick Al screen was displaced above two stacks (No.I and No.2) to cover one of them depending on the value of proton flux incident upon the instrument. In the region of the Brasil magnetic anomaly when the proton flux ex-

ceeded IO^2 $cm^{-2}sec^{-I}$ the screen covered the stack No.I and the nuclei were detected with the stack No.2. Outside the Brasil magnetic anomaly the screen covered the stack No.2 and the nuclei were detected with No.I. The stack No.3 was open throughout the exposure time. The overall weight of the instrument with the self-contained power supply and detectors was ~ 2 kg.

The instrument was delivered into the orbit on August I5, I984, On September I9 the instrument was installed in the Salyut-7 lock--chamber and was exposed to space. The exposure time was I32 hours. On October 2, I984 the detectors were returned to the Earth.

3. Analysis. The detectors were etched and the developed tracks were analysed. In each stack we revealed about a hundred of nuclei most of which got into the stacks during the 43-day storage within the station. These so-called "background" tracks are produced by the nuclei with an energy of several hundreds of MeVs per nucleon in outer space. Being decelerated in the walls and matter of the station elements, some nuclei possessing an energy < 25 MeV per nucleon, arrived at the detectors and came to rest in the cellulose nitrate film. The density of background nuclei is the same throughout the depth of relatively thin stacks. Owing to this fact we succeeded in identifying the nuclei detected in outer space as excess tracks fixed in the upper sheets of the stacks.

4. Preliminary results. On the number of tracks detected with the stack No.3 the flux of nuclei with $Z \geq 6$ at an energy of I2 MeV per nucleon is estimated to be $2 \cdot IO^{-3}$ $(m^2 s.st.MeV/nucleon)^{-I}$. In this case the energy was estimated from the range-energy dependence for oxygen nuclei and the detection time was associated with the exposure time, I32 hours. The data from the stack No.I and No.2 show that the significant part of nuclei were observed in the region of an increased proton flux, i.e. in the Brasil magnetic anomaly, but the statistical errors of these data are high.

5. Discussion. Comparing the present experimental data and the results /3/ we conclude that the flux of nuclei in September, I984

is by a factor of about 50 less than that of in May, I98I. This difference under identical experimental conditions indicates the large time fluctuations of the flux intensity observed in the orbit. These fluctuations can explain the result /5/ that the flux of oxygen nuclei with an energy ~IO MeV per nucleon in the same orbit in I978/79 years was IO^{-2} (m^2 s. st. MeV/nucleon)$^{-I}$ which is 20 times as small as the value we obtained in May, I98I at the same solar activity.

6. Acknowledgements. We are grateful to cosmonauts N.D.Kisim, V.A. Soloviev, and O.Yu.Atikov for the work done to expose the instrument and also to S.P.Tretyakova for the etching of the stacks.

References.

I. Biswas, S., Durgaprasad, N., (I980), Skylab Measurements of Low Energy Cosmic Rays, Space Science Reviews, v.25, No.3, pp.285-326

2. Fisk, L.A., Kozlovsky, B., Rematy, R., (I974), An Interpretation of Observed Oxygen and Nitrogen Enhancement in Low-Energy Cosmic Rays, Ap. J., I90, I35.

3. Bobrovskaya, V.V., Gorchakov, E.V., Grigorov, N.L., Nymmik, R.A., Tretyakova, Ch.A., Marin, A., Haiduc, M., Hasegan, D., (I983), The Measurement of the Fluxes of Medium Nuclei (C,N,O) With an Energy of IO-25 MeV per Nucleon in the Near-Earth Space, (I983), I8th Int. Conf. Cosmic Rays, Bangalore, India, v.2, p.2

4. Chan, I.H., Price, P.B., (I975), Composition and Energy Spectra of Heavy Nuclei of Unknown Origin Detected on Skylab, Phys. Review Letters, v.35, No.8, p.538.

5. Gagarin, Yu.F., Gordeev, I.V., Ivanova, N.S., Lyagushin, V.I., Smirnov, A.B., Soloviev, A.V., Khilyuto, I.G., Yakubovskii, E.A., (I983), Anomalous Fluxes of Low-Energy Nuclei in the Salyut-6 Orbit, Izv. Akad. Nauk SSSR, ser. fiz., 47, №9, p.I844.

SH 10.1-6

MEASUREMENT OF LOW ENERGY COSMIC RAYS ABOARD SPACELAB-1

R.Beaujean, K.Oschlies, and W.Enge
Institut für Reine und Angewandte Kernphysik
der Universität Kiel, 23 Kiel, W.-Germany

Abstract

In December 1983 the first Spacelab mission was launched for a duration of 10 days. Aboard was the Kiel experiment "Isotopic Stack" designed for measurement of heavy cosmic ray nuclei with nuclear charge equal to or greater than 3 and energies up to some 100MeV/nuc. One part of the stack was rotated in well defined steps registered by an angle encoder to receive information on impact times of the nuclei. Using this time resolving system "geomagnetically forbidden" particles can be detected.
In this work the chemical composition and energy spectra of mainly CNO particles are examined using a rotated 300µm thick CR-39 foil beneath a fixed 100µm thick Kodak-Cellulose Nitrate foil. About 600cm^2 have been scanned yielding nearly 100 nuclear tracks within an energy range of approximately 8 to 30 MeV/nuc.
The calibration is done by means of a postflight irradiation with 410 MeV/nuc ^{56}Fe at Berkeley Laboratory, California, USA.
Relative abundances and energy spectra will be presented.

Keywords : Spacelab-1, heavy cosmic rays, plastic track detectors

SH 10.1-7

HEAVY COSMIC RAY MEASUREMENT ABOARD SPACELAB-1

R.Beaujean, J.Krause, E.Fischer, and W.Enge
Institut für Reine und Angewandte Kernphysik
der Universität Kiel, 23 Kiel, W.-Germany

Abstract

A stack of CR-39 plastic track detectors was exposed to the cosmic radiation during the 10 days mission aboard Spacelab-1. A part of the stack was rotated one revolution within 7 days. The impact time of most of the particles was correlated with the orbit position of the shuttle and thus with geomagnetic field parameters. In this work we report on the analysis of heavy particles with charge $Z \geqslant 6$ in the energy range 50-150 MeV per nucleon with special emphasis on "geomagnetically forbidden" particles.

Keywords: Spacelab 1, heavy cosmic rays, geomagnetic field effects, plastic track detectors

SPORADIC RADIO EMISSION CONNECTED WITH A DEFINITE MANIFESTATION OF SOLAR ACTIVITY IN THE NEAR EARTH SPACE

Dudnic A.V., Zaljubovsky I.I., Kartashev V.M., Shmatko E.S.

Kharkov State University, USSR.

Sporadic radio emission of near earth space at the frequency of 38 MHz is shown to appear in case of fast development of instabilities in ionospheric plasma. The instabilities are generated due to primary ionospheric disturbances occuring under the influence of solar chromospheric flares.

During the period close to 21st cycle maximum of solar activity the investigation of sporadic radio emission in the near earth space [1] was carried out at the frequency of 38 MHz using the experimental installation of Kharkov State University [2]. The results of the experiment confirmed the existance of sporadic radio emission in the meter radio wave range [3], in its long wave range in particular. All the types of noise radio emission mentioned in [1] were observed. Fig. 1 presents some examples of the short-time events (0,5 ÷ 7m) detected at the frequency of 38 MHz. Attention was focused on existance of short-time cosmic noise absorptions with sudden onset and end (5,6). There phenomena are not observed at the dm and cm ranges and can't be identified as ionospheric disturbances of SCNA types [4]. Bursts andabsorptions with fine oscillatory structure can also be attributed to the type of events unobser-

vable in [1].

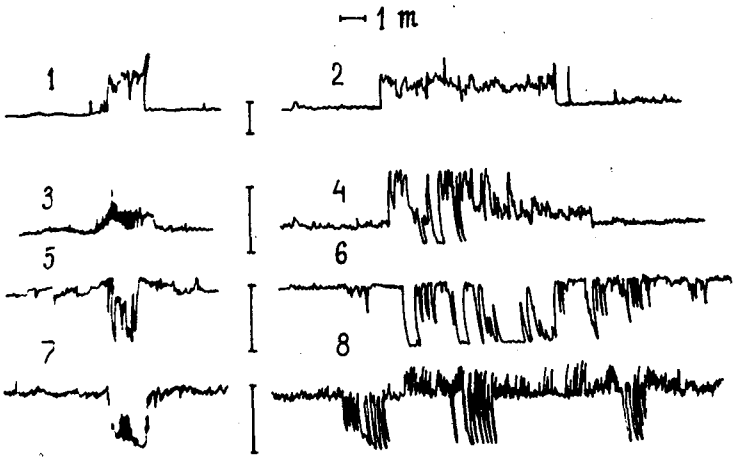

Fig. 1. Characteristic examples of radio emission bursts of near earth space and sudden short-time cosmic noise absorption (SCNA) detected at the frequency of 38 MHz. 1,2 – Sporadic bursts of overage power. 3 – Sporadic bursts with oscillating fine structure. 4 – Sporadic bursts with short-time cosmic noise absorptions. 5,6,7– Short-time sporadic of cosmic noise with oscillating fine structure. 8 – Series of sporadic absorptions of cosmic noise with oscillating fine structure.

Vertical intercepts show radio emission flow equal to $6 \cdot 10^{-22} W/m^2 Hz$.

The data about sporadic radio emission in near earth space at the frequency of 38 MHz obtained in spring and summer of 1981 were compared with solar data [5] in order to

find correlation with specific manifestations of solar activity. Figure 2 shows some eamples of the comparison.

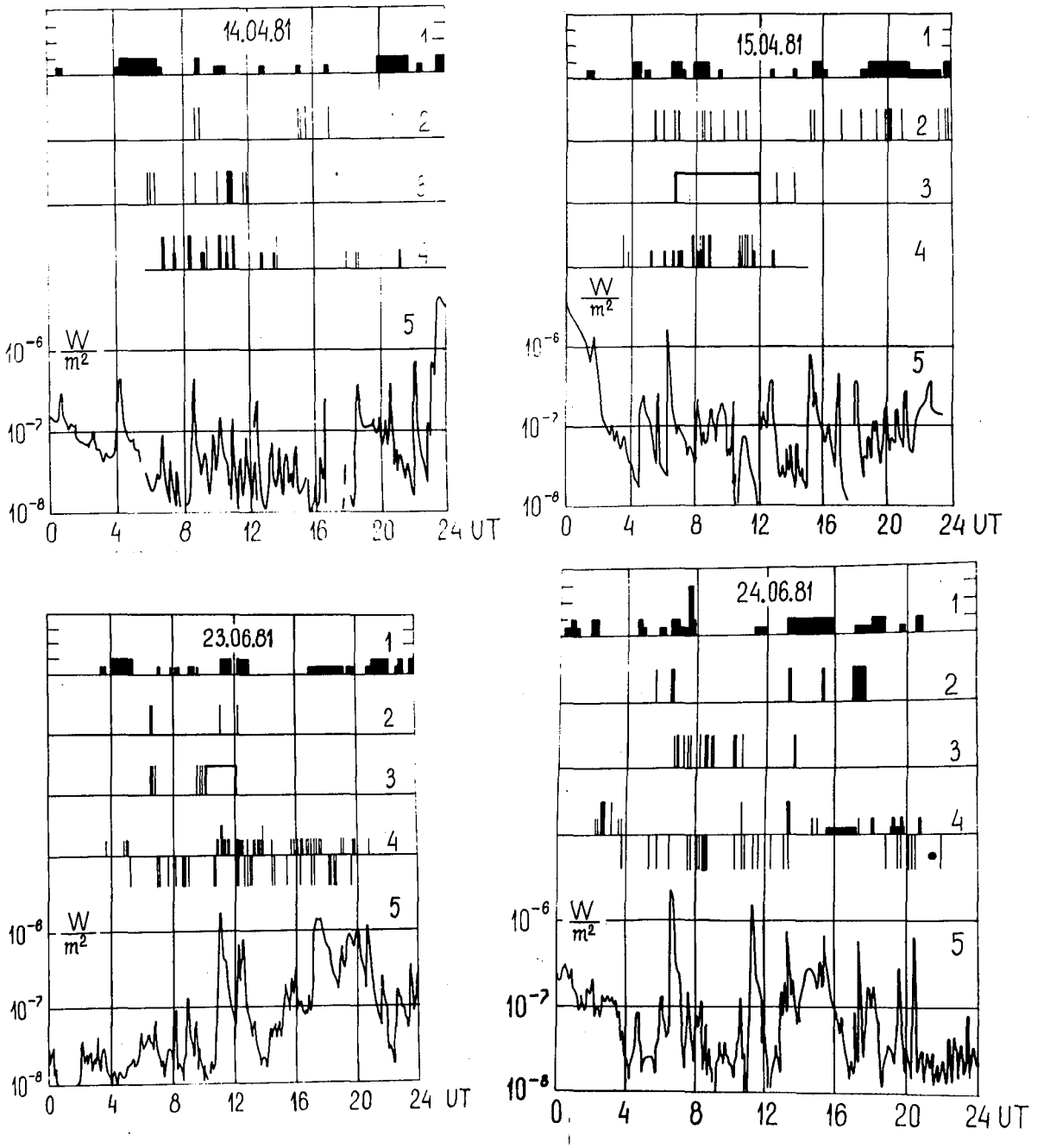

Fig. 2. Time run of solar activity and near earth space spo-

radic bursts and sporadic absorptions during a sinle day and night period at the frequency of 38 MHz. UT - universal time. 1 - Chromosperic flares on the sun 1 + 3 balls. Small flares - 0.5 div. [5]. 2 - Solar radio emission bursts in cm wave range with intensity more than 1.10^{-20} W/m^{2}Hz [5]. 3 - Distinctive events on the sun in meter radio wave range [5]. 4 - Sporadic radio emission bursts (at the top) and absorptions (at the bottom) at the frequency of 38 MHz. Short vertical intercepts at the top part corresponds to radio emission bursts with signal/noise ratio less than 2. Long intercepts corresponds to radio emission bursts with signal/noise ratio $\geq$ 2. Horisontal black rectangle corresponds to noise storms. 5 - X-Ray solar emission intensity is in the spectral interval of 0.5 + 4.0 Å [5].

The main peculiarities of the events observed at the frequency of 38 MHz are the following:
1) the member of events in increased with the growth of solar activivity as is shown in [1]; 2) the rise of chromospheric flares and X-ray bursts at the Sun but there was no full coinsidence in all details; 3) there is no detailed coinsidence with distinctive solar events in radio frequency range; 4) probability of short-time sporadic absorption occurences in winter is lower than in summer; 5) series of quasiperiodic cosmic noise absorptions and quasiperiodic bursts with small signal/noise ratio are observed; 6) at day-time the probability of event occurences is higher than at night.

A detailed analysis of all peculiarities of the phenome-

NEAR EARTH SPACE SPORADIC RADIO EMISSION BUSTS OCCURING DURING SUNRISE

Dudnik A.V., Zaljubovskaja I.I., Kartashev V.M., Lasarev A.V., Shmatko E.S.

Kharkov State University, USSR

During the period of low solar activity sunrise effect of sporadic high frequency near earth space radio emission was experimentally discovered at middle lattitudes. The possible mechanism of its origin in discussed.

Since September 1984 during the period of low solar activity the study of sporadic near earth space radio emission at middle lattitudes [1] has been carried out at the experimental installation of Kharkov University [2]. The radio telescope with operating frequency of 38 MHz described in [2] was in addition provided with a mirror parabolic antenna having an effective area ~ 16 m^2 radiation pattern width $\sim 12^\circ$ and receiving radio emission independently at the frequency of 325 MHz with East - West and North - South polarization; dual - channel radio frequency tract having the transmission band of ~ 4 MHz regulation sensitivity threshold being $2 \cdot 10^{-21}$ w/m^2 Hz for each channel. Tracing of signals was carried out with minimizing rate of 0.2 mm/s and integration time was not more than 1 s.

The analisis of experimental results proves that in

the vicinity of the moment of morning shadow - light boundary passage through the local meridium series of radio high frequency emission burts arise diurnally at the frequecy of 325 MHz (fig. 1).

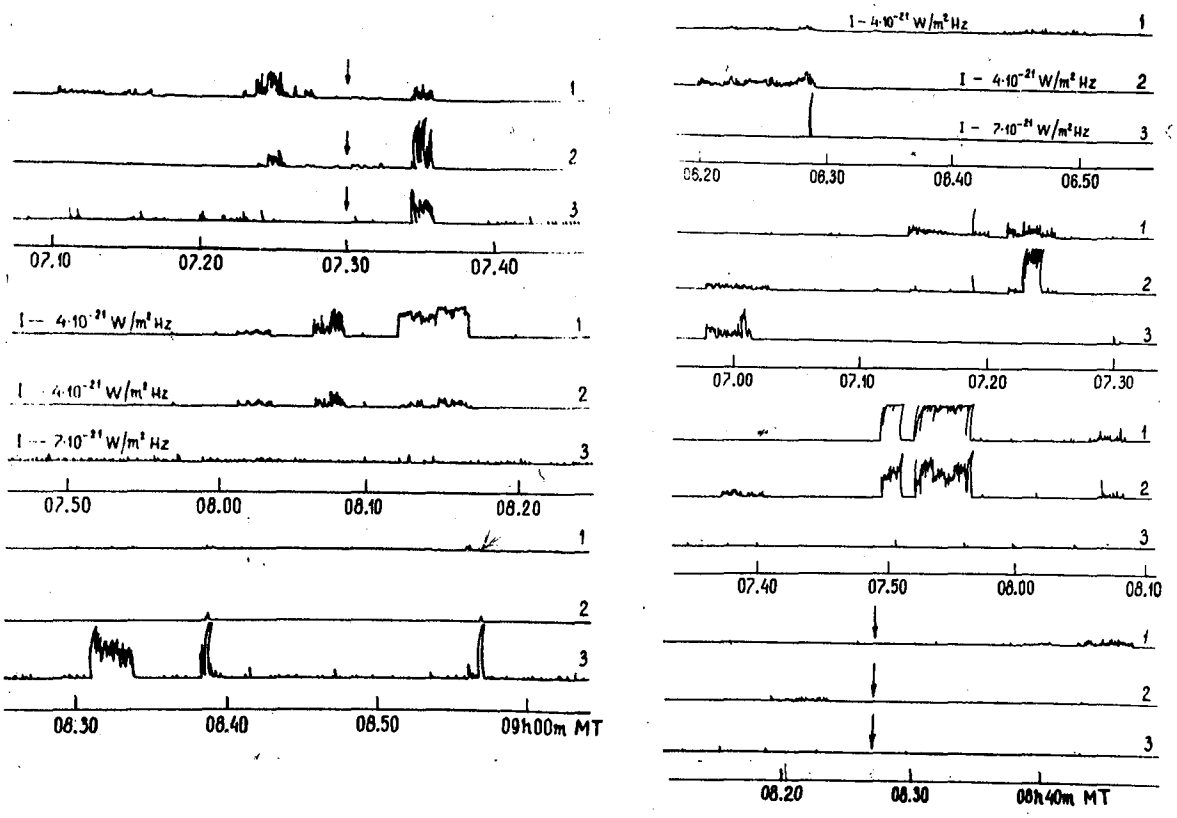

a) b)

Fig. 1. Characteristic examples of high frequency radio emission bursts series emerging during sunrise. MT - Moscow Time. Arrows show the moment of sunrise at a definite place of observation. 1 - Operating frequency of 325 MHz, East - West polarization. 2 - Operating frequency of 325 MHz, North - South polarization. 3 - Operating frequency of 38 MHz, East - West polarization. a) Morning recordig part September 28, 1984.

b) Morning recording part December 13, 1984.
The most probable duration of bursts is in the interval of 0.5 ÷ 4 m. The bursts growth and fall times are usually less than 5 s. Morning radio bursts tend to aries quasiperiodically. The quasiperiod of each bursts series is equal to 5 ÷ 20 m with mean value for full observation time being ~ 10 m. The character of sporadic radio emission polarization does not often remain unchanged even within a single series of bursts. Fine structure of bursts is irregular in most details has a period of ~0.01 ÷ 0.02 s with characteristic time of irregular modulation ~0.15 ÷ 0.5 s. The radio emission bursts coinsiding in time at the frequency of 38 and 325 MHz appeared to have similar minimal scale of fine structure details but they do not coinside in all the details of modulation.

Average diurnal course of sporadic radio emission bursts density (a number of bursts per an hour) at a frequency of 325 MHz during the autumnal equinox (1) and the winter solstice (2) is shown in fig. 2, where the sunrise and sunset are considered to take place at 6 and 18 o'clock of local time independently on the season respectively. The presence of strongly pronounced bursts density maximum during sunrise and its seasonal shift are worth emphasizing.

The observed morning effect is suggested to be connected with an excitation of internal gravity waves (IGW) by the solar terminator [3] moving in neutral atmosphere. Oscillations of IGW in neutral atmosphere draw in the ionospheric plasma and initiate its primary density disturbances. At some phase of primary disturbance in magnetized ionospheric plasma in-

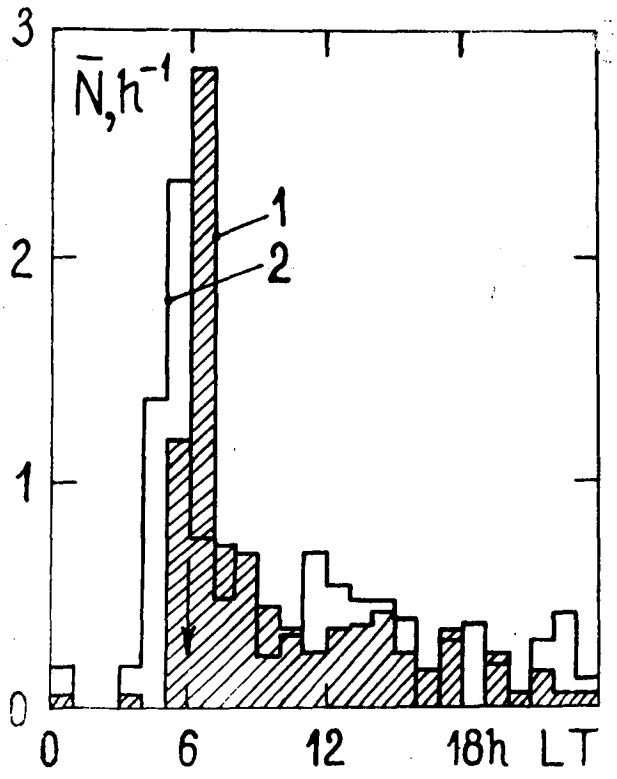

Fig. 2. Average diurnal run of near earth space sporadic radio emission reduced to equinox; $\bar{N}$ is a number of radio bursts per hour; the arrow shows the moment of sunrise; operating frequency is 325 MHz; LT is a local time. 1) September, October 1984; mean withrespect to 25 days period of observations. 2) December 1984, January 1985; mean with respect to 20 days of observations.

stabilities begin to swing quickly [4], for instance, gradient - cyclotron ion instabilities reach saturation and in this state remain unchanged during the time corres ponding to the sporadic radio emission burst duration. The instability can generate radio emission either of braking or dipole natu-

AUTHOR INDEX

BIBLIOGRAPHIC DATA SHEET

1. Report No.	2. Government Accession No.	3. Recipient's Catalog No.
NASA CP-2376 Volume 5		

4. Title and Subtitle	5. Report Date
19th International Cosmic Ray Conference Conference Papers	August 1985
	6. Performing Organization Code 665

7. Author(s)	8. Performing Organization Report No.
Frank C. Jones, compiler	

9. Performing Organization Name and Address	10. Work Unit No.
Laboratory for High Energy Astrophysics Goddard Space Flight Center Greenbelt, MD 20771	11. Contract or Grant No.
	13. Type of Report and Period Covered Conference Publication
12. Sponsoring Agency Name and Address National Aeronautics and Space Administration Washington, D. C. 20546	14. Sponsoring Agency Code

15. Supplementary Notes

16. Abstract

These volumes contain papers submitted for presentation at the 19th International Cosmic Ray Conference, held on the campus of the University of California, San Diego in La Jolla, CA., August 11-23, 1985. The conference is held every other year. The present volume contains papers with Paper Codes SH 4.3 through SH 10.1 and deals with cosmic-ray gradients in the heliosphere, siderial, diurnal and long term modulation, geomagnetic and atmospheric effects, cosmogenic nuclides, solar neutrinos.

17. Key Words (Selected by Author(s))	18. Distribution Statement
gradients, colar neutrinos, geomagnetic effects, atmospheric effects, cosmogenic nuclides	Unclassified - Unlimited Subject Category - 93

19. Security Classif. (of this report)	20. Security Classif. (of this page)	21. No. of Pages	22. Price*
Unclassified	Unclassified		

*For sale by the National Technical Information Service, Springfield, Virginia

GSFC 25-44 (10/77)

National Aeronautics and
Space Administration

Goddard Space Flight Center
Greenbelt, Maryland 20771